TECHNICAL REPORTS SERIES NO. 473

Nuclear Data for the Production of Therapeutic Radionuclides

Technical Editors
S.M. Qaim, F. Tárkányi, R. Capote

IAEA
International Atomic Energy Agency

NUCLEAR DATA FOR THE PRODUCTION OF THERAPEUTIC RADIONUCLIDES

The following States are Members of the International Atomic Energy Agency:

AFGHANISTAN
ALBANIA
ALGERIA
ANGOLA
ARGENTINA
ARMENIA
AUSTRALIA
AUSTRIA
AZERBAIJAN
BAHRAIN
BANGLADESH
BELARUS
BELGIUM
BELIZE
BENIN
BOLIVIA
BOSNIA AND HERZEGOVINA
BOTSWANA
BRAZIL
BULGARIA
BURKINA FASO
BURUNDI
CAMBODIA
CAMEROON
CANADA
CENTRAL AFRICAN REPUBLIC
CHAD
CHILE
CHINA
COLOMBIA
CONGO
COSTA RICA
CÔTE D'IVOIRE
CROATIA
CUBA
CYPRUS
CZECH REPUBLIC
DEMOCRATIC REPUBLIC OF THE CONGO
DENMARK
DOMINICAN REPUBLIC
ECUADOR
EGYPT
EL SALVADOR
ERITREA
ESTONIA
ETHIOPIA
FINLAND
FRANCE
GABON
GEORGIA
GERMANY
GHANA
GREECE
GUATEMALA
HAITI
HOLY SEE
HONDURAS
HUNGARY
ICELAND
INDIA
INDONESIA
IRAN, ISLAMIC REPUBLIC OF
IRAQ
IRELAND
ISRAEL
ITALY
JAMAICA
JAPAN
JORDAN
KAZAKHSTAN
KENYA
KOREA, REPUBLIC OF
KUWAIT
KYRGYZSTAN
LAO PEOPLE'S DEMOCRATIC REPUBLIC
LATVIA
LEBANON
LESOTHO
LIBERIA
LIBYA
LIECHTENSTEIN
LITHUANIA
LUXEMBOURG
MADAGASCAR
MALAWI
MALAYSIA
MALI
MALTA
MARSHALL ISLANDS
MAURITANIA
MAURITIUS
MEXICO
MONACO
MONGOLIA
MONTENEGRO
MOROCCO
MOZAMBIQUE
MYANMAR
NAMIBIA
NEPAL
NETHERLANDS
NEW ZEALAND
NICARAGUA
NIGER
NIGERIA
NORWAY
OMAN
PAKISTAN
PALAU
PANAMA
PARAGUAY
PERU
PHILIPPINES
POLAND
PORTUGAL
QATAR
REPUBLIC OF MOLDOVA
ROMANIA
RUSSIAN FEDERATION
SAUDI ARABIA
SENEGAL
SERBIA
SEYCHELLES
SIERRA LEONE
SINGAPORE
SLOVAKIA
SLOVENIA
SOUTH AFRICA
SPAIN
SRI LANKA
SUDAN
SWEDEN
SWITZERLAND
SYRIAN ARAB REPUBLIC
TAJIKISTAN
THAILAND
THE FORMER YUGOSLAV REPUBLIC OF MACEDONIA
TUNISIA
TURKEY
UGANDA
UKRAINE
UNITED ARAB EMIRATES
UNITED KINGDOM OF GREAT BRITAIN AND NORTHERN IRELAND
UNITED REPUBLIC OF TANZANIA
UNITED STATES OF AMERICA
URUGUAY
UZBEKISTAN
VENEZUELA
VIETNAM
YEMEN
ZAMBIA
ZIMBABWE

The Agency's Statute was approved on 23 October 1956 by the Conference on the Statute of the IAEA held at United Nations Headquarters, New York; it entered into force on 29 July 1957. The Headquarters of the Agency are situated in Vienna. Its principal objective is "to accelerate and enlarge the contribution of atomic energy to peace, health and prosperity throughout the world".

TECHNICAL REPORTS SERIES No. 473

NUCLEAR DATA FOR THE PRODUCTION OF THERAPEUTIC RADIONUCLIDES

Technical Editors
S.M. QAIM, F. TÁRKÁNYI, R. CAPOTE

INTERNATIONAL ATOMIC ENERGY AGENCY
VIENNA, 2011

Printed by the IAEA in Austria
December 2011
STI/DOC/010/473

IAEA Library Cataloguing in Publication Data

Nuclear data for the production of therapeutic radionuclides. — Vienna : International Atomic Energy Agency, 2011.
p. ; 24 cm. — (Technical reports series, ISSN 0074–1914 ; no. 473)
STI/DOC/010/473
ISBN 978–92–0–115010–3
Includes bibliographical references.

1. Radioisotopes — Therapeutic use. 2. Data compilation. 3. Nuclear data collections. 4. Isotope production. 5. Radiotherapy. I. International Atomic Energy Agency. II. Series: Technical reports series (International Atomic Energy Agency) ; 473.

IAEAL 11–00706

FOREWORD

This technical report summarizes and concludes an IAEA coordinated research project (CRP) devoted to comprehensive measurements and evaluations of neutron and charged particle induced cross-sections for the production of therapeutic radionuclides for medical applications. Nuclear reactors, cyclotrons and accelerators are used for the production of radionuclides for both diagnostic and therapeutic purposes in nuclear medicine. The physical basis of their production routes is described through the interaction of neutrons and charged particles with matter. These processes have to be well understood in order to produce radionuclides of high purity in an efficient manner. The concerted and collaborative efforts described here deal specifically with the production and use of therapeutic radionuclides. An earlier IAEA CRP was devoted to diagnostic radionuclides and monitoring reactions (IAEA-TECDOC-1211).

Although some of the production methods are well established, there are no evaluated and recommended nuclear data sets available. This situation has been emphasized at specific IAEA meetings. Over the previous 30 years, many laboratories have reported a significant body of experimental data relevant to medical radionuclide production, and charged particle data centres have compiled most of these data. However, no systematic effort had been devoted to their standardization and assembly. Under these circumstances, the IAEA decided to undertake and organize a CRP on nuclear data for the production of therapeutic radionuclides. The project was initiated in 2003, and focused on production data of radionuclides for therapeutic purposes, embracing current and possible future needs.

The assembly of a credible database involved new measurements on the production of some specific radionuclides via charged particle induced reactions, and the evaluation of cross-section data to quantify both neutron and charged particle induced reactions. Adoption and development of calculational tools in order to predict unknown cross-section data were also required.

The CRP involved nine experts from nine institutes and national radionuclide production centres. Participants met at three research coordination meetings held in Vienna. This publication constitutes the final report of the CRP.

The CRP produced a much needed database both for reactor and accelerator production, as well as this handbook covering reactions used for medically important therapeutic radionuclides. These recommended cross-sections are now accurate enough to meet the demands of all current applications and foreseen developments, although further improvements in the evaluation methodology may lead to future updates. The database is available free of cost on the following web site: http:/www-nds.iaea.org/radionuclides/.

The IAEA wishes to thank all of the participants of the CRP for their invaluable contributions to the preparation of the database. Guidance was provided throughout the project by S.M. Qaim (Germany), and extensive coordination work was undertaken by F. Tárkányi (Hungary). The contributions of R.A. Forrest, J. Kopecky, R.W. Mills, O. Serot and V. Zerkin are also acknowledged. The IAEA officers responsible for this publication were R. Paviotti-Corcuera and R. Capote of the Division of Physical and Chemical Sciences.

EDITORIAL NOTE

CONTENTS

1. INTRODUCTION

S.M. Qaim

1.1. GENERAL REMARKS

Radioactivity plays an important role in medical science in terms of beneficial applications in both diagnosis and therapy. The former entails the introduction of a short lived radionuclide attached to a suitable pharmaceutical into the patient, and measurement of the accumulation and movement of activity from outside. This process is called emission tomography and involves the measurement of either a single low energy γ ray (i.e. single photon computed emission tomography) or coincidences between the two 511 keV photons formed in the annihilation of a positron (i.e. positron emission tomography (PET)). The major governing principle in all diagnostic studies is that the radiation dose to the patient is as low as possible.

Two modalities exist in the therapeutic use of radioactivity. The first and most commonly followed procedure involves the use of external beams of electrons, X rays and γ rays from radioactive sources (e.g. ^{60}Co), high energy γ rays from accelerators, and hadrons (e.g. neutrons, protons and heavy ions). The second modality involves the introduction of certain radionuclides to a given part of the body (e.g. joints, organ and tumour) either mechanically or via a biochemical pathway. Mechanical introduction is called brachytherapy, whereas the biochemical pathway is known as endoradiotherapy.

External radiation therapy is outside the scope of the present studies. The concerted and collaborative efforts described here deal specifically with the production and use of radionuclides. An earlier coordinated research project (CRP) of the IAEA was devoted to diagnostic radionuclides [1.1]. The present effort is related to therapeutic radionuclides.

1.2. CRITERIA FOR CHOICE OF A THERAPEUTIC RADIONUCLIDE

The major criteria for the choice of a radionuclide for endotherapeutic use are suitable decay characteristics and appropriate biochemical reactivity [1.2]. As regards decay properties, the desired half-life is between 6 h and 7 d, and the emitted corpuscular radiation should have a suitable linear energy transfer and range in the tissue. The ratio of non-penetrating (corpuscular radiation) to penetrating (photon) radiation should be high, and the daughter should be short lived or stable. As regards biochemical reactivity, the situation is more stringent

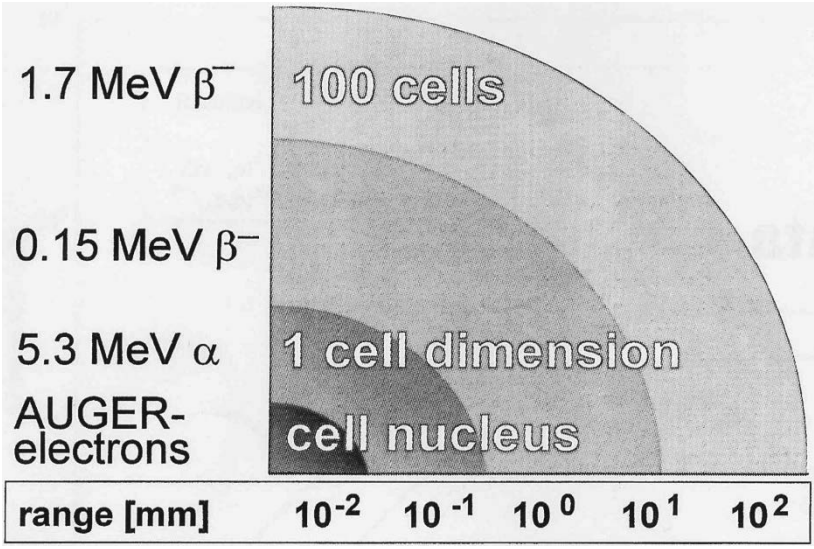

FIG. 1.1. Correlation between type and energy of corpuscular radiation, and the range in tissue (adapted from Refs [1.2–1.4]).

than for a diagnostic radiopharmaceutical, since the stability of the therapeutic entity is demanded over a much longer time period than in the case of a diagnostic pharmaceutical. Thus, the basis for successful endoradiotherapy [1.2] incorporates:

— Selective concentration and prolonged retention of the therapeutic radionuclide in the tumour;
— Minimum uptake in normal tissue.

As a result of the above criteria, the choice falls on about 30 radionuclides. Most of them are β^- emitters although several are α rays, X rays and Auger or conversion electron emitters. The ranges of the various types of emitted corpuscular radiation in the tissue are shown in Fig. 1.1.

Auger electrons have a range of about 10 μm and can only have a therapeutic effect if they reach the cell nucleus, e.g. by bringing the radioactive atoms to the DNA. On the other hand, α particles have a range of about 100 μm and can have a therapeutic effect if they reach the cell membrane, e.g. by attachment of the α emitter to a receptor ligand. β^- particles have ranges of about 1 mm and more, depending upon their energies, leading to therapeutic effects even if they reach the cell environment. Achieving beneficial therapeutic effects with Auger electrons and α particles involves a very subtle approach and

demands great skill in biochemistry, radiopharmacology and production of the radiotherapeutical. Therapeutic applications have been more straightforward, though not very specific, in the case of β^- particles.

1.3. SIGNIFICANCE OF NUCLEAR DATA

Radioactive decay data play a key role in the therapeutic application of a radionuclide [1.4, 1.5], and knowledge of the energy and intensity of the ionizing radiation is crucial. The effect of low energy, high intensity electrons emitted following EC and IT decay is not negligible. Therefore, for widely used therapeutic radionuclides, all sources of secondary electrons must be taken into account.

Overall, the available database on decay characteristics of radionuclides used in radiotherapy is extensive [1.6, 1.7], although there may be some deficiencies for individual radioisotopes. Thus, the Auger electron spectra are occasionally not known to the desired accuracy, and some of the positron emitters introduced recently as therapeutic radionuclides may have uncertain β^+ branching ratios. A few therapeutic radionuclides emit very low intensity rays (e.g. ^{64}Cu, ^{103}Pd and ^{211}At) — those γ rays are of little significance in therapy, although some experimentalists tend to choose them for nuclear reaction cross-section measurements. However, the data obtained need to be treated with some caution, and would benefit from specific measurements and evaluations. A recent study of this type dealt with the radionuclide ^{64}Cu [1.8], and similar work to clarify the decay data would be beneficial.

Whereas the radioactive decay data are of prime importance in the choice of a radionuclide for therapeutic application, the nuclear reaction data are of great significance in the optimization of the production processes, i.e. achieving the maximum yield of desired radionuclide combined with the minimum level of impurities. Since the radionuclides are produced using both reactors and cyclotrons, accurate knowledge of the relevant neutron as well as charged particle induced reaction cross-section data are essential.

The most important reaction for the production of radionuclides in a nuclear reactor is the (n, γ) process. However, during irradiation, only a small fraction of the target nuclei is activated and the radionuclide formed is of low specific activity (i.e. activity/unit mass is low). Many therapeutic radionuclides, such as ^{153}Sm ($T_{½}$ = 46.3 h) and ^{192}Ir ($T_{½}$ = 73.8 d) are produced via this route, and, therefore, their specific activity remains rather low. The same problem applies to the product of the double neutron capture process, e.g. ^{188}W formed in the sequence ^{186}W(n, γ)^{187}W(n, γ)^{188}W ($T_{½}$ = 69.0 d). The specific activity is enhanced if the daughter product is used instead of the (n, γ) reaction product.

Two important therapeutic radionuclides, ^{131}I ($T_{½}$ = 8.0 d) and ^{125}I ($T_{½}$ = 59.4 d), are produced with high specific activity via the reaction sequences $^{130}Te(n, \gamma)^{131m,g}Te \xrightarrow{\beta^-} {}^{131}I$ and $^{124}Xe(n, \gamma)^{125}Xe \xrightarrow{EC} {}^{125}I$, respectively. Another possibility involves the preparation of a generator system, for example, the generator system $^{188}W \xrightarrow{\beta^-} {}^{188}Re$, whereby the short lived daughter ^{188}Re ($T_{½}$ = 17.0 h) is periodically milked from the parent.

Two other processes, namely nuclear fission and the (n, p) reaction, are also occasionally used for the production of therapeutic radionuclides. The two most prominent therapy related radionuclides produced via fission are ^{131}I ($T_{½}$ = 8.0 d) and ^{90}Sr ($T_{½}$ = 28.6 a) — the former is used directly in endoradiotherapy and the latter is utilized in the preparation of the $^{90}Sr/^{90}Y$ generator system. As far as the (n, p) reaction is concerned, the fission neutron spectrum-averaged cross-section is generally low, although the process is in common use with regard to the production of ^{32}P and ^{89}Sr via the $^{32}S(n, p)^{32}P$ and $^{89}Y(n, p)^{89}Sr$ reactions, respectively.

As far as the cyclotron production of therapeutic radionuclides is concerned, a large number of processes may be utilized. Data requirements are stringent since many competing reactions occur. While radionuclide production data using protons, deuterons, ^{3}He and α particles are commonly available, protons and deuterons have been most commonly utilized because these reactions lead to higher yields. The ultimate choice of a production process depends upon the availability of a suitable cyclotron and the required target material.

Copper-64 ($T_{½}$ = 12.7 h) is an important emerging therapeutic nuclide that constitutes an excellent example to elucidate all the points discussed above. This radionuclide decays via three modes, namely β^- emission (38.4%), β^+ emission (17.8%) and EC (43.8%). The β^+ branching and intensity of the weak 1346 keV γ rays have been recently determined with higher precision, and the known decay characteristics allow a combination of radioimmunotherapy and PET. As far as production is concerned, the $^{63}Cu(n, \gamma)^{64}Cu$ reaction was originally used but this process has been abandoned and the $^{64}Zn(n, p)^{64}Cu$ reaction has been adopted. Although the fission spectrum-averaged cross-section of this reaction is low (69 mb), good purity product in sufficient yield is obtained if highly enriched ^{64}Zn is used as the target material. On the other hand, if ^{nat}Zn is used as the target material, the resulting ^{64}Cu is contaminated with large quantities of ^{67}Cu. Several other methods for the production of high specific activity ^{64}Cu have been suggested utilizing a cyclotron, as listed in Table 1.1. The (p, n) and (d, 2n) reactions on high enriched ^{64}Ni lead to high yield and high purity ^{64}Cu, but the target material is expensive. Sufficient ^{64}Cu is produced from the ^{68}Zn (p, αn) reaction, although a very clean separation from the much stronger matrix ^{67}Ga activity is mandatory. Furthermore, if the proton energy exceeds 35 MeV, the amount of co-produced ^{67}Cu becomes excessive.

TABLE 1.1. ROUTES FOR PRODUCTION OF HIGH SPECIFIC ACTIVITY ^{64}Cu

Production route	Suitable energy range (MeV)	Calculated integral yield (MBq/μA·h)
$^{64}Zn(n, p)^{64}Cu$	fission spectrum	14.5[a]
$^{64}Ni(d, 2n)^{64}Cu$	19 → 15	389
$^{64}Ni(p, n)^{64}Cu$	12 → 9	241[b]
$^{66}Zn(d, \alpha)^{64}Cu$	13 → 7	6.6
$^{nat}Zn(d, x)^{64}Cu$	25 → 10	50
$^{68}Zn(p, \alpha n)^{64}Cu$	35 → 20	~100

[a] Activity/mg Zn at $\Phi_n = 8.7 \times 10^{13}$ n cm^{-2} s^{-1} for 150 h.
[b] Presently the method of choice.

Similarly, the $^{66}Zn(d, \alpha)^{64}Cu$ and $^{64}Zn(d, 2p)^{64}Cu$ reactions also appear to be suitable methods of production. The $^{nat}Zn(d, x)^{64}Cu$ reactions at $E_d \leq 25$ MeV are particularly noteworthy — the use of ^{nat}Zn would lead to considerable savings in the cost of the target material. A significant number of production routes are feasible for the production of ^{64}Cu. Nonetheless, the preferred choice lies with the $^{64}Ni(p, n)^{64}Cu$ reaction, despite the high cost of the target material, because of the high yield and high purity produced by means of a small cyclotron.

1.4. SCOPE OF EVALUATION WORK

Nuclear reaction data are important for medical applications and no concerted efforts are being made to define the most appropriate reactions and optimum conditions. Thus, the IAEA established the following three CRPs in a sequential manner:

(a) Data for production of diagnostic radionuclides and for charged particle beam monitoring — the CRP has been completed and the final document was published as IAEA-TECDOC-1211 in 2001 [1.1] (the database is updated periodically);
(b) Data for production of therapeutic radionuclides — the CRP was completed in 2006 (this publication represents a primary outcome of this particular piece of work);
(c) Data for external radiation therapy — the CRP has just begun.

The studies undertaken in connection with the CRP on therapeutic radionuclides focused on the evaluation of production data. Participants at an IAEA consultants meeting recommended the evaluation of production data for about 25 radionuclides. During the course of the resulting CRP, further radionuclides were added to the list of requirements. All of those radionuclides were divided into two groups:

(a) Well established and commonly used therapeutic radionuclides;
(b) Emerging therapeutic radionuclides that are potentially important — their application in medicine has been demonstrated at least once but further medical work is needed to establish them fully.

As has been discussed above, therapeutic radionuclides are produced by means of both nuclear reactors and cyclotrons. Evaluations are, therefore, required of both neutron and charged particle induced reactions. Although many reactions can be applied to the production of a radionuclide (especially charged particle irradiations), only one or two reactions are either commonly used or are potentially useful for each radionuclide. Thus, emphasis has been placed on the more important reactions.

Each radionuclide needs to be treated individually. First, the reactor methods of production are considered (i.e. neutron induced reactions) and, thereafter, the cyclotron methods of production (i.e. charged particle induced reactions). Data for all three processes in reactor production, namely (n, γ), (n, f) and (n, p), were considered. Data for proton and deuteron induced reactions up to approximately 70 MeV are needed, and α particle induced reaction data are also required in a few special cases.

The major aim of the present work has been to evaluate the production data of all reactor and cyclotron produced therapeutic radionuclides, whether of direct importance today or of potential interest in the future. However, emphasis was placed on the most effective routes of production, i.e. preferably on reactions meeting the four basic criteria of high yield, high radionuclide purity, high chemical purity and high specific activity.

1.5. EVALUATION METHODOLOGY

The assembly of a credible database involved the evaluation of cross-section data to quantify both neutron and charged particle induced reactions. While the evaluation procedures for neutron data are well established, the equivalent methodology for charged particle data is still developing. The methodology used during the previous CRP on diagnostic radionuclides was

followed for the charged particle data. Evaluation work consisted of the following steps:

1.5.1. Compilation of data and new experimental studies

Most of the experimental data are available in EXFOR and, therefore, significant reliance was placed on that database. However, for completeness, extensive literature surveys were also performed, and data not available in EXFOR were compiled. New measurements were also undertaken. All of the available data were then considered in a comprehensive evaluation.

1.5.2. Nuclear model calculations

Standard model calculations were performed when evaluating the (n, γ), (n, p) and (n, f) reactions, and the recommended cross-sections are based on the methodology used in energy related work (e.g. files on fission and activation products, and dosimetry).

Two types of calculational code were used for the evaluations of the charged particle data: pre-compound exciton model (ALICE-IPPE code) and the Hauser–Feshbach formalism incorporating pre-compound effects (GNASH, STAPRE and EMPIRE II codes).

1.5.3. Fitting of data

Averaging and fitting methods were employed in the evaluation of all charged particle induced reactions. Only partial success was achieved in reproducing the experimental data by model calculations and, therefore, more reliance was placed on the data fitting methods.

1.6. STRUCTURE

The CRP was initiated in 2003 and brought to completion at the end of 2006. This technical publication summarizes the results of the CRP and presents the evaluated data for general use. New experimental data that were measured during the course of the CRP are described in Chapter 2, while the nuclear model calculations and fitting procedure are considered in Chapters 3, 4 and 5. Detailed results of all of the evaluations are summarized in Chapters 6 and 7 — these chapters constitute the main body of the report, and quantify the major features of the CRP. Both well established therapeutic radionuclides and emerging radionuclides have been specified and quantified in this report.

All of the collected experimental data are given for each individual charged particle induced reaction. After careful analysis, only the most reliable and concordant data were considered in the evaluations. Thereafter, the results of various calculations and evaluations are described and compared with the selected experimental data. Recommended curves are presented which agree very closely with the experimental data; the recommended numerical values of the reaction cross-sections have also been tabulated based on these curves. As well as the major production routes, some other reactions that generate adjacent impurities have been treated in the same way. Since many users prefer information on integral production yields rather than cross-sections, the expected yields of various products were calculated from the recommended excitation functions. The recommended cross-sections and yields are believed to be accurate enough to meet the demands of most of the presently envisaged applications.

The evaluated excitation curves for the two types of neutron induced reactions are presented and the integrated cross-sections for fission neutron spectra are deduced. These cross-sections can be used with confidence to calculate the activation of various materials. Accurate cumulative yields are also given for radionuclides formed via the fission process.

Only scanty cross-section information was available for some nuclear processes. Several reactor produced low specific activity radionuclides required investigation by alternative cyclotron production routes. Thus, a considerable amount of new experimental data were obtained during the course of the CRP, as given separately in Chapter 2. Publications based on the CRP work are also listed.

1.7. AVAILABILITY OF DATA

The database developed during this project and the resulting evaluated data are given in graphical and numerical form within the present report. Calculated yields of the cyclotron produced radionuclides are also given.

All of these data can be obtained electronically from the web site http://www-nds.iaea.org/radionuclides/. The data are also available from the IAEA's ENDF retrieval interface at http://www-nds.iaea.org/exfor/endf.htm (see special libraries).

REFERENCES

[1.1] INTERNATIONAL ATOMIC ENERGY AGENCY, Charged Particle Cross-Section Database for Medical Radioisotope Production: Diagnostic Radioisotopes and Monitor Reactions, IAEA-TECDOC-1211, IAEA, Vienna (2001).

[1.2] QAIM, S.M., Therapeutic radionuclides and nuclear data, Radiochim. Acta **89** (2001) 297–302.

[1.3] LEWINGTON, V.J., Targeted radionuclide therapy for bone metastases, Eur. J. Nucl. Med. Mol. Imaging **20** (1993) 66–74.

[1.4] STÖCKLIN, G., QAIM, S.M., RÖSCH, F., The impact of radioactivity on medicine, Radiochim. Acta **70/71** (1995) 249–272.

[1.5] VOLKERT, W.A., GOECKLER, W.F., ERHARDT, G.J., KETERING, A.R., Therapeutic radionuclides: Production and decay property considerations, J. Nucl. Med. **32** (1991) 174–185.

[1.6] BROWNE, E., FIRESTONE, R.B., Table of Radioactive Isotopes, SHIRLEY, V.S. (Ed.), Wiley, London (1986).

[1.7] Nuclear Data Sheets, Elsevier, Orlando, Florida, US, ENSDF database (Evaluated Nuclear Structure Data File), www.nndc.bnl.gov/ensdf

[1.8] QAIM, S.M., BISINGER, T., HILGERS, K., NAYAK, D., COENEN, H.H., Positron emission intensities in the decay of ^{64}Cu, ^{76}Br and ^{124}I, Radiochim. Acta **95** (2007) 67–73.

2. NEW EXPERIMENTAL DATA

F. Tárkányi and S.M. Qaim

During the course of the compilation process, the compilers noted that the available experimental information for some charged particle induced production routes was not satisfactory for the preparation of recommended data:

- Available information on the related production cross-section data was so inadequate that the evaluation process proved to be impossible to implement;
- There were significant contradictions between the reported experimental data, which could not be resolved on the basis of the information in the reports;
- Isotopic cross-section data could be checked by measuring excitation functions on targets with natural isotopic composition;
- During the evaluation process, new candidate reactions arose for which information on the available cross-section data was inadequate.

Although a few new experiments were performed, these studies were limited by the available time and financial resources concerning the procurement of enriched target materials. The irradiations involved charged particle beams at different cyclotrons in Debrecen, Jülich, Brussels and Sendai by means of the stacked foil irradiation technique. Particle fluxes were determined with the aid of well measured monitor reactions, and the resulting activities were determined by means of γ ray, X ray or α particle spectrometry, with or without chemical separation. Nuclear data used during the evaluations were taken from the latest on line databases. 'New measurements' involved experimental work on nuclear reactions recommended by the CRP, and covered the period 2003–2007.

A summary of the new cross-section and yield measurements performed as part of the CRP is given in Table 2.1. Only one study involved the measurement of new decay data for ^{64}Cu and ^{124}I (Qaim et al. (2007)).

A few measurements were also undertaken on (n, p) reactions leading to the formation of the ^{32}P, ^{64}Cu, ^{67}Cu, ^{89}Sr, ^{90}Y and ^{153}Sm therapeutic radionuclides. A 14 MeV d(Be) broad neutron spectrum, as generated at the Jülich cyclotron CV 28, was used. Those integral measurements served as a basis for testing the evaluated excitation functions of the respective (n, p) reactions.

TABLE 2.1. SUMMARY OF EXPERIMENTS ON CROSS-SECTION MEASUREMENTS

Author reference	Reaction	Target	Beam monitoring	Activity measurement	Stopping power (sp); Decay data (dd)	Energy range (MeV); No. of points	Reference; EXFOR entry No.
Hilgers et al. (2003)	^{68}Zn(p, αn)^{64}Cu	^{68}Zn(98%) electrodeposition on Au foil	^{nat}Cu(p, x)^{62,65}Zn, ^{nat}Ti(p, x)^{48}V	511-HPGe, chemical separation	sp: Williamson (1966); dd: Firestone (1998)	8.5–44.6; 22	D0069
Hilgers et al. (2003)	^{66}Zn(d, α)^{64}Cu	^{66}Zn(99%) electrodeposition on Au foil	^{nat}Ni(d, x)^{61}Cu, ^{nat}Fe(d, x)^{56}Co	511-HPGe, chemical separation	sp: Williamson (1966); dd: Firestone (1998)	5.4–13.8; 10	D0069
Hilgers et al. (2003)	^{nat}Zn(d, x)^{64}Cu	^{nat}Zn electrodeposition on Au foil	^{nat}Ni(d, x)^{61}Cu, ^{nat}Fe(d, x)^{56}Co	511-HPGe, chemical separation	sp: Williamson (1966); dd: Firestone (1998)	8.9–13.2; 8	D0069
Groppi et al. (2004)	^{nat}Zn(d, x)^{64}Cu	^{nat}Zn foil	^{27}Al(d, x)^{24}Na, ^{nat}Ti(d, x)^{48}V	γ-HPGe, no chemical separation	sp: SRIM (2000); dd: Firestone (1998)	5–19; 17 +yield	O0778
Spahn et al. (2004)	^{64}Zn(n, p)^{64}Cu, ^{67}Zn(n, p)^{67}Cu, ^{89}Y(n, p)^{89}Sr	Oxide pellets	14 MeV d(Be) break-up neutrons ^{27}Al(n, α)^{24}Na	γ-HPGe, chemical separations	dd: Firestone (1998)	Spectrum averaged σ	no EXFOR entry compiled
Tárkányi et al. (2004)	^{nat}Zn(d, x)^{64}Cu, ^{nat}Zn(d, x)^{67}Cu	^{nat}Zn foil	^{nat}Ni(d, x)^{61}Cu, ^{nat}Cu(d, x)^{65}Zn, ^{nat}Al(d, x)^{24}Na	γ-HPGe, no chemical separation	sp: Andersen (1977); dd: Lund database	15.5–48.9; 19 15.5–48.9; 19	D4144

TABLE 2.1. SUMMARY OF EXPERIMENTS ON CROSS-SECTION MEASUREMENTS (cont.)

Author reference	Reaction	Target	Beam monitoring	Activity measurement	Stopping power (sp); Decay data (dd)	Energy range (MeV); No. of points	Reference; EXFOR entry No.
Tárkányi et al. (2005)	$^{nat}Zn(p, x)^{64}Cu$, $^{nat}Zn(p, x)^{67}Ga$	^{nat}Zn foil	$^{nat}Al(p, x)^{22,24}Na$, $^{nat}Cu(p, x)^{56,58}Co$, $^{62,65}Zn$	γ-HPGe, no chemical separation	sp: Andersen (1977); dd: NUDAT	25.6–67.4; 9 25.6–67.4; 9	E1921 O1310 O1351 D4149
Tárkányi et al. (2005)	$^{114}Cd(p, n)^{114m}In$	^{114}Cd(99%) electrodeposition on Cu and Al foils	$^{nat}Cu(p, x)^{62,65}Zn$, IAEA-TECDOC-1211	γ-HPGe, no chemical separation	sp: Andersen (1977); dd: NUDAT	4.89–35.75; 38	D4160
Tárkányi et al. (2005)	$^{114}Cd(d, 2n)^{114m}In$	^{114}Cd(99%) electrodeposition on Cu foil	$^{nat}Ti(d, x)^{48}V$, $^{nat}Fe(d, x)^{56}Co$, $^{nat}Cu(d, x)^{65}Zn$, IAEA-TECDOC-1211	γ-HPGe, no chemial separation	sp: Andersen (1977); dd: NUDAT	6.41–20.74; 16	D4160
Tárkányi et al. (2005)	$^{116}Cd(p, 3n)^{114m}In$	^{nat}Cd foil	$^{nat}Cu(p, x)^{62,65}Zn$, IAEA-TECDOC-1211	γ-HPGe, no chemical separation	sp: Andersen (1977); dd: NUDAT	19–50; 32	D4160
Tárkányi et al. (2005)	$^{nat}Cd(p, x)^{114m}In$ $^{nat}Cd(p, x)^{111}In$	^{nat}Cd foil	$^{nat}Cu(p, x)^{56}Co$, $^{62,65}Zn$, $^{nat}Cd(p, x)^{22,24}Na$, IAEA-TECDOC-1211	γ-HPGe, no chemical separation	sp: Andersen (1977); dd: NUDAT	7.5–74.5; 40 7.5–74.5; 47	D4160
Spahn et al. (2005)	$^{169}Tm(p, n)^{169}Yb$	Tm_2O_3 sedimentation on Al foil	$^{nat}Cu(p, x)^{62,65}Zn$, IAEA-TECDOC-1211	γ-HPGe, no chemical separation	sp: Williamson (1966); dd: Firestone (1998)	4.8–44.9; 27	D4148

TABLE 2.1. SUMMARY OF EXPERIMENTS ON CROSS-SECTION MEASUREMENTS (cont.)

Author reference	Reaction	Target	Beam monitoring	Activity measurement	Stopping power (sp); Decay data (dd)	Energy range (MeV); No. of points	Reference; EXFOR entry No.
Hilgers et al. (2005)	^{192}Os(p, n)^{192}Ir	^{192}Os(84.5%) electrodeposition on Ni foil	^{nat}Cu(p, x)^{62,65}Zn, ^{nat}Ti(p, x)^{48}V, IAEA-TECDOC-1211	γ-HPGe, no chemical separation	sp: Williamson (1966); dd: Firestone (1998)	6.4–13.8; 20	O1274
Hermanne et al. (2005)	^{209}Bi(α, 2n)^{211}At ^{209}Bi(α, 3n)^{210}At	Bi evaporation on Cu foil	^{nat}Cu(α, x)^{67}Ga, ^{65}Zn, IAEA-TECDOC-1211	α-Si, γ-HPGe, no chemical separation	sp: Andersen (1977); dd: Browne (1986)	21.1–39.9; 21 31.0–39.9; 14	O1272
Kozempel et al. (2006)	^{64}Zn(d, 2p)^{64}Cu	^{64}Zn(99.4%) disk	^{nat}Ti(d, x)^{48}V, IAEA-TECDOC-1211	γ-HPGe, no chemical separation	sp: SRIM (2003); dd: Firestone (1998)	12.9–18.2	O1508
Tárkányi et al. (2006)	^{186}W(p, n)^{186}Re	^{nat}W	^{nat}Cu(p, x)^{62,65}Zn, IAEA-TECDOC-1211	γ-HPGe, no chemical separation	sp: Andersen (1977); dd: NUDAT	5.66–33.41; 29	D4163
Alfarano et al. (2006)	^{209}Bi(α, 2n)^{211}At	Bi foil covered by Al	^{nat}Cu(α, x)^{67}Ga, ^{65}Zn, IAEA-TECDOC-1211	α-Si, γ-HPGe, chemical separation	Firestone (1998)	yield	D0413

TABLE 2.1. SUMMARY OF EXPERIMENTS ON CROSS-SECTION MEASUREMENTS (cont.)

Author reference	Reaction	Target	Beam monitoring	Activity measurement	Stopping power (sp); Decay data (dd)	Energy range (MeV); No. of points	Reference; EXFOR entry No.
Al Abyad et al. (2006)	$^{64}Zn(n, p)^{64}Cu$, $^{32}S(n, p)^{32}P$, $^{90}Zr(n, p)^{90}Y$, $^{153}Eu(n, p)^{153}Sm$, $^{67}Zn(n, p)^{67}Cu$	^{nat}S, $^{nat}ZrO_2$, $^{nat}Eu_2O_3$, ^{nat}Zn	14 MeV d(Be) break-up neutrons $^{27}Al(n, \alpha)^{24}Na$	γ-HpGe, no chemical separation		Spectrum averaged σ	22857
Tárkányi et al. (2007)	$^{nat}Cd(d, x)^{114m}In$	^{nat}Cd foil	$^{nat}Al(d, x)^{22,24}Na$, $^{nat}Fe(d, x)^{56}Co$, $^{nat}Cu(d, x)^{65}Zn$, IAEA-TECDOC-1211	γ-HPGe, no chemical separation	sp: Andersen (1977); dd: NUDAT	6.5–39.8; 26	D4179
Tárkányi et al. (2007)	$^{169}Tm(d, 2n)^{169}Yb$	Tm_2O_3 sedimentation on Al foil	$^{nat}Ti(d, x)^{48}V$, IAEA-TECDOC-1211	γ-HPGe, no chemical separation	sp: Andersen (1977); dd: NUDAT	4.41–20.51; 19	D4180
Tárkányi et al. (2007)	$^{192}Os(d, 2n)^{192}Ir$	^{192}Os(84.5%) electrodeposition on Ni foil	$^{nat}Ti(d, x)^{48}V$, $^{nat}Cu(d, x)^{61}Cu$, IAEA-TECDOC-1211	γ-HPGe, no chemical separation	sp: Andersen (1977); dd: NUDAT	5.2–20.7; 12	D4192
Tárkányi et al. (2007)	$^{nat}Cd(d, x)^{111}In$	^{nat}Cd foil	$^{nat}Al(d, x)^{22,24}Na$, $^{nat}Fe(d, x)^{56}Co$, $^{nat}Cu(d, x)^{65}Zn$, IAEA-TECDOC-1211	γ-HPGe, no chemical separation	sp: Andersen(1977); dd: NUDAT	4.9–39.8; 27	No Cd(d, x)

TABLE 2.1. SUMMARY OF EXPERIMENTS ON CROSS-SECTION MEASUREMENTS (cont.)

Author reference	Reaction	Target	Beam monitoring	Activity measurement	Stopping power (sp); Decay data (dd)	Energy range (MeV); No. of points	Reference; EXFOR entry No.
Tárkányi et al. (2007)	$^{186}W(p, n)^{186}Re$	^{nat}W	$^{nat}Ti(p, x)^{48}V$, IAEA-TECDOC-1211	γ-HPGe, no chemical Separation	sp: Andersen (1977); dd: NUDAT	5.57–31.07; 33	D4193
Hermanne et al. (2007)	$^{64}Ni(d, 2n)^{64}Cu$	^{nat}Ni	$^{nat}Ti(d, x)^{48}V$, IAEA-TECDOC-1211	γ-HPGe, no chemical separation	sp: Andersen (1977); dd: NUDAT	4.2–20.4; 24	D4182
Hermanne et al. (2007)	$^{169}Tm(d, 2n)^{169}Yb$	Tm_2O_3 sedimentation on Al foil	$^{nat}Al(d, x)^{22,24}Na$, $^{nat}Cu(d, x)^{65}Zn$, IAEA-TECDOC-1211	γ-HPGe, no chemical separation	sp: Andersen (1977); dd: NUDAT	19.71–38.55; 9	no
Hermanne et al. (2007)	$^{116}Cd(p, 3n)^{114m}In$	^{116}Cd(99%) electrodeposition on Cu foil	$^{nat}Cu(p, x)^{62,63,65}Zn$, IAEA-TECDOC-1211	γ-HPGe, no chemical separation	sp: Andersen (1977); dd: NUDAT	18.0–37.0; 15	D4229
Qaim et al. (2007)	$^{150}Nd(\alpha, n)^{153}Sm$	$^{nat}Nd_2O_3$ sedimentation on Al foil	$^{nat}Ti(\alpha, x)^{51}Cr$, IAEA-TECDOC-1211	γ-HPGe, no chemical separation	sp: Williamson (1966); dd: Firestone (1998)	15.0–25.0	D4191

BIBLIOGRAPHY

AL-ABYAD, M., et al., Nuclear data for production of the therapeutic radionuclides ^{32}P, ^{64}Cu, ^{67}Cu, ^{89}Sr, ^{90}Y and ^{153}Sm via the (n,p) reaction: Evaluation of excitation function and its validation via integral cross-section measurement using a 14 MeV d(Be) neutron source, Appl. Radiat. Isot. **64** (2006) 717–724.

ALFARANO, A., et al., Thick target yield measurement of ^{211}At through the nuclear reaction ^{209}Bi(α, 2n), J. Phys.: Conf. Ser. **41** (2006) 115–122.

CAPOTE NOY, R., et al., "IAEA Coordinated Research Programme: Nuclear data for the production of therapeutic radionuclides", Int. Conf. Nuclear Data for Science and Technology, ND 2007, Nice, France 22–27 April 2007.

GROPPI, F., et al., Thin-target excitation functions and optimisation of NCA ^{64}Cu and ^{66,67}Ga production by deuteron induced nuclear reactions on natural zinc target, for radiometabolic therapy and for PET, Nucl. Instrum. Methods B **213** (2004) 373–377.

HERMANNE, A., "Excitation functions for production of medically relevant radioisotopes in deuteron irradiations of Pr and Tm targets", 17th Int. Symp. Radiopharmaceutical Sciences, ISRS 17, Aachen, Germany, 30 April–4 May 2007.

HERMANNE, A., et al., "Excitation functions for production of medically relevant radioisotopes in deuteron irradiations of Pr and Tm targets", 9th Int. Symp. Synthesis and Applications of Isotopes and Isotopically Labelled Compounds (Proc. Edinburgh, 2006), J. Labelled Compd Radiopharm. Suppl. **50** (2007) 102.

HERMANNE, A., et al., "Experimental study of the cross sections of reactions induced by alpha-particles on ^{209}Bi", Int. Conf. Nuclear Data for Science and Technology, Santa Fe, USA, 26 September–1 October 2004 (Abstract: LA-UR-04-5900, Los Alamos, p. 124).

HERMANNE, A., et al., Deuteron-induced reactions on Yb: Measured cross sections and rationale for production pathways of carrier-free, medically relevant radionuclides, Nucl. Instrum. Methods B **247** (2006) 223–231.

HERMANNE, A., et al., Experimental study of the cross sections of alpha-particle induced reactions on ^{209}Bi, Appl. Radiat. Isot. **63** (2005) 1–9.

HERMANNE, A., TÁRKÁNYI, F., TAKÁCS, S., KOVALEV, S.F., IGNATYUK, A., Activation cross sections of the ^{64}Ni(d,2n) reaction for the production of the medical radionuclide ^{64}Cu, Nucl. Instrum. Methods B **258** (2007) 308–312.

HERMANNE, A., TÁRKÁNYI, F., TAKÁCS, S., KOVALEV, S.F., IGNATYUK, A., "Activation cross sections of the ^{64}Ni(d,2n) reaction for the production of the medical radionuclide ^{64}Cu", 9th Int. Symp. Synthesis and Applications of Isotopes and Isotopically Labelled Compounds, Edinburgh, UK, 16–20 July 2006 (Book of Abstracts: p. 136).

HERMANNE, A., TÁRKÁNYI, F., TAKÁCS, S., SZÛCS, Z., "Experimental study of the cross sections of alpha-particle induced reactions on ^{209}Bi", Int. Conf. Nuclear Data for Science and Technology (Proc. Santa Fe, NM, 2004), HAIGHT, R.C., CHADWICK, M.B., TALOU, P., KAWANO, T. (Eds), AIP Conf. Proc. 769, Part 1, Melville, New York (2005) 957–960.

HILGERS, K., STOLL, T., SKAKUN, Y., COENEN, H.H., QAIM, S.M., Cross-section measurements of the nuclear reactions ^{nat}Zn(d,x)^{64}Cu, ^{66}Zn(d,α)^{64}Cu and ^{68}Zn(p,αn)^{64}Cu, Appl. Radiat. Isot. **59** (2003) 343–351.

HILGERS, K., SUDÁR, S., QAIM, S.M., Experimental study and nuclear model calculations on the ^{192}Os(p,n)^{192}Ir reaction: Comparison of reactor and cyclotron production of the therapeutic radionuclide ^{192}Ir, Appl. Radiat. Isot. **63** (2005) 93–98.

KIRÁLY, B., TÁRKÁNYI, F., TAKÁCS, S., KOVÁCS, Z., "Measurements of excitation functions of proton induced nuclear reactions on elemental tellurium up to 18 MeV for validation of isotopic cross sections", 15th Radiochemical Conf., Mariánské Lázne, Czech Republic, 23–28 April 2006 (Booklet of abstracts: P5–6, p. 206).

KIRÁLY, B., TÁRKÁNYI, F., TAKÁCS, S., KOVÁCS, Z., Excitation functions of proton induced nuclear reactions on natural tellurium up to 18 MeV for validation of isotopic cross sections, J. Radioanal. Nucl. Chem. **270** (2006) 369–378.

KOZEMPEL, J., et al., A novel method for N.C.A. ^{64}Cu production by the Zn(d,2p)^{64}Cu reaction and dual ion-exchange column chromatography, Appl. Radiat. Isot. **64** (2006) 1001–1005.

NORTIER, F.M., et al., "Nuclear data for production of therapeutic radionuclides", 229th American Chemical Soc. Natl Mtg and Exposition, San Diego, CA, USA, 13–17 March 2005.

QAIM, S.M., BISINGER, T., HILGERS, K., NAYAK D., COENEN H.H., Positron emission intensities in the decay of ^{64}Cu, ^{76}Br and ^{124}I, Radiochim. Acta **95** (2007) 67–73.

QAIM, S.M., SPAHN, I., KANDIL, S.A., COENEN, H.H., Nuclear data for production of ^{88}Y, ^{140}Nd, ^{153}Sm and ^{169}Yb via novel routes, Radiochim. Acta **95** (2007) 313–317.

SPAHN, I., COENEN, H.H., QAIM, S.M., Enhanced production possibility of the therapeutic radionuclides ^{64}Cu, ^{67}Cu and ^{89}Sr via (n,p) reactions induced by fast spectral neutron, Radiochim. Acta **92** (2004) 183–186.

SPAHN, I., et al., "Kernreaktionsdaten neuer Produktionswege für die Therapienuklide ^{32}P, ^{64,67}Cu, ^{89}Sr, ^{169}Yb und ^{192}Ir", 13. Arbeitstagung der AG Radiochemie/Radiopharmazie, Seefeld/Tirol, Austria, 6–8 October 2005 (Abstract: p. 27).

SPAHN, I., et al., "Nuclear reaction data for new production routes of the therapeutic radionuclides ^{32}P, ^{89}Sr, ^{153}Sm, ^{169}Yb and ^{192}Ir", 7th Int. Symp. Technetium in Chemistry and Nuclear Medicine (Proc. Bressanone, 2006), MAZZI, U. (Ed.), Padova, SGEP (2006) 577.

SPAHN, I., et al., “Nuclear reaction data for new production routes of the therapeutic radionuclides ^{32}P, ^{89}Sr, ^{153}Sm, ^{169}Yb and ^{192}Ir”, 7th Int. Symp. Technetium in Chemistry and Nuclear Medicine, Bressanone, Italy, 6–9 September 2006.

SPAHN, I., et al., Cross-section measurement of the ^{169}Tm(p,n) reaction for the production of the therapeutic radionuclide ^{169}Yb and comparison with its reactor-based generation, Appl. Radiat. Isot. **63** (2005) 235–239.

SPAHN, I., HILGERS, K., TÁRKÁNYI, F. , COENEN, H.H., QAIM, S.M., “New production routes for some therapeutic radionuclides”, 16th Int. Symp. Radiopharmaceutical Chemistry, Iowa City, IA, USA, 24–28 June 2005 (J. Labelled Compd. Radiopharm., Supplement, Vol. 48 (2005) S106).

SPAHN, I., HILGERS, K., TÁRKÁNYI, F., COENEN, H.H., QAIM, S.M., “Neue Produktionswege für einige Therapienuklide”, Annu. Mtg Soc. German Chemists, Düsseldorf, Germany, 11–14 September 2005 (Abstract: GDCh-Jahrestagung 2005, Chemie schafft neue Strukturen, Kurzreferate, p. 503).

TAKÁCS, S., TÁRKÁNYI, F., HERMANNE, A., “Evaluation of deuteron induced nuclear reactions on copper and nickel”, 6th Int. Mtg Industrial Radiation and Radioisotope Measurement Applications, Hamilton, Ontario, Canada, 20–24 June 2005 (Abstract: p. 56).

TAKÁCS, S., TÁRKÁNYI, F., KIRÁLY, B., HERMANNE, A., SONCK, M., Evaluated activation cross sections of longer-lived radionuclides produced by deuteron-induced reactions on natural copper, Nucl. Instrum. Methods B **251** (2006) 56–65.

TAKÁCS, S., TÁRKÁNYI, F., KIRÁLY, B., HERMANNE, A., SONCK, M., Evaluated activation cross sections of longer-lived radionuclides produced by deuteron induced reactions on natural nickel, Nucl. Instrum. Methods B **260** (2007) 495–507.

TÁRKÁNYI, F., et al., “Activation cross sections of proton induced nuclear reactions on cadmium up to 80 MeV”, European Physical Soc., 19th Nuclear Physics Divisional Conf. New Trends in Nuclear Physics Applications and Technologies, ENPDC 19, Pavia, Italy, 5–9 September 2005 (Europhysics Conf. Abstracts: Vol. 29F (2005) p. 127).

TÁRKÁNYI, F., et al., “Activation cross sections of the ^{169}Tm(d,2n) reaction for the production of the therapeutic radionuclide”, 15th Radiochemical Conf., Mariánské Lázne, Czech Republic, 23–28 April 2006 (Booklet of abstracts: p. 184).

TÁRKÁNYI, F., et al., “Compilation and evaluation of nuclear reaction cross sections for production of therapeutic radionuclides”, 5th Int. Conf. Isotopes, Brussels, Belgium, 25–29 April 2005 (Abstract: p. 51).

TÁRKÁNYI, F., et al., “Excitation functions of proton induced reactions on ^{nat}Sn and ^{nat}Cd relevance to the production of ^{111}In and ^{114m}In for medical applications”, Int. Conf. Nuclear Data for Science and Technology, Santa Fe, USA, 26 September–1 October 2004 (Abstract: LA-UR-04-5900, Los Alamos, p. 279).

TÁRKÁNYI, F., et al., “Excitation functions of proton-induced reactions on ^{nat}Sn and ^{nat}Cd: Relevance to the production of ^{111}In and ^{114m}In for medical applications”, Int. Conf. Nuclear Data for Science and Technology (Proc. Santa Fe, NM, 2004), HAIGHT, R.C., CHADWICK, M.B., KAWANO, T., TALOU, P. (Eds), AIP Conf. Proc. 769, Part 2, Melville, New York (2005) 1662–1665.

TÁRKÁNYI, F., et al., “Investigation of charged particle induced routes for production of ^{103}Pd”, MARC-VII Methods and Applications of Radioanalytical Chemistry, Kailua-Kona, HI, USA, 3–7 April 2006 (Abstract: p. 135).

TÁRKÁNYI, F., et al., “Investigation of new routes for production of the therapeutic radionuclides ^{169}Yb and ^{165}Er”, 9th Int. Symp. Synthesis and Applications of Isotopes and Isotopically Labelled Compounds (Proc. Edinburgh, 2006), J. Labelled Compd Radiopharm. Suppl. **50** (2007) 99.

TÁRKÁNYI, F., et al., “Investigation of new routes for production of the therapeutic radionuclides ^{169}Yb and ^{165}Er”, 17th Int. Symp. Radiopharmaceutical Sciences, ISRS 17, Aachen, Germany, 30 April–4 May 2007.

TÁRKÁNYI, F., et al., “Investigation of the production of therapeutic radioisotopes at cyclotrons”, 18th Int. Conf. Cyclotrons and their Applications, Giardini Naxos, Italy, 30 September–5 October 2007 (Book of abstracts: p. 98 THXCR04).

TÁRKÁNYI, F., et al., “Nuclear reaction cross section database for production of therapeutic radioisotopes”, Asia-Pacific Symp. Radiochemistry-05, APSORC-05, Peking, China, 17–21 October 2005 (Abstracts book: S6-O-03 p. 209).

TÁRKÁNYI, F., et al., “Nuclear reaction cross section database for production of therapeutic radioisotopes”, 11th Int. Workshop on Targetry and Target Chemistry, Cambridge, UK, 28–31 August 2006 (Abstract: pp. 108–109).

TÁRKÁNYI, F., et al., “Nuclear reaction databases for production of diagnostic and therapeutic radioisotopes”, 15th Radiochemical Conf., Mariánské Lázne, Czech Republic, 23–28 April 2006 (Booklet of abstracts: p. 297).

TÁRKÁNYI, F., et al., Activation cross sections of long-lived products of proton-induced nuclear reactions on zinc, Appl. Radiat. Isot. **62** (2005) 73–81.

TÁRKÁNYI, F., et al., Activation cross sections of the ^{169}Tm(d,2n) reaction for production of the therapeutic radionuclide ^{169}Yb, Appl. Radiat. Isot. **65** (2007) 663–668.

TÁRKÁNYI, F., et al., Activation cross sections on cadmium: Deuteron induced nuclear reactions up to 40 MeV, Nucl. Instrum. Methods B **259** (2007) 817–828.

TÁRKÁNYI, F., et al., Activation cross sections on cadmium: Proton induced nuclear reactions up to 80 MeV, Nucl. Instrum. Methods B **245** (2006) 379–394.

TÁRKÁNYI, F., et al., Excitation functions of deuteron induced nuclear reactions on natural tungsten up to 50 MeV, Nucl. Instrum. Methods B **211** (2003) 319–330.

TÁRKÁNYI, F., et al., Excitation functions of deuteron induced nuclear reactions on natural zinc up to 50 MeV, Nucl. Instrum. Methods B **217** (2004) 531–550.

TÁRKÁNYI, F., et al., Excitation functions of proton induced nuclear reactions on natural tungsten up to 34 MeV, Nucl. Instrum. Methods B **252** (2006) 160–174.

TÁRKÁNYI, F., et al., Investigation of the production of the therapeutic radioisotope ^{114m}In through proton and deuteron induced nuclear reactions on cadmium, Radiochim. Acta **93** (2005) 561–569.

TÁRKÁNYI, F., et al., New measurement and evaluation of the excitation function of the ^{186}W(p,n) nuclear reaction for production of the therapeutic radioisotope ^{186}Re, Nucl. Instrum. Methods B **264** (2007) 389–394.

TÁRKÁNYI, F., et al., Study of the ^{192}Os(d,2n) reaction for production of the therapeutic radionuclide ^{192}Ir in no-carrier added form, Appl. Radiat. Isot. **65** (2007) 1215–1220.

TÁRKÁNYI, F., TAKÁCS, S., HERMANNE, A., VAN DEN WINKEL, P., VAN DER ZWART, R., "Investigation of the production of the therapeutic radioisotope ^{114m}In through proton and deuteron induced nuclear reactions on cadmium", 6th Int. Conf. Nuclear and Radiochemistry, NRC6, Aachen, Germany, 29 August–3 September 2004.

3. NUCLEAR REACTION MODELLING: PARTICLE EMISSION

A.V. Ignatyuk, Yu.N. Shubin, R. Capote

Theoretical models of nuclear processes play an important role in all stages of nuclear data evaluation for both a general understanding of the physical phenomena related to the analysed data and to estimate the required cross-sections in cases where data are contradictive or not fully available. A brief description is given of the models and codes used in the studies for the present project. The ALICE, GNASH and EMPIRE codes were used for most calculations, while the TALYS code was used for some neutron capture cases and will be explained in the next chapter. All employed nuclear reaction codes are based on rather similar models of nuclear processes but differ essentially in their detail and input parameters. A discussion of the main differences between the calculated cross-sections is given in the final section.

3.1. NUCLEAR REACTION MODELS

Nuclear reaction theory is based, to a significant extent, on the compound nucleus model proposed by Bohr more than 70 years ago [3.1]. A nuclear reaction can be considered as proceeding in two stages: the formation of the compound nucleus by the collision of a projectile with a target nucleus and the decay of the resulting compound nucleus into pairs of reaction products. The corresponding reaction cross-section can be expressed by the following equation:

$$\sigma(a,b) = \sigma_c(a) P_b \Big/ \sum_{b'} P_{b'} \tag{3.1}$$

where $\sigma_c(a)$ is the cross-section for the compound nucleus formed by projectile a, and P_b is the probability of the compound nucleus decaying into the corresponding outgoing channel b. The denominator of Eq. (3.1) includes the sum over all possible decay channels. The decay probability of the compound nucleus can be given in the form:

$$P_b(e_b) = \frac{g_b \mu_b e_b \sigma_c^*(e_b)}{\pi^2 \hbar^3} \frac{\rho_b(U_b)}{\rho_c(U_c)} \tag{3.2}$$

where e_b is the energy of the emitted particle, $g_b = 2s_b+1$ is the statistical factor connected with the spin s_b of the particle, μ_b is the reduce mass, $\sigma_c^*(e_b)$ is the cross-section for the inverse reaction, and ρ_b and ρ_c are the level densities for the residual and compound nucleus at the corresponding excitation energies. All component energies are connected by the relationship $U_c = U_b + B_b + e_b$, where B_b is the binding energy of the particle in the compound nucleus. The sum of the decay probabilities over all channels, including the integrals over energies of emitted particles, determines directly the inverse value of the average lifetime of the compound nucleus with the given excitation energy.

Equation (3.2) demonstrates the evident statistical form of the nuclear reaction description. All specific features of the dynamics of the nuclear process are related to the inverse reaction cross-section, while other components estimate the phase space accessible for the reaction products. Such a description is very similar to the particle evaporation from a liquid surface and, for this reason, the above description is referred to as the evaporation model or Weisskopf–Ewing formula [3.2].

A more rigorous consideration of the nuclear process defines compound reaction cross-sections in terms of the Hauser–Feshbach–Moldauer formula [3.3–3.5]:

$$\sigma(a,b) = \pi \lambda\!\!\!^{-}{}_a^2 \sum_{J\pi} g_s^J \frac{T_a^{J\pi} T_b^{J\pi}}{\sum_c T_c^{J\pi}} F_{ab,c}^{J,\pi} \tag{3.3}$$

where $\lambda\!\!\!^{-}{}_a$ is the wavelength of the incident particle, $T_a^{J\pi}$ are the transmission coefficients for the given angular momentum J and parity π, and $F_{ab,c}^{J,\pi}$ is the width fluctuation correction for differences between the averaged ratio of fluctuating decay widths and the ratio of the averaged widths [3.5]. This correction is only important for low energies of incident particles when the number of open reaction channels is rather small.

Consider a large number of channels in which the sum of the transmission coefficients in the numerator and denominator of Eq. (3.3) can be replaced by integrals of the form:

$$\sum_c T_c = \sum_{l,j,I} \int_0^{U_{\max}} T_{lj}(E_c)\rho(U,I)dU \tag{3.4}$$

which contain the level densities of the residual nuclei. The sum in Eq. (3.4) is taken over all combinations of the angular momentums and spins of the reaction

products, including the given quantum characteristics of the compound nucleus. With an increase in the number of channels, the level density plays an increasingly important role in the correct description of reaction cross-sections that pass through the compound nucleus stage.

The transmission coefficients are usually calculated by means of the optical model [3.4] and such an approach has been used successfully by many authors to describe a large amount of experimental data on neutron induced reaction cross-sections at energies below 10 MeV. At higher energies, the influence of the angular momentum conservation law on the selection of reaction channels decreases particularly for the light-particle reactions, and the descriptions of reaction cross-sections on the basis of the evaporation model (Eq. (3.2)) and the more rigorous formulae (Eq. (3.3)) become very similar.

An increase of projectile energy above several MeV increases the probability that the projectile or some products of the intranuclear collisions escape from the nucleus before the compound nucleus stage considered above. Such occurrences are usually referred to as pre-compound or pre-equilibrium processes. The simplest correspond to the first projectile collisions or excitation of low lying collective nuclear levels, and are defined as direct reactions that have been well developed as the distorted wave born approximation or the coupled-channel (CC) approaches [3.6, 3.7].

Nucleon emission from more complex pre-equilibrium transitions has been considered by adopting the exciton model [3.8] as proposed by Griffin. The intermediate states of the excited nucleus in this model can be classified by the number of excited particles and holes or quasi-particles ($n = p + h$), and the emission of nucleons from each intermediate state can be described by equations, which differ from those of the evaporation model (Eqs (3.1) and (3.2)) through the explicit definition of n-exciton states:

$$P_n(e_b) = \frac{g_b \mu_b e_b \sigma_c^*(e_b)}{\pi^2 \hbar^3} \frac{\rho_{n-1}(U_b)}{\rho_n(U_c)} \tag{3.5}$$

where $\rho_n(U)$ are the densities of the corresponding states with a given excitation energy. The total probability of the pre-equilibrium nucleon emission can be obtained as the sum over all pre-equilibrium states for the product of Eq. (3.5) and the average lifetime of the n-exciton states τ_n. This lifetime can be estimated as the inverse of the transition rate from n-exciton states to more complex $n + 2$ exciton states, and can be written as the equation:

$$\tau_n^{-1}(U_c) \approx \lambda_{n \to n+2} = \frac{2\pi}{\hbar} |M|^2 \rho_{n,f}(U_c) \tag{3.6}$$

where $|M|^2$ is the averaged matrix element for the corresponding transitions, and $\rho_{n,f}$ is the density of the corresponding final states [3.9].

Various modifications of the pre-equilibrium model were proposed in Refs [3.10–3.16]. These publications include more detailed discussions of the corresponding relationships for the level densities and transition rates, as well as examples of applications of such models to the analysis of numerous experimental data. A more substantial list of references and applications can be found in the monograph on pre-equilibrium nuclear reactions [3.17].

Combined pre-equilibrium plus compound models have been incorporated into many computer codes, the most popular of which are ALICE, GNASH, and the recently released EMPIRE and TALYS codes. All of these programs were used to calculate the reaction cross-sections included in the present studies. We will discuss the main features of these codes, which are important in understanding the divergence between calculations, and represent a means of estimating the uncertainties of such calculations.

3.2. ALICE-91 AND ALICE-IPPE

ALICE-91 is one of the more recent versions of the widely distributed ALICE code developed by Blann [3.18], and based on the hybrid pre-equilibrium model and Weisskopf–Ewing formulas. The hybrid model considers explicitly the transition rates for colliding particles instead of averaging over all n-exciton states. The corresponding relationship of the hybrid model may be written as follows:

$$\frac{d\sigma_{ab}}{de_b} = \sigma_c(e_a) \sum_{n=n_0}^{\bar{n}} \frac{X_b^n \rho_{n-1}(U_b)}{\rho_n(U_c)} \frac{\lambda_{con}(e_b)}{\lambda_{con}(e_b) + \lambda_+(e_b)} D_n de_b \tag{3.7}$$

where X_b^n is the relative contribution of an emitted particle (proton or neutron) to the density of n-exciton states, λ_{con} is the rate of nucleon emission in the continuum, λ_+ is the competing rate for a transition after two-body collisions to more complex $n + 2$ exciton states, and the factor D_n is a depletion factor which represents the fraction of the population surviving decay prior to reaching the n-exciton configuration. The summation term in Eq. (3.7) covers configurations from n_0 to equilibrium corresponding to the number of excitons $\bar{n} \approx 2gt$, where g is the single-particle density of nucleons and t is the temperature of the excited nucleus. The continuum emission rate is determined by the common relationship:

$$\lambda_{con}(e) = \frac{g_s m e \sigma_c^*(e)}{\pi^2 \hbar^3 g} \tag{3.8}$$

where all quantities are the same as in Eq. (3.2).

Blann has estimated the rate of transition to more complex states on the basis of nucleon mean free path calculations through the equation:

$$\lambda_+(e) = [1.4 \cdot 10^{21}(e + B_\nu) - 6.0 \cdot 10^{18}(e + B_\nu)^2]\ \mathrm{s}^{-1} \tag{3.9}$$

where B_ν is the nucleon (proton or neutron) binding energy in the nucleus and all energies are given in MeV.

Comparing Eqs (3.7), (3.8) and (3.9) with Eqs (3.5) and (3.6), it can be seen that the main difference between the hybrid and standard pre-equilibrium models relates to the determination of the matrix elements responsible for the transition to more complex states. However, this difference has a relatively weak influence on the results of most calculations because, for both models, the strength of the matrix element $|M|^2$ is adjusted to the available experimental data on spectra of emitted nucleons. Analysis of such data shows that λ_+ should be reduced by a factor of five relative to Eq. (3.9) to achieve an agreement of the hybrid model calculations with experimental data [3.12].

A more consistent consideration of the two-body collisions was obtained for the geometry dependent hybrid model [3.19], in which the dependence of the mean free path and the density of particle–hole excitations on the diffuse distribution of nuclear matter in nuclei was taken into account. A much better description of the emitted nucleon spectra was achieved for this model.

The ALICE-91 code contains both versions of the hybrid model, although only the nucleon emission was included at the pre-equilibrium stage. Alpha particle and deuteron (or other light cluster) emissions are possible from the equilibrium compound stage solely. Gamma ray emission from the compound nucleus was added in ALICE-91 to improve the description of the excitation functions for the charged particle induced reactions at near threshold regions.

ALICE-91 uses two simple models for the level density of the compound nuclei: the standard Fermi gas model, with the corresponding pairing correction, or the back-shifted Fermi gas model. There is also the option to include level density parameters from the Kataria and Ramamurthy prescription that simulate shell effects [3.20]. Calculations of the absorption cross-sections by the optical model normally use the default parameters, which have been verified by the analysis of a large amount of experimental data [3.21].

The ALICE-IPPE code is the ALICE-91 version modified by the Obninsk group to include the pre-equilibrium cluster emission and the generalized superfluid model for the nuclear level densities [3.22]. An approach developed by

Iwamoto and Harada [3.15] was used to simulate the cluster emission of α particles, deuterons and tritons. The level density model includes both the energy dependent shell effects and the corresponding collective enhancement of the level densities. A more complete description of these models can be found in the RIPL Handbook [3.23], which also contains references to the original papers and recommended model parameters. ALICE-IPPE calculations use the same optical potential parameters for neutrons and protons as ALICE-91 but for α particles and deuterons, such parameters were slightly modified to reproduce the available experimental data on the absorption cross-sections at low energies [3.24, 3.25].

3.3. GNASH

The GNASH code is based on the Hauser–Feshbach formalism plus the pre-equilibrium model with full angular momentum conservation. Calculations can be carried out with rather large schemes of low lying discrete levels, which is very important for neutron induced reactions at low energies. A reasonably complete description of the current version of GNASH is given in Ref. [3.26] — this code has been used extensively by many people to produce evaluated data for national nuclear data libraries.

All particle transmission coefficients are introduced into the GNASH calculations from the external input file that is obtained from either the spherical or coupled channel optical model. The code calculates the contribution of direct processes to the excitation functions by means of the introduction of additional input data.

Pre-equilibrium emission calculations can be undertaken by means of the PRECO-B code developed by Kalbach [3.27] and adopted in GNASH. Pre-equilibrium configurations are classified according to the number of particles and holes excited, and the exciton model involves solving a series of master equations that describe the equilibration of an excited nucleus through a series of two-body collisions producing more complex configurations of particle–hole pairs. The matrix element in expressions for the transition rates similar to Eq. (3.6) was parameterized in GNASH as the exciton number dependent function:

$$
\begin{aligned}
M^2 &= \frac{k}{A^3 e}\sqrt{\frac{e}{7MeV}}\sqrt{\frac{e}{2MeV}} && \text{for } e < 2 \text{ MeV} \\
&= \frac{k}{A^3 e}\sqrt{\frac{e}{7MeV}} && \text{for } 2 < e < 7 \text{ MeV} \\
&= \frac{k}{A^3 e} && \text{for } 7 < e < 15 \text{ MeV} \\
&= \frac{k}{A^3 e}\sqrt{\frac{15MeV}{e}} && \text{for } e > 15 \text{ MeV}
\end{aligned}
\tag{3.10}
$$

where $e = U_c/n$ and U_c is expressed in MeV; and the constant k is usually set equal to 130–160 MeV. The cluster pre-equilibrium emission was included on the basis of a phenomenological description developed by Kalbach [3.28].

The above pre-equilibrium model does not take into account angular momentum effects. Some simple approaches to estimate the spin populations of the residual nuclei following pre-equilibrium decay have been developed for GNASH. Three options are available for the population in the continuum region:

(a) The calculated compound-nucleus spin distribution weighting of the pre-equilibrium cross-section components;
(b) Pure level density spin distribution for the weighting;
(c) The particle–hole spin distributions for the corresponding weighting.

Distributions of the pre-equilibrium components among the discrete levels are obtained by extrapolating the dependency of the pre-equilibrium cross-section energy to the nuclear level energies.

GNASH provides the user with three alternative models for the determination of the level density of compound nuclei:

(a) Gilbert–Cameron approach;
(b) Back-shifted Fermi gas model;
(c) Ignatyuk form of that Fermi gas model that includes the energy dependent shell effects.

Parameters for each model can be adjusted automatically to the input data describing the density of the neutron resonances. A similar adjustment can be done for the γ ray widths.

The GNASH code used by the Obninsk group has been slightly modified to include the width fluctuation corrections of Eq. (3.3) omitted in the original version, and to add the collective enhancement into the description of the level density.

3.4. EMPIRE

The EMPIRE code includes the most full set of nuclear reaction models needed for a practical evaluation of nuclear data over a wide energy range, including the optical and direct reaction models, pre-equilibrium exciton model, and the full-featured Hauser–Feshbach model [3.29, 3.30]. A comprehensive paper on EMPIRE capabilities has recently been published [3.31] and interested readers are referred to the detailed technical information about this code contained within this particular reference.

The CC ECIS03 code [3.32] has been incorporated into EMPIRE-2.19, and was used for optical model calculations employing global potentials from the RIPL-2 database [3.22]. Pre-equilibrium emission was taken into account by the PCROSS or HMS modules [3.31]; the former features the one-component exciton model with gamma, nucleon and cluster emission (Iwamoto–Harada model), while the latter is an implementation by Chadwick of the Hybrid Monte-Carlo Simulation approach to the pre-equilibrium emission of nucleons as proposed by M. Blann [3.33].

Among the various models describing level densities implemented in EMPIRE, the present calculations adopted those described as 'EMPIRE specific'. This formalism uses the superfluid model below and the Fermi gas model above the critical excitation energy. Deformation dependent collective effects on the level densities due to nuclear vibration and rotation (rotational and vibrational enhancements, and their temperature dependent damping) are taken into account. The shell correction, pairing and asymptotic value of the level density parameter have been calculated using RIPL-2 recommendations as starting values.

3.5. COMPARISON OF MODELLING RESULTS

The cross-sections of ^{103}Rh(p, n)^{103}Pd and ^{103}Rh(d, 2n)^{103}Pd reactions are shown in Figs 3.1 and 3.2 in comparison with the available experimental data. These calculations involved the use of the same optical potential and level density parameters for all reaction channels. The cross-sections calculated for the different codes agree reasonably well for the region, where the processes for the compound nucleus dominate; however, for higher energies, in which the contributions of the pre-equilibrium processes are rather large, significant discrepancies arise between the models. These discrepancies relate either to different parameterizations of the transition rates of Eq. (3.6) or to the corresponding matrix elements of the various codes (Eq. (3.9)). The descriptions of the transition rate include some adjusted parameters in all codes, and uncertainties in these parameters are the main source of the resulting uncertainties of the calculated cross-sections.

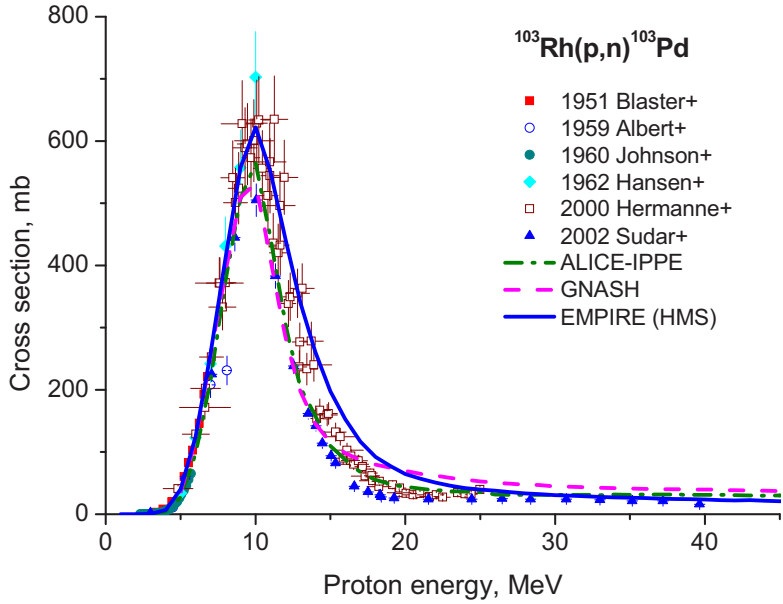

FIG. 3.1. Experimental data for the ^{103}Rh(p, n)^{103}Pd reaction cross-section in comparison with calculations by different codes: EMPIRE (HMS) uses the HMS pre-equilibrium model.

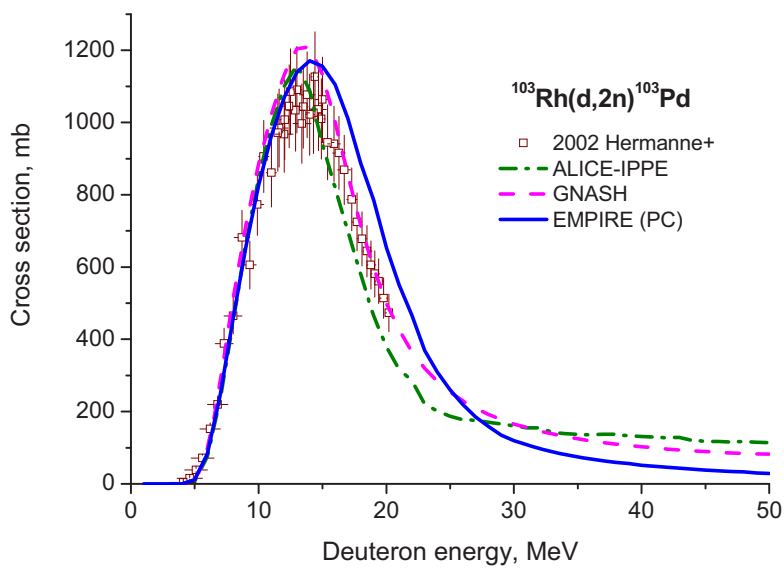

FIG. 3.2. Experimental data for the ^{103}Rh(d, 2n)^{103}Pd reaction cross-section in comparison with calculations by different codes: EMPIRE (PC) combines the PC ROSS exciton model and Kalbach's parameterization of deuteron breakup and pickup.

REFERENCES

[3.1] BOHR, N., Neutron capture and nuclear constitution, Nature **137** (1936) 344–348.

[3.2] WEISSKOPF, V.F., EWING, D.H., On the yield of nuclear reactions with heavy elements, Phys. Rev. **57** (1940) 472–485.

[3.3] HAUSER, W., FESHBACH, H., The inelastic scattering of neutrons, Phys. Rev. **87** (1952) 366–373.

[3.4] FESHBACH, H., PORTER, C.E., WEISKOPF, V.F., Model for nuclear reactions with neutrons, Phys. Rev. **96** (1954) 448–464.

[3.5] MOLDAUER, P., Theory of average neutron reaction cross section in the resonance region, Phys. Rev. **123** (1961) 968–978.

[3.6] AUSTERN, N., Direct Nuclear Reaction Theories, Wiley-Interscience, New York (1970).

[3.7] SATCHLER, G.R., Direct Nuclear Reactions, Clarendon, Oxford (1983).

[3.8] GRIFFIN, J.J., Statistical model of intermediate structure, Phys. Rev. Lett. **17** (1966) 478–481.

[3.9] WILLIAMS, F.C., Particle-hole state density in the uniform spacing model, Nucl. Phys. A **166** (1971) 231–240.

[3.10] BLANN, M., Extensions of Griffin's statistical model for medium-energy nuclear reactions, Phys. Rev. Lett. **21** (1968) 1357–1360.

[3.11] HARP, G.D., MILLER, J.M., Precompound decay from a time-dependent point of view, Phys. Rev. C **3** (1971) 1847–1855.

[3.12] BLANN, M., Hybrid model for pre-equilibrium decay in nuclear reactions, Phys. Rev. Lett. **27** (1971) 337–340.

[3.13] GADIOLI, E., GADIOLI-ERBA E., SONA P.G., Intermediate-state decay rates in the exciton model, Nucl. Phys. A **217** (1973) 589–610.

[3.14] FESHBACH, H., KERMAN, A., KOONIN, S., Statistical theory of multi-step compound and direct reactions, Ann. Phys. **125** (1980) 429–476.

[3.15] IWAMOTO, A., HARADA, K., Mechanism of cluster emission in nucleon-induced preequilibrium reactions, Phys. Rev. C **26** (1982) 1821–1834.

[3.16] NISHIOKA, H., WEIDENMULLER, H.A., YOSHIDA, S., Statistical theory of precompound reactions: The multistep direct process, Ann. Phys. **183** (1988) 166–187.

[3.17] GADIOLI, E., HODGSON, P.E., Pre-equilibrium Nuclear Reactions, Clarendon Press, Oxford (1992).

[3.18] BLANN, M., Recent Progress and Current Status of Preequilibrium Reaction Theories and Computer Code ALICE, Technical Rep. UCRL-JC-109052 (1991).

[3.19] BLANN, M., Hybrid model for pre-equilibrium decay in nuclear reactions, Phys. Rev. Lett. **27** (1972) 337–340.

[3.20] KATARIA, S.K., RAMAMURTHY, V.S., Macroscopic systematics of nuclear level densities, Nucl. Phys. A **349** (1980) 10–28.

[3.21] BLANN, M., VONACH, H.K., Global test of modified precompound decay models, Phys. Rev. C **28** (1983) 1475–1492.

[3.22] DITYUK, A.I., KONOBEYEV, A.YU., LUNEV, V.P., SHUBIN, Yu.N., New Advanced Version of Computer Code ALICE – IPPE, Rep. INDC(CCP)-410, IAEA, Vienna (1998).

[3.23] BELGYA, T., et al., Handbook For Calculations of Nuclear Reaction Data, RIPL-2, IAEA-TECDOC-1506, IAEA, Vienna (2006), http://www-nds.iaea.org/RIPL-2/
[3.24] AUCE, A., et al., Reaction cross-sections for 38, 65, and 97 MeV deuterons on targets from ^{9}Be to ^{208}Pb, Phys. Rev. C **53** (1996) 2919–2925.
[3.25] AVRIGEANU, M., OERTZEN, W., PLOMPEN, A.J.M., Optical model potentials for alpha-particles scattering around the Coulomb barrier on A~100 nuclei, Nucl. Phys. A **723** (2003) 104–126.
[3.26] YOUNG, P.G., ARTHUR, E.D., CHADWICK, M.B., in Nuclear Reaction Data and Nuclear Reactors, GANDINI, A., REFFO, G. (Eds), World. Sci., Singapore (1996) 227–404.
[3.27] KALBACH, C., PRECOA: Programme for Calculating Pre-equilibrium Particle Energy Spectra, Rep. CEN-DPh-N/BE/74/3 (1974).
[3.28] KALBACH, C., The Griffin model, complex particles and direct nuclear reactions, Z. Phys. A **283** (1977) 401–411.
[3.29] HERMAN, M., "EMPIRE-II statistical model code for nuclear reaction calculations", ICTP Lecture Notes, Workshop on Nuclear Reaction Data and Nuclear Reactors: Physics, Design and Safety (Trieste, 2000) (PAVER, N., HERMAN, M., GANDINI, A., Eds), ICTP, Trieste Vol. 5 (2001) 137–230.
[3.30] HERMAN, M., et al., EMPIRE 2.19 release, http://www.nndc.bnl.gov/empire
[3.31] HERMAN, M., et al., EMPIRE: Nuclear reaction model code system for data evaluation, Nucl. Data Sheets **108** (2007) 2657–2717.
[3.32] RAYNAL, J., "Optical model and coupled-channels calculations in nuclear physics", Computing as a Language of Physics, ICTP Int. Sem. Course (Trieste, 1971), IAEA, Vienna (1972), J. Raynal, ECIS code, distributed by NEA DATA BANK, OECD, Paris, p. 281.
[3.33] BLANN, M., New precompound decay model, Phys. Rev. C **54** (1996) 1341–1349.

4. NUCLEAR REACTION MODELLING: CAPTURE REACTIONS

E. Běták

4.1. INTRODUCTION

The (n, γ) reactions can serve as the means of production of some radiopharmaceuticals, either directly (^{89}Sr, ^{103}Pd, ^{153}Sm and others) or via suitable generators and/or precursors (e.g. ^{125}Xe serves as a precursor for ^{125}I). This reactor-based method of production is well established in some cases (^{89}Sr and ^{125}I) but more often, the necessary radionuclide is preferentially produced by other reactions (e.g. see Refs [4.1, 4.2]). A primary aim is not only to create the desired radionuclide but to produce sufficient amounts that are uncontaminated by other isotopes that arise from either the target impurities or competing reactions.

Nuclear reactions evolve through several very different regions with increasing incident energy, beginning with the thermal and resonance regions before reaching the continuum. Whereas the thermal and, especially, the resonance regions are of vital importance to isotope production in reactors where the (n, γ) reactions take practically the whole strength, the continuum region is of much less interest because of the very low cross-sections, the main strength being taken away by the open nucleon channels. Correspondingly, experimental data in the continuum are rare, so that reliable predictions of the excitation functions based on model calculations are very important.

4.2. GAMMA EMISSION IN THE MeV REGION

EMPIRE-II version 2.19 [4.3] and TALYS [4.4, 4.5] represent suitable computer codes for the calculation of nuclear reactions, and they represent significant improvements over previously employed codes, such as PEQAG [4.6] and DEGAS [4.7], as well as older versions of EMPIRE-II (e.g. version 2.18 [4.8]). At excitation energies above 10 MeV, both EMPIRE and TALYS are based on the pre-equilibrium single-particle radiative mechanism, which has been elaborated in previous codes. However, whereas one can use simple exciton model codes at nucleon energies exceeding 10 MeV and sufficiently far from the closed shells, such as the simple PEQAG code [4.6] or the spin-dependent successor DEGAS [4.7], sophisticated nuclear reaction codes can now be used with confidence to include an extensive number of approaches and cover rather

wide energy ranges. Such complex coding systems are coupled to large libraries of parameters if estimates are required for reactions that are not just tailored to simple statistical pre-equilibrium calculations. Two codes of this type have been recently released, namely EMPIRE-II (version 2.18 in 2002 [4.8] and version 2.19 three years later [4.3][1]) and TALYS in 2005 and at the end of 2006 [4.4, 4.5, 4.9]. They possess similar underlying physics at the pre-equilibrium stage (e.g. the same single nucleon radiative mechanism formula for the γ emission is used both in EMPIRE and in TALYS), and both of them use very extensive tables of the various recommended parameters.

The single-particle radiative mechanism has proved to be very successful at incident energies below about 30 MeV [4.10, 4.11], and also gives a reliable description at energies as low as about 5 MeV [4.12, 4.13]. Therein, the γ emission is associated with a decrease of the exciton number[2] n ($\Delta = -2$) or leaves this quantity unchanged ($\Delta n = 0$), and the emission rates can be expressed as follows:

$$\lambda_\gamma(n,E,\varepsilon_\gamma) = \frac{\varepsilon_\gamma^2 \sigma_{GDR}(\varepsilon_\gamma)}{\pi^2 \hbar^3 c^2} \frac{\sum_{m=n,n-2} b(m,\varepsilon_\gamma)\omega(m,E-\varepsilon_\gamma)}{\omega(n,E)}, \tag{4.1}$$

where E denotes the excitation energy of the nucleus (composite system), ε_γ is the γ energy, $\sigma_{GDR}(\varepsilon_g)$ is the photo-absorption cross-section, ω are the exciton state densities, and the branching ratios are defined as follows:

$$\begin{aligned} b(n-2,\varepsilon_\gamma) &= \frac{\omega(2,\varepsilon_\gamma)}{g(n-2)+\omega(2,\varepsilon_\gamma)} \\ b(n,\varepsilon_\gamma) &= \frac{gn}{gn+\omega(2,\varepsilon_\gamma)}. \end{aligned} \tag{4.2}$$

However, with the inclusion of spin, the above expressions become much more complicated. Fortunately, the branching ratios factorize [4.14]:

[1] The main differences between the two versions of EMPIRE-II may be characterized as the replacement of the data libraries by more recent versions, addition of further subroutines and elimination of some minor bugs.

[2] Exciton number n is the sum of the excited particles p above and holes h below the Fermi level, $n = p + h$.

$$b_{mS}^{nJ} = \frac{y_m^n x_{mS}^{nJ}}{y_m^m x_{mS}^{mJ} + y_m^{m+2} x_{mS}^{m+2J}}, \tag{4.3}$$

where y are the energy dependent functions that are identical to Eq. (4.2) that becomes:

$$y_n^n = gn,$$

$$y_n^{n+2} = g^2 \varepsilon_\gamma, \tag{4.4}$$

in the case of the equidistant spacing scheme, and x arise from the spin couplings (for details, see Ref. [4.14]).

The photo-absorption cross-section σ_{GDR} is usually defined in the form of the giant dipole resonance (GDR) approximated by the corresponding Lorentzian (or double-humped Lorentzian in the case of deformed nuclei).

Important differences for the pre-equilibrium stage of the reaction may be summarized as follows:

— The basic approach to the pre-equilibrium stage consists of the two components in TALYS (i.e. distinguishing between the neutrons and the protons), whereas a one-component formulation with a charge factor is used in EMPIRE;
— A one-particle radiation mechanism is used for the γ emission in EMPIRE but TALYS includes the quasi-deuteron (two-particle)[3], which may cause some differences at excitation energies above about 30 MeV (albeit very small);
— Although the level densities using the default option are the same in both codes (with parameters taken from RIPL [4.15, 4.16]), different semi-microscopic approaches are available for advanced users;
— The classical optical model is used to calculate the particle transmission coefficients T_l in EMPIRE with parameters from the libraries, and the local and global parametrization of Koning and Delaroche [4.17] is employed in TALYS (this difference influences the γ emission only via the competition with that of the particles).

Previous pre-equilibrium calculations of the radiative capture reactions in the MeV region were undertaken by means of the PEQAG code [4.6].

[3] The quasi-deuteron mechanism is also included in EMPIRE-II version 2.19 but is considered for the photonuclear reactions only and not for the γ emission.

Generalizations with spin PEGAS and DEGAS [4.7] as well as the EMPIRE code (version 2.18 Mondovi) [4.8] demonstrated the level of sensitivity of the calculations to the details of the level density parameters (necessary for the evaluation of the state densities (ω)) and also to facets of GDR. Overall, calculations are reasonably reliable for reactions far from the closed shells and close enough to the line of beta stability, and somewhat questionable near closed and even doubly-closed shells, where one has to pay the utmost care to the proper choice of level densities (e.g. see Ref. [4.12]). There is no straightforward solution for nuclei close to the drip lines, and the spread of calculations performed with different model assumptions and/or codes may suitably serve as a rough estimate as to how reliable or weak the prediction of cross-sections and related quantities may be.

4.3. REACTIONS — GENERAL

The need to produce isotopes for diagnostic and therapeutic purposes has stimulated calls for further measurements and evaluations of the (n, γ) reactions at energies below 20 MeV. Within the IAEA coordinated research project, some very desirable isotopes for therapeutic needs have been identified and studied [4.18–4.20]. With public access to two excellent codes being granted in 2005, one has the opportunity to predict the excitation curves with much improved reliability than ever before. Generally, there are not many data defining (n, γ) reactions in the continuum region [4.21]. Studies up to about 3 MeV exist for neutron reactions on ^{152}Sm and ^{191}Ir, and experimental data up to nearly 20 MeV are available for the ^{165}Ho(n, γ) reaction for which the cross-sections referring to the ground and isomeric states can be separated.

Data are presented together with calculations of TALYS [4.4, 4.5] and two versions of EMPIRE-II (version 2.18 [4.8] and version 2.19 [4.3]) in a subsequent section of this report. Essentially, the default parameters in EMPIRE were kept, while allowing for full inclusion of pre-equilibrium emission and γ cascades. Details of the form of the GDR (which enters calculations of the γ emission via the detailed balance principle) and other parameters did not exhibit much influence on the resulting excitation functions calculated using EMPIRE-II version 2.18 [4.18] and, therefore, we also applied this approach to version 2.19 and TALYS[4].

[4] It is essential to include the γ cascades at all stages of the process but the details of the GDR form are only of marginal influence at our energies [4.18, 4.20]; GDR parameters taken from the RIPL-2 recommendations [4.15, 4.16] give the best overall fit, although other GDR parameters are also available for some of the nuclei.

4.4. BASIC PARAMETERS OF THE CALCULATIONS

Reliable data are needed for at least 21 nuclei (three nuclei for each reaction considered, the composite system, plus two nuclei after the neutron and after the proton emissions). Assuming that the best available up to date information is contained in RIPL-2 [4.15, 4.16] and other IAEA NDS libraries [4.21], both EMPIRE and TALYS are able to access and use these available parameters. When the recommended values in RIPL-2 are not applicable, other data have to be sought and used. We have studied the influence of different level densities and the form of the GDR[5], and found that they are not essential for the reactions studied [4.18, 4.20] — these calculations were not undertaken within the critical region of doubly magic nuclei, and other less certain input data can be suitably adopted in such studies.

4.5. CONCLUSIONS

We have carried out calculations of the excitation curves of (n, γ) reactions on seven selected targets leading to medically-suitable therapeutic isotopes at energies above the resonance region up to 20 MeV. These calculations have shown the influence of different level densities on the calculated production cross-sections (albeit rather small).

A combination of different computer codes is necessary[6], together with cross-checking of all of the adopted parameters against the available data for other reactions by the same projectiles that have been more frequently measured. This complex approach minimizes the uncertainties of the parameters and increases the predictive validity of the calculations when there are insufficient experimental data (as typically the situation for these reactions).

---

[5] Also includes recent recommendations for GDR parameters by Varlamov et al. [4.22].

[6] Both TALYS and EMPIRE-II are not single computer codes but sophisticated systems able to switch from one mechanism (and code) to another in accord with the specific conditions.

REFERENCES

[4.1] QAIM, S.M., Therapy related radioisotopes, SMR-1148-38, ICTP, Trieste (1999).

[4.2] RURARZ, E., TYS, J., Mozliwosci produkcji radioizotopow medycznych z wykorzystaniem Warszawskiego cyklotronu, Warsaw (1998).

[4.3] HERMAN, M., et al., EMPIRE modular system for nuclear reaction calculations (version 2.19, Lodi), NNDC, Brookhaven Natl Lab., Upton, New York (2005).

[4.4] KONING, A.J., HILAIRE, S., DUIJVESTIJN, M.C., "TALYS: comprehensive nuclear reaction modelling", Int. Conf. Nuclear Data for Science and Technology (Proc. Santa Fe, NM, 2004, HAIGHT, R.C., CHADWICK, M.B., KAWANO, T., TALOU, P. (Eds), AIP Conf. Proc. 769, Part II, Melville, New York (2005) 1154–1159.

[4.5] KONING, A.J., HILAIRE, S., DUIJVESTIJN, M.C., TALYS: a nuclear reaction program, 21297/04.62741/P FAI/AK/AK, NRG, Petten (2004).

[4.6] BĚTÁK, E., PEQAG: a PC version of fully pre-equilibrium computer code with gamma emission, INDC(CSR)-016, IAEA, Vienna (1989).

[4.7] BĚTÁK, E., OBLOŽINSKÝ, P., PEGAS: Pre-equilibrium-equilibrium gamma-and-spin code (PC version), INDC(SLK)-001, IAEA, Vienna (1993).

[4.8] HERMAN, M., EMPIRE-II statistical model code for nuclear reaction calculations (version 2.18, Mondovi), IAEA-NDS-CD-10, IAEA, Vienna (2002).

[4.9] KONING, A.J., HILAIRE, S., DUIJVESTIJN, M., TALYS — what is TALYS? http://www.talys.eu/

[4.10] BĚTÁK, E., DOBEŠ, J., Gamma emission in the pre-equilibrium exciton model, Phys. Lett. **84B** (1979) 368–370.

[4.11] AKKERMANS, J.M., GRUPPELAAR, H., Analysis of continuum gamma-ray emission in precompound-decay reactions, Phys. Lett. **157B** (1985) 95–100.

[4.12] BĚTÁK, E., KOPECKY, J., CVELBAR, F., Another possible manifestation of the energy-dependent width of the giant dipole resonance, Phys. Rev. C **46** (1992) 945–951.

[4.13] CVELBAR, F., BĚTÁK, E., LIKAR, A., Pre-equilibrium and direct-semi-direct model calculations of nucleon radiative capture excitation functions on heavy nuclei, J. Phys. G **21** (1995) 377–384.

[4.14] OBLOŽINSKÝ, P., Pre-equilibrium γ rays with angular momentum coupling, Phys. Rev. C **35** (1987) 407–414.

[4.15] INTERNATIONAL ATOMIC ENERGY AGENCY, Handbook for Calculations of Nuclear Reaction Data, Reference Input Parameter Library, IAEA-TECDOC-1034, IAEA, Vienna (1998).

[4.16] BELGYA, T., et al., Handbook for Calculations of Nuclear Reaction Data, RIPL-2, Reference Input Parameter Library-2, IAEA-TECDOC-1506, IAEA, Vienna (2006), http://www-nds.iaea.org/RIPL-2/

[4.17] KONING, A.J., DELAROCHE, J.P., Local and global nucleon optical models from 1 keV to 200 MeV, Nucl. Phys. A **713** (2003) 231–310.

[4.18] SUBLET, J.-Ch., CAPOTE NOY, R., Nuclear Data for the Production of Therapeutic Radionuclides, Summary Rep. 2nd Research Coordination Mtg (IAEA, Vienna, 2004), INDC(NDS)-465, IAEA, Vienna (2004).

[4.19] SUBLET, J.-Ch., CAPOTE NOY, R., Nuclear Data for the Production of Therapeutic Radionuclides, Summary Rep. Third Research Coordination Mtg (IAEA, Vienna, 2006), INDC(NDS)-0501, IAEA, Vienna (2006).

[4.20] SUBLET, J.-Ch., PAVIOTTI-CORCUERA, R., Nuclear Data for the Production of Therapeutic Radionuclides, Summary Rep. 1st Research Coordination Mtg (IAEA, Vienna, 2003), INDC(NDS)-444, IAEA, Vienna (2003).
[4.21] EXFOR-CINDA for applications, database and retrieval systems, version 1.63i (CD-ROM), IAEA, Vienna (2004), http://www-nds.iaea.org/exfor/
[4.22] VARLAMOV, A.V., VARLAMOV, V.V., RUDENKO, D.S., STEPANOV, M.E., Atlas of Giant Dipole Resonances, Parameters and Graphs of Photonuclear Reaction Cross Sections, INDC(NDS)-394, IAEA, Vienna (1999).

5. METHODS OF FITTING

A.V. Ignatyuk and Yu.N. Shubin

The status of an experimental data set is judged appropriate for statistical analysis when a reasonable number of independent measurements have been published that do not show inexplicable discrepancies and reliable error estimations are available for all points. Often, such fits use analytical functions, the most prominent being polynomials. A more general class of analytical functions is rational functions defined as the ratio of two polynomials. These functions have a capability to approximate nuclear reaction cross-sections in the resonance region, behaviour exhibited in the present project by several light nuclei. A method of fitting has been developed by the IPPE group, Obninsk, and applied to the data in the present project, as described below.

5.1. PADÉ FIT

The approximation proposed by Padé over one hundred years ago [5.1] has become one of the most important interpolation techniques of statistical mathematics [5.2–5.4]. A Padé approximant for a function *f(x)* is the rational function:

$$p_L(x) = R_L(x) / Q_L(x) \tag{5.1}$$

where *R* and *Q* are the polynomials described by *L* coefficients that exactly match the function *f(x)* in *L* points:

$$p_L(x_j) = f(x_j),\ \mathrm{j} = 1, 2, \ldots L \tag{5.2}$$

We do not show the degrees of the polynomials R and Q explicitly since the description is based on the recurrent solution where these degrees are defined internally. Until recently, two obstacles hindered an application of the Padé approximation to data processing and analysis: (1) difficulty of realization since rational approximants unlike polynomials lead to complicated nonlinear systems of equations in the least squares method (LSM); (2) a special form of approximant instability — possible real pole–zero pairs (noise doublets).

Both of these difficulties can be circumvented by undertaking a recursive calculation of many approximants differing by a choice of interpolation knots along with their statistical optimization by discrete sorting.

Equations (5.1) and (5.2) result in a system of linear equations for coefficients which may be solved using either determinants or recurrent expressions. The simplest recurrent expression is represented by the following equation:

$$p_L(x) = \frac{R_{L-1}(x) + \gamma_L(x - x_{L-1})R_{L-2}}{Q_{L-1}(x) + \gamma_L(x - x_{L-1})Q_{L-2}} \tag{5.3a}$$

where the coefficient L can be readily determined from the condition:

$$p_L(x_L) = f(x_L) \tag{5.3b}$$

and the initial polynomials are constant:

$$R_0(x) = 0, \quad R_1(x) = f(x_1), \quad Q_0(x) = 1, \quad Q_1(x) = 1 \tag{5.3c}$$

Equation (5.3) satisfies the definition (Eq. (5.1)) and condition (Eq. (5.2)).

For an experimental data set with N points, essential stages of the Padé approximation for these data are defined as the following:

— An initial set of L supporting points (interpolation knots) among the experimental data points ($L << N$) is chosen;
— The recurrent algorithm (Eq. (5.3)) to these L points is applied and interpolated with a rational function $p_L(x)$;
— $p_L(x)$ is computed for all experimental points and the deviation functional minimized:

$$\chi^2 = \sum_{j=1}^{N} (p_L(x_j) - f_j)^2 / \sigma_j^2 \tag{5.4}$$

Minimization is carried out by adopting an iteration using the concept of discrete optimization (sorting). Thus, one goes over all possibilities of choosing L points from the available experimental points N, constructs corresponding approximants, computes Eq. (5.4) and determines the minimum. Once this process is completed, L is changed and the iteration is repeated until an overall minimum is found from among all discrete possibilities available.

One of the advantages of the discrete optimization technique as compared to the continuous LSM is the possibility of using manifold functionals. Theoretical estimates show that the mean quadratic deviation of the approximant

(found by the discrete optimization) from the continuous LSM solution is about $(N/L)^{1/2}$ times less than the LSM deviation from the exact curve (valid for $L << N$). Thus, the approximant is statistically equivalent to the LSM solution.

As a rational function, the Padé approximant can be expressed by a set of polynomial coefficients or by a set of coefficients of the pole expansion. The last expansion is based on the analytical properties of the rational functions in the complex plane. One uses a complex variable $z = x + iy$ and replaces $p_L(x)$ by $p_L(z)$ which can be defined as the following:

$$p_L(z) = c + \sum_l \frac{a_l}{z - \eta_l} + \sum_k \frac{\alpha_k (z - \varepsilon_k) + \beta_k}{(z - \varepsilon_k)^2 + \gamma_k^2} \tag{5.5}$$

This equation can also be called the resonance expansion, in which ε_k and γ_k are the energy and the total half-width of the k-th resonance level, and α_k and β_k are the partial widths and interference parameters. The first sum corresponds to the real poles, while the second sum relates to the complex poles.

A prominent disturbing feature of the numerically generated rational approximants is the appearance of real poles (zero denominators) inside the approximation interval, which is physically meaningless and makes the approximant unusable. These poles are closely accompanied by real zeros of the numerator, constituting noise doublets that prevented wide use of Padé approximants in data fitting.

The noise doublets are not only neutralized but become useful, corresponding to the terms with $z \approx \eta_\ell$ inside the interval of approximation with relatively small coefficients a_l in the first sum of Eq. (5.5). These terms are cancelled in the present method and eliminated from the sum, and the regularization generates satisfactory results. Normally, the noise doublets appear with increasing L at the final stages of the approximation and indicate, together with statistical criteria, that the analytical information is exhausted.

The situation may be different if some points in the input experimental data deviate abnormally from the general trend. Under such circumstances, the noise doublets appear at relatively low L near such 'bad' points, describing them by local singularities rather than by smooth components. When the singularities are eliminated, the resulting regularized curve ignores the particularly bad points — this approach identifies points with aberrations automatically. From the point of view of statistical mathematics, the method of discrete optimization is equivalent to the least squares technique and, therefore, the experimental data set must be statistically consistent. When there are several sets of experimental data and discrepancies between different sets are significantly larger than their declared uncertainties, the statistical processing of the data is possible only after data

selection by an expert. This situation was found to occur fairly frequently in the present project, so that critical analysis and selection of experimental data had to be applied to all reactions.

The Padé code constructs the approximating rational function and calculates the coefficients of the pole expansion for each resonance (Eq. (5.5)). Thus, we have an analytical expression which can be easily calculated at any energy point. A simple version of the Padé code is applicable to cases with a limited number of experimental points, parameters and span of experimental data ($N \leq 500$, $L \leq 40$, $F^{max}/F^{min} \leq 10^6$), and is already suitable for many practical situations. The method is also very convenient for calculations of error bands and covariance matrices. A more detailed description of the method can be found in Ref. [5.5], with more general outlines in Refs [5.6, 5.7].

REFERENCES

[5.1] PADÉ, H.E., Sur la représentation d'une fonction par des fractions rationnelles, Ann. L'École Norm. **9**(3) (1892) 3–93.

[5.2] BAKER Jr., G.A., GAMMEL, J.L. (Eds), The Padé Approximants in Theoretical Physics, Academic Press, New York (1970).

[5.3] GRAVES-MORRIS, P.R. (Ed.), Padé Approximants and their Applications, Academic Press, New York (1973).

[5.4] BAKER Jr., G.A., Essentials of Padé Approximants, Academic Press, New York (1975).

[5.5] VINOGRADOV, V.N., GAI, E.V., RABOTNOV, N.S., Analytical Approximation of Data in Nuclear and Neutron Physics, Energoatomizdat, Moscow (1987) (in Russian).

[5.6] BADIKOV, S.A., GAI, E.V., GUSEINOV, M.A., RABOTNOV, N.S., "Padé — approximants in curve fitting and resonance analysis", 3rd IMSL User Group Europe (Proc. Conf. Bologna, 1990), p. B11.

[5.7] BADIKOV, S.A., GAI, E.V., GUSEINOV, M.A., RABOTNOV, N.S., "Nuclear data processing, evaluation, transformation and storage with Padé — Approximants", Nuclear Data for Science and Technology (Proc. Int. Conf. Jülich, 1991), QAIM, S.M. (Ed.), Springer-Verlag, Berlin (1992) 182–187.

6. PRODUCTION OF THERAPEUTIC RADIONUCLIDES BY MEANS OF NUCLEAR REACTORS

J.-Ch. Sublet, B.V. Carlson, A.D. Caldeira, F.B. Guimarães, P. Pompeia, H.D. Choi, S.K. Kim, S.M. Qaim, R. Capote

6.1. INTRODUCTION

This chapter deals with nuclear data for reactor production of about 20 radionuclides distributed over the whole chart of the nuclides. They are either already routinely used in radionuclide therapy or show some potential for therapeutic applications. Among them, ^{131}I ($T_{½}$ = 8.02 d) is by far the most important therapeutic radionuclide, having an established place in the management of follicular thyroid carcinoma. The other radioiodine, ^{125}I ($T_{½}$ = 59.41 d), is commonly used in brachytherapy but more important is its use in Auger electron therapy, provided suitable chemical compounds can be proposed.

Four radionuclides, namely ^{32}P ($T_{½}$ = 14.26 d), ^{89}Sr ($T_{½}$ = 50.5 d), ^{153}Sm ($T_{½}$ = 1.91 d) and ^{186}Re ($T_{½}$ = 3.72 d), are often used in metastatic bone pain treatment. The radionuclide ^{186}Re as well as another radiorhenium, ^{188}Re ($T_{½}$ = 16.98 h), being analogues of technetium, are also potentially useful for many other applications since they form good metal chelates. The same is valid for ^{64}Cu ($T_{½}$ = 12.7 h) and ^{67}Cu ($T_{½}$ = 2.58 d). They are of great therapeutic interest, especially in radioimmunotherapy because they can form diversified metal chelates. The radionuclide ^{64}Cu has an added advantage of combining positron emission tomography (PET) with internal radionuclide therapy.

The radionuclide ^{90}Y ($T_{½}$ = 2.67 d) has been used for radiation synovectomy in the arthritides and for labelling monoclonal antibodies (WAbs) and glass microspheres for intracavity therapy. Several other trivalent metal radionuclides, such as ^{149}Pm ($T_{½}$ = 2.21 d), ^{166}Ho ($T_{½}$ = 1.12 d), ^{169}Yb ($T_{½}$ = 32.0 d) and ^{177}Lu ($T_{½}$ = 6.71 d), find some application in metastatic bone marrow treatment.

The radionuclides ^{103}Pd ($T_{½}$ = 16.96 d) and ^{192}Ir ($T_{½}$ = 73.83 d) are commonly used in brachytherapy, the former in the form of seeds for treatment of prostate cancer and the latter as wires for treating deep lying tumours. The long lived ^{137}Cs ($T_{½}$ = 30.17 a) finds application as an external source of low energy β^- particles for irradiation of the retina or some other soft tissue.

The radionuclide ^{105}Rh ($T_{½}$ = 1.47 d) is used in labelling of WAbs, and the radionuclide ^{114m}In ($T_{½}$ = 49.5 d), being an analogue of ^{111}In, is of potential interest in Auger electron therapy. The radionuclide ^{213}Bi ($T_{½}$ = 45.6 min) is an α emitter. It can be attached to WAbs and is then best suited for treatment of rapidly accessible cancer cells or leukaemia.

The radionuclide ^{126}I ($T_{½}$ = 13.11 d), also treated in this chapter, is not a therapeutic radionuclide. Its production is discussed only because it could be a disturbing activity in the soft radiation emitting therapeutic radionuclide ^{125}I.

The production of radionuclides in a nuclear reactor generally utilizes the (n, γ) process. The yields achieved are generally high but the desired product is of low specific radioactivity (defined as the radioactivity per unit mass of the product). It is a disadvantage since most therapeutic applications demand radionuclides with as little mass of the inactive element as possible. Higher specific radioactivity is achieved if the radioactive daughter of a neutron capture product, rather than the capture product itself, is of therapeutic interest. Several such cases are:

$^{104}Ru(n, \gamma)^{105}Ru(\beta^-)^{105}Rh$
$^{124}Xe(n, \gamma)^{125}Xe(EC)^{125}I$
$^{130}Te(n, \gamma)^{131m,g}Te(\beta^-)^{131}I$
$^{164}Dy(n, \gamma)^{165m,g}Dy(n, \gamma)^{166}Dy(\beta^-)^{166}Ho$
$^{176}Yb(n, \gamma)^{177}Yb(\beta^-)^{177}Lu$
$^{186}W(n, \gamma)^{187}W(n, \gamma)^{188}W(\beta^-)^{188}Re$

The radionuclides ^{105}Rh, ^{125}I, ^{131}I and ^{188}Re are really produced via the indirect route but the radionuclides ^{166}Ho and ^{177}Lu are partly produced via the indirect route and partly via the direct (n, γ) reaction, the resulting specific radioactivity in the latter case being appreciably lower.

For achieving higher specific radioactivity, in production of some radionuclides, either the (n, p) reaction or the fission process is used. The radionuclides ^{32}P and ^{89}Sr, for example, are preferentially produced via the (n, p) reaction, and the radionuclides ^{90}Sr and ^{137}Cs are obtained via the fission process. The purified ^{90}Sr is used for preparing a ^{90}Sr (^{90}Y) generator. In the case of ^{131}I, on the other hand, both fission and the indirect (n, γ) process (mentioned above) are commonly used.

For some therapeutic radionuclides, charged particle induced reactions have proven to be superior to the reactor irradiations, both in terms of practical yield and specific radioactivity. They are ^{64}Cu, ^{67}Cu, ^{103}Pd, ^{114m}In and ^{186}Re. On the other hand, no meaningful alternative charged particle induced reaction was found for the (n, γ) produced radionuclides ^{153}Sm, ^{169}Yb, ^{177}Lu and ^{192}Ir. In the case of ^{213}Bi, the presently used method involves the chemical isolation of this product from the nuclear waste. A charged particle induced reaction process on the radioactive target material ^{226}Ra is in development. All of the charged particle induced reactions, whether of real practical value in the production of therapeutic radionuclides or only of academic interest with regard to production, are treated in Chapter 7.

The present chapter comprises five reactions. The radionuclides produced via the fission process are discussed in Section 6.2 and those via the (n, p) reaction in Section 6.6. The (n, γ) produced radionuclides are given in Sections 6.3, 6.4 and 6.5. The grouping of the radionuclides into those three sections is arbitrary and related to the assignment undertaken by three different groups. As a result, some differences in style and presentation were inevitable. For ^{213}Bi, only decay data were considered but it is placed in Section 6.4 along with the other cases studied by Carlson et al.

6.2. EVALUATION OF FISSION YIELDS FOR THE PRODUCTION OF ^{90}Y, ^{131}I AND ^{137}Cs RADIONUCLIDES

Many of the therapeutic radionuclides used worldwide can be produced as fragments emitted from the fissioning of actinides. The usual fissile isotope is ^{235}U although other fissionable isotopes can be used in the same manner. Energy dependent fission yields for more than a thousand fission fragments have been quantified and stored in tabulated form as special purpose files within the major nuclear applications libraries, such as JEFF-3.1 [6.1], JENDL-3.3 [6.2] and ENDF/B-VII [6.3]. Typical two-peaked energy dependent mass and charge distributions of these fission products are shown in Figs 6.1 to 6.4 — strontium radionuclides can be found in the light fragment peak, while iodine and caesium are located in the heavy fragment peak. As shown in these figures, rather good agreement exists between theory and measurement for those fragments in the peaks with the higher yields, while rather large discrepancies occur for the lower probability fragments. All of the radionuclides under investigation are to be found in the better characterized regions of the fission yield curves. One may note that when defined in terms of charge, strontium is even, while iodine and caesium are odd, with lower yields due to the odd–even effect (although this phenomenon is greatly reduced with increasing neutron energy to give higher fission yields). However, the majority of radionuclide production centres rely on facilities that operate in the thermal energy range. One needs to differentiate between the independent and cumulative yields listed in the data files:

— Independent yields represent nuclide production directly from fission;
— Cumulative yields account for the production of the nuclei both directly from fission and from the decay of other nuclides produced by fission.

The cumulative yields are of interest in radionuclide production rather than the more academic independent yields.

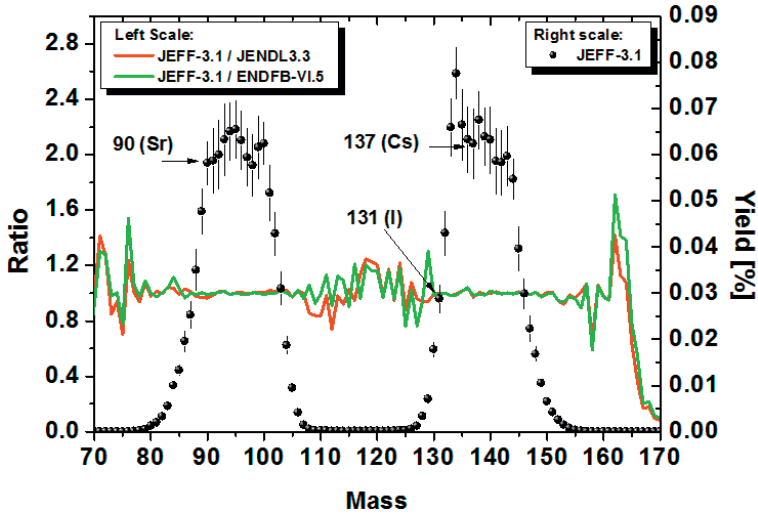

FIG. 6.1. Fission yield mass distribution of ^{235}U at thermal neutron energy.

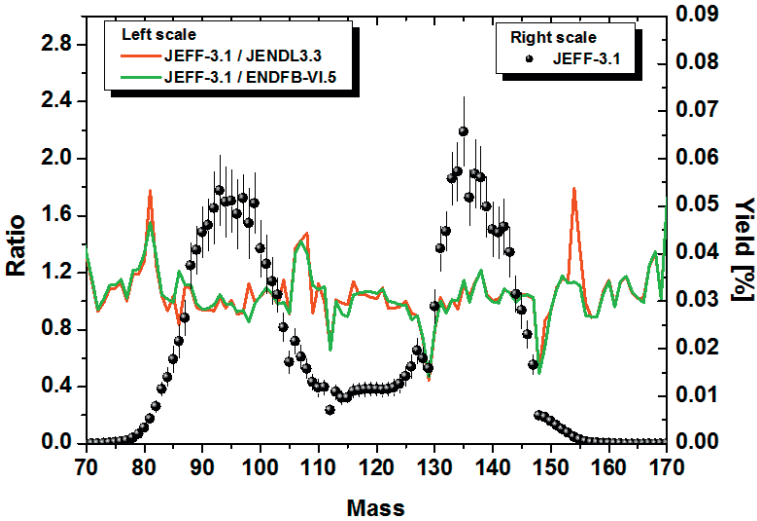

FIG. 6.2. Fission yield mass distribution of ^{235}U at 14 MeV neutron energy.

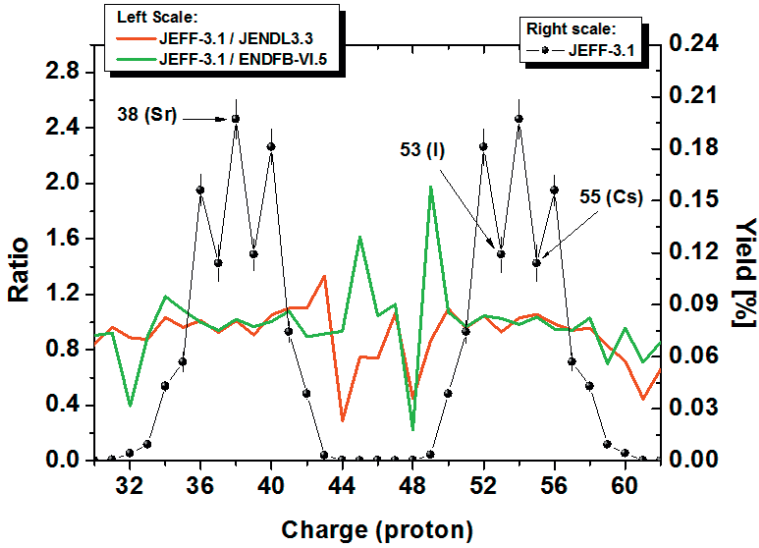

FIG. 6.3. Fission yield charge distribution of ^{235}U at thermal neutron energy.

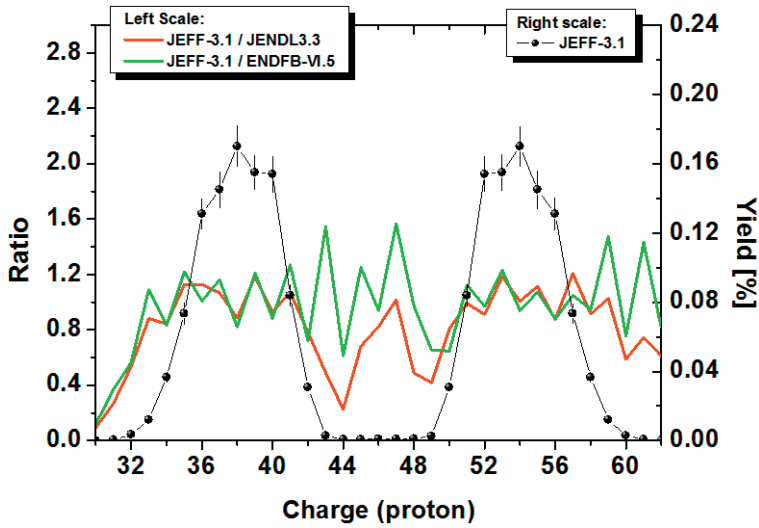

FIG. 6.4. Fission yield charge distribution of ^{235}U at 400 keV neutron energy.

Data uncertainties can be derived from two different sources: (1) evaluated fission yield files or (2) analysis of the experimental chain and cumulative yields, such as the compilation from Nexia Solutions Ltd [6.4]. Uncertainty data in the evaluated files are rather poorly defined and are largely related to the evaluation processes and constraints, the date of the evaluation, etc. The second data source is judged to be more reliable and forms the basis of the recommendation made in this work. Table 6.1 lists the thermal 400 keV and 14 MeV fission yields, and uncertainties for the radionuclides of interest from all selected libraries. The quoted uncertainties of the independent yields are noticeably larger than the cumulative yields as would be expected but, in some cases, the cumulative yields appear too precise given the available measurements.

Strontium-90 undergoes 100% beta decay to ^{90}Y with a half-life of 28.869 a. Strontium-89 undergoes beta decay to stable ^{89}Y with a half-life of 50.57 d, and a 20% lower cumulative yield; thus, this possible impurity will not cause any serious problems in the preparation of the ^{90}Y generator.

^{90}Y decay properties: $T_{½}$ = 2.671 d ± 0.12%; 100% β^- (^{90}Zr), with an average <β> energy of 933.82 keV and average <γ> energy of 1.236 eV.

^{131}I decay properties: $T_{½}$ = 8.023 d ± 0.02%; β^- 98.91% (^{131g}Xe), 1.09% (^{131m}Xe), with an average <β> energy of 192.43 keV and average <γ> energy of 381.54 keV.

^{137}Cs decay properties: $T_{½}$ = 30.041 d ± 0.10%; β^- 5.6% (^{137g}Ba), 94.4% (^{137m}Ba), with an average <β> energy of 187.87 keV and average <γ> energy of 1.6443 eV.

The recommended cumulative yields are given in Table 6.2, with a new set of uncertainties derived from reliable experimental chain and cumulative yields. These data have the advantage of being based on a retrievable source, and satisfy a set of statistically correct criteria. Although higher than 1.0% at thermal neutron energies, they rely on a set of published measurements and statistical analysis without adjustments that enforce consistency with physical constraints.

6.3. NUCLEAR DATA FOR THE PRODUCTION OF ^{64}Cu, ^{114m}In, ^{166}Ho, ^{169}Yb, ^{177}Lu, ^{186}Re AND ^{188}Re RADIONUCLIDES THROUGH CAPTURE CHANNELS AND DECAY

Newly evaluated cross-sections have been reviewed below, including consideration of the decay schemes of the specified nuclides. The evaluated data files are produced in ENDF format [6.5] for neutron energies up to 60 MeV, and include uncertainty data. This experimental information has been retrieved from the EXFOR database [6.6] by means of the original ENDVER/Gui package [6.7] and the SAFEPAQ-II application [6.8]. All of the data processing and

TABLE 6.1. FISSION YIELDS AT THERMAL (th), FISSION (.4, .5 and 1. MeV) AND 14 MeV (14.) NEUTRON ENERGIES FOR ^{235}U

Source files	Radionuclide Z	A	Independent yield	Uncertainty	%	Cumulative yield	Uncertainty	%
	38-Sr-89							
JEFF-3.1 (th)	38	89	2.183E–05	8.003E–06	36.7%	4.689E–02	5.678E–03	12.1%
	38-Sr-90							
JEFF-3.1 (th)	38	90	3.134E–04	1.180E–04	37.7%	5.729E–02	1.319E–03	2.3%
JEFF-3.1 (.4)	38	90	1.248E–04	4.608E–05	36.9%	5.221E–02	1.830E–03	3.5%
JEFF-3.1 (14)	38	90	2.109E–03	7.407E–04	35.1%	4.408E–02	1.808E–03	4.1%
JENDL-3.3 (th)	38	90	3.560E–04			5.900E–02		
JENDL-3.3 (1.)	38	90	2.190E–04			5.430E–02		
JENDL-3.3 (14.)	38	90	7.600E–04			4.660E–02		
ENDF/B-VII.0 (th)	38	90	7.371E–04	4.422E–05	6.0%	5.781E–02	5.781E–04	1.0%
ENDF/B-VII.0 (.5)	38	90	3.431E–04	1.544E–04	45.0%	5.465E–02	3.825E–04	0.7%
ENDF/B-VII.0 (14)	38	90	1.123E–03	7.191E–04	64.0%	4.592E–02	1.837E–03	4.0%
	53-I-131							
JEFF-3.1 (th)	53	131	1.364E–05	4.745E–06	34.8%	2.878E–02	3.166E–04	1.1%
JEFF-3.1 (.4)	53	131	4.434E–05	1.671E–05	37.7%	3.365E–02	5.384E–04	1.6%
JEFF-3.1 (14)	53	131	2.678E–03	9.195E–04	34.3%	4.110E–02	1.356E–03	3.3%
JENDL-3.3 (th)	53	131	4.150E–05			2.880E–02		
JENDL-3.3 (1.)	53	131	3.200E–05			3.180E–02		

TABLE 6.1. FISSION YIELDS AT THERMAL (th), FISSION (.4, .5 and 1. MeV) AND 14 MeV (14.) NEUTRON ENERGIES FOR ^{235}U (cont.)

Source files	Radionuclide Z	A	Independent yield	Uncertainty	%	Cumulative yield	Uncertainty	%
JENDL-3.3 (14.)	53	131	1.050E–03			3.990E–02		
ENDF/B-VII.0 (th)	53	131	3.915E–05	4.307E–06	11.0%	2.890E–02	2.890E–04	1.0%
ENDF/B-VII.0 (.5)	53	131	1.080E–05	6.918E–06	64.1%	3.219E–02	4.507E–04	1.4%
ENDF/B-VII.0 (14.)	53	131	1.201E–03	7.690E–04	64.0%	4.101E–02	1.640E–03	4.0%
	55-Cs-137							
JEFF-3.1 (th)	55	137	7.225E–04	2.557E–04	35.4%	6.221E–02	6.936E–04	1.1%
JEFF-3.1 (.4)	55	137	1.225E–03	4.398E–04	35.9%	5.889E–02	9.572E–04	1.6%
JEFF-3.1 (14.)	55	137	1.138E–02	3.203E–03	28.1%	5.567E–02	1.308E–02	23.5%
JENDL-3.3 (th)	55	137	1.580E–03			6.270E–02		
JENDL-3.3 (1.)	55	137	2.990E–03			6.200E–02		
JENDL-3.3 (14.)	55	137	8.890E–03			4.920E–02		
ENDF/B-VII.0 (th)	55	137	5.999E–04	6.599E–05	11.0%	6.188E–02	3.094E–04	0.5%
ENDF/B-VII.0 (.5)	55	137	2.283E–03	7.307E–04	32.0%	6.221E–02	3.110E–04	0.5%
ENDF/B-VII.0 (14.)	55	137	9.475E–03	3.032E–03	32.0%	4.926E–02	2.955E–03	6.0%

TABLE 6.2. RECOMMENDED FISSION YIELDS AND UNCERTAINTIES OF ^{235}U

Radionuclide Z	A	Cumulative yield	Uncertainty %	Number of experiments	Weighted mean
38-Sr-90		**28.869 y ± 0.19%**			
38	90 (th)	5.729E–02	7.0%	7+	5.77E–02
38	90 (.4)	5.221E–02	6.0%	4+	5.27E–02
38	90 (14.)	4.408E–02	4.0%	3+	4.41E–02
53-I-131		**8.040 d ± 0.12%**			
53	131 (th)	2.878E–02	9%	15+	2.88E–02
53	131 (.4)	3.365E–02	5%	11+	3.36E–02
53	131 (14.)	4.110E-02	5.0%	5+	4.09E–02
55-Cs-137		**30.172 y ± 0.54%**			
55	137 (th)	6.221E–02	8.0%	11+	6.21E–02
55	137 (.4)	5.889E–02	8.0%	7+	6.02E–02
55	137 (14.)	5.567E–02	10.0%	1+	5.90E–02

Note: 7+ means seven direct experimental studies of the isotope; + refers to measurements on the element that are also relevant.

Values in parentheses are the corresponding incident neutron energy (from JEFF-3.1 nuclear data library).

manipulation were performed using the NJOY-99, ENDF Utility and PREPRO-2007 codes [6.9, 6.10]. The differential experimental data are plotted as excitation functions, while the integral data are derived and compared with integral experimental information [6.11–6.13], whenever possible.

6.3.1. Rhenium-186 production: $^{185}Re(n, \gamma)^{186}Re$ reaction

The $^{185}Re(n, \gamma)^{186}Re$ reaction channel is present in many evaluated nuclear application libraries and model code calculations. Existing evaluations have been analysed, and demonstrate good agreement for the thermal neutron capture cross-sections, and resonance integrals between evaluations and measurements (Tables 6.3 and 6.4). A long lived isomer exists with a relatively low production cross-section at thermal energy (~0.3 b) that decays by isomeric transition only. The recommended neutron capture cross-sections and uncertainty bands are shown as functions of neutron energy in Fig. 6.5 for the $^{185}Re(n, \gamma)^{186g+m}Re$, ^{186g}Re and ^{186m}Re reactions, along with various measurements.

TABLE 6.3. THERMAL NEUTRON CAPTURE CROSS-SECTION OF ^{185}Re

Laboratory-year	σ (b)	Δσ (b)	σ^m (Δσ) (b)
ANL-1947	101	20	—
ORL-1960	127	36	—
GA-1968	114	30	—
LRL-1978	116	6	—
MU-2006	112	2	0.34 (0.1)
KfK Chart	—	—	0.34
This work	112	10%	0.34

Note: m means metastable.

TABLE 6.4. RESONANCE INTEGRAL FOR THE CAPTURE CROSS-SECTION OF ^{185}Re

Laboratory-year	Min. energy (eV)	RI (b)	ΔRI (b)
STF-1966	0.5	1650	90
LRC-1968	0.5	1790	60
GHT-1974	0.5	1419	77
LRL-1978	0.5	1810	150
MU-2006	—	1727	50
This work		1729	5%

^{186}Re decay properties: $T_{½}$ = 3.77 d ± 0.19%; 93.1% β^- (^{186}Os), 6.9% β^+ (^{186}W), with an average <β> energy of 337.26 keV and average <γ> energy of 20.305 keV. This radionuclide possesses indices for ingestion and inhalation of 1.5×10^{-9} and 1.1×10^{-9} Sv/Bq, respectively.

^{186m}Re decay properties: $T_{½}$ = 200 000 a ± 25.4%; 100% IT (^{186}Re).

Rhenium-186 has several current and potential applications, including investigations as a pain palliant for cancerous metastases in bones and for antibody labelling in targeted radiotherapy.

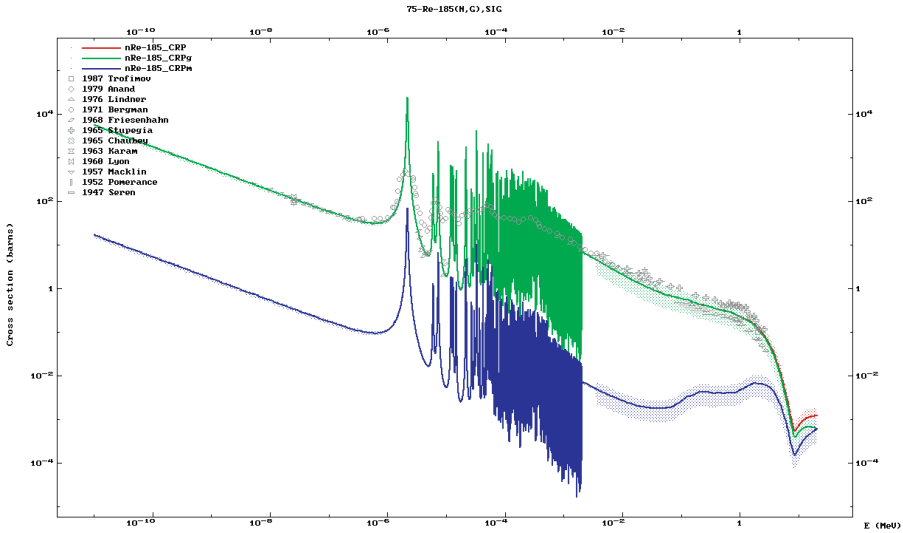

FIG. 6.5. ^{185}Re neutron capture cross-section — shaded areas constitute the uncertainty bands.

6.3.2. Rhenium-188 production: ^{186}W(n, γ)^{187}W(n, γ)^{188}W(β$^-$)^{188}Re double capture and beta decay reaction

The double neutron capture and decay channel is important in the production of ^{188}Re when no carrier is added. While the first capture reaction has been evaluated and validated by both differential and integral measurements (Tables 6.5 and 6.6), the second reaction is based purely on theoretical model calculations, with only one known study of the resonance integral and thermal cross-section. An uncertainty of 10% in the ^{187}W(n, γ) cross-section of 71 b at thermal neutron energy is acceptable for production purposes. A single level Breit–Wigner formalism has been used to represent a single resonance while maintaining the thermal cross-section [6.14].

^{188}Re decay properties: $T_{½}$ = 16.98 h ± 0.12%; 100% β$^-$ (^{188}Os), with an average <β> energy of 780.20 keV and average <γ> energy of 57.881 keV. This radionuclide is identified with indices for ingestion and inhalation of 1.4×10^{-9} and 5.4×10^{-10} Sv/Bq, respectively.

^{187}W decay properties: $T_{½}$ = 23.85 h ± 0.34%; 100% β$^-$ (^{187}Re).
^{188}W decay properties: $T_{½}$ = 69.78 d ± 0.07%; 100% β$^-$ (^{188}Re).

TABLE 6.5. THERMAL NEUTRON CAPTURE CROSS-SECTION OF ^{186}W

Laboratory-year	σ (b)	Δσ (b)
AGA-1966	37.8	1.2
MOL-1967	35.4	8.0
ORL-1977	37.0	1.5
MUN-1987	38 .5	8.0
MU-2006	38.1	0.5
This work	37.5	5%

TABLE 6.6. RESONANCE INTEGRAL FOR THE CAPTURE CROSS-SECTION OF ^{186}W

Laboratory-year	Min. energy (eV)	RI (b)	ΔRI (b)
BGK-1969	0.5	345	99
GHT-1974	0.5	410	4.
ORL-1977	0.5	490	15
LRL-1978	0.5	426	32
MU-2006	—	480	15
This work		519	25%

The first capture channel has been validated through experimental integral studies involving many different neutron spectra, including fusion, fission and high energy, as demonstrated by the highly satisfactory calculated/experimental (C/E) values depicted in Fig. 6.6 [6.11]. Uncertainty in the cross-section is shown as a shaded band around the C/E = 1 value, while each C/E value has an uncertainty range that corresponds to the experimental uncertainty.

Recommended neutron capture cross-sections and uncertainty bands for the ^{186}W(n, γ)^{187}W and ^{187}W(n, γ)^{188}W reactions are shown as functions of neutron energy in Figs 6.7 and 6.8, respectively, along with various measurements. (Tables 6.7 and 6.8).

6.3.3. Copper-64 production: ^{63}Cu(n, γ)^{64}Cu reaction

Cross-section data for the ^{63}Cu(n, γ)^{64}Cu reaction in many libraries have been carefully evaluated because this reaction has been adopted as a standard in dosimetry. The decay scheme has been re-evaluated at Jülich to produce the following recommended data: 38.4% β^-, 17.8% β^+ and 43.8% electron capture, and

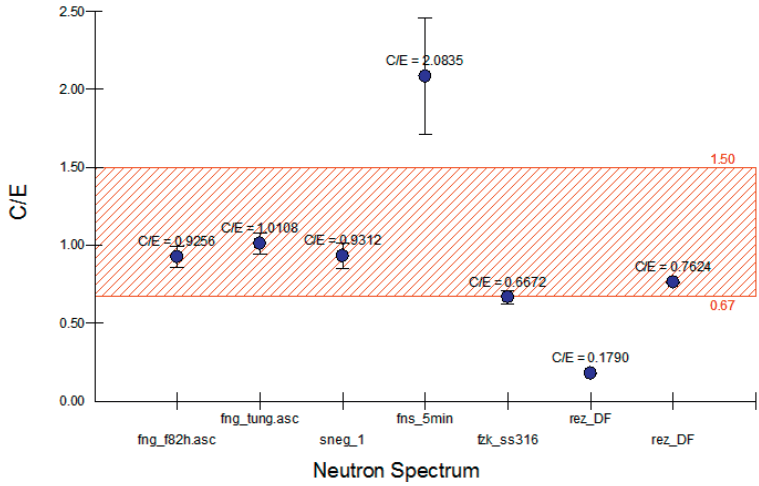

FIG. 6.6. C/E values for the $^{186}W(n, \gamma)$ reaction.

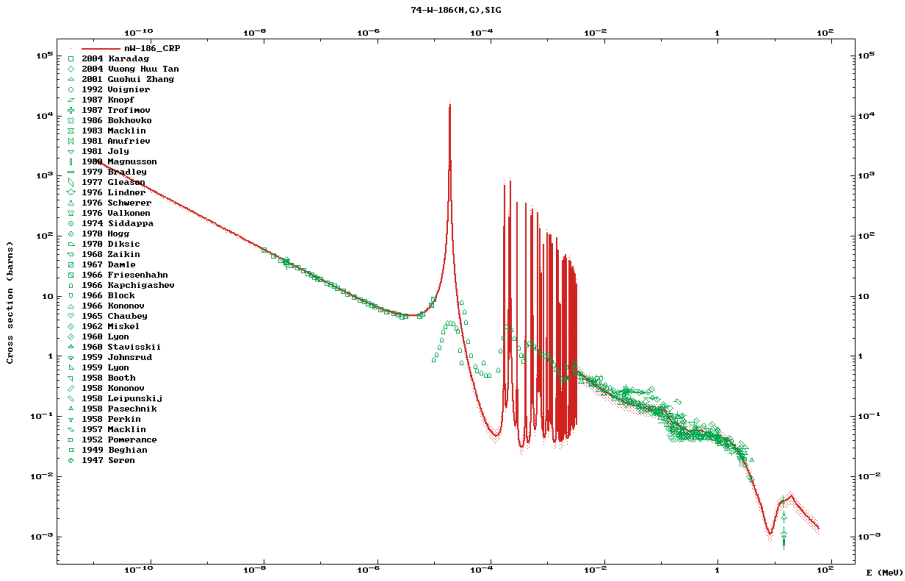

FIG. 6.7. ^{186}W neutron capture cross-section — shaded area constitutes the uncertainty band.

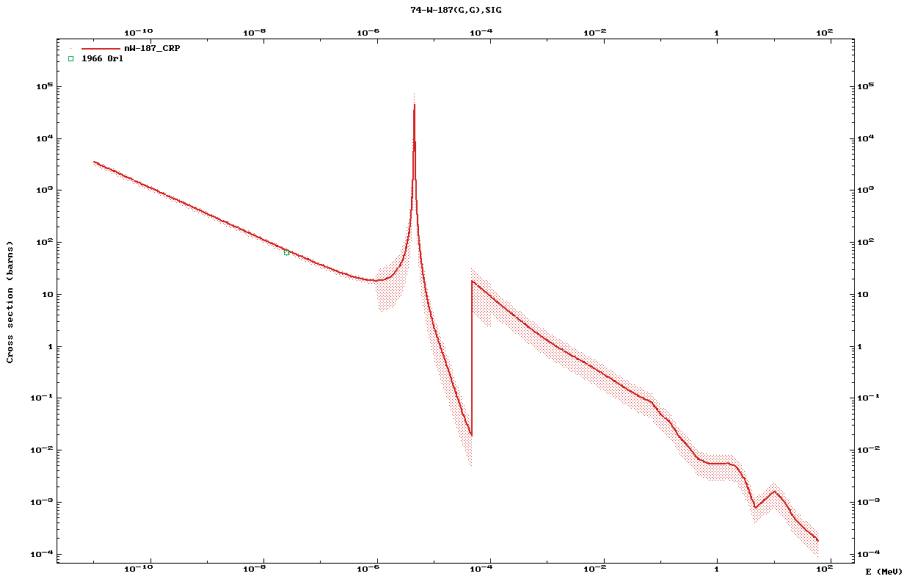

FIG. 6.8. ^{187}W neutron capture cross-section — shaded area constitutes the uncertainty band.

an emission probability of 0.54% for the 1346 keV γ ray emission. The ^{63}Cu(n, γ)^{64}Cu reaction is still occasionally used and a high flux reactor can lead to reasonable yields although the preferred production route is by means of a cyclotron.

^{64}Cu decay properties: $T_{½}$ = 12.701 h ± 0.02%; 38.4% β^- (^{64}Zn), 43.8% electron capture and 17.8% β^+ (^{64}Ni), with an average <β> energy of 125.88 keV and average <γ> energy of 190.08 keV. This radionuclide possesses indices for ingestion and inhalation of 1.2×10^{-10} and 1.2×10^{-10} Sv/Bq, respectively.

Copper-64 is one of the most important emerging therapeutic radionuclides that can be adopted to undertake a combination of radiotherapy and PET.

Only one resonance parameter file exists, with the resolved resonance parameters for multi level Breit–Wigner taken mainly from the work of Mughabghab up to 153 keV [6.12], with a 50 keV cut-off for JENDL-3.2 (JENDL-3.3, 99D) and a 99.5 keV cut-off for ENDF/B-VI revision 2 (revisions 6 and 8 up to 150 MeV). A 50 keV cut-off has been made because many levels are missing above 50 keV — only the total widths have been measured (Rohr et al. (1968) [6.15]), and γ–γ data are non-existent. The 100 keV cut-off in ENDF/B-VII has been adopted because an even poorer fit occurs above this energy. Nevertheless, a thermal value of 4.50 ± 0.2 b from Mughabghab [6.12] is consistent with other thermal measurements, and the IRDF-2002 resonance integral of 4.92 b with a thermal cross-section of 4.47 b is perfectly acceptable (see Tables 6.9 and 6.10).

TABLE 6.7. RESONANCE INTEGRAL FOR THE CAPTURE CROSS-SECTION OF ^{187}W

Laboratory-year	Min. energy (eV)	RI (b)	ΔRI (b)
ORL-1966	0.5	2760	550
This work		1652	75%

TABLE 6.8. THERMAL NEUTRON CAPTURE CROSS-SECTION OF ^{187}W

Laboratory-year	σ (b)	Δσ (b)
ORL-1966	64	10
ORL-1977	70	10
This work	71	10%

TABLE 6.9. RESONANCE INTEGRAL FOR THE CAPTURE CROSS-SECTION OF ^{63}Cu

Laboratory-year	Min. energy (eV)	RI (b)	ΔRI (b)
ANL-1964	0.55	5.0	—
GHT-1972	0.55	4.7	0.3
NPL-1974	0.1	2.79	0.18
ORL-1977	0.5	5.3	0.1
LRL-1978	0.5	5.15	0.10
MU-2006	—	4.97	0.08
This work		4.92	5%

TABLE 6.10. THERMAL NEUTRON CAPTURE CROSS-SECTION OF ^{63}Cu

Laboratory-year	σ (b)	Δσ (b)
ORL-1960	4.66	±0.5
NPL-1974	4.44	±0.2
ORL-1977	4.45	±0.5
MU-2006	4.50	±0.2
This work	4.47	2%

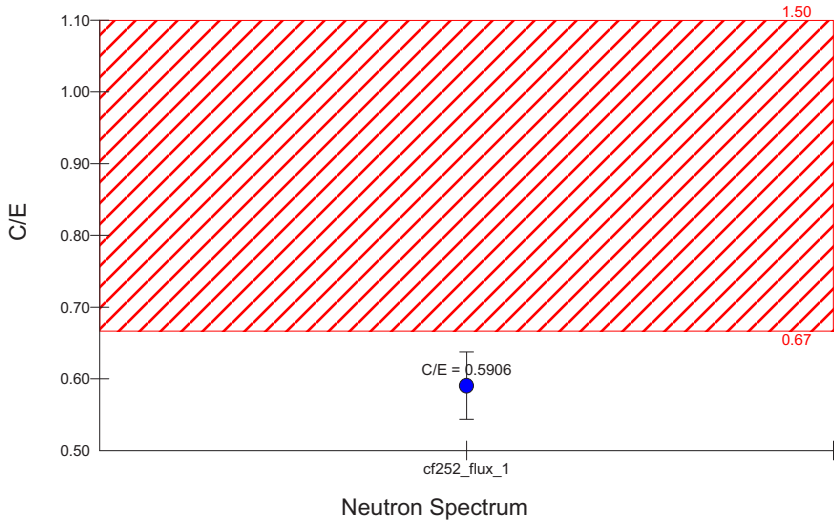

FIG. 6.9. Integral validation of experimental study of ^{63}Cu neutron capture.

A single 'calculated integral experiment' (C/E) value in the ^{252}Cf spontaneous fission spectrum for the capture channel, as shown in Fig. 6.9 [6.11], does not reflect the confidence that one can place in this reaction channel based on comparison with the differential measurements. The experimental uncertainty does not seem to be realistic, while the cross-section appears to be reasonably well founded. The recommended neutron capture cross-sections and uncertainty band for the ^{63}Cu(n, γ)^{64}Cu reaction are shown as a function of neutron energy in Fig. 6.10, along with various measurements.

6.3.4. Indium-114m production: ^{113}In(n, γ)^{114m}In reaction

Data quantifying the ^{113}In(n, γ)^{114}In (^{114m}In) reaction channel exist in many evaluated libraries although this particular reaction channel is rarely defined in terms of the two branches apart from in EAF [6.14] and JENDL-3.2/A, where the energy dependent branching ratio has been calculated from systematics. However, experimental information in the thermal and MeV ranges points to a different branching ratio of 0.42 at thermal energy increasing to 0.5 at 14 MeV. The first metastable channel has been better measured than the ground channel although the existence of other metastable levels does seem to be supported in the literature (^{114m}In with a half-life of 42 ms). A total thermal cross-section of 12.0 ± 1.1 b from Mughabghab [6.12] agrees reasonably well with the various measurements (Table 6.11). The proposed total resonance integral fits well with the calculated

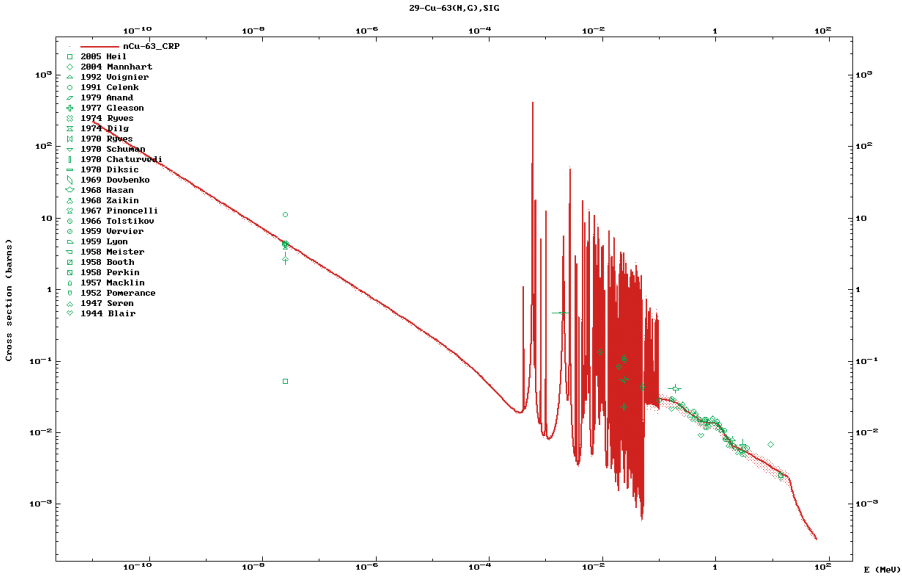

FIG. 6.10. ^{63}Cu neutron capture cross-section — shaded area constitutes the uncertainty band.

TABLE 6.11. THERMAL NEUTRON CAPTURE CROSS-SECTION OF ^{113}In

Laboratory-year	σ (b)	Δσ (b)	σ^m (b)
MTR-1963m	—	0.8	8.1
MTR-1963g	3.9	0.4	—
ROS-1968m	—	0.7	7.5
ROS-1968g	3.1	0.7	—
GHT-1972m	—	0.4	9.45
MU-2006	12.0	1.1	—
This work	12	10%	7.8

Note: m means metastable.

value although the metastable resonance integral would appear to be high (Table 6.12).

^{114m}In decay properties: $T_{½}$ = 50.0 d ± 0.4%; 3.5% β^+ (^{114}Cd), 96.5% IT (^{114}In), with an average <β> energy of 140.90 keV and average <γ> energy of 88.989 keV. This radionuclide is associated with indices for ingestion and inhalation of 4.1 × 10^{-9} and 9.3 × 10^{-9} Sv/Bq, respectively.

TABLE 6.12. RESONANCE INTEGRAL FOR THE CAPTURE CROSS-SECTION OF ^{113}In

Laboratory-year	Min. energy (eV)	RI (b)	ΔRI (b)
GHT-1969	0.55	258	10
CNE-1970	0.5	243	29
GHT-1973	0.55	258	18
MU-2006	—	320	30
MU-2006m	—	220	15
This work		321	10%
g		112	
m		209	

TABLE 6.13. EXPERIMENTAL (m/g) BRANCHING RATIO OF ^{113}In

Laboratory-year	Energy (eV)	m/g branching ratio	Δbranching ratio
MTR-1963	2.53E–01	2.1	0.1
KFK-1966	7.80E+03	2.1	0.3
KFK-1966	3.00E+04	2.7	0.5
KFK-1966	6.40E+04	5.1	1.0
ROS-1968	2.53E–01	2.6	0.1
LOK-1968	3.68E+05	3.2	0.3
LOK-1968	1.00E+06	3.5	0.3

^{114}In decay properties: $T_{½}$ = 1.198 m ± 0.1%; 99.5% β^-, 0.5% β^+, with an average <β> energy of 769.23 keV and average <γ> energy of 4.369 keV.

Without further experimental measurements in the resonance range, the total capture cross-section has been adopted directly from EAF-2007 [6.14], while the branching ratio has been modified to follow more precisely the experimental information available at high energies (Table 6.13).

The recommended neutron capture cross-sections and uncertainty bands are shown as functions of neutron energy in Fig. 6.11 for the ^{113}In(n, γ)$^{114g+m}$In, ^{114g}In and ^{114m}In reactions, along with various measurements.

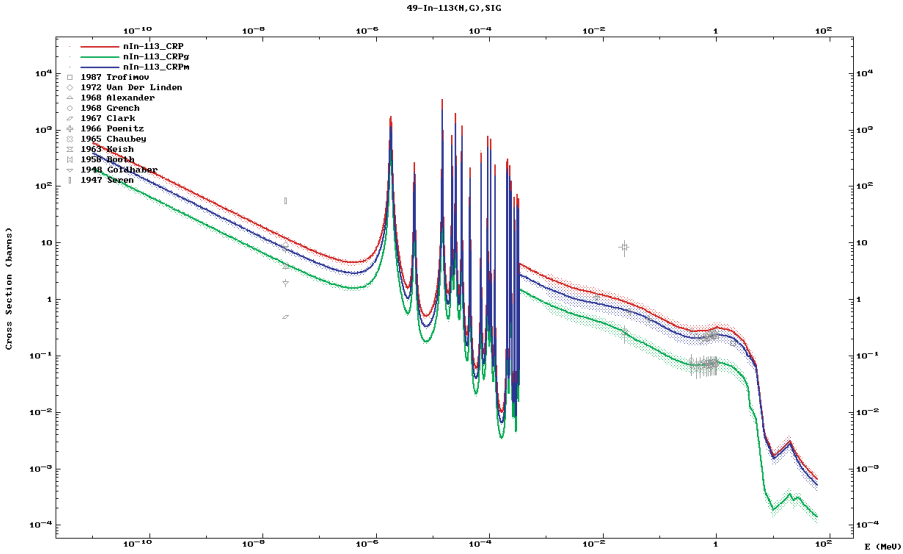

FIG. 6.11. ^{113}In neutron capture cross-section — shaded areas constitute the uncertainty bands. The ground state (green), metastable (blue) and total (red) are shown.

6.3.5. Holmium-166 production: ^{164}Dy(n, γ)^{165}Dy(n, γ)^{166}Dy(β$^-$)^{166}Ho double capture and beta decay reaction

While the ^{164}Dy(n, γ)^{165}Dy reaction channel has been well studied and exists in many libraries (Tables 6.14 and 6.15) (Figs 6.13 and 6.14). The ^{165}Dy(n, γ)^{166}Dy reaction channel is much more ill-defined (Tables 6.16 and 6.17) and can only be derived by means of model calculations. The capture reaction for the first branch has been validated by both differential and integral measurements of the metastable product with surprisingly good agreement for such an exotic radionuclide. Under such reassuring circumstances, a C/E ratio of 0.85 is judged to be reliable (Fig. 6.12 [6.11]), despite the lack of knowledge of the experimental neutron flux below 1 keV at the fusion neutron source in JAERI where the integral experiment was performed. Unexpectedly, the experimental and effective cross-section uncertainties agree rather well for such an exotic cross-section.

^{166}Ho decay properties: $T_{½}$ = 1.117 d ± 0.07%; 100% β$^-$ (^{166}Er), with an average <β> energy of 69.475 keV and average <γ> energy of 30.211 keV. This radionuclide is associated with indices for ingestion and inhalation of 1.4×10^{-9} and 6.5×10^{-10} Sv/Bq, respectively.

TABLE 6.14. THERMAL NEUTRON CAPTURE CROSS-SECTION OF ^{164}Dy

Laboratory-year	σ (b)	Δσ (b)	σ^m (Δσ) (b)
MNZ-1954	507	—	—
MAU-1962g	951	—	—
OSL-1962g	1100	—	—
OSL-1972	2800	140	—
OSL-1972m	—	—	1700 (240)
NPL-1974	2700	100	—
SAC-1977	2695	—	—
ANR-1991g	1056	—	—
MU-2006	2650	70	—
This work	2650	15%	1669

Note: m means metastable.

TABLE 6.15. RESONANCE INTEGRAL FOR THE CAPTURE CROSS-SECTION OF ^{164}Dy

Laboratory-year	Min. energy (eV)	RI (b)	ΔRI (b)
GHT-1974m	0.5	470	20
KJL-1975	0.5	335	27
KTO-2001	0.5	649	24
ANR-2005	0.5	527	89.
MU-2006	—	341	20
This work		342	50%

TABLE 6.16. THERMAL NEUTRON CAPTURE CROSS-SECTION OF ^{165}Dy

Laboratory-year	σ^g (b)	Δσ (b)
OSL-1972	3900	—
JAE-1981	2000	—
JAE-1981	3530	300
MU-2006	3600	300
This work	3573	10%

TABLE 6.17. RESONANCE INTEGRAL FOR THE CAPTURE CROSS-SECTION OF ^{165}Dy

Laboratory-year	Min. energy (eV)	RI (b)	ΔRI (b)
OSL-1972	0.5	22000	3000
MU-2006	—	22000	3000
This work		20181	15%

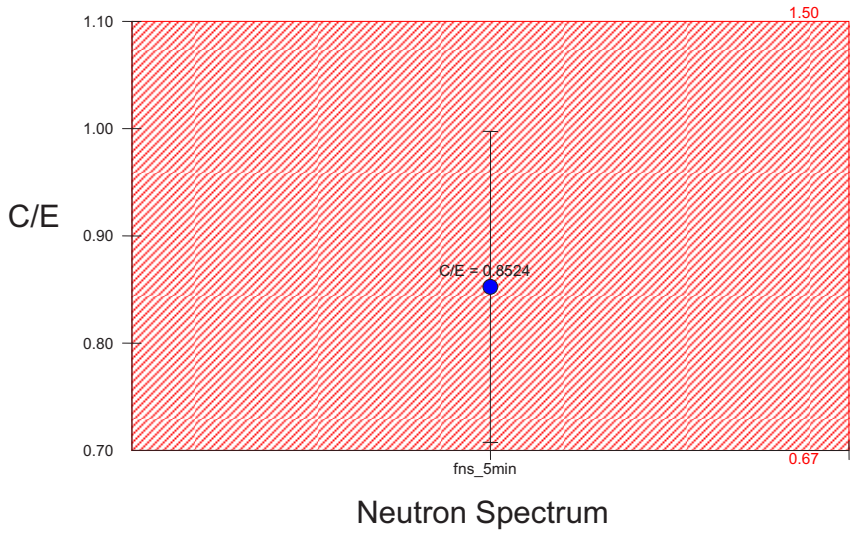

FIG. 6.12. Integral validation of experimental study of ^{164}Dy neutron capture.

^{165}Dy decay properties: $T_{½}$ = 2.33 h ± 0.26%; 100% β^-.
^{165m}Dy decay properties: $T_{½}$ = 1.26 m ± 0.48%; 2.4% β^- and 97.6% IT.
^{166}Dy decay properties: $T_{½}$ = 3.40 d ± 0.12%; 100% β^-.

6.3.6. Ytterbium-169 production: ^{168}Yb(n, γ)^{169}Yb reaction

The ^{168}Yb(n, γ)^{169}Yb reaction channel exists in only a few libraries, and the excitation function is mainly based on model calculations.

^{169}Yb decay properties: $T_{½}$ = 32.01 d ± 0.6%; 100% β^+ (^{169}Tm), with an average <β> energy of 111.80 keV and average <γ> energy of 313.26 keV. This radionuclide is associated with indices for ingestion and inhalation of 7.1×10^{-10} and 3.0×10^{-9} Sv/Bq, respectively.

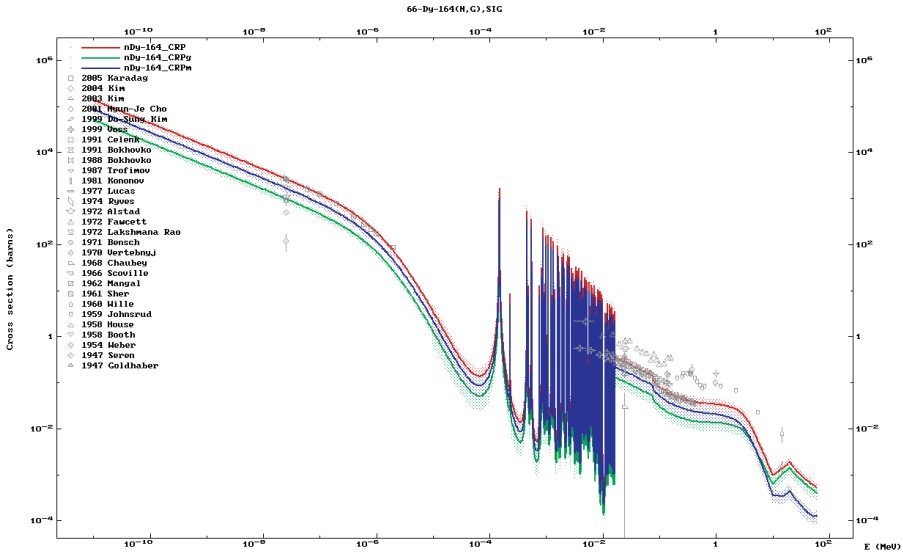

FIG. 6.13. ^{164}Dy neutron capture cross-section — shaded areas constitute the uncertainty bands. The ground state (green), metastable (blue) and total (red) are shown.

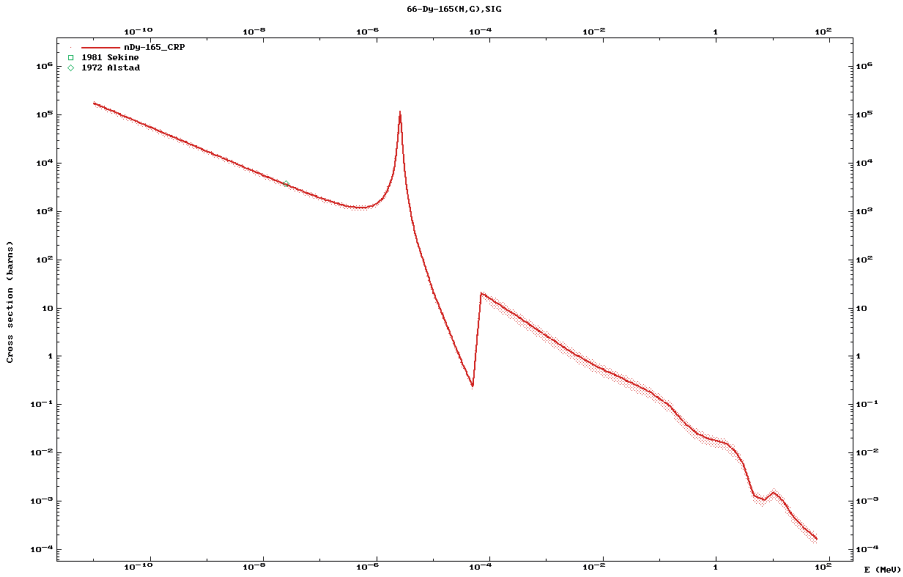

FIG. 6.14. ^{165}Dy neutron capture cross-section — shaded area constitutes the uncertainty band.

^{169m}Yb decay properties: $T_{½}$ = 46.0 s ± 4%; IT 100%, with an average <β> energy of 24.2 keV.

^{169}Yb is an Auger electron emitter that is gaining interest for therapeutic applications.

An evaluation was performed by means of a model calculation [6.14] and systematically derived branches (set at a ratio of 0.5 up to a neutron energy of 30 keV, and increasing to 0.8 thereafter). Rather elderly reduced sets of experimental differential measurements were used, and the thermal cross-section has been renormalized to specific studies (Tables 6.18 and 6.19).

TABLE 6.18. THERMAL NEUTRON CAPTURE CROSS-SECTION OF ^{168}Yb

Laboratory-year	σ (b)	Δσ (b)
TNC-1961	5500	2640
LAS-1968	2840	600
CPO-1970	3660	50
OSL-1970	4400	200
LRL-1978	2600	60
MU-2006	2300	170
This work	3658	20%

TABLE 6.19. RESONANCE INTEGRAL FOR THE CAPTURE CROSS-SECTION OF ^{168}Yb

Laboratory-year	Min. energy (eV)	RI (b)	ΔRI (b)
KJL-1969	0.5	14 700	1900
CNE-1970	—	35 706	1714
OSL-1970	—	38 000	2000
CPO-1970	0.55	19 800	4200
CPO-1970	0.55	21 000	4200
GHT-1973	—	23 040	5440
LRL-1978	0.5	16 600	1700
MU-2006	—	21 300	1000
This work		21 238	25%

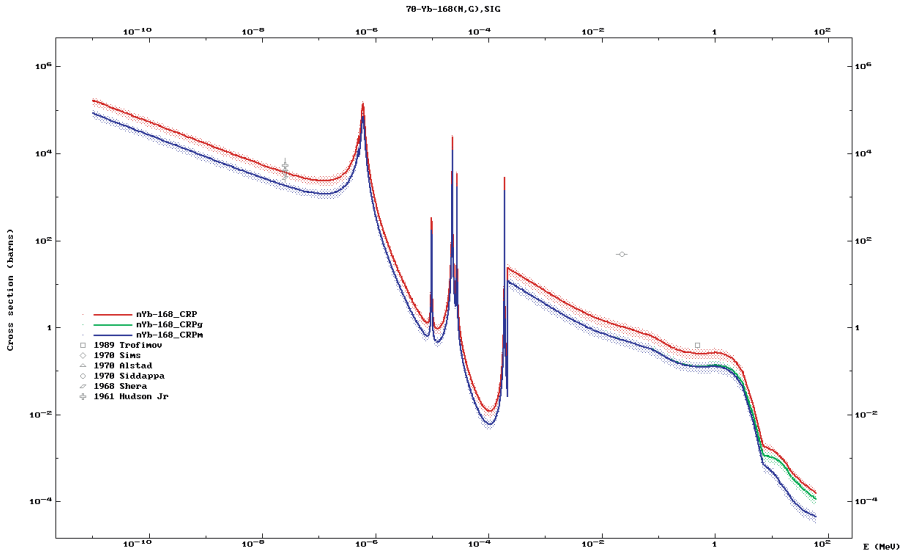

FIG. 6.15. ^{168}Yb neutron capture cross-section — shaded areas constitute the uncertainty bands. The ground state (green), metastable (blue) and total (red) are shown.

Recommended neutron capture cross-sections and uncertainty bands for the ^{168}Yb(n, γ)$^{169g+m}$Yb, ^{169g}Yb and ^{169m}Yb reactions are shown as functions of neutron energy in Fig. 6.15, along with various measurements.

6.3.7. Lutetium-177 production: ^{176}Yb(n, γ)^{177}Yb(β$^-$)^{177}Lu and ^{176}Lu(n, γ)^{177}Lu reactions

The ^{176}Yb(n, γ)^{177}Yb reaction channel exists in specific libraries and is mainly based on model calculations. All data have been assessed, and specific evaluations selected for the ground and metastable states.

^{177}Lu decay properties: $T_{½}$ = 6.64 d ± 0.3%; 100% β$^-$ (^{177}Hf) with an average <β> energy of 147.34 keV and average <γ> energy of 33.423 keV. This radionuclide is associated with indices for ingestion and inhalation of 5.3 × 10^{-10} and 1.2 × 10^{-9} Sv/Bq, respectively.

^{177m}Lu decay properties: $T_{½}$ = 160.3 d ± 2.5%; 77.4% β$^-$ and 22.6% IT (^{177}Lu) with an average <β> energy of 82.07 keV and average <γ> energy of 167.77 keV.

^{177n}Lu has been observed with a $T_{½}$ of 7.0 m; 50% β$^-$ and 50% IT (^{177}Lu) with an average <β> energy of 276.76 keV and average <γ> energy of 1741.7 keV.

^{177}Yb decay properties: $T_{½}$ = 1.911 h ± 6%; 100% β^- (^{177}Lu) with an average <β> energy of of 420.0 keV and average <γ> energy of 199.13 keV.

^{177m}Yb decay properties: $T_{½}$ = 6.41 s ± 0.3%; 100% IT with an average <β> energy of 178.2 keV and average <γ> energy of 150.0 keV.

Lutetium-177 is used in palliative therapy via interstitial implantation as a liquid gel injection.

An evaluation of the ^{176}Yb(n, γ)^{177}Yb reaction was performed by means of a model calculation [6.14] and systematically derived branches (set at a ratio of 0.5 up to a neutron energy of 30 keV, and increasing to 0.76 thereafter). A reliable set of experimental differential measurements were adopted, particularly above the resonance region. There is room for improvement in this evaluation with respect to the branching ratio and resonance integral if new experimental studies are performed (see Tables 6.20 and 6.21).

TABLE 6.20. THERMAL NEUTRON CAPTURE CROSS-SECTION OF ^{176}Yb

Laboratory-year	σ (b)	Δσ (b)
OSL-1970	2.40	0.2
LRL-1978	3.02	0.5
MU-2006	2.85	0.5
This work	2.85	17.5%

TABLE 6.21. RESONANCE INTEGRAL FOR THE CAPTURE CROSS-SECTION OF ^{176}Yb

Laboratory-year	Min. energy (eV)	RI (b)	ΔRI (b)
LRL-1970	0.5	1.33	0.13
OSL-1970	0.4	2.7	0.3
GHT-1973	0.55	14.4	1.2
KJL-1975	0.5	9.2	1.8
MU-2006	—	6.9	0.6
This work		6.77	10%

The $^{176}Lu(n, \gamma)^{177}Lu$ reaction channel exists in a few libraries, and is mainly based on model calculations. First resonances and keV region measurements provide confidence in the predicted excitation function (Tables 6.22 and 6.23), and the cross-section of the longer lived metastable state has been measured at thermal neutron energy. However, the ^{176}Yb route of production of ^{177}Lu is recommended because of the carrier-free nature of the end product.

Recommended neutron capture cross-sections and uncertainty bands for the $^{176}Yb(n, \gamma)^{177g+m}Yb$, ^{177g}Yb and ^{177m}Yb reactions are shown as functions of neutron energy in Fig. 6.16, along with various measurements, while the equivalent data for the $^{176}Lu(n, \gamma)^{177g+m}Lu$, ^{177g}Lu and ^{177m}Lu reactions are depicted in Fig. 6.17.

TABLE 6.22. THERMAL NEUTRON CAPTURE CROSS-SECTION OF ^{176}Lu

Laboratory-year	σ (b)	Δσ (b)	σ^m (b)
ANL-1947	3640	728	—
HAR-1960	2100	150	—
LRL-1967m	—	2.0	7.0
MUN-1976m	—	0.7	2.1
MU-2006	2020	70	—
MU-2006	—	0.7	2.8
This work	2097	8%	2.1

Note: m means metastable.

TABLE 6.23. RESONANCE INTEGRAL FOR THE CAPTURE CROSS-SECTION OF ^{176}Lu

Laboratory-year	Min. energy (eV)	RI (b)	ΔRI (b)
GH-1974	0.55	1069	41
MUN-1976m	0.55	3.8	1
LRL-1978	0.5	1480	80
MU-2006	—	1087	40
MU-2006m	—	4.7	1.4
This work		919	10%
m		0.9	

Note: m means metastable.

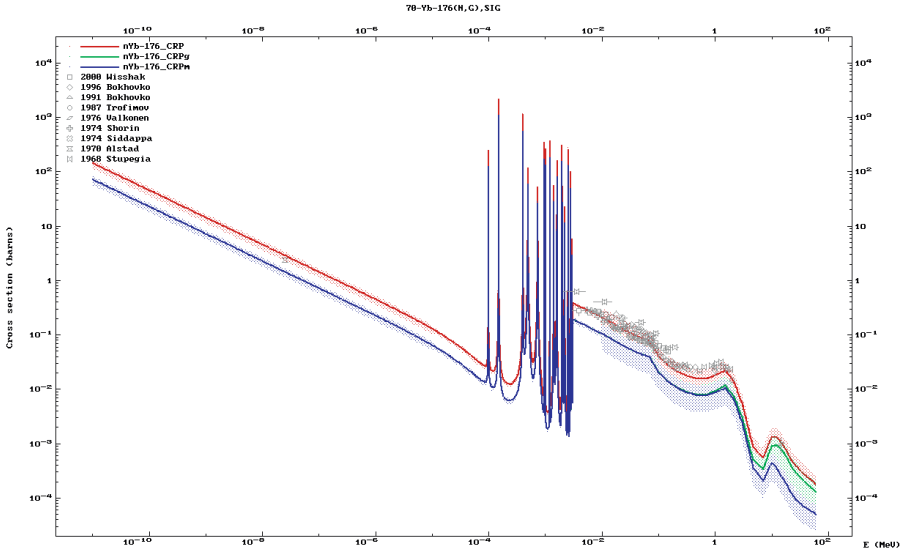

FIG. 6.16. ^{176}Yb neutron capture cross-section — shaded areas constitute the uncertainty bands. The ground state (green), metastable (blue) and total (red) are shown.

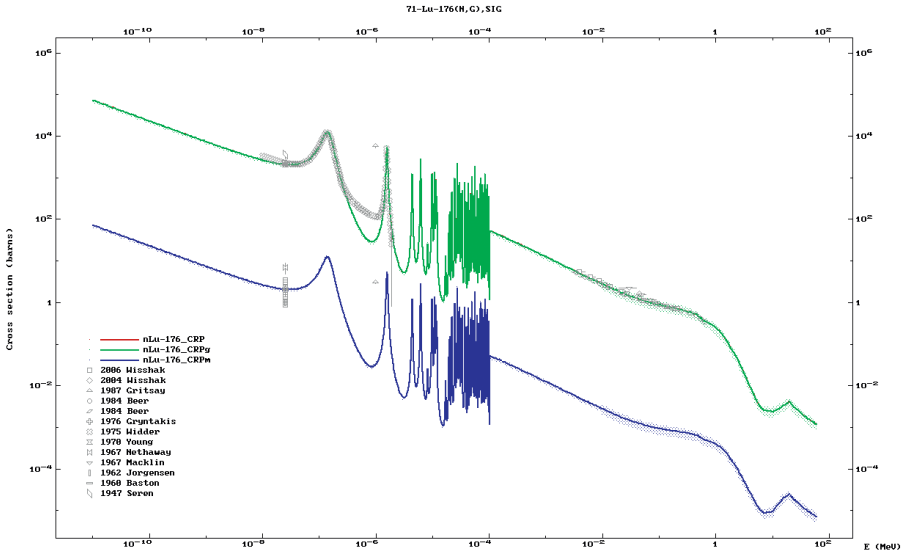

FIG. 6.17. ^{176}Lu neutron capture cross-section — shaded areas constitute the uncertainty bands. The ground state (green), metastable (blue) and total (red) are shown.

6.4. NUCLEAR DATA FOR THE PRODUCTION OF ^{90}Y, ^{103}Pd, ^{125}I, ^{126}I, ^{149}Pm, ^{153}Sm, ^{188}Re AND ^{213}Bi RADIONUCLIDES THROUGH CAPTURE CHANNELS AND DECAY

6.4.1. Introduction

We have examined the experimental and evaluated data for the neutron capture reactions that produce the radioactive isotopes ^{90}Y, ^{103}Pd, ^{125}I (from the β^- decay of ^{125}Xe), ^{126}I, ^{149}Pm (from the β–decay of ^{149}Nd), ^{153}Sm and ^{188}Re, along with the ^{213}Bi-producing decay chain initiated by the decay of ^{233}U. The experimental data available in the EXFOR library [6.6, 6.15] for the neutron capture reactions were initially compiled and checked for their normalization to standards. These data were then compared with theoretical calculations using the EMPIRE-II code [6.16] and with previous evaluations in the ENDF-formatted libraries using the NJOY99 code [6.17]. BROND-2, JENDL-3.3 [6.2, 6.19], JEFF-3.1 [6.1] and ENDF/B-VI databases were used in the comparison, with the ENDF/B-VII library [6.3] added to these data sets on release. The unshielded spectrum-averaged capture cross-sections were also calculated using the PREPRO processing codes [6.10] and the ENDF-formatted libraries. The resulting capture resonance integrals, along with the thermal capture cross-sections from the various evaluations, were compared with the experimental data, as well as with the evaluated values of Mughabghab [6.12, 6.18].

No serious discrepancies were observed between the EMPIRE-II calculations [6.16, 6.20] and the available evaluations — these particular comparisons were between the experimental data from the EXFOR library and the available evaluations. The evaluation that described the experimental data most precisely was recommended although small adjustments were sometimes made in attempts to improve agreement. Since only one evaluation of neutron induced reactions on ^{125}I was found in the ENDF-formatted libraries, a new evaluation was prepared that was based on the behaviour expected from the scarce experimental data in the thermal region, from systematics in the resonance region and from EMPIRE-II calculations based on systematics in the continuum region [6.20]. A crude capture cross-section covariance file was included in all evaluations, except for ^{89}Y where the ENDF/B-VII evaluation provides a reasonably detailed covariance file [6.3]. Our covariance files were prepared solely to reproduce the uncertainty (variance) in the spectrum-averaged capture cross-section in the thermal, resonance and continuum region, and are not intended for wider use.

We examined the information in the ENDF-formatted decay data libraries [6.21] for the decay of the radionuclides of interest: ^{90}Y, ^{103}Pd, ^{125}Xe, ^{125}I, ^{149}Nd, ^{149}Pm, ^{153}Sm, ^{188}Re, ^{213}Bi and the α emitting decay chain

$^{225}Ac \rightarrow ^{221}Fr \rightarrow ^{217}At \rightarrow ^{213}Bi$, as well as the decay chain that produces ^{225}Ac ($^{233}U \rightarrow ^{229}Th \rightarrow ^{225}Ra \rightarrow ^{225}Ac$).

6.4.2. Production of ^{90}Y by means of the $^{89}Y(n, \gamma)^{90}Y$ reaction

Yttrium-90 has a $J^{\pi} = 2^{-}$ ground state with a half-life of $T_{1/2} = 64.053(20)$ h that decays only by β^{-} emission. There is also a $J^{\pi} = 7^{+}$ isomeric state at $E_x = 682.04(6)$ keV with a half-life of $T_{1/2} = 3.19(6)$ h that undergoes decay almost exclusively to the ground state but possesses an extremely small branching ratio of 1.8×10^{-5} for β^{-} emission. The Q-value of the β^{-} decay of ^{90}Y is 2280.1(16) keV, with an average light particle (electron) energy of 933.614(13) keV and negligible γ ray energy. The most recent version of the radioactive decay file can be found in the ENDF/B-VII nuclear applications library, based on the ENSDF evaluation of Browne (Fig. 6.18) [6.22].

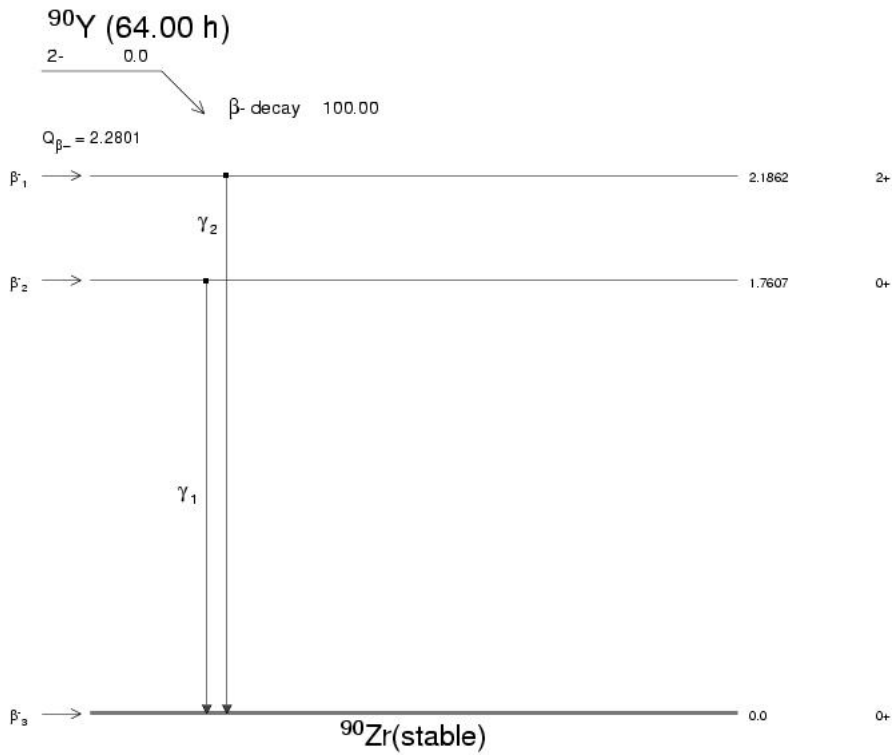

FIG. 6.18. Decay scheme of ^{90}Y from the MIRD library.

Experimental values of the thermal capture cross-section and capture resonance integral are available from EXFOR (Tables 6.24 and 6.25). A simple weighted mean of the experimental values of the thermal capture cross-section furnishes the value adopted by Mughabghab. However, the adopted value for the resonance capture integral is about twice the weighted mean of the two available data determinations.

JENDL-3.3, JEFF-3.1, ENDF/B-VI and ENDF/B-VII evaluations were compared with the experimental (n, tot), (n, el), (n, γ), (n, p), (n, α), (n, 2n) and (n, inl) data found in the EXFOR library. The JEFF-3.1 evaluation is essentially identical to that of ENDF/B-VI, and all four evaluations agree well with respect to total, elastic, (n, α) and (n, 2n) cross-section data; the JENDL-3.3 evaluation shows slightly better agreement with the available inelastic data, while the

TABLE 6.24. THERMAL NEUTRON CAPTURE CROSS-SECTION DATA OF ^{89}Y *(extracted from EXFOR [6.23–6.29])*

Lead author	Publication date	(n, γ) (b)
Seren	1947	1.24 (0.25)
Pomerance	1951	1.38 (0.14)
Benoist	1951	1.25 (0.20)
Lyon	1956	1.26 (0.08)
Rustad	1966	1.28 (0.01)
Ryves	1971	1.21 (0.05)
Takiue	1978	1.31 (0.04)
This work	—	1.28 (0.01)
Mughabghab	2006	1.28 (0.02)

TABLE 6.25. CAPTURE RESONANCE INTEGRAL DATA OF ^{89}Y *(extracted from EXFOR [6.28–6.30])*

Lead author	Publication date	RI (b)
Harris	1950	0.72 (0.22)
Ryves	1971	0.44 (0.06)
This work	—	0.46 (0.06)
Mughabghab	2006	1.00 (0.10)

TABLE 6.26. SPECTRUM-AVERAGED CAPTURE CROSS-SECTIONS FROM EVALUATIONS OF ^{89}Y

Library	Resonance integral (b)	Maxwellian fission integral (mb)
ENDF/B-VI.8	0.892	4.76
ENDF/B-VII.0	0.840	6.34
JEFF-3.1	0.895	4.77
JENDL-3.3	0.840	6.34

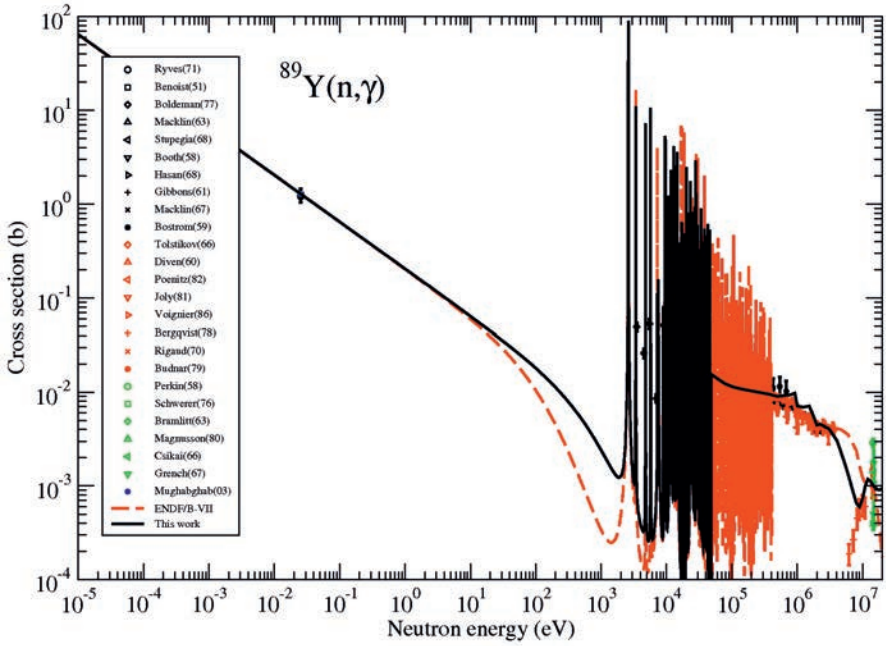

FIG. 6.19. ^{89}Y(n, γ) capture cross-section for the production of ^{90}Y; EXFOR data are plotted as symbols [6.25, 6.28, 6.31–6.52].

JEFF-3.1 and ENDF/B evaluations are in better agreement with the (n, p) data. All evaluations provide a reasonably good description of the capture cross-section (Fig. 6.19) but underestimate the accepted value of the capture resonance integral by 10 to 15% (Table 6.26).

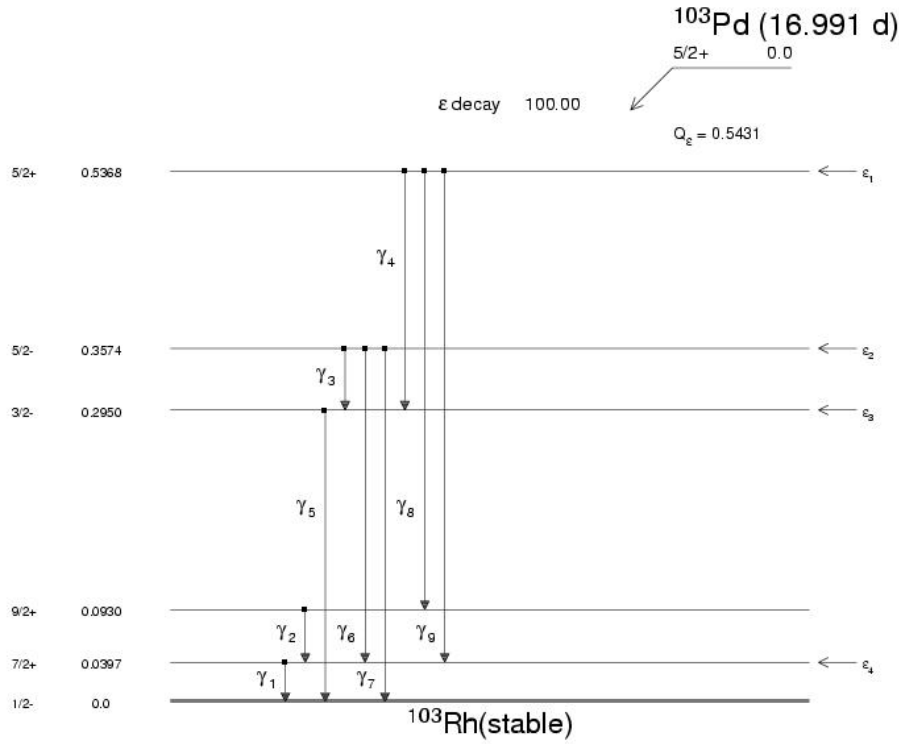

FIG. 6.20. Decay scheme of ^{103}Pd from the MIRD library.

6.4.3. Production of ^{103}Pd by means of the ^{102}Pd(n, γ)^{103}Pd reaction

Palladium-103 is a low energy X ray emitter used increasingly for brachytherapy. The $J^{\pi} = 5/2^{+}$ ground state decays exclusively by electron capture with a half-life of $T_{1/2}$ = 16.991(19) d. The Q-value for this decay mode is 543.1(8) keV, with an average light particle (electron) energy of 4.90(14) keV and an average γ ray energy of 14.4(3) keV. The most recent version of the radioactive decay file can be found in the ENDF/B-VII library, based on the ENSDF evaluation of De Frenne and Jacobs [6.53] (Fig. 6.20).

The single experimental value of the thermal capture cross-section found in EXFOR [6.54] as well as the experimental values of the thermal capture cross-section and the capture resonance integral published by Duncan and Krane [6.55] are given in Tables 6.27 and 6.28. The values of Duncan and Krane were adopted by Mughabghab.

JENDL-3.3, JEFF-3.1, ENDF/B-VI and ENDF/B-VII evaluations were compared with the (n, 2n) and (n, p) data found in the EXFOR library, as well as

TABLE 6.27. THERMAL NEUTRON CAPTURE CROSS-SECTION DATA OF ^{102}Pd *(extracted from EXFOR [6.54, 6.55])*

Lead author	Publication date	(n, γ) (b)
Meinke	1953	4.80 (1.44)
Duncan	2005	1.82 (0.20)
This work	—	1.88 (0.20)
Mughabghab	2006	1.82 (0.20)

TABLE 6.28. CAPTURE RESONANCE INTEGRAL DATA OF ^{102}Pd *(extracted from EXFOR [6.55])*

Lead author	Publication date	RI (b)
Duncan	2005	23.0 (4.0)
This work	—	23.0 (4.0)
Mughabghab	2006	23.0 (4.0)

with the newly recommended values of the thermal capture cross-section and resonance integral. JENDL-3.3 overestimates the (n, 2n) cross-section data slightly, while the ENDF/B-VII evaluation underestimates them slightly. The JENDL-3.3 evaluation best describes the anomalously small (n, p) cross-section data. However, only ENDF/B-VII reproduces the newly accepted value of the thermal capture cross-section, whereas none of the evaluations reproduce the accepted value of the capture resonance integral (Table 6.29). An attempt was made to improve the agreement with the experimental value of the resonance integral by adding the JENDL-3.3 data in the unresolved resonance region to the ENDF/B-VII file, which contains no such data. The unresolved resonance region was taken to extend from 820 eV (just above the last resolved resonance) to 100 keV, and the p- and d-wave strength functions were increased slightly within the systematics. This approach resulted in the capture resonance integral *decreasing* from 17.0 to 16.7 b, about one and a half standard deviations below the accepted value of 23 ± 4 b. Further changes in the unresolved resonance parameters would take the data beyond the range expected from systematics and would only increase the resonance integral slightly — this representation is the best that can be achieved with the available data. The ENDF/B-VII capture cross-

TABLE 6.29. SPECTRUM AVERAGED CAPTURE CROSS-SECTIONS FROM EVALUATIONS OF ^{102}Pd

Library	Resonance integral (b)	Maxwellian fission integral (mb)
ENDF/B-VI.8	8.969	130.0
ENDF/B-VII.0	16.98	130.0
JEFF-3.1	13.08	47.26
JENDL-3.3	19.41	109.8
This work	16.73	111.3

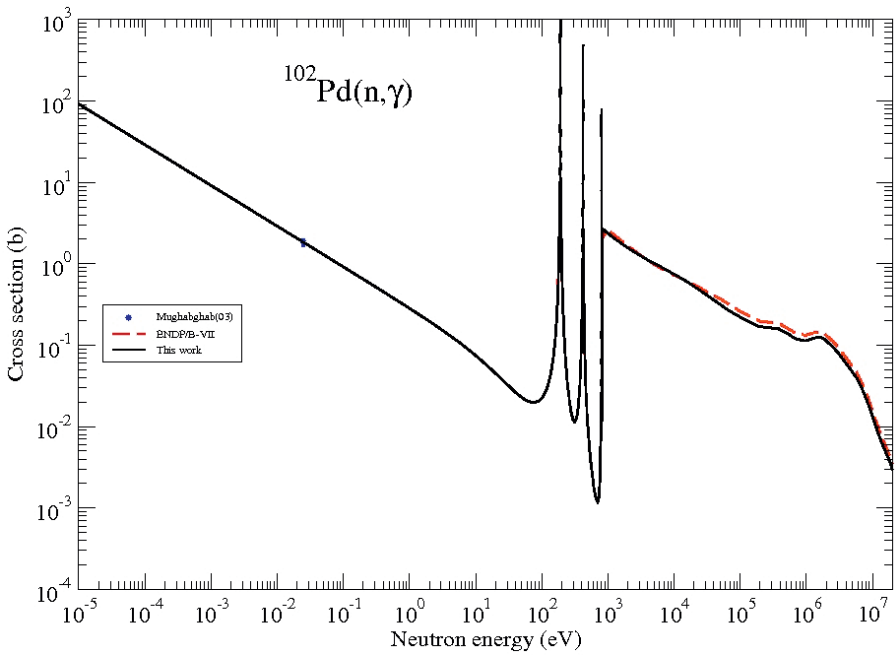

FIG. 6.21. ^{102}Pd(n, γ) capture cross-section for the production of ^{103}Pd.

section for the ^{102}Pd(n, γ)^{103}Pd reaction and the modified data described above are shown in Fig. 6.21.

6.4.4. Production of ^{125}I by means of the ^{124}Xe(n, γ)^{125}Xe reaction and subsequent β$^+$/EC decay

With $J^\pi = 1/2^{(+)}$ and a half-life of $T_{1/2}$ = 16.9(2) h, ^{125}Xe decays by β$^+$ emission/electron capture. A short lived $J^\pi = 9/2^{(-)}$ isomeric state also exists at

E_x = 252.60(14) keV with a half-life of $T_{1/2}$ = 56.9(9) s that undergoes IT decay exclusively to the ground state. Both ^{125}Xe and the ^{125}I decay product are of interest — the latter has been tested as a treatment for hyperthyroidism and lung cancer. Iodine-125 has a $J^{\pi} = 5/2^{+}$ ground state with a half-life of $T_{1/2}$ = 59.400(10) d, and also decays by β^{+} emission/electron capture. The Q-value of the ^{125}I β^{+}/EC decay mode is 185.77(6) keV, with an average light particle (electron) energy of 16.51(19) keV and average γ ray energy of 41.07(62) keV. The most recent version of the ^{125}I radioactive decay file can be found in the ENDF/B-VII library [6.3], based on the ENSDF evaluation of Katakura (Fig. 6.22) [6.56].

The experimental values of the thermal capture cross-section and capture resonance integral taken from the EXFOR library are given in Tables 6.30 and 6.31. Mughabghab adopts the more recent value of Bresesti et al. for the resonance capture integral, and increases the uncertainty slightly. He also

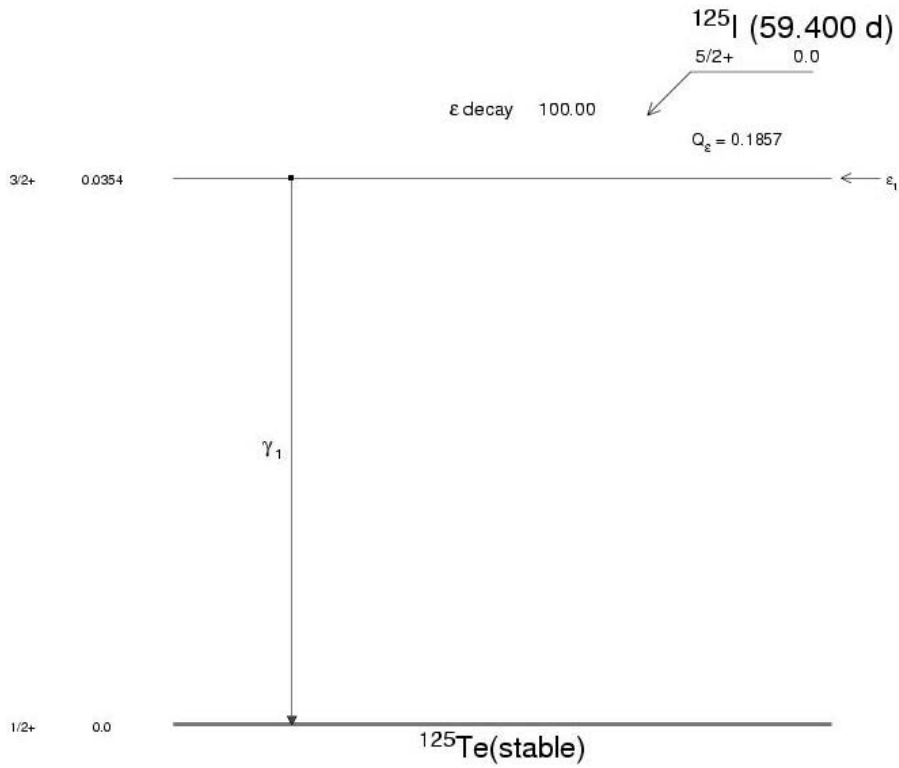

FIG. 6.22. Decay scheme of ^{125}I from the MIRD library.

recommends a thermal cross-section value larger than the experimental values we obtained from the EXFOR library.

JENDL-3.3, JEFF-3.1, ENDF/B-VI and ENDF/B-VII evaluations were compared with the (n, 2n) data found in the EXFOR library, as well as with the accepted values of the thermal capture cross-section and resonance integral. The JEFF-3.1 evaluation is essentially identical to that of ENDF/B-VI, and all four evaluations reproduce the thermal capture cross-section, while the JENDL-3.3 and ENDF/B-VII evaluations give improved fits to the experimental (n, 2n) data. Although ENDF/B-VII best reproduces the accepted value of the capture

TABLE 6.30. THERMAL NEUTRON CAPTURE CROSS-SECTION DATA OF ^{124}Xe *(extracted from EXFOR [6.57–6.61])*

Lead author	Publication date	σ(n, γ) (b)
Tobin	1958	74.4
Harper	1961	115
Eastwood	1963	94 (9.4)
Bresesti	1964	110 (11)
Kondaiah	1968	144 (11)
This work	—	114 (11)
Mughabghab	2006	165 (11)

TABLE 6.31. CAPTURE RESONANCE INTEGRAL DATA OF ^{124}Xe *(extracted from EXFOR [6.59, 6.60])*

Lead author	Publication date	RI (b)
Eastwood	1963	2100 (210)
Bresesti	1964	3600 (500)
this work	—	2300 (200)
Mughabghab	2006	3600 (700)

TABLE 6.32. SPECTRUM AVERAGED CAPTURE CROSS-SECTIONS FROM EVALUATIONS OF ^{124}Xe

Library	Resonance integral (b)	Maxwellian fission integral (mb)
ENDF/B-VI.8	3048	106.9
ENDF/B-VII.0	3189	444.3
JEFF-3.1	3050	92.59
JENDL-3.3	2964	570.6
This work	3191	444.3

resonance integral (Table 6.32), an anomalously low thermal elastic cross-section results. Comparison with the other evaluations revealed this behaviour to be the result of not including a negative energy resonance. The ENDF/B-VI value for the thermal elastic cross-section can be recovered by re-introducing the negative energy resonance at −100 eV with a neutron width of 2.05 eV and a radiative width of 0.11 eV (modifications of the capture cross-section that result are negligible). Both the ENDF/B-VII capture cross-section for the ^{124}Xe(n, γ)^{125}Xe reaction in the production of ^{125}Xe and the modified data described above are shown in Fig. 6.23.

6.4.5. Production of ^{126}I by means of the ^{125}I(n, γ)^{126}I reaction

Iodine-126 has a $J^{\pi} = 2^{-}$ ground state with a half-life of $T_{1/2}$ = 12.93(5) h that undergoes 52.7% decay by β^{+} emission/electron capture with a Q-value of 2155(4) keV, and by 47.3% β^{-} emission with a Q-value of 1258(5) keV. As the neutron capture production cross-section for ^{126}I is extremely large, this radionuclide could be an important contaminant of ^{125}I, when produced by means of reactor irradiation such as in the ^{124}Xe(n, γ)^{125}Xe→^{125}I reaction (see Section 6.4.4). The two existing experimental values for the thermal capture cross-section and the one known value of the capture resonance integral are listed in Tables 6.33 and 6.34. Spectrum averaged evaluated cross-sections are given in Table 6.35.

No ^{125}I reaction data other than the values tabulated above were found in the EXFOR library, and only one evaluation was found in the JEFF-3.1A library. Therefore, we attempted to prepare an alternative set of data:

— Above 100 keV, the EMPIRE-II code [6.16] was used with default input parameters obtained from the RIPL-2 library;

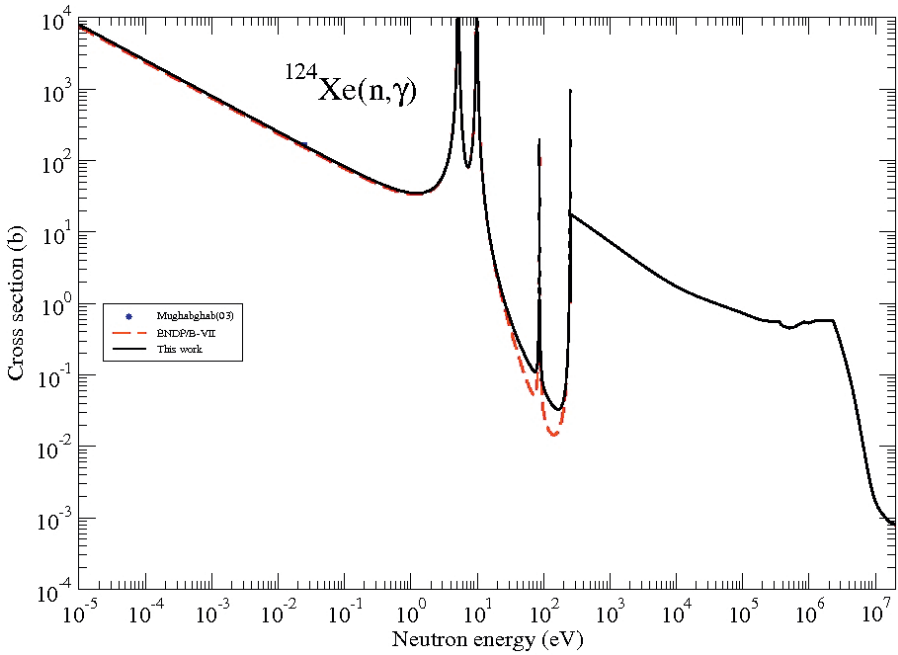

FIG. 6.23. ^{124}Xe(n, γ) capture cross-section for the production of ^{125}I.

TABLE 6.33. THERMAL NEUTRON CAPTURE CROSS-SECTION DATA OF ^{125}I *(extracted from EXFOR [6.58, 6.62])*

Lead author	Publication date	σ(n, γ) (b)
Harper	1961	890
Bresesti	1964	894 (90)
This work	—	892 (90)

TABLE 6.34. CAPTURE RESONANCE INTEGRAL DATA OF ^{125}I *(extracted from EXFOR [6.62])*

Lead author	Publication date	RI (b)
Bresesti	1964	13 730 (2000)

TABLE 6.35. CAPTURE RESONANCE INTEGRAL DATA FROM EVALUATIONS OF ^{125}I

Library	Resonance integral (b)
JEFF-3.1A	14 910
This work	9 300

— The unresolved resonance parameters of the ENDF/B-VII evaluation of ^{131}I were adopted in the energy range from 20 to 100 keV;
— A negative-energy resonance and a single, artificial positive-energy resolved resonance were used in the resonance region in order to obtain a thermal capture cross-section in agreement with the experimental observation, along with a resonance integral as large as possible (9300 b, which is still about 30% below the experimental value).

JEFF-3.1/A also reproduces the thermal capture cross-section but furnishes a capture resonance integral of 14 910 b, which is about 10% larger than the experimental value although within the defined uncertainty. The latter is generated in a somewhat artificial manner, as can be seen in the plot of the capture cross-section ^{125}I(n, γ)^{126}I of the two evaluations shown in Fig. 6.24. However, if the objective of the evaluation is to reproduce the experimental values of the spectrum averaged production cross-sections, the JEFF-3.1A evaluation is adequate and can be recommended.

6.4.6. Production of ^{149}Pm by means of the ^{148}Nd(n, γ)^{149}Nd reaction and subsequent β^- decay

Neodymium-149 has a $J^\pi = 5/2^-$ ground state with a half-life of $T_{1/2}$ = 1.728(1) h that decays exclusively by β^- emission with a Q-value of 1690(3) keV. The ^{149}Pm decay product of interest has been tested as a treatment for hyperthyroidism and lung cancer. Promethium-149 has a $J^\pi = 7/2^+$ ground state with a half-life of $T_{1/2}$ = 53.08(5) h, and also decays exclusively by β^- emission. The Q-value of the ^{149}Pm β^- decay mode is 1071(4) keV, with an average light-particle (electron) energy of 364.7(14) keV and average γ ray energy of 11.9(8) keV. The most complete recent version of the ^{149}Pm radioactive decay file can be found in the JEFF3.1 library, based on the ENSDF evaluation of Szucs, Johns and Singh [6.63] (Fig. 6.25).

Experimental values of the thermal capture cross-section and the capture resonance integral that are available in the EXFOR library are listed in

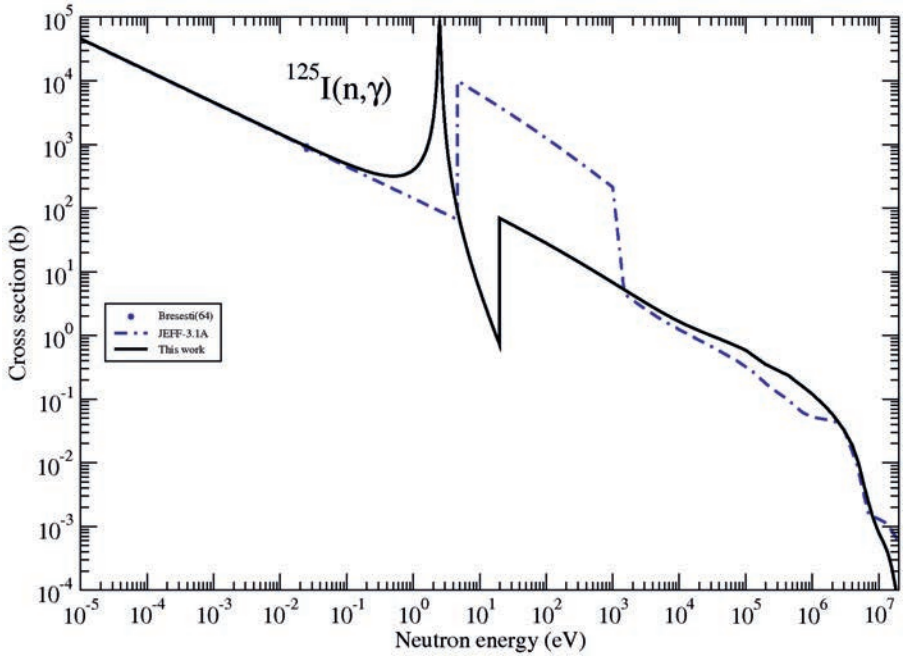

FIG. 6.24. $^{125}I(n, \gamma)$ capture cross-section for the production of ^{126}I.

Tables 6.36 and 6.37. Simple weighted means of the experimental thermal capture cross-sections and capture resonance integrals furnish values close to those adopted by Mughabghab but with approximately half of the adopted uncertainty.

JENDL-3.3, JEFF-3.1, ENDF/B-VI and ENDF/B-VII evaluations were compared with the experimental (n, tot), (n, el), (n, γ), (n, p), (n, α) and (n, 2n) data found in the EXFOR library. All evaluations agree well with the measured total and elastic cross-section data but only the JENDL-3.3 and ENDF/B-VII files are in good agreement with the (n, 2n) data, and the small (n, p) and (n, α) experimental cross-sections. The ENDF/B-VII evaluation provides a slightly better description of the experimental data above the resonance region, as can be seen in Fig. 6.26, and also uses the most recent resonance parameters set. Johnsrud et al. [6.80] capture data were renormalized by a factor of 2.58/3.7 to take into account the accepted value of the ^{148}Nd thermal neutron capture cross-section. Only the evaluated data in JENDL-3.3 yield a result in agreement with the accepted value of the capture resonance integral, while the ENDF/B-VII evaluation furnishes a result that is approximately 10% too high (Table 6.38). However, if the radiative width of the first physical resonance at 155 eV can be

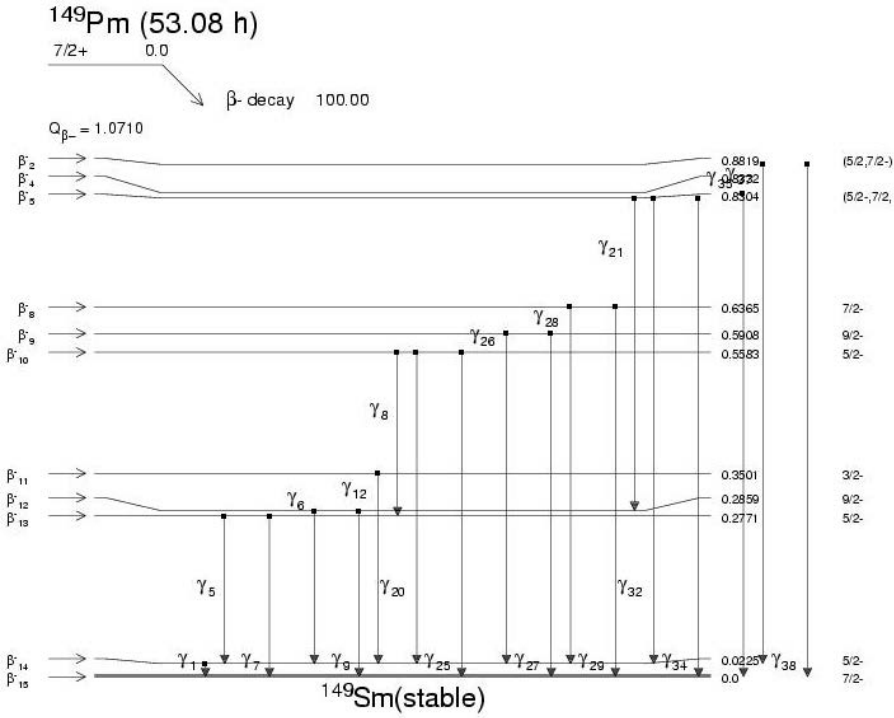

FIG. 6.25. Decay scheme of ^{149}Pm from the MIRD library.

TABLE 6.36. THERMAL NEUTRON CAPTURE CROSS-SECTION DATA OF ^{148}Nd *(extracted from EXFOR [6.64–6.69])*

Lead author	Publication date	σ(n, γ) (b)
Pomerance	1952	3.30 (0.99)
Walker	1953	3.70 (0.90)
Ruiz	1964	2.54 (0.18)
Alstad	1967	2.50 (0.20)
Gryntakis	1976	2.45 (0.14)
Heft	1978	2.58 (0.07)
This work	—	2.56 (0.06)
Mughabghab	2006	2.58 (0.14)

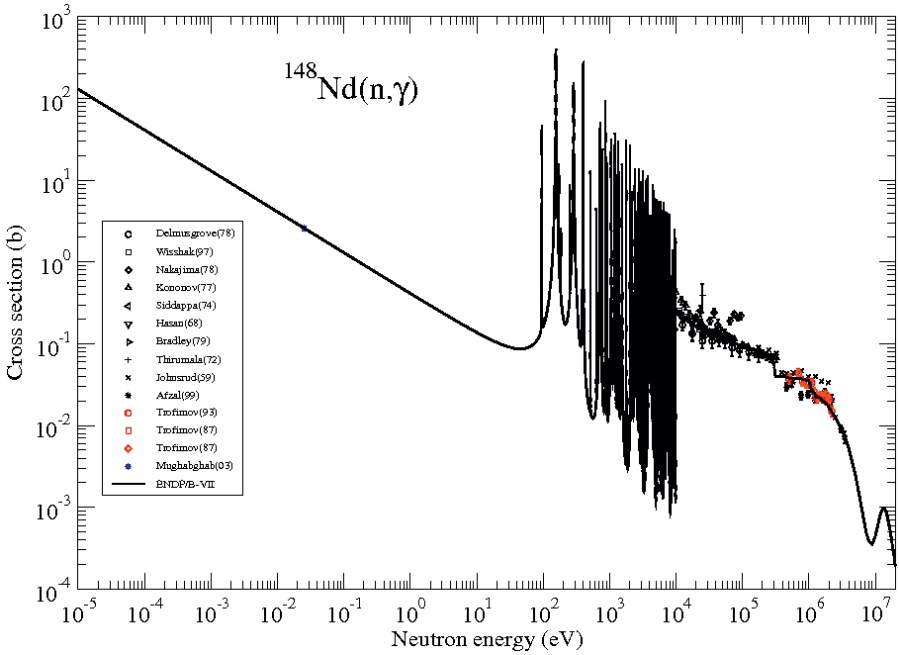

FIG. 6.26. ^{148}Nd(n, γ) capture cross-section for the production of ^{149}Nd; EXFOR data are plotted as symbols [6.73–6.84].

TABLE 6.37. CAPTURE RESONANCE INTEGRAL DATA OF ^{148}Nd *(extracted from EXFOR [6.66–6.72])*

Lead author	Publication date	RI (b)
Ruiz	1964	18.7 (0.5)
Alstad	1967	14.0 (2.0)
Ricabarra	1973	11.7 (1.0)
Van Der Linden	1974	14.0 (0.7)
Steinnes	1975	14.1 (1.3)
Gryntakis	1976	13.8 (1.0)
Heft	1978	16.5 (3.0)
This work	—	14.0 (0.5)
Mughabghab	2006	14.0 (1.0)

TABLE 6.38. SPECTRUM-AVERAGED CAPTURE CROSS-SECTIONS FROM EVALUATIONS OF ^{148}Nd

Library	Resonance integral (b)	Maxwellian fission integral (mb)
ENDF/B-VI.8	19.44	58.75
ENDF/B-VII.0	15.96	25.04
JEFF-3.1	19.84	35.81
JENDL-3.3	14.68	27.63
This work	14.65	25.04

reduced from 52 ± 8 to 44 MeV, as suggested by Mughabghab, a slight increase of the capture width of the negative energy resonance from 39 to 48.5 MeV recovers the agreement with the thermal capture cross-section. The calculated capture resonance integral of the modified ENDF/B-VII evaluation is 14.65 b, well within the uncertainty limits of the Mughabghab value.

6.4.7. Production of ^{153}Sm by means of the ^{152}Sm(n, γ)^{153}Sm reaction

Samarium-153 exhibits promise as an analgesic for use in painful bone metastases. This radionuclide has a $J^{\pi} = 3/2^{+}$ ground state with a half-life of $T_{1/2} = 46.284(4)$ h that decays exclusively by β^{-} emission. There is also a short lived $J^{\pi} = 11/2^{-}$ isomeric state at $E_x = 98.4(2)$ keV with a half-life of $T_{1/2} = 10.6(2)$ ms that undergoes 100% IT decay to the ground state. The Q-value for β^{-} decay is 807.6(7) keV, with an average light-particle (electron) energy of 266.3(63) keV and an average γ ray energy of 61.2(4) keV. The most recent version of the radioactive decay file can be found in the ENDF/B-VII library [6.3], based on the ENSDF evaluation of Helmer [6.85] (Fig. 6.27).

The experimental values of the thermal capture cross-section and capture resonance integral available in the EXFOR library are listed in Tables 6.39 and 6.40. Simple weighted means of these data furnish values close to those adopted by Mughabghab but with approximately half of the adopted uncertainty.

BROND-2 JENDL-3.3, JEFF-3.1, ENDF/B-VI and ENDF/B-VII evaluations were compared with the experimental (n, tot), (n, γ), (n, p), (n, α) and (n, 2n) data found in the EXFOR library. All five evaluations agree well with the total cross-section data but only the BROND-2, JENDL-3.3 and ENDF/B-VII evaluations are in good agreement with the (n, 2n) data. The experimental (n, p) and (n, α) cross-section data are small at approximately 5 and 2 mb,, respectively,

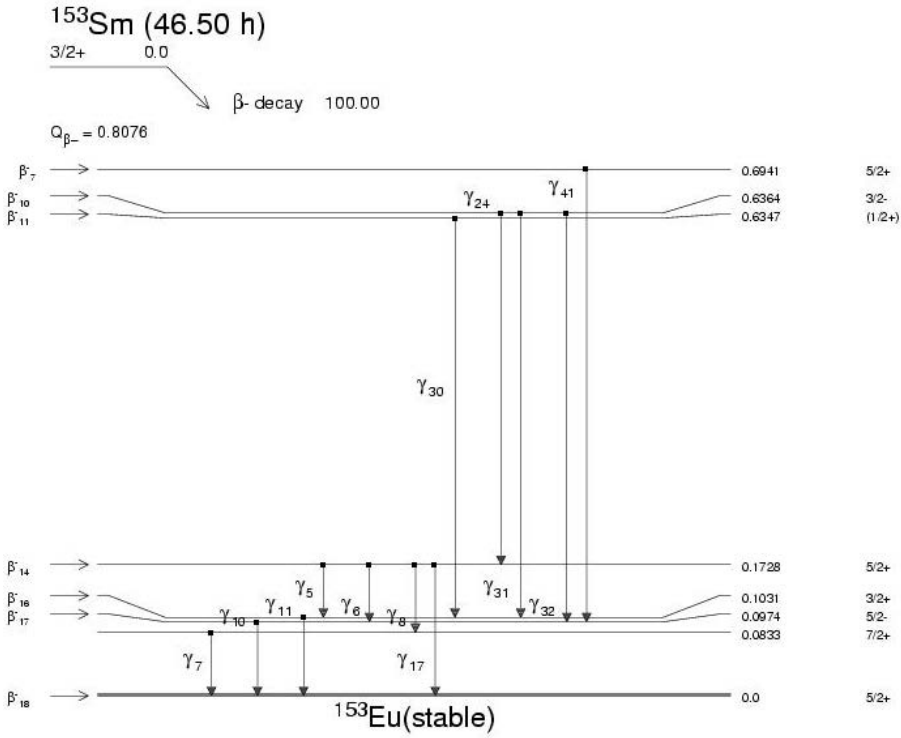

FIG. 6.27. Decay scheme of ^{153}Sm from the MIRD library.

TABLE 6.39. THERMAL NEUTRON CAPTURE CROSS-SECTION DATA OF ^{152}Sm *(extracted from EXFOR [6.23, 6.69, 6.86–6.90])*

Lead author	Publication date	σ(n, γ) (b)
Seren	1947	138 (28)
Walker	1956	250 (50)
Pattenden	1958	200 (60)
Fehr	1960	215 (10)
Tattersall	1960	224 (7)
Cabell	1962	209 (9)
Heft	1978	204 (9)
This work	—	213 (4)
Mughabghab	2006	206 (6)

TABLE 6.40. CAPTURE RESONANCE INTEGRAL DATA OF ^{152}Sm *(extracted from EXFOR [6.30, 6.69, 6.71, 6.88–6.92])*

Lead author	Publication date	RI (b)
Harris	1950	1560 (138)
Fehr	1960	2740 (150)
Tattersall	1960	2850 (300)
Cabell	1962	3160 (104)
Hayodom	1969	2920
Steinnes	1972	2530 (150)
Van Der Linden	1974	3140 (157)
Heft	1978	3050 (360)
This work	—	2940 (60)
Mughabghab	2006	2970 (100)

for 14 MeV, and are well described by the JENDL-3.3 and ENDF/B-VII evaluations but not considered in BROND-2. All three of these evaluations recommend data that provide a good description of the experimental capture cross-section. Peto et al. [6.103] data at 3 MeV were renormalized by a factor of 25.42/35.2 to take into account the accepted value for the ^{197}Au neutron capture cross-section at that energy. Only BROND-2 and ENDF/B-VII yield results in agreement with the accepted value of the capture resonance integral (Table 6.41). The ENDF/B-VII evaluation provides a much more extensive set of resolved resonances, while the BROND-2 evaluation gives a slightly better description of the data at high energies (Fig. 6.28). We recommend the ENDF/B-VII evaluation because this file contains a more extensive set of resolved resonances and is more complete at higher energies.

6.4.8. Production of ^{188}Re by means of the ^{187}Re(n, γ)^{188}Re reaction

Rhenium-188 has a $J^{\pi} = 1^{-}$ ground state with a half-life of $T_{1/2}$ = 17.0040(22) h and decays exclusively by β^{-} emission. There is also a short lived $J^{\pi} = (6)^{-}$ isomeric state at E_x = 0.172 MeV with a half-life of $T_{1/2}$ = 18.59(4) m that undergoes 100% IT decay to the ground state. The Q value for β^{-} decay is 2120.4(4) keV, with an average light particle (electron) energy of 777.6(54) keV and an average γ ray energy of 61.3(3) keV. The most recent version of the radioactive decay file can be found in the ENDF/B-VII library, based on the ENSDF evaluation of Singh [6.104] (Fig. 6.29).

TABLE 6.41. SPECTRUM AVERAGED CAPTURE CROSS-SECTIONS FROM EVALUATIONS OF ^{152}Sm

Library	Resonance integral (b)	Maxwellian fission integral (mb)
BROND-2	2963	88.80
ENDF/B-VI.8	2975	90.28
ENDF/B-VII.0	2975	69.77
JEFF-3.1	2976	91.14
JENDL-3.3	2761	99.58
This work	2975	69.77

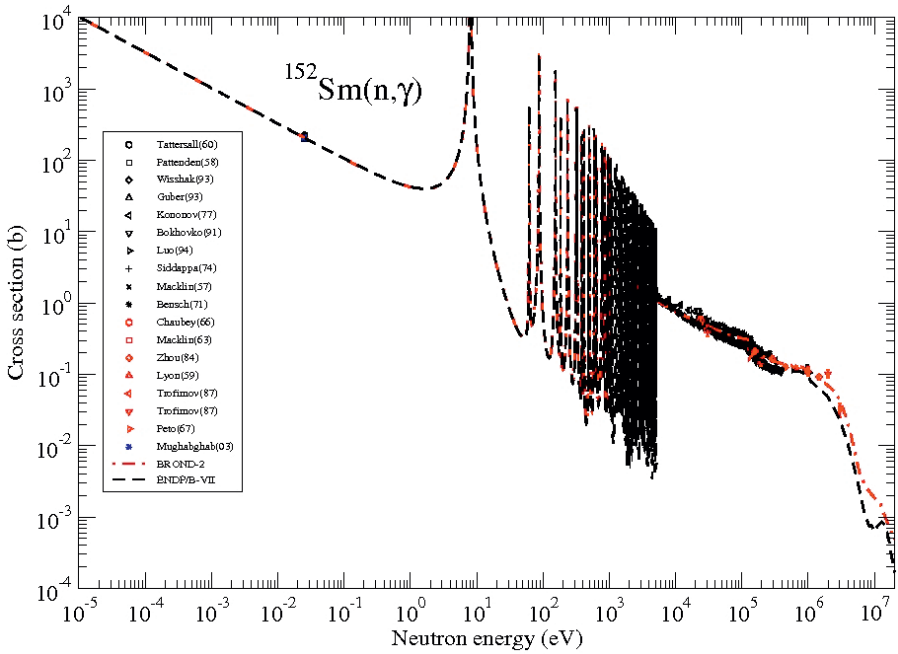

FIG. 6.28. ^{152}Sm(n, γ) capture cross-section for the production of ^{153}Sm; EXFOR data are plotted as symbols [6.87, 6.89, 6.93–6.103].

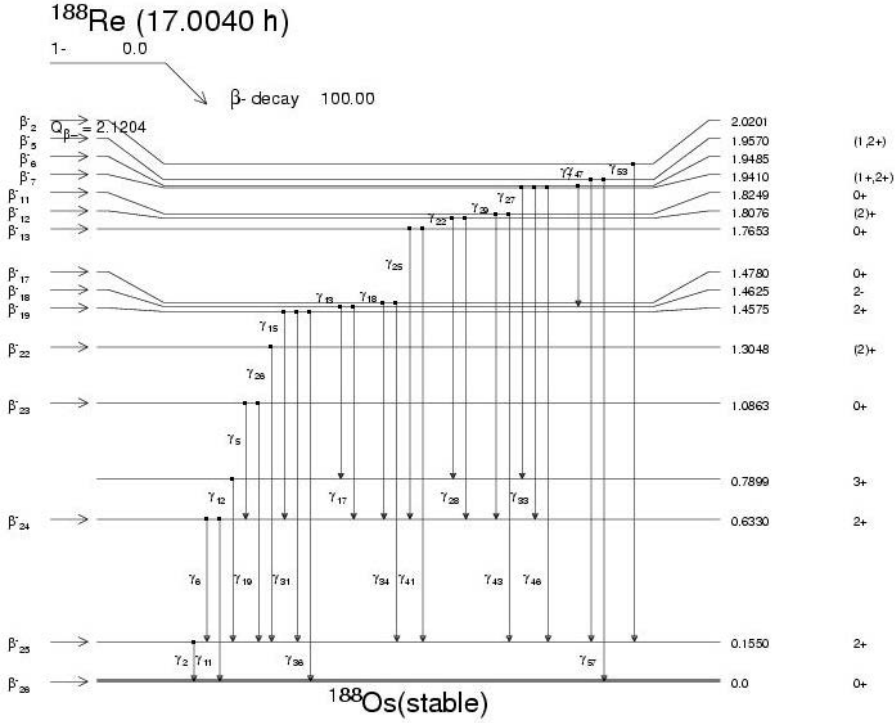

FIG. 6.29. Decay scheme of ^{188}Re from the MIRD library.

Experimental values of the thermal capture cross-section and capture resonance integral taken from the EXFOR library are listed in Tables 6.42 and 6.43. Simple weighted means of these data furnish values close to those adopted by Mughabghab although the uncertainty of the capture resonance integral is approximately a factor of two lower (±12 compared with ±20 b).

The three most recent evaluations are essentially identical (JEFF-3.1, ENDF/B-VI and ENDF/B-VII), and have been compared with the experimental (n, tot), (n, γ) and (n, 2n) data found in the EXFOR database. These three evaluations agree well with the total cross-section data and reasonably well with the (n, 2n) data, which is difficult to measure due to the extremely long lived isomeric state of ^{186}Re ($T_{1/2}$ = 2.0 × 10^5 a). The evaluations also agree reasonably well with the capture cross-section, as shown in Fig. 6.30. Data determined by Stupegia et al. [6.111] were renormalized by a factor of 76.4/110, to take into account the accepted value of the thermal cross-section used as the monitor in this particular measurement. These evaluations are also in excellent agreement with the accepted values for the thermal capture cross-section and the capture resonance integral, as noted in Tables 6.43 and 6.44. Experimental (n, p) and (n, α) cross-sections of

TABLE 6.42. THERMAL NEUTRON CAPTURE CROSS-SECTION DATA OF ^{187}Re *(extracted from EXFOR [6.23, 6.64, 6.69, 6.105–6.107])*

Lead author	Publication date	σ(n, γ) (b)
Seren	1947	75.3 (15.0)
Pomerance	1952	63.0 (5.0)
Lyon	1960	67.0 (6.7)
Karam	1963	88.0 (14.0)
Friesenhahn	1968	75.0 (4.0)
Heft	1978	75.0 (1.0)
This work	—	74.5 (0.9)
Mughabghab	2006	76.4 (1.0)

TABLE 6.43. CAPTURE RESONANCE INTEGRAL DATA OF ^{187}Re *(extracted from EXFOR [6.30, 6.69, 6.71, 6.108, 6.109])*

Lead author	Publication date	RI (b)
Harris	1950	275 (83)
Sher	1966	308 (20)
Pierce	1968	323 (20)
Van Der Linden	1974	311 (30)
Heft	1978	318 (50)
This work	—	314 (12)
Mughabghab	2006	300 (20)

approximately 4 and 1 mb, respectively, at about 14 MeV can also be found in the EXFOR database but they have not been included in the evaluations due to their low values. Given the good agreement of the evaluations with the existing experimental data, any one of them could be taken as a reference.

6.4.9. Production of ^{213}Bi by means of the decay chains ^{233}U → ^{229}Th → ^{225}Ra → ^{225}Ac and ^{225}Ac → ^{221}Fr → ^{217}At → ^{213}Bi

Bismuth-213 has a $J^{\pi} = 9/2^{-}$ ground state with a half-life of $T_{1/2}$ = 45.59(6) m, and undergoes 97.91(3)% β^{-} decay with a Q value of 1422(9) keV, and

TABLE 6.44. SPECTRUM AVERAGED CAPTURE CROSS-SECTIONS FROM EVALUATIONS OF ^{187}Re

Library	Resonance integral (b)	Maxwellian fission integral (mb)
ENDF/B-VI.8	292.8	117.1
ENDF/B-VII.0	292.8	117.1
JEFF-3.1	287.1	120.3
This work	292.8	117.1

TABLE 6.45. HALF-LIVES AND DECAY MODES OF THE ^{233}U → ^{213}Bi DECAY CHAIN

Radionuclide	Half-life ($T_{1/2}$)	Decay modes
U-233	$1.592(2) \times 10^5$ a	α 100%, SF < 6×10^{-9}%
Th-229	7340(160) a	α 100%
Ra-225	14.9(2) d	β^- 100%
Ac-225	10.0(1) d	α 100%
Fr-221	4.9(2) m	α 100%, β^- < 0.1%
At-217	32.3(4) ms	α 99.993(3)%, β^- 0.007(3)%
Bi-213	45.59(6) m	β^- 97.91(3)%, α 2.09(3)%

2.09(3)% α emission with a Q value of 5982(6) keV. The average light-particle (electron) energy is 442.9(24) keV, while the average γ ray energy is 127.4(13) keV and the average α energy is 124.5(29) keV. The most recent version of the radioactive decay file can be found in the ENDF/B-VII library, based on the ENSDF evaluation of Akovali [6.115] (Fig. 6.31).

Decay data for the other radionuclides in the decay chain are well described by the corresponding ENDF/B-VII data files, all based on evaluations by Akovali [6.116–6.119] (except for ^{233}U which is best described by the JEFF-3.1 data file) [6.120] (Table 6.45).

The primary production route for ^{213}Bi is through purification of ^{229}Th from reactor produced ^{233}U, but the demand for ^{213}Bi could soon exhaust the limited supply of ^{229}Th. Direct production of ^{229}Th through irradiation of ^{226}Ra in a high flux reactor seems to offer a promising alternative but requires more study [6.11, 6.122].

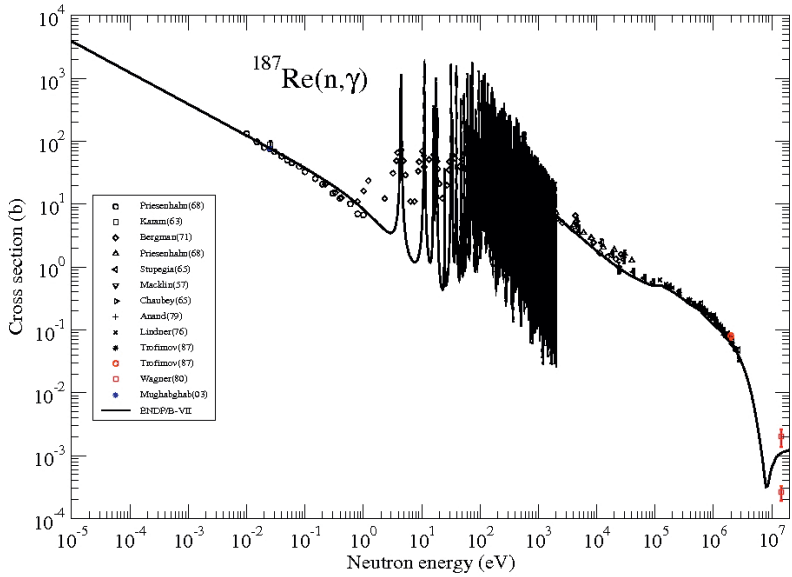

FIG. 6.30. ^{188}Re(n, γ) capture cross-section for the production of ^{188}Re; EXFOR data are plotted as symbols [6.83, 6.84, 6.97, 6.99, 6.106, 6.107, 6.110–6.114].

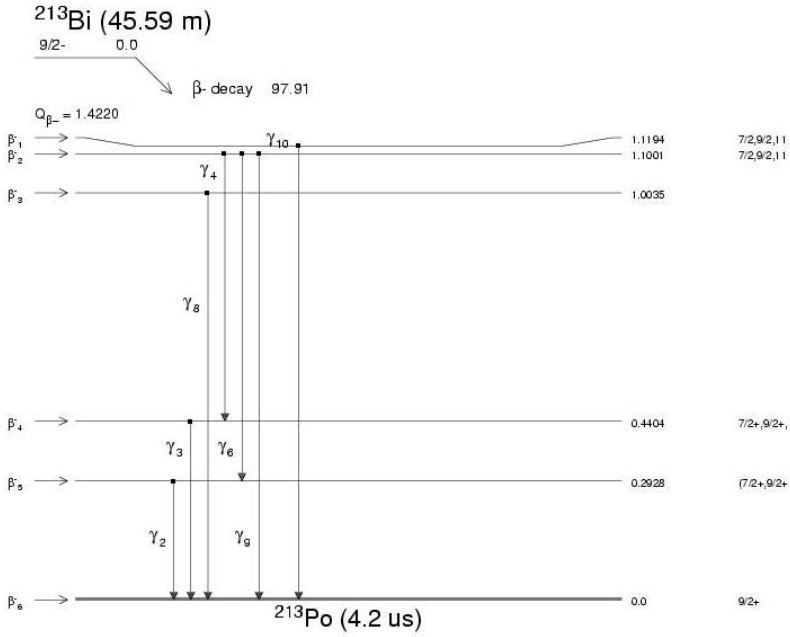

FIG. 6.31. Decay scheme of ^{213}Bi from the MIRD library.

6.5. CALCULATION AND EVALUATION OF (n, γ) CAPTURE CROSS-SECTIONS FOR THE PRODUCTION OF ^{32}P, ^{105}Rh, ^{131}I AND ^{192}Ir RADIONUCLIDES

Developments in the application of radionuclides within nuclear medicine have enhanced their adoption as external irradiation sources and internal treatments including brachytherapy, metabolic therapy and radioimmunotherapy. The present work is concerned with the evaluation of specific (n, γ) cross-sections that are required for the production of the therapeutic isotopes of ^{32}P, ^{105}Rh, ^{131}I and ^{192}Ir in a nuclear reactor spectrum. ^{32}P, ^{131}I and ^{192}Ir are well established radioisotopes in routine clinical use, while ^{105}Rh is a β^--decaying transition metal with the potential to emerge as a suitable isotope for medical application.

Nuclear structure and decay data have been adopted from the ENSDF library [6.21] along with relevant publications therein, and summaries are given in the various figures and tables. The experimental reaction data were obtained from EXFOR [6.15]. Significant quantities of experimental cross-section data exist over the thermal and resonance region for all of the reactions in this work, while few data exist in the high energy region above 1 MeV. Nuclear isomeric states formed in the $^{130}Te(n, \gamma)^{131}Te(\beta^-)^{131}I$ and $^{191}Ir(n, \gamma)^{192}Ir$ reactions are of great concern, and measured cross-sections are scarce except for a few at thermal neutron energy. Under these circumstances, isomeric (n, γ) cross-sections were theoretically predicted by means of the TALYS code [6.123]. The thermal neutron capture cross-section at 2200 m/s was obtained by weighted averaging of the experimental data on the basis of inverse variance. Calculated cross-sections in the thermal and resolved resonance regions were produced by NJOY [6.17] using the resonance parameters of Mughabghab et al. [6.124] and those in the selected library. The unresolved resonance cross-sections were taken from the existing ENDF/B-VI [6.5] or JENDL-3.3 [6.125] libraries. TALYS calculations were carried out for the high energy region above resonance by fitting and fine tuning the available experimental data to the optical model potentials (OMPs).

Evaluated data were produced in ENDF format for neutron energies up to 20 MeV. Integral data were produced and compared with the library whenever possible in order to validate the recommended data.

6.5.1. Evaluation methods

Experimental data were taken from EXFOR and plotted by means of the IAEA utility codes ENDVER [6.126] and ZVView [6.127]. Original references were traced for each EXFOR entry in order to check the data input if the publication was accessible. All of the EXFOR items are listed in the present documentation, while some of the data were not considered in the evaluation process because no

uncertainties had been assigned or the data were outliers. Overall, two errors were found in EXFOR, and were reported in the description section.

The (n, γ) reaction cross-sections were evaluated in three energy regions:

(a) Thermal energy region — there were many experimental data sets at the thermal neutron energy of 2200 m/s. An average cross-section was produced by weighting the inverse variance. Resolved cross-sections for the final isomeric states of the ^{130}Te(n, γ)^{131}Te and ^{191}Ir(n, γ)^{192}Ir reactions were also considered. While resolved measured data for the 2200 m/s cross-section were few and widely discrepant ($\sigma_{\gamma 0}{}^{g}$, $\sigma_{\gamma 0}{}^{m}$ for ^{131}Te and $\sigma_{\gamma 0}{}^{g}$, $\sigma_{\gamma 0}{}^{m1}$, $\sigma_{\gamma 0}{}^{m2}$ for ^{192}Ir), EXFOR data for the isomeric branching ratio (δ_2) were available to derive meaningful average data for the ^{130}Te(n, γ)^{131}Te reaction. Data for the isomeric branching ratio (δ_2) of ^{192m2}Ir had to be re-calculated from the latest half-life value. Resolved isomeric cross-sections for the 2200 m/s neutron were produced from the total radiative capture cross-section and branching ratios.

(b) Resonance region — any new attempt to improve the parameters was beyond the scope of our work and, hence, the established parameters of Mughabghab et al. [6.124] and FILE 2 of ENDF/B-VI [6.5] or JENDL-3.3 [6.125] were adopted for each reaction to produce the resolved resonance cross-section and equivalent data in the thermal energy region by means of the Breit–Wigner formula. The ambiguous gamma widths of any negative resonances were slightly tuned to produce the 2200 m/s cross-section determined in this work. Apart from ^{105}Ru, unresolved resonance regions were not evident in the experimental data sets, and could, therefore, be treated as high energy regions in the TALYS calculations.

(c) High energy region — TALYS predictions were performed on the basis of the default OMPs, level densities and nuclear structure information required to calculate scattering and reaction equilibrium of the Hauser–Feshbach type and pre-equilibrium theories. Results were compared with the experimental data sets. When the prediction needed to be improved, least squares fits to the experimental data were performed for total and/or (n, γ) cross-sections by means of the following equation:

$$\frac{\chi^2}{\nu} = \frac{1}{\nu}\sum_i \frac{[N\sigma_{cal}(E_i) - \sigma_{\exp}(E_i)]^2}{\delta_i^2} \tag{6.1}$$

where $\sigma_{exp}(E_i)$ and $\sigma_{cal}(E_i)$ are the experimental and calculated cross-sections at the *i*-th energy, respectively, δ_i is the associated uncertainty, N is the normalization factor and ν is the degree of freedom for the fit. Since an

automatic parameter search is not yet available in TALYS [6.123], a manual fit by a combination of grid search and estimate has been undertaken through a process of modifying the potential depths of the real, imaginary and spin-orbit components of the spherical OMPs and normalizing the cross-sections [6.128]. When the fit was unsatisfactory, slight changes to the radius and diffuseness parameters were attempted. When no experimental cross-sections were available, predictions were performed by adopting the data set in TALYS. As a consequence of the significant predictive power of TALYS, only modest amounts of work were required for most of the reactions in this study.

6.5.2. ^{32}P production

Phosphorus-32 has a half-life of 14.262(14) d, and decays 100% by β^- emission with no concomitant γ rays. The Q-value for β^- decay is 1710.66(21) keV, and the average β^- energy is 694.9(3) keV. Reaction cross-sections for the ^{31}P(n, γ)^{32}P reaction are listed in Table 6.46. The thermal (n, γ) cross-section ($\sigma_{\gamma 0}$) is 172(4) mb and is based on the eight data sets in EXFOR [6.15] and a recent measurement [6.129]. All of the retrieved EXFOR data and the recommended excitation function are shown in Fig. 6.32.

Thermal and resonance cross-sections were produced by using the parameters in JENDL-3.3. The gamma width for negative energy resonance at

TABLE 6.46. THERMAL NEUTRON CAPTURE CROSS-SECTION OF ^{31}P *(data taken from EXFOR)*

Author	Year of publication	Thermal (n, γ) cross-section (b)
Seren	1947	0.230 (46)
Pomerance	1951	0.150 (15)
Grimeland	1955	0.19 (2)
Jozefowitz	1963	0.172 (8)
Kappe	1966	0.1850 (74)
Ishikawa	1973	0.17 (1)
Salama	1986	0.143 (12)
Zeng	1989	0.177 (5)
Sun (unpublished) [6.129]	2003	0.166 (2)
Mughabghab evaluation	1981	0.172 (6)
This work	Average cross-section	0.172 (4)

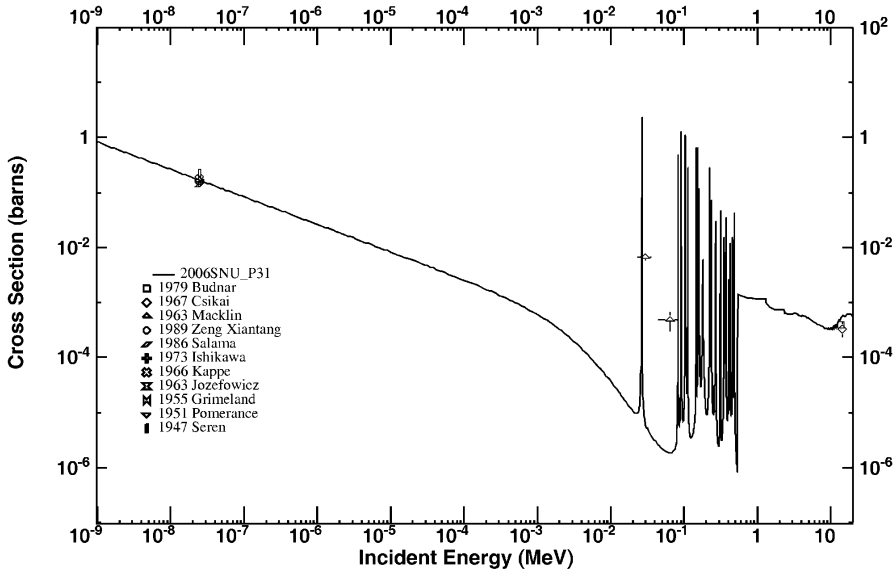

FIG. 6.32. $^{31}P(n, \gamma)^{32}P$ cross-sections, with EXFOR data plotted as symbols.

~5.9 keV was slightly modified to 2.07 eV in order to tune the thermal cross-section. Over the energy region of 545 keV to 20 MeV, the cross-sections were determined by TALYS calculation on the basis of the default parameters, including local OMPs taken from Koning [6.130] and RIPL [6.131]. Consistency between the calculations and measured data at 14 MeV is reasonable, and improvement on the existing libraries is evident. EXFOR data by Macklin and Mughabghab at 30 keV [6.132] are consistent with calculation although there were EXFOR compilation errors involving the energy and data uncertainty. The derived integral cross-section is of astrophysical interest, whereby the spectrum comprises a Maxwellian of T = 30 keV multiplied by v/<v>, in which v is the velocity of the neutron [6.132]. Stepping features that appear in the cross-section between 1.5 and 7 MeV arise from the thresholds of new channels that include inelastic scattering.

6.5.3. ^{105}Rh production

Rhodium-105 decays to ^{105}Pd by β^- decay with a half-life of 35.36(6) h. The Q-value for β^- decay is 566.2(29) keV, and the average β^- energy is 152.3(18) keV. Rhodium-105 was selected for evaluation because of the therapeutic medical applications of this isotope [6.133] and, therefore, the

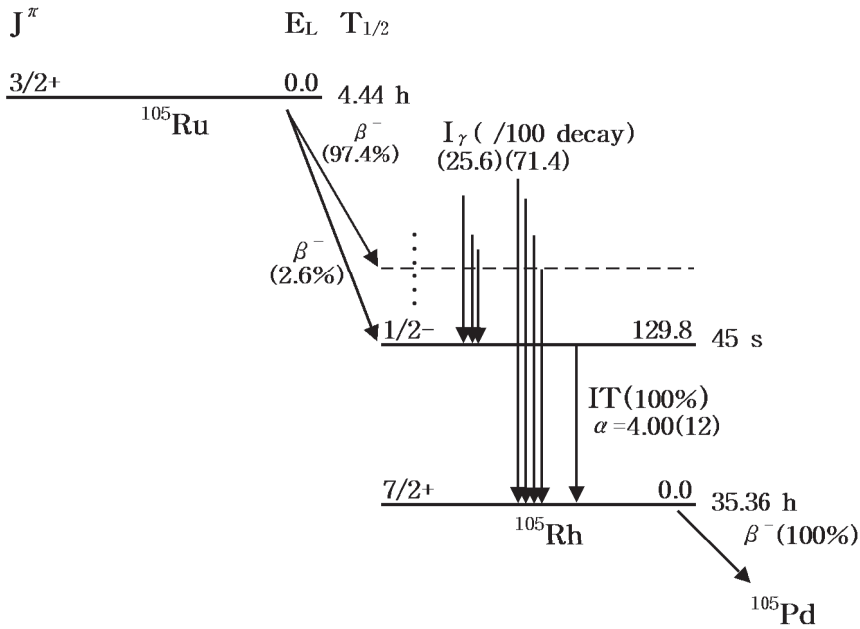

FIG. 6.33. Partial decay scheme of ^{105}Ru and ^{105}Rh from the ^{104}Ru(n, γ)^{105}Ru reaction.

^{104}Ru(n, γ)^{105}Ru reactor based reaction was considered in detail. The partial decay scheme for ^{105}Ru and ^{105}Rh is shown in Fig. 6.33.

Even though an extensive set of experimental data was retrieved from EXFOR in the resonance and high energy range above 10 keV, only two experimental data points exist for the 2200 m/s thermal cross-section [6.69, 6.134]. Since they are consistent, the most recent thermal cross-section value of 466(15) mb was adopted [6.69]. Both the thermal and resonance cross-sections were derived from the parameters of Mughabghab et al. [6.124], with a modification to the gamma width (0.14 eV) for the negative energy resonance (–941 eV). Data from the JENDL library were adopted in the unresolved resonance region of 11 to 300 keV [6.125]. Over the energy region from 0.3 to 20 MeV, a TALYS calculation was normalized to the experimental data set by adopting a normalization factor of 1.9 (reduced χ^2 of 9.6) and combining smoothly within the unresolved resonance region. The calculated cross-section at 14 MeV is 3 mb which is larger than the most recent experimental value of 0.86 (15) mb by Wagner and Warhanek [6.114] although close to the average of all available data including the two previous measurements [6.47, 6.135]. Figure 6.34 shows the data fitted to the experimental data set.

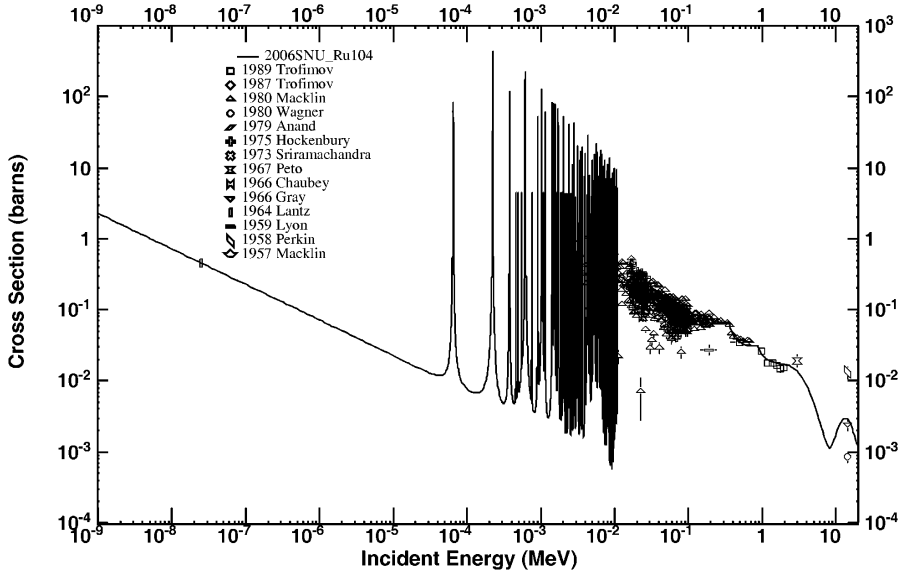

FIG. 6.34. ^{104}Ru(n, γ)^{105}Ru cross-sections for the production of ^{105}Rh, with EXFOR data plotted as symbols.

6.5.4. ^{131}I production

Iodine-131 can be produced by fission product extraction from ^{235}U burnt in a nuclear reactor (see Section 6.2) or from the ^{130}Te(n, γ)^{131}Te reaction. Iodine-131 undergoes 100% β^- decay with a half-life of 8.0207(1) d. Isomeric and ground states of ^{131}Te are produced from the ^{130}Te(n, γ)^{131}Te reaction: ^{131m}Te (182.25 keV, 11/2$^-$, $T_{½}$ = 30 h) has a longer half-life than ^{131g}Te (3/2$^+$, $T_{½}$ = 25 min). Figure 6.35 shows the decay scheme of ^{131}Te, while Table 6.47 lists a brief summary of the decay data.

The cross-sections retrieved from the existing libraries are plotted in Fig. 6.36. ENDF/B-VI, JENDL-3.3 and JEFF-3.1 libraries give the total capture cross-sections without resolving the final states of ground and isomeric ^{131}Te [6.136]. The JEFF library adopts data to be found in ENDF/B-VI, while JENDL contains re-calculated cross-sections in the resonance and high energy regions.

Experimental data for the 2200 m/s capture cross-sections were taken from EXFOR. Measured data for the total ($\sigma_{\gamma 0}$) or individual final state ($\sigma_{\gamma 0}{}^{g}$ and $\sigma_{\gamma 0}{}^{m}$) exist with derived quantities based on the isomeric ratios (δ_1, δ_2) as defined by:

$$\delta_1(E) = \frac{\sigma_\gamma^g(E)}{\sigma_\gamma^m(E)} \quad \text{and} \quad \delta_2(E) = \frac{\sigma_\gamma^m(E)}{\sigma_\gamma^g(E) + \sigma_\gamma^m(E)} \tag{6.2}$$

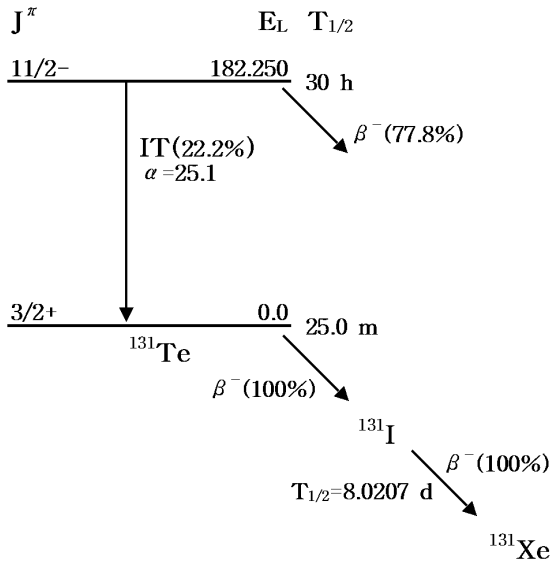

FIG. 6.35. Decay scheme of ^{131}Te from the ^{130}Te(n, γ)^{131}Te reaction for the production of ^{131}I.

TABLE 6.47. DECAY DATA FOR GROUND AND ISOMERIC STATES OF ^{131}Te AND FOR ^{131}I *(data taken from ENSDF)*

Radionuclide	Half-life	Decay mode	Radiation	Energy (keV) Branching ratio (%)
Te-131m	30 (2) h	β^- (77.8%)		
		IT (22.2%)	γ ray	182.25 (0.85%)
			ce	ce-K, 150.4 (14.4%)
				ce-L, 177.3 (5.44%)…
Te-131g	25.0 (1) m	β^- (100%)	<β^->	381.1 (9.96%)
				614.9 (21.7%)
				817.3 (59.3%)…
			γ rays	149.7 (68.8%)
				452.3 (18.2%)…
I-131	8.02070 (11) d	β^- (100%)	<β^->	96.6 (7.3%)
				192 (90%)…
			γ rays	364.5 (82%)
				637 (7.2%)…

Note: IT: isomeric transition; ce: conversion electron; <β^->: average β^- energy.

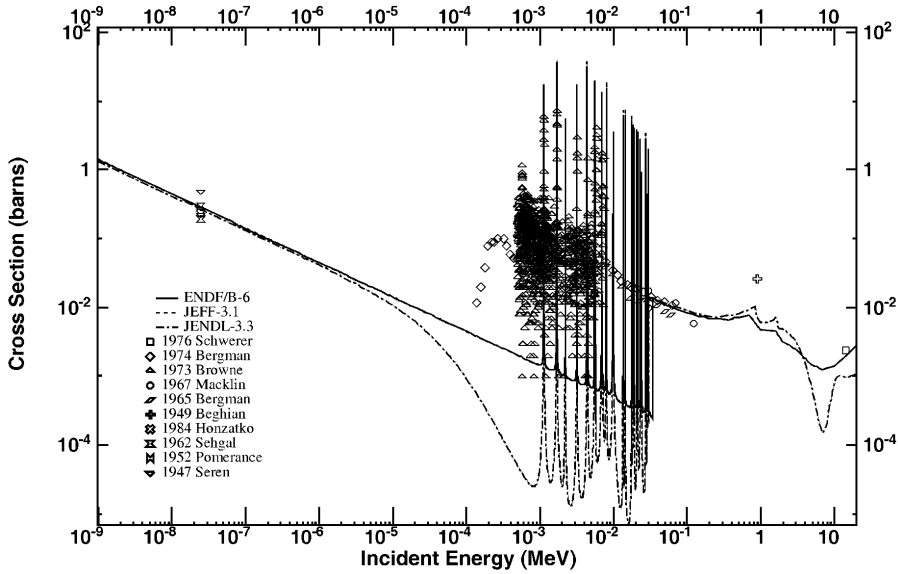

FIG. 6.36. $^{130}Te(n,\gamma)^{131}Te$ reaction cross-section retrieved from existing libraries — EXFOR data are plotted as symbols.

where $\sigma_\gamma^g(E)$ and $\sigma_\gamma^m(E)$ are the capture cross-sections for the final ground and isomeric states, respectively, at neutron energy E. Seven EXFOR data points also exist for the isomeric branching ratio (δ_2) at a neutron energy of 2200 m/s. Weighted averages of the total ($\sigma_{\gamma 0}$) cross-section and isomeric branching ratio (δ_2) at 25.3 meV (thermal point) were calculated after excluding all data with no assigned uncertainty: $\sigma_{\gamma 0}$ of 204(10) mb and δ_2 (25.3 meV) of 0.058(3). Seren et al. [6.23] and Sehgal [6.137] were not considered in this averaging process for the isomeric branching ratio (δ_2) because their data possessed no uncertainties. Thermal $\sigma_{\gamma 0}^g$, $\sigma_{\gamma 0}^m$ and δ_1 were derived, as listed in Tables 6.48 and 6.49.

Resonance cross-sections were produced by adopting the parameters in JENDL-3.3 [6.125]. A modification to the gamma width (0.06 eV) of the negative energy resonance of −89.5 eV reproduced the thermal cross-section. Over the energy region of 31 keV to 20 MeV, TALYS calculations were undertaken to obtain $\sigma_\gamma^{g+m}(E)$, $\sigma_\gamma^g(E)$ and $\sigma_\gamma^m(E)$, and fine tuning of the spherical OMP was carried out to fit $\sigma_{tot}(E)$ manually to derive values that were within 2% of the global OMPs (Fig. 6.37). Predictions involving the inelastic channel and comparisons with experimental data have been performed by noting that the low lying excited states (2^+ and 3^-) of ^{130}Te are deformed and can be described by the one-phonon vibrational model [6.138–6.140]. Hence, a coupled channel calculation based on the harmonic vibrational model was performed by means of

TABLE 6.48. THERMAL NEUTRON CAPTURE CROSS-SECTIONS OF ^{130}Te *(data taken from EXFOR)*

Author	Year of publication	Thermal neutron capture cross-section (mb)		
		$\sigma_{\gamma 0}$	$\sigma_{\gamma 0}{}^{g}$	$\sigma_{\gamma 0}{}^{m}$
Seren [6.23]	1947	230 (44)	222 (44)	<8 (3)
Pomerance	1952	500 (250)	—	—
Sehgal [6.137]	1962	310 (61)	270 (60)	40 (10)
Mangal	1962	—	161 (24)	—
Honzatko	1984	193 (20)	—	—
Tomandl-1	2003	186 (13)	—	—
Tomandl-2	2003	240 (20)	—	—
Mughabghab evaluation	1981	290 (61)	270 (60)	20 (10)
This study	Average cross-section	204 (10)	192 (10)	12 (1)

TABLE 6.49. ISOMERIC RATIOS FOR THERMAL NEUTRON CAPTURE CROSS-SECTION OF ^{130}Te *(data taken from EXFOR)*

Author	Year of publication	Isomeric ratios for thermal neutron capture	
		δ_1	δ_2
Seren [6.23]	1947	27.8	0.03
Sehgal [6.137]	1962	6.8	0.13
Mangal	1962	20.4	—
Namboodiri	1966	—	0.059 (3)
Bondarenko	2000	—	0.053 (5)
Reifarth	2002	—	0.067 (5)
Tomandl-I	2003	—	0.054 (2)
Tomandl-II	2003	—	0.059 (4)
Mughabghab evaluation	1981	13.5	0.07 (4)
This study	Average	16	0.058 (3)

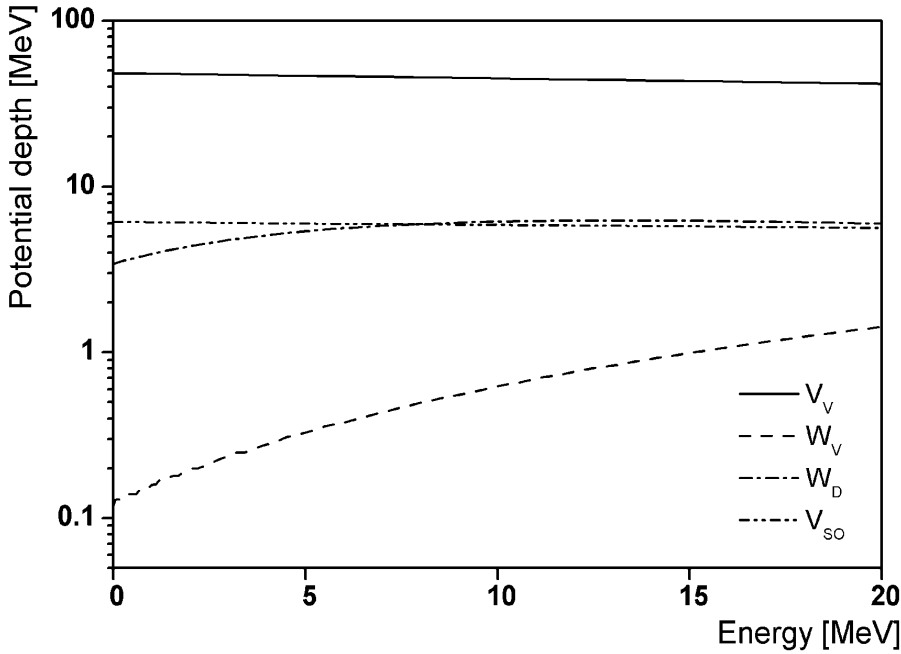

FIG. 6.37. Energy variation of the depth of the optical model potential — other parameters were fixed during the fit (a = 0.665 fm, r = 1.22 fm, etc.).

the TALYS code. Deformation parameters of the 2^+ state at 839.5 keV and the 3^- state at 2.73 MeV were taken from RIPL-2 [6.141], and the tuned OMPs from this work were used for the spherical component of the potential. The γ ray strength function of Kopecky and Uhl was used for the E1 transition, while the Brink–Axel function was adopted for the other transitions to evaluate the capture cross-section [6.123]. This analysis demonstrated that the $\sigma_\gamma^{g+m}(E)$ and $\sigma_\gamma^{g}(E)$ cross-sections in the radiative capture channels were rather insensitive to the choice of OMPs and the coupling strengths of the inelastic channel.

Slight improvements in the calculation of $\sigma_\gamma^{g+m}(E)$ and $\sigma_\gamma^{g}(E)$ were achieved by tuning the normalization factor and level density parameter *a*. The EXFOR data set originating from Dovbenko et al. [6.142] for $\sigma_\gamma^{g}(E)$ had erroneously been defined as millibarns, and was used in the data analysis after being corrected to barns. The resulting fit improved the TALYS prediction for all reaction channels of ^{130}Te + n including inelastic and (n, γ). Figure 6.38 shows the results of the model calculation for the capture channel, along with the EXFOR data. Although the discrepancy between the calculation and experimental $\sigma_\gamma^{g}(E)$ around 2 MeV could not be eliminated, the overall consistency has been improved and an isomeric excitation function was derived. Total capture cross-

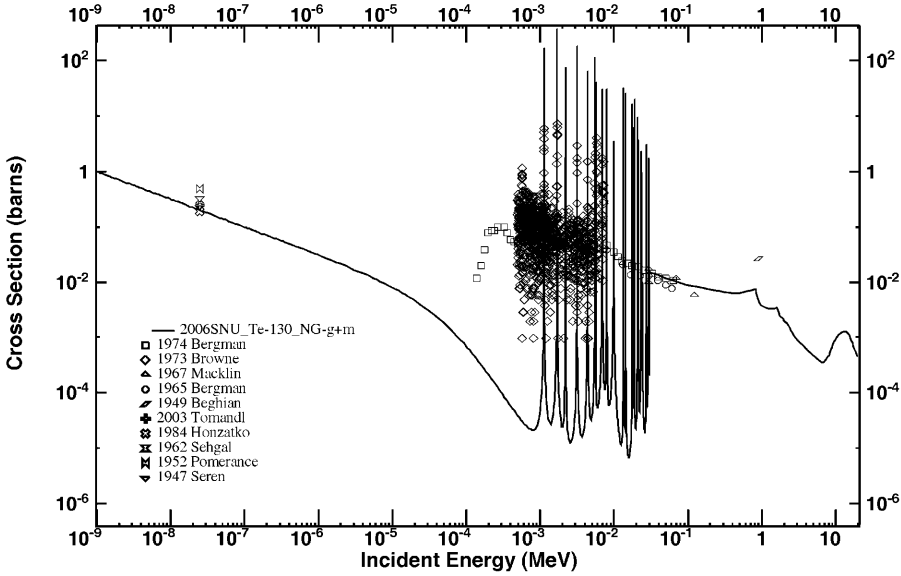

FIG. 6.38(a). Total capture cross-section $\sigma_{\gamma}^{g+m}(E)$ of the $^{130}Te(n, \gamma)^{131}Te$ reaction — EXFOR data plotted as symbols.

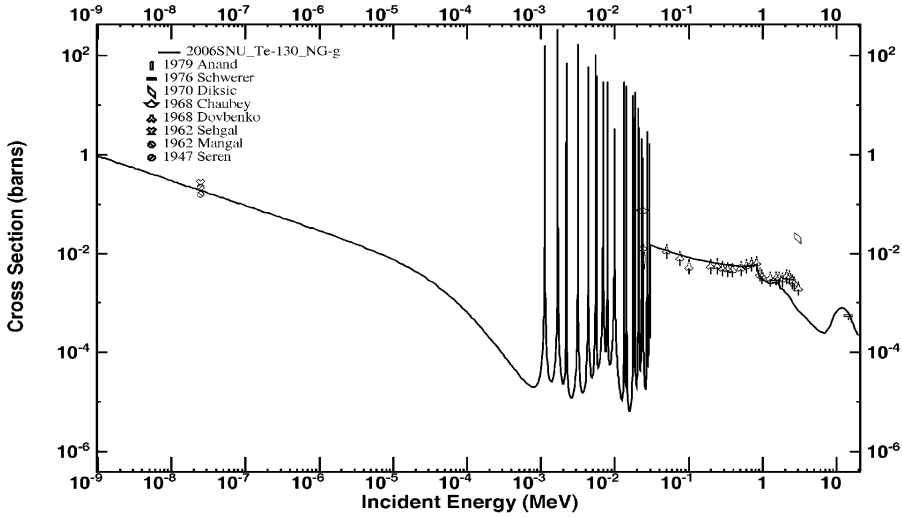

FIG. 6.38(b). Capture cross-section for the ground state $\sigma_{\gamma}^{g}(E)$ of the $^{130}Te(n, \gamma)^{131}Te$ reaction — EXFOR data plotted as symbols.

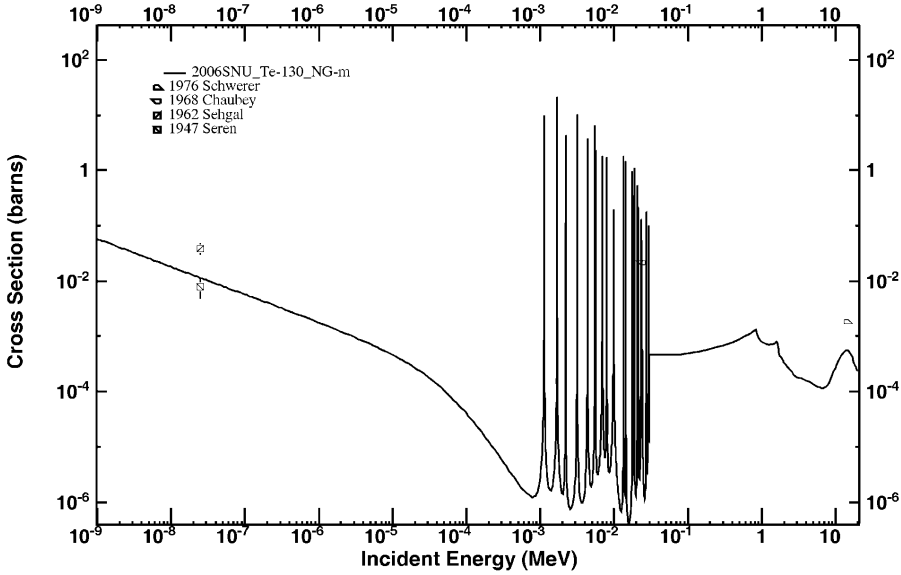

FIG. 6.38(c). Capture cross-section for the isomeric state $\sigma_{\gamma}^{m}(E)$ of the $^{130}Te(n, \gamma)^{131}Te$ reaction — EXFOR data plotted as symbols.

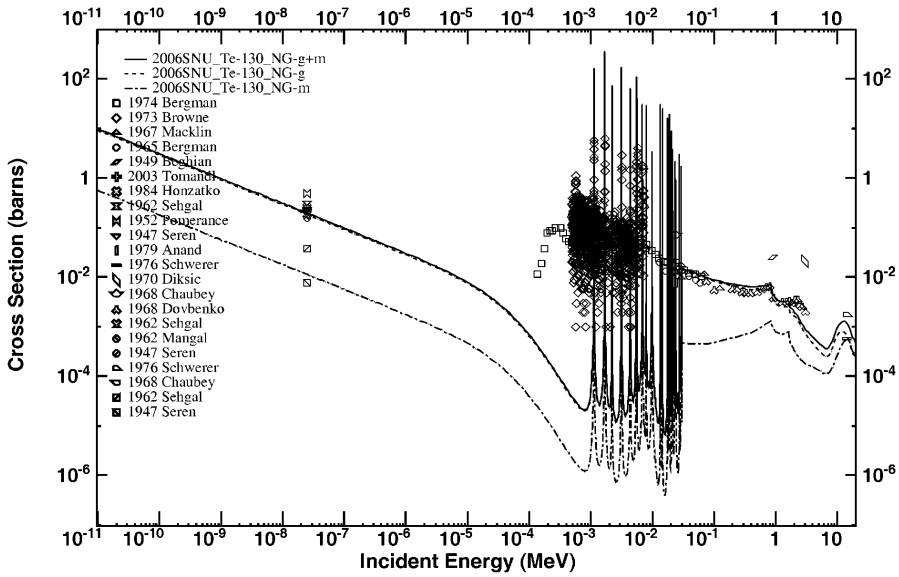

FIG. 6.38(d). $^{130}Te(n, \gamma)^{131}Te$ reaction cross-sections plotted on a single scale, together with EXFOR data as symbols.

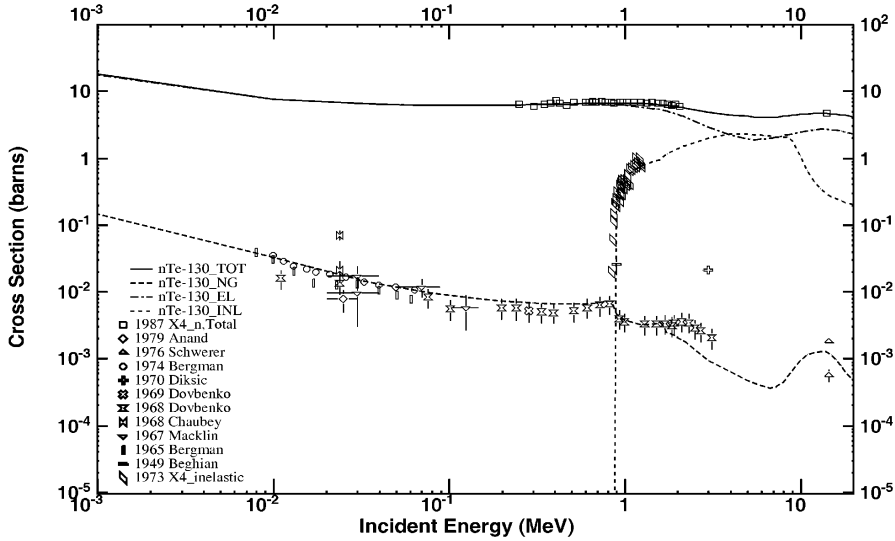

FIG. 6.39. Cross-sections $\sigma_{tot}(E)$, $\sigma_{el}(E)$, $\sigma_{inel}(E)$ and $\sigma_{\gamma}^{g+m}(E)$ for the ^{130}Te + n reaction from 1 keV to 20 MeV shown as continuous, dot-dashed, dotted and dashed lines, respectively — EXFOR data are shown as symbols.

sections $\sigma_{\gamma}^{g+m}(E)$ over the energy range 10 keV to 1 MeV are consistent with the data of Bergman and Romanov [6.143], Macklin and Gibbons [6.37], and Dovbenko et al. [6.142], even though the calculation underpredicts the sparse measurements in the region above 1 MeV. The oldest measurement by Beghian and Halban [6.144] has a large uncertainty (~50%) and deviates significantly from the observed trend. Ground state cross-sections in the high energy region are consistent with the studies of Dovbenko et al. [6.142]. TALYS calculations are also in good agreement with both sets of experimental data at 14 MeV. Experimental isomeric cross-section data over the entire energy range are sparse, with no assignment of uncertainties. The 14.6 MeV data by Schwerer et al. [6.48] are defined as ≤1.85 mb and, therefore, direct comparison is not feasible. Figure 6.39 shows calculations of the total cross-section and EXFOR data for the elastic, inelastic and (n, γ) channels, while the resulting isomeric branching ratios are defined as a function of neutron energy in Fig. 6.40. The thermal isomeric branching ratio (δ_2) remains fairly constant up to 30.5 keV, which supports the use of this value for data normalization at these energies.

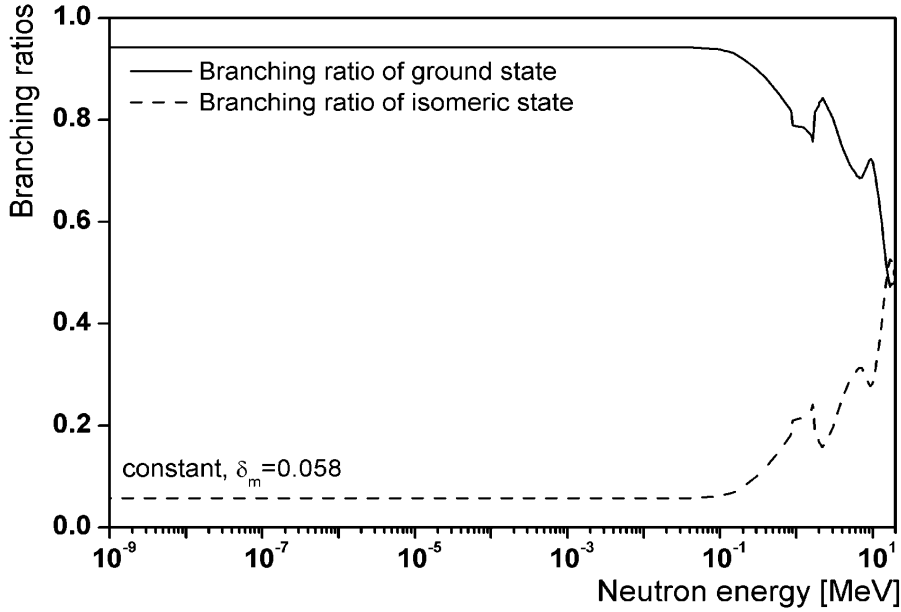

FIG. 6.40. Branching ratios for the $^{130}Te(n, \gamma)^{131}Te$ reaction.

6.5.5. ^{192}Ir production

Iridium-192 is commonly used for non-destructive testing in a wide range of industrial applications. More recent medical studies have resulted in the successful adoption of this radionuclide in the field of brachytherapy. Reactor production by means of the $^{191}Ir(n, \gamma)^{192}Ir$ reaction results in the formation of the ground and two isomeric states of ^{192}Ir although few measurements exist to quantify the cross-sections of the isomeric states.

Simplified structure and decay data for ^{192}Ir are summarized in Fig. 6.41 and Table 6.50 [6.21, 6.145]. The deformed ground state (4^+) of the odd–odd ^{192}Ir nucleus has a half-life of 73.827(13) d and decays mainly to ^{192}Pt by β^- decay (95.13%) and ^{192}Os by electron capture decay (4.87%), while the first isomeric state (56.720 keV, 1^-) has a half-life of 1.45(5) min and decays mainly to the ground state by a single isomeric transition (99.9825%). The spin-parity, level energy and decay characteristics of the ground and the first isomeric states are well defined [6.145, 6.146].

Experimental studies of the second isomeric state are scarce following the first observation of this radionuclide in 1959 [6.147]. This isomeric state (168.14 keV, 11^-) has a reasonably long half-life of 241(9) a and is reported to undergo 100% decay to a low lying state (12.984 keV, 6^+) through a highly

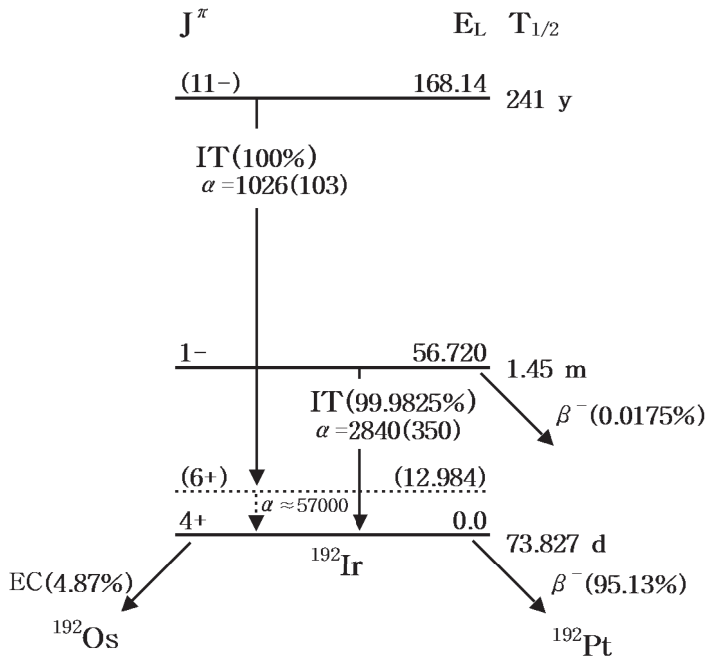

FIG. 6.41. Decay scheme of ^{192}Ir produced from the ^{191}Ir(n, γ)^{192}Ir reaction.

converted isomeric transition [6.145]. Although the spin-parity and decay scheme remain uncertain, the most recent evaluation recommends 11^-, 168.14 keV [6.145] nuclear level, based on an assumed decay to a predicted state at 12.984 keV (6^+) by the Nilsson model [6.148] and multipolarity of E5 [6.149] as shown in Fig. 6.41. However, the most extensive measurement suggests that the second isomeric state has an energy and spin-parity of 155.16 keV and 9^+, with M5 IT decay to the ground state defined from IBFFM predictions [6.150]. No experimental observations exist to clarify the feeding transitions to the second isomeric state, even though an unmatched neighbouring state exists at 173 keV. Further experimental studies are merited to determine the spin-parity, energy and decay of the second isomeric state, including the activation cross-section and quantification of the low lying 6^+ state.

There are five EXFOR entries that address the total capture cross-section at 25.3 meV, while five data sets also exist in the high energy region from keV to several MeV. Resolved measurements for the individual isomeric states are scarce, and the existing data libraries do not provide resolved isomeric and ground cross-sections in a consistent manner. For example, ENDF/B-VI and JEFF-3.1 contain total capture cross-sections, while the RNAL database gives

TABLE 6.50. DECAY DATA FOR GROUND AND ISOMERIC STATES OF ^{192}Ir *(data are from ENSDF)*

Radionuclide	Half-life	Decay mode	Main radiation	Energy (keV) Branching ratio (%)
Ir-192m2	241 (9) a	IT (100%)	γ ray	155.16 (0.0974%)
			ce	ce-L, 142 (74.6%)
				ce-M+, 153 (24.6%)
				ce-K, 79.1 (0.65%)
Ir-192m1	1.45 (5) min	β^- (0.0175%)		
		IT (99.9825%)	ce	ce-L, 43.3 (72.4%)
				ce-M, 53.5 (21%)
				ce-N+, 56.0 (6.5%)
			γ ray	56.71 (0.003%)
Ir-192g	73.827 (13) d	β^- (95.13%)	<β^->	
		EC (4.87%)		71.6 (5.6%)
				162.1 (41.4%)
				209.9 (48%)…
			γ rays	296.0 (28.7%)
				308.5 (29.7%)
				316.5 (82.7%)
				468.1 (47.8%)…

Note: IT: isomeric transition; ce: conversion electron; EC: electron capture; <β^->: average β^- energy.

only the cross-section for the second isomeric state [6.151]. NGATLAS [6.152] and EAF [6.153] quantify all of the resolved cross-sections separately although their descriptions of the thermal and high energy cross-sections are inadequate.

Table 6.51 lists all of the thermal cross-section data retrieved from EXFOR and some of the evaluated values extracted from specific libraries. Averaged experimental data for the total (n, γ) cross-section ($\sigma_{\gamma 0}$) at 25.3 meV give a value of 962(11) mb. The most recent data by Masyanov et al. [6.154] were excluded in the averaging process since this derived cross-section is a resonance measurement and represents the contribution of positive energy resonances to thermal neutron capture. Only two data sets exist that resolve the first isomeric and ground states at a neutron energy of 2200 m/s although they are totally inconsistent (Keish [6.155], Arino et al. [6.156]).

TABLE 6.51. THERMAL NEUTRON CAPTURE CROSS-SECTIONS OF ^{191}Ir
(experimental data taken from EXFOR)

Author		Year of publication	Thermal neutron capture cross-section (b)			
			$\sigma_{\gamma 0}$	$\sigma_{\gamma 0}^{g}$	$\sigma_{\gamma 0}^{m1}$	$\sigma_{\gamma 0}^{m2}$
Seren		1947	1000 (200)	—	260 (104)	
Harbottle		1963	—	—	—	0.38 ($^{+24}_{-11}$)
Keisch		1963	910 (67)	300 (30)	610 (60)	—
Arino		1964	—	1200 (300)	300 (50)	—
Sims		1968	1120 (25)	—	—	—
Heft		1978	922 (13)	—	—	—
Masyanov		1992	279 (3)	—	—	—
Evaluations	Mughabghab	1984	954 (10)	309 (30)	645 (32)	0.16 (7)
	NGATLAS	1997	954	309	645	0.16
	EAF	2001	965	273	692	0.16
	This work		962 (11)	317 (58)	645 (120)	0.13 (6)

Experimental data for the second isomeric state are limited to the study of Harbottle [6.157], which is based on a half-life of 650 (+430/–90) a. A simple estimate of the thermal neutron capture cross-section generates a recommended half-life of 241 a to give a $\sigma_{\gamma 0}^{m2}$ of 0.13 b that is similar to the values to be found in NGATLAS and EAF. Due to the scarcity and inconsistency of the experimental data set for the $\sigma_{\gamma 0}^{g}$ and $\sigma_{\gamma 0}^{m1}$ cross-sections, the data of Keish [6.155] have been adopted for the isomeric ratio to determine the resolved, first isomeric and ground state cross-sections. This procedure results in thermal cross-sections of $\sigma_{\gamma 0}$ 962(11), $\sigma_{\gamma 0}^{g}$ 317(58) and $\sigma_{\gamma 0}^{m1}$ 645(120) b.

Resonance cross-sections were adopted from the parameters in ENDF/B-VI. A minor modification was made to the gamma width (0.0837 eV) of the negative energy resonance (–0.854 eV) in order to match the thermal cross-section. Over the range from 0.3 keV to 20 MeV, experimental total cross-sections $\sigma_{\gamma}(E)$ have been tuned by means of the OMPs and adoption of a normalization factor of 1.524 (reduced χ^2 of 1.3). Since no experimental data exist for $\sigma_{tot}(E)$ or $\sigma_{el}(E)$ in this region, only capture cross-section data were included in the fit. Hence, $\sigma_{\gamma}^{g}(E)$, $\sigma_{\gamma}^{m1}(E)$ and $\sigma_{\gamma}^{m2}(E)$ were predicted from the calculated branching ratios. Figure 6.42 depicts the recommended cross-sections, while Fig. 6.43 shows the branching ratios. The total cross-section data of Sriramachandra et al. were defined as outliers [6.158], and there are few or no experimental data in the high energy region for comparison with the calculated $\sigma_{\gamma}^{g}(E)$, $\sigma_{\gamma}^{m1}(E)$ and $\sigma_{\gamma}^{m2}(E)$.

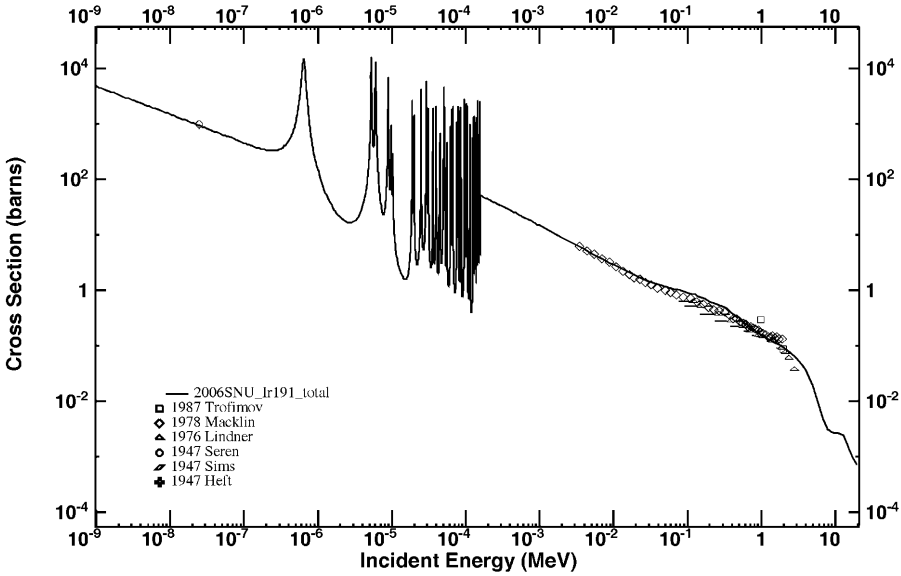

FIG. 6.42(a). Total capture cross-section $\sigma_{\gamma}^{g+m}(E)$ of the $^{191}Ir(n, \gamma)^{192}Ir$ reaction — EXFOR data are plotted as symbols.

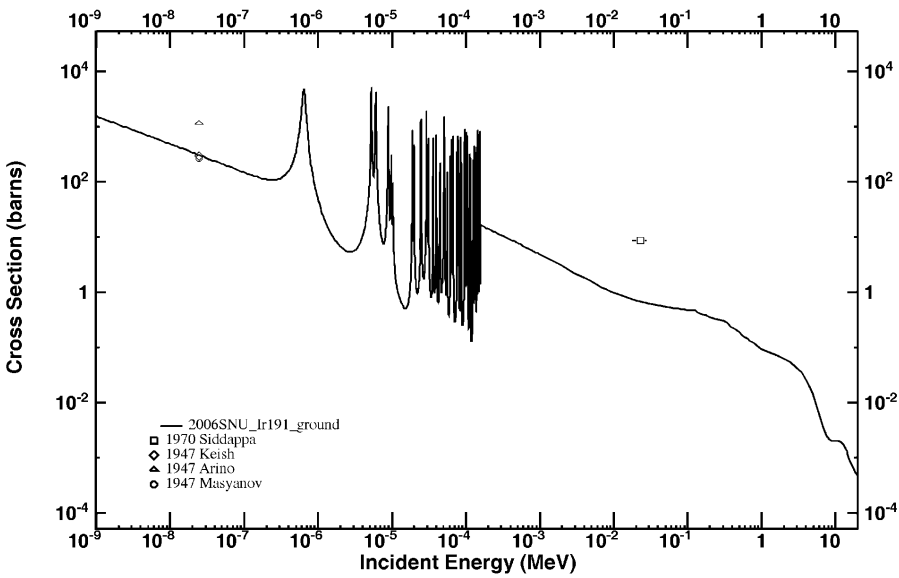

FIG. 6.42(b). Capture cross-section of the ground state $\sigma_{\gamma}^{g}(E)$ of the $^{191}Ir(n, \gamma)^{192}Ir$ reaction — EXFOR data are plotted as symbols.

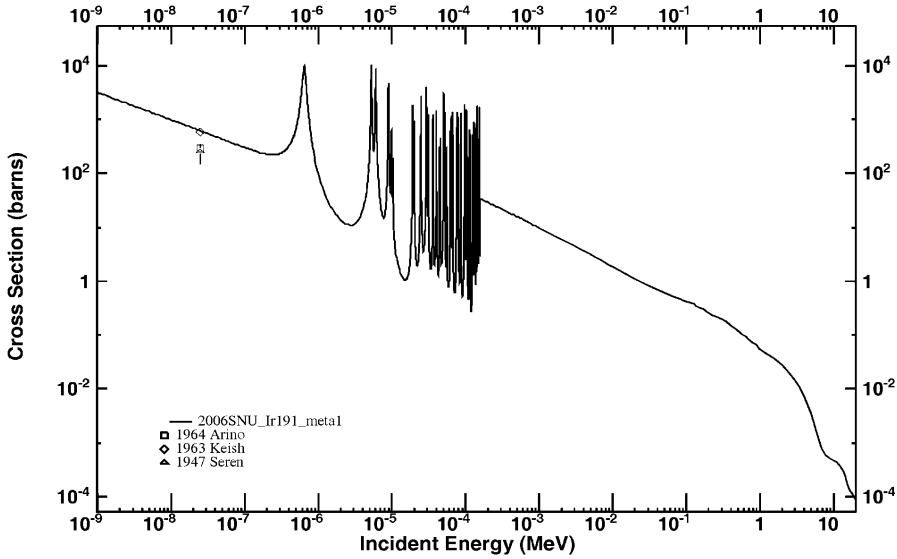

FIG. 6.42(c). Capture cross-section of the first isomeric state $\sigma_{\gamma}^{m1}(E)$ of the $^{191}Ir(n, \gamma)^{192}Ir$ reaction — EXFOR data are plotted as symbols.

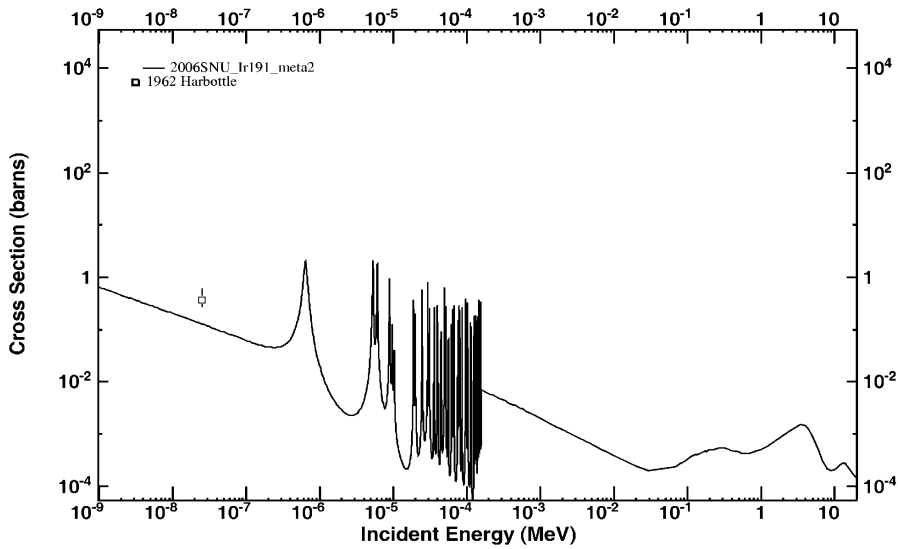

FIG. 6.42(d). Capture cross-section of the second isomeric state $\sigma_{\gamma}^{m2}(E)$ of the $^{191}Ir(n, \gamma)^{192}Ir$ reaction — EXFOR datum is plotted as a symbol.

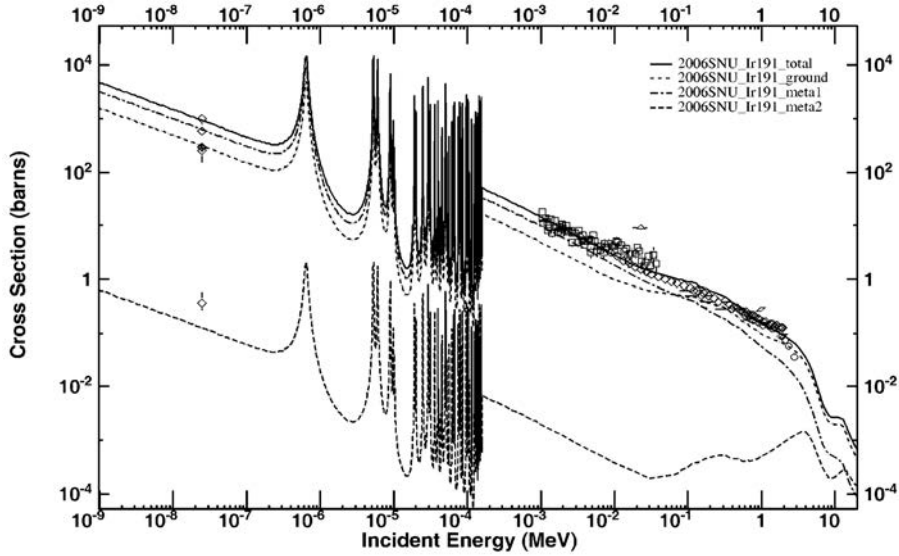

FIG. 6.42(e). Proposed cross-sections of the $^{191}Ir(n, \gamma)^{192}Ir$ reaction — EXFOR data are plotted as symbols.

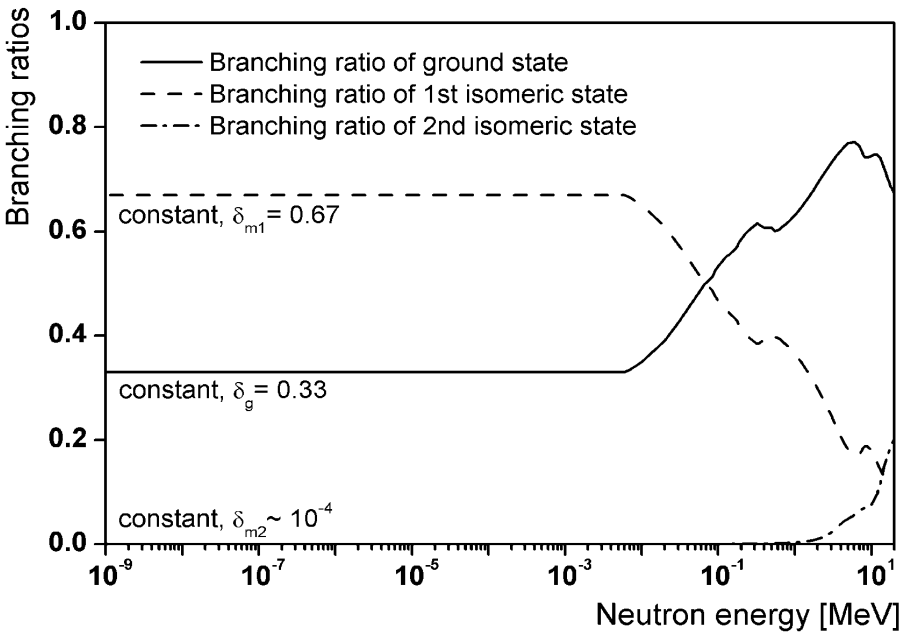

FIG. 6.43. Predicted branching ratios of the $^{191}Ir(n, \gamma)^{192}Ir$ reaction as determined by TALYS.

6.5.6. Validation and derived integral quantities

Integral quantities for the Maxwellian and fission neutron spectra and resonance integrals were produced by means of INTER [6.159]. The temperature for the Maxwellian spectrum was defined by T = 300 K and integration was limited from 10^{-5} to 10 eV. A Maxwellian fission spectrum with an effective temperature T = 1.35 MeV was adopted, and integration was implemented from 1 keV to 20 MeV. The 1/E spectrum was adopted for the resonance integral over the energy range from 0.55 eV to 2 MeV. The data are compared with the experimental studies to be found in EXFOR and other sources: Tables 6.52 to 6.55 show the quantities derived from the cross-sections produced in this work as compared with the values taken from various national libraries and experimental studies.

The resonance integral derived for the $^{31}P(n, \gamma)^{32}P$ reaction would appear to be inconsistent with the relatively elderly measurements, underlining the need for new measurements and re-assessments of the resonance parameters. Quantification of the resonance integral for the $^{104}Ru(n, \gamma)^{105}Ru$ reaction is tentatively based on only one EXFOR entry because the various measurements are inconsistent by multiples of their uncertainties. Similar inconsistentencies in the resonance integrals are seen in the $^{130}Te(n, \gamma)^{131}Te$ reaction that may arise from the inability to reproduce the resonance structure in the lower energy region below 1 keV. A better set of resonance parameters for this reaction would be

TABLE 6.52. INTEGRAL QUANTITIES FOR THE CROSS-SECTION OF THE $^{31}P(n, \gamma)^{32}P$ REACTION AS DERIVED IN THIS WORK AND COMPARED WITH VARIOUS OTHER DATA SOURCES INCLUDING EXFOR

Sources	$\sigma_{\gamma 0}$ (2200 m/s) (b)	$<\sigma_\gamma>$ Maxwellian (300 K) (b)	Resonance integral (b)	Fast cross-section (b)	
				Fission spectrum	14 MeV
Mughabghab evaluation	0.172 (6)	—	0.085 (10)	—	—
ENDF/B-VI	0.199	0.197	0.149	1.47×10^{-3}	3.00×10^{-3}
JENDL-3.3	0.166	0.166	0.0765	1.01×10^{-3}	9.90×10^{-4}
This work	0.172 (4)	0.172	0.0785	8.65×10^{-4}	5.49×10^{-4}
EXFOR Harris 1950			~0.10		
EXFOR Macklin 1956			0.092		
EXFOR Hayodom 1969			0.144 (10)		

TABLE 6.53. INTEGRAL QUANTITIES FOR THE CROSS-SECTION OF THE $^{104}Ru(n, \gamma)^{105}Ru$ REACTION

Sources		$\sigma_{\gamma 0}$ (2200 m/s) (b)	$<\sigma_\gamma>$ Maxwellian (300 K) (b)	Resonance integral (b)	Fast cross-section (b)	
					Fission spectrum	14 MeV
Mughabghab evaluation		0.32 (2)	—	4.3 (1)	—	—
ENDF/B-VI		0.437	0.437	6.54	3.19×10^{-2}	9.09×10^{-4}
JENDL-3.3		0.323	0.323	6.53	3.23×10^{-2}	1.09×10^{-3}
This work		0.466 (15)	0.466	6.58	2.51×10^{-2}	3.04×10^{-3}
EXFOR	Lantz 1964			4.6 (4)		
	Linden 1972			6.5 (3)		
	Ricabarra 1972			4.36		
	Bereznai 1977			5.9 (25)		
	Heft 1978			7.70 (65)		

TABLE 6.54. INTEGRAL QUANTITIES FOR THE CROSS-SECTION OF THE $^{130}Te(n, \gamma)^{131}Te$ REACTION

Sources		$\sigma_{\gamma 0}$ (2200 m/s) (b)	$<\sigma_\gamma>$ Maxwellian (300 K) (b)	Resonance integral (b)	Fast cross-section (b)	
					Fission spectrum	14 MeV
Mughabghab evaluation (total)		0.290 (61)	—	0.46 (5)	—	—
ENDF/B-VI (total)		0.290	0.290	0.344	4.48×10^{-3}	1.95×10^{-3}
JENDL-3.3 (total)		0.270	0.270	0.275	5.56×10^{-3}	1.00×10^{-3}
This work	total	0.204 (10)	0.204	0.239	2.47×10^{-3}	1.40×10^{-3}
	ground	0.192 (10)	0.192	0.225	2.08×10^{-3}	8.09×10^{-4}
	isomeric	0.012 (1)	0.012	0.015	3.88×10^{-3}	5.94×10^{-4}
EXFOR	Ricabarra 1968			0.48 (14)		
	Browne 1973			0.258 (32)		
	Linden 1974			0.34 (3)		

TABLE 6.55. INTEGRAL QUANTITIES FOR THE CROSS-SECTION OF THE $^{191}Ir(n, \gamma)^{192}Ir$ REACTION

Libraries		$\sigma_{\gamma 0}$ (2200 m/s) (b)	$<\sigma_\gamma>$ Maxwellian (300 K) (b)	Resonance integral I_0 (b)	Fast cross-section (b)	
					Fission spectrum	14 MeV
Mughabghab (evaluation)		954 (10)	—	3500 (100)	—	—
ENDF/B-VI		955	952	3424	0.185	6.08×10^{-3}
JEFF-3.1		958	954	3423	0.185	6.08×10^{-3}
This work	total	962 (11)	959	3429[a,b]	0.181	2.06×10^{-3}
	ground	317 (58)	316	1132[a]	0.110	1.50×10^{-3}
	meta1	645 (120)	642	2296[a,c]	0.070	2.79×10^{-4}
	meta2	0.13 (6)	0.13	0.46[a]	8.04×10^{-4}	2.78×10^{-4}
EXFOR	Harris 1950			3270 (230)[d]		
	Sims 1968			4800 (240)[d]		
	Koehler 1968			4074 (285)[e] 940 (160)[f]		
	Linden 1974			3480 (382)[a]		
	Heft 1978			5320 (480)[d]		
	Masyanov 1992 [6.154]			3410 (70)[d]		

[a] Lower limit of resonance integral of 0.55 eV.
[b] $I_0^{tot}(0.50\ eV) = 3558$ b, $I_0^{tot}(0.62\ eV) = 2940$ b.
[c] $I_0^{m1}(0.62\ eV) = 1969$ b.
[d] Lower limit of resonance integral of 0.5 eV.
[e] Lower limit of resonance integral of 0.62 eV.
[f] Value for the first isomeric state with lower integral limit of 0.62 eV.

extremely useful [6.12]. Resonance integrals have been obtained for $^{191}Ir(n, \gamma)^{192g}Ir$, $^{192m1}Ir$, and $^{192m2}Ir$, with their associated cross-section data. The lowest positive energy resonance is located at 0.65 eV, which is close to the Cd cut-off energy, such that the measured resonance integral depends strongly on the thickness of the cadmium used in such studies. Hence, three resonance integrals were calculated with lower limits of integration of 0.50, 0.55 and 0.62 eV as tabulated in Table 6.55 for comparison with the EXFOR data. The resonance integral for the total (n, γ) reaction channel is consistent with the values of Masyanov et al. [6.154] and van der Linden et al. [6.71]. However, the predicted cross-sections for the final isomeric states are highly marginal since few or no experimental data exist in the resonance and high energy regions.

6.6. NUCLEAR DATA FOR THE PRODUCTION OF ^{32}P, ^{64}Cu, ^{67}Cu, ^{89}Sr, ^{90}Y AND ^{153}Sm RADIONUCLIDES THROUGH THE CHARGE-EXCHANGE (n, p) CHANNEL

Radionuclides emitting low range highly ionizing radiation (β^- and α particles, Auger and conversion electrons) are of increasing significance in internal radiotherapy. Most of them are produced at nuclear reactors but new possibilities for production in spallation neutron sources are also being explored. Usually, the neutron capture production is employed in nuclear reactors. Another important production process is the fission of ^{235}U, which gives rise to 'no-carrier-added' products. The (n, p) reaction is also utilized in the reactor production to obtain a product of high specific activity although cross-sections with fission neutrons are rather low. Four such radionuclides are ^{32}P ($T_{½}$ = 14.3 d), ^{64}Cu ($T_{½}$ = 12.7 h), ^{67}Cu ($T_{½}$ = 61.9 h) and ^{89}Sr ($T_{½}$ = 50.5 d); they are produced via the (n, p) reaction on the target nuclei ^{32}S, ^{64}Zn, ^{67}Zn and ^{89}Y, respectively. Over recent years, the production of ^{64}Cu and ^{67}Cu has shifted mainly to cyclotrons but ^{32}P and ^{89}Sr are still produced via the (n, p) reaction at nuclear reactors. Two other therapeutic radionuclides, namely ^{90}Y ($T_{½}$ = 64.8 h) and ^{153}Sm ($T_{½}$ = 46.75 h), are available via the fission produced $^{90}Sr/^{90}Y$ generator system and the $^{152}Sm(n, \gamma)$-reaction, respectively although the latter is of low specific activity. They could also possibly be generated via the (n, p) reaction on ^{90}Zr and ^{153}Eu, respectively. The production of these six radionuclides via the charge-exchange (n, p) reaction will be covered in this section.

6.6.1. $^{67}Zn(n, p)^{67}Cu$ reaction

Cross-sections for the $^{67}Zn(n, p)^{67}Cu$ reaction in the production of ^{67}Cu are shown in Fig. 6.44. While experimental data also exist at thermal neutron energy, much of the experimental data appear to be incorrect. The three sources of evaluated cross-section data originate from JEFF-3.1/A [6.136], JENDL-Activation File [6.160] and the file calculated and assembled by Qaim and co-workers for this project [6.161]. A combination of $1/\sqrt{E}$ in the thermal and resonance region with calculated data in the fast neutron region was used by Qaim et al. to produce their curve for the excitation function. JEFF-3.1/A also includes thermal and resonance regions, while the Japanese evaluation is restricted to the fast neutron region. There are big discrepancies among the different evaluations for neutron energies above 14 MeV.

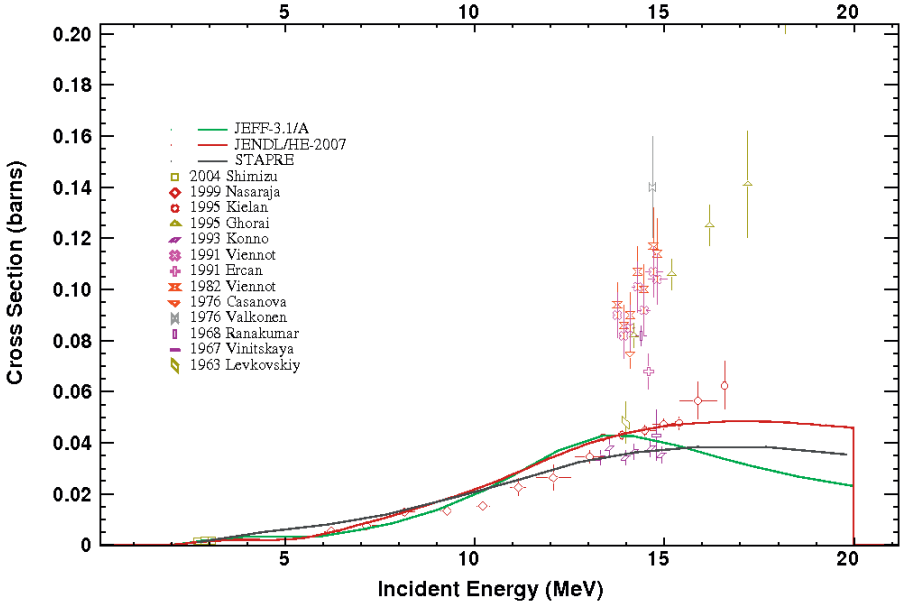

FIG. 6.44. Cross-section data of the $^{67}Zn(n, p)^{67}Cu$ reaction — EXFOR data [6.15] are plotted as symbols.

TABLE 6.56. INTEGRAL QUANTITIES FOR THE CROSS-SECTION OF THE $^{67}Zn(n, p)^{67}Cu$ REACTION COMPARED WITH VALUES FROM VARIOUS OTHER DATA SOURCES INCLUDING EXFOR

Sources		Spectrum-averaged cross-section (mb)		
		Fission	Cf-252[a]	Others
Library	Qaim calculation, STAPRE [6.161]	1.32	1.48	35.8[b]
	JEFF-3.1/A [6.136]	1.02	1.13	42.8[b]
	JENDL-Activation [6.160]	1.02	1.15	36.4[b]
Evaluation	Calamand 1974 [6.13]	1.07 (4)	—	—
Measurement	Horibe 1989 [6.162]	1.01 (9)	—	—
	Brodskaja 1977 [6.15]	0.92 (7)	—	—

[a] Cf-252 neutron spectrum, with effective temperature T = 1.42 MeV and integration limits from 1 keV to 20 MeV.

[b] 14 MeV neutron spectrum, with the same integration limits.

Integral experimental data for spectrum-averaged cross-sections are listed for the ^{67}Zn(n, p)^{67}Cu reaction in Table 6.56. The cross-sections from JEFF-3.1/A were used as an input for INTER to obtain spectrum averaged fission cross-sections. $<\sigma_{n,p}>$ = 1.02 mb for the ^{67}Zn(n, p) reaction, which is consistent with the latest measurement by Horibe et al. [6.162]. Similar results were derived for the JENDL-activation library. However, the Qaim et al. evaluation overestimates both fission and ^{252}Cf spectrum averaged cross-sections.

Considering the integral benchmarks performance and the existence of thermal and resonance data, we recommend that the JEFF-3.1/A evaluation be adopted for this reaction. The recommended data are available on-line at the IAEA web site (http://www-nds.iaea.org/exfor/endf.htm, special libraries).

6.6.2. ^{64}Zn(n, p)^{64}Cu reaction

Cross-sections for the ^{64}Zn(n, p) reaction in the production of ^{64}Cu are shown in Fig. 6.45(a). Data sets derived by Qaim et al. (RNAL) [6.161] and Zolotarev in his update for the IRDF-2002 [6.165] dosimetry evaluation [6.165, 6.166] are included along with other data files and the raw EXFOR data.

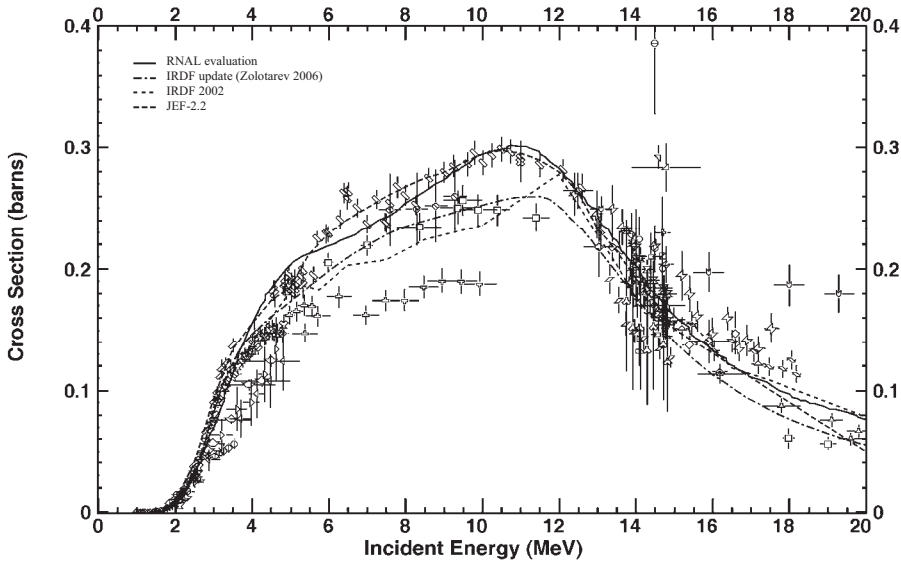

FIG. 6.45(a). Evaluated cross-section data of the ^{64}Zn(n, p)^{64}Cu reaction in comparison with IRDF-2002 and uncorrected experimental data [6.15].

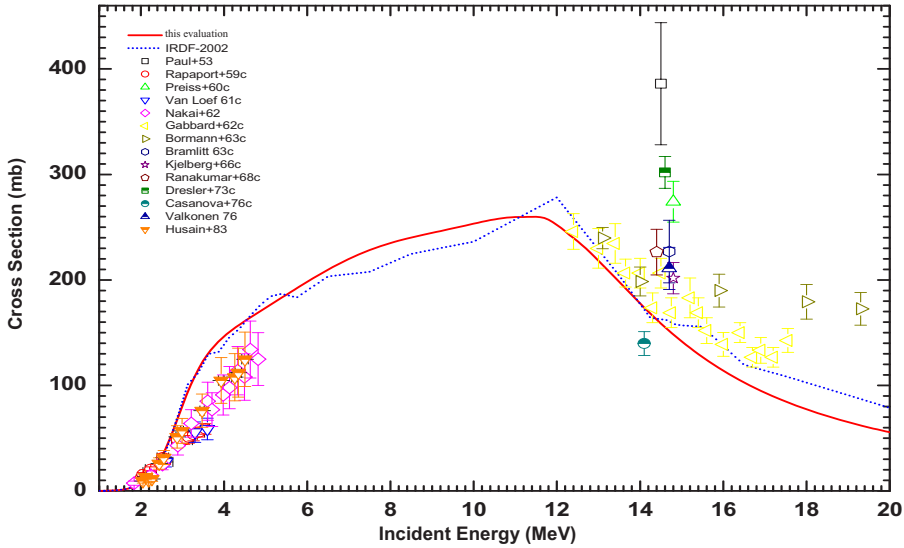

FIG. 6.45(b). Recommended cross-section data of the $^{64}Zn(n, p)^{64}Cu$ reaction in comparison with IRDF-2002 and rejected experimental data [6.15] (reprinted from Ref. [6.166]).

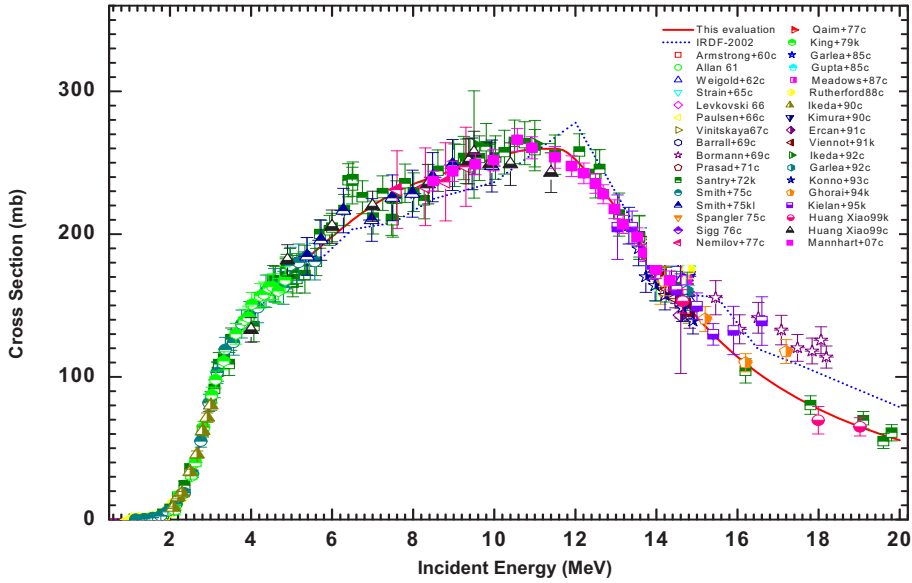

FIG. 6.45(c). Recommended cross-section data of the $^{64}Zn(n, p)^{64}Cu$ reaction in comparison with IRDF-2002 and experimental data (reprinted from Ref. [6.166]).

Zolotarev carried out a very careful selection and correction/normalization of available experimental data [6.166] — experimental data rejected by Zolotarev are shown in Fig. 6.45(b). Differences between raw and corrected experimental data are significant as shown in Figs 6.45(a) and 6.45(c). Some discrepancies remain above 14 MeV but the experimental database used in Zolotarev's evaluation (Fig. 6.45(c)) is more consistent than the original uncorrected set (Fig. 6.45(a)). Thus, we recommend the Zolotarev evaluation [6.165, 6.166] be adopted, which is listed in Table 6.57.

Spectrum-averaged cross-sections for the ^{64}Zn(n, p)^{64}Cu reaction are shown in Table 6.58. Since all of the experimental data before the 1980s were considered in the evaluations by Calamand [6.13] and Mannhart [6.168, 6.169], only measurements reported afterwards have been listed in this table. The latest evaluations for the ^{64}Zn(n, p) reaction recommend $<\sigma_{n,p}>$ in the ^{235}U thermal fission spectra of approximately 40 mb, which is supported by the most recent measurement of Cohen et al. [6.167].

6.6.3. ^{90}Zr(n, p)^{90}Y reaction

Experimental cross-sections for the ^{90}Zr(n, p)^{90}Y reaction given in the EXFOR database are reproduced in Fig. 6.46. Ignatyuk and co-workers carried out a new evaluation in 2005 to update the Russian dosimetry library, RRDF-2006 [6.170, 6.171]. The excitation function from threshold to 21 MeV was obtained by means of a theoretical model calculation with the modified GNASH code that was guided by available experimental data [6.172–6.178]; all experimental data were corrected to the new standards. Data of Bayhurst and Prestwood [6.172], Mukherjee and Bakhru [6.173], and Carroll and Stooksberry [6.174], measured above 12 MeV, were corrected for the contribution from the ^{91}Zr(n, x) ^{90}Y^{m+g} reaction as these measurements used natural targets. Data from Refs [6.172, 6.174] were renormalized to the factors Fc = 0.76391 and Fc = 0.77555, respectively. Experimental data of Nemilov and Trofimov [6.176] were renormalized to the theoretically calculated integral of the cross-sections over the energy range from 7.60 to 9.30 MeV, resulting in a correction factor of Fc = 0.49621. All corrected experimental data sets were fitted using Padé functions. Data measured by Qaim et al. [6.178] were found to be the most consistent. The resulting RRDF-06 dosimetry file was adopted as the recommended data set for the ^{90}Zr(n, p)^{90}Y reaction, and is shown in Fig. 6.46.

TABLE 6.57. EVALUATED CROSS-SECTIONS AND THEIR UNCERTAINTIES FOR THE $^{64}Zn(n, p)^{64}Cu$ REACTION IN THE NEUTRON ENERGY RANGE FROM THRESHOLD TO 20 MeV

Neutron energy (MeV) from to	Cross-section (mb)	Uncertainty (%)	Neutron energy (MeV) from to	Cross-section (mb)	Uncertainty (%)
0.500–1.750	0.435	11.81	7.750–8.000	233.431	2.43
1.750–2.000	4.528	4.25	8.000–8.500	237.672	2.31
2.000–2.250	10.941	3.61	8.500–9.000	242.455	2.13
2.250–2.500	23.187	3.24	9.000–9.500	246.769	2.00
2.500–2.750	42.689	2.93	9.500–10.000	251.112	2.06
2.750–3.000	67.682	2.74	10.000–11.000	257.083	2.20
3.000–3.250	93.146	2.69	11.000–11.500	259.162	2.32
3.250–3.500	114.482	2.71	11.500–12.000	254.580	2.37
3.500–3.750	130.332	2.73	12.000–12.500	243.880	2.36
3.750–4.000	141.779	2.68	12.500–13.000	227.746	2.27
4.000–4.250	150.467	2.55	13.000–13.500	208.260	2.12
4.250–4.500	157.680	2.36	13.500–14.000	187.776	1.92
4.500–4.750	164.211	2.18	14.000–14.500	168.057	1.81
4.750–5.000	170.482	2.06	14.500–15.000	150.067	2.01
5.000–5.250	176.690	2.02	15.000–15.500	134.146	2.49
5.250–5.500	182.896	2.07	15.500–16.000	120.273	3.06
5.500–5.750	189.089	2.18	16.000–16.500	108.258	3.58
5.750–6.000	195.213	2.31	16.500–17.000	97.857	3.99
6.000–6.250	201.193	2.42	17.000–17.500	88.831	4.34
6.250–6.500	206.949	2.50	17.500–18.000	80.964	4.68
6.500–6.750	212.400	2.55	18.000–18.500	74.072	5.13
6.750–7.000	217.481	2.56	18.500–19.000	68.001	5.81
7.000–7.250	222.141	2.55	19.000–19.500	62.625	6.79
7.250–7.500	226.351	2.52	19.500–20.000	57.839	8.11
7.500–7.750	230.107	2.48			

TABLE 6.58. INTEGRAL QUANTITIES FOR THE CROSS-SECTION OF THE ^{64}Zn(n, p)^{64}Cu REACTION COMPARED WITH VALUES FROM VARIOUS OTHER DATA SOURCES INCLUDING EXFOR

	Sources	Spectrum-averaged cross-section (mb)		
		Fission	Cf-252[a]	Others
Library	RNAL (Qaim) [6.161]	40.4	44.5	201[b]
	JEF-2.2	44.2	48.4	193[b]
	IRDF-2002 [6.164]	38.7	42.4	177[b]
	RRDF-2006 [6.165, 6.166]	39.3/38.9	43.1/42.7	178[b]
Evaluation	Calamand 1974 [6.13]	31.0 (23)	—	—
	Mannhart 1989 [6.168]	—	40.47 (75)	—
	Mannhart 2003 [6.169]	35.39 (1.07)	40.59 (67)	—
	Zolotarev 2008 [6.166]	38.9 (2.8)	42.3 (0.9)	—
Measurement	Cohen 2005 [6.167]	37.4 (14)	—	—
	Kobayashi 1990	31.7 (18)	—	—
	Benabdallah 1985	—	38.2 (15)	—
	Kobayashi 1984	—	41.8 (17)	—
	Spahn 2004 [6.163]	—	—	132 (25)[c]

[a] Cf-252 neutron spectrum, with effective temperature T = 1.42 MeV and integration limits from 1 keV to 20 MeV.
[b] 14 MeV neutron spectrum, with the same integration limits.
[c] 14 MeV d(Be) neutron spectrum.

6.6.4. ^{89}Y(n, p)^{89}Sr reaction

The experimental cross-section data for the ^{89}Y(n, p)^{89}Sr reaction are plotted in Fig. 6.47 (all from EXFOR) as a function of neutron energy. The results of Tewes et al. (1960) are rather low, and they cannot be checked because no details are available; furthermore, the Csikai and Nagy (1967) value is rather high. Both sets of data have been rejected. There are several experimental data points around 14 MeV but only two data sets exist over wide energy ranges (Bayhurst et al. [6.172] and Klopries et al. [6.179]). All of these data are consistent. STAPRE calculations reported by Klopries et al. [6.179] and EMPIRE 2.19 studies are also shown in Fig. 6.47. There is very good agreement between experiment and model calculations. Therefore, we adopted the STAPRE curve as the standard excitation function of the ^{89}Y(n, p)^{89}Sr reaction. The recommended data are available on

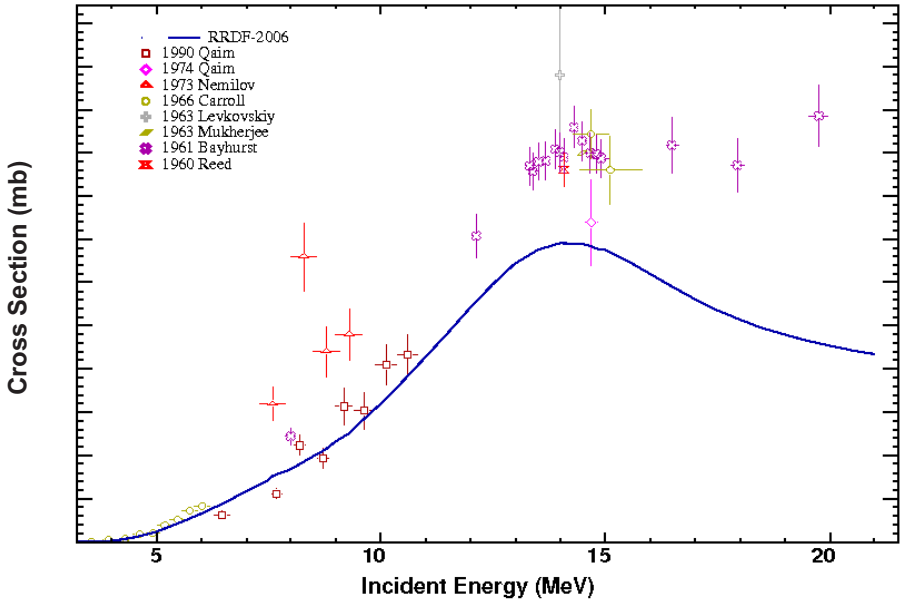

FIG. 6.46. Excitation function of the $^{90}Zr(n, p)^{90}Y$ reaction – EXFOR contains references to experimental data.

line at the IAEA Nuclear Data Section web site (see http://www-nds.iaea.org/exfor/endf.htm, special libraries).

Integral experimental data for spectrum-averaged cross-sections for the $^{89}Y(n, p)^{89}Sr$ reaction have been measured [6.161], in which the fast neutron field was generated via break-up of 14 MeV deuterons on a thick beryllium target. An experimentally determined cross-section of 0.91 ± 0.20 mb agrees within uncertainty with the calculated integral value of 1.05 mb based on the recommended STAPRE calculation.

6.6.5. $^{153}Eu(n, p)^{153}Sm$ reaction

Only a few data points around 14 MeV have been reported for the $^{153}Eu(n, p)^{153}Sm$ reaction (Fig. 6.48). Experimental data together with the results of STAPRE and EMPIRE 2.19 calculations are shown in Fig. 6.49 as a function of neutron energy. The encircled data of Coleman et al. (1959) and Pruys et al. (1975) appear to be rather high and were, therefore, rejected. Data represented by the curve given by the STAPRE calculation were adopted as the recommended excitation function of the $^{153}Eu(n, p)^{153}Sm$ reaction.

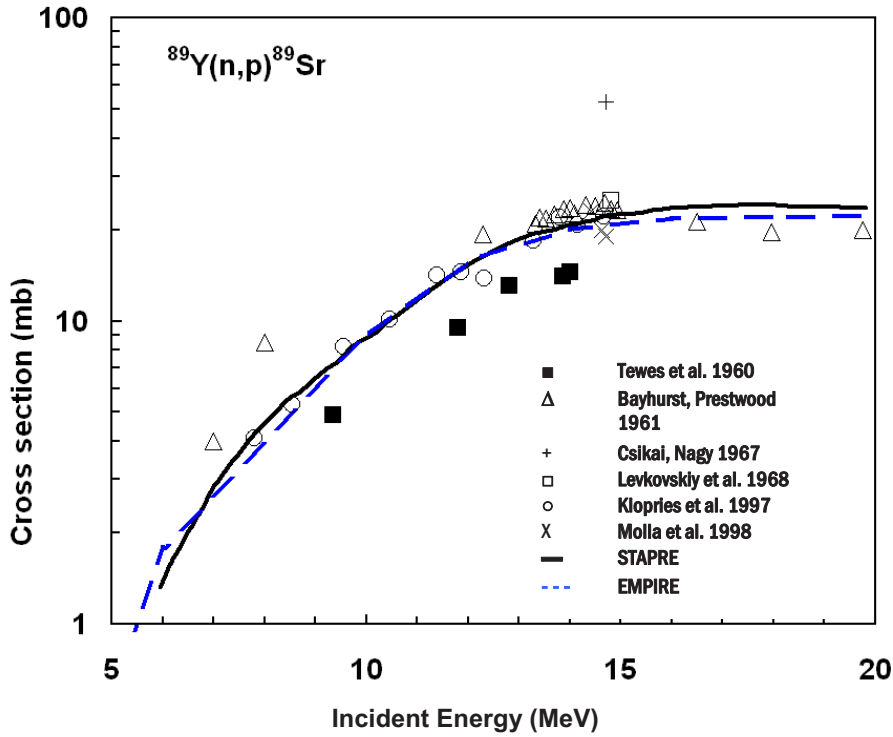

FIG. 6.47. Excitation function of the ^{89}Y(n, p)^{89}Sr reaction — EXFOR contains references to experimental data.

The spectrum-averaged cross-section of the ^{153}Eu(n, p)^{153}Sm reaction induced by 14 MeV d(Be) break-up neutrons was measured via the activation technique [6.161]. An experimentally determined cross-section of 0.26 ± 0.04 mb agrees within uncertainty with the calculated integral value of 0.30 mb based on the recommended STAPRE calculation.

6.6.6. ^{32}S(n, p)^{32}P reaction

The excitation function for the ^{32}S(n, p)^{32}P reaction is shown in Fig. 6.49(a). References to all raw experimental data are to be found in the EXFOR database. While nuclear model calculations with STAPRE and EMPIRE 2.19 codes describe the overall trend of the excitation function, they do not reproduce the fine structures as expected from statistical model codes. A better fit of the experimental data was achieved in the IRDF-2002 evaluation [6.164].

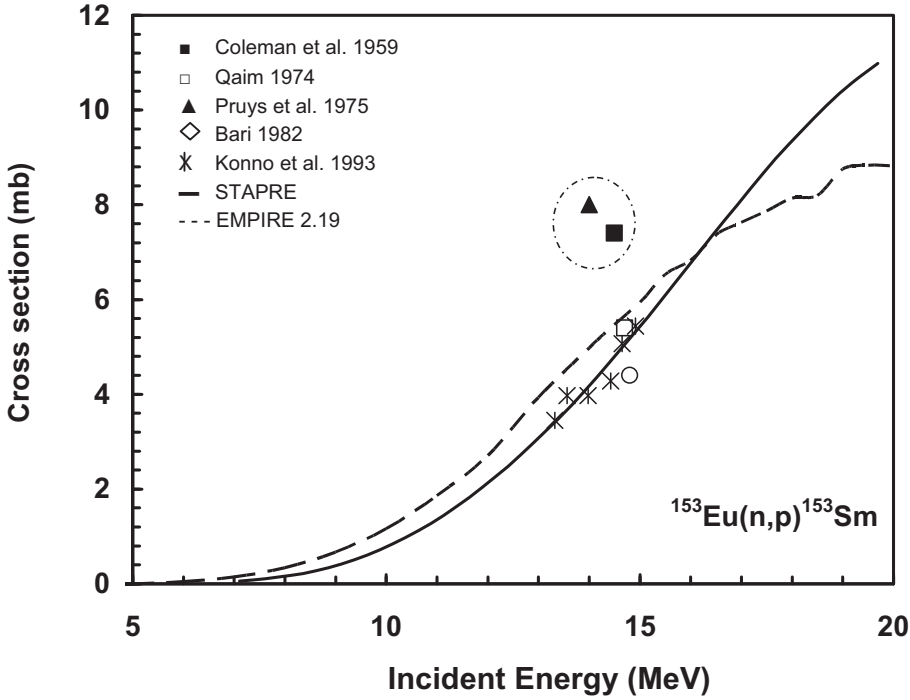

FIG. 6.48. Excitation function of the ^{153}Eu(n, p)^{153}Sm reaction — EXFOR contains references to experimental data.

Zolotarev has re-evaluated the excitation function in order to update the IRDF-2002 library [6.164, 6.166]. A careful selection and correction/normalization of available experimental data was undertaken [6.166]. Figure 6.49(b) shows the re-evaluated excitation function for the ^{32}S(n, p)^{32}P reaction over the neutron energy range from 1.0 to 5.0 MeV, and Fig. 6.49(c) the equivalent data from threshold to 21.0 MeV, compared with the cross-sections of IRDF-2002 and experimental data. Over the neutron energy range from 1.5 to 20 MeV, the re-evaluated excitation function is in better agreement with the corrected experimental data than the IRDF-2002 evaluation; therefore, we recommend the Zolotarev evaluation [6.165, 6.166] to be adopted as the standard excitation function of this reaction. The recommended data are listed in Table 6.59.

Evaluated excitation functions for the ^{32}S(n, p)^{32}P reaction have been tested against integral experimental data from Refs [6.180] and [6.181]. Calculated average cross-sections for ^{235}U thermal fission and ^{252}Cf spontaneous fission neutron spectra are compared with the IRDF-2002 and experimental data

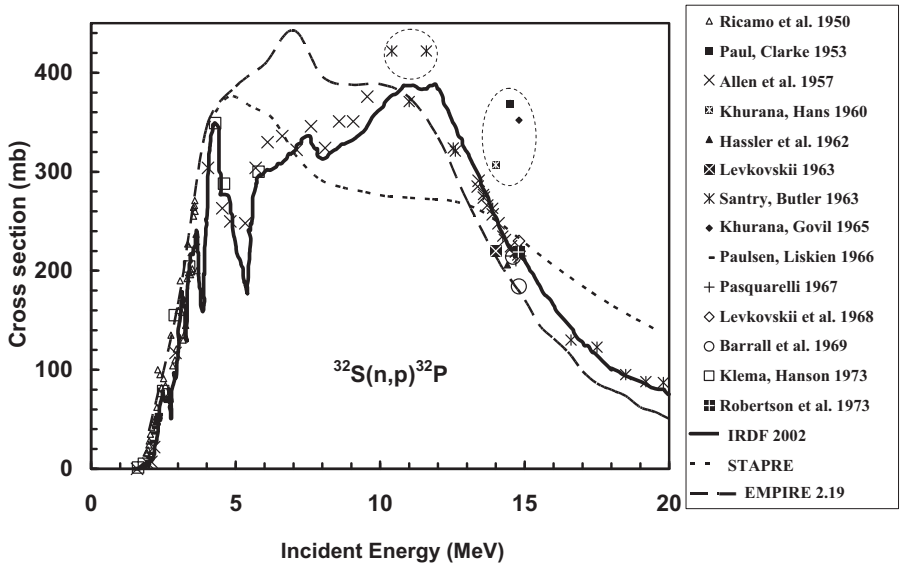

FIG. 6.49(a). Excitation function of the $^{32}S(n, p)^{32}P$ reaction — EXFOR contains references to experimental data. Discrepant data are circled, and the results of STAPRE and EMPIRE 2.19 model calculations and the curve given in the IRDF-2002 dosimetry file are also shown.

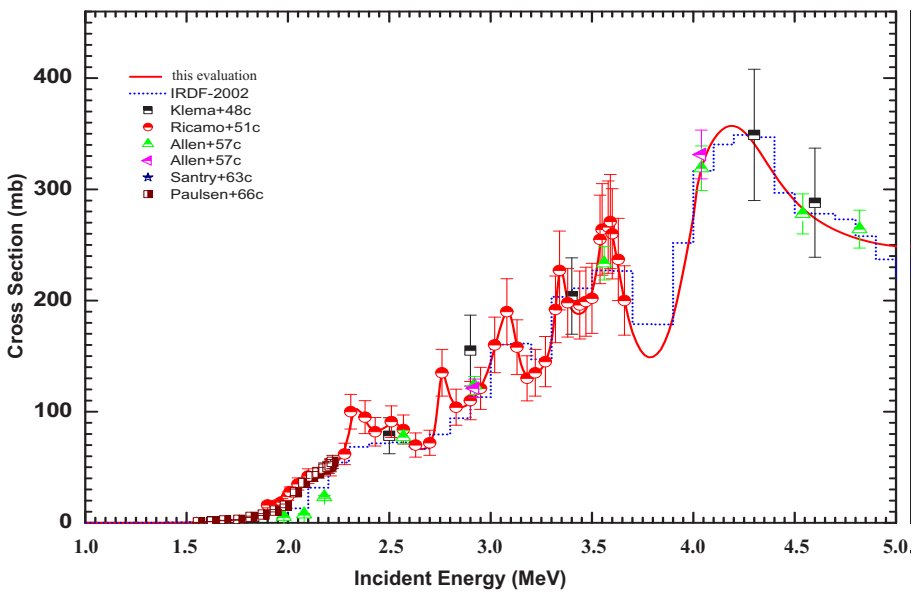

FIG. 6.49(b). Re-evaluated excitation function of the $^{32}S(n, p)^{32}P$ reaction in the energy range from threshold to 5 MeV in comparison with IRDF-2002 and selected experimental data (reprinted from Ref. [6.166]).

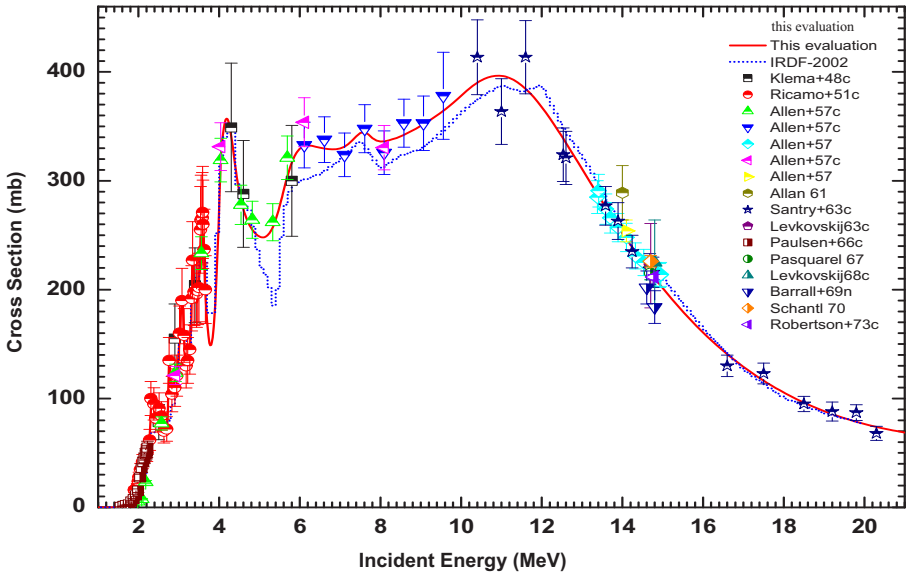

FIG. 6.49(c). Re-evaluated excitation function of the $^{32}S(n, p)^{32}P$ reaction in the energy range from threshold to 20 MeV in comparison with IRDF-2002 and experimental data (reprinted from Ref. [6.166]).

in Table 6.60. Data calculated from the re-evaluated excitation functions for ^{235}U thermal fission and ^{252}Cf spontaneous fission neutron spectra agree well with the experimental data, while discrepancies exist between the IRDF-2002 and experimental data of about 6.4% and 3.2% for the ^{235}U and ^{252}Cf spectra, respectively.

TABLE 6.59. EVALUATED CROSS-SECTIONS AND THEIR UNCERTAINTIES FOR THE $^{32}S(n, p)^{32}P$ REACTION IN THE NEUTRON ENERGY RANGE FROM THRESHOLD TO 21 MeV

Neutron energy (MeV) from to	Cross-section (mb)	Uncertainty (%)	Neutron energy (MeV) from to	Cross-section (mb)	Uncertainty (%)
0.958–2.000	2.266	10.94	8.000–8.500	337.897	
2.000–2.200	37.243	3.72	8.500–9.000	345.442	2.95
2.200–2.400	77.314	3.33	9.000–9.500	356.385	3.04
2.400–2.600	84.928	3.32	9.500–10.000	370.121	3.06
2.600–2.800	88.674	3.27	10.000–10.500	385.822	2.99
2.800–3.000	114.865	3.34	10.500–11.000	395.288	2.81
3.000–3.200	161.191	3.37	11.000–11.500	393.101	2.57
3.200–3.400	172.418	3.86	11.500–12.000	378.428	2.32
3.400–3.600	220.489	3.43	12.000–12.500	354.514	2.08
3.600–3.800	183.632	3.88	12.500–13.000	325.756	1.86
3.800–4.000	194.915	4.44	13.000–13.500	295.609	1.65
4.000–4.200	336.752	4.22	13.500–14.000	266.173	1.46
4.200–4.400	339.058	3.95	14.000–14.500	238.544	1.33
4.400–4.600	291.271	3.58	14.500–15.000	213.217	1.31
4.600–4.800	264.011	3.45	15.000–15.500	190.365	1.41
4.800–5.000	251.888	3.55	15.500–16.000	169.985	1.58
5.000–5.200	248.468	3.78	16.000–16.500	151.989	1.77
5.200–5.400	255.711	3.99	16.500–17.000	136.237	1.94
5.400–5.600	276.922	3.97	17.000–17.500	122.564	2.08
5.600–5.800	304.713	3.68	17.500–18.000	110.792	2.20
5.800–6.000	324.063	3.33	18.000–18.500	100.742	2.34
6.000–6.500	331.551	3.11	18.500–19.000	92.239	2.52
6.500–7.000	329.358	2.96	19.000–20.000	82.158	2.96
7.000–7.500	335.908	2.84	20.000–21.000	72.418	3.98
7.500–8.000	340.682	2.83			

TABLE 6.60. CALCULATED AND MEASURED AVERAGED CROSS-SECTIONS FOR THE $^{32}S(n, p)^{32}P$ REACTION IN ^{235}U THERMAL FISSION AND ^{252}Cf SPONTANEOUS FISSION NEUTRON SPECTRA

Type of neutron field	Average cross-section (mb)		C/E [6.181]
	Calculated	Measured	
U-235 thermal fission neutron spectrum	68.195[a] 64.501[b]	69.080 ± 1.361 [6.181]	0.9872 0.9337
Cf-252 spontaneous fission neutron spectrum	74.106[a] 70.230[b]	73.240 ± 2.695 [6.180] 72.540 ± 2.532 [6.181]	1.0216 0.9682

[a] Present evaluation.
[b] IRDF-2002 (IRDF-90 version 2), Ref. [6.164].

REFERENCES

[6.1] The JEFF-3.1 library, JEFF Rep. 21, NEA/OECD No. 6190 (2006), http://www.nea.fr/html/dbdata/projects/nds_jef.htm

[6.2] Descriptive Data of JENDL-3.3 (Part I and II), SHIBATA, K. (Ed.), JAERI-Data/Code 2002-026 (2003), http://wwwndc.tokai-sc.jaea.go.jp/jendl/j33/j33.html

[6.3] CHADWICK, M.B., et al., ENDF/B-VII.0: Next generation evaluated nuclear data library for Nuclear Science and Technology, Nucl. Data Sheets **107** (2006) 2931–3060, http://www.nndc.bnl.gov/exfor7/endf00.htm

[6.4] MILLS, R.W., Nexia Solutions Ltd., personal communication, 2006.

[6.5] HERMAN, M. (Ed.), ENDF-6 Data Formats and Procedures for the Evaluated Nuclear Data File ENDF/B-VI and ENDF/B-VII (Rev. June 2005), Rep. BNL-NCS-44945-05-Rev., National Nuclear Data Center, Brookhaven Natl Lab. (2005), http://www.nndc.bnl.gov/endf/

[6.6] Experimental Nuclear Reaction Data — EXFOR, http://www-nds.iaea.org/exfor/exfor00.htm

[6.7] ENDVER/Gui — ENDF File Verification Support Package, http://www-nds.iaea.org/ndspub/endf/endver/

[6.8] FORREST, R.A., SAFEPAQ-II User Manual, UKAEA FUS **454**(7), January 2007, http://www.fusion.org.uk/easy2007/index.html

[6.9] RSICC peripheral shielding routine collection — NJOY-99.0, PSR-480 code package, http://www-rsicc.ornl.gov/

[6.10] ENDF Utility Codes — Release 7.02 and Pre-processing Code PREPRO-2007, http://www.nndc.bnl.gov/nndcscr/endf/

[6.11] FORREST, R.A., et al., Validation of EASY-2005 using integral measurements, UKAEA FUS 526, January 2006, http://www.fusion.org.uk/easy2007/index.html

[6.12] MUGHABGHAB, S.F., Atlas of Neutron Resonances, Elsevier Science (2006).

[6.13] INTERNATIONAL ATOMIC ENERGY AGENCY, Handbook on Nuclear Activation Cross-sections, Technical Reports Series No. 156, IAEA, Vienna (1974) 273–324.

[6.14] FORREST, R.A., KOPECKY, J., SUBLET, J.-Ch., The European Activation File: EAF-2007 neutron-induced cross section library, UKAEA FUS 535, January 2007, http://www.fusion.org.uk/easy2007/index.html
[6.15] ZERKIN, V. (Ed.), EXFOR+CINDA for Applications: Database and Retrieval System, Version 1.70, January 2005, CD-ROM, Nuclear Data Section, IAEA, Vienna (2003), http://www.nndc.bnl.gov/exfor3/
[6.16] HERMAN, M., EMPIRE-II — A modular system for nuclear reaction calculations, http://www.nndc.bnl.gov/empire219/
[6.17] MacFARLANE, R.E., NJOY99: Code System for Producing, Pointwise and Multigroup Neutron and Photon Cross Sections from ENDF/B Data, PSR-480(NJOY99.0), LANL (2000).
[6.18] MUGHABGHAB, S.F., Thermal Neutron Capture Cross Sections, Resonance Integrals and g-Factors, INDC(NDS)-440, IAEA, Vienna (2003).
[6.19] SHIBATA, K., et al., Japanese Evaluated Nuclear Data Library, Version 3, Revision-3: JENDL-3.3, J. Nucl. Sci. Technol. **39** (2002) 1125–1136.
[6.20] YOUNG, P.G., Handbook for Calculation of Nuclear Reaction Data: Reference Input Parameter Library, IAEA-TECDOC-1034, IAEA, Vienna (1998) 41–63.
[6.21] TULI, J.K., Evaluated Nuclear Structure Data File - A Manual for Preparation of Data Sets, Rep. BNL-NCS-51655-01/02-Rev. (2001), National Nuclear Data Center, Brookhaven Natl Lab., Upton, NY, http://www.nndc.bnl.gov/nndc/ensdf/
[6.22] BROWNE, E., Nuclear data sheets for A = 90, Nucl. Data Sheets **82** (1997) 379.
[6.23] SEREN, L., FRIEDLANDER, H.N., TURKEL, S.H., Thermal neutron activation cross sections, Phys. Rev. **72** (1947) 888–901.
[6.24] POMERANCE, H., Thermal neutron capture cross sections, Phys. Rev. **83** (1951) 641–645.
[6.25] BENOIST, P., KOWARSKI, L., NETTER, F., Measurement of thermal neutron absorption measurement by pile oscillation, J. Phys. **12** (1951) 584–589.
[6.26] LYON, W.S., REYNOLDS, S.A., Oak Ridge Natl Lab., personal communication to EXFOR, 1956.
[6.27] RUSTAD, B.M., MELKONIAN, E., HAVENS Jr., W.W., Coherent, incoherent and capture cross sections of ^{89}Y, New York Ops. Off. Rep. NYO-72-28 (1966).
[6.28] RYVES, T.B., PERKINS, D.R., Further activation thermal neutron capture cross sections and resonance integrals, J. Nucl. Energy **25** (1971) 129–131.
[6.29] TAKIUE, M., ISHIKAWA, H., Thermal neutron reaction cross section measurements for fourteen nuclides with a liquid scintillation spectrometer, Nucl. Instrum. Meth. Phys. Res. **148** (1978) 157.
[6.30] HARRIS, S.P., MUEHLHAUSE, C.O., THOMAS, G.E., Low energy neutron resonance scattering and absorption, Phys. Rev. **79** (1950) 11–18.
[6.31] BOLDEMAN, J.W., ALLEN, B.J., DE L. MUSGROVE, A.R., MACKLIN, R.L., The neutron capture cross-section of ^{89}Y, Nucl. Sci. Eng. **64** (1977) 744–748.
[6.32] MACKLIN, R.L., GIBBONS, J.H., INADA, T., Neutron capture cross sections near 30 keV using a Moxon-Rae detector, Nucl. Phys. **43** (1963) 353–362.
[6.33] STUPEGIA, D.C., SCHMIDT, M., REEDY, C.R., MADSON, A.A., Neutron capture between 5 keV and 3 MeV, J. Nucl. Energy **22** (1968) 267–281.
[6.34] BOOTH, R., BALL, W.P., MacGREGOR, M.H., Neutron activation cross sections at 25 keV, Phys. Rev. **112** (1958) 226–229.

[6.35] HASAN, S.S., CHAUBEY, A.K., SEHGAL, M.L., Neutron activation cross-sections at 24 keV, Nuovo Cimento B **58** (1968) 402–406.
[6.36] GIBBONS, J.H., MACKLIN, R.L., MILLER, P.D., NEILER, J.H., Average radiative capture cross sections for 7- to 170-keV neutrons, Phys. Rev. **122** (1961) 182–201.
[6.37] MACKLIN, R.L., GIBBONS, J.H., Capture-cross-section studies for 30- to 220-keV neutrons using a new technique, Phys. Rev. **159** (1967) 1007–1012.
[6.38] BOSTROM, N.A., MORGAN, I.L., PRUD'HOMME, J.T., OKHUYSEN, P.L., HUDSON Jr., O.M., Neutron Interactions in Lithium, Carbon, Nitrogen, Aluminum, Argon, Manganese, Yttrium, Zirconium, Radiolead and Bismuth, Wright Air Devel. Centre Rep. WADC-TN-59-107 (1959).
[6.39] TOLSTIKOV, V.A., KOROLEVA, V.P., KOLESOV, V.E., DOVBENKO, A.G., Fast neutron radiative capture by ^{89}Y, Atomnaya Energiya (USSR) **21** (1966) 506–507.
[6.40] DIVEN, B.C., TERRELL, J., HEMMENDINGER, A., Radiative capture cross sections for fast neutrons, Phys. Rev. **120** (1960) 556–569.
[6.41] POENITZ, W.P., Fast-neutron capture-cross-section measurements with the Argon National Laboratory large-liquid-scintillator tank, Argonne Natl Lab., Rep. ANL-83-4 (1982) 239–247.
[6.42] JOLY, S., VOIGNER, J., GRENIER, G., DRAKE, D.M., NILSSON, L., Measurements of Fast Neutron Capture Cross Sections Using a NaI Spectrometer, Centre d'Etudes Nucleaires Saclay Rep. CEA-R-5089 (1981).
[6.43] VOIGNIER, J., JOLY, S., GRENIER, G., Capture cross sections and gamma-ray spectra from the interaction of 0.5 to 3.0 MeV neutron with nuclei in the mass range A = 63 to 209, Nucl. Sci. Eng. **112** (1992) 87–94.
[6.44] BERGQVIST, I., et al., Radiative capture of fast neutrons by ^{89}Y and ^{140}Ce, Nucl. Phys. A **295** (1978) 256–268.
[6.45] RIGAUD, F., et al., Radiative neutron capture on Si, Rb, Sr and Y in the dipole giant resonance region, Nucl. Phys. A **154** (1970) 243–260.
[6.46] BUDNAR, M., et al., Prompt Gamma-ray Spectra and Integrated Cross Sections for the Radiative Capture of 14 MeV Neutrons for 28 Natural Targets in the Mass Region from 12 to 208, INDC(YUG)-6 (1979).
[6.47] PERKIN, J.L., O'CONNOR, L.P., COLEMAN, R.F., Radiative capture cross sections for 14.5 MeV neutrons, Proc. Phys. Soc. **72** (1958) 505–513.
[6.48] SCHWERER, O., WINKLER-ROHATSCH, M., WARHANEK, H., WINKLER, G., Measurement of cross sections for 14 MeV neutron capture, Nucl. Phys. A **264** (1976) 105–114.
[6.49] BRAMLITT, E.T., FINK, R.W., Rare nuclear reactions induced by 14.7-MeV neutrons, Phys. Rev. **131** (1963) 2649–2663.
[6.50] MAGNUSSON, G., ANDERSSON, P., BERQUIST, I., 14.7 MeV neutron capture cross section measurements with activation technique, Phys. Scrip. **21** (1980) 21–26.
[6.51] CSIKAI, J., PETO, G., BUCZKO, M., MILLIGY, Z., EISSA, N., Radiative capture cross-sections for 14.7-MeV neutrons, Nucl. Phys. A **95** (1967) 229–234.
[6.52] GRENCH, H.A., COOP, K.L., MENLOVE, H.O., VAUGHN, F.J., A study of the spin dependence of the nuclear level density by means of the ^{89}Y(n,γ)^{90g,90m}Y reactions with fast neutrons, Nucl. Phys. A **94** (1967) 157–176.
[6.53] DE FRENNE, D., JACOBS, E., Nuclear data sheets for A = 103, Nucl. Data Sheets **93** (2001) 447.

[6.54] MEINKE, W., Half-life of ^{109}Pd and neutron activation cross section of ^{102}Pd, Phys. Rev. **90** (1953) 410–412.
[6.55] DUNCAN, C.L., KRANE, K.S., Neutron capture cross section of ^{102}Pd, Phys. Rev. C **71** (2005) 054322:1–5.
[6.56] KATAKURA, J., nuclear data sheets for A = 125, Nucl. Data Sheets **86** (1999) 955.
[6.57] TOBIN, J.M., SAKO, J.H., Thermal neutron absorption cross section of xenon-124, J. App. Phys. **29** (1958) 1373.
[6.58] HARPER, P.V., SIEMENS, W.D., LATHROP, K.A., ENDLICH, H., Production and Use of ^{125}I, Argonne Cancer Res. Hospital Rep. (1961).
[6.59] EASTWOOD, T., BROWN, F., Neutron Capture Cross Sections for Kr and Xe isotopes, Canadian Rep. to EANDC (1963).
[6.60] BRESESTI, M., CAPPELLANI, F., DEL TURCO, A.M., ORVINI, E., The thermal neutron capture cross-section and the resonance capture integral of ^{124}Xe, J. Inorg. Nucl. Chem. **26** (1964) 9–14.
[6.61] KONDAIAH, E., RANAKUMAR, N., FINK, R.W., Thermal neutron activation cross sections for Kr and Xe isotopes, Nucl. Phys. A **120** (1968) 329–336.
[6.62] BRESESTI, M., BRESESTI DEL TURCO, A.M., NEUMANN, H., ORVINI, E., The thermal neutron capture cross-section and resonance integral of ^{125}I, J. Inorg. Nucl. Chem. **26** (1964) 1625–1631.
[6.63] SZUCS, J.A., JOHNS, M.W., SINGH, B., Nuclear data sheets for A = 129, Nucl. Data Sheets **46** (1985) 1.
[6.64] POMERANCE, H., Thermal neutron capture cross sections, Phys. Rev. **88** (1952) 412–413.
[6.65] WALKER, W.H., THODE, H.G., Relative abundances and neutron capture cross sections of the neodymium isotopes, Phys. Rev. **90** (1953) 447–448.
[6.66] RUIZ, C.P., PETERSON Jr., J.P., RIDER, B.F., Thermal-neutron cross section and resonance capture integral of neodymium-148, Trans. Am. Nucl. Soc. **7** (1964) 270–271.
[6.67] ALSTAD, J., JAHNSEN, T., PAPPAS, A.C., Thermal neutron capture cross sections and resonance capture integrals of the lanthanide nuclei ^{140}Ce, ^{142}Ce, ^{146}Nd, ^{148}Nd, ^{150}Nd and ^{159}Tb, J. Inorg. Nucl. Chem. **29** (1967) 2155–2160.
[6.68] GRYNTAKIS, E.M., Examination of the dependence of the effective cross section from the neutron temperature, measurements of the neutron temperature and determination of some cross sections for neutron capture and neutron fission, Technical University Munich, personal communication, 1976.
[6.69] HEFT, R.E., "A consistent set of nuclear-parameter values for absolute instrumental neutron activation analysis", Conf. Computers in Activ. Analysis and Gamma-ray Spectroscopy (Proc. Conf. Mayaguez, Puerto Rico, 1978), Trans. Am. Nucl. Soc. Suppl. **28** (1978) 43–44.
[6.70] RICABARRA, M.D., TURJANSKI, R., RICABARRA, G.H., Measurement and evaluation of the activation resonance integral of ^{146}Nd, ^{148}Nd and ^{150}Nd, Can. J. Phys. **51** (1973) 1454–1462.
[6.71] VAN DER LINDEN, R., DE CORTE, F., HOSTE, J., A compilation of infinite dilution resonance integrals II, J. Radioanal. Chem. **20** (1974) 695–706.
[6.72] STEINNES, E., Resonance activation integrals of some lanthanide nuclides, J. Inorg. Nucl. Chem. **37** (1975) 1591–1592.

[6.73] DE L. MUSGROVE, A.R., ALLEN, B.J., BOLDEMAN, J.W., MACKLIN, R.L., "Non-statistical effects in the radiative capture cross-sections of the neodymium isotopes", Int. Conf. Neutron Phys. Nucl. Data, Harwell (1978).
[6.74] WISSHAK, K., et al., Stellar Neutron Capture Cross Sections of the Nd Isotopes, FZKA-5967 (1997).
[6.75] NAKAJIMA, Y., ASAMI, A., KAWARASAKI, Y., FURUTA, Y., "Neutron capture cross section measurements of ^{143}Nd, ^{145}Nd, ^{146}Nd and ^{148}Nd", Int. Conf. Neutron Phys. Nucl. Data, Harwell (1978).
[6.76] KONONOV, V.N., JURLOV, B.D., POLETAEV, E.D., TIMOKHOV, V.M., MANTUROV, G.N., Average neutron radiative capture cross-section in the energy range 5–30 keV for Ta, Au and Nd, Sm, Eu, Gd, Er isotopes, Yad. Konst. **22** (1977) 29.
[6.77] SIDDAPPA, K., SRIRAMACHANDRA MURTY, M., RAMA RAO, J., Neutron activation cross-sections in rare earths and heavier nuclei, Ann. Phys. **83** (1974) 355–366.
[6.78] BRADLEY, T., PARSA, Z., STELTS, M.L., CHRIEN, R.E., "Stellar nucleosynthesis and the 24-keV neutron capture cross sections of some heavy nuclei", Int. Conf. Nucl. Cross Sections for Technol. (Knoxville, TN, 1979), Brookhaven Natl Lab., BNL-26885 (1979).
[6.79] THIRUMALA RAO, B.V., RAMA RAO, J., KONDAIAH, E., Neutron capture cross sections at 25 keV, J. Phys. Mathematical+General A **5** (1972) 468–470.
[6.80] JOHNSRUD, A.E., SILBERT, M.G., BARSCHALL, H.H., Energy dependence of fast-neutron activation cross section, Phys. Rev. **116** (1959) 927–936.
[6.81] AFZAL ANSARI, M., SINGH, R.K.Y., GAUTAM, R.P., KAILAS, S., Fast neutron radiative capture cross-sections in fission product isotopes of neodymium, Ann. Nucl. Energy **26** (1999) 553–558.
[6.82] TROFIMOV, Yu.N., Neutron radiation capture cross-sections for even neodim isotopes in the energy range 0.5 - 2.0 MeV, Vop. At. Nauki i Tekhn. Ser. Yad. Konst. (1993) 17.
[6.83] TROFIMOV, Yu.N., "Neutron radiation capture cross-sections for nuclei of medium and large masses at the neutron energy 1 MeV", 1st Int. Conf. Neutron Physics, (Proc. Conf. Kiev, 1987), Vol. 3 (1987) 331.
[6.84] TROFIMOV, Yu.N., Activation cross-sections for 31 nuclei at the neutron energy 2 MeV, Vop. At. Nauki i Tekhn. Ser. Yad. Konst. **4** (1987) 10.
[6.85] HELMER, R.G., Nuclear data sheets for A = 153, Nucl. Data Sheets **107** (2006) 507.
[6.86] WALKER, W.H., The relative abundances and pile neutron capture cross sections of the isotopes of samarium, gadolinium, dysprosium and ytterbium, Phd Thesis, McMaster University, Hamilton, Ontario (1956).
[6.87] PATTENDEN, N.J., Some neutron cross sections of importance to reactors — ^{99}Tc, ^{143}Nd, ^{145}Nd, ^{149}Sm, ^{152}Sm, ^{151}Eu, ^{153}Eu, ^{155}Gd, ^{157}Gd, ^{240}Pu, 2nd Int. At. Energy Conf., Geneva (1958).
[6.88] FEHR, E., HANSEN, E., Fission-Product Cross-Section Measurements, Knolls Atomic Power Lab. Rep. (1960).
[6.89] TATTERSALL, R.B., ROSE, H., PATTENDEN, S.K., JOWITT, D., Pile oscillator measurements of resonance absorption integrals, J. Nucl. Energy A **12** (1960) 32–46.
[6.90] CABELL, M.J., Neutron capture cross-section data for ^{152}Sm, J. Inorg. Nucl. Chem. **24** (1962) 749–753.

[6.91] HAYODOM, V., BOONKONG, W., MAHAPANYAWONG, S., CHAIMONKON, C., Resonance Integral Measurements, Atomic Energy for Peace, Bangkok Rep. (1969).
[6.92] STEINNES, E., Resonance activation integrals of some nuclides of interest in neutron activation analysis, J. Inorg. Nucl. Chem. **34** (1972) 2699–2703.
[6.93] WISSHAK, K., GUBER, K., VOSS, F., KAEPPELER, F., REFFO, G., Neutron capture in ^{148,150}Sm — a sensitive probe of the s-process neutron density, Phys. Rev. C **48** (1993) 1401–1419.
[6.94] GUBER, K., Experimental determination of the stellar neutron capture cross sections of ^{148}Sm and ^{150}Sm and the consequences for the s-process, Kernforschungszentrum Karlsruhe, KFK-5170 (1993).
[6.95] BOKHOVKO, M.V., et al., Neutron Radiation Cross-section, Neutron Transmission and Average Resonance Parameters for Some Fission Product Nuclei, Fiz.-Energ Institut Obninsk Rep. (1991).
[6.96] LUO XIAO-BING, XIA YI-JUN, YANG ZHI-HUA, LIU MAN-TIAN, Measurement of neutron capture cross section for ^{152}Sm, Chin. J. Nucl. Phys. **16** (1994) 275–277.
[6.97] MACKLIN, R.L., LAZAR, N.H., LYON, W.S., Neutron activation cross sections with Sb-Be neutrons, Phys. Rev. **107** (1957) 504–508.
[6.98] BENSCH, F., LEDERMANN, H., The activation cross section of several nuclides for neutrons of intermediate energies, Rep. to EANDC (1971).
[6.99] CHAUBEY, A.K., SEHGAL, M.L., Test of statistical theory of nuclear reactions at 24 keV, Phys. Rev. **152** (1966) 1055–1061.
[6.100] MACKLIN, R.L., GIBBONS, J.H., INADA, T., Neutron capture in the samarium isotopes and the formation of the elements of the solar system, Nature **197** (1963) 369–370.
[6.101] ZHOU ZUYING, CHEN YING, JIANG SONGSHENG, LUO DEXING, Measurements of 0.1-0.5 MeV neutron capture cross section for ^{180}Hf and ^{152}Sm, Chin. J. Nucl. Phys. **6** (1984) 174.
[6.102] LYON, W.S., MACKLIN, R.L., Neutron activation at 195 keV, Phys. Rev. **114** (1959) 1619–1620.
[6.103] PETO, G., MILLIGY, Z., HUNYADI, I., Radiative capture cross-sections for 3 MeV neutrons, J. Nucl. Energy **21** (1967) 797–801.
[6.104] SINGH, B., Nuclear data sheets for A = 188, Nucl. Data Sheets **95** (2002) 387.
[6.105] LYON, W.S., Reactor neutron activation cross sections for a number of elements, Nucl. Sci. Eng. **8** (1960) 378–380.
[6.106] MENGE, E.E., ELLIS, W.H., KARAM, R.A., PARKINSON, T.F., The Nuclear Properties of Rhenium, Technical Rep. NP-13807 (1963).
[6.107] FRIESENHAHN, S.J., GIBBS, D.A., HADDAD, E., FROHNER, F.H., LOPEZ, W.M., Neutron capture cross sections and resonance parameters of rhenium from 0.01 eV to 30 keV, J. Nucl. Energy **22** (1968) 191–210.
[6.108] SHER, R., LE SAGE, L., CONNOLLY, T.J., BROWN, H.L., The resonance integrals of rhenium and tungsten, Trans. Am. Nucl. Soc. **9** (1966) 248–249.
[6.109] PIERCE, C.R., SHOOK, D.F., BOGART, D., Resonance Integrals of Rhenium for a Wide Range of Sample Sizes, NASA-Lewis Research Center, Cleveland, OH, NASA-TN-D-4938 (1968).

[6.110] BERGMAN, A.A., KAIPOV, D.K., KONKS, V.A., ROMANOV, S.A., "Radiative capture of neutrons by rhenium isotopes", Neutron Phys. Conf., Kiev (1971).
[6.111] STUPEGIA, D.C., SCHMIDT, M., MADSON, A.A., Fast neutron capture in Rhenium, J. Nucl. Energy A+B **19** (1965) 767–773.
[6.112] ANAND, R.P., BHATTACHARYA, D., JHINGAN, M.L., KONDAIAH, E., Measurement of isotopic neutron capture cross-sections for ^{51}V, ^{63}Cu, ^{71}Ga, ^{74}Ge, ^{75}As, ^{98}Mo, ^{100}Mo, ^{104}Ru, ^{115}In, ^{128}Te, ^{130}Te, ^{140}Ce, ^{142}Ce, ^{165}Ho at the neutron energy of (25 ± 5) keV, Nuovo Cimento A **50** (1979) 274.
[6.113] LINDNER, M., NAGLE, R.J., LANDRUM, J.H., Neutron capture cross-sections from 0.1 to 3 MeV by activation measurements, Nucl. Sci. Eng. **59** (1976) 381–394.
[6.114] WAGNER, M., WARHANEK, H., Activation measurements of neutron capture cross sections at 14.6 MeV and a critical survey of such data in the literature, Acta Phys. Austriaca **52** (1980) 23–37.
[6.115] AKOVALI, Y.A., Nuclear data sheets for A = 213, Nucl. Data Sheets **66** (1992) 237.
[6.116] AKOVALI, Y.A., Nuclear data sheets for A = 229, Nucl. Data Sheets **55** (1989) 555.
[6.117] AKOVALI, Y.A., Nuclear data sheets for A = 225, Nucl. Data Sheets **60** (1990) 617.
[6.118] AKOVALI, Y.A., Nuclear data sheets for A = 221, Nucl. Data Sheets **61** (1990) 623.
[6.119] AKOVALI, Y.A., Nuclear data sheets for A = 217, Nucl. Data Sheets **100** (2003) 141.
[6.120] NICHOLS, A.L., JEFF-3.1 decay data library (1979).
[6.121] SONZOGNI, A.A., private communication, Brookhaven Natl Lab. (2007).
[6.122] BOLL, R.A., GARLAND, M., MIRZADEH, S., "Reactor production of thorium-229", Int. Conf. Nuclear Data for Science and Technology (Proc. Int. Conf. Santa Fe, NM, 2004), HAIGHT, R.C., CHADWICK, M.B., TALOU, P., KAWANO, T. (Eds), **769** (2005) 1674–1675.
[6.123] KONING, A.J., HILAIRE, S., DUIJVESTIJN, M.C., "TALYS: Comprehensive nuclear reaction modeling", Int. Conf. Nuclear Data for Science and Technology (Proc. Int. Conf. Santa Fe, NM, 2004), **769** (2005) 1154–1159.
[6.124] MUGHABGHAB, S.F., DIVADEENAM, M., HOLDEN, N.E., Neutron Cross Sections, Vol. 1: Neutron Resonance Parameters and Thermal Cross Sections, Part A, Z = 1 - 60, Academic Press, New York (1981).
MUGHABGHAB, S.F., Neutron Cross Sections, Vol. 1: Neutron Resonance Parameters and Thermal Cross Sections, Part B, Z = 61–100, Academic Press, New York (1984).
[6.125] SHIBATA, K., et al., Japanese Evaluated Nuclear Data Library Version 3 Revision-3: JENDL-3.3, J. Nucl. Sci. Technol. **39** (2002) 1125–1136.
[6.126] TRKOV, A., Program ENDVER, IAEA-NDS-77 Rev.0, Nuclear Data Section, IAEA, Vienna (2001), http://www-nds.iaea.org/ndspub/endf/endver/
[6.127] ZERKIN, V., ZVView — Graphic Software for Nuclear Data Analysis, Version 9.7, Nuclear Data Section, IAEA, Vienna (2003), http://www-nds.iaea.org/ndspub/zvview/
[6.128] KIM, S.K., PhD Thesis, Department of Nuclear Engineering, Seoul National University (2006).
[6.129] SUN, G.M., PhD Thesis, Department of Nuclear Engineering, Seoul National University (2004).
[6.130] KONING, A.J., DELAROCHE, J.P., Local and global nucleon optical models from 1 keV to 200 MeV, Nucl. Phys. A **713** (2003) 231–310.

[6.131] INTERNATIONAL ATOMIC ENERGY AGENCY, Handbook for Calculation of Nuclear Reaction Data: Reference Input Parameter Library, IAEA-TECDOC-1034, IAEA, Vienna (1998) 41–63.
[6.132] MACKLIN, R.L., MUGHABGHAB, S.F., Neutron capture by ^{31}P, Phys. Rev. C **32** (1985) 379-383.
[6.133] SUBLET, J.-Ch., CAPOTE NOY, R., Nuclear Data for the Production of Therapeutic Radionuclides, Summary Rep. Second Res. Coordination Mtg, INDC(NDS)-465, IAEA, Vienna (2004) 14.
[6.134] LANTZ, P., Thermal-Neutron Cross Section and Resonance Integral of Ru-104, Chemistry Division Annu. Prog. Rep. for Period Ending 20 June 1964, ORNL-3679, Oak Ridge Natl Lab. (1964) 11, EXFOR item 11929003.
[6.135] GRAY, P.R., ZANDER, A.R., EBREY, T.G., Activation cross sections for reactions of Rh and Ru with 14.7 MeV neutrons, Nucl. Phys. **75** (1966) 215–225.
[6.136] KONING, A.J., et al., "Status of the JEFF Nuclear Data Library", Int. Conf. Nuclear Data for Science and Technology (Proc. Int. Conf. Santa Fe, NM, 2004), Vol. 769, Melville, NY (2005) 177–182, http://www.nea.fr/html/dbdata/JEFF/
[6.137] SEHGAL, M.L., Isomeric cross-section ratios in (n,γ) reactions, Phys. Rev. **128** (1962) 761–767.
[6.138] RAMAN, S., NESTOR, J.C.W., TIKKANEN, P., Transition probability from the ground to the first-excited 2+ state of even-even nuclides, At. Data Nucl. Data Tables **78** (2001) 11–28.
[6.139] KIBÉDI, T., SPEAR, R.H., Transition probability from the ground to the first-excited 2^+ state of even-even nuclides reduced electric-octupole transition probabilities, $B(E3;0_1^+ \rightarrow 3_1^-)$ — an update, At. Data Nucl. Data Tables **80** (2002) 35–82.
[6.140] MAKOFSKE, W., SAVIN, W., OGATA, H., KRUSE, T.H., Elastic and inelastic proton scattering from even isotopes of Cd, Sn, and Te, Phys. Rev. **174** (1968) 1429–1441.
[6.141] BELGYA, T., et al., Handbook for Calculations of Nuclear Reaction Data, RIPL-2, Reference Input Parameter Library-2, IAEA-TECDOC-1506, Vienna (2006), http://www-nds.iaea.or.at/ripl-2/
[6.142] DOVBENKO, A.G., KOLESOV, V.E., KOROLEVA, V.P., TOLSTIKOV, V.A., SHUBIN, Yu.N., Cross sections for radiative capture of 0.2-3 MeV neutrons by Te^{128} and Te^{130}, Sov. At. Energy **25** (1968) 1367–1368.
[6.143] BERGMAN, A.A., ROMANOV, S.A., Study of the cross sections for radiative capture of neutrons by tellurium isotopes and their application to the theory of the origin of the elements, Sov. J. Nucl. Phys. **20** (1975) 133–137.
[6.144] BEGHIAN, L.E., HALBAN, H.H., Absorption cross section measurement, Nature **163** (1949) 366–367.
[6.145] BAGLIN, C.M., Nuclear data sheets for A = 192, Nucl. Data Sheets **84** (1998) 717–900.
[6.146] SHIRLEY, V.S., Nuclear data sheets for A = 192, Nucl. Data Sheets **64** (1991) 205–322.
[6.147] SCHARFF-GOLDHABER, G., McKEOWN, M., Triple isomerism in Ir^{192}, Phys. Rev. Lett. **3** (1959) 47–50.

[6.148] BALODIS, M., "The revised Nilsson model interpretation of transitional nucleus ^{192}Ir", 9th Int. Symp. Capture Gamma-ray Spectroscopy and Related Topics, (Proc. Int. Symp. Budapest, 1996) Vol. 1, Springer Hungarica (1997) 147–153.

[6.149] SCHARFF-GOLDHABER, G., Multipole order and enhancement factor of long-lived isomeric transition in ^{192}Ir, Bull. Am. Phys. Soc. **22** (1977) 545, BG1.

[6.150] KERN, J., et al., Nuclear levels in ^{192}Ir, Nucl. Phys. A **534** (1991) 77–127.

[6.151] IAEA NUCLEAR DATA SECTION, Reference Neutron Activation Library, IAEA-TECDOC-1285, IAEA, Vienna (2002).

[6.152] KOPECKY, J. (Ed.), Atlas of Neutron Capture Cross Sections, INDC(NDS)-362, Nuclear Data Section, IAEA, Vienna (1997), http://www-nds.iaea.org/nngatlas2/

[6.153] FORREST, R.A., KOPECKY, J., SUBLET, J.-Ch., The European Activation File: EAF-2003 Cross Section Library, UKAEA FUS 486, EURATOM/UKAEA Fusion Association (2002).

[6.154] MASYANOV, S.M., ANUFRIEV, V.A., SIVUKHA, V.I., Resonance parameters of ^{191}Ir, ^{193}Ir, and ^{192g}Ir, At. Energy **73** (1992) 686–688.

[6.155] KEISCH, B., Yield ratios of isomers produced by neutron activation, Phys. Rev. **129** (1963) 769–775.

[6.156] ARINO, H., KRAMER, H.H., MOLINSKI, V.J., TILSBURY, R.S., Research in Activation Analysis, New York Operation Office Rep., NYO-10175, Union Carbide Corporation, Tuxedo, New York (1964), EXFOR item 11817021.

[6.157] HARBOTTLE, G., The half-lives of Tl^{204}, Au^{195}, Ir^{192} and its long-lived isomer Ir^{192m2}, Nucl. Phys. **41** (1963) 604–607.

[6.158] SRIRAMACHANDRA MURTY, M., SIDDAPPA, K., RAMA RAO, J., "p-wave neutron capture in heavy nuclei at 25 keV", Nuclear Physics and Solid State Physics Symp. (Proc. Symp. Madurai, 1970), Vol. II — Nuclear Physics, Department of Atomic Energy, Government of India (1970) 29–32.

[6.159] PERRY, R.J., DEAN, C.J., "Version 6.8w of the INTER code at Winfrith", JEFDOC-487, AEA Technology (1994) http://www.nndc.bnl.gov/nndcscr/endf/

[6.160] NAKAJIMA, Y., "Status of the JENDL activation file", Symp. Nuclear Data (Proc. Symp. Tokai, 1995), JAERI-Conf 06-008 (1996) 50, http://wwwndc.tokai-sc.jaea.go.jp/jendl/jendl.html

[6.161] QAIM, S.M., Coordinated Research Project on Nuclear Data for Production of Therapeutic Radionuclides, Institut für Nuklearchemie, Forschungszentrum Jülich, private communication, 2005.
AL-ABYAD, et al., Nuclear data for the production of the therapeutic radionuclides ^{32}P, ^{64}Cu, ^{67}Cu, ^{89}Sr, ^{90}Y And ^{153}Sm via the (n,p) reaction: Evaluation of excitation function and its validation via integral cross section measurement using a 14-MeV d(Be) neutron source, Appl. Radiat. Isot. **64** (2006) 717–724.

[6.162] HORIBE, O., MIZUMOTO, Y., KUSAKABE, T., CHATANI, H., U-235 Fission Neutron Spectrum Averaged Cross Sections Measured for Some Threshold Reactions on Mg, Al, Ca, Sc, Ti, Fe, Co, Ni, Zn, Sr, Mo, Rh, In and Ce, 50 Years with Nuclear Fission (Proc. 1989), Vol. 2, American Nuclear Soc. (1989) 923–930 (EXFOR 22140012).

[6.163] SPAHN, I., COENEN, H.H., QAIM, S.M., Enhanced production possibility of the therapeutic radionuclides ^{64}Cu, ^{67}Cu and ^{89}Sr via (n,p) reactions induced by fast spectral neutrons, Radiochim. Acta **92** (2004) 183–186.

[6.164] BERSILLON, O., et al., International Reactor Dosimetry File 2002 (IRDF-2002), Technical Reports Series No. 452, IAEA, Vienna (2006).
[6.165] ZOLOTAREV, K.I., Recommended Russian Dosimetry File RRDF-2006(BROND-3) MAT 3025, IPPE, Obninsk, personal communication to the IAEA, 2006.
[6.166] ZOLOTAREV, K.I., Re-evaluation of the Excitation Functions for the ^{24}Mg(n,p)^{24}Na, ^{32}S(n,p)^{32}P, ^{60}Ni(n,p)$^{60m+g}$Co, ^{63}Cu(n,2n)^{62}Cu, ^{65}Cu(n,2n)^{64}Cu, ^{64}Zn(n,p)^{64}Cu, ^{115}In(n,2n)^{114m}In, ^{127}I(n,2n)^{126}I, ^{197}Au(n,2n)^{196}Au and ^{199}Hg(n,n')^{199m}Hg Reactions, Technical Rep. INDC(NDS)-0526, IAEA, Vienna (2008).
[6.167] COHEN, I.M., et al., Determination of nuclear constants of reactions induced on zinc by short irradiations with the epithermal and fast components of a reactor neutron spectrum, Radiochim. Acta **93** (2005) 543–546.
[6.168] MANNHART, W., "Status of the Cf-252 fission neutron spectrum evaluation with regard to recent experiments", Proc. Consultants' Meeting on Physics of Neutron Emission in Fission, INDC(NDS)-220/L, IAEA, Vienna (1989) 305–336; INTERNATIONAL ATOMIC ENERGY AGENCY, Handbook on Nuclear Activation Data, Technical Reports Series No. 273, IAEA, Vienna (1987) 413–437.
[6.169] MANNHART, W., Response of Activation Reactions in the Neutron Field of Spontaneous Fission of ^{252}Cf, Summary Rep. Final Technical Mtg on International Reactor Dosimetry File, IRDF-2002, INDC(NDS)-448, IAEA, Vienna (2003) 61–71.
[6.170] IGNATYUK, A.V., ZOLOTAREV, K.I., LUNEV, V.P., MANOKHIN, V.N., TERTYCHNYJ, G.Y.A., Analysis and evaluation of the spectra and production cross-sections of gamma-rays. VANT, Ser. Yadernye Konstanty, Issue 1–2 (2002) 3–44.
[6.171] ZOLOTAREV, K.I., Recommended Russian Dosimetry File RRDF-2006 (BROND-3) MAT 4025, IPPE, Obninsk, personal communication to the IAEA, 2006.
[6.172] BAYHURST, B.P., PRESTWOOD, R.J., (n,p) and (n,alpha) excitation functions of several nuclei from 7.0 to 19.8 MeV, J. Inorg. Nucl. Chem. **23** (1961) 173 (EXFOR 11462.010).
[6.173] MUKHERJEE, S.K., BAKHRU, H., "Some (n,alpha) reaction cross-sections and the resulting radio-isotopes", Nuclear and Solid State Physics Symp. (Proc. Symp. Bombay, 1963) (EXFOR 31330.002), p. 244.
[6.174] CARROLL, E.E., STOOKSBERRY, R.W., Zirconium (n,p) cross-section measurements, Nucl. Sci. Eng. **25** (1966) 285.
[6.175] LEVKOVSKIY, V.N., VINITSKAYA, G.P., KOVEL'SKAYA, G.E., STEPANOV, G.E., Empirical regularities in the (n,p) reaction cross-sections at the neutron energy 14-15 MeV, Zhurnal Eksperimental'noi I Teoret. Fiziki **45** (1963) 305 (EXFOR 40016.010).
[6.176] NEMILOV, Ju.A., TROFIMOV, Ju.N., Cross section of the ^{90}Zn(n,p)^{90}Y reaction, Vopr. At. Nauki i Tekhn., Serija Yadernye Konstanty **12** (1973) 61 (EXFOR 40211.002).
[6.177] QAIM, S.M., STÖCKLIN, G., "Measurement and systematics of cross sections for common and low yield 14 MeV neutron induced nuclear reactions on structural materials and transmuted species", 8th Symp. Fusion Technology (Proc. Symp. Noordwijkerhout, 1974), Rep. EUR-5182E (1974) 939 (EXFOR 20513.010).
[6.178] QAIM, S.M., IBN MAJAH, M., WÖLFLE, R., STROHMAIER, B., Excitation functions and isomeric cross-section ratios for the ^{90}Zr(n,p)^{90m,g}Y and ^{91}Zr(n,p)^{91m,g}Y processes, Phys. Rev. **C42** (1990) 363.

[6.179] KLOPRIES, R.M., DÓCZI, R., SUDÁR, S., CSIKAI, J., QAIM, S.M., Excitation functions of some neutron threshold reactions on ^{89}Y in the energy range of 7.8 to 14.7 MeV, Radiochim. Acta **77** (1997) 3–9.

[6.180] KOBAYASHI, K., KIMURA, I., GOTOH, H., TOMINAGA, H., Measurement of Average Cross Sections for some Threshold Reactions of Ti, Cr and Pb in the Californium-252 Spontaneous Fission Neutron Spectrum Field, NEANDC(J)-106/U, Japan Atomic Energy Research Institute, Tokai-mura, Ibaraki-ken (1984) 41–44.

[6.181] MANNHART, W., Validation of Differential Cross Sections with Integral Data, Summary Rep. of the Technical Mtg on Int. Reactor Dosimetry File IRDF-2002, GREENWOOD, L.R., PAVIOTTI-CORCUERA, R. (Eds), IAEA Rep. INDC(NDS)-435, IAEA, Vienna (2002) 59–64.

7. CHARGED PARTICLE PRODUCTION OF ^{64,67}Cu, ^{67}Ga, ^{86g}Y, ^{102}Rh, ^{103}Pd, ^{111g,114m}In, ^{124,125}I, ^{169g}Yb, ^{177g}Lu, ^{186g}Re, ^{192g}Ir, ^{210,211}At AND ^{225}Ac

F. Tárkányi, S.M. Qaim, M. Nortier, R. Capote, A.V. Ignatyuk, B. Scholten, S.F. Kovalev, B. Kiraly, E. Menapace, Yu.N. Shubin

This chapter is devoted to the evaluation of reaction cross-sections for the most important accelerator produced radioisotopes used in internal radiotherapy. The chapter is divided into 15 parts, each corresponding to one radionuclide, as given below:

7.1. Cu-64
7.2. Cu-67
7.3. Ga-67
7.4. Y-86g
7.5. Pd-103, Rh-102 (impurity)
7.6. In-111g
7.7. In-114m
7.8. I-124
7.9. I-125
7.10. Yb-169g
7.11. Lu-177g
7.12. Re-186g
7.13. Ir-192g
7.14. At-211, At-210 (impurity)
7.15. Ac-225

All of the experimental data have been assembled and evaluated for each charged particle induced reaction considered. After detailed assessment, only the most reliable data were used in the evaluations, as described below. Recommended excitation functions are presented that agree closely with measurements. Other important reactions that generate impurities have also been treated in the same manner.

Averaging and fitting methods were adopted in the evaluation of the charged particle induced reactions. However, only partial success was achieved in reproducing the experimental data by modelling calculations and, therefore, greater reliance was placed on the data fitting methods.

The resulting evaluated data in this section are given in graphical and numerical form. Calculated yields of these cyclotron-produced radionuclides are also given.

7.1. CHARGED PARTICLE PRODUCTION OF ^{64}Cu

Copper-64 is one of the most important emerging therapeutic radionuclides. This radionuclide is normally used as a dual purpose agent, permitting the combination of therapy and positron emission tomography (PET). Several hypoxin (^{64}Cu-ASTM), blood perfusion (^{64}Cu-PTSM) and cancer imaging tracers (^{64}Cu labelled antibodies and peptides) have been studied.

A. Decay data

The decay scheme for ^{64}Cu has recently been evaluated [7.1], and the applicable updates to the decay data are incorporated in this assessment. A simplified decay scheme is shown in Fig. 7.1 and the main emissions, as defined in Table 7.1, were taken from NuDat 2.4 [7.3].

B. Production routes

Copper-64 was originally produced by means of the ^{63}Cu(n, γ)^{64}Cu reaction (an evaluation of the data for this reaction is given in Section 6.3.3). However, the low specific activity achieved in this process has resulted in alternative routes of production being developed, as specified in Table 7.2.

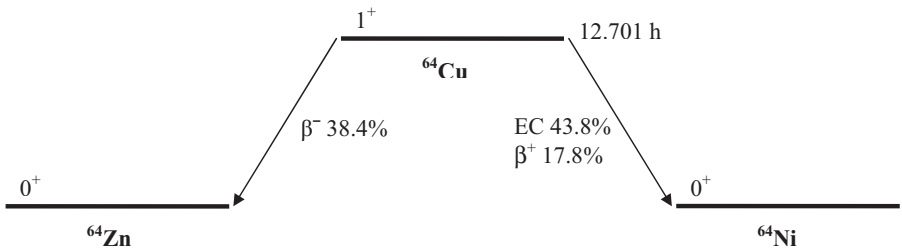

FIG. 7.1. Simplified decay scheme of ^{64}Cu [7.1, 7.3].

TABLE 7.1. MAIN EMISSIONS [7.1–7.3]

Cu-64	Decay mode:	EC 43.8% β^+ 17.8% [7.1] β^- 38.4%
	$T_{1/2}$:	12.701 h
Radiation	Intensity	Energy (MeV)
β^+	1.78×10^{-01} [7.1]	2.782×10^{-01} [a] 6.531×10^{-01} [b]
$\gamma^{\pm}$	3.45×10^{-01} [7.1]	5.110×10^{-01}
γ 1	5.4×10^{-03} [7.1]	1.346
$K_{\alpha 1}$ X ray	9.47×10^{-02}	7.478×10^{-03}
$K_{\alpha 2}$ X ray	4.85×10^{-02}	7.461×10^{-03}
K_{β} X ray	1.97×10^{-02}	8.260×10^{-03} [a]
L X ray	4.86×10^{-03}	8.500×10^{-04} [a]
Auger-K	2.24×10^{-01}	6.540×10^{-03} [a]
Auger-L	5.74×10^{-01}	8.400×10^{-04} [a]
β^-	3.84×10^{-01} [7.1]	1.902×10^{-01} [a] 5.787×10^{-01} [b]

[a] Average energy (MeV).
[b] End point energy (MeV).

TABLE 7.2. INVESTIGATED PRODUCTION ROUTES [7.3, 7.4]

Target isotope	Natural abundance	Reaction	Q-value (MeV)	Threshold energy (MeV)
Ni-64	0.926%	(p, n)	–2.5	2.5
		(d, 2n)	–4.7	4.8
Zn-nat	^{64}Zn 48.63%	(d, 2p)	–2.0	2.1
	^{66}Zn 27.90%	(d, α)	7.2	0.0
	^{67}Zn 4.10%	(d, αn)	0.2	0.0
	^{68}Zn 18.75%	(d, α2n)	–10.0	10.3
	^{70}Zn 0.62%	(d, α4n)	–25.7	26.5
Zn-68	18.75%	(p, αn)	–7.8	7.9

C. ^{64}Ni(p, n)^{64}Cu reaction

BIBLIOGRAPHY, EVALUATION AND SELECTION

Cross-sections

BLASER, J.P., BOEHM, F., MARMIER, P., SCHERRER, P., Anregungsfunktionen und Wirkungsquerschnitte der (p,n)-Reaktion (II), Helv. Phys. Acta **24** (1951) 441–464.
EXFOR: P0033

BLOSSER, H.G., HANDLEY, T.H., Survey of (p,n) reactions at 12 MeV, Phys. Rev. **100** (1955) 1340–1344.
EXFOR: B0052
Detected particles: β^+ and β^- (Σ 58%). A single data point at 12 MeV was given with a large uncertainty (37%) and too high a value; therefore, data were rejected.

TANAKA, S., FURUKAWA, M., Excitation functions for (p,n) reactions with titanium, vanadium, chromium, iron and nickel up to 14 MeV, J. Phys. Soc. Jpn **14** (1959) 1269–1275.
EXFOR: B0043
Detected particles: β^+ and β^- (Σ 57%). Rejected because of energy shift and scattered values.

TREYTL, W.J., CARETTO Jr., A.A., Study of (p,n) reactions between 100 and 400 MeV, Phys. Rev. **146** (1966) 836–840.
EXFOR: C0389
Measuring method: β–γ coincidence. This cross-section measurement above 100 MeV proton energy was rejected.

GUZHOVSKIJ, B.Ja., et al., Isospin mixing of isobar analog resonances observed for the ^{59,61,63,65}Cu nuclei, Izv. Rossiiskoi Akademii Nauk, Ser. Fiz. **33** (1969) 129–144.
EXFOR: F0704
Scintillation detector.

TANAKA, S., FURUKAWA, M., CHIBA, M., Nuclear reactions of nickel with protons up to 56 MeV, J. Inorg. Nucl. Chem. **34** (1972) 2419–2426.
Exfor: B0020
Detected particles: β^+ (19%), β^- (38%) and annihilation radiation.

NEMASHKALO, B.A., MEL'NIK, Yu.P., STORIZHKO, V.E., SHEBEKO, K.V., Radiative capture of protons by ^{54}Cr and ^{64}Ni near the (p,n) threshold, Sov. J. Nucl. Phys. (Engl. Transl.) **37** (1983) 1–6.
EXFOR: A0112
Detected radiation: γ photon. Data in EXFOR are given incorrectly in μb (should be mb) and, therefore, are a factor of 1000 too low. Partial (p, nγ_i) cross-sections were measured near the threshold of the reaction for three prompt γ energies. This data set was set aside from the compilation. Nevertheless, after fitting the three partial excitation functions and summing these data, the cross-sections supported the other measurements.

SEVIOR, M.E., MITCHELL, L.W., ANDERSON, M.R., TINGWELL, C.W., SARGOOD, D.G., Absolute cross sections of proton induced reactions on ^{65}Cu, ^{64}Ni, ^{63}Cu, Aust. J. Phys. **36** (1983) 463–471.
EXFOR: A0198
Detected particle: neutron.

LEVKOVSKIJ, V.N., "Activation cross-section nuclides of average masses (A = 40 - 100) by protons and alpha-particles with average energies (E = 10 - 50 MeV)", Activation Cross Section by Protons and Alphas, Moscow (1991).
EXFOR: A0510
Ge(Li) detector.
*Cross-sections must be normalized by a factor of 0.8 as noted by Takács, S., Tárkányi, F., Sonck, M., Hermanne, A., Investigation of the ^{nat}Mo(p,x)^{96mg}Tc nuclear reaction to monitor proton beams: New measurements and consequences on the earlier reported data, Nucl. Instrum. Methods B **198** (2002) 183–196.*

ANTROPOV, A.E., et al., Total cross sections of (p,n) reaction on the nuclei of isotopes nickel and zinc at e/p = 5 - 6 MeV, Izv. Rossiiskoi Akademii Nauk, Ser. Fiz. **56** (1992) 198–205.
EXFOR: A0543
Detected radiation: 1346 keV γ photon. Data are only given around the sharp resonance at about 5.1 MeV.

SZELECSÉNYI, F., BLESSING, G., QAIM, S.M., Excitation functions of proton induced nuclear reactions on enriched ^{61}Ni and ^{64}Ni: Possibility of production of no-carrier-added ^{61}Cu and ^{64}Cu at a small cyclotron, Appl. Radiat. Isot. **44** (1993) 575–580.
EXFOR: D4020
Detected radiation: annihilation radiation (36%).
*Data of ^{nat}Cu(p, x)^{62}Zn monitor reaction were taken from IAEA report INDC(NDS)-218/GZ (1989) which needed to be updated. These original data were multiplied by a factor of 1.15 in agreement with the authors and according to the studies of Takács, S., Tárkányi, F., Sonck, M., Hermanne, A., New cross sections and intercomparison of proton monitor reactions on Ti, Ni and Cu, Nucl. Instrum. Methods B **188** (2002) 106–111.*

Yield

NICKLES, R.J., A shotgun approach to the chart of the nuclides: Radiotracer production with an 11 MeV proton cyclotron, Acta Radiologica Suppl. **376** (1991) 69–71.
EXFOR: no
Target: natural Ni.

McCARTHY, D.W., et al., Efficient production of high specific activity ^{64}Cu using a biomedical cyclotron, Nucl. Med. Biol. **24** (1997) 35–43.
EXFOR: no

OBATA, A., et al., Production of therapeutic quantities of ^{64}Cu using a 12-MeV cyclotron, Nucl. Med. Biol. **30** (2003) 535–539.
EXFOR: no

AVILA-RODRIGUEZ, M.A., NYE, J.A., NICKLES, R.J., Simultaneous production of high specific activity ^{64}Cu and ^{61}Co with 11.4 MeV protons on enriched ^{64}Ni nuclei, Appl. Radiat. Isot. **65** (2007) 1115–1120.
EXFOR: no

All experimental cross-section data are shown in Fig. 7.2, and the selected measurements are compared with the resulting statistical fit to these data in Fig. 7.3. Excitation functions have been calculated by means of the ALICE-IPPE, EMPIRE and GNASH nuclear reaction modelling codes, and results are compared with all of the selected experimental data in Fig. 7.4. Yields determined from the recommended cross-sections are presented in Fig. 7.5, while corresponding numerical values for the recommended cross-sections and yields are listed in Table 7.3.

D. ^{64}Ni(d, 2n)^{64}Cu reaction

Only one set of experimental data is available in the literature before 2007 for the ^{64}Ni(d, 2n)^{64}Cu reaction (Zweit et al. (1991)). Cross-sections were measured by the authors for deuterons incident on ^{nat}Ni. Monitor cross-section

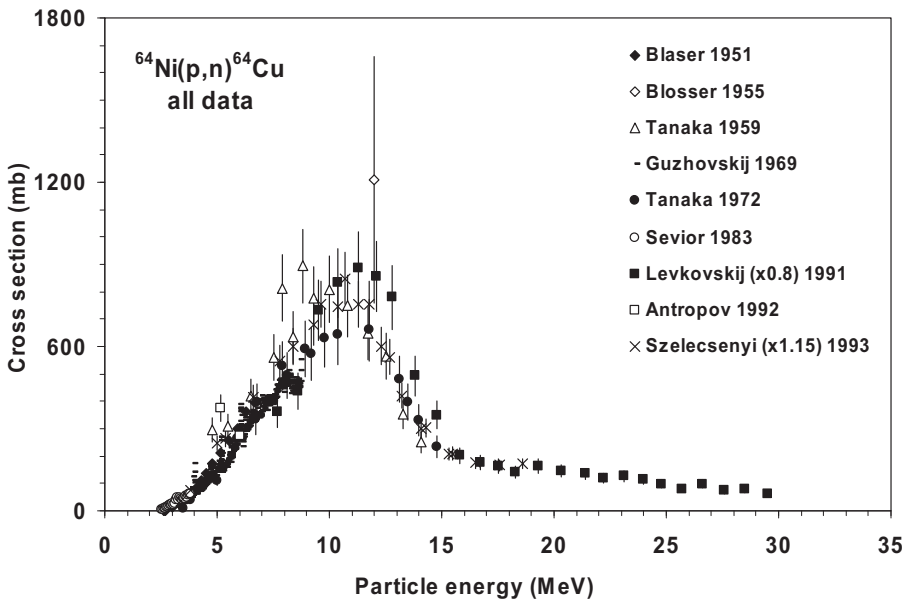

FIG. 7.2. All experimental data.

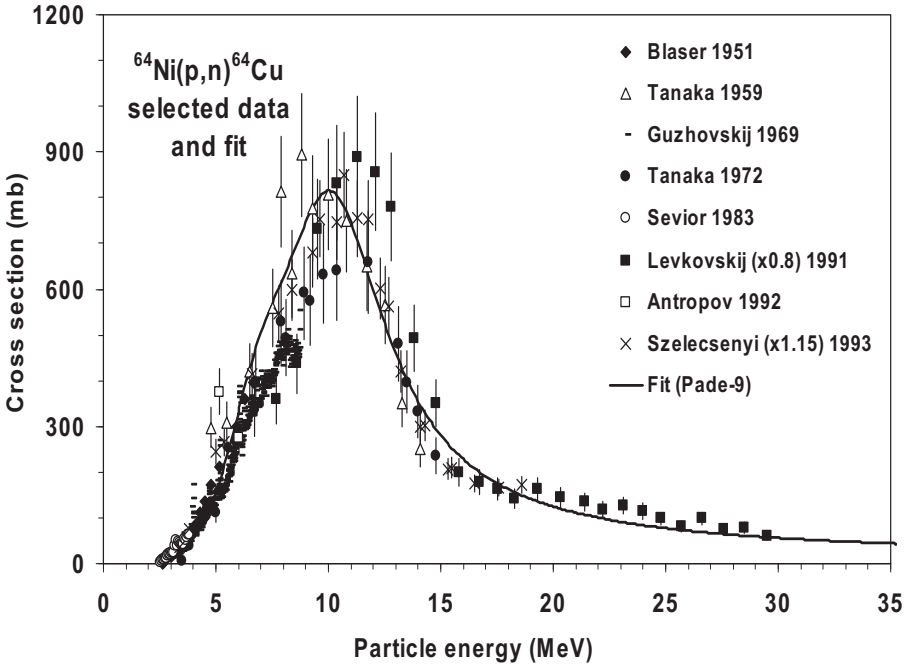

FIG. 7.3. Selected experimental data and the recommended curve (fit).

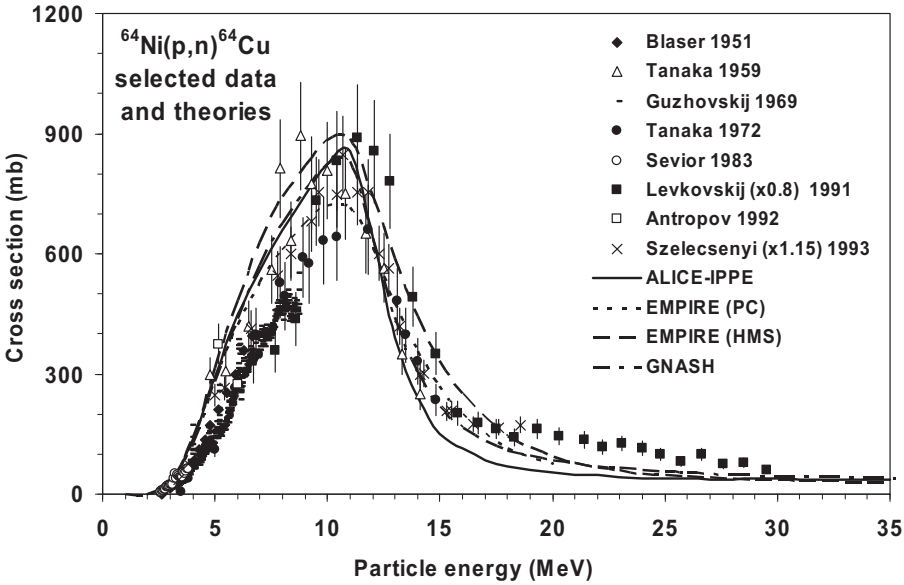

FIG. 7.4. Selected experimental data and theoretical calculations.

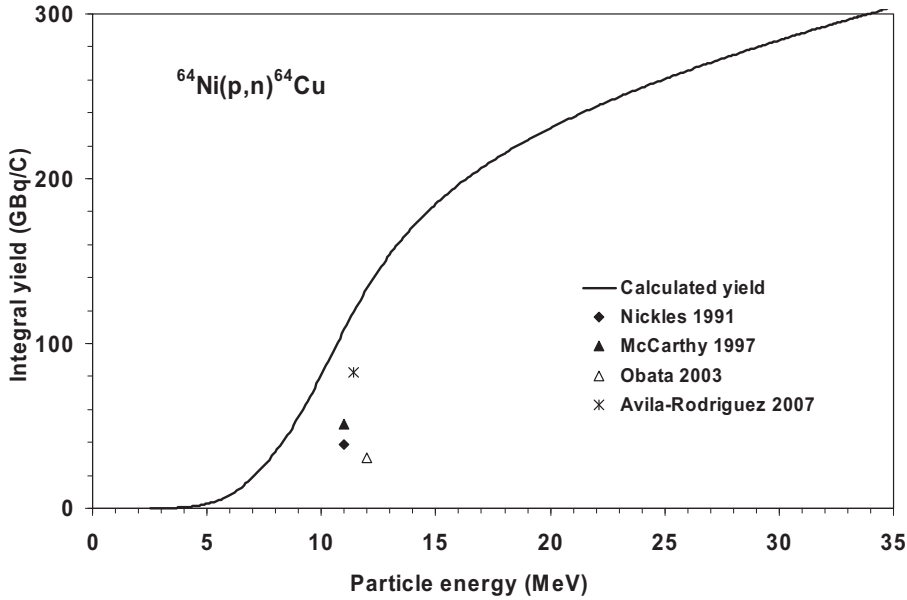

FIG. 7.5. Calculated integral yield curve based on the recommended cross-sections.

TABLE 7.3. RECOMMENDED CROSS-SECTIONS AND INTEGRAL YIELDS

^{64}Ni(p, n)^{64}Cu energy (MeV)	Cross-section (mb)	Integral yield	
		(μCi/μAh)	(GBq/C)
2.5	0	0	0
3.0	10	3	0
3.5	29	19	0
4.0	56	56	1
4.5	97	127	1
5.0	156	254	3
5.5	236	463	5
6.0	331	786	8
6.5	425	1241	13
7.0	504	1827	19
7.5	568	2534	26
8.0	626	3356	34
8.5	687	4302	44
9.0	747	5379	55

TABLE 7.3. RECOMMENDED CROSS-SECTIONS AND INTEGRAL YIELDS (cont.)

$^{64}Ni(p, n)^{64}Cu$ energy (MeV)	Cross-section (mb)	Integral yield	
		(μCi/μAh)	(GBq/C)
9.5	795	6583	68
10.0	815	7889	81
10.5	797	9239	95
11.0	747	10 568	109
11.5	676	11 831	122
12.0	599	12 995	134
12.5	525	14 050	144
13.0	459	15 000	154
13.5	402	15 857	163
14.0	354	16 630	171
14.5	314	17 333	178
15.0	281	17 975	185
15.5	252	18 564	191
16.0	228	19 110	196
16.5	208	19 619	202
17.0	191	20 094	207
17.5	176	20 541	211
18.0	163	20 963	215
18.5	151	21 362	220
19.0	141	21 743	223
19.5	132	22 106	227
20.0	125	22 453	231
20.5	118	22 787	234
21.0	111	23 108	238
21.5	106	23 418	241
22.0	100	23 718	244
22.5	96	24 009	247
23.0	91	24 291	250
23.5	87	24 565	252
24.0	84	24832	255
24.5	80	25 092	258
25.0	77	25 347	261

data used for the determination of the deuteron flux are in good agreement with IAEA evaluated data. The cross-section data shown in Figs 7.6–7.8 are normalized for deuterons incident on enriched ^{64}Ni. Another upward adjustment of 7% was made to account for the most recently reported value of 17.8% for the total β^+ intensity of ^{64}Cu [7.1]. Old measurements agree reasonably well with newer measurements reported in 2007 (Takacs et al. (2007), Hermanne et al. (2007)). Cross-sections predicted by theoretical calculations are higher than the measured data by almost a factor of two, as can be seen in Fig. 7.8. This discrepancy is partly explained by the fact that the deuteron break-up channel is not considered in those calculations.

The same authors who reported the older set of measured cross-sections also measured ^{64}Cu yields in the 15 to 19 MeV energy window on ^{nat}Ni and 96% enriched ^{64}Ni (Zweit et al. (1991)). However, these thick-target yield measurements do not support their cross-section data. Integral ^{64}Cu yields for the 15 to 19 MeV energy range predicted on the basis of their reported cross-sections are much lower than their reported thick-target yields. At most, the relative values resulting from their yield measurements confirm the expected relative ^{64}Ni abundance in the targets used in the measurements. Therefore, users of the recommended curve for the ^{64}Ni(d, 2n)^{64}Cu reaction should be aware that

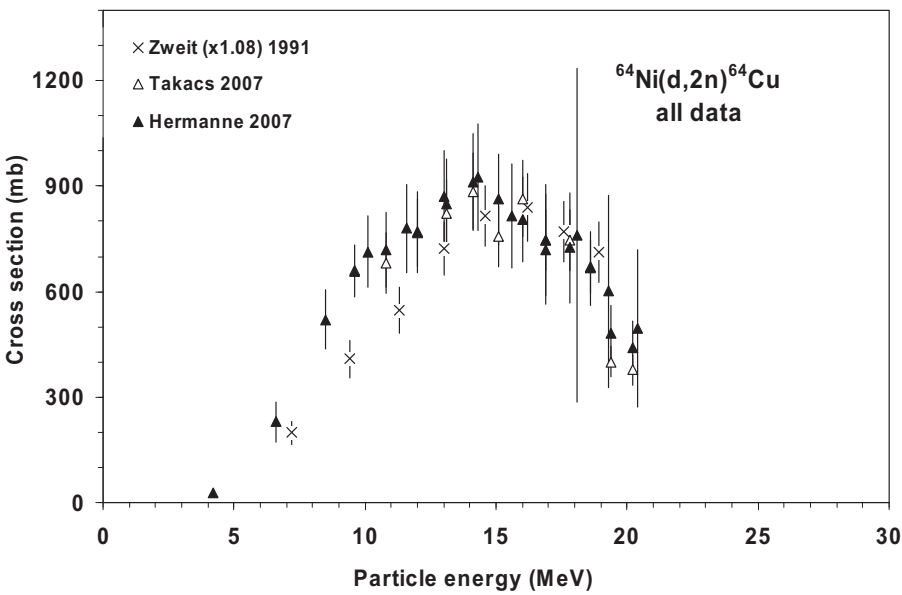

FIG. 7.6. All experimental data.

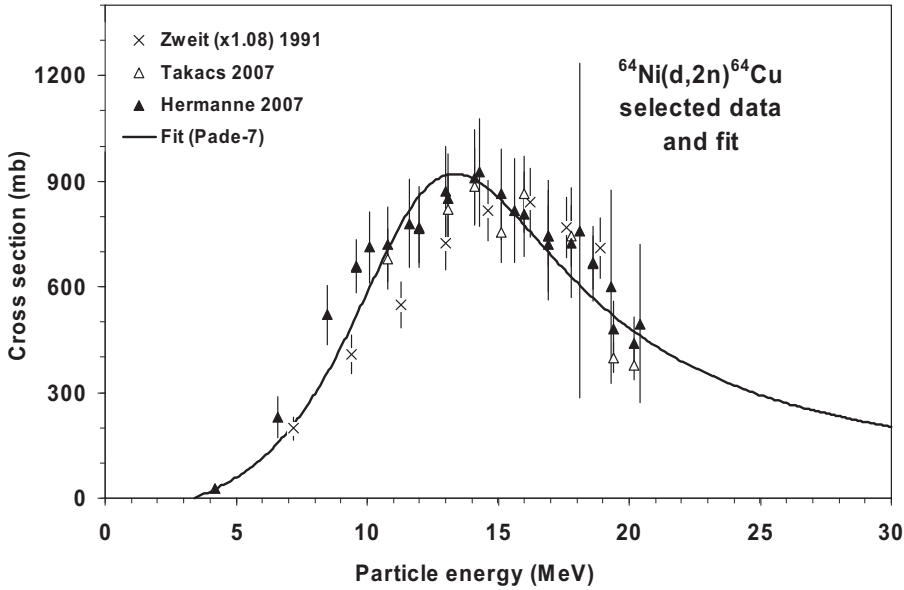

FIG. 7.7. Selected experimental data and the recommended curve (fit).

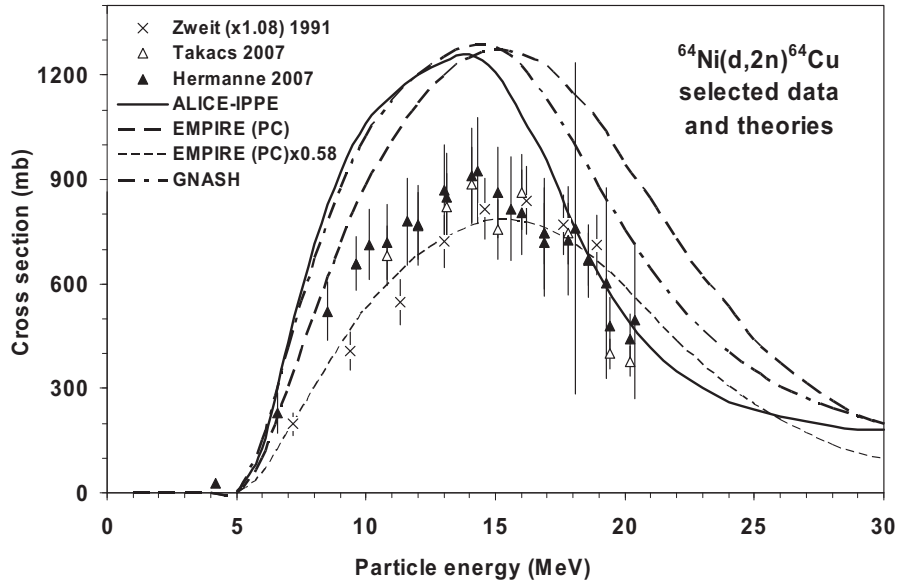

FIG. 7.8. Selected experimental data and theoretical calculations.

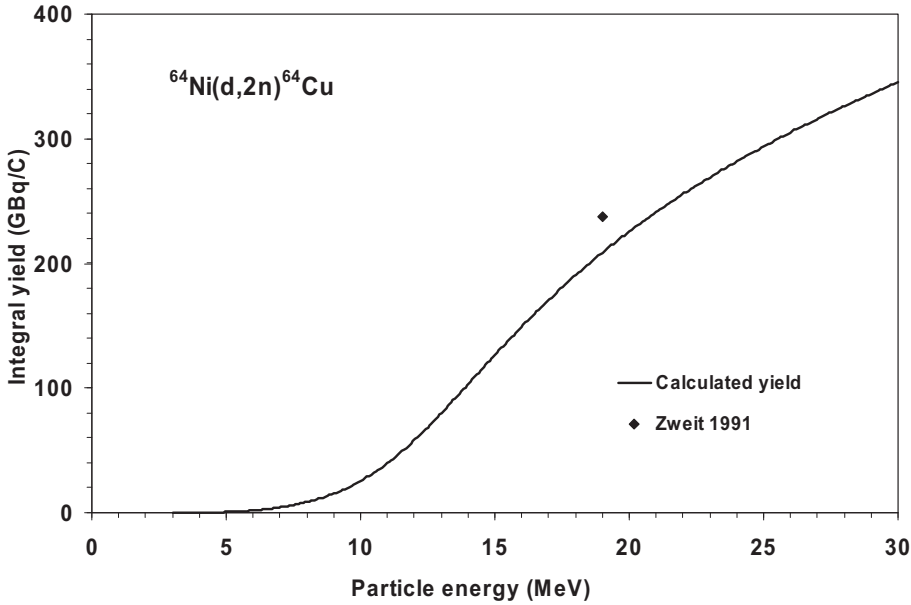

FIG. 7.9. Calculated integral yield curve based on the recommended cross-sections.

independent experimental thick-target yield measurements are still required for comparison before the present recommended data can be used with confidence. Yields determined from the recommended cross-sections are presented in Fig. 7.9, while corresponding numerical values for the recommended cross-sections and yields are listed in Table 7.4.

BIBLIOGRAPHY, EVALUATION AND SELECTION

Cross-sections

ZWEIT, J., SMITH, A.M., DOWNEY, S., SHARMA, H.L., Excitation functions for deuteron induced reactions in natural nickel: Production of no-carrier-added ^{64}Cu from enriched ^{64}Ni targets for positron emission tomography, Appl. Radiat. Isot. **42** (1991) 193–197.
EXFOR: D4056
Detected radiation: annihilation radiation (38%). Target: natural Ni.
Original data were multiplied by 1.08 in accordance with the 38/35.2 ratio of the intensity of the annihilation radiation.

TABLE 7.4. RECOMMENDED CROSS-SECTIONS AND INTEGRAL YIELDS

^{64}Ni(d, 2n)^{64}Cu energy (MeV)	Cross-section (mb)	Integral yield	
		(μCi/μAh)	(GBq/C)
3.0	0	0	0
3.5	3	0	0
4.0	19	7	0
4.5	37	24	0
5.0	58	54	1
5.5	84	102	1
6.0	114	172	2
6.5	150	271	3
7.0	191	405	4
7.5	240	582	6
8.0	295	812	8
8.5	358	1104	11
9.0	428	1469	15
9.5	504	1918	20
10.0	583	2462	25
10.5	662	3105	32
11.0	738	3851	40
11.5	805	4697	48
12.0	859	5638	58
12.5	897	6658	68
13.0	917	7740	80
13.5	921	8861	91
14.0	909	10 007	103
14.5	886	11 160	115
15.0	853	12 302	126
15.5	816	13 422	138
16.0	775	14 512	149
16.5	733	15 568	160
17.0	691	16 591	171
17.5	651	17 574	181

TABLE 7.4. RECOMMENDED CROSS-SECTIONS AND INTEGRAL YIELDS (cont.)

^{64}Ni(d, 2n)^{64}Cu energy (MeV)	Cross-section (mb)	Integral yield	
		(μCi/μAh)	(GBq/C)
18.0	613	18 518	190
18.5	577	19 425	200
19.0	543	20 294	209
19.5	512	21 132	217
20.0	483	21 937	225
20.5	456	22 710	233
21.0	432	23 455	241
21.5	409	24 172	248
22.0	389	24 864	256
22.5	369	25 533	262
23.0	352	26 181	269
23.5	335	26 808	276
24.0	320	27 416	282
24.5	306	28 005	288
25.0	293	28 578	294
25.5	281	29 134	299
26.0	270	29 676	305
26.5	259	30 205	310
27.0	250	30 721	316
27.5	240	31 225	321
28.0	232	31 716	326
28.5	224	32 197	331
29.0	216	32 667	336
29.5	209	33 128	340
30.0	202	33 579	345

TAKÁCS, S., TÁRKÁNYI, F., KIRÁLY, B., HERMANNE, A., SONCK, M., Evaluated activation cross sections of longer-lived radionuclides produced by deuteron induced reactions on natural nickel, Nucl. Instrum. Methods B **260** (2007) 495–507.
EXFOR: D4178
Detected radiation: 1345.8 keV γ (0.473%). Target: natural Ni.

HERMANNE, A., TÁRKÁNYI, F., TAKÁCS, S., KOVALEV, S.F., IGNATYUK, A., Activation cross sections of the ^{64}Ni(d,2n) reaction for the production of the medical radionuclide ^{64}Cu, Nucl. Instrum. Methods B **258** (2007) 308–312.
EXFOR: D4182
Detected radiation: 1345 keV γ (0.47%). Target: natural Ni.

Yield

ZWEIT, J., SMITH, A.M., DOWNEY, S., SHARMA, H.L., Excitation functions for deuteron induced reactions in natural nickel: Production of no-carrier-added ^{64}Cu from enriched ^{64}Ni targets for positron emission tomography, Appl. Radiat. Isot **42** (1991) 193–197.
EXFOR: D4056

E. ^{nat}Zn(d, x)^{64}Cu reaction

Five groups reported measurements on ^{nat}Zn for the ^{nat}Zn(d, x)^{64}Cu production route (Williams et al. (1963), Hilgers et al. (2003), Bonardi et al. (2003), Groppi et al. (2004) and Tárkányi et al. (2004)) and data are presented in Fig. 7.10. The Italian group (Bonardi et al. (2003) and Groppi et al. (2004)) and Tárkányi et al. (2004) counted the irradiated foils directly by means of the 1346 keV gamma line. Hilgers et al. (2003) performed chemical separations and counted the samples using coincidence counting of the 511 keV gamma emission. The cross-section values were adjusted to account for the most recent ^{64}Cu decay data [7.1]. Significant discrepancies exist with the Hilgers data, especially near the threshold of the reaction. Following communication with the authors of the Hilgers et al. (2003) paper, their measurements on ^{nat}Zn were ignored. The remaining four data sets were selected for Padé fit as shown in Fig. 7.11. Figure 7.12 compares the four selected data sets with a theoretical curve obtained by means of the ALICE-IPPE code. While all four data sets are accepted for the determination of the recommended curve, users are reminded to use the recommended data with caution near the threshold. The recommended integral yield shows good agreement with Dmitriev et al. (1982) thick-target measurements as seen in Fig. 7.13, while corresponding numerical values for the recommended cross-sections and yields are listed in Table 7.5.

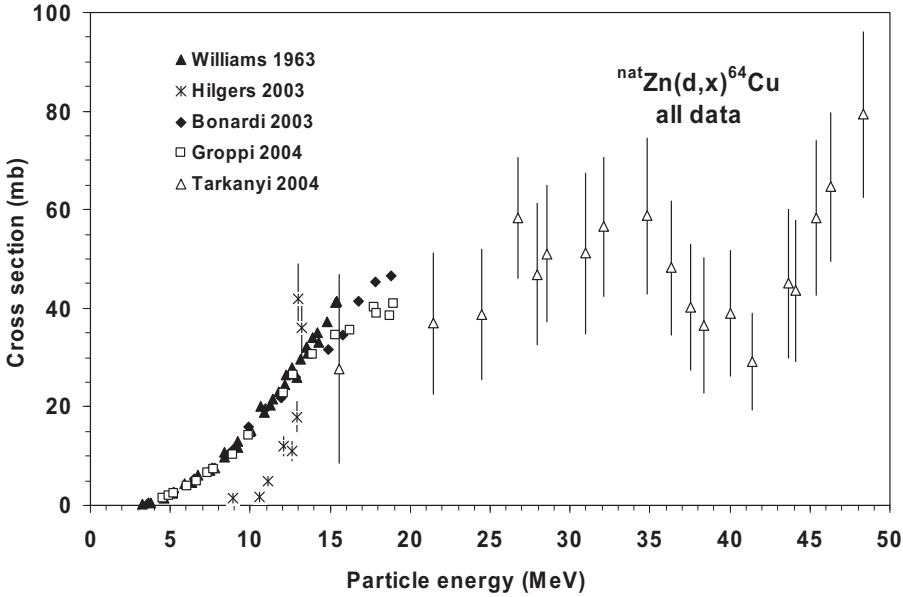

FIG. 7.10. All experimental data.

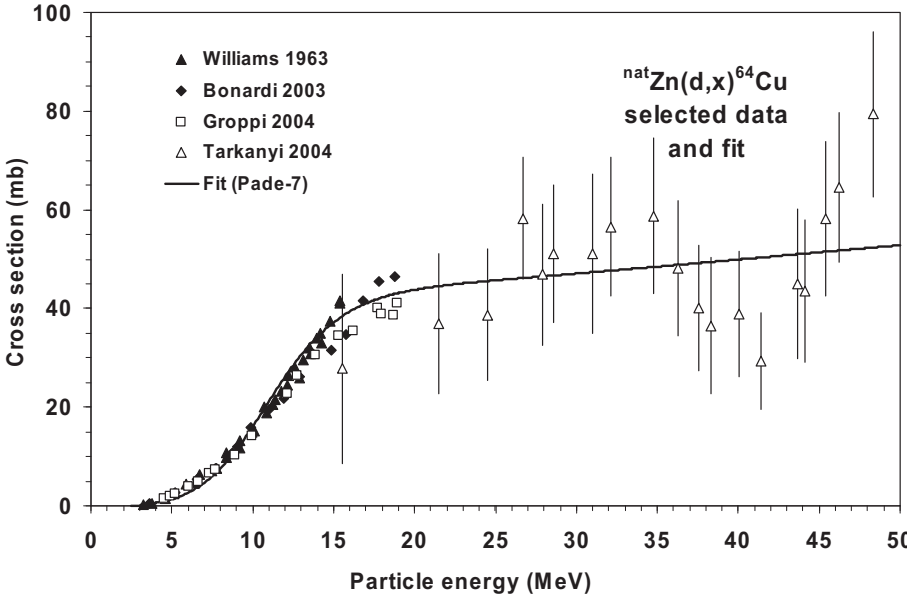

FIG. 7.11. Selected experimental data and the recommended curve (fit).

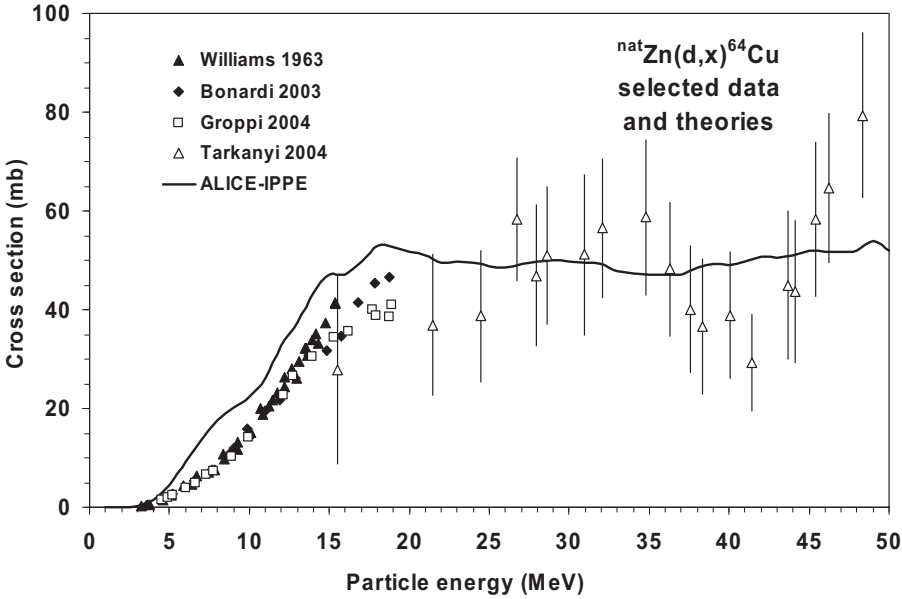

FIG. 7.12. Selected experimental data and theoretical calculations.

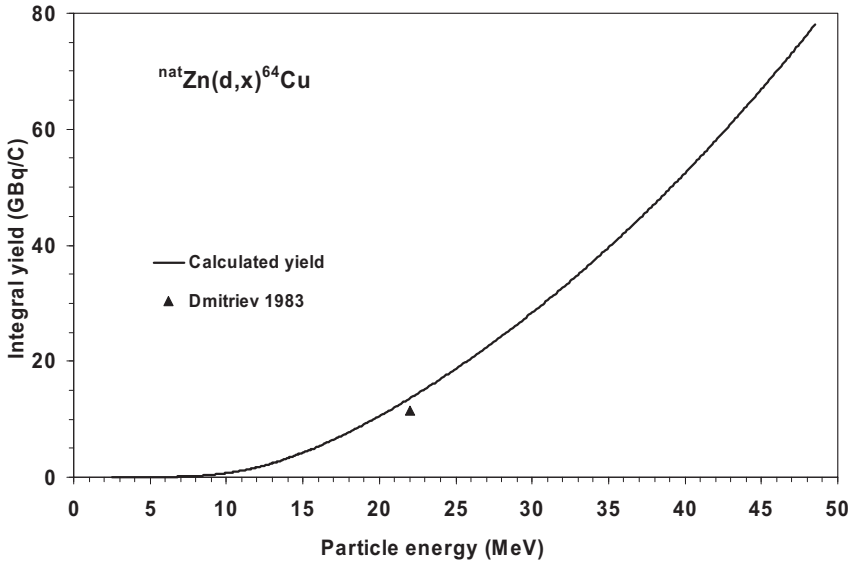

FIG. 7.13. Calculated integral yield curve based on the recommended cross-section.

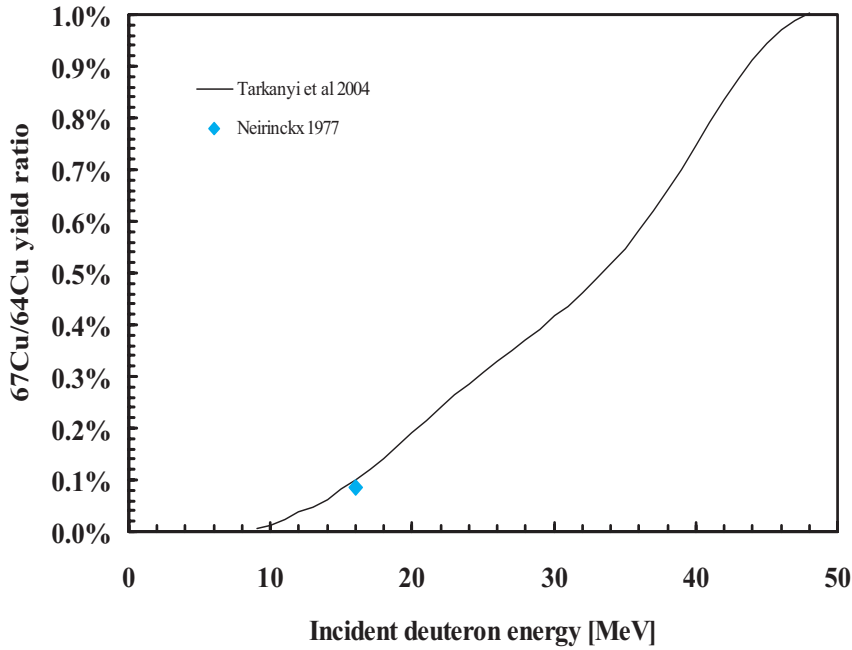

FIG. 7.14. $^{67}Cu/^{64}Cu$ thick-target yield ratio for the $^{nat}Zn(d, x)^{64}Cu$ reaction.

The co-production of ^{67}Cu is of concern in the case of the $^{nat}Zn(d, x)^{64}Cu$ reaction and, therefore, thick-target yield curves were calculated from the data of Tárkányi et al. (2004) in order to evaluate the expected impurity levels. These curves and the thick-target yield measurement by Neirinckx et al. (1977) were used in the impurity evaluation. The ^{67}Cu impurity levels obtained on a thick target are presented in Fig. 7.14 and show good agreement. These data show that ^{64}Cu purity of >99% is achievable up to 48 MeV deuteron energy for short irradiations. However, when longer bombardment times and appropriate decay times are required, the useful energy range to maintain a 99% purity level shifts to lower values and must be taken into account by the user.

BIBLIOGRAPHY, EVALUATION AND SELECTION

Cross-sections

WILLIAMS, D.C., IRVINE Jr., J.W., Nuclear excitation functions and thick-target yields: Zn+d and $^{40}Ar(d,\alpha)$, Phys. Rev. **130** (1963) 265–271.
EXFOR: R0038

TABLE 7.5. RECOMMENDED CROSS-SECTIONS AND INTEGRAL YIELDS

$^{nat}Zn(d, x)^{64}Cu$ energy (MeV)	Cross-section (mb)	Integral yield	
		(μCi/μAh)	(GBq/C)
2.5	0.0	0	0.00
3.0	0.1	0	0.00
3.5	0.3	0	0.00
4.0	0.6	0	0.00
4.5	0.9	1	0.01
5.0	1.4	2	0.02
5.5	1.9	3	0.03
6.0	2.7	5	0.05
6.5	3.6	7	0.08
7.0	4.7	11	0.11
7.5	6.0	16	0.16
8.0	7.6	22	0.22
8.5	9.4	30	0.31
9.0	11.5	40	0.41
9.5	13.7	53	0.54
10.0	16.1	68	0.70
10.5	18.6	87	0.89
11.0	21.2	109	1.12
11.5	23.7	134	1.38
12.0	26.2	163	1.68
12.5	28.5	196	2.01
13.0	30.6	232	2.38
13.5	32.6	271	2.79
14.0	34.3	314	3.23
14.5	35.8	360	3.70
15.0	37.2	409	4.20
15.5	38.4	460	4.73
16.0	39.4	514	5.29
16.5	40.3	571	5.87
17.0	41.0	630	6.47
17.5	41.7	691	7.10

TABLE 7.5. RECOMMENDED CROSS-SECTIONS AND INTEGRAL YIELDS (cont.)

$^{nat}Zn(d, x)^{64}Cu$ energy (MeV)	Cross-section (mb)	Integral yield	
		(μCi/μAh)	(GBq/C)
18.0	42.2	754	7.75
18.5	42.7	819	8.42
19.0	43.1	886	9.11
19.5	43.5	955	9.81
20.0	43.8	1025	10.54
20.5	44.0	1097	11.28
21.0	44.3	1171	12.04
21.5	44.5	1247	12.81
22.0	44.7	1324	13.61
22.5	44.9	1402	14.41
23.0	45.1	1482	15.24
23.5	45.3	1564	16.07
24.0	45.4	1647	16.93
24.5	45.6	1732	17.80
25.0	45.7	1818	18.68
25.5	45.9	1906	19.58
26.0	46.0	1995	20.50
26.5	46.1	2085	21.43
27.0	46.3	2177	22.38
27.5	46.4	2271	23.34
28.0	46.5	2366	24.32
28.5	46.7	2462	25.31
29.0	46.8	2560	26.31
29.5	46.9	2660	27.34
30.0	47.1	2761	28.37
30.5	47.2	2863	29.43
31.0	47.4	2967	30.50
31.5	47.5	3073	31.58
32.0	47.6	3180	32.68
32.5	47.8	3289	33.80
33.0	47.9	3399	34.93

TABLE 7.5. RECOMMENDED CROSS-SECTIONS AND INTEGRAL YIELDS (cont.)

$^{nat}Zn(d, x)^{64}Cu$ energy (MeV)	Cross-section (mb)	Integral yield	
		(μCi/μAh)	(GBq/C)
33.5	48.1	3510	36.08
34.0	48.2	3623	37.24
34.5	48.3	3738	38.42
35.0	48.5	3854	39.61
35.5	48.6	3972	40.82
36.0	48.8	4091	42.05
36.5	48.9	4212	43.29
37.0	49.0	4334	44.55
37.5	49.2	4458	45.82
38.0	49.3	4584	47.11
38.5	49.5	4711	48.42
39.0	49.6	4840	49.74
39.5	49.8	4970	51.08
40.0	49.9	5102	52.43
40.5	50.1	5235	53.80
41.0	50.2	5370	55.19
41.5	50.4	5507	56.60
42.0	50.5	5645	58.02
42.5	50.7	5785	59.45
43.0	50.8	5928	60.93
43.5	50.9	6071	62.40
44.0	51.1	6214	63.86
44.5	51.2	6360	65.37
45.0	51.4	6508	66.89
45.5	51.5	6658	68.43
46.0	51.7	6811	70.01
46.5	51.8	6962	71.55
47.0	52.0	7116	73.14
47.5	52.1	7273	74.75
48.0	52.2	7433	76.39
48.5	52.4	7590	78.01

HILGERS, K., STOLL, T., SKAKUN, Y., COENEN, H.H., QAIM, S.M., Cross-section measurements of the nuclear reactions $^{nat}Zn(d,x)^{64}Cu$, $^{66}Zn(d,\alpha)^{64}Cu$ and $^{68}Zn(p,\alpha n)^{64}Cu$ for production of ^{64}Cu and technical developments for small-scale production of ^{67}Cu via the $^{70}Zn(p,\alpha)^{67}Cu$ process, Appl. Radiat. Isot. **59** (2003) 343–351.
EXFOR: D0069
Detected radiation: annihilation radiation (38%). Measurements on ^{nat}Zn were rejected because of the large disagreement with other equivalent data.

BONARDI, M.L., et al., Thin-target excitation functions and optimization of simultaneous production of NCA copper-64 and gallium-66,67 by deuteron induced nuclear reactions on a natural zinc target, J. Radioanal. Nucl. Chem. **257** (2003) 229–241.
EXFOR: no
Detected radiation: 1345.84 keV γ photon (0.473%). Measured yields were converted to cross-section data.

GROPPI, F., et al., Thin-target excitation functions and optimisation of NCA ^{64}Cu and $^{66,67}Ga$ production by deuteron induced nuclear reactions on natural zinc target, for radiometabolic therapy and for PET, Nucl. Instrum. Methods B **213** (2004) 373–377.
EXFOR: O0778 (data of ^{61}Cu and ^{64}Cu are mixed up in the EXFOR database)
Detected radiation: 1345.84 keV γ photon (0.473%). Measured yields were converted to cross-section data.

TÁRKÁNYI, F., et al., Excitation functions of deuteron induced nuclear reactions on natural zinc up to 50 MeV, Nucl. Instrum. Methods B **217** (2004) 531–550.
EXFOR: D4144
Detected radiation: 1345.84 keV γ photon (0.473%).

Yield

DMITRIEV, P.P., KRASNOV, M.N., MOLIN, G.A., Yields of Radioactive Nuclides Formed by Bombardment of a Thick Target with 22-MeV Deuterons, INDC(CCP)-210/L (1983), translation from Nuclear Constants **4**(48) (1982) 38.
EXFOR: A0194

NEIRINCKX, R.D., Simultaneous production of ^{67}Cu, ^{64}Cu and ^{67}Ga and labelling of bleomycin with ^{67}Cu or ^{66}Cu, Int. J. Appl. Radiat. Isot. **28** (1977) 802–804.

F. ^{68}Zn(p, 2p3n)^{64}Cu reaction

The ^{68}Zn(p, x)^{64}Cu reaction has been evaluated mainly as a possible route for ^{64}Cu impurity in the production of ^{67}Cu via the ^{68}Zn(p, 2p)^{67}Cu reaction. However, this reaction can also be utilized for the production of ^{64}Cu. Three measured cross-section data sets exist for the ^{68}Zn(p, x)^{64}Cu reaction (Levkovskij et al. (1991), Hilgers et al. (2003) and Szelecsényi et al. (2005)) and are shown in Figs 7.15 and 7.16. All of the data were adjusted in order to account for the most recent ^{64}Cu decay data [7.1]. The measurements by Levkovskij were also adjusted downwards by 20%. The data of Hilgers et al. (2003) in the energy range of 23 to 35 MeV were deleted due to systematic errors in that energy range (information from authors). Figure 7.17 compares an ALICE-IPPE and EMPIRE-HMS calculation with the measured data, and demonstrates that there is generally good agreement. Due to the production of the ^{67}Cu impurity at higher energies, the user should be aware that the useful energy range for the production of ^{64}Cu is below 40 MeV. Yields determined from the recommended cross-sections are presented in Fig. 7.18, while corresponding numerical values for the recommended cross-sections and yields are listed in Table 7.6.

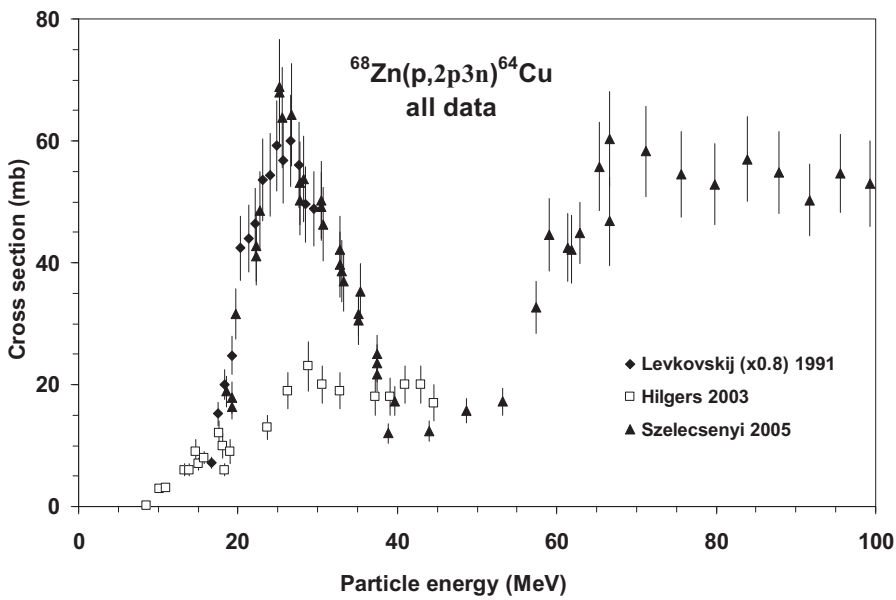

FIG. 7.15. All experimental data.

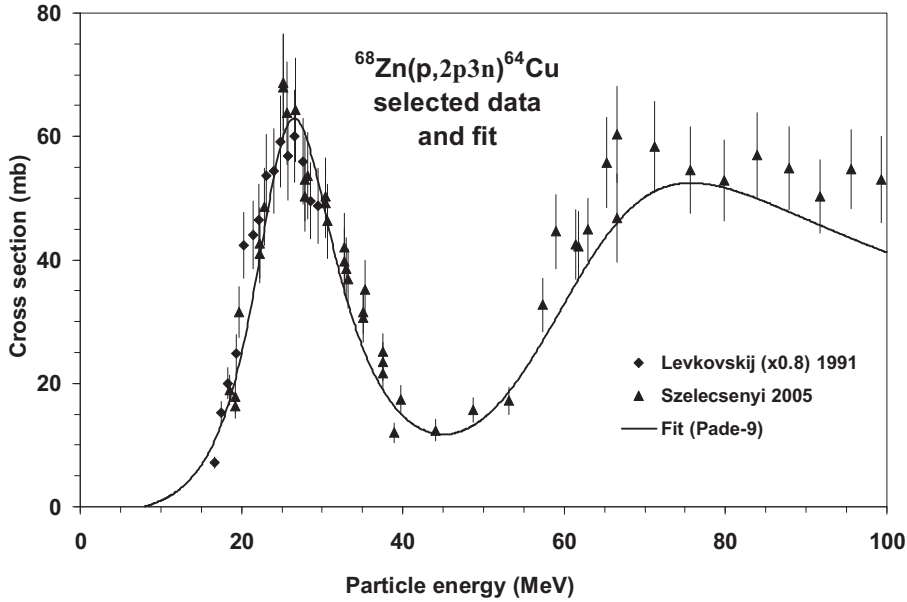

FIG. 7.16. Selected experimental data and the recommended curve (fit).

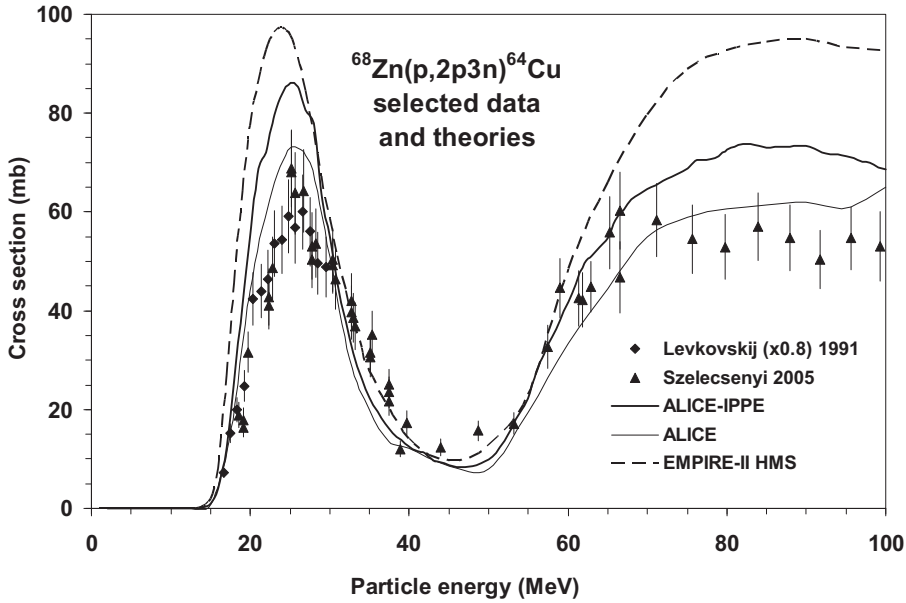

FIG. 7.17. Selected experimental data and theoretical calculations.

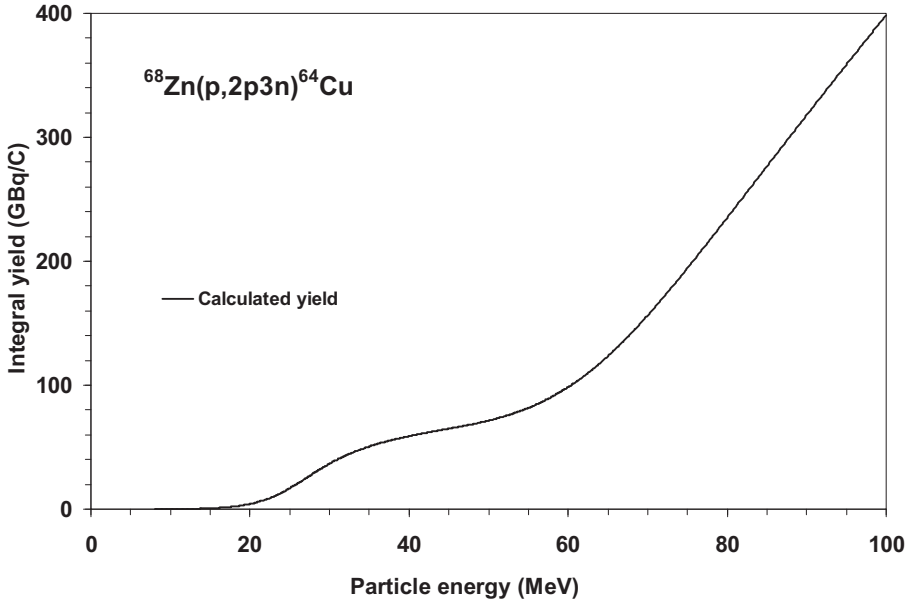

FIG. 7.18. Calculated integral yield curve based on the recommended cross-sections.

TABLE 7.6. RECOMMENDED CROSS-SECTIONS AND INTEGRAL YIELDS

^{68}Zn(p, 2p3n)^{64}Cu energy (MeV)	Cross-section (mb)	Integral yield	
		(μCi/μAh)	(GBq/C)
8.0	0.0	0	0.00
8.5	0.2	0	0.00
9.0	0.4	1	0.01
9.5	0.7	2	0.02
10.0	1.0	3	0.03
10.5	1.3	5	0.05
11.0	1.7	7	0.07
11.5	2.1	10	0.11
12.0	2.5	14	0.15
12.5	3.0	19	0.20
13.0	3.6	26	0.26
13.5	4.2	33	0.34

TABLE 7.6. RECOMMENDED CROSS-SECTIONS AND INTEGRAL YIELDS (cont.)

$^{68}Zn(p, 2p3n)^{64}Cu$ energy (MeV)	Cross-section (mb)	Integral yield	
		(μCi/μAh)	(GBq/C)
14.0	5.0	42	0.44
14.5	5.8	53	0.55
15.0	6.7	66	0.68
15.5	7.7	82	0.84
16.0	8.9	100	1.03
16.5	10.2	121	1.25
17.0	11.7	146	1.50
17.5	13.3	176	1.80
18.0	15.1	210	2.15
18.5	17.2	249	2.56
19.0	19.5	295	3.03
19.5	22.0	347	3.57
20.0	24.8	408	4.19
20.5	27.8	477	4.90
21.0	31.1	556	5.72
21.5	34.6	646	6.64
22.0	38.3	747	7.68
22.5	42.2	862	8.86
23.0	46.1	988	10.15
23.5	49.8	1128	11.59
24.0	53.4	1281	13.16
24.5	56.6	1446	14.86
25.0	59.2	1623	16.68
25.5	61.2	1810	18.61
26.0	62.5	2004	20.60
26.5	62.9	2204	22.65
27.0	62.6	2406	24.72
27.5	61.6	2608	26.81
28.0	60.0	2809	28.87
28.5	57.9	3006	30.89
29.0	55.4	3198	32.87

TABLE 7.6. RECOMMENDED CROSS-SECTIONS AND INTEGRAL YIELDS (cont.)

$^{68}Zn(p, 2p3n)^{64}Cu$ energy (MeV)	Cross-section (mb)	Integral yield	
		(μCi/μAh)	(GBq/C)
29.5	52.7	3383	34.77
30.0	49.9	3561	36.60
30.5	47.0	3731	38.35
31.0	44.1	3893	40.01
31.5	41.4	4047	41.59
32.0	38.7	4193	43.09
32.5	36.2	4331	44.51
33.0	33.8	4461	45.85
33.5	31.6	4585	47.13
34.0	29.5	4702	48.33
34.5	27.6	4813	49.46
35.0	25.9	4917	50.54
35.5	24.2	5017	51.56
36.0	22.8	5111	52.53
36.5	21.4	5200	53.45
37.0	20.1	5285	54.32
37.5	19.0	5366	55.16
38.0	18.0	5444	55.95
38.5	17.0	5518	56.71
39.0	16.2	5589	57.44
39.5	15.4	5658	58.15
40.0	14.8	5724	58.83
40.5	14.2	5788	59.48
41.0	13.6	5849	60.12
41.5	13.2	5910	60.74
42.0	12.8	5969	61.35
42.5	12.4	6027	61.94
43.0	12.2	6084	62.53
43.5	12.0	6141	63.11
44.0	11.8	6197	63.69
44.5	11.7	6254	64.27

TABLE 7.6. RECOMMENDED CROSS-SECTIONS AND INTEGRAL YIELDS (cont.)

$^{68}Zn(p, 2p3n)^{64}Cu$ energy (MeV)	Cross-section (mb)	Integral yield	
		(μCi/μAh)	(GBq/C)
45.0	11.7	6310	64.86
45.5	11.7	6367	65.44
46.0	11.8	6425	66.04
46.5	11.9	6484	66.64
47.0	12.1	6545	67.26
47.5	12.4	6606	67.90
48.0	12.6	6670	68.56
48.5	13.0	6736	69.24
49.0	13.4	6805	69.94
49.5	13.8	6876	70.67
50.0	14.3	6951	71.44
50.5	14.9	7029	72.24
51.0	15.5	7111	73.08
51.5	16.1	7196	73.96
52.0	16.8	7286	74.89
52.5	17.6	7381	75.86
53.0	18.4	7481	76.89
53.5	19.2	7586	77.97
54.0	20.1	7697	79.11
54.5	21.0	7814	80.31
55.0	22.0	7937	81.57
55.5	23.0	8066	82.91
56.0	24.0	8203	84.31
56.5	25.0	8346	85.78
57.0	26.1	8497	87.33
57.5	27.2	8655	88.96
58.0	28.3	8821	90.66
58.5	29.5	8995	92.45
59.0	30.6	9178	94.32
59.5	31.8	9368	96.28
60.0	32.9	9567	98.32

TABLE 7.6. RECOMMENDED CROSS-SECTIONS AND INTEGRAL YIELDS (cont.)

$^{68}Zn(p, 2p3n)^{64}Cu$ energy (MeV)	Cross-section (mb)	Integral yield	
		(μCi/μAh)	(GBq/C)
60.5	34.0	9773	100.45
61.0	35.2	9989	102.67
61.5	36.3	10 213	104.97
62.0	37.4	10 445	107.36
62.5	38.5	10 686	109.83
63.0	39.5	10 935	112.39
63.5	40.6	11 193	115.04
64.0	41.6	11 459	117.77
64.5	42.5	11 733	120.58
65.0	43.4	12 014	123.48
65.5	44.3	12 303	126.45
66.0	45.1	12 601	129.51
66.5	45.9	12 904	132.63
67.0	46.7	13 215	135.82
67.5	47.4	13 533	139.09
68.0	48.0	13 857	142.42
68.5	48.6	14 188	145.82
69.0	49.2	14 524	149.27
69.5	49.7	14 866	152.79
70.0	50.2	15 213	156.36
70.5	50.6	15 566	159.98
71.0	50.9	15 923	163.66
71.5	51.3	16 285	167.37
72.0	51.5	16 651	171.13
72.5	51.8	17 021	174.93
73.0	52.0	17 394	178.78
73.5	52.1	17 771	182.65
74.0	52.3	18 151	186.56
74.5	52.4	18 535	190.50
75.0	52.4	18 920	194.46
75.5	52.5	19 308	198.45

TABLE 7.6. RECOMMENDED CROSS-SECTIONS AND INTEGRAL YIELDS (cont.)

$^{68}Zn(p, 2p3n)^{64}Cu$ energy (MeV)	Cross-section (mb)	Integral yield	
		(μCi/μAh)	(GBq/C)
76.0	52.5	19 699	202.46
76.5	52.4	20 091	206.49
77.0	52.4	20 485	210.54
77.5	52.3	20 881	214.61
78.0	52.2	21 279	218.70
78.5	52.1	21 678	222.80
79.0	52.0	22 077	226.91
79.5	51.8	22 478	231.02
80.0	51.6	22 879	235.15
80.5	51.5	23 281	239.28
81.0	51.3	23 684	243.42
81.5	51.1	24 088	247.57
82.0	50.8	24 491	251.72
82.5	50.6	24 895	255.87
83.0	50.4	25 299	260.02
83.5	50.1	25 703	264.17
84.0	49.9	26 108	268.33
84.5	49.6	26 512	272.49
85.0	49.4	26 916	276.64
85.5	49.1	27 319	280.78
86.0	48.8	27 722	284.93
86.5	48.5	28 126	289.07
87.0	48.3	28 529	293.21
87.5	48.0	28 931	297.35
88.0	47.7	29 333	301.48
88.5	47.4	29 734	305.60
89.0	47.1	30 135	309.72
89.5	46.9	30 536	313.84
90.0	46.6	30 935	317.95
90.5	46.3	31 335	322.05
91.0	46.0	31 734	326.15

TABLE 7.6. RECOMMENDED CROSS-SECTIONS AND INTEGRAL YIELDS (cont.)

$^{68}Zn(p, 2p3n)^{64}Cu$ energy (MeV)	Cross-section (mb)	Integral yield	
		(μCi/μAh)	(GBq/C)
91.5	45.7	32 132	330.24
92.0	45.4	32 529	334.33
92.5	45.2	32 926	338.40
93.0	44.9	33 322	342.48
93.5	44.6	33 718	346.54
94.0	44.3	34 112	350.60
94.5	44.1	34 506	354.65
95.0	43.8	34 899	358.69
95.5	43.5	35 292	362.72
96.0	43.3	35 684	366.75
96.5	43.0	36 075	370.77
97.0	42.7	36 465	374.78
97.5	42.5	36 855	378.79
98.0	42.2	37 245	382.79
98.5	42.0	37 633	386.79
99.0	41.7	38 021	390.77
99.5	41.5	38 408	394.75
100.0	41.2	38 794	398.72

BIBLIOGRAPHY, EVALUATION AND SELECTION

Cross-sections

LEVKOVSKIJ, V.N., "Activation cross-section nuclides of average masses (A = 40 - 100) by protons and alpha-particles with average energies (E = 10 - 50 MeV)", Activation Cross Section by Protons and Alphas, Moscow (1991).
EXFOR: A0510
Cross-sections must be normalized by a factor of 0.8 as pointed out by Takács, S., Tárkányi, F., Sonck, M., Hermanne, A., Investigation of the $^{nat}Mo(p,x)^{96mg}Tc$ nuclear reaction to monitor proton beams: New measurements and consequences on the earlier reported data, Nucl. Instrum. Methods B ***198*** *(2002) 183–196.*

HILGERS, K., STOLL, T., SKAKUN, Y., COENEN, H.H., QAIM, S.M., Cross-section measurements of the nuclear reactions $^{nat}Zn(d,x)^{64}Cu$, $^{66}Zn(d,\alpha)^{64}Cu$ and $^{68}Zn(p,\alpha n)^{64}Cu$ for production of ^{64}Cu and technical developments for small-scale production of ^{67}Cu via the $^{70}Zn(p,\alpha)^{67}Cu$ process, Appl. Radiat. Isot. **59** (2003) 343–351.
EXFOR: D0069
Detected radiation: annihilation radiation (38%). Data were rejected because of the large disagreement with other equivalent data.

SZELECSÉNYI, F., et al., Investigation of the $^{66}Zn(p,2pn)^{64}Cu$ and $^{68}Zn(p,x)^{64}Cu$ nuclear processes up to 100 MeV: Production of ^{64}Cu, Nucl. Instrum. Methods B **240** (2005) 625–637.
EXFOR: O1351
Detected radiation: 1345.8 keV γ photon (0.48%) and annihilation radiation (38%).

Yield

No data were found.

7.2. CHARGED PARTICLE PRODUCTION OF ^{67}Cu

Copper-67 is the longest lived copper radionuclide, with practical application in therapy. With a half-life of 2.6 d, ^{67}Cu emits β particles with energy maxima ranging from 0.4 to 0.6 MeV that are ideal for cancer therapy. Along with 100% beta emission, ^{67}Cu also emits gamma photons of 92 and 184 keV that are suitable for gamma scintigraphy. This combination of suitable half-life, beta and gamma emissions makes ^{67}Cu a highly attractive radioisotope for cancer therapy; in particular, the short range of emitted β particles and the capability of copper to form stable chemical complexes (with antibodies, peptides, etc.) make this radionuclide potentially very useful for internal radiotherapy. A simplified decay scheme is shown in Fig. 7.19 and the main emissions, as defined in Table 7.7, were taken from NuDat 2.4 [7.3].

A. Decay data

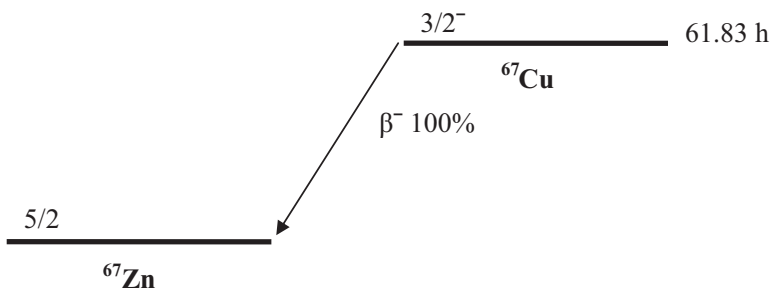

FIG. 7.19. Simplified decay scheme of ^{67}Cu [7.3].

TABLE 7.7. MAIN EMISSIONS [7.2, 7.3]

Cu-67	Decay mode: $T_{1/2}$	β^- 100% 61.83 h
Radiation	Intensity	Energy (MeV)
β^- 1	1.10×10^{-02}	5.100×10^{-02} [a] 1.820×10^{-01} [b]
β^- 2	5.70×10^{-01}	1.210×10^{-01} [a] 3.910×10^{-01} [b]
β^- 3	2.20×10^{-01}	1.540×10^{-01} [a] 4.830×10^{-01} [b]
β^- 4	2.00×10^{-01}	1.890×10^{-01} [a] 5.760×10^{-01} [b]
γ 1	7.00×10^{-02}	9.127×10^{-02}
ce-K, γ 1	4.62×10^{-03}	8.161×10^{-02}
ce-L, γ 1	5.32×10^{-04}	9.007×10^{-02} [c]
γ 2	1.61×10^{-01}	9.331×10^{-02}
ce-K, γ 2	1.24×10^{-01}	8.365×10^{-02}
ce-L, γ 2	1.48×10^{-02}	9.212×10^{-02} [c]
γ 3	4.87×10^{-01}	1.846×10^{-01}
ce-K, γ 3	7.60×10^{-03}	1.749×10^{-01}
ce-L, γ 3	8.04×10^{-04}	1.834×10^{-01} [c]
γ 4	1.15×10^{-03}	2.090×10^{-01}
ce-K, γ 4	9.25×10^{-06}	1.993×10^{-01}
ce-L, γ 4	9.43×10^{-07}	2.078×10^{-01} [c]
γ 5	7.97×10^{-03}	3.002×10^{-01}
γ 6	2.20×10^{-03}	3.935×10^{-01}
$K_{\alpha 1}$ X ray	3.83×10^{-02}	8.639×10^{-03}
$K_{\alpha 2}$ X ray	1.97×10^{-02}	8.616×10^{-03}
K_{β} X ray	8.22×10^{-03}	9.570×10^{-03} [a]
L X ray	2.13×10^{-03}	1.010×10^{-03} [a]
Auger-K	7.00×10^{-02}	7.530×10^{-03} [a]
Auger-L	1.95×10^{-01}	9.900×10^{-04} [a]

[a] Average energy (MeV).
[b] End point energy (MeV).
[c] Maximum energy (MeV) for the subshell.

B. Production routes

TABLE 7.8. INVESTIGATED PRODUCTION ROUTES [7.3, 7.4]

Target isotope	Natural abundance	Reaction	Q-value (MeV)	Threshold energy (MeV)
Zn-68	18.75%	(p, 2p)	–10.0	10.1
Zn-70	0.62%	(p, α)	2.6	0.0

C. ^{68}Zn(p, 2p)^{67}Cu reaction

Eight data sets are available in the literature for proton energies up to 200 MeV and are shown in Fig. 7.20. Five selected data sets up to 100 MeV are presented in Fig. 7.21. The selected data are compared with theoretical curves in Fig. 7.22, and show that results from the ALICE and EMPIRE codes disagree significantly and represent poor descriptions of the experimental data. Yields determined from the recommended cross-sections are presented in Fig. 7.23, while corresponding numerical values for the recommended cross-sections and yields are listed in Table 7.9. An important point to emphasize in practical production runs

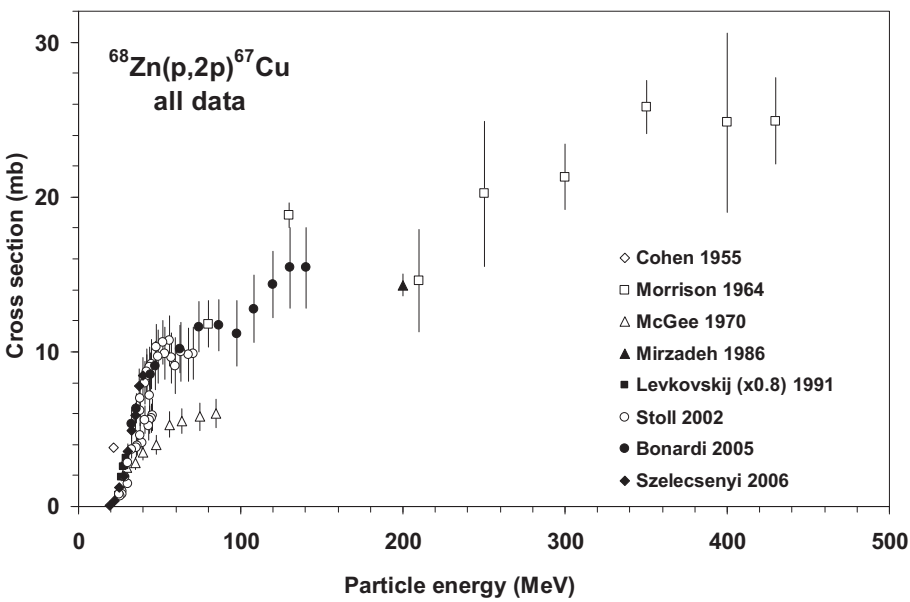

FIG. 7.20. All experimental data.

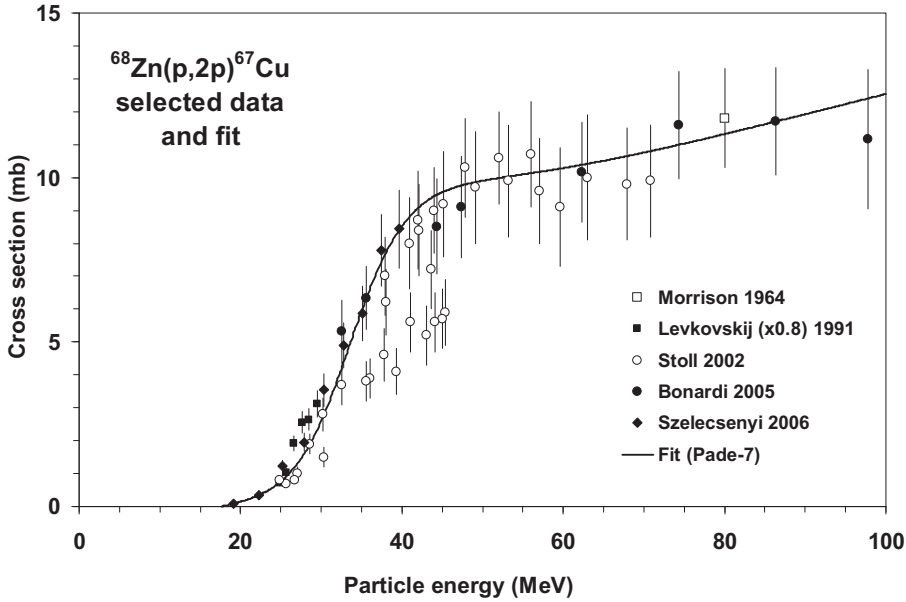

FIG. 7.21. Selected experimental data and the recommended curve (fit).

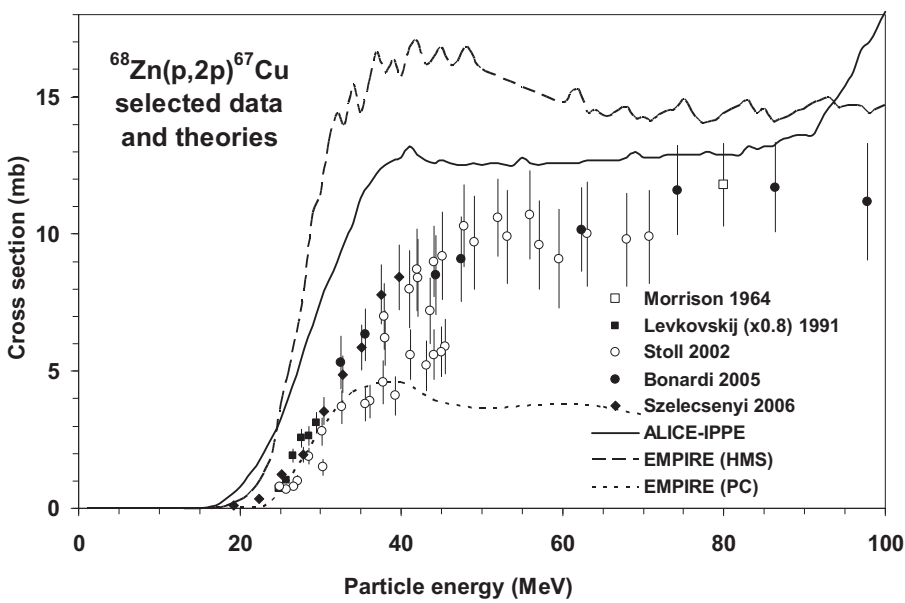

FIG. 7.22. Selected experimental data and theoretical calculations.

with thick targets is that a significant flux of energetic secondary neutrons is generated. This additional neutron flux often contributes to the production of the primary isotope or to some of the impurities. Thus, the formation of ^{67}Cu via the ^{68}Zn(n, d) and ^{68}Zn(n, np) reactions is also expected to contribute to the overall yield when producing this radioisotope via the ^{68}Zn(p, 2p)^{67}Cu reaction.

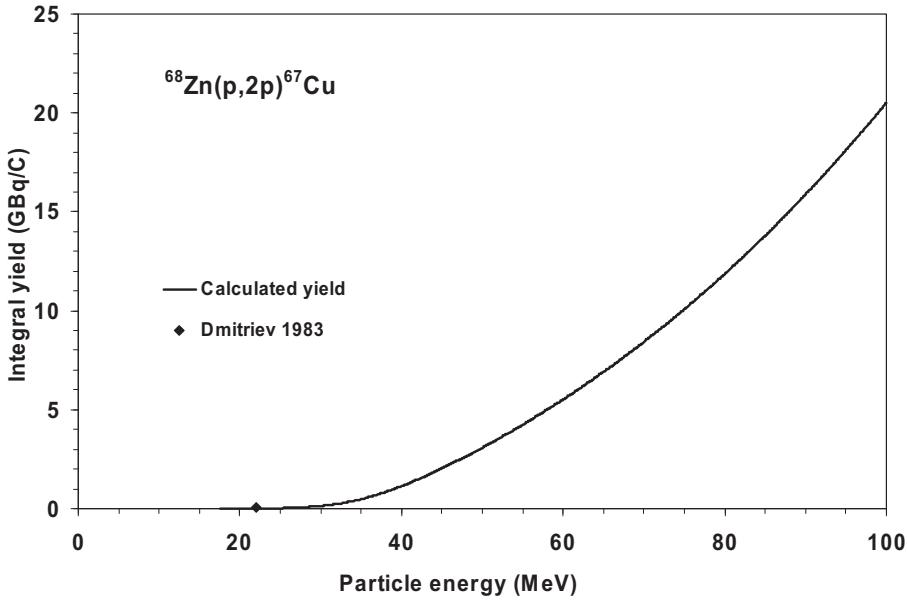

FIG. 7.23. Calculated integral yield curve based on the recommended cross-sections.

TABLE 7.9. RECOMMENDED CROSS-SECTIONS AND INTEGRAL YIELDS

^{68}Zn(p, 2p)^{67}Cu energy (MeV)	Cross-section (mb)	Integral yield	
		(μCi/μAh)	(GBq/C)
17.5	0.00	0.0	0.000
18.0	0.02	0.0	0.000
18.5	0.05	0.0	0.000
19.0	0.08	0.1	0.001
19.5	0.11	0.1	0.001
20.0	0.14	0.2	0.002
20.5	0.18	0.3	0.003
21.0	0.22	0.4	0.004

TABLE 7.9. RECOMMENDED CROSS-SECTIONS AND INTEGRAL YIELDS (cont.)

$^{68}Zn(p, 2p)^{67}Cu$ energy (MeV)	Cross-section (mb)	Integral yield	
		(μCi/μAh)	(GBq/C)
21.5	0.27	0.5	0.005
22.0	0.31	0.7	0.007
22.5	0.37	0.9	0.009
23.0	0.43	1.1	0.011
23.5	0.50	1.4	0.014
24.0	0.58	1.7	0.018
24.5	0.66	2.1	0.022
25.0	0.76	2.6	0.026
25.5	0.87	3.1	0.032
26.0	0.99	3.7	0.038
26.5	1.13	4.4	0.045
27.0	1.29	5.2	0.053
27.5	1.46	6.1	0.063
28.0	1.65	7.2	0.074
28.5	1.86	8.4	0.086
29.0	2.08	9.8	0.101
29.5	2.33	11.4	0.117
30.0	2.60	13.2	0.135
30.5	2.89	15.2	0.156
31.0	3.19	17.4	0.179
31.5	3.51	20.0	0.205
32.0	3.84	22.7	0.234
32.5	4.19	25.8	0.266
33.0	4.54	29.2	0.300
33.5	4.89	32.9	0.339
34.0	5.24	37.0	0.380
34.5	5.59	41.4	0.425
35.0	5.94	46.0	0.473
35.5	6.27	51.1	0.525
36.0	6.59	56.4	0.580
36.5	6.90	62.1	0.638
37.0	7.18	68.1	0.700

TABLE 7.9. RECOMMENDED CROSS-SECTIONS AND INTEGRAL YIELDS (cont.)

$^{68}Zn(p, 2p)^{67}Cu$ energy (MeV)	Cross-section (mb)	Integral yield	
		(μCi/μAh)	(GBq/C)
37.5	7.46	74.4	0.765
38.0	7.71	81.0	0.832
38.5	7.94	87.8	0.903
39.0	8.15	95.0	0.976
39.5	8.35	102.4	1.052
40.0	8.52	110.0	1.131
40.5	8.68	117.9	1.211
41.0	8.83	125.9	1.294
41.5	8.96	134.2	1.380
42.0	9.07	142.7	1.467
42.5	9.18	151.4	1.556
43.0	9.27	160.2	1.647
43.5	9.35	169.2	1.739
44.0	9.43	178.4	1.833
44.5	9.49	187.7	1.929
45.0	9.55	197.2	2.026
45.5	9.60	206.8	2.125
46.0	9.65	216.5	2.225
46.5	9.69	226.4	2.326
47.0	9.73	236.4	2.429
47.5	9.76	246.5	2.533
48.0	9.80	256.7	2.639
48.5	9.83	267.1	2.745
49.0	9.85	277.6	2.853
49.5	9.88	288.2	2.962
50.0	9.90	298.9	3.072
50.5	9.92	309.7	3.183
51.0	9.94	320.6	3.295
51.5	9.96	331.7	3.409
52.0	9.98	342.8	3.523
52.5	10.00	354.1	3.639
53.0	10.02	365.4	3.756

TABLE 7.9. RECOMMENDED CROSS-SECTIONS AND INTEGRAL YIELDS (cont.)

$^{68}Zn(p, 2p)^{67}Cu$ energy (MeV)	Cross-section (mb)	Integral yield	
		(μCi/μAh)	(GBq/C)
53.5	10.04	376.9	3.874
54.0	10.06	388.5	3.993
54.5	10.08	400.2	4.113
55.0	10.09	412.0	4.235
55.5	10.11	423.9	4.357
56.0	10.13	436.0	4.481
56.5	10.15	448.1	4.605
57.0	10.17	460.3	4.731
57.5	10.19	472.7	4.858
58.0	10.21	485.2	4.986
58.5	10.23	497.7	5.116
59.0	10.25	510.4	5.246
59.5	10.27	523.3	5.378
60.0	10.29	536.2	5.511
60.5	10.31	549.2	5.645
61.0	10.33	562.4	5.780
61.5	10.35	575.6	5.916
62.0	10.37	589.0	6.054
62.5	10.39	602.5	6.192
63.0	10.41	616.1	6.332
63.5	10.44	629.9	6.474
64.0	10.46	643.7	6.616
64.5	10.48	657.7	6.760
65.0	10.51	671.8	6.905
65.5	10.53	686.0	7.051
66.0	10.55	700.4	7.198
66.5	10.58	714.8	7.347
67.0	10.60	729.4	7.497
67.5	10.63	744.1	7.648
68.0	10.65	758.9	7.800
68.5	10.68	773.9	7.954
69.0	10.70	789.0	8.109

TABLE 7.9. RECOMMENDED CROSS-SECTIONS AND INTEGRAL YIELDS (cont.)

$^{68}Zn(p, 2p)^{67}Cu$ energy (MeV)	Cross-section (mb)	Integral yield	
		(μCi/μAh)	(GBq/C)
69.5	10.73	804.2	8.265
70.0	10.76	819.6	8.423
70.5	10.78	835.0	8.582
71.0	10.81	850.6	8.743
71.5	10.84	866.4	8.904
72.0	10.86	882.2	9.067
72.5	10.89	898.2	9.232
73.0	10.92	914.3	9.397
73.5	10.95	930.6	9.565
74.0	10.97	947.0	9.733
74.5	11.00	963.5	9.903
75.0	11.03	980.2	10.074
75.5	11.06	997.0	10.247
76.0	11.09	1013.9	10.421
76.5	11.12	1030.9	10.596
77.0	11.14	1048.2	10.773
77.5	11.17	1065.5	10.951
78.0	11.20	1083.0	11.131
78.5	11.23	1100.6	11.312
79.0	11.26	1118.4	11.494
79.5	11.29	1136.2	11.678
80.0	11.32	1154.3	11.863
80.5	11.35	1172.4	12.050
81.0	11.38	1190.8	12.238
81.5	11.41	1209.2	12.428
82.0	11.44	1227.8	12.619
82.5	11.47	1246.6	12.812
83.0	11.50	1265.5	13.006
83.5	11.53	1284.5	13.202
84.0	11.56	1303.7	13.399
84.5	11.59	1323.0	13.597
85.0	11.62	1342.5	13.797

TABLE 7.9. RECOMMENDED CROSS-SECTIONS AND INTEGRAL YIELDS (cont.)

$^{68}Zn(p, 2p)^{67}Cu$ energy (MeV)	Cross-section (mb)	Integral yield	
		(μCi/μAh)	(GBq/C)
85.5	11.65	1362.1	13.999
86.0	11.68	1381.8	14.202
86.5	11.71	1401.7	14.407
87.0	11.74	1421.8	14.613
87.5	11.77	1442.0	14.820
88.0	11.80	1462.3	15.030
88.5	11.83	1482.8	15.240
89.0	11.86	1503.5	15.452
89.5	11.89	1524.3	15.666
90.0	11.92	1545.2	15.881
90.5	11.95	1566.3	16.098
91.0	11.98	1587.6	16.317
91.5	12.01	1609.0	16.537
92.0	12.05	1630.6	16.758
92.5	12.08	1652.3	16.982
93.0	12.11	1674.1	17.206
93.5	12.14	1696.2	17.433
94.0	12.17	1718.3	17.661
94.5	12.20	1740.7	17.890
95.0	12.23	1763.1	18.121
95.5	12.26	1785.8	18.354
96.0	12.29	1808.6	18.588
96.5	12.32	1831.5	18.824
97.0	12.35	1854.6	19.061
97.5	12.38	1877.9	19.300
98.0	12.41	1901.3	19.541
98.5	12.45	1924.9	19.784
99.0	12.48	1948.6	20.028
99.5	12.51	1972.5	20.273
100.0	12.54	1996.6	20.521

BIBLIOGRAPHY, EVALUATION AND SELECTION

Cross-sections

COHEN, B.L., NEWMAN, E., HANDLEY, T.H., (p,pn)+(p,2n) and (p,2p) cross sections in medium weight elements, Phys. Rev. **99** (1955) 723–727.
EXFOR: B0049
Data were rejected. Authors state that the uncertainty for the ^{67}Cu cross-sections is much higher than the 25% estimated for other cross-sections.

MORRISON, D.L., CARETTO Jr., A.A., Recoil study of the ^{68}Zn(p,2p)^{67}Cu reaction, Phys. Rev. **133** (1964) B1165–B1170.
EXFOR: R0047

McGEE, T., RAO, C.L., SAHA, G.B., YAFFE, L., Nuclear interactions of ^{45}Sc and ^{68}Zn with protons of medium energy, Nucl. Phys. A **150** (1970) 11–29.
EXFOR: B0053
Data needed adjustment in order to account for improved IAEA monitor data. After adjustment, the resulting data still do not reproduce the expected shape of the excitation function and, therefore, they were rejected.

MIRZADEH, S., MAUSNER, L.F., SRIVASTAVA, S.C., Production of no-carrier added ^{67}Cu, Appl. Radiat. Isot. **37** (1986) 29–36.
EXFOR: 12970
One data point at 200 MeV — not considered in the fitting process.

LEVKOVSKIJ, V.N., "Activation cross-section nuclides of average masses (A = 40 - 100) by protons and alpha-particles with average energies (E = 10 - 50 MeV)", Activation Cross Section by Protons and Alphas, Moscow (1991).
EXFOR: A0510
*Cross-sections must be normalized by a factor of 0.8 as pointed out by Takács, S., Tárkányi, F., Sonck, M., Hermanne, A., Investigation of the ^{nat}Mo(p,x)^{96mg}Tc nuclear reaction to monitor proton beams: New measurements and consequences on the earlier reported data, Nucl. Instrum. Methods B **198** (2002) 183–196.*

STOLL, T., et al., Excitation functions of proton induced reactions on ^{68}Zn from threshold up to 71 MeV with specific reference to the production of ^{67}Cu, Radiochim. Acta **90** (2002) 309–313.
EXFOR: O1002
Data in the energy range 35 to 45 MeV were deleted due to systematic errors in that energy range (information from authors).

BONARDI, M.L., et al., Cross-section studies on ^{64}Cu with zinc target in the proton energy range from 141 down to 31 MeV, J. Radioanal. Nucl. Chem. **264** (2005) 101–105.
EXFOR: O1310

SZELECSÉNYI, F., et al., "New cross-section data on the ^{68}Zn(p,2p)^{67}Cu nuclear reaction: Production possibility of ^{67}Cu used for internal radiotherapy", 15th Pacific Basin Nuclear Conf. (Proc. Conf. Sydney, 2006), CD-ROM.
EXFOR: no

Yield

DMITRIEV, P.P., Systematics of nuclear reaction yields for thick target at 22 MeV proton energy, Vop. At. Nauki i Tekhn., Ser. Yad. Konst. **2** (1983) 57–61.
EXFOR: A0195

The co-production of ^{64}Cu via ^{68}Zn(p, x)^{64}Cu reactions is of concern. Evaluated experimental cross-section data for the production of this impurity via the ^{68}Zn(p, x)^{64}Cu reaction are presented in the Section 7.1. Based upon the good agreement between theoretical calculations and measurements for ^{64}Cu production and the reasonable similarity in trends observed in Fig. 7.22, ALICE data were used as a means of defining the first order impurity level in the calculation of the ^{64}Cu/^{67}Cu yield ratios. Instantaneous thin-target and thick-target yield ratios for ^{64}Cu/^{67}Cu are shown in Fig. 7.24, as a function of the incident proton energy, indicating that the useful production energies are above 40 MeV. Also, for short bombardments and incident energies above 40 MeV, sufficient time must still be allowed after EOB for the ^{64}Cu to decay to acceptable impurity levels (i.e. several ^{64}Cu half-lives). Shorter decay times are also required for longer bombardment times. An exit proton energy of about 40 MeV or slightly higher is recommended.

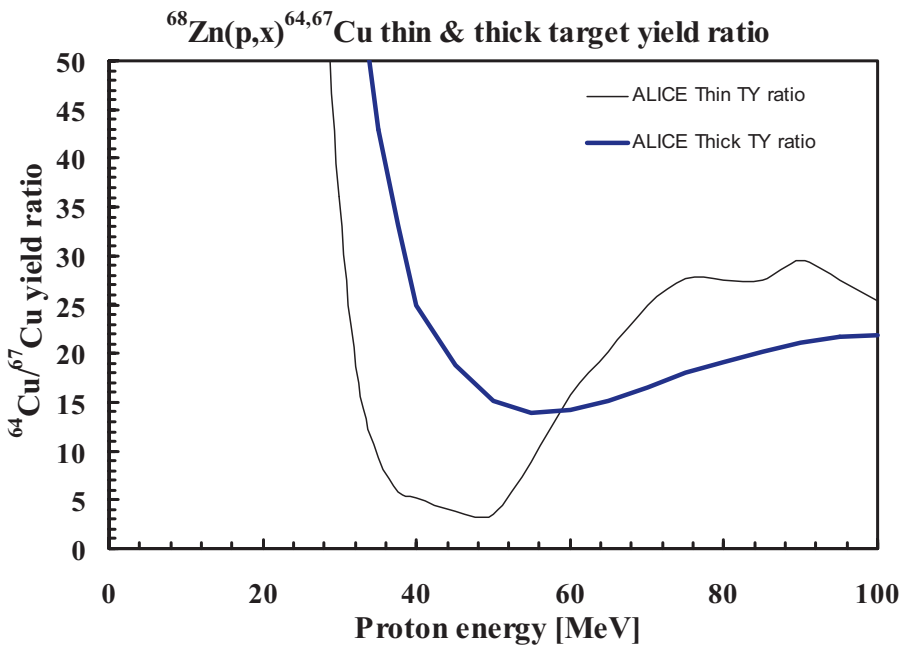

FIG. 7.24. Instantaneous thin-target and thick-target ^{64}Cu/^{67}Cu yield ratios obtained in the proton bombardment of enriched ^{68}Zn.

D. $^{70}Zn(p, \alpha)^{67}Cu$ reaction

All experimental cross-section data are shown in Fig. 7.25, and the selected measurements are compared with the resulting statistical fit to these data in Fig. 7.26. Excitation functions have been calculated by means of the ALICE-IPPE, EMPIRE and GNASH nuclear reaction modelling codes, and results are compared with all of the selected experimental data in Fig. 7.27. Yields determined from the recommended cross-sections are presented in Fig. 7.28, while corresponding numerical values for the recommended cross-sections and yields are listed in Table 7.10.

BIBLIOGRAPHY, EVALUATION AND SELECTION

Cross-sections

LEVKOVSKIJ, V.N., "Activation cross-section nuclides of average masses (A = 40 - 100) by protons and alpha-particles with average energies (E = 10 - 50 MeV)", Activation Cross Section by Protons and Alphas, Moscow (1991).
EXFOR: A0510
Cross-sections must be normalized by a factor of 0.8 as pointed out by Takács, S., Tárkányi, F., Sonck, M., Hermanne, A., Investigation of the $^{nat}Mo(p,x)^{96mg}Tc$ nuclear reaction to monitor proton beams: New measurements and consequences on the earlier reported data, Nucl. Instrum. Methods B ***198*** *(2002) 183–196.*

KASTLEINER, S., COENEN, H.H., QAIM, S.M., Possibility of production of ^{67}Cu at a small-sized cyclotron via the (p,α) reaction on enriched ^{70}Zn, Radiochim. Acta **84** (1999) 107–110.
EXFOR: O0738

Yield

No data were found.

7.3. CHARGED PARTICLE PRODUCTION OF ^{67}Ga

This radionuclide has been in use as a diagnostic single photon emission computed tomography radionuclide for several decades. Its production cross-sections have been evaluated (IAEA-TECDOC-1211). In view of its recent application in Auger electron therapy, new and updated evaluations of the two major production reactions are given below. A simplified decay scheme is shown in Fig. 7.29 and the main emissions, as defined in Table 7.11, were taken from NuDat 2.4 [7.3].

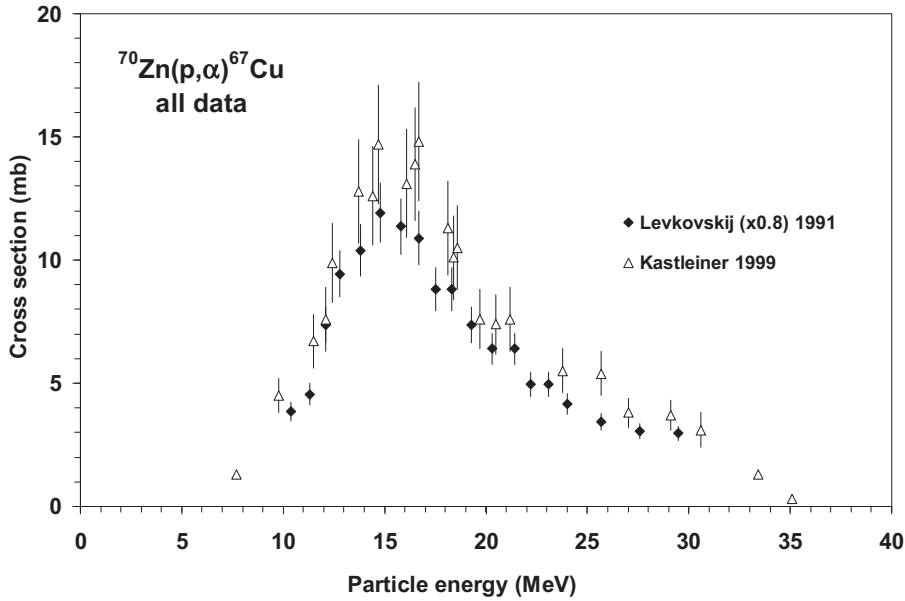

FIG. 7.25. All experimental data.

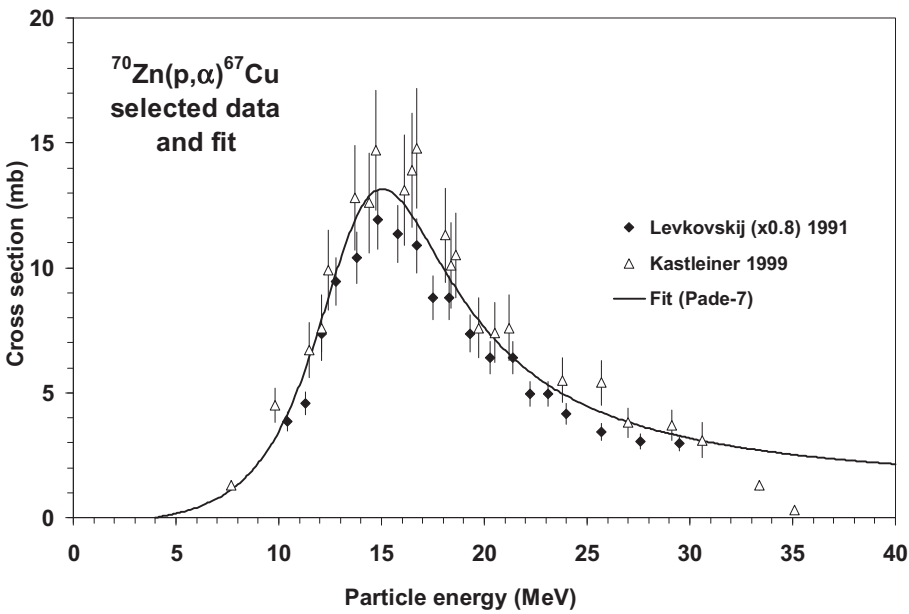

FIG. 7.26. Selected experimental data and the recommended curve (fit).

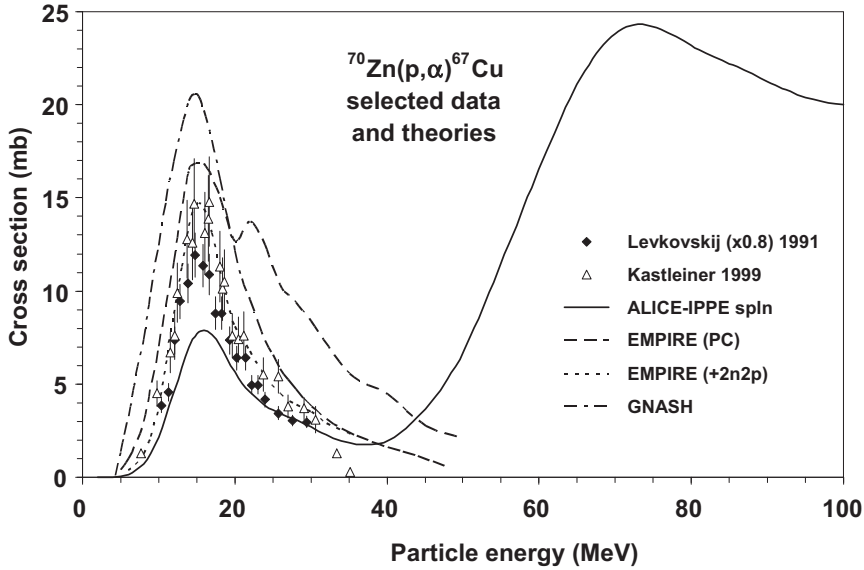

FIG. 7.27. Selected experimental data and theoretical calculations.

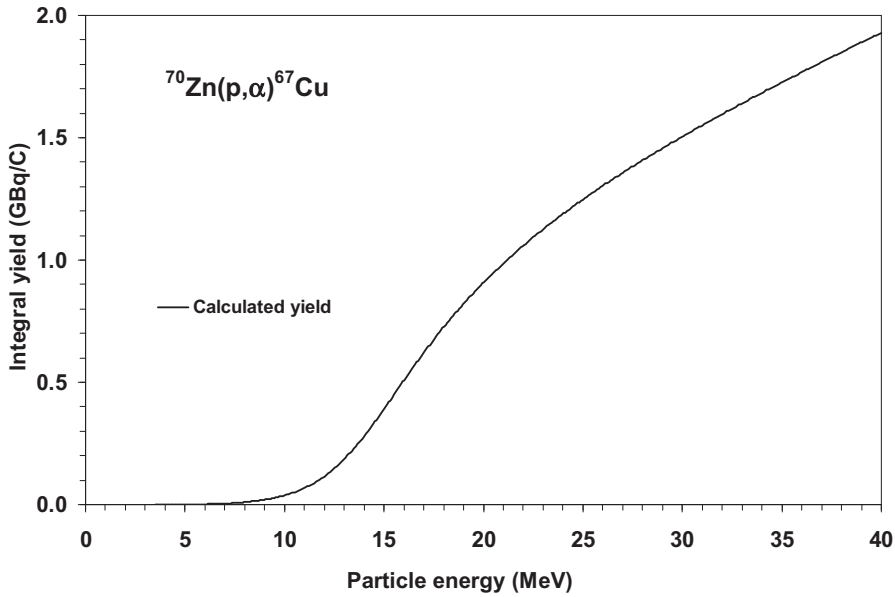

FIG. 7.28. Calculated integral yield curve based on the recommended cross-sections.

TABLE 7.10. RECOMMENDED CROSS-SECTIONS AND INTEGRAL YIELDS

$^{70}Zn(p, \alpha)^{67}Cu$ energy (MeV)	Cross-section (mb)	Integral yield	
		(μCi/μAh)	(GBq/C)
3.5	0.00	0.0	0.000
4	0.01	0.0	0.000
4.5	0.07	0.0	0.000
5	0.16	0.0	0.000
5.5	0.26	0.1	0.001
6	0.40	0.2	0.002
6.5	0.56	0.3	0.003
7	0.76	0.5	0.005
7.5	1.01	0.6	0.006
8	1.31	1.0	0.010
8.5	1.70	1.4	0.014
9	2.17	2.0	0.020
9.5	2.75	2.7	0.028
10	3.45	3.7	0.038
10.5	4.28	5.0	0.051
11	5.28	6.6	0.068
11.5	6.43	8.6	0.089
12	7.70	11.3	0.115
12.5	9.03	14.3	0.148
13	10.33	18.1	0.185
13.5	11.50	22.4	0.230
14	12.40	27.3	0.280
14.5	12.96	32.5	0.334
15	13.16	38.1	0.391
15.5	13.02	43.7	0.449
16	12.63	49.4	0.508
16.5	12.06	55.0	0.565
17	11.39	60.4	0.621
17.5	10.69	65.6	0.674
18	10.00	70.6	0.725
18.5	9.33	75.3	0.774

TABLE 7.10. RECOMMENDED CROSS-SECTIONS AND INTEGRAL YIELDS (cont.)

$^{70}Zn(p, \alpha)^{67}Cu$ energy (MeV)	Cross-section (mb)	Integral yield	
		(μCi/μAh)	(GBq/C)
19	8.70	79.8	0.821
19.5	8.13	84.2	0.865
20	7.61	88.3	0.907
20.5	7.14	92.2	0.948
21	6.71	95.9	0.986
21.5	6.32	99.5	1.023
22	5.97	103.0	1.058
22.5	5.65	106.4	1.093
23	5.36	109.5	1.126
23.5	5.10	112.6	1.157
24	4.87	115.7	1.188
24.5	4.65	118.5	1.219
25	4.46	121.3	1.247
25.5	4.28	124.1	1.276
26	4.11	126.8	1.303
26.5	3.96	129.4	1.330
28.5	3.47	139.4	1.433
29	3.36	141.8	1.457
29.5	3.26	144.1	1.481
30	3.17	146.4	1.505
30.5	3.09	148.7	1.528
31	3.01	150.9	1.551
31.5	2.93	153.1	1.573
32	2.86	155.3	1.596
32.5	2.80	157.4	1.618
33	2.74	159.6	1.640
33.5	2.68	161.6	1.661
34	2.62	163.8	1.683
34.5	2.57	165.9	1.705
35	2.52	167.9	1.725
35.5	2.48	169.9	1.747

TABLE 7.10. RECOMMENDED CROSS-SECTIONS AND INTEGRAL YIELDS (cont.)

$^{70}Zn(p, \alpha)^{67}Cu$ energy (MeV)	Cross-section (mb)	Integral yield	
		(μCi/μAh)	(GBq/C)
36	2.43	172.0	1.768
36.5	2.39	174.0	1.788
37	2.35	176.0	1.809
37.5	2.30	178.0	1.829
38	2.27	180.0	1.850
38.5	2.23	181.9	1.870
39	2.21	183.9	1.890
39.5	2.17	185.9	1.910
40	2.14	187.7	1.930

A. Decay data

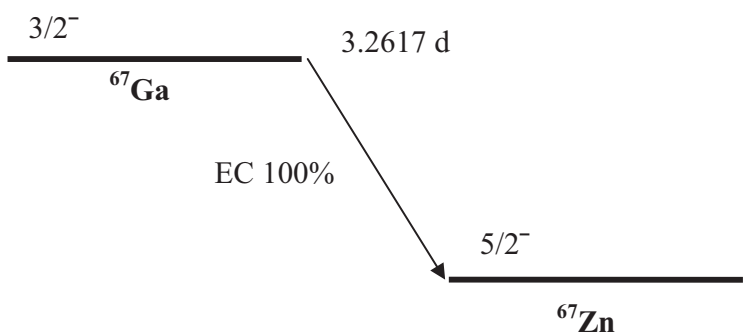

FIG. 7.29. Simplified decay scheme of ^{67}Ga [7.3].

TABLE 7.11. MAIN EMISSIONS [7.3]

Ga-67	Decay mode: $T_{1/2}$:	EC 100% 3.2617 d
Radiation	Energy (keV)	Intensity (%)
Auger L	0.99	168.3
Auger K	7.53	60.7
ce K	83.651	29.1
ce L	92.116	3.57
g	93.310	38.81
g	184.576	21.410
g	208.950	2.460
g	300.217	16.64
g	393.527	4.56

B. Production routes

Two proton induced reactions have been assessed, as specified in Table 7.12.

C. ^{67}Zn(p, n)^{67}Ga reaction

All experimental cross-section data are shown in Fig. 7.30, an d the selected measurements are compared with the resulting statistical fit to these data in Fig. 7.31. Excitation functions have been calculated by means of the ALICE-IPPE, HF and SPEC nuclear reaction modelling codes, and results are compared with all of the selected experimental data in Fig. 7.32. Yields determined from the recommended cross-sections are presented in Fig. 7.33, while corresponding numerical values for the recommended cross-sections and yields are listed in Table 7.13.

TABLE 7.12. INVESTIGATED PRODUCTION ROUTES [7.3, 7.4]

Target isotope	Natural abundance	Reaction	Q-value (MeV)	Threshold energy (MeV)
Zn-67	4.10%	(p, n)	–1.8	1.8
Zn-68	18.75%	(p, 2n)	–12.0	12.2

BIBLIOGRAPHY, EVALUATION AND SELECTION

Cross-sections

BLASER, J.-P., BOEHM, F., MARMIER, P., PEASLEE, D.C., Fonctions d'excitation de la reaction (p,n) I, Helv. Phys. Acta **24** (1951) 3–38.
EXFOR: B0048

JOHNSON, C.H., GALONSKY, A., INSKEEP, C.N., Cross sections for (p,n) reactions in intermediate-weight nuclei, Oak Ridge Natl Lab. Rep. ORNL-2910 (1960) 25 (unpublished).
EXFOR: T0135
Same as Johnson et al. (1964).

JOHNSON, C.H., TRAIL, C.C., GALONSKY, A., Thresholds for (p,n) reactions on 26 intermediate-weight nuclei, Phys. Rev. B **136** (1964) 1719–1729.
EXFOR: T0126

BARRANDON, J.N., DEBRUN, J.L., KOHN, A., SPEAR, R.H., The yield of Ti, V, Cr, Fe, Ni, Cu and Zn through activation by protons of energies limited to 20 MeV, Nucl. Instrum. Methods **127** (1975) 269–278.
EXFOR: O0086
Target: natural Zn. Data were rejected — despite the very good agreement with the results of other groups up to 10 MeV, the rapid decrease of the excitation function in the tail is unusual for a (p, n) reaction in this energy region.

BONARDI, M., BIRATTARI, C., Optimization of irradiation parameters for ^{67}Ga production from ^{nat}Zn(p,xn) nuclear reactions, J. Radioanal. Chem. **76** (1983) 311–318.
EXFOR: O1062
Target: natural Zn. Yield data were converted to cross-section data.

LITTLE, F.E., LAGUNAS-SOLAR, M.C., Cyclotron production of ^{67}Ga. Cross sections and thick-target yields for the ^{67}Zn(p,n) and ^{68}Zn(p,2n) reactions, Int. J. Appl. Radiat. Isot. **34** (1983) 631–637.
EXFOR: A0321
Data were rejected because of an energy shift.

KOPECKÝ, P., Cross sections and production yields of ^{66}Ga and ^{67}Ga for proton reactions in natural zinc, Appl. Radiat. Isot. **41** (1990) 606–608.
EXFOR: D0089
Target: natural Zn.

TÁRKÁNYI, F., SZELECSENYI, F., KOVACS, Z., SUDAR, S., Excitation functions of proton induced nuclear reactions on enriched ^{66}Zn, ^{67}Zn and ^{68}Zn. Production of ^{67}Ga and ^{66}Ga, Radiochim. Acta **50** (1990) 19–26.
EXFOR: D4004

LEVKOVSKIJ, V.N., "Activation cross-section nuclides of average masses (A = 40 - 100) by protons and alpha-particles with average energies (E = 10 - 50 MeV)", Activation Cross Section by Protons and Alphas, Moscow (1991).
EXFOR: A0510
Cross-sections must be normalized by a factor of 0.8 as noted by Takács, S., Tárkányi, F., Sonck, M., Hermanne, A., Investigation of the $^{nat}Mo(p,x)^{96mg}Tc$ nuclear reaction to monitor proton beams: New measurements and consequences on the earlier reported data, Nucl. Instrum. Methods B ***198*** *(2002) 183–196.*

NORTIER, F.M., MILLS, S.J., STEYN, G.F., Excitation functions and yields of relevance to the production of ^{67}Ga by proton bombardment of ^{nat}Zn and ^{nat}Ge up to 100 MeV, Appl. Radiat. Isot. **42** (1991) 353–359.
EXFOR: A0498
Target: natural Zn.

HERMANNE, A., Evaluated cross section and thick target yield data of Zn+p processes for practical applications, private communication (1997).
EXFOR: D4093
Target: natural Zn. Since the data are 'estimated' values above 12 MeV based on a 'tail-fitting' procedure, the results are only used up to this energy.

SZELECSÉNYI, F., BOOTHE, T.E., TAKÁCS, S., TÁRKÁNYI, F., TAVANO, E., Evaluated cross section and thick target yield data bases of Zn+p processes for practical applications, Appl. Radiat. Isot. **49** (1998) 1005–1032.
EXFOR: C0506

AL-ABYAD, M.E., Nuclear reactions studies on some natural targets using cyclotron, Masters Thesis, Ain Shams University (2003).
EXFOR: no
Target: natural Zn.

BONARDI, M.L., et al., Cross-section studies on ^{64}Cu with zinc target in the proton energy range from 141 down to 31 MeV, J. Radioanal. Nucl. Chem. **264** (2005) 101–105.
EXFOR: O1310
Target: natural Zn. Data were rejected because they are above the threshold of the $^{68}Zn(p, 2n)$ reaction.

TÁRKÁNYI, F., et al., Activation cross sections of long-lived products of proton-induced nuclear reactions on zinc, Appl. Radiat. Isot. **62** (2005) 73–81.
EXFOR: D4149, E1921
Target: natural Zn. Data were rejected because they are above the threshold of the $^{68}Zn(p, 2n)$ reaction.

AL-SALEH, F.S., AL MUGREN, K.S., AZZAM, A., Excitation function measurements and integral yields estimation for ^{nat}Zn(p,x) reactions at low energies, Appl. Radiat. Isot. **65** (2007) 1101–1107.
EXFOR: O1547
Target: natural Zn.

UDDIN, M.S., KHANDAKER, M.U., KIM, K.S., LEE, Y.S., KIM, G.N., Excitation functions of the proton induced nuclear reactions on ^{nat}Zn up to 40 MeV, Nucl. Instrum. Methods B **258** (2007) 313–320.
EXFOR: O1600
Target: natural Zn.

Yield

KRASNOV, N.N., KONSTANTINOV, I.O., TUEV, V.M., DMITRIEV, P.P., KONYAKHIN, N.A., Yields of ^{67}Ga produced by a cyclotron, Isot. USSR **27** (1972) 11–14.
EXFOR: no

INTRATOR, T.P., PETERSON, R.J., ZAIDINS, C.S., ROUGHTON, N.A., Determination of proton spectra by thick target radioactive yields, Nucl. Instrum. Methods **188** (1981) 347–352.
EXFOR: no
Data were not adopted because they differed from all other values by some orders of magnitude.

MAHUNKA, I., SZELECSENYI, F., ANDO, L., Radioisotope Production at the MGC Cyclotron, INDC(HUN)-027/G, IAEA, Vienna (1989) 7.
EXFOR: no

TÁRKÁNYI, F., SZELECSENYI, F., KOVACS, Z., SUDAR, S., Excitation functions of proton induced nuclear reactions on enriched ^{66}Zn, ^{67}Zn and ^{68}Zn. Production of ^{67}Ga and ^{66}Ga, Radiochim. Acta **50** (1990) 19–26.
EXFOR: D4004

NICKLES, R.J., A shotgun approach to the chart of the nuclides: Radiotracer production with an 11 MeV proton cyclotron, Acta Radiologica, Suppl. **376** (1991) 69–71.
EXFOR: no
Target: natural Zn.

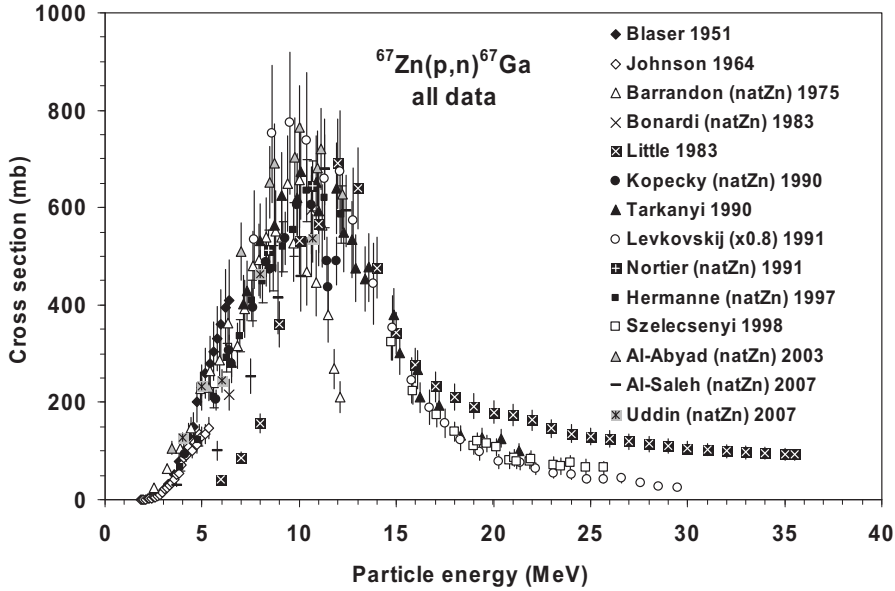

FIG. 7.30. All experimental data.

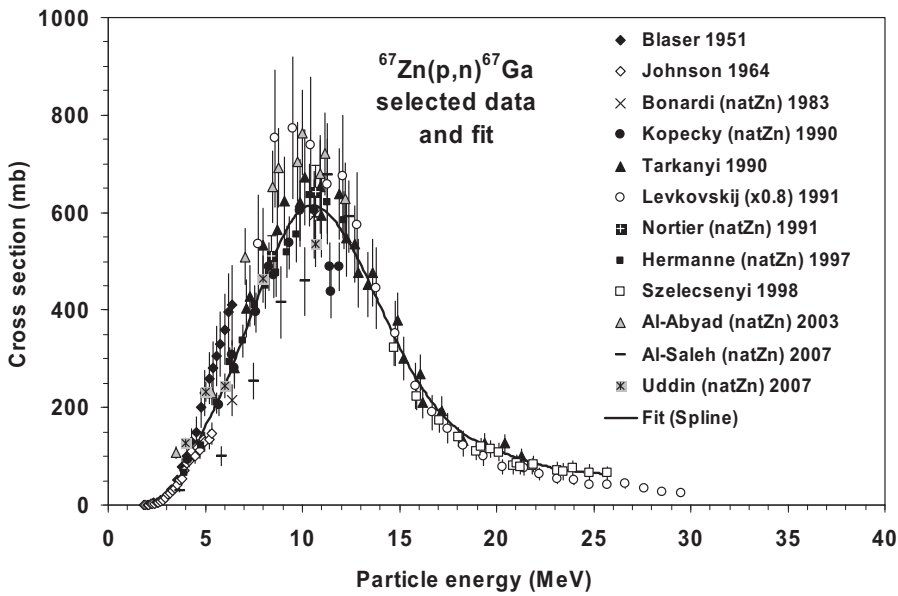

FIG. 7.31. Selected experimental data and the recommended curve (fit).

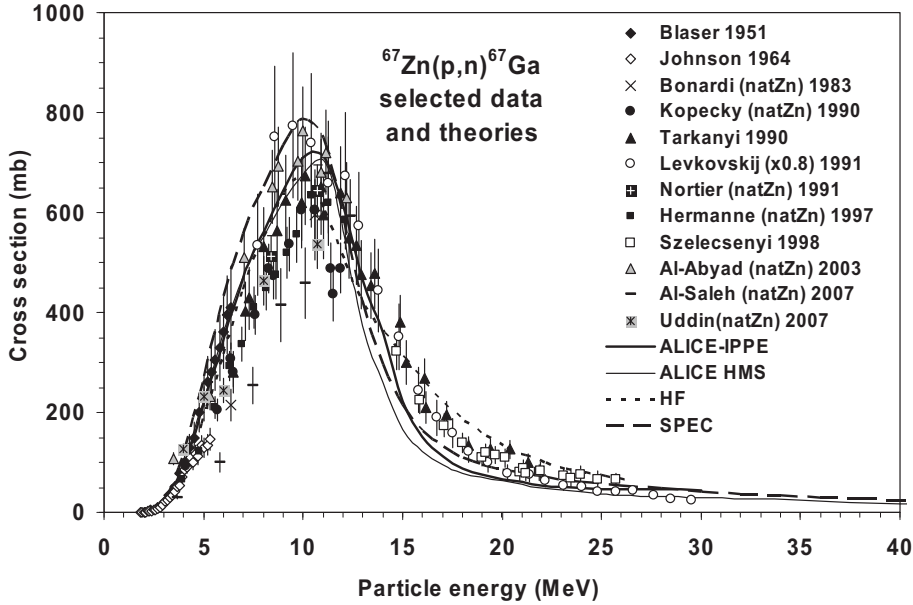

FIG. 7.32. Selected experimental data and theoretical calculations.

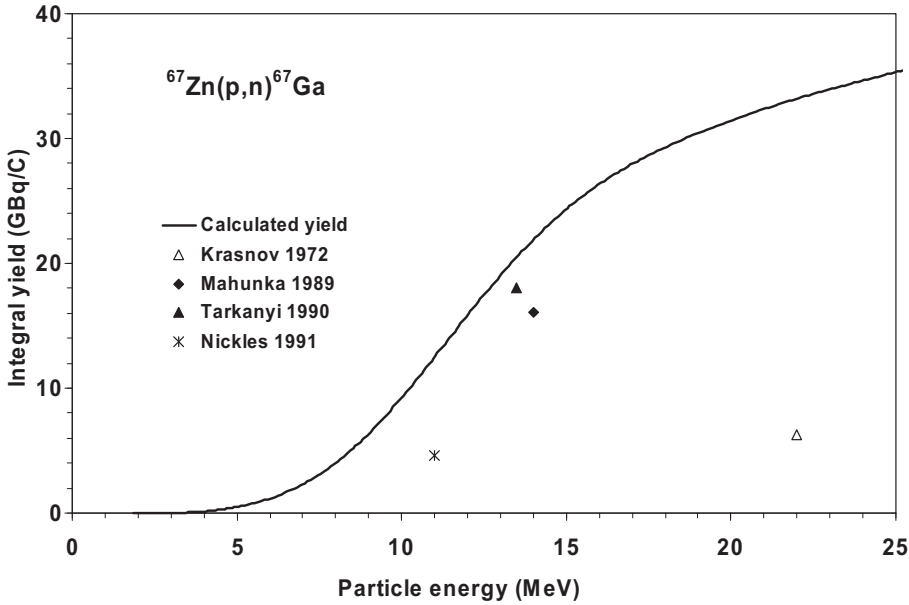

FIG. 7.33. Calculated integral yield curve based on the recommended cross-sections.

TABLE 7.13. RECOMMENDED CROSS-SECTIONS AND INTEGRAL YIELDS

$^{67}Zn(p, n)^{67}Ga$ energy (MeV)	Cross-section (mb)	Integral yield	
		(μCi/μAh)	(GBq/C)
2.0	0	0	0.00
2.5	4	0	0.00
3.0	15	1	0.01
3.5	38	4	0.04
4.0	70	11	0.12
4.5	110	24	0.25
5.0	159	44	0.45
5.5	196	73	0.75
6.0	240	110	1.13
6.5	290	158	1.62
7.0	344	218	2.24
7.5	399	292	3.00
8.0	452	381	3.92
8.5	503	486	4.99
9.0	547	605	6.22
9.5	583	739	7.59
10.0	607	885	9.10
10.5	614	1040	10.69
11.0	609	1201	12.34
11.5	593	1364	14.02
12.0	567	1526	15.68
12.5	535	1684	17.31
13.0	498	1837	18.88
13.5	457	1982	20.37
14.0	414	2118	21.77
14.5	370	2243	23.05
15.0	328	2358	24.23
15.5	289	2461	25.29
16.0	254	2554	26.25
16.5	223	2638	27.12
17.0	197	2714	27.89

TABLE 7.13. RECOMMENDED CROSS-SECTIONS AND INTEGRAL YIELDS (cont.)

$^{67}Zn(p, n)^{67}Ga$ energy (MeV)	Cross-section (mb)	Integral yield	
		(μCi/μAh)	(GBq/C)
17.5	175	2782	28.60
18.0	157	2845	29.24
18.5	143	2903	29.83
19.0	131	2957	30.39
19.5	122	3008	30.91
20.0	114	3056	31.41
20.5	106	3102	31.88
21.0	98	3145	32.33
21.5	92	3187	32.75
22.0	86	3226	33.16
22.5	81	3264	33.54
23.0	76	3299	33.91
23.5	72	3334	34.26
24.0	70	3367	34.61
24.5	68	3401	34.95
25.0	66	3433	35.29
25.5	64	3466	35.62

D. ^{68}Zn(p, 2n)^{67}Ga reaction

Results of measurements for the ^{nat}Zn(p, xn)^{67}Ga process can be used for evaluations between 17 and 30 MeV. Over this energy range, the contribution of the ^{67}Zn(p, n)^{67}Ga reaction can be ignored due to the low isotopic abundance of ^{67}Zn in a natural zinc matrix and the small cross-section of the ^{67}Zn(p, n)^{67}Ga reaction. The influence of the ^{70}Zn(p, 4n)^{67}Ga process to the production cross-sections is also negligible because of the very low isotopic abundance of ^{70}Zn in natural zinc (0.62%).

BIBLIOGRAPHY, EVALUATION AND SELECTION

Cross-sections

COHEN, B.L., NEWMAN, E., HANDLEY, T.H., (p,pn) + (p,2n) and (p,2p) cross sections in medium weight elements, Phys. Rev. **99** (1955) 723–727.
EXFOR: B0050

McGEE, T., RAO, C.L., SAHA, G.B., YAFFE, L., Nuclear interactions of ^{45}Sc and ^{68}Zn with protons of medium energy, Nucl. Phys. A **150** (1970) 11–29.
EXFOR: B0053
Data were rejected because of the very low cross-section values.

BARRANDON, J.N., DEBRUN, J.L., KOHN, A., SPEAR, R.H., Study of the yield of Ti, V, Cr, Fe, Ni, Cu and Zn through activation by protons of energies limited to 20 MeV, Nucl. Instrum. Methods **127** (1975) 269–278.
EXFOR: O0086
Target: natural Zn. Data were rejected because the measured energies were below 17 MeV.

BONARDI, M., BIRATTARI, C., Optimization of irradiation parameters for ^{67}Ga production from nat Zn(p,xn) nuclear reactions, J. Radioanal. Chem. **76** (1983) 311–318.
EXFOR: O1062
Target: natural Zn. Yields were converted to cross-section data.

LITTLE, F.E., LAGUNAS-SOLAR, M.C., Cyclotron production of ^{67}Ga. Cross sections and thick-target yields for the ^{67}Zn(p,n) and ^{68}Zn(p,2n) reactions, Appl. Radiat. Isot. **34** (1983) 631–637.
EXFOR: A0321
Target: natural Zn and enriched ^{68}Zn. Data were rejected because of an energy shift.

KOPECKÝ, P., Cross sections and production yields of ^{66}Ga and ^{67}Ga for proton reactions in natural zinc, Appl. Radiat. Isot. **41** (1990) 606–608.
EXFOR: D0089
Target: natural Zn. Data were rejected because of their significant deviations from the observed trend.

TÁRKÁNYI, F., SZELECSENYI, F., KOVACS, Z., SUDAR, S., Excitation functions of proton induced nuclear reactions on enriched ^{66}Zn, ^{67}Zn and ^{68}Zn. Production of ^{67}Ga and ^{66}Ga, Radiochim. Acta **50** (1990) 19–26.
EXFOR: D4004

LEVKOVSKIJ, V.N., "Activation cross-section nuclides of average masses (A = 40–100) by protons and alpha-particles with average energies (E = 10–50 MeV)", Activation Cross Section by Protons and Alphas, Moscow (1991).
EXFOR: A0510
*Cross-sections must be normalized by a factor of 0.8 as noted by Takács, S., Tárkányi, F., Sonck, M., Hermanne, A., Investigation of the ^{nat}Mo(p,x)^{96mg}Tc nuclear reaction to monitor proton beams: New measurements and consequences on the earlier reported data, Nucl. Instrum. Methods B **198** (2002) 183–196.*

NORTIER, F.M., MILLS, S.J., STEYN, G.F., Excitation functions and yields of relevance to the production of ^{67}Ga by proton bombardment of ^{nat}Zn and ^{nat}Ge up to 100 MeV, Appl. Radiat. Isot. **42** (1991) 353–359.
EXFOR: A0498
Target: natural Zn.

HERMANNE, A., WALRAVENS, N., CICCHELLI, O., Optimization of isotope production by cross-section determination, personal communication, 1991.
EXFOR: A0494
Data were rejected because of their significant deviation from the observed trend.

HERMANNE, A., Evaluated cross section and thick target yield data of Zn+p processes for practical applications, private communication, 1997.
EXFOR: D4093
Target: natural Zn and enriched ^{68}Zn.

SZELECSÉNYI, F., BOOTHE, T.E., TAKÁCS, S., TÁRKÁNYI, F., TAVANO, E., Evaluated cross section and thick target yield data bases of Zn+p processes for practical applications, Appl. Radiat. Isot. **49** (1998) 1005–1032.
EXFOR: C0506

HERMANNE, A., et al., New cross-section data on ^{68}Zn(p,2n)^{67}Ga and ^{nat}Zn(p,xn)^{67}Ga nuclear reactions for the development of a reference data base, J. Radioanal. Nucl. Chem. **240** (1999) 623–630.
EXFOR: D4088
Target: natural Zn and enriched ^{68}Zn.

STOLL, T., et al., Excitation functions of proton induced reactions on ^{68}Zn from threshold up to 71 MeV, with specific reference to the production of ^{67}Cu, Radiochim. Acta **90** (2002) 309–113.
EXFOR: O1002

SZELECSÉNYI, F., et al., New cross-section data for the ^{66}Zn(p,n)^{66}Ga, ^{68}Zn(p,3n)^{66}Ga, ^{nat}Zn(p,x)^{66}Ga, ^{68}Zn(p,2n)^{67}Ga and ^{nat}Zn(p,x)^{67}Ga nuclear reactions up to 100 MeV, Nucl. Instrum. Methods B **234** (2005) 375–386.
EXFOR: E1935
Target: natural Zn and enriched ^{68}Zn.

Yield

DMITRIEV, P.P., Systematics of nuclear reaction yields for thick target at 22 MeV proton energy, Vop. At. Nauki i Tekhn., Ser. Yad. Konst. **2** (1983) 57–61.
EXFOR: A0195

KOPECKY, P., KONRAD, L., MELICHAR, F., Research, development and production of cyclotron produced radionuclides for diagnostic nuclear medicine, Jad. Energ. **31** (1985) 186–189.
EXFOR: no
Target thickness: 33 → 12 MeV.

HUPF, H.B., TISCHER, S.D., AL-WATBAN, F., The cyclotron radionuclide program at King Faisal Specialist Hospital and Research Centre, Nucl. Instrum. Methods B **10/11** (1985) 967–968.
EXFOR: no

KRASNOV, N.N., et al., "Radionuclide production on cyclotron of Institute of Physics and Power Engineering", 4th Int. Workshop on Targetry and Target Chemistry (Proc. 4th Int. Workshop Villigen, 1991), PSI, Villigen (1992) 54–56.
EXFOR: no

All experimental cross-section data are shown in Fig. 7.34, and the selected measurements are compared with the resulting statistical fit to these data in Fig. 7.35. Excitation functions have been calculated by means of the ALICE-IPPE, HF and SPEC nuclear reaction modelling codes, and results are compared with all of the selected experimental data in Fig. 7.36. Yields determined from the recommended cross-sections are presented in Fig. 7.37, while corresponding numerical values for the recommended cross-sections and yields are listed in Table 7.14.

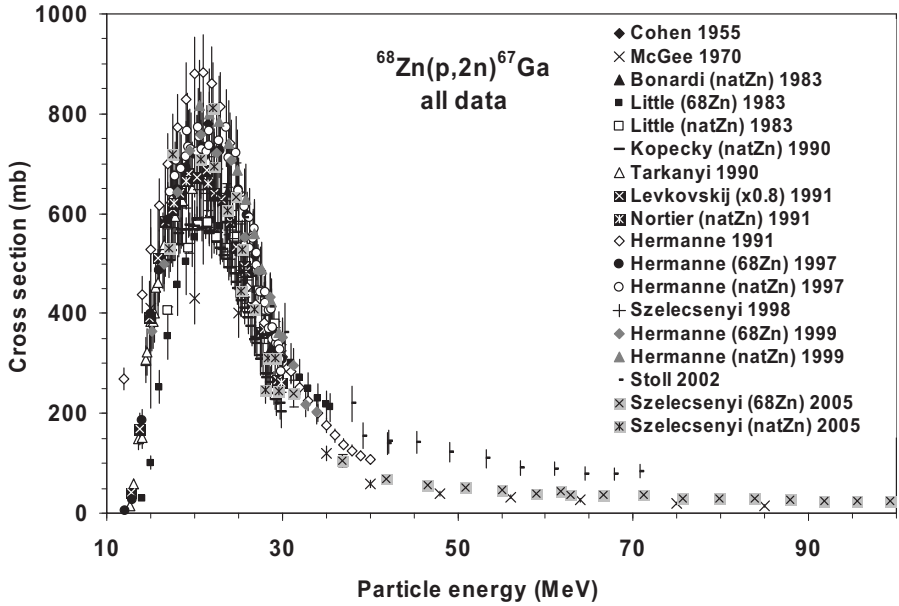

FIG. 7.34. All experimental data.

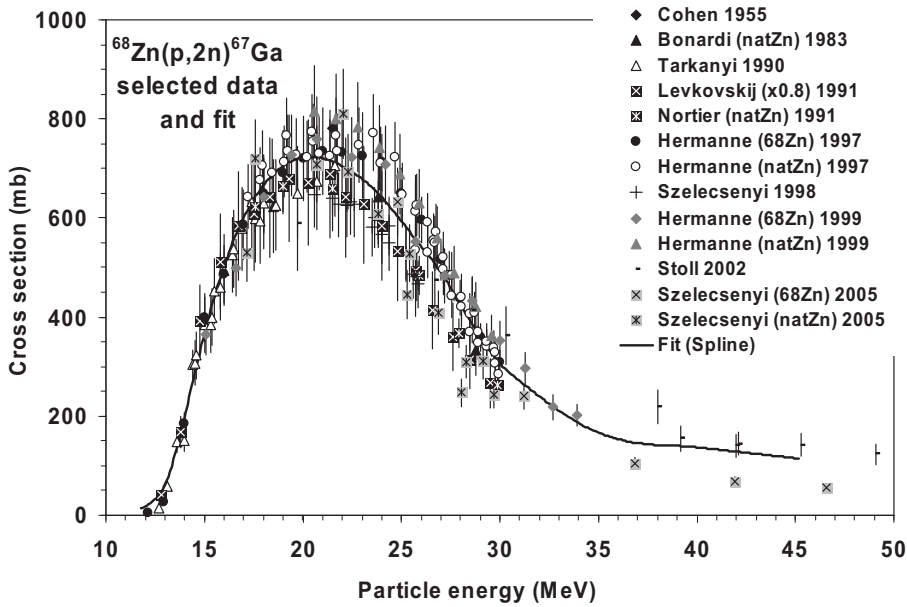

FIG. 7.35. Selected experimental data and the recommended curve (fit).

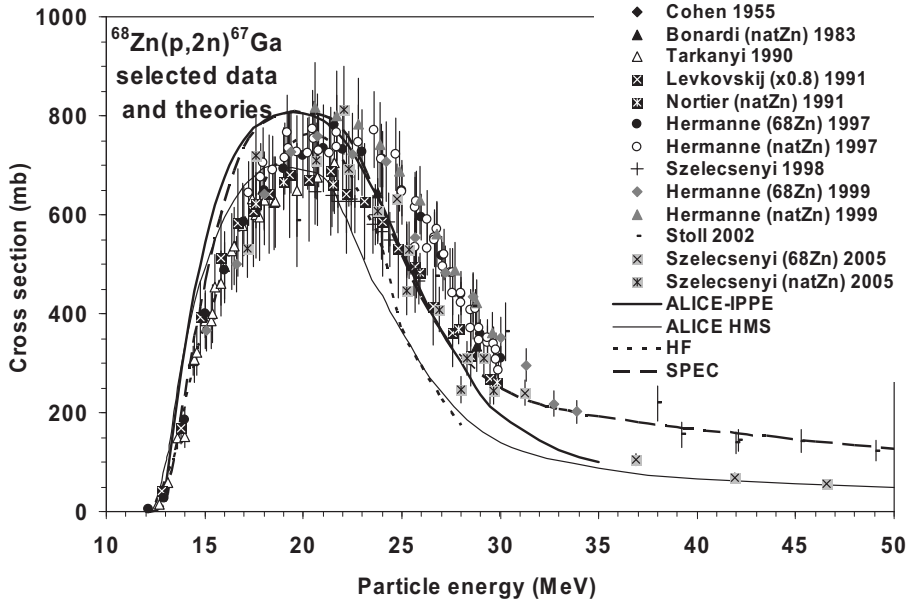

FIG. 7.36. Selected experimental data and theoretical calculations.

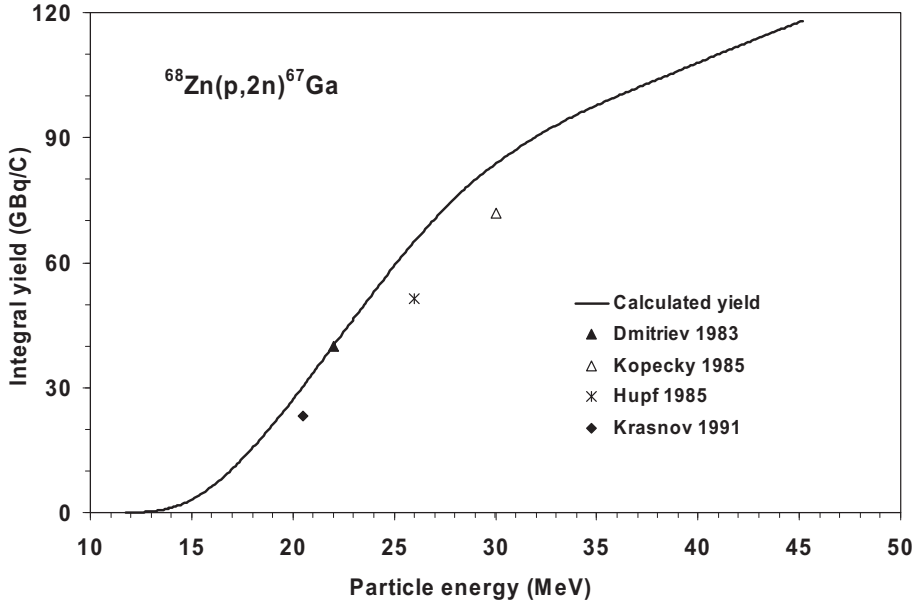

FIG. 7.37. Calculated integral yield curve based on the recommended cross-sections.

TABLE 7.14. RECOMMENDED CROSS-SECTIONS AND INTEGRAL YIELDS

$^{68}Zn(p, 2n)^{67}Ga$ energy (MeV)	Cross-section (mb)	Integral yield	
		(μCi/μAh)	(GBq/C)
12.0	17	3	0.0
12.5	31	10	0.1
13.0	59	24	0.2
13.5	114	51	0.5
14.0	191	102	1.0
14.5	276	181	1.9
15.0	358	290	3.0
15.5	432	427	4.4
16.0	497	593	6.1
16.5	552	784	8.1
17.0	598	997	10.2
17.5	634	1230	12.6
18.0	663	1480	15.2
18.5	686	1745	17.9
19.0	704	2023	20.8
19.5	716	2313	23.8
20.0	722	2612	26.8
20.5	724	2918	30.0
21.0	721	3229	33.2
21.5	715	3544	36.4
22.0	705	3860	39.7
22.5	694	4180	43.0
23.0	681	4495	46.2
23.5	664	4810	49.4
24.0	644	5121	52.6
24.5	621	5427	55.8
25.0	597	5726	58.8
25.5	570	6018	61.9
26.0	545	6300	64.7
26.5	521	6573	67.6
27.0	494	6837	70.3

TABLE 7.14. RECOMMENDED CROSS-SECTIONS AND INTEGRAL YIELDS (cont.)

$^{68}Zn(p, 2n)^{67}Ga$ energy (MeV)	Cross-section (mb)	Integral yield	
		(μCi/μAh)	(GBq/C)
27.5	462	7089	72.9
28.0	428	7326	75.3
28.5	395	7548	77.6
29.0	363	7755	79.7
29.5	333	7947	81.7
30.0	309	8127	83.5
30.5	289	8297	85.3
31.0	272	8459	86.9
31.5	257	8614	88.5
32.0	241	8761	90.0
32.5	226	8901	91.5
33.0	212	9034	92.9
33.5	199	9160	94.1
34.0	187	9280	95.4
34.5	177	9394	96.6
35.0	168	9504	97.7
35.5	160	9609	98.8
36.0	154	9712	99.8
36.5	149	9812	100.8
37.0	146	9910	101.9
37.5	143	10 008	102.9
38.0	142	10 105	103.9
38.5	141	10 203	104.9
39.0	140	10 301	105.9
39.5	139	10 399	106.9
40.0	137	10 498	107.9
40.5	135	10 596	108.9
41.0	133	10 693	109.9
41.5	131	10 790	110.9
42.0	129	10 886	111.9
42.5	126	10 982	112.9

TABLE 7.14. RECOMMENDED CROSS-SECTIONS AND INTEGRAL YIELDS (cont.)

$^{68}Zn(p, 2n)^{67}Ga$ energy (MeV)	Cross-section (mb)	Integral yield	
		(μCi/μAh)	(GBq/C)
43.0	124	11 076	113.8
43.5	122	11 170	114.8
44.0	120	11 263	115.8
44.5	118	11 355	116.7
45.0	116	11 447	117.6

7.4. CHARGED PARTICLE PRODUCTION OF ^{86g}Y

A combination of β^- emitting ^{90}Y and β^+ emitting ^{86g}Y represents a means of undertaking PET and radiotherapy — dosimetry and therapy planning can be better quantified. A simplified decay scheme is shown in Fig. 7.38, and the main emissions, as defined in Table 7.15, were taken from NuDat 2.4 [7.3].

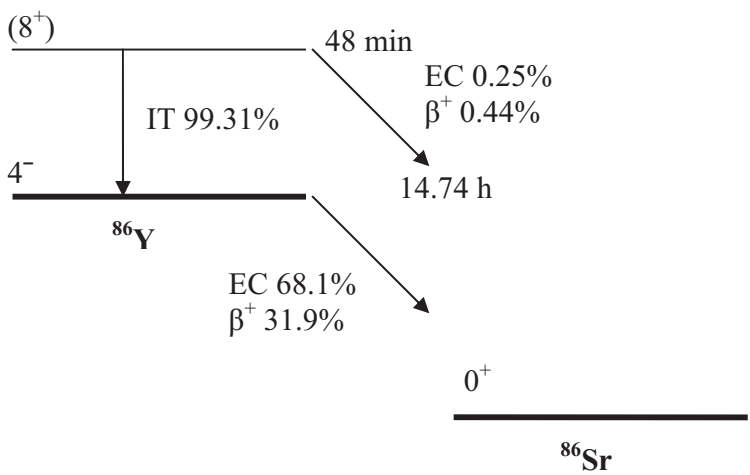

FIG. 7.38. Simplified decay scheme of ^{86}Y [7.3].

A. Decay data

TABLE 7.15. MAIN EMISSIONS [7.3]

Y-86g	Decay mode: $T_{1/2}$:	EC 68.1% β^+ 31.9% 14.74 h	
Radiation	Energy (keV)	End point energy (keV)	Intensity (%)
β^+	114	249	0.0038
β^+	126	275	0.0029
β^+	133	292	0.035
β^+	156	346	0.0035
β^+	173	387	0.22
β^+	197	443	0.0110
β^+	201	452	0.26
β^+	235	531	0.057
β^+	252	573	0.31
β^+	375	856	0.180
β^+	394	900	1.10
β^+	406	927	0.043
β^+	452	1033	1.9
β^+	509	1162	1.33
β^+	535	1221	11.9
β^+	589	1340	0.69
β^+	629	1430	0.05
β^+	681	1545	5.6
β^+	695	1576	0.05
β^+	768	1736	1.7
β^+	883	1988	3.6
β^+	1078	2364	0.9
β^+	1437	3141	2.0
g	443.13		16.9
g	511.0	Annihilation	64
g	627.72		32.6
g	703.33		15.4
g	777.37		22.4
g	1076.63		82.5
g	1153.05		30.5
g	1854.38		17.2
g	1920.72		20.8

B. Production routes

Large scale production of ^{86}Y is undertaken via the (p, n) reaction on highly enriched ^{86}Sr targets, as specified in Table 7.16.

TABLE 7.16. INVESTIGATED PRODUCTION ROUTE [7.3, 7.4]

Target isotope	Natural abundance	Reaction	Q-value (MeV)	Threshold energy (MeV)
Sr-86	9.86%	(p, n)	–6.0	6.1

C. $^{86}Sr(p, n)^{86}Y$ reaction

Two experimental data sets exist in the literature for the isotopic cross-section on ^{86}Sr. Levkovskij et al. (1991) measured the excitation function of the $^{86}Sr(p, n)^{86}Y$ reaction up to 30 MeV and Rösch et al. (1993) up to 17 MeV. Skakun et al. (1980) measured the isomer reaction for the production of the two isomeric states up to 9 MeV. Michel et al. (1997) measured excitation functions on $^{nat}Sr(p, xn)^{86}Y$ from 15.2 MeV to high energies. Taking into account that the threshold of the $^{87}Sr(p, 2n)^{86}Y$ reaction is 14.62 MeV, the first measured point of Michel et al. (1997) at 15.2 MeV can be used (after normalization to the isotopic abundance of ^{86}Sr in ^{nat}Sr). Thick-target yields on enriched $SrCO_3$ and SrO targets were measured by Yoo et al. (2005), using low intensity proton beams, and compared with the theoretical yields.

BIBLIOGRAPHY, EVALUATION AND SELECTION

Cross-sections

SKAKUN, E.A., et al., Excitation of isomeric pairs for reactions $^{86}Sr(p,n)^{86m,g}Y$ and $^{87}Sr(p,n)^{87m,g}Y$, 30th Conf. Nuclear Spectrometry and Nuclear Structure (Proc. Conf. Leningrad, 1980), AN SSSR, Moscow, 325.
EXFOR: A0074
Only isomeric ratio.

LEVKOVSKIJ, V.N., "Activation cross-section nuclides of average masses (A = 40 - 100) by protons and alpha-particles with average energies (E = 10 - 50 MeV)", Activation Cross Section by Protons and Alphas, Moscow (1991).
EXFOR: A0510

Cross-sections must be normalized by a factor of 0.8 as pointed out by Takács, S., Tárkányi, F., Sonck, M., Hermanne, A., Investigation of the $^{nat}Mo(p,x)^{96mg}Tc$ nuclear reaction to monitor proton beams: New measurements and consequences on the earlier reported data, Nucl. Instrum. Methods B 198 (2002) 183-196.

RÖSCH, F., QAIM, S.M., STÖCKLIN, G., Nuclear data relevant to the production of the positron emitting radioisotope ^{86}Y via the $^{86}Sr(p,n)$- and $^{nat}Rb(^{3}He,xn)$-processes, Radiochim. Acta **61** (1993) 1–8.
EXFOR: D4030

QAIM, S.M., UHL, M., ROSCH, F., SZELECSENYI, F., Excitation functions of (p,α) reactions on ^{64}Ni, ^{78}Kr, and ^{86}Sr, Phys. Rev. C **52** (1995) 733–739.
EXFOR: D4015
Same data as in Rösch (1993).

MICHEL, R., et al., Cross sections for the production of residual nuclides by low- and medium-energy protons from the target elements C, N, O, Mg, Al, Si, Ca, Ti, V, Mn, Fe, Co, Ni, Cu, Sr, Y, Zr, Nb, Ba and Au, Nucl. Methods B **129** (1997) 153–193.
EXFOR: O0276
Measured on natural Y target; therefore, only one (first) point has been retained in this evaluation.

Yield

ZATOLOKIN, B.V., KONSTANTINOV, I.O., KRASNOV, N.N., Use of 11-MeV protons for activation analysis, Atomnaya Energiya **42** (1977) 311–314.
EXFOR: no
Target: natural Sr.

NICKLES, R.J., A shotgun approach to the chart of the nuclides: Radiotracer production with an 11 MeV proton cyclotron, Acta Radiologica Suppl. **376** (1991) 69–71.
EXFOR: no
Target: natural Sr.

YOO, J., et al., Preparation of high specific activity ^{86}Y using a small biomedical cyclotron, Nucl. Med. Biol. **32** (2005) 891–897.
The measured experimental yields are 60–70% of the yields calculated from cross-section data of Rösch et al. (1993). Results of this paper are not plotted on the yield graph because the proton beam did not terminate in the target — thick-target yields and not integral yields were published.

All experimental cross-section data are shown in Fig. 7.39, and the selected measurements are compared with the resulting statistical fit to these data in Fig. 7.40. Excitation functions have been calculated by means of the ALICE-IPPE and EMPIRE nuclear reaction modelling codes, and results are compared with all of the selected experimental data in Fig. 7.41. Yields determined from the recommended cross-sections are presented in Fig. 7.42, while corresponding numerical values for the recommended cross-sections and yields are listed in Table 7.17.

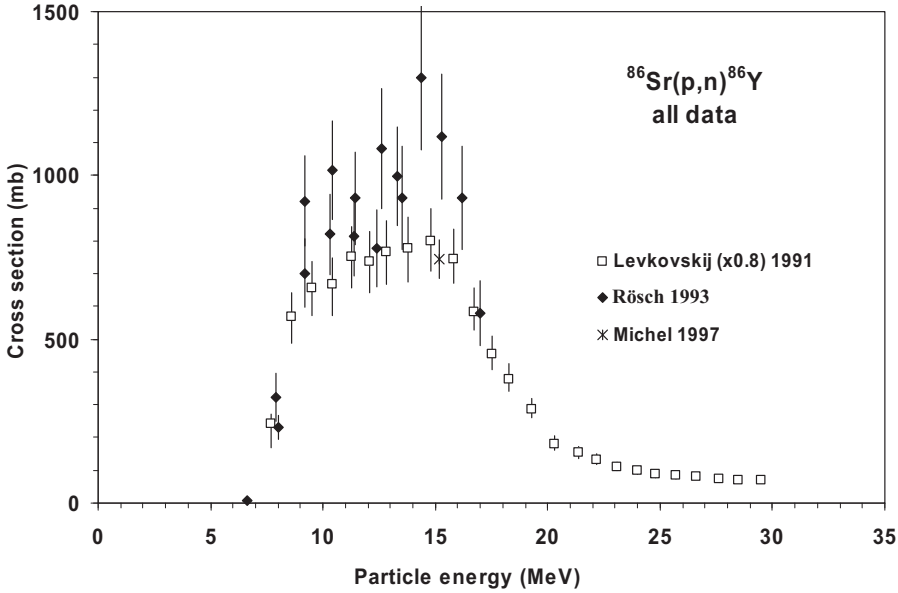

FIG. 7.39. All experimental data.

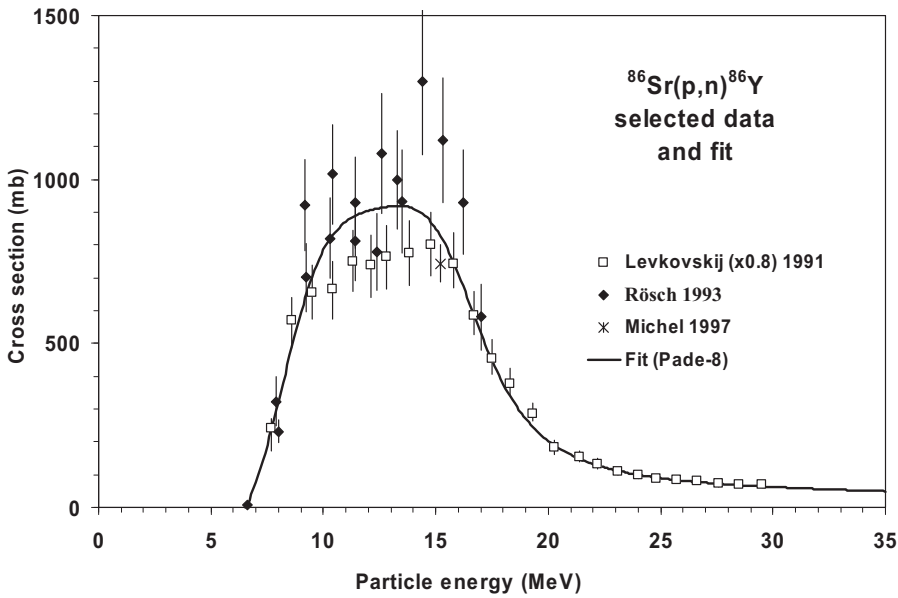

FIG. 7.40. Selected experimental data and the recommended curve (fit).

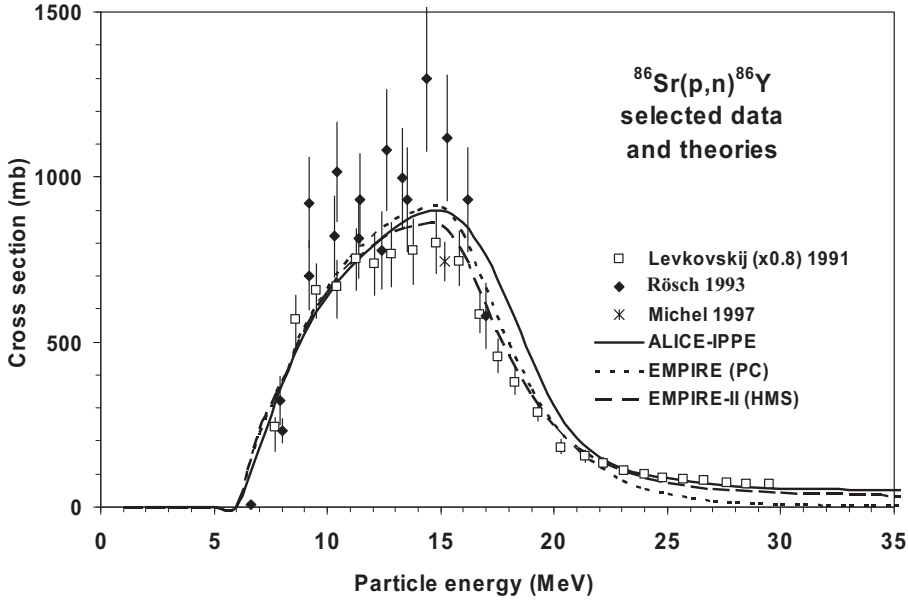

FIG. 7.41. Selected experimental data and theoretical calculations.

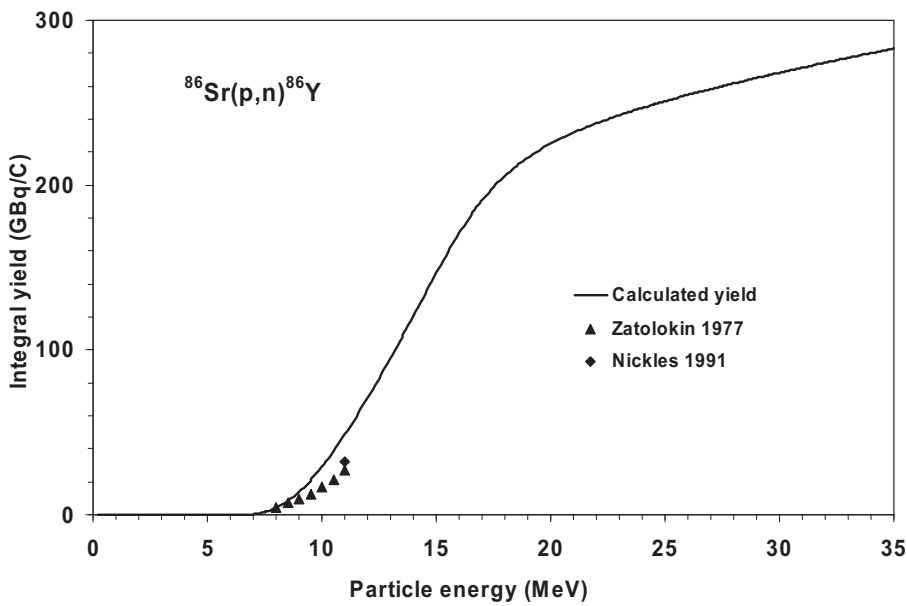

FIG. 7.42. Calculated integral yield curve based on the recommended cross-sections.

TABLE 7.17. RECOMMENDED CROSS-SECTIONS AND INTEGRAL YIELDS

$^{86}Sr(p, n)^{86}Y$ energy (MeV)	Cross-section (mb)	Integral yield	
		(μCi/μAh)	(GBq/C)
6.5	0	0	0
7.0	78	34	0
7.5	190	160	2
8.0	323	406	4
8.5	463	795	8
9.0	595	1337	14
9.5	704	2023	21
10.0	785	2835	29
10.5	839	3749	39
11.0	872	4740	49
11.5	892	5794	60
12.0	904	6901	71
12.5	913	8054	83
13.0	918	9248	95
13.5	919	10 481	108
14.0	911	11 743	121
14.5	890	13 016	134
15.0	850	14 274	147
15.5	789	15 486	159
16.0	710	16 624	171
16.5	621	17 648	181
17.0	531	18 552	191
17.5	448	19 335	199
18.0	377	20 007	206
18.5	318	20 585	212
19.0	270	21 084	217
19.5	232	21 520	221
20.0	202	21 904	225
20.5	179	22 248	229
21.0	159	22 560	232
21.5	144	22 845	235

TABLE 7.17. RECOMMENDED CROSS-SECTIONS AND INTEGRAL YIELDS (cont.)

$^{86}Sr(p, n)^{86}Y$ energy (MeV)	Cross-section (mb)	Integral yield	
		(μCi/μAh)	(GBq/C)
22.0	132	23 108	238
22.5	121	23 354	240
23.0	113	23 586	242
23.5	105	23 806	245
24.0	99	24 015	247
24.5	94	24 216	249
25.0	89	24 409	251
25.5	85	24 596	253
26.0	81	24 777	255
26.5	78	24 953	256
27.0	75	25 125	258
27.5	72	25 293	260
28.0	70	25 458	262
28.5	68	25 619	263
29.0	66	25 777	265
29.5	64	25 933	267
30.0	62	26 086	268
30.5	60	26 237	270
31.0	59	26 386	271
31.5	57	26 533	273
32.0	56	26 679	274
32.5	55	26 823	276
33.0	54	26 965	277
33.5	52	27 106	279
34.0	51	27 245	280
34.5	50	27 383	281
35.0	49	27 521	283

7.5. CHARGED PARTICLE PRODUCTION OF ^{103}Pd

Palladium-103 is extensively used in the treatment of prostate cancer and ocular melanoma, and is mostly applied in the form of sealed seeds (brachytherapy). This radioisotope has a suitable half-life of 16.9 d and decays almost exclusively by EC to ^{103m}Rh, which de-excites by means of a heavily converted internal transition. As a result of both processes (EC and IT), X rays and Auger electrons are emitted which are ideally suited for brachytherapy. ^{102}Rh is a relevant impurity. Simplified decay schemes for ^{103,102}Rh radionuclides are shown in Figs 7.43(a) and 7.43(b), and the main emissions, as defined in Tables 7.18(a), 7.18(b) and 7.18(c), were taken from NuDat 2.4 [7.3].

A. Decay data

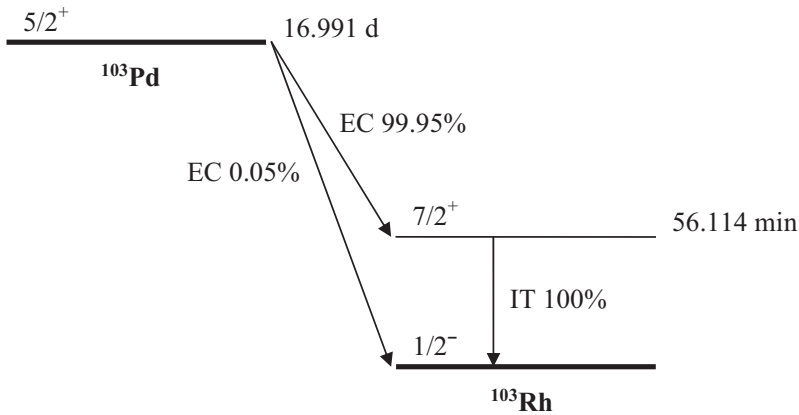

FIG. 7.43(a). Simplified decay scheme of ^{103}Pd [7.3, 7.4].

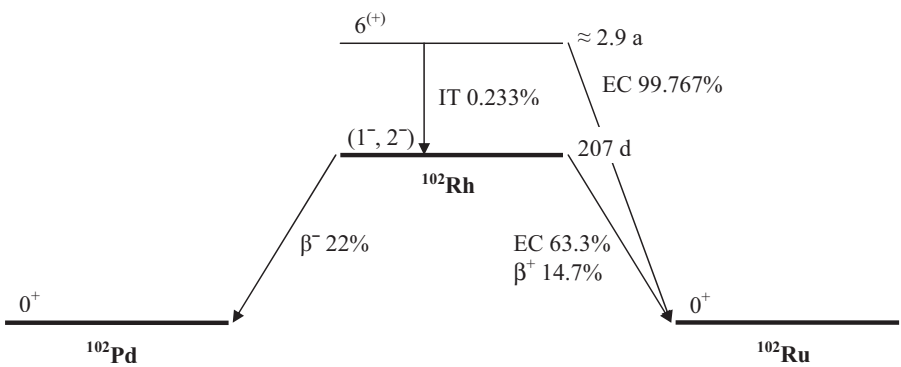

FIG. 7.43(b). Simplified decay scheme of ^{102m}Rh and ^{102}Rh [7.3].

TABLE 7.18(a). MAIN EMISSIONS [7.3]

Pd-103	Decay mode: $T_{1/2}$	EC 100% 16.991 d
Radiation	Energy (keV)	Intensity (%)
Auger L	2.39	168.0
ce K	16.528	9.52
Auger K	17.0	18.2
ce L	36.336	71.2
ce M	39.121	14.38
X-L	2.7	8.73
X-Kα2	20.074	22.4
X-Kα1	20.216	42.5
X-Kβ3	22.699	3.54
X-Kβ1	22.724	6.85
X-Kβ2	23.172	1.64
g	39.748	0.0683
g	357.45	0.0221

TABLE 7.18(b). MAIN EMISSIONS [7.3]

Rh-102g	Decay mode:	EC 63.3%, β^+ 14.7%
	$T_{1/2}$	207 d
Radiation	Energy (keV)	Intensity (%)
g	475.06	46
γ annihilation	511.0	29.4

TABLE 7.18 (c). MAIN EMISSIONS [7.3]

Rh-102m	Decay mode: $T_{1/2}$	EC 99.767% ≈ 2.9 a
Radiation	Energy (keV)	Intensity (%)
g	475.06	95
g	631.29	56.0
g	697.49	44.0
g	766.84	34.0
g	1046.59	34.0
g	1112.84	19.0

B. Production routes

Palladium-103 was originally produced via the ^{102}Pd(n, γ)^{103}Pd reaction (an evaluation of the data for this reaction is given in Section 6.3). The low specific activity achieved in this process resulted in the development of alternative routes of production, as defined in Table 7.19. Since ^{102}Rh is a disturbing impurity, its production data were also evaluated.

C. ^{103}Rh(p, n)^{103}Pd reaction

Eight experimental sets of cross-section data were found in the literature. Hermanne et al. (2000) and Sudár et al. (2002) measured cross-sections by counting both the X rays and the 357 keV gamma emission. The two methods gave different results, whereby the gamma ray study was systematically higher.

TABLE 7.19. INVESTIGATED PRODUCTION ROUTES [7.3, 7.4]

Target isotope	Natural abundance	Reaction	Q-value (MeV)	Threshold energy (MeV)
Rh-103	100%	(p, n)^{103}Pd	–1.3	1.3
Rh-103	100%	(p, pn)^{102}Rh (p, d)^{102}Rh impurity	–9.3 –7.1	9.4 7.2
Rh-103	100%	(d, 2n)^{103}Pd	–3.6	3.6
Rh-103	100%	(d, p2n)^{102}Rh (d, dn)^{102}Rh (d, t)^{102}Rh impurity	–11.5 –9.3 –3.1	11.8 9.5 3.1

BIBLIOGRAPHY, EVALUATION AND SELECTION

Cross-sections

BLASER, J.P., BOEHM, F., MARMIER, P., SCHERRER, P., Anregungsfunktionen und Wirkungsquerschnitte der (p,n)-Reaktion (II), Helv. Phys. Acta **24** (1951) 441–464.
EXFOR: P0033

ALBERT, R.D., (p,n) cross section and proton optical-model parameters in the 4 to 5.5 MeV energy region, Phys. Rev. **115** (1959) 925–927.
EXFOR: T0130
Detected particle: neutrons.

JOHNSON, C.H., GALONSKY, A., INSKEEP, C.N., Cross Sections for (p,n) Reactions in Intermediate-Weight Nuclei, Oak Ridge Natl Lab., Rep. ORNL-2910 (1960) 25 (unpublished).
EXFOR: T0135
Detected particle: neutrons.

HARPER, P.V., LATHROP, K., NE ED, J.L., The thick target yield and excitation function for the reaction ^{103}Rh(p,n)^{103}Pd, Oak Ridge Natl Lab., Rep. ORNL-LR-DWG 51564 (1961) 124–128.
EXFOR: no

HANSEN, L.F., ALBERT, R.D., Statistical theory predictions for 5 to 11 MeV (p,n) and (p,p') nuclear reactions in ^{51}V, ^{59}Co, ^{63}Cu, ^{65}Cu and ^{103}Rh, Phys. Rev. **128** (1962) 291–299.
EXFOR: B0066
Detected particle: neutrons.

MUKHAMMEDOV, S., VASIDOV, A., Determination of rhodium by proton-activation technique using the (p,n) reaction at a cyclotron, Izv. Akad. Nauk. Uzb. SSR Ser. Fiz.-Mat. **2** (1984) 329 or 2 (1986) 90 (in Russian).
EXFOR: no
Rejected because of the differences in shape compared with all other excitation functions just above the threshold energy.

HERMANNE, A., SONCK, M., FENYVESI, A., DARABAN, L., Study on production of ^{103}Pd and characterisation of possible contaminants in the proton irradiation of ^{103}Rh up to 28 MeV, Nucl. Instrum. Methods B **170** (2000) 281–292.
EXFOR: D4108, O0843
Detected particle: X rays and γ photons.
Data measured by means of the 357 keV gamma ray emission were rejected.

SUDAR, S., CSERPAK, F., QAIM, S.M., Measurements and nuclear model calculation on proton-induced reactions on ^{103}Rh up to 40 MeV: Evaluation of the excitation function of the ^{103}Rh(p,n)^{103}Pd reaction relevant to the production of the therapeutic radionuclide ^{103}Pd, Appl. Radiat. Isot. **56** (2002) 821–831.
EXFOR: D4125, O1010
Detected particle: X rays and γ photons.

Yield

DMITRIEV, P.P., PANARIN, M.V., MOLIN, G.A., Production of ^{103}Pd by the ^{103}Rh(p,n) and ^{103}Rh(d,2n) reactions, Atomnaya Energiya **82** (1982) 53.
EXFOR: S0033

DMITRIEV, P.P., Systematics of nuclear reaction yields for thick target at 22 MeV proton energy, Vop. At. Nauki i Tekhn., Ser. Yad. Konst. **2** (1983) 57–61.
EXFOR: A0195

MUKHAMMEDOV, S., VASIDOV, A., PARDAEV, E., Application of proton and deuteron activation method of analysis in the determination of elements with Z greater than 42, Atomnaya Energiya **56** (1984) 50–53.
EXFOR: A0212

All experimental cross-section data are shown in Fig. 7.44, and the selected measurements are compared with the resulting statistical fit to these data in Fig. 7.45. Excitation functions have been calculated by means of the ALICE-IPPE, EMPIRE and GNASH nuclear reaction modelling codes, and results are compared with all of the selected experimental data in Fig. 7.46. Yields determined from the recommended cross-sections are presented in Fig. 7.47, while corresponding numerical values for the recommended cross-sections and yields are listed in Table 7.20.

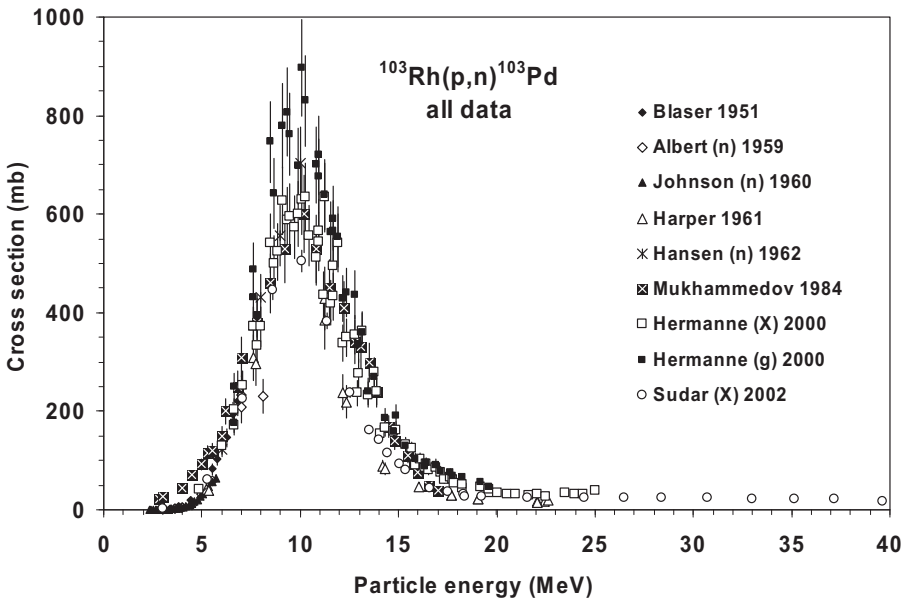

FIG. 7.44. All experimental data.

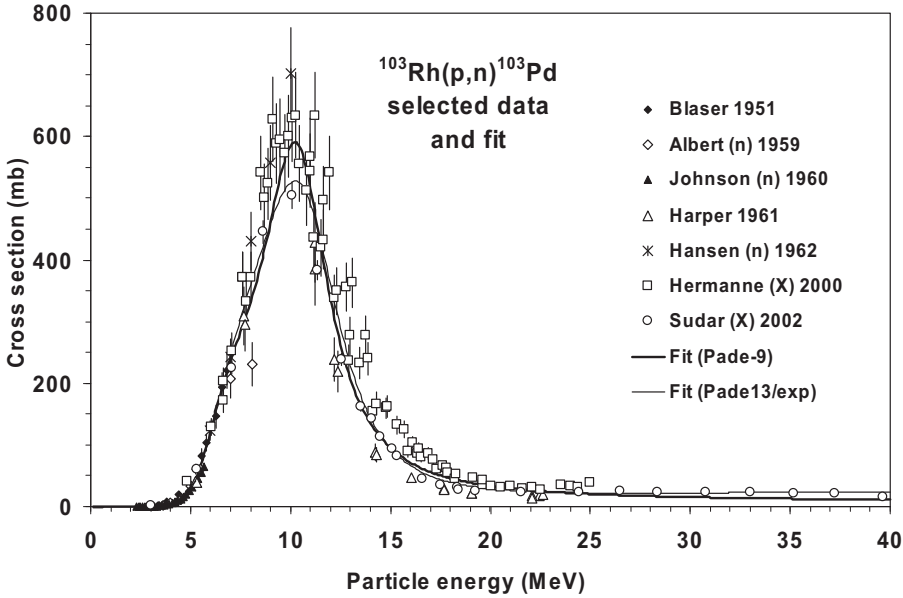

FIG. 7.45. Selected experimental data and the recommended curve (fit).

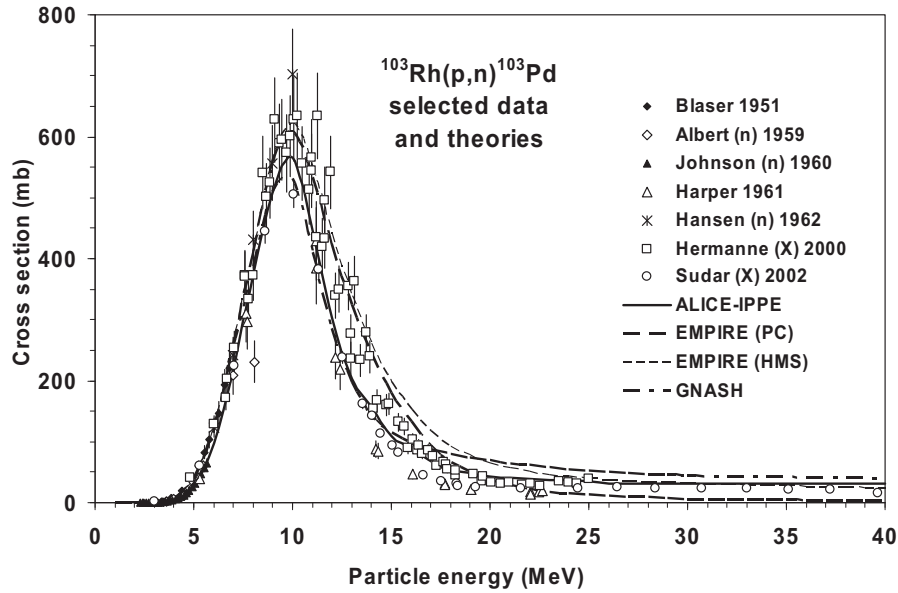

FIG. 7.46. Selected experimental data and theoretical calculations.

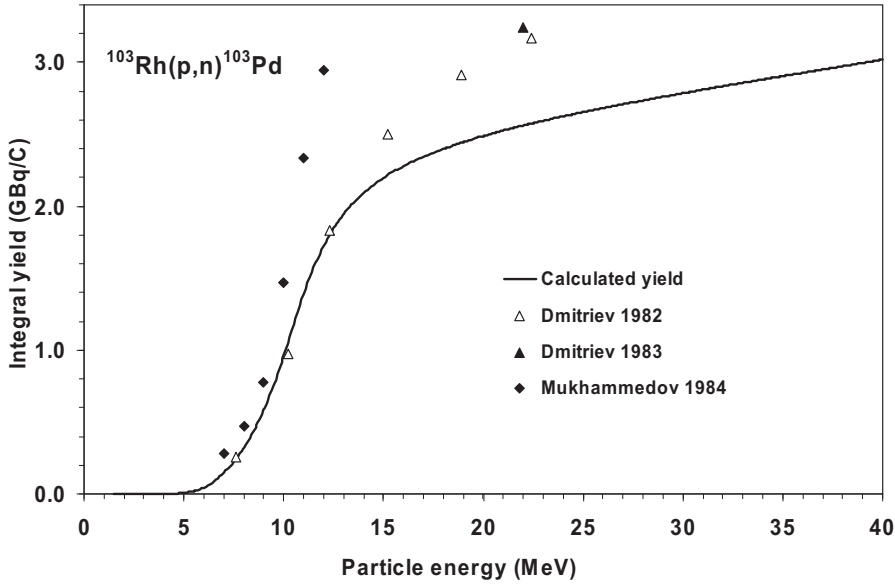

FIG. 7.47. Calculated integral yield curve based on the recommended cross-sections.

TABLE 7.20. RECOMMENDED CROSS-SECTIONS AND INTEGRAL YIELDS

^{103}Rh(p, n)^{103}Pd energy (MeV)	Cross-section (mb)	Integral yield	
		(μCi/μAh)	(GBq/C)
1.5	0.0	0.0	0.00
2.0	0.1	0.0	0.00
2.5	0.0	0.0	0.00
3.0	0.3	0.0	0.00
3.5	1.5	0.0	0.00
4.0	4.7	0.1	0.00
4.5	12.5	0.3	0.00
5.0	30.3	0.7	0.01
5.5	65.8	1.9	0.02
6.0	121.6	4.3	0.04
6.5	184.2	8.4	0.09
7.0	237.8	14.3	0.15
7.5	283.5	21.9	0.23

TABLE 7.20. RECOMMENDED CROSS-SECTIONS AND INTEGRAL YIELDS (cont.)

$^{103}Rh(p, n)^{103}Pd$ energy (MeV)	Cross-section (mb)	Integral yield	
		(μCi/μAh)	(GBq/C)
8.0	331.6	31.2	0.32
8.5	390.5	42.6	0.44
9.0	461.7	56.6	0.58
9.5	535.5	73.7	0.76
10.0	585.2	93.6	0.96
10.5	580.0	114.8	1.18
11.0	516.3	135.2	1.39
11.5	424.2	153.1	1.57
12.0	334.7	167.8	1.72
12.5	261.7	179.7	1.85
13.0	206.4	189.2	1.94
13.5	165.5	197.1	2.03
14.0	135.1	203.6	2.09
14.5	112.4	209.1	2.15
15.0	95.1	213.9	2.20
15.5	81.8	218.0	2.24
16.0	71.3	221.7	2.28
16.5	62.9	225.1	2.31
17.0	56.1	228.1	2.34
17.5	50.5	230.8	2.37
18.0	45.9	233.4	2.40
18.5	42.0	235.8	2.42
19.0	38.7	238.0	2.45
19.5	35.8	240.1	2.47
20.0	33.4	242.1	2.49
20.5	31.3	244.0	2.51
21.0	29.4	245.8	2.53
21.5	27.8	247.5	2.54
22.0	26.4	249.2	2.56
22.5	25.1	250.8	2.58
23.0	23.9	252.4	2.59
23.5	22.9	253.9	2.61
24.0	21.9	255.4	2.62

TABLE 7.20. RECOMMENDED CROSS-SECTIONS AND INTEGRAL YIELDS (cont.)

$^{103}Rh(p, n)^{103}Pd$ energy (MeV)	Cross-section (mb)	Integral yield	
		(μCi/μAh)	(GBq/C)
24.5	21.1	256.8	2.64
25.0	20.3	258.2	2.65
25.5	19.6	259.6	2.67
26.0	19.0	260.9	2.68
26.5	18.4	262.3	2.70
27.0	17.8	263.6	2.71
27.5	17.3	264.9	2.72
28.0	16.9	266.1	2.74
28.5	16.4	267.4	2.75
29.0	16.0	268.6	2.76
29.5	15.7	269.8	2.77
30.0	15.3	271.0	2.79
30.5	15.0	272.2	2.80
31.0	14.7	273.4	2.81
31.5	14.4	274.6	2.82
32.0	14.1	275.7	2.83
32.5	13.8	276.9	2.85
33.0	13.6	278.1	2.86
33.5	13.4	279.2	2.87
34.0	13.2	280.3	2.88
34.5	12.9	281.5	2.89
35.0	12.7	282.6	2.90
35.5	12.6	283.7	2.92
36.0	12.4	284.9	2.93
36.5	12.2	286.0	2.94
37.0	12.1	287.1	2.95
37.5	11.9	288.2	2.96
38.0	11.8	289.3	2.97
38.5	11.6	290.4	2.98
39.0	11.5	291.5	3.00
39.5	11.4	292.6	3.01
40.0	11.2	293.7	3.02

D. ^{103}Rh(p, x)^{102}Rh reaction: radioisotope impurity

Rhodium-102 is an important radioisotopic impurity generated during the production of ^{103}Pd when Pd is not separated from the irradiated Rh target. The long lived isomer deserves special attention (see also Subsection F for deuteron induced production).

BIBLIOGRAPHY, EVALUATION AND SELECTION

Cross-sections

HERMANNE, A., SONCK, M., FENYVESI, A., DARABAN, L., Study on production of ^{103}Pd and characterisation of possible contaminants in the proton irradiation of ^{103}Rh up to 28 MeV, Nucl. Instrum. Methods B **170** (2000) 281–292.
EXFOR: O0843
Measured isomeric states: metastable (^{102m}Rh) and ground state (^{102g}Rh). The data in Table 5 of the original publication are inverted by mistake. Column ^{102m}Rh belongs to ^{102g}Rh and vice versa (information from the authors). Data are shown correctly in Fig. 3 of the paper.

Yield

DMITRIEV, P.P., Systematics of nuclear reaction yields for thick target at 22 MeV proton energy, Vop. At. Nauki i Tekhn., Ser. Yad. Konst. **2** (1983) 57–61.
EXFOR: A0195

All experimental cross-section data are shown in Fig. 7.48, and the selected measurements are compared with the resulting statistical fit to these data in Fig. 7.49. Excitation functions have been calculated by means of the ALICE-IPPE nuclear reaction modelling code, and results are compared with all of the selected experimental data in Fig. 7.50. Yields determined from the recommended cross-sections are presented in Fig. 7.51, while corresponding numerical values for the recommended cross-sections and yields are listed in Tables 7.21(a) and 7.21(b).

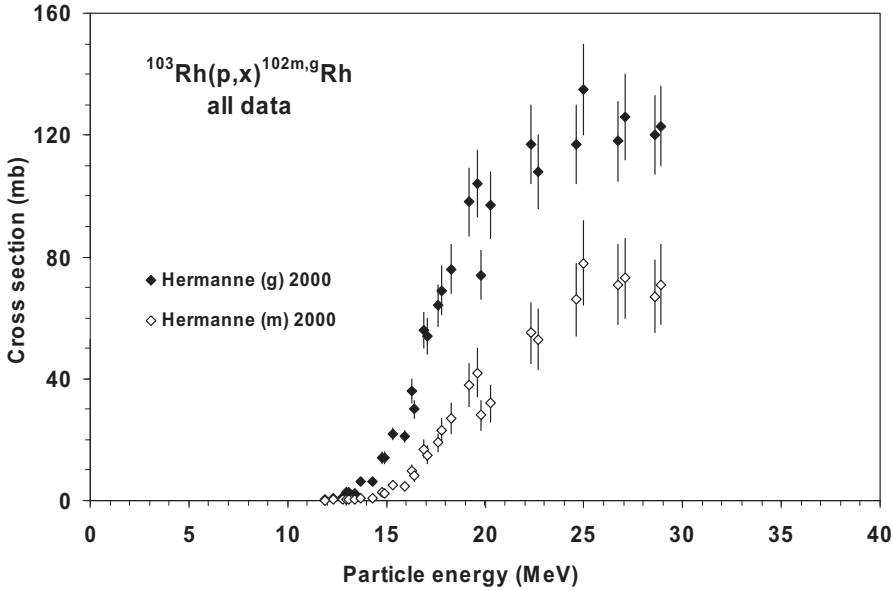

FIG. 7.48. All experimental data.

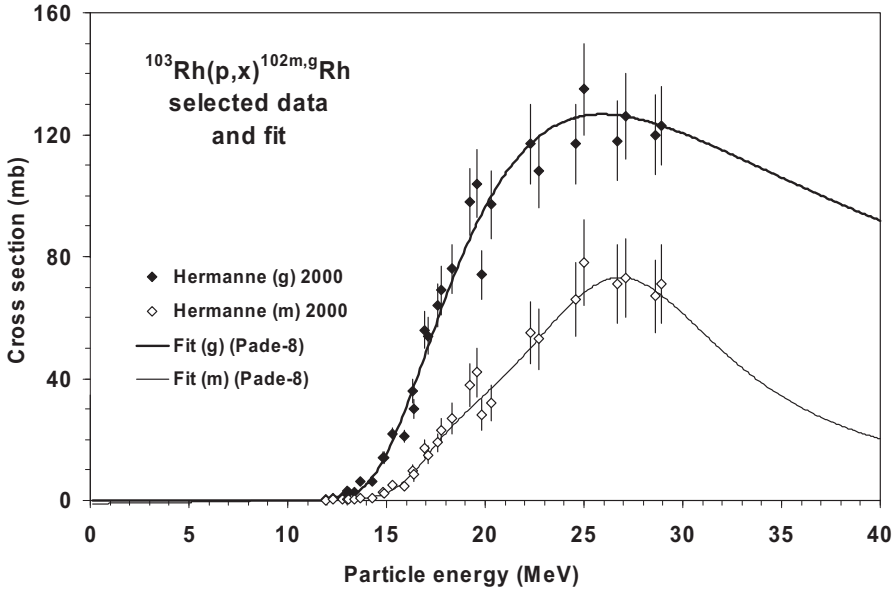

FIG. 7.49. Selected experimental data and the recommended curve (fit).

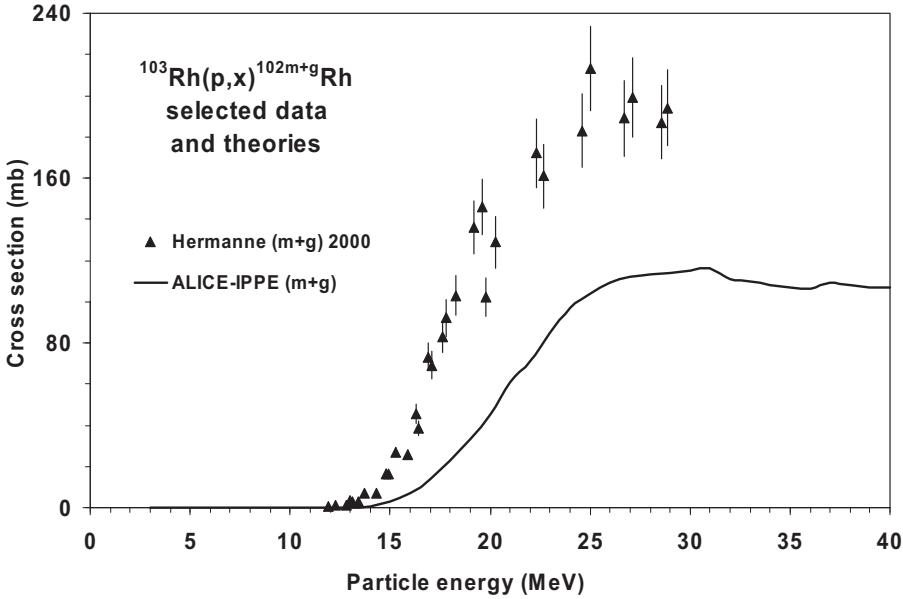

FIG. 7.50. Selected experimental data and theoretical calculations.

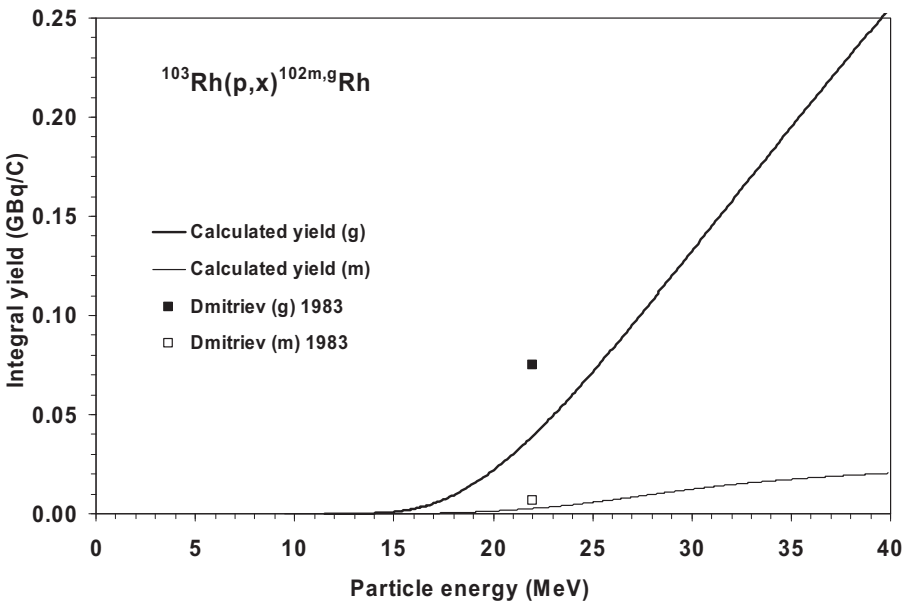

FIG. 7.51. Calculated integral yield curve based on the recommended cross-sections.

TABLE 7.21(a). RECOMMENDED CROSS-SECTIONS AND INTEGRAL YIELDS FOR ^{102g}Rh PRODUCTION

^{103}Rh(p, x)^{102g}Rh energy (MeV)	Cross-section (mb)	Integral yield	
		(μCi/μAh)	(GBq/C)
11.5	0.0	0.00	0.000
12.0	0.5	0.00	0.000
12.5	1.1	0.00	0.000
13.0	1.7	0.01	0.000
13.5	2.9	0.01	0.000
14.0	5.4	0.03	0.000
14.5	9.5	0.05	0.001
15.0	15.3	0.09	0.001
15.5	22.5	0.15	0.002
16.0	30.7	0.24	0.002
16.5	39.6	0.36	0.004
17.0	48.7	0.51	0.005
17.5	57.8	0.70	0.007
18.0	66.6	0.92	0.009
18.5	74.9	1.17	0.012
19.0	82.7	1.46	0.015
19.5	89.8	1.79	0.018
20.0	96.2	2.14	0.022
20.5	102.0	2.52	0.026
21.0	107.0	2.93	0.030
21.5	111.4	3.37	0.035
22.0	115.1	3.83	0.039
22.5	118.2	4.31	0.044
23.0	120.7	4.80	0.049
23.5	122.7	5.32	0.055
24.0	124.3	5.85	0.060
24.5	125.4	6.40	0.066
25.0	126.2	6.95	0.071
25.5	126.6	7.52	0.077
26.0	126.7	8.10	0.083
26.5	126.5	8.68	0.089

TABLE 7.21(a). RECOMMENDED CROSS-SECTIONS AND INTEGRAL YIELDS FOR ^{102g}Rh PRODUCTION (cont.)

^{103}Rh(p, x)^{102g}Rh energy (MeV)	Cross-section (mb)	Integral yield	
		(μCi/μAh)	(GBq/C)
27.0	126.1	9.27	0.095
27.5	125.5	9.87	0.101
28.0	124.7	10.47	0.108
28.5	123.8	11.07	0.114
29.0	122.8	11.67	0.120
29.5	121.6	12.28	0.126
30.0	120.4	12.89	0.132
30.5	119.1	13.50	0.139
31.0	117.7	14.11	0.145
31.5	116.3	14.72	0.151
32.0	114.9	15.33	0.158
32.5	113.4	15.94	0.164
33.0	111.9	16.55	0.170
34.0	108.9	17.76	0.183
34.5	107.4	18.36	0.189
35.0	105.9	18.97	0.195
35.5	104.4	19.57	0.201
36.0	103.0	20.16	0.207
36.5	101.5	20.76	0.213
37.0	100.1	21.35	0.219
37.5	98.6	21.94	0.226
38.0	97.2	22.53	0.232
38.5	95.8	23.12	0.238
39.0	94.5	23.70	0.244
39.5	93.1	24.28	0.250
33.5	110.4	17.15	0.176

TABLE 7.21(b). RECOMMENDED CROSS-SECTIONS AND INTEGRAL YIELDS FOR ^{102m}Rh PRODUCTION

^{103}Rh(p, x)^{102m}Rh energy (MeV)	Cross-section (mb)	Integral yield	
		(μCi/μAh)	(GBq/C)
9.5	0.0	0.000	0.00000
10.0	0.0	0.000	0.00000
10.5	0.1	0.000	0.00000
11.0	0.1	0.000	0.00000
11.5	0.2	0.000	0.00000
12.0	0.2	0.000	0.00000
12.5	0.3	0.000	0.00000
13.0	0.3	0.001	0.00001
13.5	0.5	0.001	0.00001
14.0	0.8	0.001	0.00001
14.5	1.4	0.002	0.00002
15.0	2.5	0.003	0.00003
15.5	4.2	0.005	0.00005
16.0	6.8	0.009	0.00009
16.5	10.3	0.014	0.00015
17.0	14.2	0.023	0.00023
17.5	18.2	0.034	0.00035
18.0	22.0	0.048	0.00049
18.5	25.5	0.065	0.00067
19.0	28.8	0.084	0.00087
19.5	31.8	0.107	0.00110
20.0	34.9	0.132	0.00135
20.5	38.0	0.159	0.00164
21.0	41.2	0.190	0.00195
21.5	44.5	0.223	0.00229
22.0	48.0	0.260	0.00267
22.5	51.6	0.300	0.00308
23.0	55.2	0.344	0.00353
23.5	58.8	0.391	0.00402
24.0	62.2	0.442	0.00455
24.5	65.4	0.497	0.00511

TABLE 7.21(b). RECOMMENDED CROSS-SECTIONS AND INTEGRAL YIELDS FOR ^{102m}Rh PRODUCTION (cont.)

^{103}Rh(p, x)^{102m}Rh energy (MeV)	Cross-section (mb)	Integral yield	
		(μCi/μAh)	(GBq/C)
25.0	68.2	0.555	0.00571
25.5	70.4	0.616	0.00633
26.0	72.1	0.680	0.00699
26.5	72.9	0.745	0.00766
27.0	73.1	0.812	0.00835
27.5	72.5	0.879	0.00904
28.0	71.2	0.947	0.00973
28.5	69.3	1.013	0.01041
29.0	66.9	1.078	0.01108
29.5	64.2	1.142	0.01174
30.0	61.3	1.204	0.01237
30.5	58.2	1.263	0.01298
31.0	55.1	1.320	0.01356
31.5	52.1	1.374	0.01412
32.0	49.1	1.426	0.01466
32.5	46.2	1.475	0.01516
33.0	43.5	1.523	0.01565
33.5	41.0	1.567	0.01611
34.0	38.6	1.610	0.01655
34.5	36.3	1.651	0.01697
35.0	34.2	1.690	0.01736
35.5	32.3	1.726	0.01774
36.0	30.5	1.762	0.01811
36.5	28.8	1.795	0.01845
37.0	27.3	1.828	0.01878
37.5	25.9	1.858	0.01910
38.0	24.6	1.888	0.01940
38.5	23.3	1.916	0.01969
39.0	22.2	1.943	0.01997
39.5	21.2	1.969	0.02024

E. ^{103}Rh(d, 2n)^{103}Pd reaction

BIBLIOGRAPHY, EVALUATION AND SELECTION

All experimental cross-section data are shown in Fig. 7.52, and the selected measurements are compared with the resulting statistical fit to these data in Fig. 7.53. Excitation functions have been calculated by means of the ALICE-IPPE, EMPIRE and GNASH nuclear reaction modelling codes, and results are compared with all of the selected experimental data in Fig. 7.54. Yields determined from the recommended cross-sections are presented in Fig. 7.55, while corresponding numerical values for the recommended cross-sections and yields are listed in Table 7.22.

Cross-sections

HERMANNE, A., SONCK, M., TAKACS, S., TÁRKÁNYI, F., SHUBIN, Y., Study on alternative production of ^{103}Pd and characterisation of contaminants in the deuteron irradiation of ^{103}Rh up to 21 MeV, Nucl. Instrum. Methods B **187** (2002) 3–14.
EXFOR: D4097
Detected particle: X rays and γ photons. Data measured by means of the 357 keV gamma ray emission were rejected.

HERMANNE, A., et al., Deuteron bombardment of ^{103}Rh: a new promising pathway for the production of ^{103}Pd, J. Nucl. Sci. Technol. Suppl. **2** (2002) 1286–1289.
Same as the above.

Yield

DMITRIEV, P.P., PANARIN, M.V., MOLIN, G.A., Production of ^{103}Pd by the ^{103}Rh(p,n) and ^{103}Rh(d,2n) reactions, Atomnaya Energiya **53** (1982) 198.
EXFOR: S0033

DMITRIEV, P.P., KRASNOV, M.N., MOLIN, G.A., Yields of radioactive nuclides formed by bombardment of a thick target with 22-MeV deuterons, INDC(CCP)-210/L (1983), translation from Nuclear Constants **4** (1982) 38.
EXFOR: A0194

MUKHAMMEDOV, S., VASIDOV, A., PARDAEV, E., Application of proton and neutron activation method of analysis for the determination of elements with Z greater than 42, Atomnaya Energiya **56** (1984) 50–53.
EXFOR: A0212

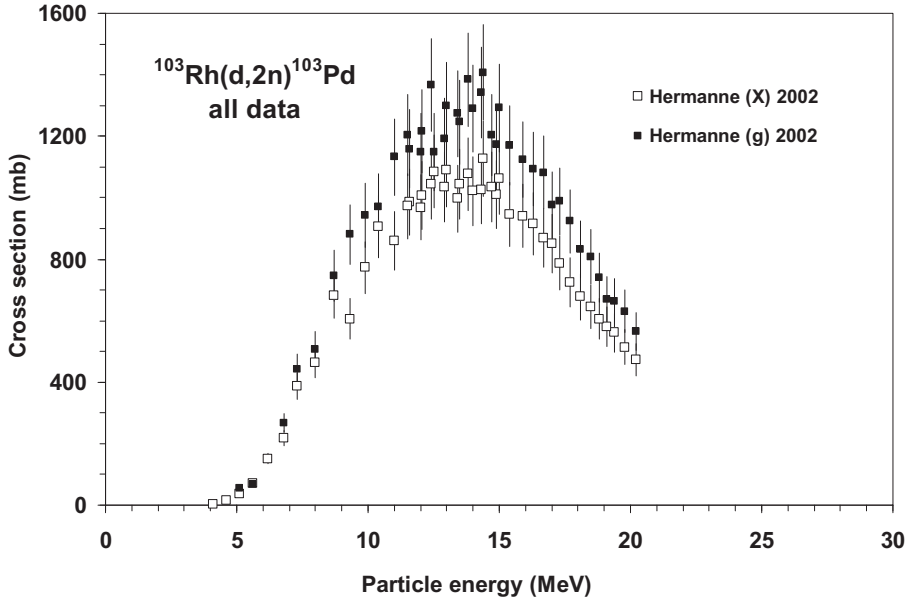

FIG. 7.52. All experimental data.

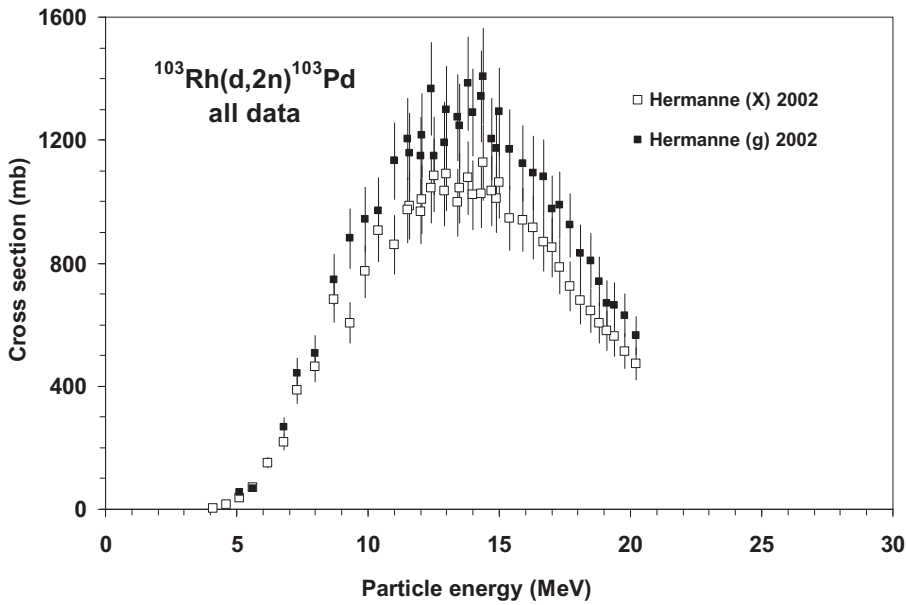

FIG. 7.53. Selected experimental data and the recommended curve (fit).

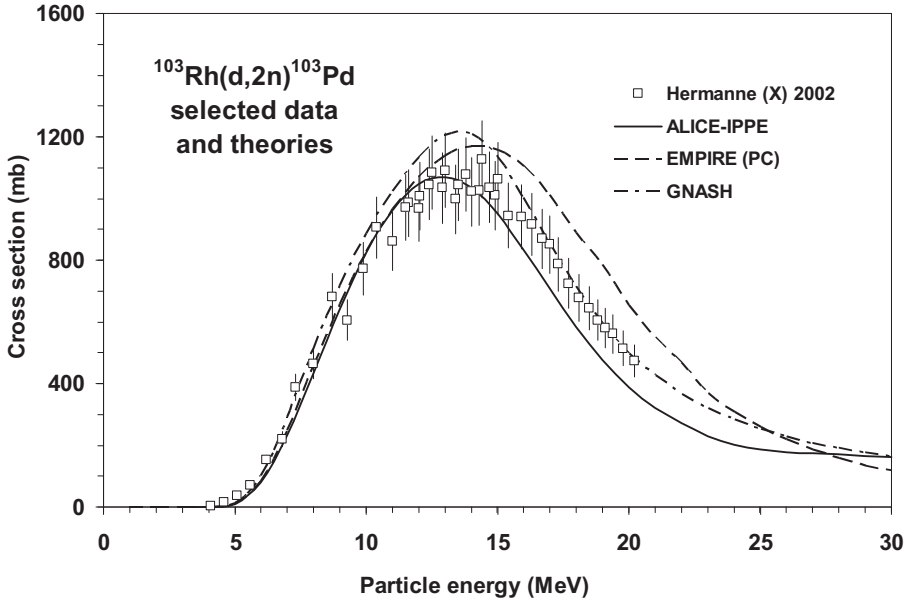

FIG. 7.54. Selected experimental data and theoretical calculations.

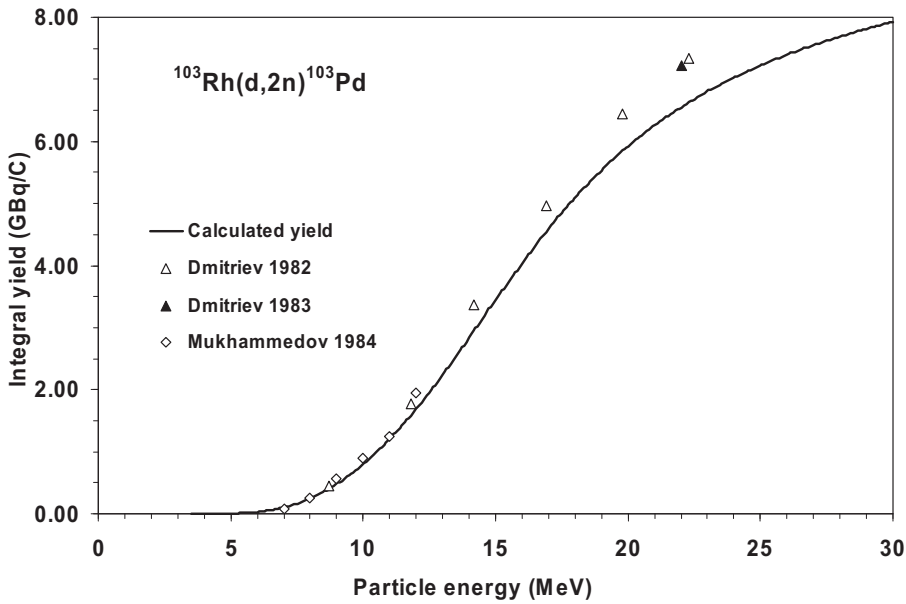

FIG. 7.55. Calculated integral yield curve based on the recommended cross-sections.

TABLE 7.22. RECOMMENDED CROSS-SECTIONS AND INTEGRAL YIELDS

^{103}Rh(d, 2n)^{103}Pd energy (MeV)	Cross-section (mb)	Integral yield	
		(μCi/μAh)	(GBq/C)
3.5	0	0	0.00
4.0	3	0	0.00
4.5	12	0	0.00
5.0	32	0	0.00
5.5	68	1	0.01
6.0	121	3	0.03
6.5	193	5	0.06
7.0	278	10	0.10
7.5	371	16	0.16
8.0	465	24	0.25
8.5	555	34	0.35
9.0	639	47	0.48
9.5	716	61	0.63
10.0	787	78	0.80
10.5	851	96	0.99
11.0	909	117	1.20
11.5	960	140	1.44
12.0	1003	164	1.69
12.5	1036	190	1.96
13.0	1058	218	2.24
13.5	1067	246	2.53
14.0	1063	276	2.83
14.5	1046	305	3.14
15.0	1016	335	3.44
15.5	976	364	3.74
16.0	928	393	4.04
16.5	874	420	4.32
17.0	816	447	4.59
17.5	758	472	4.85
18.0	700	496	5.09
18.5	644	518	5.32

TABLE 7.22. RECOMMENDED CROSS-SECTIONS AND INTEGRAL YIELDS (cont.)

^{103}Rh(d, 2n)^{103}Pd energy (MeV)	Cross-section (mb)	Integral yield	
		(μCi/μAh)	(GBq/C)
19.0	591	539	5.54
19.5	542	558	5.74
20.0	496	576	5.92
20.5	454	593	6.10
21.0	416	609	6.26
21.5	382	624	6.41
22.0	350	637	6.55
22.5	322	650	6.68
23.0	297	662	6.80
23.5	274	673	6.92
24.0	253	684	7.03
24.5	234	693	7.13
25.0	217	703	7.22
25.5	202	711	7.31
26.0	188	720	7.40
26.5	175	727	7.48
27.0	163	735	7.55
27.5	153	742	7.62
28.0	143	748	7.69
28.5	134	754	7.75
29.0	126	760	7.81
29.5	119	766	7.87
30.0	112	771	7.93

F. ^{103}Rh(d, x)^{102}Rh reaction: impurity radioisotope

Rhodium-102 is an important radioisotopic impurity generated during the production of ^{103}Pd when Pd is not separated from the irradiated Rh target. The long lived isomer deserves special attention (see also Subsection D for proton induced production).

BIBLIOGRAPHY, EVALUATION AND SELECTION

Cross-sections

HERMANNE, A., SONCK, M., TAKACS, S., TARKANYI, F., SHUBIN, Y., Study on alternative production of ^{103}Pd and characterisation of contaminants in the deuteron irradiation of ^{103}Rh up to 21 MeV, Nucl. Instrum. Methods B **187** (2002) 3–14.
EXFOR: D4097
Measured isomeric states: metastable (^{102m}Rh) and ground state (^{102g}Rh).

HERMANNE, A., et al., Deuteron bombardment of ^{103}Rh: a new promising pathway for the production of ^{103}Pd, J. Nucl. Sci. Technol. Suppl. **2** (2002) 1286–1289.
Same as the above.

Yield

DMITRIEV, P.P., KRASNOV, M.N., MOLIN, G.A., Yields of radioactive nuclides formed by bombardment of a thick target with 22-MeV deuterons, INDC(CCP)-210/L (1983), translation from Nuclear Constants **4** (1982) 38.
EXFOR: A0194

All experimental cross-section data are shown in Fig. 7.56, and the selected measurements are compared with the resulting statistical fit to these data in Fig. 7.57. Excitation functions have been calculated by means of the EMPIRE and ALICE-IPPE nuclear reaction modelling codes, and results are compared with all of the selected experimental data in Figs 7.58 and 7.59. Yields determined from the recommended cross-sections are presented in Fig. 7.60, while corresponding numerical values for the recommended cross-sections and yields are listed in Tables 7.23(a) and 7.23(b).

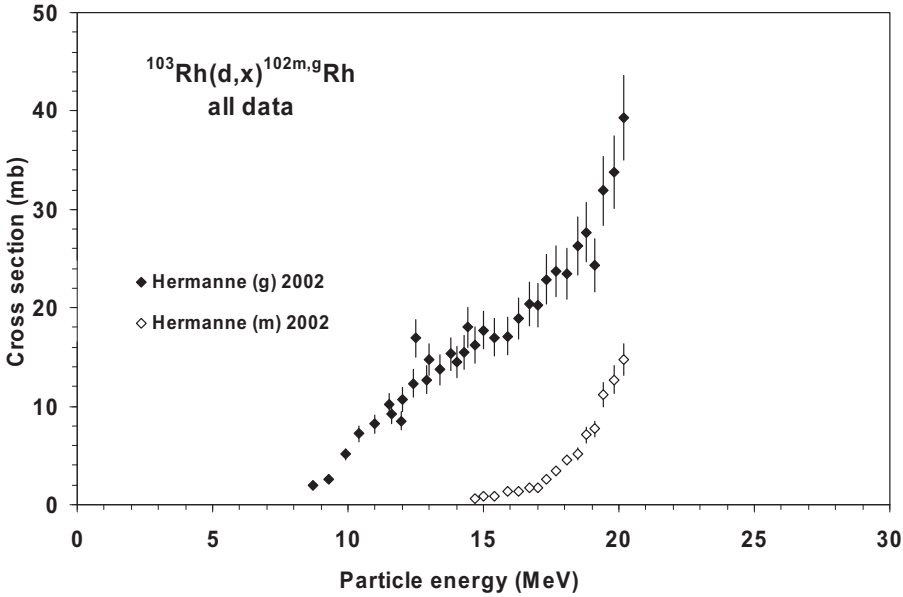

FIG. 7.56. All experimental data.

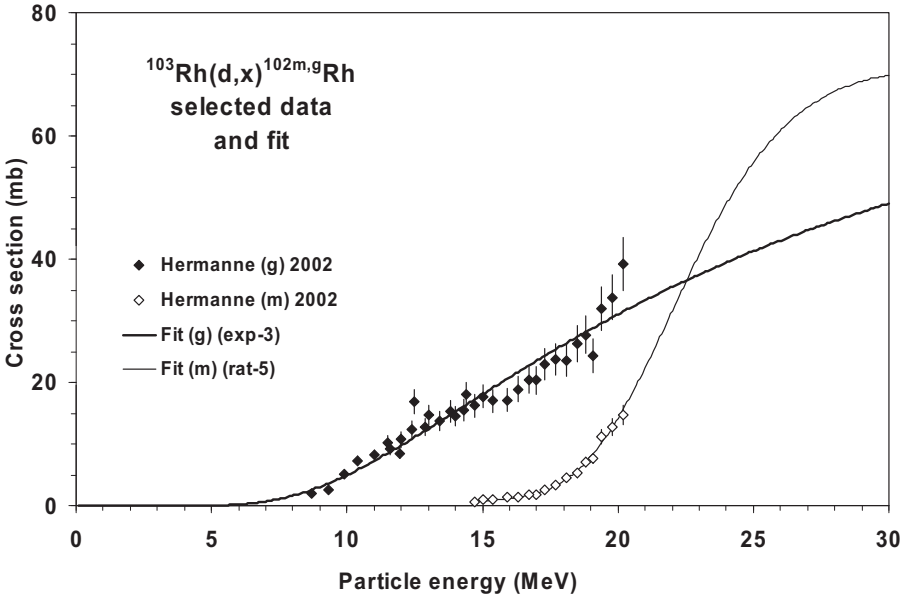

FIG. 7.57. Selected experimental data and the recommended curve (fit).

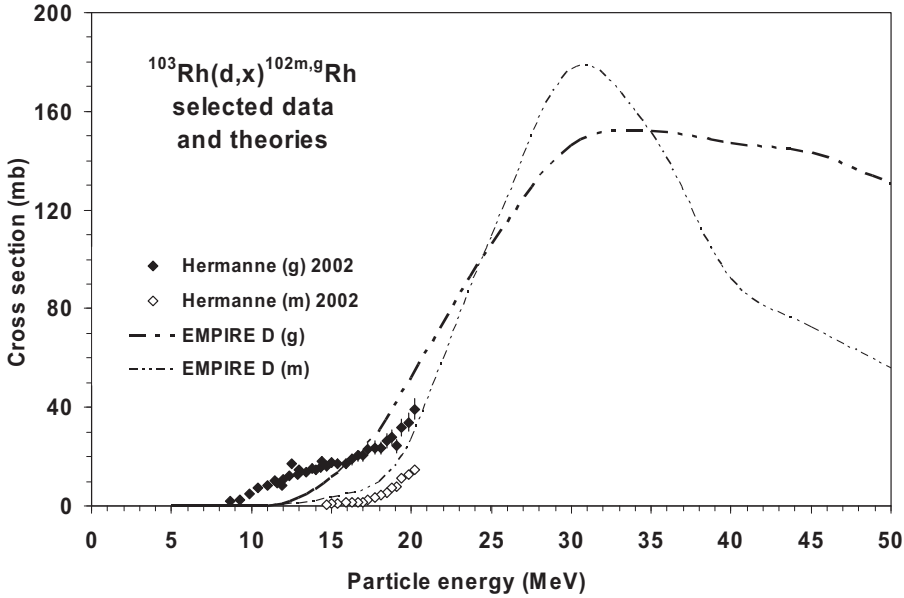

FIG. 7.58. Selected experimental data and theoretical calculations.

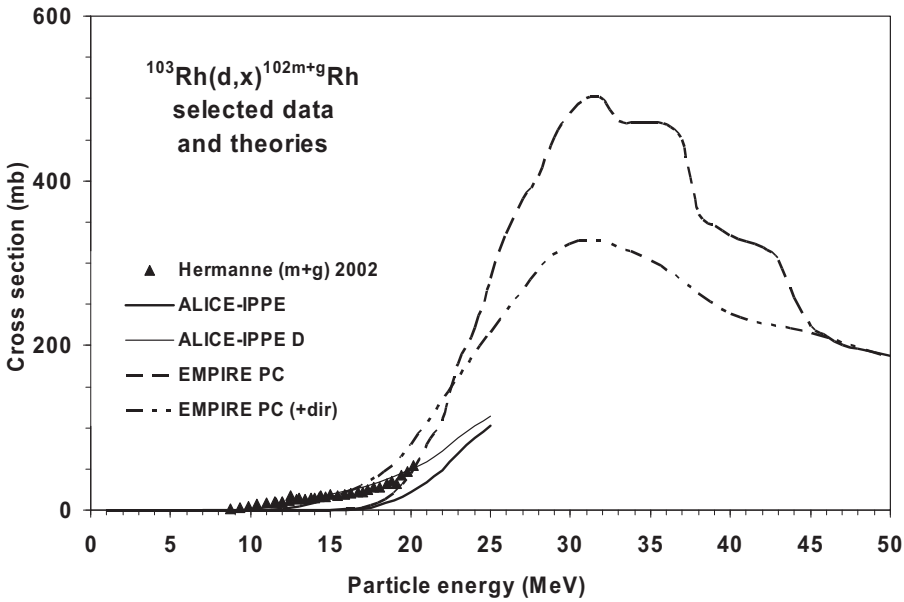

FIG. 7.59. Selected experimental data and theoretical calculations.

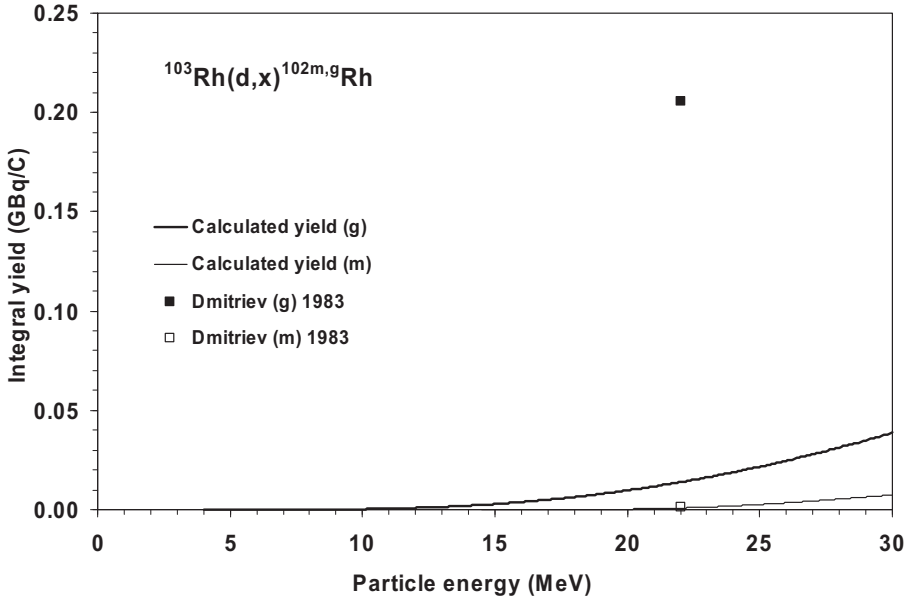

FIG. 7.60. Calculated integral yield curve based on the recommended cross-sections.

TABLE 7.23(a). RECOMMENDED CROSS-SECTIONS AND INTEGRAL YIELDS FOR ^{102g}Rh PRODUCTION

^{103}Rh(d, x)^{102g}Rh energy (MeV)	Cross-section (mb)	Integral yield	
		(μCi/μAh)	(GBq/C)
4.0	0.00	0.00	0.0000
4.5	0.01	0.00	0.0000
5.0	0.03	0.00	0.0000
5.5	0.08	0.00	0.0000
6.0	0.19	0.00	0.0000
6.5	0.37	0.00	0.0000
7.0	0.66	0.00	0.0000
7.5	1.06	0.00	0.0000
8.0	1.59	0.00	0.0001
8.5	2.25	0.01	0.0001
9.0	3.03	0.01	0.0001
9.5	3.93	0.02	0.0002
10.0	4.94	0.03	0.0003

TABLE 7.23(a). RECOMMENDED CROSS-SECTIONS AND INTEGRAL YIELDS FOR ^{102g}Rh PRODUCTION (cont.)

^{103}Rh(d, x)^{102g}Rh energy (MeV)	Cross-section (mb)	Integral yield	
		(μCi/μAh)	(GBq/C)
10.5	6.03	0.04	0.0004
11.0	7.21	0.05	0.0005
11.5	8.45	0.07	0.0007
12.0	9.75	0.08	0.0009
12.5	11.08	0.11	0.0011
13.0	12.45	0.13	0.0014
13.5	13.84	0.16	0.0017
14.0	15.23	0.19	0.0020
14.5	16.63	0.23	0.0024
15.0	18.03	0.27	0.0028
15.5	19.42	0.32	0.0033
16.0	20.80	0.37	0.0038
16.5	22.16	0.42	0.0044
17.0	23.50	0.48	0.0050
17.5	24.82	0.55	0.0056
18.0	26.11	0.62	0.0063
18.5	27.38	0.69	0.0071
19.0	28.62	0.77	0.0079
19.5	29.83	0.85	0.0088
20.0	31.02	0.94	0.0097
20.5	32.17	1.03	0.0106
21.0	33.30	1.13	0.0116
21.5	34.39	1.24	0.0127
22.0	35.46	1.34	0.0138
22.5	36.50	1.46	0.0150
23.0	37.51	1.58	0.0162
23.5	38.49	1.70	0.0175
24.0	39.45	1.83	0.0188
24.5	40.38	1.96	0.0202
25.0	41.28	2.10	0.0216
25.5	42.16	2.24	0.0231
26.0	43.01	2.39	0.0246
26.5	43.84	2.55	0.0262

TABLE 7.23(a). RECOMMENDED CROSS-SECTIONS AND INTEGRAL YIELDS FOR ^{102g}Rh PRODUCTION (cont.)

^{103}Rh(d, x)^{102g}Rh energy (MeV)	Cross-section (mb)	Integral yield	
		(μCi/μAh)	(GBq/C)
27.0	44.65	2.71	0.0278
27.5	45.43	2.87	0.0295
28.0	46.19	3.04	0.0312
28.5	46.93	3.21	0.0330
29.0	47.65	3.39	0.0349
29.5	48.35	3.58	0.0367
30.0	49.03	3.76	0.0387

TABLE 7.23(b). RECOMMENDED CROSS-SECTIONS AND INTEGRAL YIELDS FOR ^{102m}Rh PRODUCTION

^{103}Rh(d, x)^{102m}Rh energy (MeV)	Cross-section (mb)	Integral yield	
		(μCi/μAh)	(GBq/C)
14.5	0.0	0.000	0.00000
15.0	0.8	0.000	0.00000
15.5	0.9	0.001	0.00001
16.0	1.1	0.001	0.00001
16.5	1.4	0.002	0.00002
17.0	2.0	0.003	0.00003
17.5	2.8	0.004	0.00004
18.0	4.1	0.006	0.00006
18.5	5.7	0.009	0.00009
19.0	8.0	0.012	0.00013
19.5	10.7	0.018	0.00018
20.0	14.1	0.025	0.00026
20.5	18.0	0.034	0.00035
21.0	22.3	0.046	0.00048
21.5	26.8	0.061	0.00063
22.0	31.5	0.079	0.00081
22.5	36.2	0.100	0.00103
23.0	40.7	0.125	0.00128
23.5	45.0	0.152	0.00156
24.0	48.9	0.183	0.00188

TABLE 7.23(b). RECOMMENDED CROSS-SECTIONS AND INTEGRAL YIELDS FOR ^{102m}Rh PRODUCTION (cont.)

^{103}Rh(d, x)^{102m}Rh energy (MeV)	Cross-section (mb)	Integral yield	
		(μCi/μAh)	(GBq/C)
24.5	52.5	0.216	0.00222
25.0	55.7	0.252	0.00259
25.5	58.5	0.291	0.00299
26.0	60.9	0.331	0.00341
26.5	62.9	0.374	0.00385
27.0	64.6	0.419	0.00431
27.5	66.0	0.466	0.00479
28.0	67.2	0.514	0.00528
28.5	68.1	0.563	0.00579
29.0	68.9	0.614	0.00631
29.5	69.4	0.665	0.00684
30.0	69.8	0.718	0.00738

7.6. CHARGED PARTICLE PRODUCTION OF ^{111g}In

A simplified decay scheme is shown in Fig. 7.61, and the main emissions, as defined in Table 7.24, were taken from NuDat 2.4 [7.3].

A. Decay data

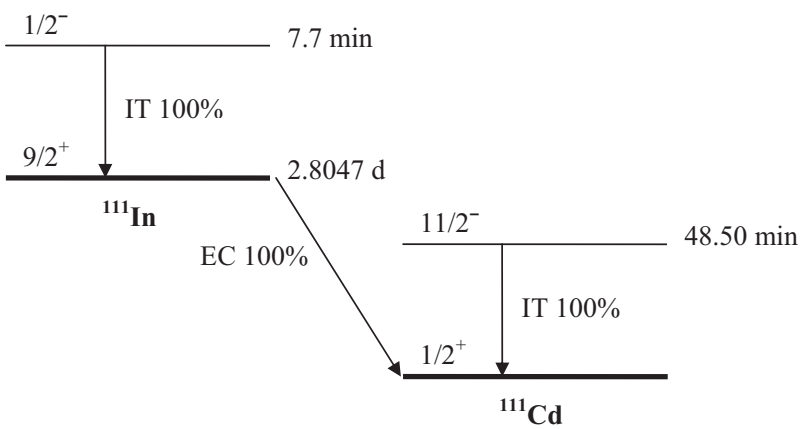

FIG. 7.61. Simplified decay scheme of ^{111}In [7.3].

TABLE 7.24. MAIN EMISSIONS [7.3]

In-111g	Decay mode: $T_{1/2}$	EC 100% 2.8047 d
Radiation	Energy (keV)	Intensity (%)
Auger L	2.72	100.4
Auger K	19.3	15.5
ce K	144.57	8.07
ce K	218.64	4.95
g	171.28	90.7
g	245.35	94.1

B. Production routes

Two proton induced reactions have been assessed, as specified in Table 7.25.

TABLE 7.25. INVESTIGATED PRODUCTION ROUTES [7.3, 7.4]

Target isotope	Natural abundance	Reaction	Q-value (MeV)	Threshold energy (MeV)
Cd-111	12.80%	(p, n)	–1.6	1.7
Cd-112	24.13%	(p, 2n)	–11.0	11.1

C. ^{111}Cd(p, n)^{111}In reaction

BIBLIOGRAPHY, EVALUATION AND SELECTION

Cross-sections

BLASER, J.-P., BOEHM, F., MARMIER, P., PEASLEE, D.C., Fonctions d'excitation de la reaction (p,n) I, Helv. Phys. Acta **24** (1951) 3–38.
EXFOR: B0048

BLOSSER, H.G., HANDLEY, T.H., Survey of (p,n) reactions at 12 MeV, Phys. Rev. **100** (1955) 1340–1344.
EXFOR: B0052

WING, J., HUIZENGA, J.R., (p,n) cross sections of ^{51}V, ^{52}Cr, ^{63}Cu, ^{65}Cu, ^{107}Ag, ^{109}Ag, ^{111}Cd, ^{114}Cd, and ^{139}La from 5 to 10.5 MeV, Phys. Rev. **128** (1962) 280–290.
EXFOR: T0124

OTOZAI, K., et al., Excitation functions for the reactions induced by protons on Cd up to 37 MeV, Nucl. Phys. **80** (1966) 335–348.
EXFOR: P0019

NIECKARZ Jr., W.J., CARETTO Jr., A.A., Production of ^{111}In and ^{114m}In from the separated isotopes of cadmium using 70- to 400-MeV protons, Phys. Rev. **178** (1969) 1887–1893.
EXFOR: C0345
Target: natural Cd and ^{111}Cd. Data were not adopted because they were measurements in the higher energy region.

SKAKUN, E.A., KLJUCHAREV, A.P., RAKIVNENKO, Yu.N., ROMANIJ, I.A., Excitation functions of (p,n)- and (p,2n)-reactions on cadmium isotopes, Izv. Rossiiskoi Akademii Nauk, Ser. Fiz. **39** (1975) 24–30.
EXFOR: A0001

SKAKUN, E.A., et al., Excitation functions and isomeric ratios for ^{111}Cd(p,n)^{111m,g}In and ^{113}Cd(p,n)^{113m}In reactions, 29th Conf. on Nuclear Spectroscopy and Nuclear Structure (Proc. Conf. Riga, 1979) 290.
EXFOR: A0135

MARTEN, M., SCHURING, A., SCOBEL, W., Pre-equilibrium neutron emission in ^{109}Ag(^{3}He,xn) and ^{111}Cd(p,xn) reactions, Z. Phys. A **322** (1985) 93–103.
EXFOR: A0335

NORTIER, F.M., MILLS, S.J., STEYN, G.F., Excitation functions and production rates of relevance to the production of ^{111}In by proton bombardment of ^{nat}Cd and ^{nat}In up to 100 MeV, Appl. Radiat. Isot. **41** (1990) 1201–1208.
EXFOR: A0500
Target: natural Cd.

ZAITSEVA, N.G., et al., Excitation functions and yields for ^{111}In production using ^{113,114,nat}Cd(p,xn)^{111}In reactions with 65 MeV protons, Appl. Radiat. Isot. **41** (1990) 177–183.
EXFOR: D4070, A0569
Target: natural Cd. Data were rejected because they are above the threshold of the ^{112}Cd(p, 2n) reaction.

TÁRKÁNYI, F., et al., Cross sections of proton induced nuclear reactions on enriched ^{111}Cd and ^{112}Cd for the production of ^{111}In for use in nuclear medicine, Appl. Radiat. Isot. **45** (1994) 239–249.
EXFOR: D4027

TÁRKÁNYI, F., et al., Activation cross sections on cadmium: Proton induced nuclear reactions up to 80 MeV, Nucl. Instrum. Methods B **245** (2006) 379–394.
EXFOR: D4170
Target: natural Cd.

Yield

BROWN, L.C., BEETS, A.L., Cyclotron production of carrier-free ^{111}In, Int. J. Appl. Radiat. Isot. **23** (1972) 57–63.
EXFOR: no

DMITRIEV, P.P., DMITRIEVA, Z.P., KRASNOV, N.N., MOLIN, G.A., PANARIN, M.V., Yields of ^{111}In and ^{114m}In in nuclear reactions with protons, deuterons and alpha particles, Atomnaya Energiya **37** (1974) 496–497.
EXFOR: no

DMITRIEV, P.P., Systematics of nuclear reaction yields for thick target at 22 MeV proton energy, Vop. At. Nauki i Tekhn., Ser. Yad. Konst. **2** (1983) 57–61.
EXFOR: A0195

MUKHAMMEDOV, S., VASIDOV, A., PARDAEV, E., Application of proton and neutron activation method of analysis for the determination of elements with Z greater than 42, Atomnaya Energiya **56** (1984) 50–53.
EXFOR: A0212

ISSHIKI, M., FUKUDA, Y., IGAKI, K., Proton activation analysis of trace impurities in purified cobalt, J. Radioanal. Nucl. Chem. **82** (1984) 135–142.
EXFOR: A0287, S0030, E1965

ZAITSEVA, N.G., et al., Excitation functions and yields for ^{111}In production using ^{113,114,nat}Cd(p,xn)^{111}In reactions with 65 MeV protons, Appl. Radiat. Isot. **41** (1990) 177–183.
EXFOR: D4070, A0569
Target: natural Cd. Data were rejected because they are above the threshold of the ^{112}Cd(p, 2n) reaction.

NICKLES, R.J., A shotgun approach to the chart of the nuclides: Radiotracer production with an 11 MeV proton cyclotron, Acta Radiologica Suppl. **376** (1991) 69–71.
EXFOR: no
Target: natural Cd. It is assumed that the result given in the article is incorrect by one order of magnitude.

All experimental cross-section data are shown in Fig. 7.62, and the selected measurements are compared with the resulting statistical fit to these data in Fig. 7.63. Excitation functions have been calculated by means of the ALICE nuclear reaction modelling code, and results are compared with all of the selected experimental data in Fig. 7.64. Yields determined from the recommended cross-sections are presented in Fig. 7.65, while corresponding numerical values for the recommended cross-sections and yields are listed in Table 7.26.

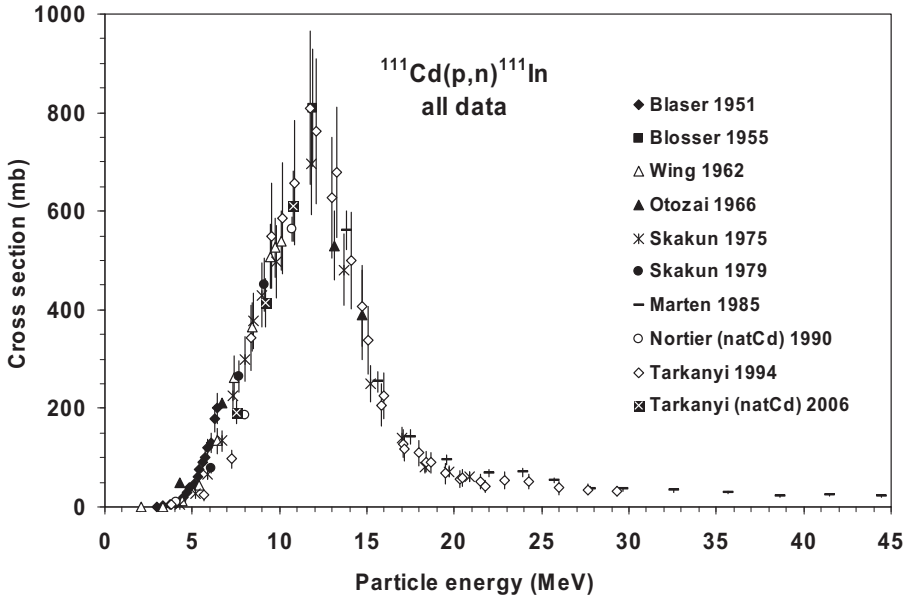

FIG. 7.62. All experimental data.

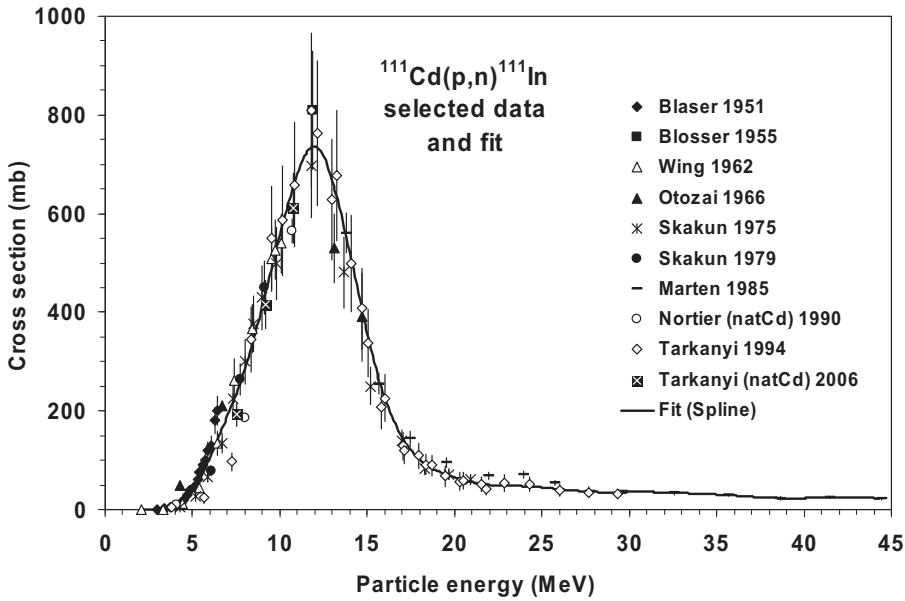

FIG. 7.63. Selected experimental data and the recommended curve (fit).

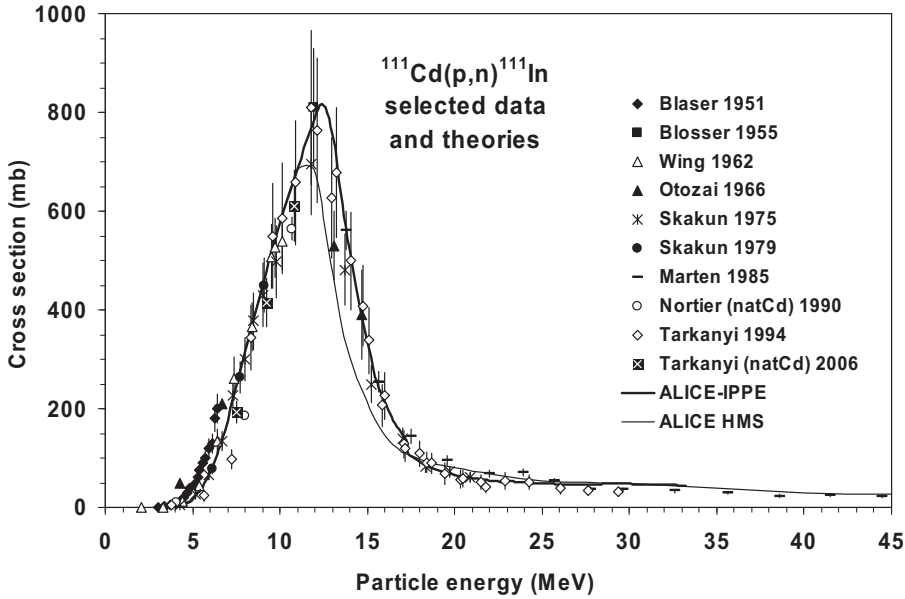

FIG. 7.64. Selected experimental data and theoretical calculations.

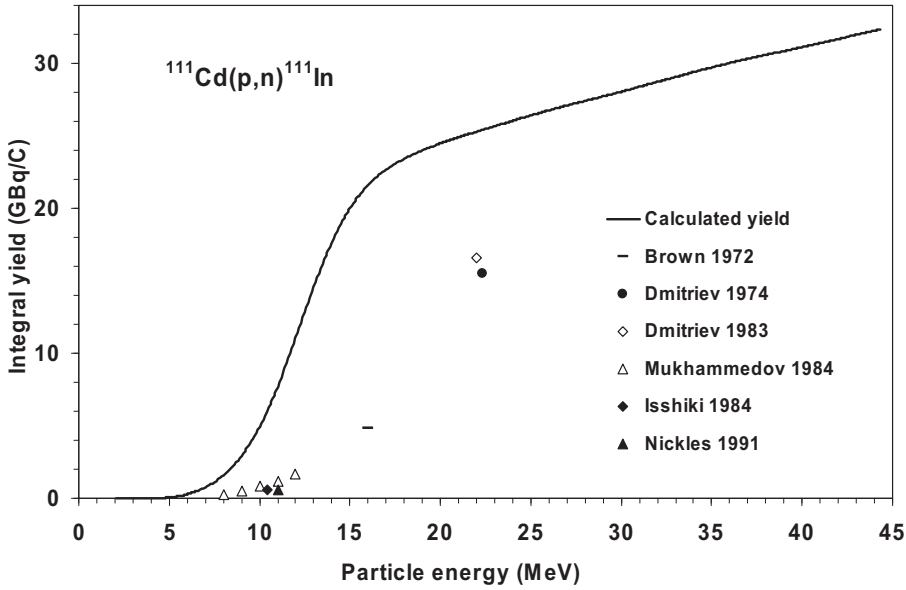

FIG. 7.65. Calculated integral yield curve based on the recommended cross-section.

TABLE 7.26. RECOMMENDED CROSS-SECTIONS AND INTEGRAL YIELDS

$^{111}Cd(p, n)^{111}In$ energy (MeV)	Cross-section (mb)	Integral yield	
		(μCi/μAh)	(GBq/C)
2.0	0.0	0	0.00
2.5	0.2	0	0.00
3.0	0.4	0	0.00
3.5	2.3	0	0.00
4.0	8.2	1	0.01
4.5	13.1	2	0.02
5.0	39.4	5	0.06
5.5	69.3	13	0.13
6.0	105.2	26	0.27
6.5	148.1	45	0.47
7.0	191.2	73	0.75
7.5	234.9	109	1.12
8.0	285.4	155	1.59
8.5	346.6	212	2.18
9.0	415.2	285	2.93
9.5	486.4	374	3.85
10.0	556.6	481	4.95
10.5	622.5	606	6.23
11.0	680.5	749	7.69
11.5	722.2	907	9.32
12.0	736.5	1076	11.05
12.5	715.6	1248	12.82
13.0	666.9	1415	14.55
13.5	599.5	1573	16.16
14.0	521.0	1715	17.62
14.5	438.0	1839	18.90
15.0	357.4	1944	19.98
15.5	285.6	2031	20.87
16.0	226.6	2101	21.60
16.5	180.7	2159	22.19
17.0	146.2	2206	22.67

TABLE 7.26. RECOMMENDED CROSS-SECTIONS AND INTEGRAL YIELDS (cont.)

$^{111}Cd(p, n)^{111}In$ energy (MeV)	Cross-section (mb)	Integral yield	
		(μCi/μAh)	(GBq/C)
17.5	121.0	2245	23.08
18.0	101.5	2279	23.42
18.5	87.5	2308	23.72
19.0	78.5	2334	23.99
19.5	72.1	2359	24.24
20.0	65.9	2382	24.48
20.5	60.2	2403	24.69
21.0	55.5	2423	24.90
21.5	52.0	2441	25.09
22.0	50.0	2459	25.28
22.5	49.3	2477	25.46
23.0	48.9	2495	25.65
23.5	48.3	2514	25.84
24.0	47.4	2532	26.02
24.5	46.3	2550	26.21
25.0	44.9	2568	26.39
25.5	43.2	2586	26.57
26.0	41.2	2603	26.75
26.5	39.5	2619	26.92
27.0	38.0	2635	27.08
27.5	36.8	2651	27.24
28.0	35.8	2666	27.40
28.5	35.0	2681	27.56
29.0	34.6	2697	27.72
29.5	35.0	2712	27.87
30.0	35.6	2728	28.04
30.5	35.9	2744	28.21
31.0	35.7	2761	28.38
31.5	35.3	2777	28.55
32.0	34.8	2794	28.72
32.5	34.1	2810	28.88

TABLE 7.26. RECOMMENDED CROSS-SECTIONS AND INTEGRAL YIELDS (cont.)

$^{111}Cd(p, n)^{111}In$ energy (MeV)	Cross-section (mb)	Integral yield	
		(μCi/μAh)	(GBq/C)
33.0	33.5	2827	29.05
33.5	32.8	2843	29.22
34.0	32.1	2859	29.38
34.5	31.4	2875	29.55
35.0	30.5	2890	29.71
35.5	29.5	2906	29.86
36.0	28.4	2921	30.02
36.5	27.1	2935	30.17
37.0	25.9	2949	30.31
37.5	24.8	2963	30.45
38.0	23.8	2976	30.58
38.5	23.1	2988	30.71
39.0	22.8	3001	30.84
39.5	22.9	3014	30.97
40.0	23.1	3027	31.11
40.5	23.5	3040	31.24
41.0	23.9	3053	31.38
41.5	24.2	3067	31.53
42.0	24.3	3082	31.67
42.5	24.2	3096	31.82
43.0	23.9	3110	31.97
43.5	23.6	3125	32.11
44.0	23.2	3139	32.26

D. ^{112}Cd(p, 2n)^{111}In reaction

All experimental cross-section data are shown in Fig. 7.66, and the selected measurements are compared with the resulting statistical fit to these data in Fig. 7.67. Excitation functions have been calculated by means of the ALICE nuclear reaction modelling code, and results are compared with all of the selected experimental data in Fig. 7.68. Yields determined from the recommended cross-sections are presented in Fig. 7.69, while corresponding numerical values for the recommended cross-sections and yields are listed in Table 7.27.

BIBLIOGRAPHY, EVALUATION AND SELECTION

Cross-sections

OTOZAI, K., et al., Excitation functions for the reactions induced by protons on Cd up to 37 MeV, Nucl. Phys. **80** (1966) 335–348.
EXFOR: P0019

NIECKARZ Jr., W.J., CARETTO Jr., A.A., Production of ^{111}In and ^{114m}In from the separated isotopes of cadmium using 70- to 400-MeV protons, Phys. Rev. **178** (1969) 1887–1893.
EXFOR: C0345
Target: natural Cd and ^{112}Cd. Data were not adopted because they were measured in the higher energy region.

SKAKUN, E.A., KLJUCHAREV, A.P., RAKIVNENKO, Yu.N., ROMANIJ, I.A., Excitation functions of (p,n)- and (p,2n)-reactions on cadmium isotopes, Izv. Rossiiskoi Akademii Nauk, Ser. Fiz. **39** (1975) 24–30.
EXFOR: A0001

TÁRKÁNYI, F., et al., Cross sections of proton induced nuclear reactions on enriched ^{111}Cd and ^{112}Cd for the production of ^{111}In for use in nuclear medicine, Appl. Radiat. Isot. **45** (1994) 239–249.
EXFOR: D4027

Yield

MacDONALD, N.S., et al., Methods for compact cyclotron production of ^{111}In for medical use, Int. J. Appl. Radiat. Isot. **26** (1975) 631–633.
EXFOR: no
Target: natural Cd, thickness: 0.51 mm. The outcoming beam energy was 16 MeV, so estimated data were added to the measured value to derive a thick-target yield taking into account our recommended yield curve.

DMITRIEV, P.P., Systematics of nuclear reaction yields for thick target at 22 MeV proton energy, Vop. At. Nauki i Tekhn., Ser. Yad. Konst. **2** (1983) 57–61.
EXFOR: A0195

HUPF, H.B., TISCHER, S.D., AL-WATBAN, F., The cyclotron radionuclide program at King Faisal Specialist Hospital and Research Centre, Nucl. Instrum. Methods B **10/11** (1985) 967–968.
EXFOR: no

KOPECKY, P., KONRAD, L., MELICHAR, F., Research, development and production of cyclotron produced radionuclides for diagnostic nuclear medicine, Jad. Energ. **31** (1985) 186–189.
EXFOR: no
Target thickness: 33 → 11 MeV.

KRASNOV, N.N., et al., Radionuclide production on cyclotron of Institute of Physics and Power Engineering, 4th Int. Workshop on Targetry and Target Chemistry (Proc. Int. Workshop Villigen, 1991), PSI, Villigen (1992) 54–56.
EXFOR: no

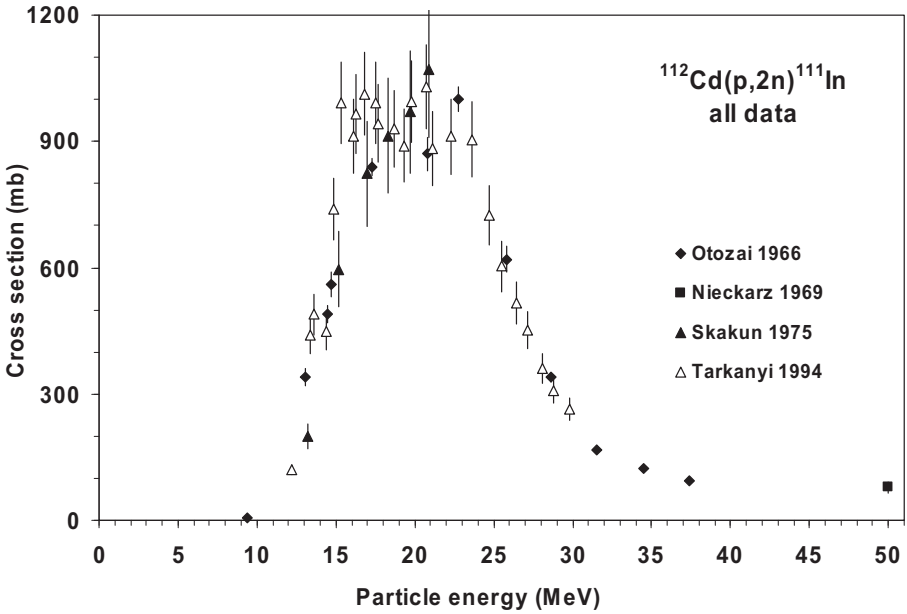

FIG. 7.66. All experimental data.

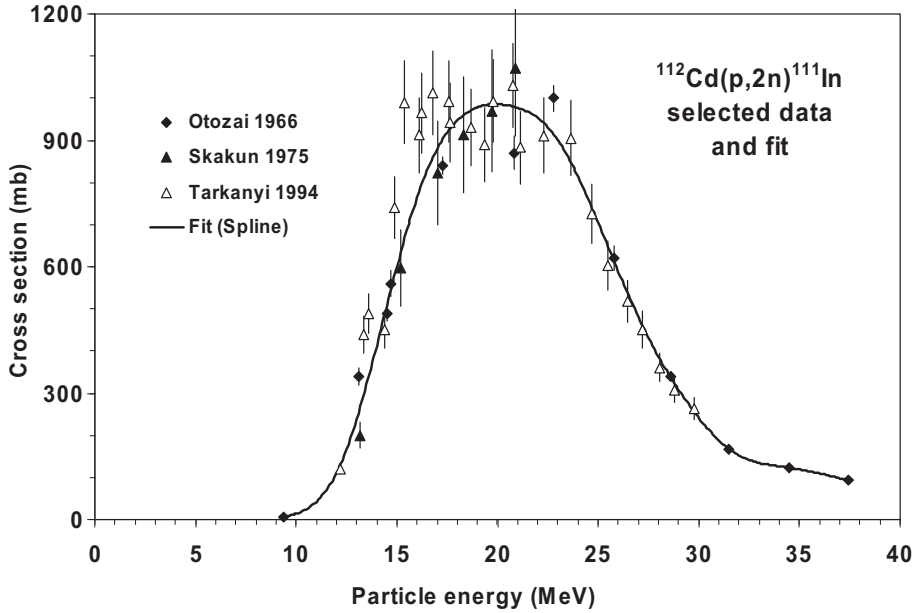

FIG. 7.67. Selected experimental data and the recommended curve (fit).

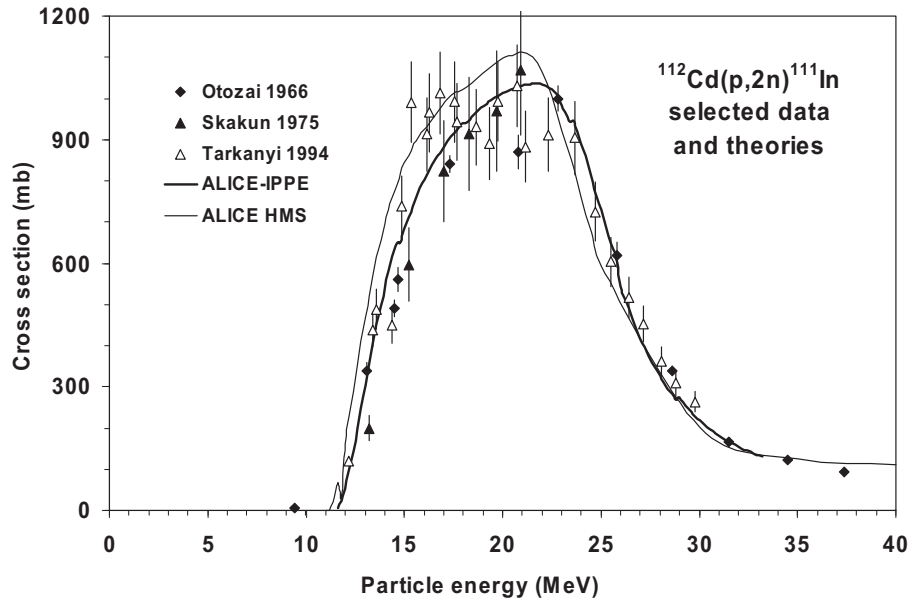

FIG. 7.68. Selected experimental data and theoretical calculations.

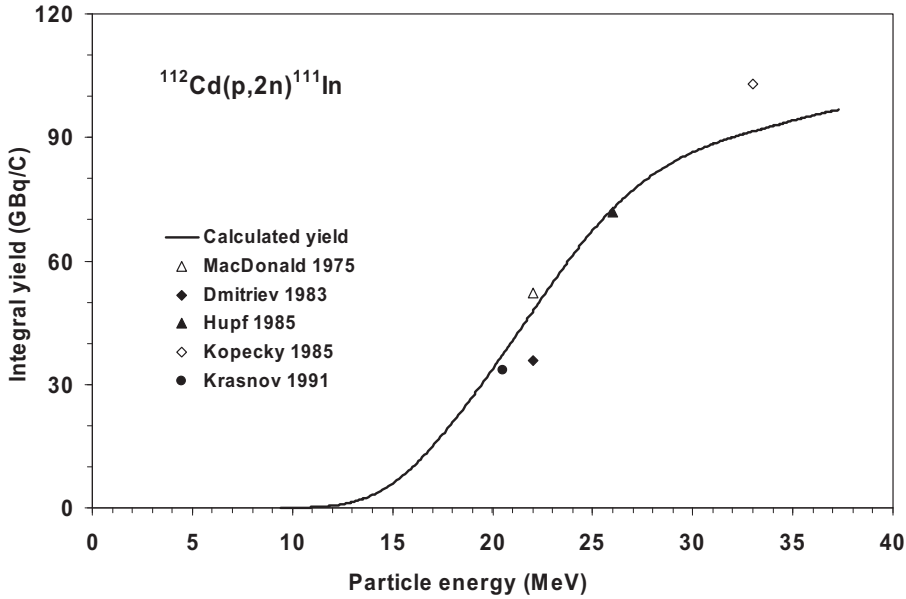

FIG. 7.69. Calculated integral yield curve based on the recommended cross-sections.

TABLE 7.27. RECOMMENDED CROSS-SECTIONS AND INTEGRAL YIELDS

^{112}Cd(p, 2n)^{111}In energy (MeV)	Cross-section (mb)	Integral yield	
		(μCi/μAh)	(GBq/C)
9.5	7	0	0.00
10.0	14	3	0.03
10.5	25	7	0.07
11.0	42	14	0.15
11.5	70	27	0.28
12.0	110	49	0.50
12.5	166	82	0.85
13.0	237	133	1.37
13.5	321	205	2.11
14.0	412	302	3.10
14.5	506	425	4.37
15.0	600	577	5.93
15.5	687	758	7.79
16.0	764	966	9.93

TABLE 7.27. RECOMMENDED CROSS-SECTIONS AND INTEGRAL YIELDS (cont.)

$^{112}Cd(p, 2n)^{111}In$ energy (MeV)	Cross-section (mb)	Integral yield	
		(μCi/μAh)	(GBq/C)
16.5	829	1199	12.32
17.0	880	1454	14.94
17.5	919	1727	17.75
18.0	947	2016	20.72
18.5	966	2318	23.83
19.0	978	2631	27.04
19.5	984	2952	30.34
20.0	986	3281	33.72
20.5	983	3615	37.15
21.0	977	3953	40.63
21.5	968	4295	44.14
22.0	953	4638	47.66
22.5	931	4982	51.21
23.0	901	5317	54.65
23.5	861	5649	58.06
24.0	814	5967	61.33
24.5	761	6270	64.44
25.0	705	6556	67.38
25.5	647	6823	70.12
26.0	589	7070	72.67
26.5	534	7298	75.01
27.0	481	7507	77.15
27.5	432	7697	79.11
28.0	386	7870	80.88
28.5	345	8026	82.49
29.0	308	8167	83.94
29.5	273	8295	85.25
30.0	241	8409	86.42
30.5	212	8510	87.47
31.0	187	8601	88.40
31.5	167	8683	89.24
32.0	152	8757	90.00
32.5	141	8826	90.72

TABLE 7.27. RECOMMENDED CROSS-SECTIONS AND INTEGRAL YIELDS (cont.)

^{112}Cd(p, 2n)^{111}In energy (MeV)	Cross-section (mb)	Integral yield	
		(μCi/μAh)	(GBq/C)
33.0	134	8893	91.40
33.5	130	8958	92.07
34.0	126	9024	92.74
34.5	123	9088	93.40
35.0	119	9151	94.05
35.5	114	9213	94.68
36.0	109	9272	95.30
36.5	104	9329	95.89
37.0	98	9384	96.45

7.7. CHARGED-PARTICLE PRODUCTION OF ^{114m}IN

This radionuclide is a longer lived conversion electron emitting analogue of ^{111}In and could be used for longer lasting therapeutic studies. Its potential has as yet not been fully demonstrated. It is also used for diagnostic applications. A simplified decay scheme is shown in Fig. 7.70, and the main emissions, as defined in Table 7.28, were taken from NuDat 2.4 [7.3].

A. Decay data

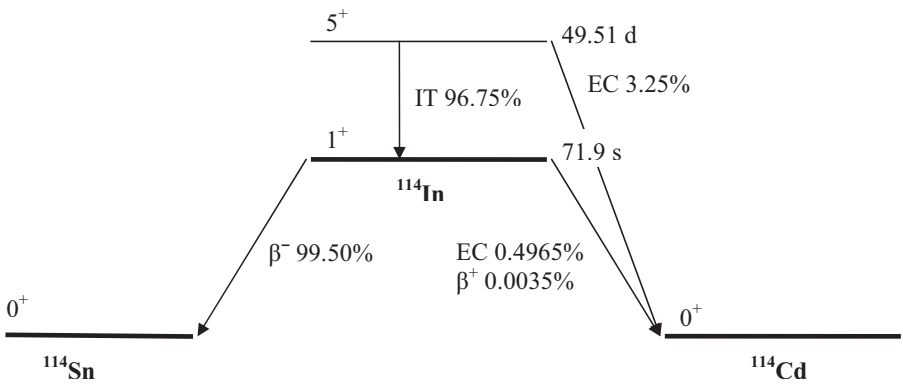

FIG. 7.70. Simplified decay scheme of ^{114}In [7.3].

TABLE 7.28. MAIN EMISSIONS [7.3]

In-114m	Decay mode: $T_{1/2}$:	IT 96.75% 49.51 d
Radiation	Energy (keV)	Intensity (%)
Auger L	2.84	65.0
Auger K	20.1	5.98
ce K	162.33	40.1
ce L	186.03	31.9
ce M	189.44	6.71
ce NP	190.15	1.351
g	190.27	15.56

B. Production routes

Originally, this radionuclide was produced via the $^{113}In(n, \gamma)^{114m}In$ reaction, which is covered in Section 6.3.4. However, alternative routes of production have been developed, as specified in Table 7.29.

TABLE 7.29. INVESTIGATED PRODUCTION ROUTES [7.3, 7.4]

Target isotope	Natural abundance	Reaction	Q-value (MeV)	Threshold energy (MeV)
Cd-114	28.73%	(p, n)	–2.2	2.3
Cd-114	28.73%	(d, 2n)	–4.5	4.5
Cd-116	7.49%	(p, 3n)	–17.1	17.2

C. $^{114}Cd(p, n)^{114m}In$ reaction

All experimental cross-section data are shown in Fig. 7.71, and the selected measurements are compared with the resulting statistical fit to these data in Fig. 7.72. Excitation functions have been calculated by means of the ALICE-IPPE, EMPIRE and GNASH nuclear reaction modelling codes, and results are compared with all of the selected experimental data in Fig. 7.73. Yields determined from the recommended cross-sections are presented in Fig. 7.74, while corresponding numerical values for the recommended cross-sections and yields are listed in Table 7.30.

BIBLIOGRAPHY, EVALUATION AND SELECTION

Cross-sections

BLASER, J.-P., BOEHM, F., MARMIER, P., PEASLEE, D.C., Fonctions d'excitation de la reaction (p,n) I, Helv. Phys. Acta **24** (1951) 3.
Exfor: B0048
Target: natural cadmium.

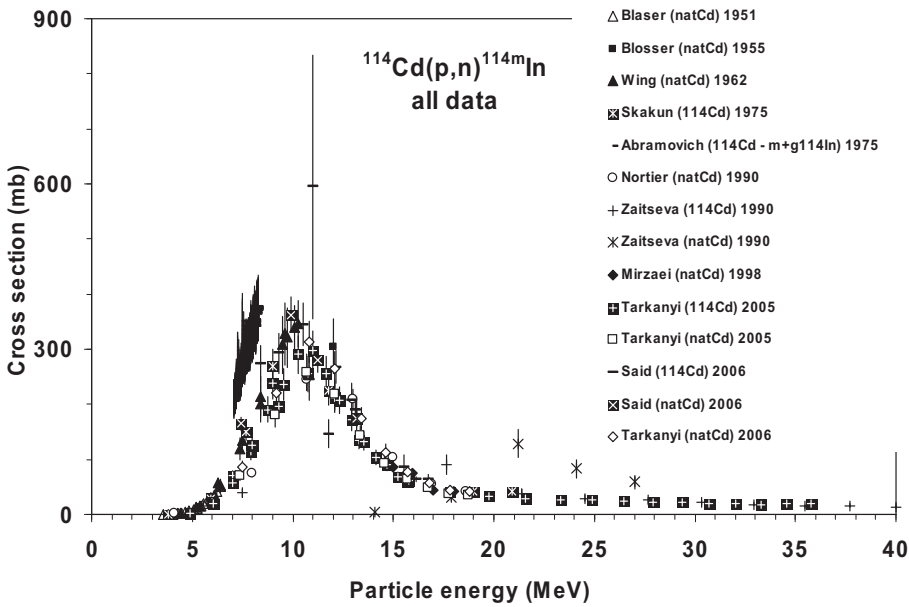

FIG. 7.71. All experimental data.

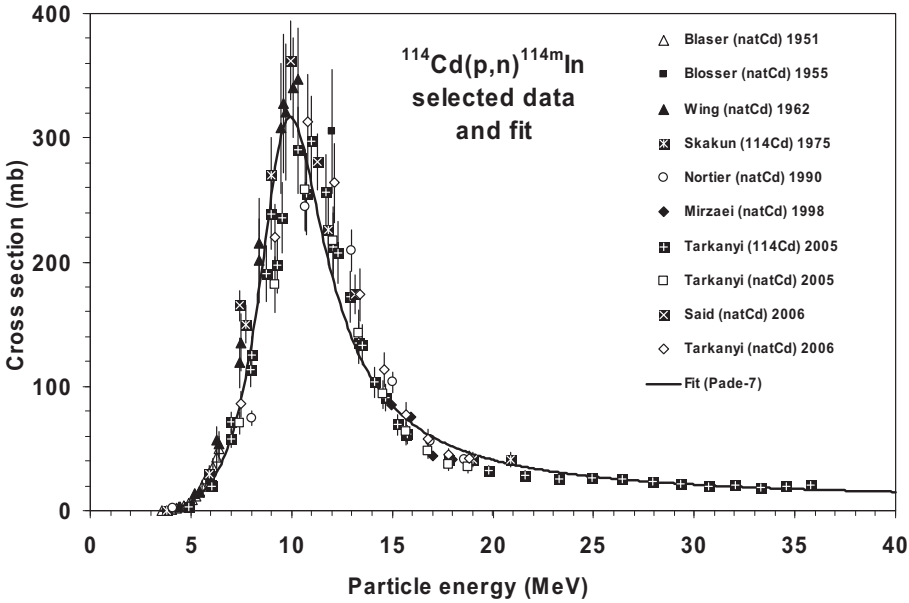

FIG. 7.72. Selected experimental data and the recommended curve (fit).

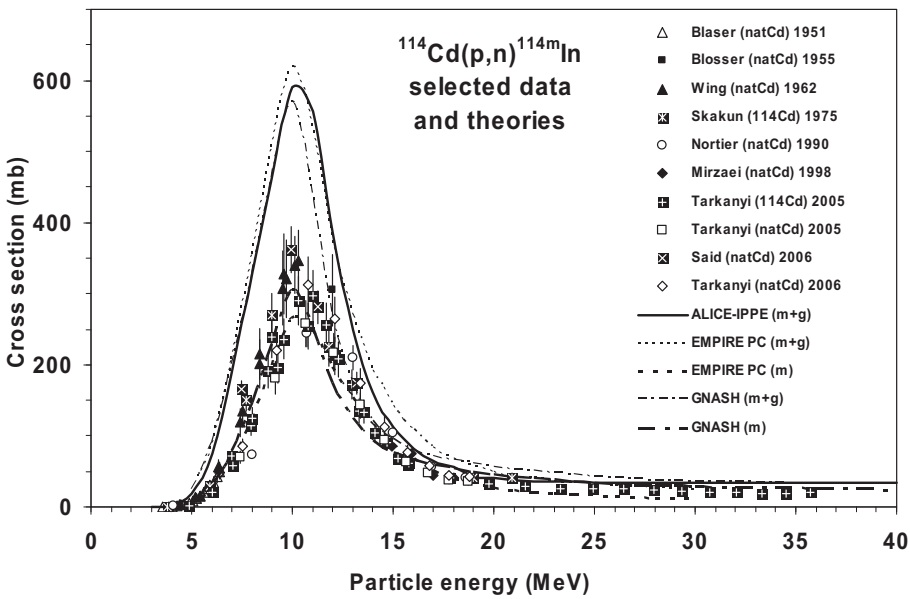

FIG. 7.73. Selected experimental data and theoretical calculations.

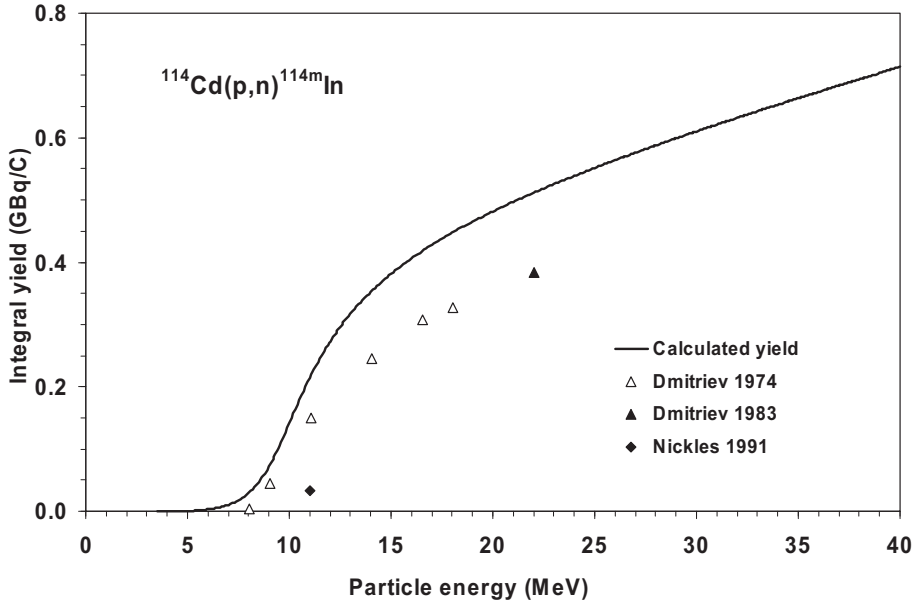

FIG. 7.74. Calculated integral yield curve based on the recommended cross-sections.

TABLE 7.30. RECOMMENDED CROSS-SECTIONS AND INTEGRAL YIELDS

^{114}Cd(p, n)^{114m}In energy (MeV)	Cross-section (mb)	Integral yield	
		(μCi/μAh)	(GBq/C)
3.5	0.0	0.0	0.000
4.0	0.5	0.0	0.000
4.5	2.9	0.0	0.000
5.0	7.1	0.1	0.001
5.5	13.5	0.1	0.001
6.0	23.2	0.3	0.003
6.5	37.6	0.6	0.006
7.0	58.9	1.0	0.010
7.5	90.1	1.7	0.018
8.0	134.4	2.9	0.029
8.5	191.9	4.6	0.047
9.0	254.5	7.0	0.072

TABLE 7.30. RECOMMENDED CROSS-SECTIONS AND INTEGRAL YIELDS (cont.)

$^{114}Cd(p, n)^{114m}In$ energy (MeV)	Cross-section (mb)	Integral yield	
		(μCi/μAh)	(GBq/C)
9.5	302.3	10.2	0.105
10.0	316.4	13.8	0.142
10.5	297.6	17.4	0.179
11.0	261.8	20.8	0.214
11.5	223.4	23.8	0.245
12.0	189.3	26.5	0.272
12.5	161.1	28.8	0.296
13.0	138.5	30.8	0.317
13.5	120.4	32.6	0.336
14.0	105.9	34.3	0.352
14.5	94.1	35.7	0.367
15.0	84.5	37.1	0.381
15.5	76.5	38.3	0.394
16.0	69.8	39.5	0.406
16.5	64.1	40.6	0.417
17.0	59.2	41.6	0.428
17.5	55.1	42.6	0.438
18.0	51.4	43.5	0.447
18.5	48.3	44.4	0.456
19.0	45.4	45.3	0.465
19.5	43.0	46.1	0.474
20.0	40.7	46.9	0.482
20.5	38.8	47.6	0.489
21.0	37.0	48.4	0.497
21.5	35.3	49.1	0.504
22.0	33.9	49.8	0.512
22.5	32.5	50.5	0.519
23.0	31.3	51.1	0.525
23.5	30.1	51.8	0.532
24.0	29.1	52.4	0.539
24.5	28.1	53.0	0.545

TABLE 7.30. RECOMMENDED CROSS-SECTIONS AND INTEGRAL YIELDS (cont.)

$^{114}Cd(p, n)^{114m}In$ energy (MeV)	Cross-section (mb)	Integral yield	
		(μCi/μAh)	(GBq/C)
25.0	27.2	53.7	0.552
25.5	26.4	54.3	0.558
26.0	25.6	54.9	0.564
26.5	24.9	55.5	0.570
27.0	24.2	56.0	0.576
27.5	23.6	56.6	0.582
28.0	23.0	57.2	0.588
28.5	22.4	57.7	0.593
29.0	21.9	58.3	0.599
29.5	21.4	58.8	0.604
30.0	21.0	59.4	0.610
30.5	20.5	59.9	0.616
31.0	20.1	60.4	0.621
31.5	19.7	60.9	0.626
32.0	19.3	61.5	0.632
32.5	18.9	62.0	0.637
33.0	18.6	62.5	0.642
33.5	18.3	63.0	0.648
34.0	18.0	63.5	0.653
34.5	17.7	64.0	0.658
35.0	17.4	64.5	0.663
35.5	17.1	65.0	0.668
36.0	16.8	65.5	0.673
36.5	16.6	66.0	0.678
37.0	16.3	66.5	0.684
37.5	16.1	67.0	0.689
38.0	15.9	67.5	0.694
38.5	15.7	68.0	0.699
39.0	15.5	68.5	0.704
39.5	15.3	68.9	0.709
40.0	15.1	69.4	0.714

BLOSSER, H.G., HANDLEY, T.H., Survey of (p,n) reactions at 12 MeV, Phys. Rev. **100** (1955) 1340–1344.
Exfor: B0052
Target: natural cadmium.

WING, J., HUIZENGA, J.R., (p,n) cross sections of ^{51}V, ^{52}Cr, ^{63}Cu, ^{65}Cu, ^{107}Ag, ^{109}Ag, ^{111}Cd, ^{114}Cd, and ^{139}La from 5 to 10.5 MeV, Phys. Rev. **128** (1962) 280–290.
Exfor: T0124
Target: natural cadmium.

NIECKARZ, W.J., CARETTO, A.A., Production of ^{111}In and ^{114m}In from the separated isotopes of cadmium using 70 to 400 MeV protons, Physical Rev. **178** (1969) 1887–1893.
Exfor: C0345
Target: enriched ^{114}Cd.
High energy measurements.

SKAKUN, Y.A., KLJUCHAREV, A.P., RAKIVNENKO, YU.N., ROMANIJ, I.A., Excitation functions of (p,n)- and (p,2n)-reactions on cadmium isotopes, Izv. Rossiiskoi Akademii Nauk, Ser. Fiz. **39** (1975) 24.
Exfor: A0001
Target: enriched ^{114}Cd.

ABRAMOVICH, S.N., GUZHOVSKIJ, B.Ya., ZVENIGORODSKII, A.G., TRUSILLO, S.V., Isobaric analog resonances appearing during elastic scattering of protons and in the (p,n) reaction of ^{110}Cd, ^{112}Cd, ^{114}Cd, ^{116}Cd nuclei, Izv. Rossiiskoi Akademii Nauk, Ser. Fiz. **39** (1975) 1688–1694.
Exfor: A0129
Target: enriched ^{114}Cd.
The data were rejected because the sum of metastable and ground states was measured.

NORTIER, F.M., MILLS, S.J., STEYN, G.F., Excitation functions and production rates of relevance to the production of ^{111}In by proton bombardment of ^{nat}Cd and ^{nat}In up to 100 MeV, Appl. Rad. Isot. **41** (1990) 1201–1208.
Exfor: A0500
Target: natural cadmium.

ZAITSEVA, N.G., et al., Excitation functions and yields for ^{111}In production using ^{113,114,nat}Cd(p,xn)^{111}In reactions with 65 MeV protons, Appl. Rad. Isot. **41** (1990) 177–183.
Exfor: A0569, D4070
Target: enriched ^{114}Cd and ^{nat}Cd.
Data were rejected due to the systematic energy shift to the higher energies.

MIRZAEI, M., AFARIDEH, H., HAJI-SAEID, S.M., ARDANEH, K., Production of ^{111}In by irradiation of natural cadmium with deuterons and protons in NRCAM cyclotron, Int. Conf. on Cyclotrons and their Applications (Proc. Int. Conf. Caen, 1998), (BARON, E., LIEUVIN, M., Eds), Institute of Physics Publishing, Bristol (1999) 65–67.
EXFOR: no
Target: natural cadmium.

TÁRKÁNYI, F., et al., Investigation of the production of the therapeutic radioisotope ^{114m}In through proton and deuteron induced nuclear reactions on cadmium, Radiochim. Acta **93** (2005) 561–570.
Exfor: D4160
Target: enriched ^{114}Cd and ^{nat}Cd.

SAID, S.A., ELMAGHRABY, E.K., ASFOUR, F.I., Experimental investigation and nuclear model calculations on proton-induced reactions on highly enriched ^{114}Cd at low energies, Appl. Rad. Isot. **64** (2006) 1655–1660.
Exfor: O1502
Target: enriched ^{114}Cd and ^{nat}Cd.
Data measured on enriched target were rejected because of the large deviation, probably caused by the unreliable target thickness determination.

TÁRKÁNYI, F., et al., Activation cross sections on cadmium: Proton induced nuclear reactions up to 80 MeV, Nucl. Instrum. Methods B **245** (2006) 379–394.
Exfor: D4170
Target: natural cadmium.

Yield

DMITRIEV, P.P., DMITRIEVA, Z.P., KRASNOV, N.N., MOLIN, G.A., PANARIN, M.V., Yields of ^{111}In and ^{114m}In in nuclear reactions with protons, deuterons and alpha particles, Atomnaya Energiya **37** (1974) 496–497.
Exfor: no
Target: natural cadmium.

DMITRIEV, P.P., MOLIN, G.A., Radioactive nuclide yields for thick target at 22 MeV proton energy, Vop. At. Nauki i Tekhn., Ser. Yad. Konst. **44** (1981) 43–50.
Exfor: A0168
Target: natural cadmium.
Rejected because the proton energy is above the threshold of the (p, 3n) reaction.

DMITRIEV, P.P., Systematics of nuclear reaction yields for thick target at 22 MeV proton energy, Vop. At. Nauki i Tekhn., Ser. Yad. Konst. **2** (1983) 57–61.
Exfor: A0195
Target: enriched ^{114}Cd.

NICKLES, R.J., A shotgun approach to the chart of the nuclides; Radiotracer production with an 11 MeV proton cyclotron, Acta Radiologica Suppl. **376** (1991) 69–71.
Exfor: no
Target: natural Cd.

D. ^{114}Cd(d, 2n)^{114m}In reaction

All experimental cross-section data are shown in Fig. 7.75, and the selected measurements are compared with the resulting statistical fit to these data in Fig. 7.76. Excitation functions have been calculated by means of the ALICE-IPPE, EMPIRE and GNASH nuclear reaction modelling codes, and results are compared with all of the selected experimental data in Fig. 7.77. Yields determined from the recommended cross-sections are presented in Fig. 7.78, while corresponding numerical values for the recommended cross-sections and yields are listed in Table 7.31.

BIBLIOGRAPHY, EVALUATION AND SELECTION

Cross-sections

NASSIFF, S.J., USHER, O.H., WASILEVSKY, C., Cross sections for the formation of ^{114m}In and ^{116m}In on bombardment of cadmium by deuterons, Radiation Phys. Chem. **13** (1979) 129–132.
EXFOR: no
Target: natural cadmium.
The excitation function has an unusual shape above the maximum — cross-sections are too high in this region and, therefore, the data were rejected.

MIRZAEI, M., AFARIDEH, H., HAJI-SAEID, S.M., ARDANEH, K., Production of ^{111}In by irradiation of natural cadmium with deuterons and protons in NRCAM cyclotron, Int. Conf. on Cyclotrons and their Applications (Proc. Int. Conf. Caen, 1998), (BARON, E., LIEUVIN, M., Eds), Institute of Physics Publishing, Bristol (1999) 65–67.
EXFOR: no
Target: natural cadmium.
Data were rejected because the absolute values are too small compared with the data of Tárkányi et al. (2005) and to Nassiff et al. (1979). The absolute values are also too small for the simultaneously measured ^{111}In.

TÁRKÁNYI, F., et al., Investigation of the production of the therapeutic radioisotope ^{114m}In through proton and deuteron induced nuclear reactions on cadmium, Radiochim. Acta **93** (2005) 561–570.
EXFOR: D4160
Target: enriched ^{114}Cd and ^{nat}Cd.
Data measured on ^{nat}Cd target contain the contribution from the ^{113}Cd(d, n)^{114m}In reaction. According to the ALICE-IPPE calculation, this contribution can be neglected. The estimated contribution of the ^{113}Cd(d, n)$^{114m+g}$In is around 5–10% in the important low energy range and is even smaller for the production of ^{114m}In. No corrections were made for this contribution on the data measured with the ^{nat}Cd target, taking into account that the data on the ^{114}Cd and ^{nat}Cd targets exhibit excellent agreement, and the uncertainties of the absolute values are in the range of 12–15% in both cases.

TÁRKÁNYI, F., et al., Activation cross sections on cadmium: Deuteron induced nuclear reactions up to 40 MeV, Nucl. Instrum. Methods B **259** (2007) 817–828.
EXFOR: D4179
Target: natural cadmium.
The evaluation was carried out before 2007 and, therefore, these measurements were not considered in the recommended data.

Yield

DMITRIEV, P.P., DMITRIEVA, Z.P., KRASNOV, N.N., MOLIN, G.A., PANARIN, M.V., Yields of ^{111}In and ^{114m}In in nuclear reactions with protons, deuterons and alpha particles, Atomnaya Energiya **37** (1974) 496.
EXFOR: no
Target: natural cadmium.

DMITRIEV, P.P., KRASNOV, M.N., MOLIN, G.A., Yields of radioactive nuclides formed by bombardment of a thick target with 22-MeV deuterons, INDC(CCP)-210/L (1983), translation from Nuclear Constants **4**(48) (1982) 38.
EXFOR: A0194
Target: natural cadmium.
Rejected because the threshold of the ^{116}Cd(d, n) reaction is at 19.6 MeV.

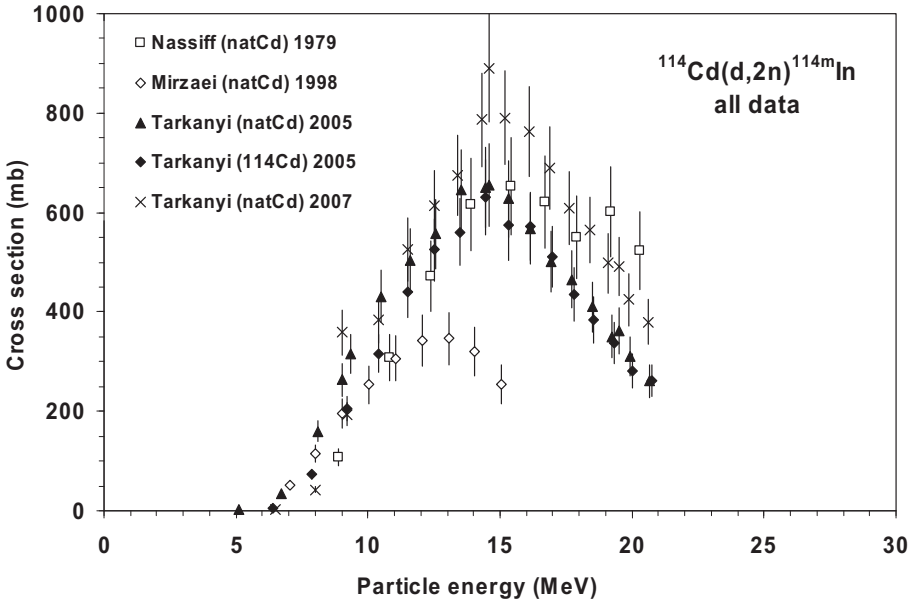

FIG. 7.75. All experimental data.

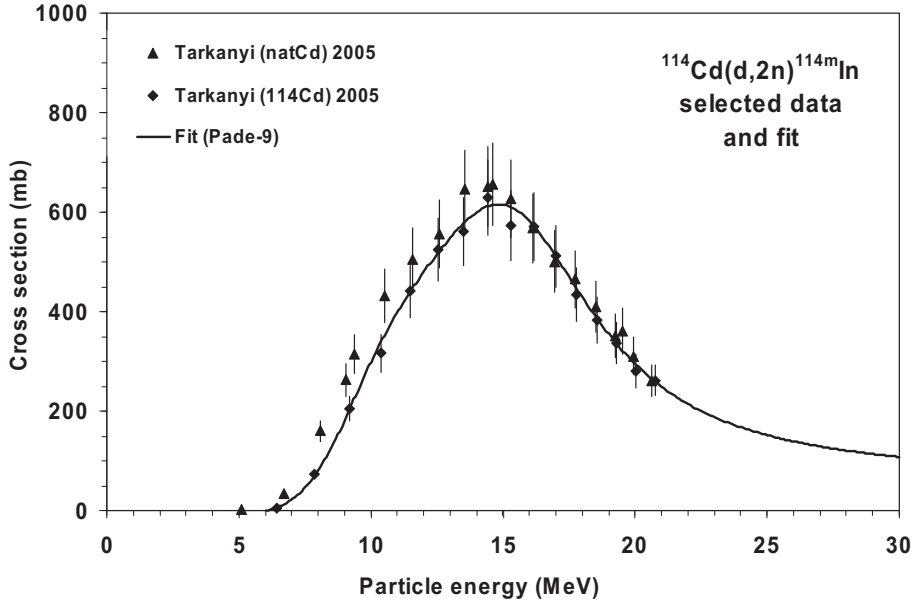

FIG. 7.76. Selected experimental data and the recommended curve (fit).

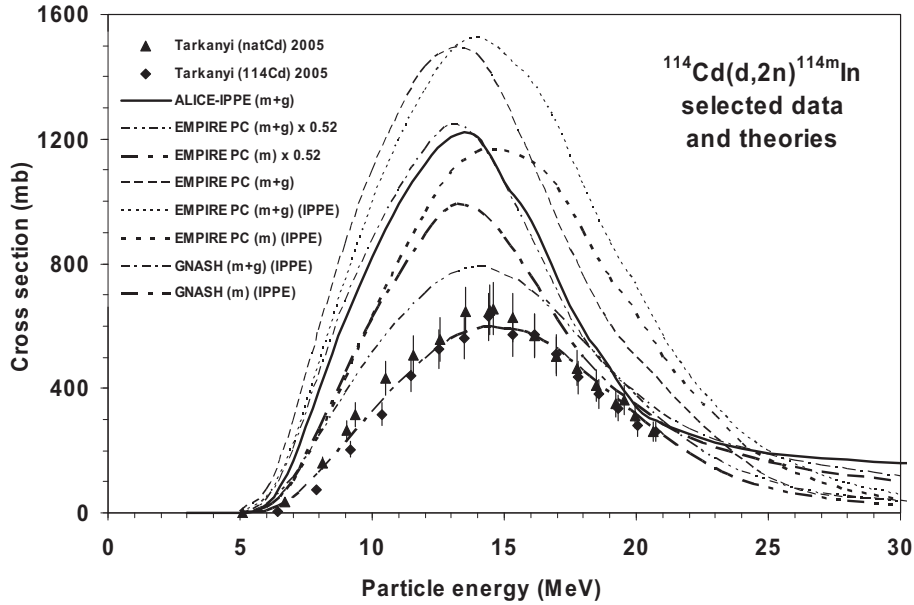

FIG. 7.77. Selected experimental data and theoretical calculations.

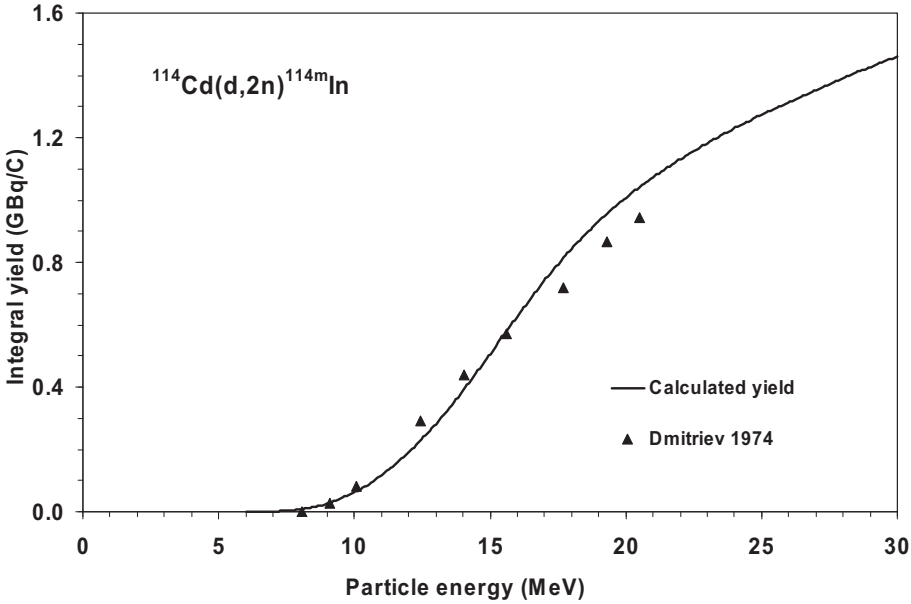

FIG. 7.78. Calculated integral yield curve based on the recommended cross-sections.

TABLE 7.31. RECOMMENDED CROSS-SECTIONS AND INTEGRAL YIELDS

^{114}Cd(d, 2n)^{114m}In energy (MeV)	Cross-section (mb)	Integral yield	
		(μCi/μAh)	(GBq/C)
6.0	0	0.0	0.00
6.5	8	0.0	0.00
7.0	22	0.1	0.00
7.5	46	0.3	0.00
8.0	80	0.7	0.01
8.5	126	1.4	0.01
9.0	181	2.5	0.03
9.5	240	4.0	0.04
10.0	298	6.0	0.06
10.5	351	8.5	0.09
11.0	399	11.4	0.12
11.5	441	14.8	0.15
12.0	479	18.6	0.19
12.5	515	22.8	0.23

TABLE 7.31. RECOMMENDED CROSS-SECTIONS AND INTEGRAL YIELDS (cont.)

$^{114}Cd(d, 2n)^{114m}In$ energy (MeV)	Cross-section (mb)	Integral yield	
		(μCi/μAh)	(GBq/C)
13.0	548	27.4	0.28
13.5	577	32.4	0.33
14.0	600	37.7	0.39
14.5	613	43.4	0.45
15.0	615	49.2	0.51
15.5	604	55.1	0.57
16.0	582	61.0	0.63
16.5	550	66.7	0.69
17.0	511	72.1	0.74
17.5	470	77.2	0.79
18.0	429	82.0	0.84
18.5	390	86.5	0.89
19.0	355	90.6	0.93
19.5	323	94.4	0.97
20.0	295	98.0	1.01
20.5	271	101.3	1.04
21.0	249	104.3	1.07
21.5	231	107.2	1.10
22.0	214	110.0	1.13
22.5	200	112.5	1.16
23.0	188	115.0	1.18
23.5	177	117.4	1.21
24.0	168	119.6	1.23
24.5	159	121.8	1.25
25.0	152	123.9	1.27
25.5	145	125.9	1.29
26.0	139	127.9	1.31
26.5	134	129.8	1.33
27.0	129	131.7	1.35
27.5	124	133.5	1.37
28.0	121	135.3	1.39
28.5	117	137.0	1.41
29.0	114	138.8	1.43
29.5	111	140.5	1.44
30.0	108	142.2	1.46

E. ^{116}Cd(p, 3n)^{114m}In reaction

Measurements are compared with the resulting statistical fit to experimental cross-section data in Fig. 7.79. Excitation functions have been calculated by means of the ALICE-IPPE, EMPIRE and GNASH nuclear reaction modelling codes, and results are compared with all of the selected experimental data in Fig. 7.80. Yields determined from the recommended cross-sections are presented in Fig. 7.81, while corresponding numerical values for the recommended cross-sections and yields are listed in Table 7.32.

BIBLIOGRAPHY, EVALUATION AND SELECTION

Cross-sections

TÁRKÁNYI, F., et al., Investigation of the production of the therapeutic radioisotope ^{114m}In through proton and deuteron induced nuclear reactions on cadmium, Radiochim. Acta **93** (2005) 561–570.
EXFOR: D4160
Target: natural cadmium.

HERMANNE, A., TÁRKÁNYI, F., TAKÁCS, S., VAN DEN WINKEL, P., REBELES, A., Investigation of the ^{116}Cd(p,3n)^{114m}In nuclear reaction: Production of the therapeutic radioisotope ^{114m}In (unpublished).
Target: enriched ^{116}Cd.
Not included in the coordinated research project (CRP).

Yield

No data were found.

7.8. CHARGED PARTICLE PRODUCTION OF ^{124}I

Iodine-124 is one of the most important emerging therapeutic radionuclides. The decay characteristics support a combination of therapy and PET, and allow precise regional dosimetry. As a result, ^{124}I is considered to be a superior therapy agent over commonly used, reactor produced ^{131}I. Since iodine forms a reasonably stable bond to the C atom, many organic compounds can be labelled with ^{124}I and used for internal radiotherapy. A simplified decay scheme is shown in Fig. 7.82, and the main emissions, as defined in Table 7.33 [7.1–7.3], were taken from NuDat 2.4 [7.3].

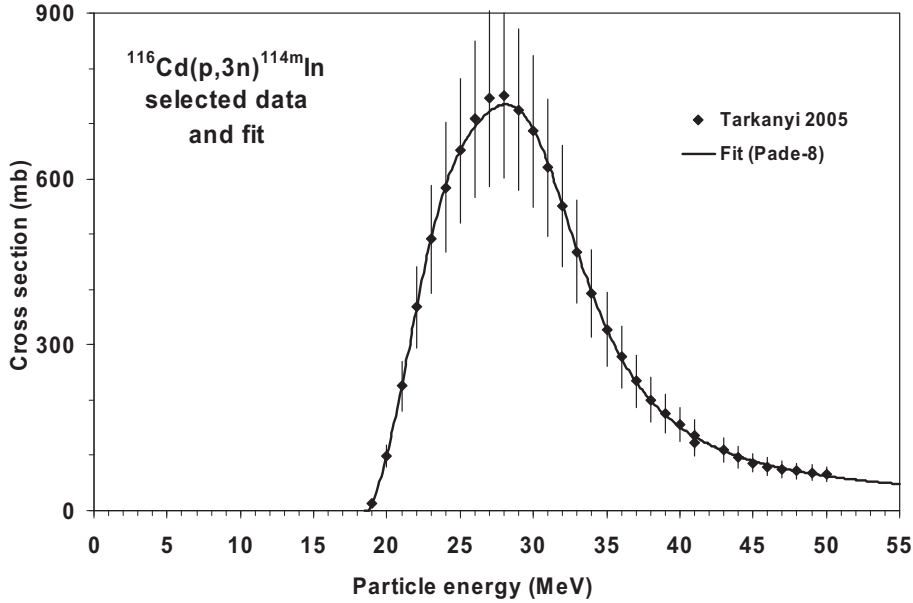

FIG. 7.79. Selected experimental data and the recommended curve (fit).

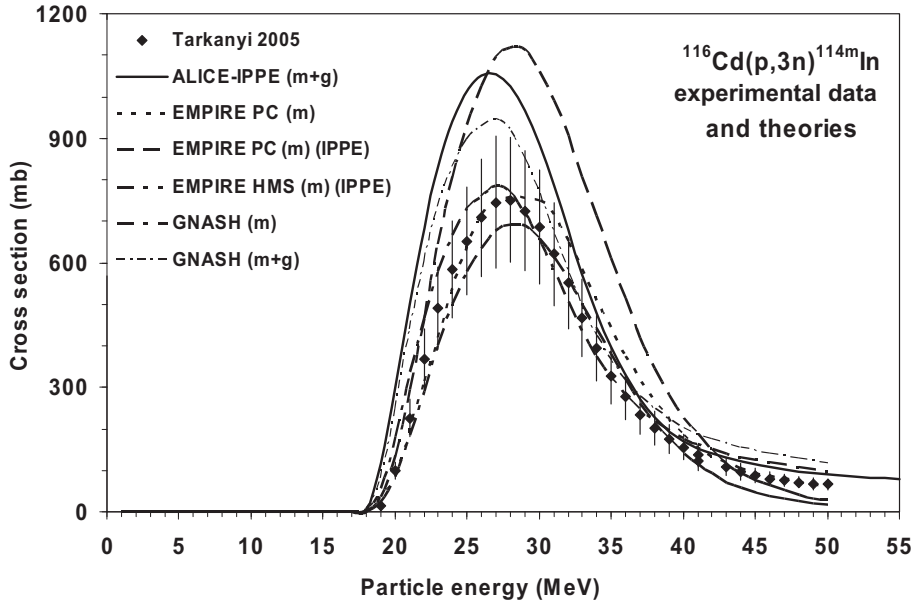

FIG. 7.80. Experimental data and theoretical calculations.

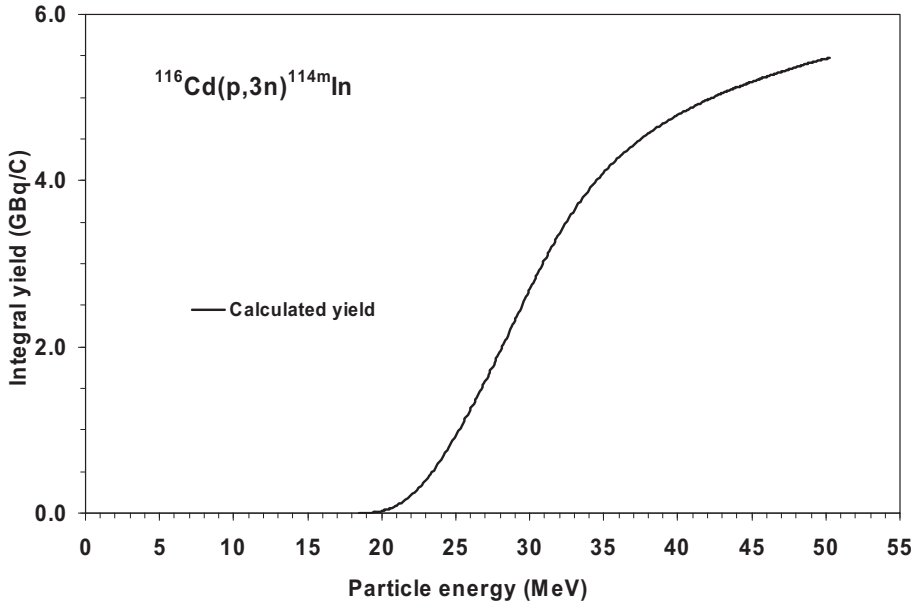

FIG. 7.81. Calculated integral yield curve based on the recommended cross-sections.

TABLE 7.32. RECOMMENDED CROSS-SECTIONS AND INTEGRAL YIELDS

^{116}Cd(p, 3n)^{114m}In energy (MeV)	Cross-section (mb)	Integral yield	
		(μCi/μAh)	(GBq/C)
18.5	0	0	0.00
19.0	14	0	0.00
19.5	53	1	0.01
20.0	101	2	0.02
20.5	158	5	0.05
21.0	223	9	0.09
21.5	293	14	0.14
22.0	363	21	0.21
22.5	430	29	0.30
23.0	491	39	0.40
23.5	543	50	0.52
24.0	587	63	0.64

TABLE 7.32. RECOMMENDED CROSS-SECTIONS AND INTEGRAL YIELDS (cont.)

$^{116}Cd(p, 3n)^{114m}In$ energy (MeV)	Cross-section (mb)	Integral yield	
		(μCi/μAh)	(GBq/C)
24.5	623	76	0.78
25.0	652	90	0.93
25.5	675	105	1.08
26.0	694	121	1.24
26.5	710	137	1.41
27.0	722	154	1.59
27.5	730	172	1.77
28.0	734	190	1.95
28.5	733	208	2.13
29.0	725	226	2.32
29.5	711	244	2.51
30.0	690	262	2.69
30.5	662	279	2.87
31.0	628	296	3.04
31.5	591	312	3.20
32.0	551	327	3.36
32.5	510	341	3.51
33.0	469	355	3.64
33.5	430	367	3.77
34.0	394	378	3.89
34.5	360	389	4.00
35.0	329	399	4.10
35.5	301	408	4.19
36.0	276	416	4.28
36.5	254	424	4.36
37.0	234	431	4.43
37.5	216	438	4.50
38.0	200	444	4.57
38.5	186	450	4.63
39.0	173	456	4.68
39.5	162	461	4.74

TABLE 7.32. RECOMMENDED CROSS-SECTIONS AND INTEGRAL YIELDS (cont.)

^{116}Cd(p, 3n)^{114m}In energy (MeV)	Cross-section (mb)	Integral yield	
		(μCi/μAh)	(GBq/C)
40.0	151	466	4.79
40.5	142	471	4.84
41.0	134	475	4.88
41.5	126	479	4.93
42.0	120	484	4.97
42.5	114	487	5.01
43.0	108	491	5.05
43.5	103	495	5.08
44.0	98	498	5.12
44.5	94	501	5.15
45.0	90	505	5.19
45.5	86	508	5.22
46.0	83	511	5.25
46.5	80	514	5.28
47.0	77	516	5.31
47.5	74	519	5.34
48.0	71	522	5.36
48.5	69	524	5.39
49.0	67	527	5.42
49.5	65	529	5.44
50.0	63	532	5.47

A. Decay data

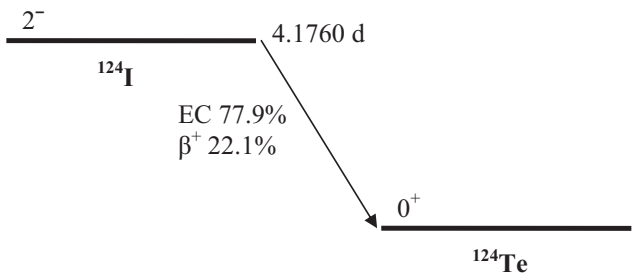

FIG. 7.82. Simplified decay scheme of ^{124}I [7.1, 7.3].

TABLE 7.33. MAIN EMISSIONS [7.1–7.3]

I-124	Decay mode:	EC 77.9% β^+ 22.1% [7.1]
	$T_{1/2}$:	4.1760 d
Radiation	Intensity	Energy (MeV)
β^+ 2	3.01×10^{-03}	3.668×10^{-01} [a] 8.121×10^{-01} [b]
β^+ 3	1.18×10^{-01}	6.871×10^{-01} [a] 1.5349 [b]
β^+ 4	1.09×10^{-01}	9.747×10^{-01} [a] 2.1376 [b]
$\gamma^{\pm}$	4.42×10^{-01} [7.1]	5.110×10^{-01}
γ 5	2.08×10^{-03}	5.412×10^{-01}
γ 7	6.29×10^{-01}	6.027×10^{-01}
ce-K, γ 7	2.64×10^{-03}	5.709×10^{-01}
ce-L, γ 7	3.59×10^{-04}	5.978×10^{-01} [c]
γ 8	9.88×10^{-03}	6.458×10^{-01}
γ 13	1.04×10^{-01}	7.228×10^{-01}
γ 21	4.35×10^{-03}	9.682×10^{-01}
γ 24	4.41×10^{-03}	1.045
γ 25	1.26×10^{-03}	1.054
γ 30	1.56×10^{-02}	1.326
γ 32	3.02×10^{-03}	1.368
γ 33	1.75×10^{-02}	1.376
γ 36	1.99×10^{-03}	1.489
γ 37	3.13×10^{-02}	1.509
γ 38	1.65×10^{-03}	1.560
γ 40	2.09×10^{-03}	1.638
γ 42	1.12×10^{-03}	1.676
γ 43	1.09×10^{-01}	1.691
γ 44	1.76×10^{-03}	1.720
γ 46	2.14×10^{-03}	1.851
γ 47	1.64×10^{-03}	1.919
γ 48	3.52×10^{-03}	2.038
γ 49	3.59×10^{-03}	2.079

TABLE 7.33. MAIN EMISSIONS [7.1–7.3] (cont.)

I-124	Decay mode:	EC 77.9% β^+ 22.1% [7.1]
	$T_{1/2}$:	4.1760 d
Radiation	Intensity	Energy (MeV)
γ 50	5.91×10^{-03}	2.091
γ 51	1.45×10^{-03}	2.099
γ 52	1.13×10^{-03}	2.144
γ 53	5.91×10^{-03}	2.232
γ 54	6.86×10^{-03}	2.283
γ 57	6.92×10^{-04}	2.454
γ 59	4.78×10^{-03}	2.747
$K_{\alpha 1}$ X ray	3.09×10^{-01}	2.747×10^{-02}
$K_{\alpha 2}$ X ray	1.66×10^{-01}	2.720×10^{-02}
K_{β} X ray	1.08×10^{-01}	3.100×10^{-02} [a]
Auger-K	8.28×10^{-02}	2.270×10^{-02} [a]
Auger-L	6.40×10^{-01}	3.190×10^{-03} [a]

[a] Average energy (MeV).
[b] End point energy (MeV).
[c] Maximum energy (MeV) for subshell.

B. Production routes

Production of ^{124}I is carried out via the (p, n) or (d, 2n) reactions on a highly enriched ^{124}Te target or by a (p, 2n) reaction on highly enriched ^{125}Te, as specified in Table 7.34.

TABLE 7.34. INVESTIGATED PRODUCTION ROUTES [7.3, 7.4]

Target isotope	Natural abundance	Reaction	Q-value (MeV)	Threshold energy (MeV)
Te-124	4.74%	(p, n)	–3.9	4.0
Te-124	4.74%	(d, 2n)	–6.2	6.3
Te-125	7.07%	(p, 2n)	–10.5	10.6

C. ^{124}Te(p, n)^{124}I reaction

All experimental cross-section data are shown in Fig. 7.83, and the selected measurements are compared with the resulting statistical fit to these data in Fig. 7.84. Excitation functions have been calculated by means of the ALICE-IPPE nuclear reaction modelling code, and results are compared with all of the selected experimental data in Fig. 7.85. Yields determined from the recommended cross-sections are presented in Fig. 7.86, while corresponding numerical values for the recommended cross-sections and yields are listed in Table 7.35.

BIBLIOGRAPHY, EVALUATION AND SELECTION

Cross-sections

ACERBI, E., BIRATTARI, C., CASTIGLIONI, M., RESMINI, F., VILLA, M., Production of ^{123}I for medical purposes at the Milan AVF cyclotron, Int. J. Appl. Radiat. Isot. **26** (1975) 741–747.
EXFOR: A0266
Target: natural Te and ^{124}Te. Data measured with a natural target were rejected because they are above the threshold energy of the ^{125}Te(p, 2n) reaction.

KONDO, K., LAMBRECHT, R.M., WOLF, A.P., ^{123}I production for radiopharmaceuticals - XX. Excitation functions of the ^{124}Te(p,2n)^{123}I and ^{124}Te(p,n)^{124}I reactions and the effect of target enrichment on radionuclidic purity, Int. J. Appl. Radiat. Isot. **28** (1977) 395–401.
EXFOR: B0090
Two data sets are available on targets with different enrichment. Both sets of data were rejected because of their energy shift towards higher energies.

VAN DEN BOSCH, R., et al., A new approach to target chemistry for the iodine-123 production via the ^{124}Te(p,2n) reaction, Int. J. Appl. Radiat. Isot. **28** (1977) 255–261.
EXFOR: B0167
Yield data were converted to cross-sections. Data were rejected because of an energy shift towards higher energies.

SCHOLTEN, B., QAIM, S.M., STÖCKLIN, G., Excitation functions of proton induced nuclear reactions on natural tellurium and enriched ^{123}Te: Production of ^{123}I via the ^{123}Te(p,n)^{123}I process at a low energy cyclotron, Appl. Radiat. Isot. **40** (1989) 127–132.
EXFOR: A0473
Target: natural Te. Data were rejected because they are above the threshold energy of the ^{125}Te(p, 2n) reaction.

ZWEIT, J., et al., Excitation functions of proton induced reactions in natural tellurium: Production of no-carrier added iodine-124 for PET applications, 4th Int. Workshop on Targetry and Target Chemistry (Proc. Int. Workshop Villigen, 1991) PSI, Villigen (1992) 76–78.
EXFOR: O1260
Target: natural Te. Rejected because the data set shows an energy shift towards higher energies.

SCHOLTEN, B., KOVÁCS, Z., TÁRKÁNYI, F., QAIM, S.M., Excitation functions of ^{124}Te(p,xn)^{124,123}I reactions from 6 to 31 MeV with special reference to the production of ^{124}I at a small cyclotron, Appl. Radiat. Isot. **46** (1995) 255–259.
EXFOR: D4019

Yield

KONDO, K., LAMBRECHT, R.M., NORTON, E.F., WOLF, A.P., Cyclotron isotopes and radiopharmaceuticals - XXII. Improved targetry and radiochemistry for production of ^{123}I and ^{124}I, Int. J. Appl. Radiat. Isot. **28** (1977) 765–771.
EXFOR: B0169

DMITRIEV, P.P., PANARIN, M.V., DMITRIEVA, Z.P., ^{123}I, ^{124}I, ^{125}I, ^{126}I, ^{130}I, ^{131}I and ^{132}I yields when irradiating tellurium with protons, deuterons and alpha particles, and antimony with alpha particles, Atomnaya Energiya **49** (1980) 329.
EXFOR: A0078
Target: natural Te.

DMITRIEV, P.P., MOLIN, G.A., Radioactive nuclide yields for thick target at 22 MeV proton energy, Vop. At. Nauki i Tekhn., Ser. Yad. Konst. **44** (1981) 43–50, INDC(CCP)-188/L (1983).
EXFOR: A0168
Target: natural Te. Data were rejected because they are above the threshold energy of the ^{125}Te(p, 2n) reaction.

DMITRIEV, P.P., Radionuclide Yield in Reactions with Protons, Deuterons, Alpha Particles and ^{3}He, Moscow, Ehnergioatomizdat (1986) and INDC(CCP)-263 (1986).
EXFOR: no
Data were rejected because they are calculated and not measured results.

NICKLES, R.J., A shotgun approach to the chart of the nuclides: Radiotracer production with an 11 MeV proton cyclotron, Acta Radiologica Suppl. **376** (1991) 69–71.
EXFOR: no
Target: natural Te.

SCHOLTEN, B., KOVÁCS, Z., TÁRKÁNYI, F., QAIM, S.M., Excitation functions of ^{124}Te(p,xn)^{124,123}I reactions from 6 to 31 MeV with special reference to the production of ^{124}I at a small cyclotron, Appl. Radiat. Isot. **46** (1995) 255–259.
EXFOR: no
Data were rejected because they are calculated and not measured results.

WEINREICH, R., KNUST, E.J., Quality control of ^{124}I, 6th Workshop on Targetry and Target Chemistry (Proc. Vancouver, BC 1995), (LINK, J.M., RUTH, T., Eds), TRIUMF (1996) 84–86.
EXFOR: no

QAIM, S.M., et al., Some optimisation studies relevant to the production of high-purity ^{124}I and ^{120g}I at a small-sized cyclotron, Appl. Radiat. Isot. **58** (2003) 69–78.
EXFOR: no

SAJJAD, M., BARS, E., NABI, H.A., Optimization of ^{124}I production via ^{124}Te(p,n)^{124}I reaction, Appl. Radiat. Isot. **64** (2006) 965–970.
EXFOR: C1462

NYE, J.A., AVILA-RODRIGUEZ, M.A., NICKLES, R.J., A new binary compound for the production of ^{124}I via the ^{124}Te(p,n)^{124}I reaction, Appl. Radiat. Isot. **65** (2007) 407–412.
EXFOR: C1517

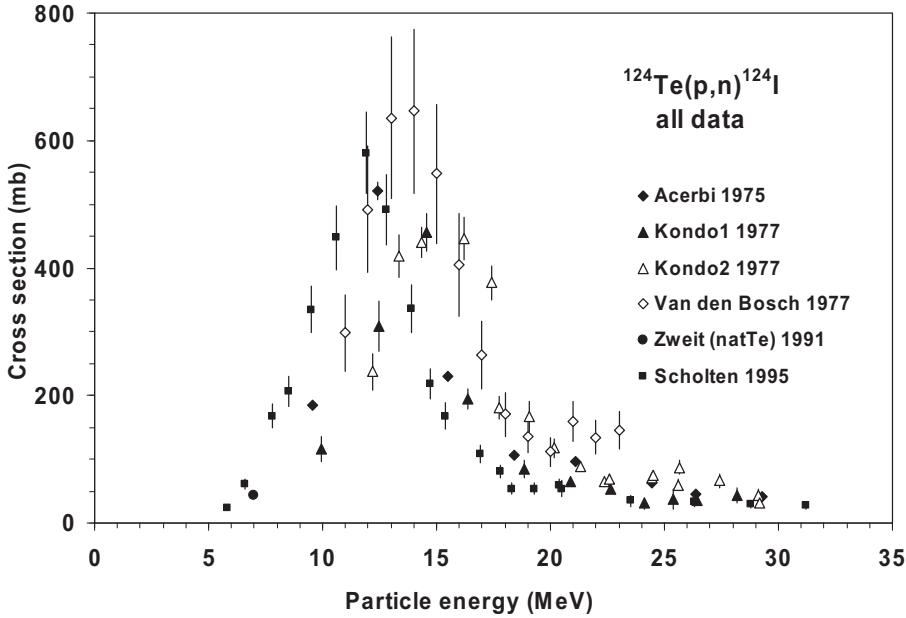

FIG. 7.83. All experimental data.

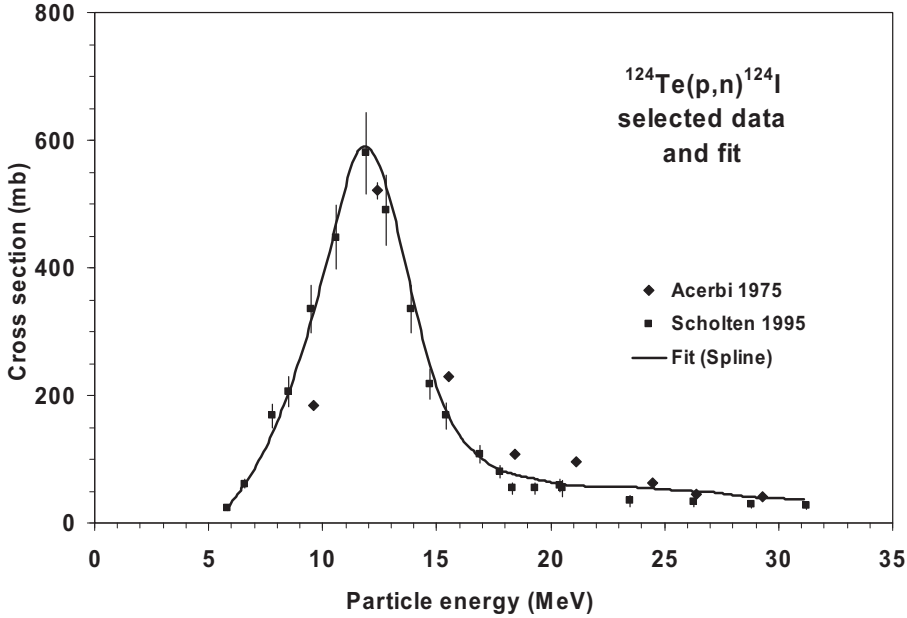

FIG. 7.84. Selected experimental data and the recommended curve (fit).

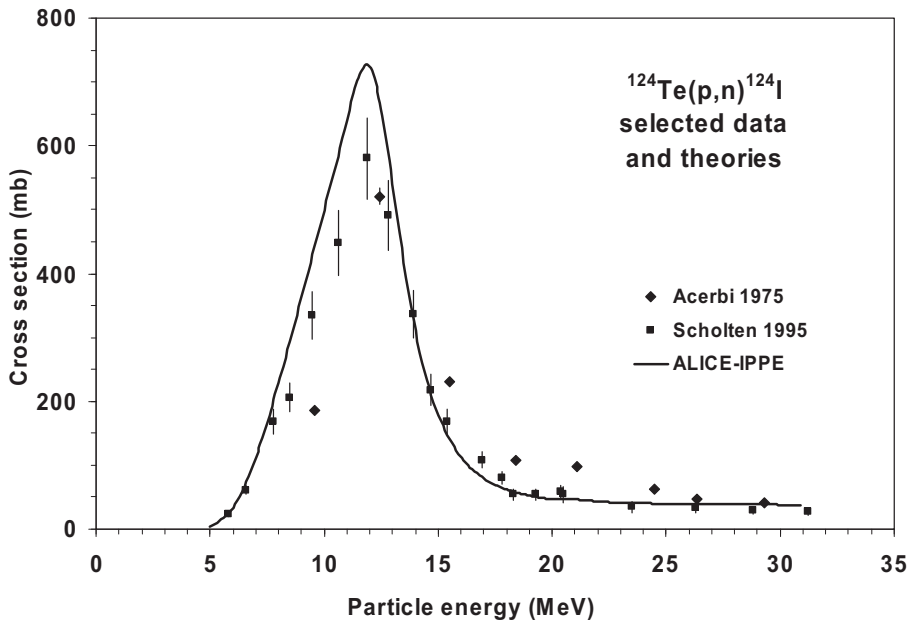

FIG. 7.85. Selected experimental data and theoretical calculations.

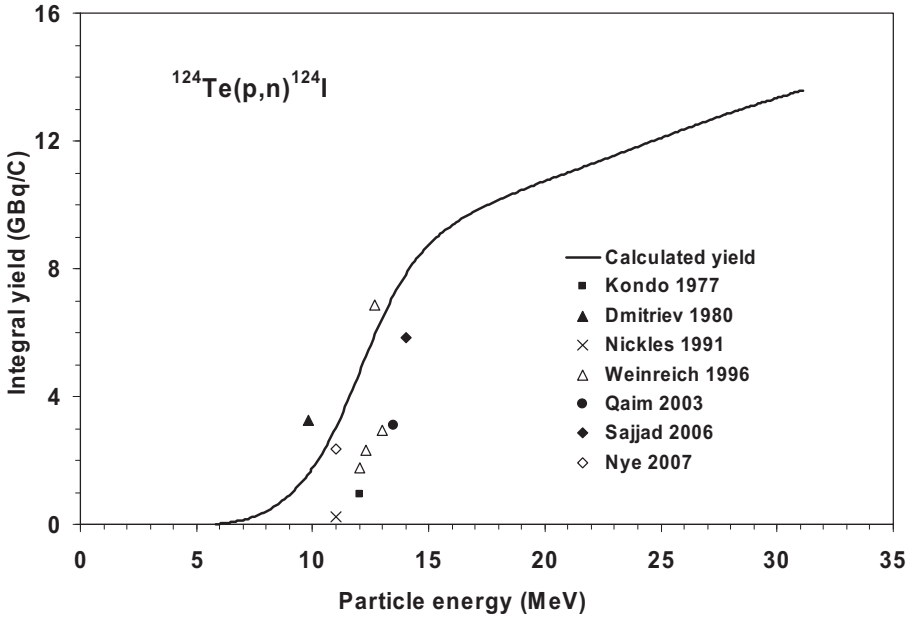

FIG. 7.86. Calculated integral yield curve based on the recommended cross-sections.

TABLE 7.35. RECOMMENDED CROSS-SECTIONS AND INTEGRAL YIELDS

^{124}Te(p, n)^{124}I energy (MeV)	Cross-section (mb)	Integral yield	
		(μCi/μAh)	(GBq/C)
6.0	32	2	0.02
6.5	56	6	0.06
7.0	85	13	0.14
7.5	118	24	0.25
8.0	158	40	0.41
8.5	204	61	0.63
9.0	257	89	0.91
9.5	317	125	1.29
10.0	383	171	1.76
10.5	455	227	2.34
11.0	528	295	3.04

TABLE 7.35. RECOMMENDED CROSS-SECTIONS AND INTEGRAL YIELDS (cont.)

$^{124}Te(p, n)^{124}I$ energy (MeV)	Cross-section (mb)	Integral yield	
		(μCi/μAh)	(GBq/C)
11.5	580	375	3.85
12.0	588	461	4.73
12.5	558	546	5.62
13.0	500	627	6.45
13.5	426	700	7.19
14.0	347	761	7.82
14.5	274	811	8.34
15.0	213	852	8.75
15.5	169	884	9.09
16.0	138	911	9.36
16.5	116	934	9.60
17.0	100	953	9.80
17.5	88	971	9.98
18.0	80	987	10.15
18.5	75	1003	10.30
19.0	71	1017	10.46
19.5	67	1031	10.60
20.0	64	1045	10.74
20.5	61	1058	10.88
21.0	59	1071	11.01
21.5	58	1084	11.14
22.0	57	1097	11.28
22.5	57	1110	11.41
23.0	57	1124	11.55
23.5	56	1137	11.69
24.0	55	1150	11.82
24.5	54	1164	11.96
25.0	53	1177	12.10
25.5	51	1190	12.23
26.0	50	1203	12.36

TABLE 7.35. RECOMMENDED CROSS-SECTIONS AND INTEGRAL YIELDS (cont.)

^{124}Te(p, n)^{124}I energy (MeV)	Cross-section (mb)	Integral yield	
		(μCi/μAh)	(GBq/C)
26.5	49	1216	12.49
27.0	49	1228	12.63
27.5	46	1241	12.76
28.0	44	1253	12.88
28.5	42	1265	13.00
29.0	40	1276	13.11
29.5	39	1287	13.23
30.0	39	1298	13.34
30.5	38	1309	13.45
31.0	37	1320	13.56

D. ^{124}Te(d, 2n)^{124}I reaction

The ^{124}Te(d, 2n)^{124}I reaction is generally considered to be an acceptable method for the production of ^{124}I. However, the user should be aware that ^{125}I is also produced as an impurity and, therefore, the ^{124}Te(d, n)^{125}I reaction has also been evaluated elsewhere in this section. Two experimental cross-section data sets for the ^{124}Te(d, 2n)^{124}I reaction are available in the literature (Firouzbakht et al. (1993), Bastian et al. (2001)), although the original cross-section values published by Firouzbakht et al. were incorrect. New cross-sections were re-calculated from the authors' thin-target yield values presented in the same paper, and these re-calculated data compare very well with those of Bastian et al. Experimental data sets are compared with the theoretical curves in Fig. 7.87, and show that all theoretical calculations are higher by a factor of two in the region around the peak area, due partly to the deuteron break-up channel not being considered in the theoretical model.

BIBLIOGRAPHY, EVALUATION AND SELECTION

Cross-sections

FIROUZBAKHT, M.L., SCHLYER, D.J., FINN, R.D., LAGUZZI, G., WOLF, A.P., ^{124}I production: Excitation function for the ^{124}Te(d,2n)^{124}I and ^{124}Te(d,3n)^{123}I reactions from 7 to 24 MeV, Nucl. Instrum. Methods B **79** (1993) 909–910.
EXFOR: no
The original cross-sections were incorrect. New cross-sections have been re-calculated from the thin-target yield values as given in the same paper.

BASTIAN, TH., COENEN, H.H., QAIM, S.M., Excitation functions of ^{124}Te(d,xn)^{124,125}I reactions from threshold up to 14 MeV: Comparative evaluation of nuclear routes for the production of ^{124}I, Appl. Radiat. Isot. **55** (2001) 303–308.
EXFOR: A0248

Yield

SHARMA, H.L., ZWEIT, J., DOWNEY, S., SMITH, A., SMITH, A.G., Production of ^{124}I for positron-emission tomography, J. Labelled Compd Radiopharm. **26** (1988) 165–167.
EXFOR: no
Integral yield at 20 MeV was deduced by adding the recommended integral yield at 15 MeV to the experimental data of Sharma et al. (15–20 MeV).

LAMBRECHT, R.M., SAJJAD, M., QURESHI, M.A., AL-YANBAWI, S.J., Production of ^{124}I, J. Radioanal. Nucl. Chem. 127 (**1988**) 143–150.
EXFOR: no

CLEM, R.G., LAMBRECHT, R.M., Enriched ^{124}Te targets for production of ^{123}I and ^{124}I, Nucl. Instrum. Methods A **303** (1991) 115–118.
EXFOR: no

All experimental cross-section data are shown in Fig. 7.88, and the selected measurements are compared with the resulting statistical fit to these data in Fig. 7.89. Excitation functions have been calculated by means of the ALICE-IPPE, EMPIRE and GNASH nuclear reaction modelling codes, and results are compared with all of the selected experimental data in Fig. 7.87. Yields determined from the recommended cross-sections are presented in Fig. 7.90, while corresponding numerical values for the recommended cross-sections and yields are listed in Table 7.36.

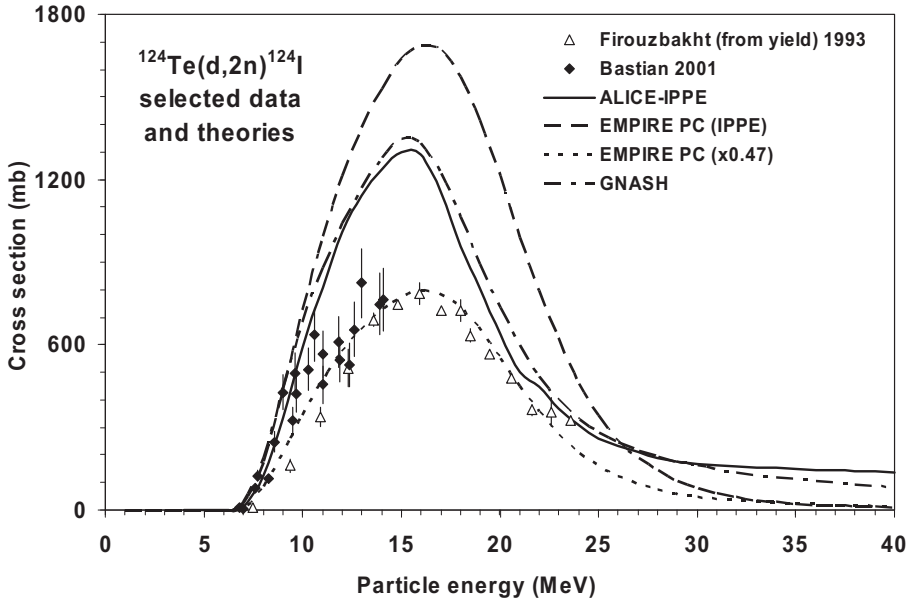

FIG. 7.87. Selected experimental data and theoretical calculations.

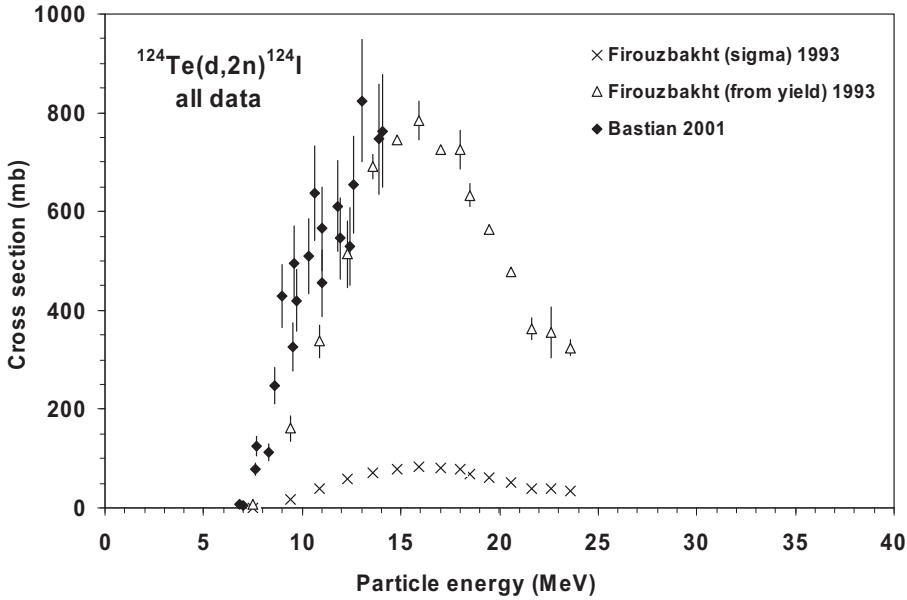

FIG. 7.88. All experimental data.

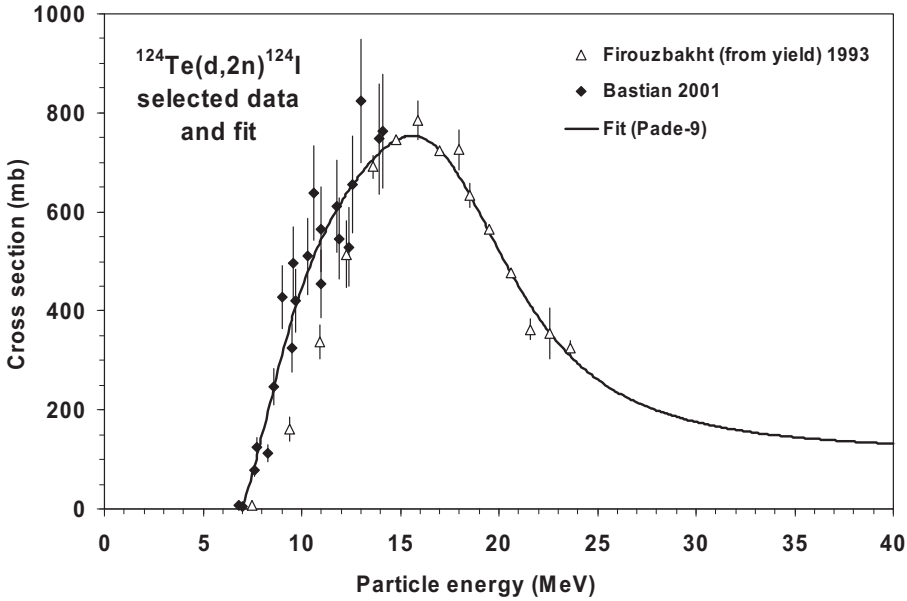

FIG. 7.89. Selected experimental data and the recommended curve (fit).

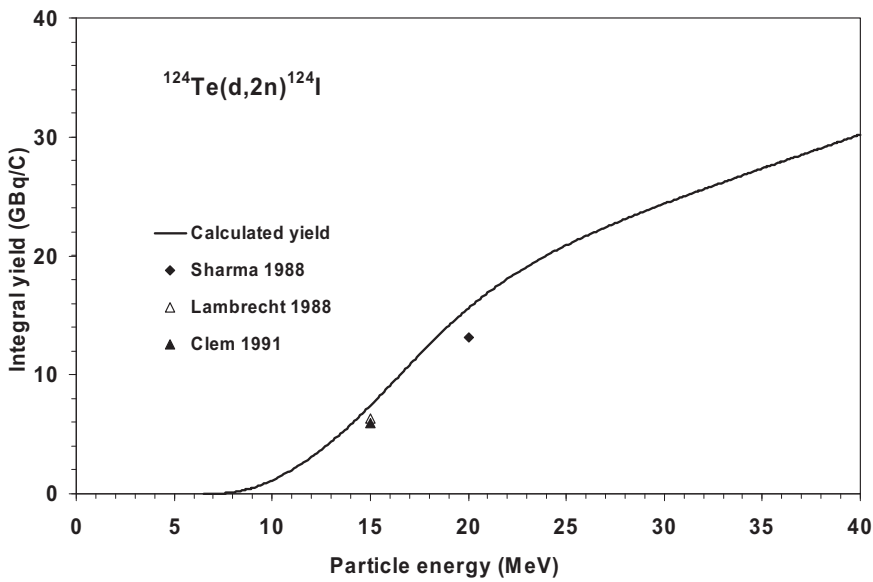

FIG. 7.90. Calculated integral yield curve based on the recommended cross-sections.

TABLE 7.36. RECOMMENDED CROSS-SECTIONS AND INTEGRAL YIELDS

$^{124}Te(d, 2n)^{124}I$ energy (MeV)	Cross-section (mb)	Integral yield	
		(μCi/μAh)	(GBq/C)
6.5	0	0	0.0
7.0	6	0	0.0
7.5	71	3	0.0
8.0	148	11	0.1
8.5	231	26	0.3
9.0	310	47	0.5
9.5	382	75	0.8
10.0	445	109	1.1
10.5	499	149	1.5
11.0	545	194	2.0
11.5	584	244	2.5
12.0	619	300	3.1
12.5	649	360	3.7
13.0	677	424	4.4
13.5	701	492	5.1
14.0	721	564	5.8
14.5	738	640	6.6
15.0	749	719	7.4
15.5	754	800	8.2
16.0	751	884	9.1
16.5	742	968	10.0
17.0	725	1053	10.8
17.5	701	1137	11.7
18.0	671	1219	12.5
18.5	636	1298	13.3
19.0	599	1374	14.1
19.5	560	1448	14.9
20.0	522	1517	15.6
20.5	485	1583	16.3
21.0	450	1645	16.9
21.5	417	1703	17.5
22.0	387	1758	18.1
22.5	360	1810	18.6
23.0	336	1859	19.1

TABLE 7.36. RECOMMENDED CROSS-SECTIONS AND INTEGRAL YIELDS (cont.)

$^{124}Te(d, 2n)^{124}I$ energy (MeV)	Cross-section (mb)	Integral yield	
		(μCi/μAh)	(GBq/C)
23.5	314	1906	19.6
24.0	294	1950	20.0
24.5	277	1992	20.5
25.0	262	2033	20.9
25.5	248	2071	21.3
26.0	236	2109	21.7
26.5	225	2145	22.0
27.0	215	2180	22.4
27.5	207	2214	22.8
28.0	199	2247	23.1
28.5	192	2279	23.4
29.0	186	2311	23.7
29.5	180	2342	24.1
30.0	175	2372	24.4
30.5	171	2402	24.7
31.0	167	2432	25.0
31.5	163	2461	25.3
32.0	160	2490	25.6
32.5	157	2519	25.9
33.0	154	2547	26.2
33.5	151	2576	26.5
34.0	149	2604	26.8
34.5	147	2632	27.0
35.0	145	2660	27.3
35.5	143	2688	27.6
36.0	141	2716	27.9
37.0	138	2771	28.5
37.5	137	2799	28.8
38.0	136	2827	29.1
38.5	135	2854	29.3
39.0	133	2882	29.6
39.5	132	2910	29.9
40.0	132	2938	30.2

As mentioned above, the co-production of an ^{125}I impurity is of concern and should be taken into account by the user. Thin-target yields were calculated from the cross-sections reported by Bastian et al. (2001), and ^{125}I /^{124}I yield ratios were derived as a function of incident deuteron energy as shown in Fig. 7.91. These data show clearly that radioisotope production at energies below 11 MeV should be avoided.

E. $^{125}Te(p, 2n)^{124}I$ reaction

Only one set of experimental data reported by Hohn et al. (2001) exists for the $^{125}I(p, 2n)^{124}I$ reaction in the energy range up to 100 MeV, and these measured data are supported very well by ALICE, EMPIRE and GNASH calculations. Figure 7.93 shows this good agreement between the theoretical curves and the experimental studies. A further attempted validation exercise involved the calculation of the thick-target yields from the experimental cross-sections. The resulting data are compared in Fig. 7.94 with thick-target yield measurements found in the literature, while corresponding numerical values for the recommended cross-sections and yields are listed in Table 7.37. The obvious discrepancies make this validation effort inconclusive. Nevertheless, the evaluator tends to favour the data set reported by Hohn et al., which is well supported by theory.

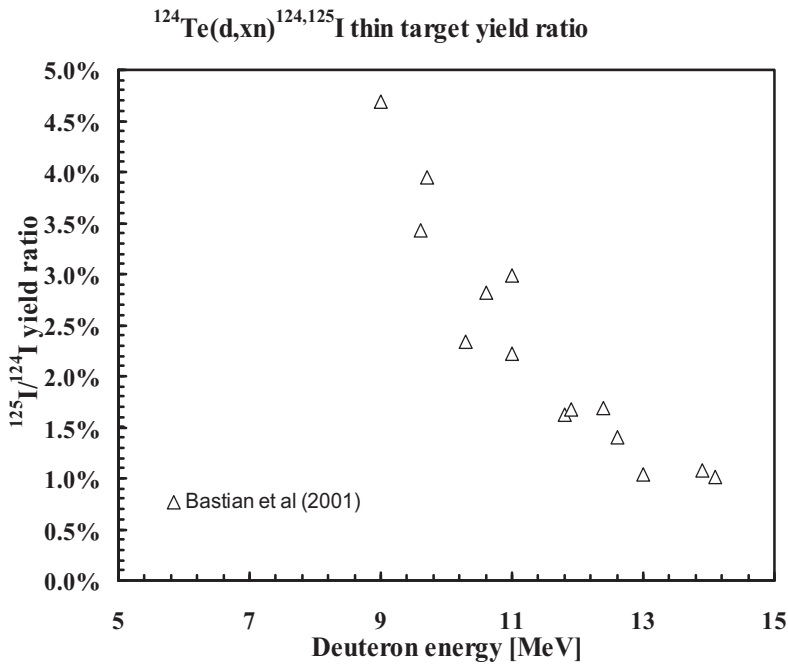

FIG. 7.91. Thin-target $^{125}I/^{124}I$ yield ratios for the $^{124}Te(d, xn)^{124,125}I$ production route.

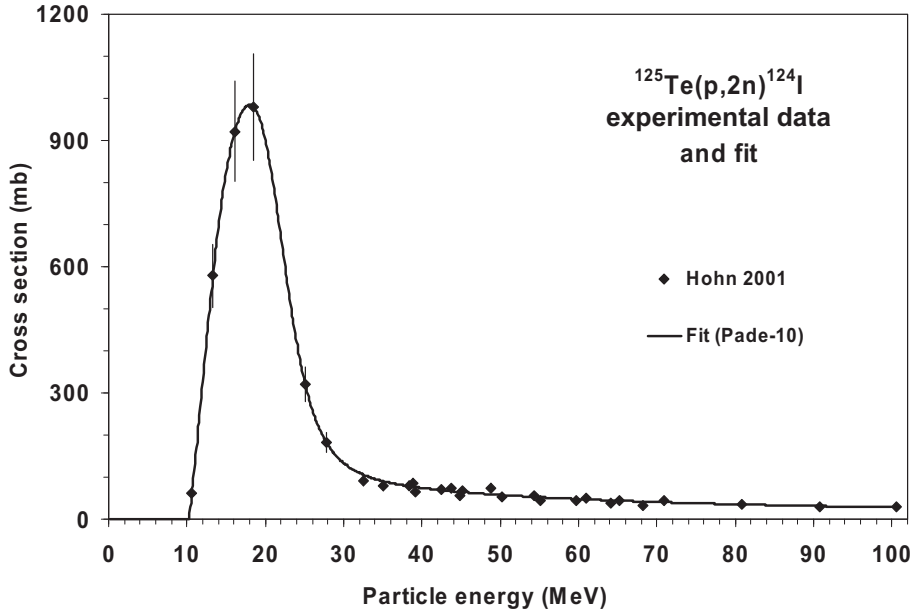

FIG. 7.92. Experimental data and the fitted curve (fit).

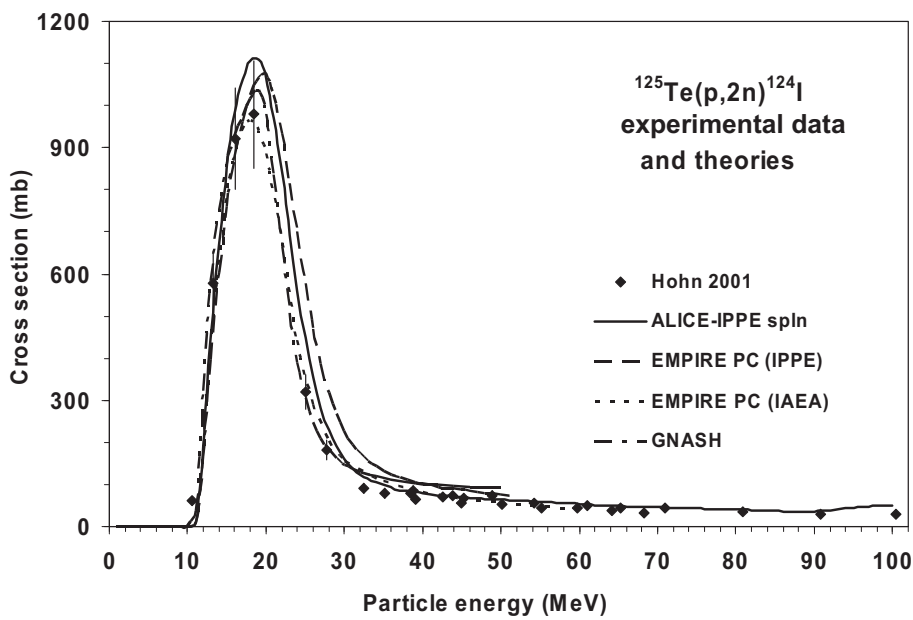

FIG. 7.93. Experimental data and theoretical calculations.

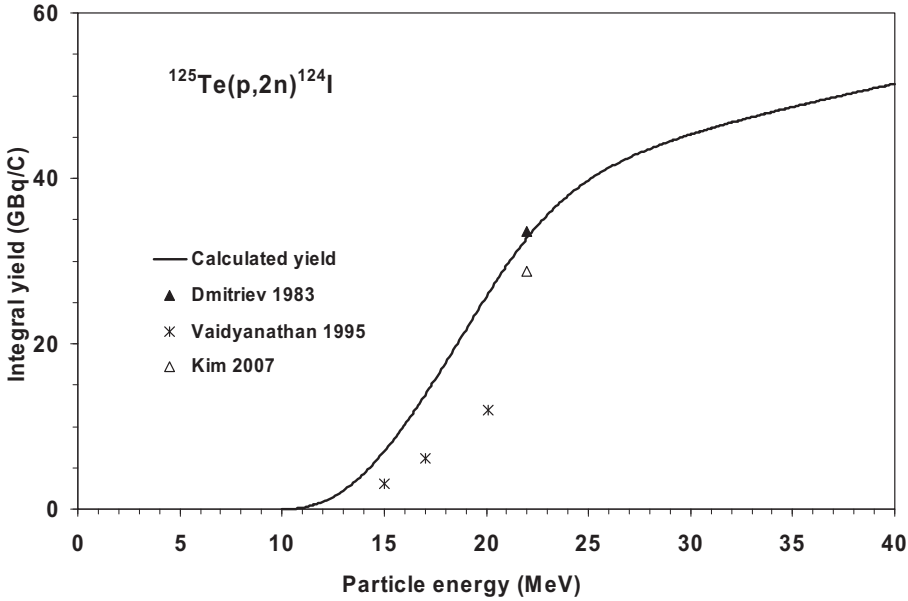

FIG. 7.94. Calculated integral yield curve based on the fitted cross-sections.

TABLE 7.37. RECOMMENDED CROSS-SECTIONS AND INTEGRAL YIELDS

^{125}Te(p, 2n)^{124}I energy (MeV)	Cross-section (mb)	Integral yield	
		(μCi/μAh)	(GBq/C)
10.0	0	0	0.0
10.5	46	2	0.0
11.0	134	16	0.2
11.5	228	43	0.4
12.0	328	85	0.9
12.5	428	143	1.5
13.0	524	218	2.2
13.5	614	309	3.2
14.0	695	417	4.3
14.5	766	540	5.6
15.0	826	678	7.0
15.5	875	827	8.5

TABLE 7.37. RECOMMENDED CROSS-SECTIONS AND INTEGRAL YIELDS (cont.)

$^{125}Te(p, 2n)^{124}I$ energy (MeV)	Cross-section (mb)	Integral yield	
		(μCi/μAh)	(GBq/C)
16.0	915	988	10.2
16.5	946	1160	11.9
17.0	967	1339	13.8
17.5	980	1527	15.7
18.0	984	1718	17.7
18.5	979	1912	19.7
19.0	964	2109	21.7
19.5	938	2305	23.7
20.0	901	2499	25.7
20.5	854	2686	27.6
21.0	798	2865	29.4
21.5	735	3034	31.2
22.0	668	3191	32.8
22.5	601	3335	34.3
23.0	536	3465	35.6
23.5	475	3584	36.8
24.0	420	3690	37.9
24.5	371	3785	38.9
25.0	328	3870	39.8
25.5	291	3947	40.6
26.0	260	4016	41.3
26.5	233	4079	41.9
27.0	211	4137	42.5
27.5	192	4190	43.1
28.0	176	4239	43.6
28.5	162	4285	44.0
29.0	151	4328	44.5
29.5	141	4368	44.9
30.0	133	4407	45.3
30.5	126	4444	45.7
31.0	120	4479	46.0

TABLE 7.37. RECOMMENDED CROSS-SECTIONS AND INTEGRAL YIELDS (cont.)

^{125}Te(p, 2n)^{124}I energy (MeV)	Cross-section (mb)	Integral yield	
		(μCi/μAh)	(GBq/C)
31.5	114	4513	46.4
32.0	110	4546	46.7
32.5	105	4579	47.1
33.0	102	4610	47.4
33.5	98	4641	47.7
34.0	95	4671	48.0
34.5	93	4700	48.3
35.0	90	4730	48.6
35.5	88	4758	48.9
36.0	86	4787	49.2
36.5	84	4815	49.5
37.0	83	4842	49.8
37.5	81	4870	50.1
38.0	79	4897	50.3
38.5	78	4924	50.6
39.0	77	4951	50.9
39.5	75	4978	51.2
40.0	74	5004	51.4

BIBLIOGRAPHY, EVALUATION AND SELECTION

Cross-sections

HOHN, A., et al., Excitation functions of ^{125}Te(p,xn)-reactions from their respective thresholds up to 100 MeV with special reference to the production of ^{124}I, Appl. Radiat. Isot. **55** (2001) 149–156.
EXFOR: A0215

Yield

DMITRIEV, P.P., Systematics of nuclear reaction yields for thick target at 22 MeV proton energy, Vop. At. Nauki i Tekhn., Ser.Yad. Konst. **2** (1983) 57–61.
EXFOR: A0195

VAIDYANATHAN, G., WIELAND, B.W., LARSEN, R.H., ZALUTSKY, M.R., High-yield production of ^{124}I using the ^{125}Te(p,2n)^{124}I reaction, S116, 6th Int. Workshop on Targetry and Target Chemistry (Proc. Int. Workshop Vancouver, BC, 1995) 87–89.
EXFOR: no
Yield results were converted to GBq/C, assuming that the data are not saturation but physical yields.

KIM, J.H., LEE, J.S., LEE, T.S., PARK, H., CHUN, K.S., Optimization studies on the production of high-purity ^{124}I using (p,2n) reaction, J. Labelled Compd Radiopharm. **50** (2007) 511–512.
EXFOR: O1538

The co-production of an ^{125}I impurity is of concern, and should be taken into account by the user. Hohn et al. (2001) measured the cross-sections for the production of both ^{124}I and ^{125}I. Thin-target yields were calculated from the reported cross-sections, and the ^{125}I /^{124}I yield ratios are shown in Fig. 7.96, as a function of the proton energy. Based upon the curves in the figure, an exit proton energy of 11 MeV or higher is recommended.

7.9. CHARGED PARTICLE PRODUCTION OF ^{125}I

Iodine-125 is an intense Auger electron emitter, and can be attached to DNA compounds, which have a chance to reach the cell nucleus and produce a

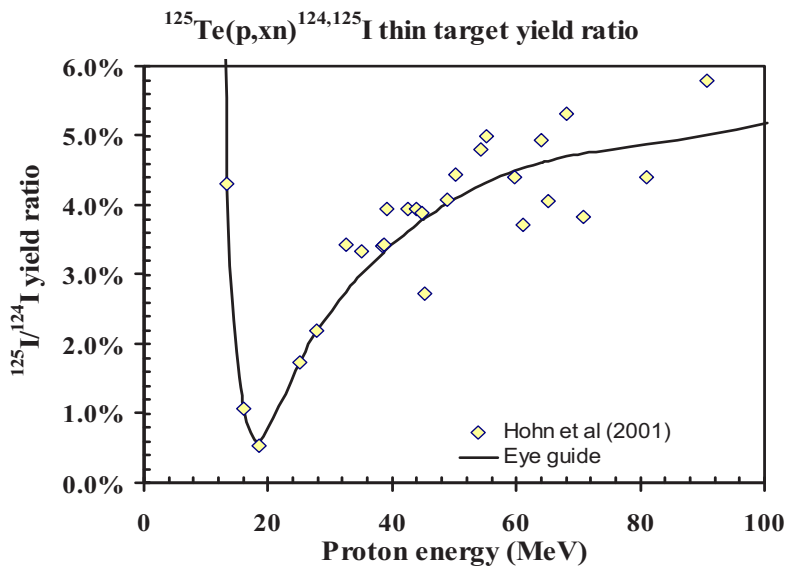

FIG. 7.95. Thin-target ^{125}I/^{124}I yield ratios for the ^{125}Te(p, xn)^{124,125}I production route.

therapeutic effect. Iodine-125 is used extensively in radio-immunoassay. It is generally produced in a nuclear reactor. Here it is considered as an impurity in the accelerator production of ^{124}I via the ^{124}Te(p, n)^{124}I, ^{124}Te(d, 2n)^{124}I and ^{125}I(p, 2n)^{124}I reactions. A simplified decay scheme is shown in Fig. 7.96, and the main emissions, as defined in Table 7.38 [7.2, 7.3], were taken from NuDat 2.4 [7.3].

A. Decay data

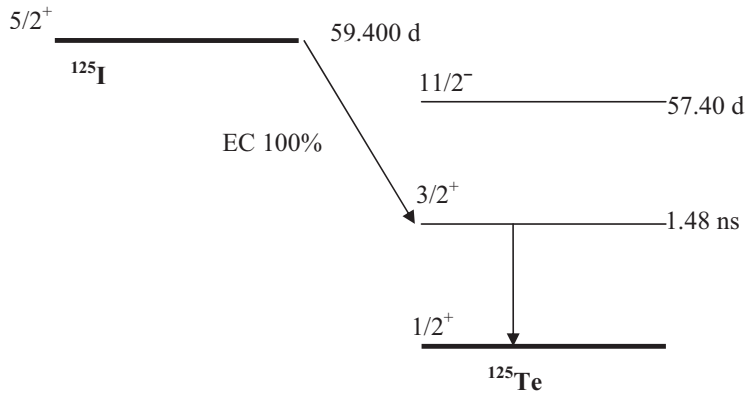

FIG. 7.96. Simplified decay scheme of ^{125}I [7.3].

TABLE 7.38. MAIN EMISSIONS [7.2, 7.3]

I-125	Decay mode: $T_{1/2}$	EC 100 % 59.400 d
Radiation	Intensity	Energy (MeV)
γ 1	6.68×10^{-02}	3.549×10^{-02}
ce-K, γ 1	8.02×10^{-01}	3.678×10^{-03}
ce-L, γ 1	1.08×10^{-01}	3.055×10^{-02} [a]
ce-M, γ 1	2.15×10^{-02}	3.449×10^{-02} [a]
$K_{\alpha 1}$ X ray	7.44×10^{-01}	2.747×10^{-02}
$K_{\alpha 2}$ X ray	4.00×10^{-01}	2.720×10^{-02}
K_{β} X ray	2.59×10^{-01}	3.100×10^{-02} [b]
L X ray	1.49×10^{-01}	3.770×10^{-03} [b]
Auger-K	2.00×10^{-01}	2.270×10^{-02} [b]
Auger-L	1.58	3.190×10^{-03} [b]

[a] Maximum energy (MeV) for subshell.
[b] Average energy (MeV).

B. Production routes

TABLE 7.39. INVESTIGATED PRODUCTION ROUTES [7.3, 7.4]

Target isotope	Natural abundance	Reaction	Q-value (MeV)	Threshold energy (MeV)
Te-125	7.07%	(p, n)	–0.97	0.98
Te-124	4.74%	(d, n)	3.4	0.0

C. ^{125}Te(p, n)^{125}I reaction

The ^{125}Te(p, n)^{125}I reaction is important in assessing the ^{125}I impurity level in ^{124}I produced via the ^{125}I(p, 2n)^{125}I reaction.

BIBLIOGRAPHY, EVALUATION AND SELECTION

Cross-sections

JOHNSON, C.H., GALONSKY, A., INSKEEP, C.N., Cross Sections for (p,n) Reactions in Cadmium And Tellurium Isotopes, Rep. ORNL-2501, Oak Ridge Natl Lab., TN (1958) 29.
EXFOR: T0138
Detected particle: neutron.

HOHN, A., et al., Excitation functions of ^{125}Te(p,xn)-reactions from their respective thresholds up to 100 MeV with special reference to the production of ^{124}I, Appl. Radiat. Isot. **55** (2001) 149–156.
EXFOR: A0215

Yield

No data were found.

Selected measurements are compared with the resulting statistical fit to these data in Fig. 7.97. Excitation functions have been calculated by means of the ALICE-IPPE, EMPIRE and GNASH nuclear reaction modelling codes, and results are compared with all of the selected experimental data in Fig. 7.98. Yields determined from the recommended cross-sections are presented in Fig. 7.99, while corresponding numerical values for the recommended cross-sections and yields are listed in Table 7.40.

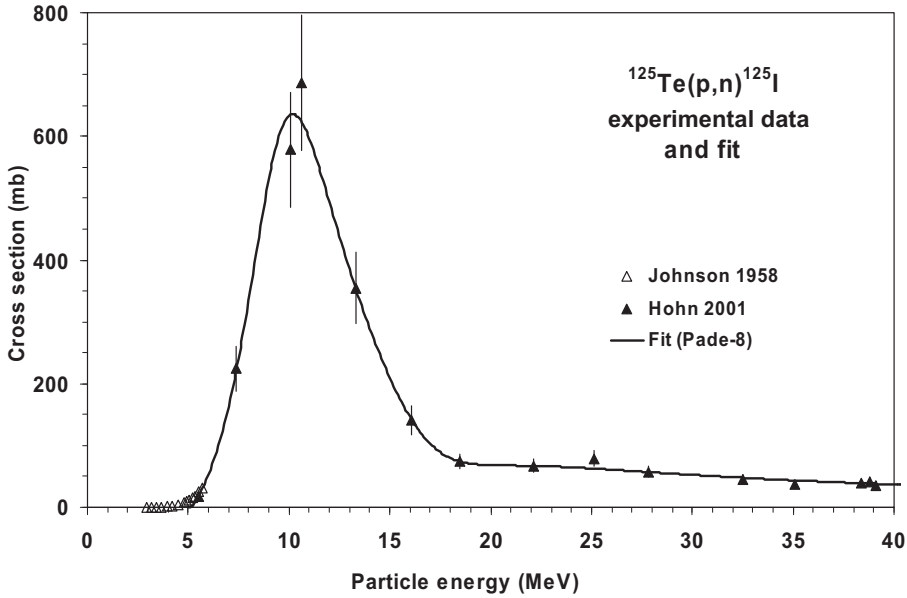

FIG. 7.97. Experimental data and the recommended curve (fit).

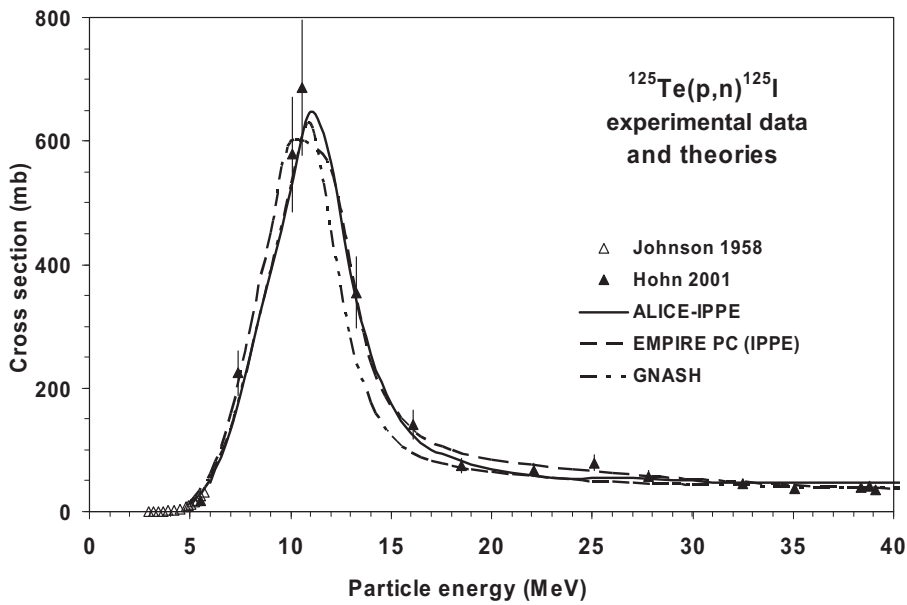

FIG. 7.98. Experimental data and theoretical calculations.

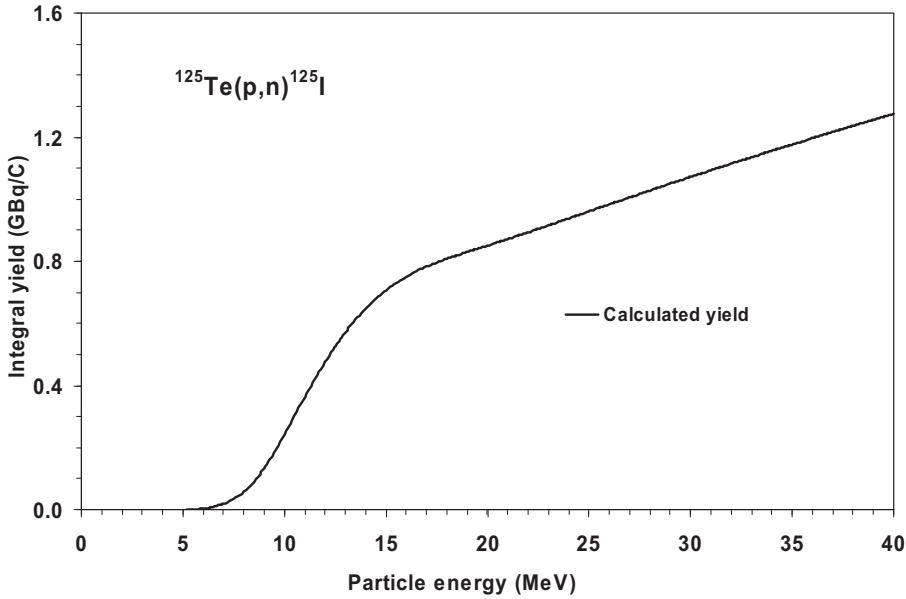

FIG. 7.99. Calculated integral yield curve based on the recommended cross-sections.

TABLE 7.40. RECOMMENDED CROSS-SECTIONS AND INTEGRAL YIELDS

^{125}Te(p, n)^{125}I energy (MeV)	Cross-section (mb)	Integral yield	
		(μCi/μAh)	(GBq/C)
5.0	0	0.0	0.00
5.5	18	0.0	0.00
6.0	53	0.3	0.00
6.5	100	0.8	0.01
7.0	162	1.8	0.02
7.5	241	3.3	0.03
8.0	335	5.6	0.06
8.5	437	8.8	0.09
9.0	531	12.9	0.13
9.5	600	17.9	0.18
10.0	633	23.5	0.24
10.5	629	29.4	0.30

TABLE 7.40. RECOMMENDED CROSS-SECTIONS AND INTEGRAL YIELDS (cont.)

$^{125}Te(p, n)^{125}I$ energy (MeV)	Cross-section (mb)	Integral yield	
		(μCi/μAh)	(GBq/C)
11.0	597	35.3	0.36
11.5	549	41.0	0.42
12.0	494	46.3	0.48
12.5	439	51.1	0.53
13.0	385	55.5	0.57
13.5	336	59.5	0.61
14.0	290	63.0	0.65
14.5	248	66.1	0.68
15.0	210	68.8	0.71
15.5	176	71.1	0.73
16.0	146	73.1	0.75
16.5	122	74.8	0.77
17.0	103	76.2	0.78
17.5	89	77.5	0.80
18.0	80	78.6	0.81
18.5	74	79.7	0.82
19.0	71	80.7	0.83
19.5	69	81.7	0.84
20.0	68	82.7	0.85
20.5	68	83.8	0.86
21.0	68	84.8	0.87
21.5	67	85.9	0.88
22.0	67	86.9	0.89
22.5	67	88.0	0.90
23.0	66	89.1	0.92
23.5	65	90.2	0.93
24.0	65	91.3	0.94
24.5	64	92.4	0.95
25.0	63	93.5	0.96
25.5	62	94.6	0.97
26.0	61	95.7	0.98

TABLE 7.40. RECOMMENDED CROSS-SECTIONS AND INTEGRAL YIELDS (cont.)

$^{125}Te(p, n)^{125}I$ energy (MeV)	Cross-section (mb)	Integral yield	
		(μCi/μAh)	(GBq/C)
26.5	60	96.8	0.99
27.0	59	97.9	1.01
27.5	58	98.9	1.02
28.0	57	100.0	1.03
28.5	56	101.1	1.04
29.0	54	102.2	1.05
29.5	53	103.2	1.06
30.0	52	104.3	1.07
30.5	51	105.3	1.08
31.0	51	106.4	1.09
31.5	50	107.4	1.10
32.0	49	108.4	1.11
32.5	48	109.4	1.12
33.0	47	110.5	1.14
33.5	46	111.5	1.15
34.0	45	112.5	1.16
34.5	44	113.5	1.17
35.0	44	114.4	1.18
35.5	43	115.4	1.19
36.0	42	116.4	1.20
36.5	42	117.4	1.21
37.0	41	118.3	1.22
37.5	40	119.3	1.23
38.0	40	120.2	1.24
38.5	39	121.2	1.25
39.0	38	122.1	1.26
39.5	38	123.1	1.26
40.0	37	124.0	1.27

D. ^{124}Te(d, n)^{125}I reaction

The ^{124}Te(d, n)^{125}I reaction is important when considering the ^{125}I impurity level ^{124}I produced via the ^{124}I(d, 2n) reaction.

BIBLIOGRAPHY, EVALUATION AND SELECTION

Cross-sections

BASTIAN, TH., COENEN, H.H., QAIM, S.M., Excitation functions of ^{124}Te(d,xn)^{124,125}I reactions from threshold up to 14 MeV: Comparative evaluation of nuclear routes for the production of ^{124}I, Appl. Radiat. Isot. **55** (2001) 303–308.
EXFOR: A0248

Yield

SHARMA, H.L., ZWEIT, J., DOWNEY, S., SMITH, A.M., SMITH, A.G., Production of ^{124}I for positron emission tomography, J. Labelled Compd Radiopharm. **26** (1989) 165–167.
EXFOR: no
Within the 15–8 MeV energy window, a 1.8 μCi/μAh yield of ^{125}I was measured on a 91.7% enriched ^{124}Te target. This value is significantly lower than the thick-target yield calculated from the recommended cross-section for the same energy range (14 μCi/μAh).

Bastian 2001 measurements are compared with the resulting statistical fit to these data in Fig. 7.100. Excitation functions have been calculated by means of the ALICE-IPPE, EMPIRE and GNASH nuclear reaction modelling codes, and results are compared with all of the selected experimental data in Fig. 7.101. Yields determined from the recommended cross-sections are presented in Fig. 7.102, while corresponding numerical values for the recommended cross-sections and yields are listed in Table 7.41.

7.10. CHARGED PARTICLE PRODUCTION OF ^{169g}Yb

All of the rare earth radionuclides considered are useful or potentially useful for the treatment of bone metastases. Ytterbium-169 has also been evaluated for use in brachytherapy. A simplified decay scheme is shown in Fig. 7.103, and the main emissions, as defined in Table 7.42, were taken from NuDat 2.4 [7.3].

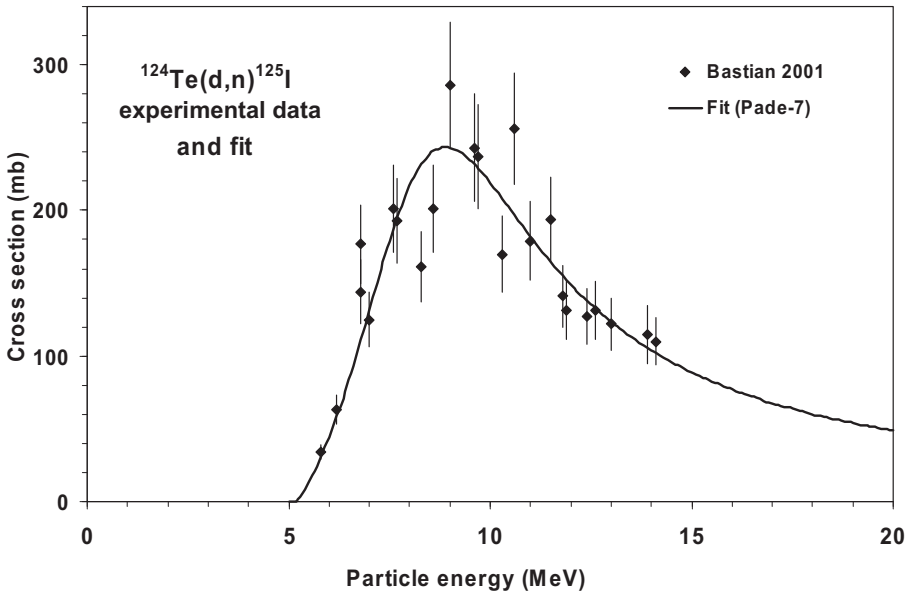

FIG. 7.100. Experimental data and the recommended curve (fit).

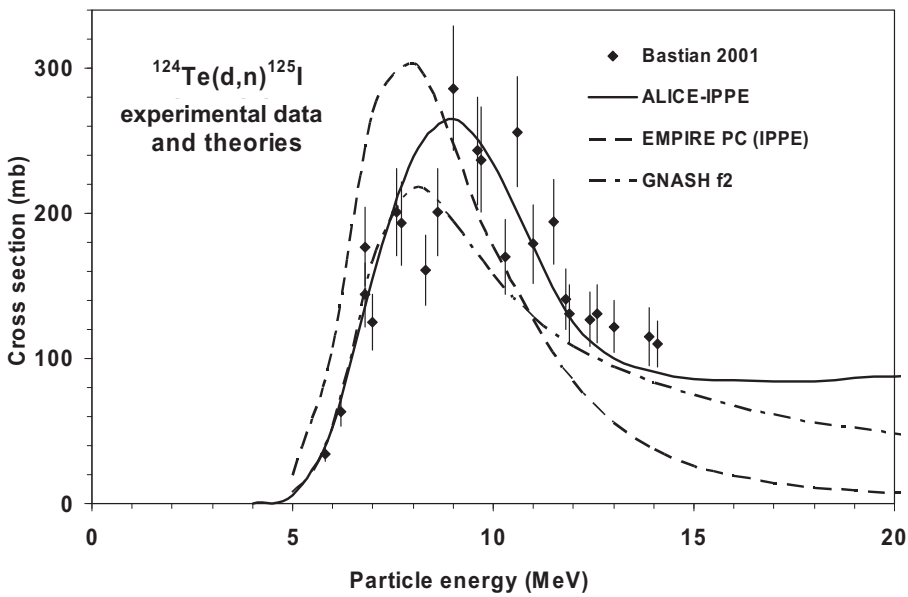

FIG. 7.101. Experimental data and theoretical calculations.

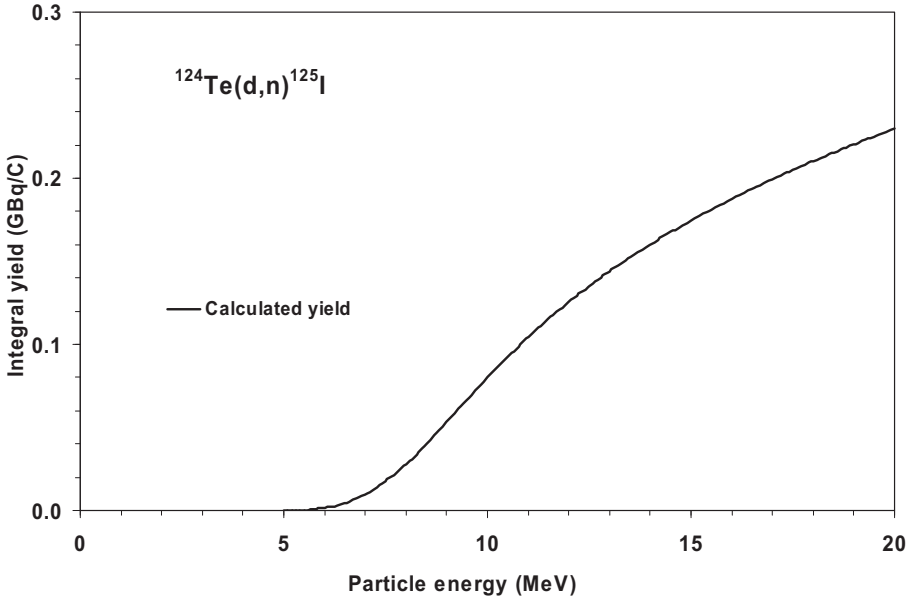

FIG. 7.102. Calculated integral yield curve based on the recommended cross-sections.

TABLE 7.41. RECOMMENDED CROSS-SECTIONS AND INTEGRAL YIELDS

^{124}Te(d, n)^{125}I energy (MeV)	Cross-section (mb)	Integral yield	
		(μCi/μAh)	(GBq/C)
5.0	0	0.0	0.000
5.5	13	0.0	0.000
6.0	44	0.1	0.002
6.5	84	0.4	0.005
7.0	131	0.9	0.010
7.5	178	1.7	0.018
8.0	217	2.7	0.028
8.5	239	3.9	0.040
9.0	243	5.2	0.053
9.5	235	6.5	0.067
10.0	219	7.8	0.080
10.5	200	9.0	0.093
11.0	182	10.1	0.104

TABLE 7.41. RECOMMENDED CROSS-SECTIONS AND INTEGRAL YIELDS (cont.)

^{124}Te(d, n)^{125}I energy (MeV)	Cross-section (mb)	Integral yield	
		(μCi/μAh)	(GBq/C)
11.5	165	11.2	0.115
12.0	149	12.2	0.125
12.5	135	13.1	0.135
13.0	123	14.0	0.144
13.5	113	14.8	0.152
14.0	104	15.6	0.160
14.5	96	16.3	0.168
15.0	89	17.0	0.175
15.5	83	17.6	0.181
16.0	77	18.2	0.188
16.5	72	18.8	0.194
17.0	68	19.4	0.199
17.5	64	19.9	0.205
18.0	60	20.5	0.210
18.5	57	21.0	0.215
19.0	54	21.4	0.220
19.5	51	21.9	0.225
20.0	49	22.4	0.230

A. Decay data

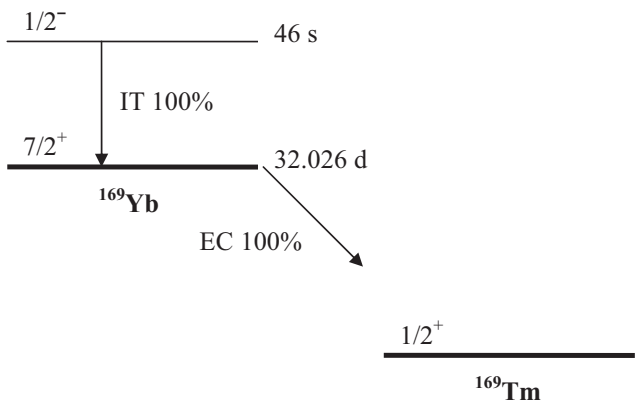

FIG. 7.103. Simplified decay scheme of ^{169}Yb [7.3].

TABLE 7.42. MAIN EMISSIONS [7.3]

Yb-169g	Decay mode: $T_{1/2}$	EC 100% 32.026 d
Radiation	Energy (keV)	Intensity (%)
ce K	3.7312	40.4
Auger L	5.67	164
ce M	6.1035	72
ce NP	7.9386	23.3
ce L	10.636	8.3
ce M	18.445	1.86
ce K	34.2255	8.24
Auger K	40.9	10.8
ce K	50.3903	34.9
ce L	53.0051	7.21
ce K	58.8006	1.32
ce M	60.8140	1.60
ce K	71.1341	6.19
ce L	83.4994	1.40
ce L	99.6642	5.70
ce M	107.4731	1.28
ce L	108.0745	1.36
ce K	117.8244	10.61
ce L	120.4080	5.28
ce M	128.2169	1.278
ce K	138.5683	13.03
ce L	167.0983	1.91
ce L	187.8422	2.15
X ray l	7.18	48.1
$K_{\alpha 2}$ X ray	49.773	53.2
$K_{\alpha 1}$ X ray	50.742	92.7
$K_{\beta 3}$ X ray	57.3	9.99
$K_{\beta 1}$ X ray	57.505	19.3
$K_{\beta 2}$ X ray	59.028	6.49
g	63.012	1.1
g	63.12077	44.2
g	93.61514	2.61
g	109.77987	17.5
g	118.19018	1.87
g	130.52368	11.31
g	177.21402	22.2
g	197.95788	35.8
g	261.07857	1.71
g	307.73757	10.05

B. Production routes

Large scale production of ^{169}Yb occurs via the (n, γ) reaction on ^{168}Yb in nuclear reactors. This route yields a product of low specific activity, especially if natural Yb targets are irradiated. Higher specific activity can be obtained by using highly enriched ^{168}Yb targets but the product will still contain significant amounts of the carrier. Therefore, alternative production routes utilizing charged particle induced processes on the mono-isotopic target ^{169}Tm (Table 7.43) or stable isotopes of erbium and ytterbium would appear to be of interest.

TABLE 7.43. INVESTIGATED PRODUCTION ROUTES [7.3, 7.4]

Target isotope	Natural abundance	Reaction	Q-value (MeV)	Threshold energy (MeV)
Tm-169	100%	(p, n)	–1.7	1.7
Tm-169	100%	(d, 2n)	–3.9	4.0

C. ^{169}Tm(p, n)^{169}Yb reaction

Two experimental data sets exist in the literature. Birattari et al. (1973) measured the excitation function of the ^{169}Tm(p, n)^{169}Yb reaction up to 44 MeV in a systematic study of the pre-equilibrium process. The second data set was measured up to 45 MeV for the CRP in a collaboration between INC FZJ (Jülich) and ATOMKI (Debrecen) to complete and verify the earlier data of Birattari et al.

The shape of the two data sets is similar but there is a factor of nearly 1.5 difference in the absolute values — no real explanation can be given for this difference. The final recommended data are based on the fitted experimental data of Spahn et al. (2005), and arise as a consequence of the more detailed cross-section measurements near the maximum and the more realistic effective threshold (Birattari et al. (1973) data at low energies are shifted towards lower energies).

BIBLIOGRAPHY, EVALUATION AND SELECTION

Cross-sections

BIRATTARI, C., et al., Pre-equilibrium processes in (p,n) reactions, Nucl. Phys. A **201** (1973) 579–592.
EXFOR: B0018
This data set was not taken into account in the fitting process.

SPAHN, I., et al., Cross section measurement of the ^{169}Tm(p,n) reaction for the production of the therapeutic radionuclide ^{169}Yb and comparison with its reactor-based generation, Appl. Radiat. Isot. **63** (2005) 235–239.
EXFOR: D4148

Yield

No data were found.

All experimental cross-section data are shown in Fig. 7.104 and the selected measurements are compared with the resulting statistical fit to these data in Fig. 7.105. Excitation functions have been calculated by means of the ALICE-IPPE, EMPIRE and GNASH nuclear reaction modelling codes, and results are compared with all of the selected experimental data in Fig. 7.106. Yields determined from the recommended cross-sections are presented in Fig. 7.107, while corresponding numerical values for the recommended cross-sections and yields are listed in Table 7.44.

D. ^{169}Tm(d, 2n)^{169}Yb reaction

Only one set of published experimental data exists up to 20 MeV as measured by Tárkányi et al. (2006) on the recommendation of the CRP. New data have been measured recently by Hermanne et al. (2007) up to 40 MeV but only preliminary data exist.

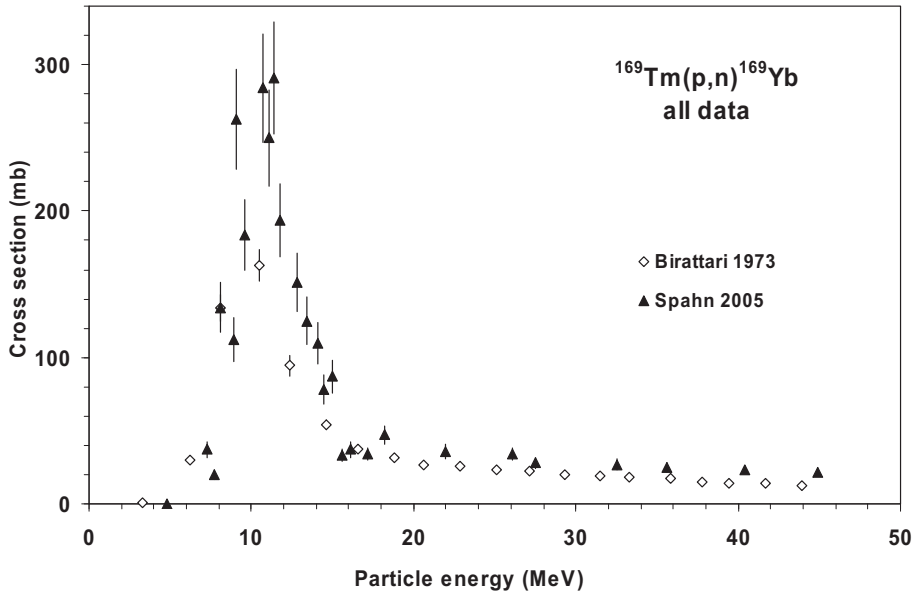

FIG. 7.104. All experimental data.

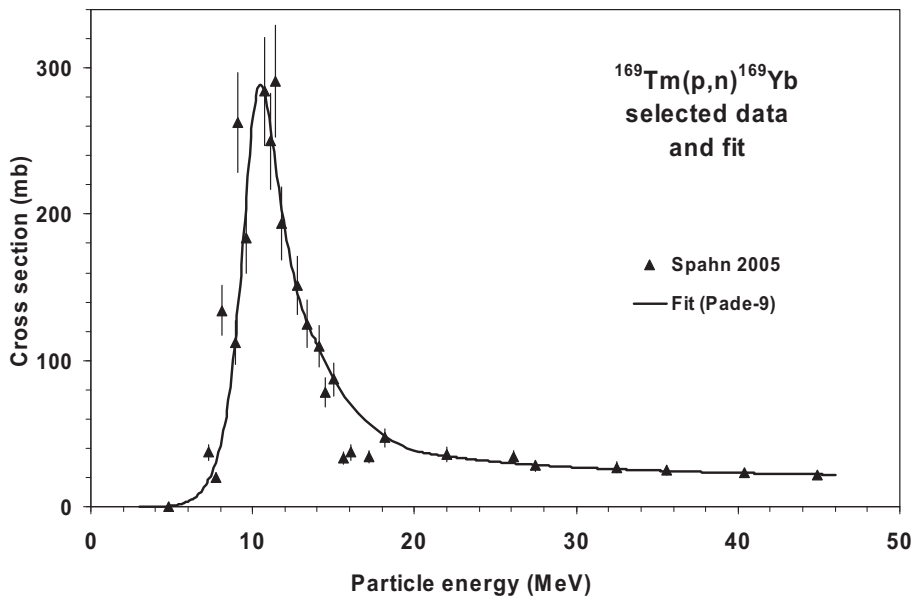

FIG. 7.105. Selected experimental data and the recommended curve (fit).

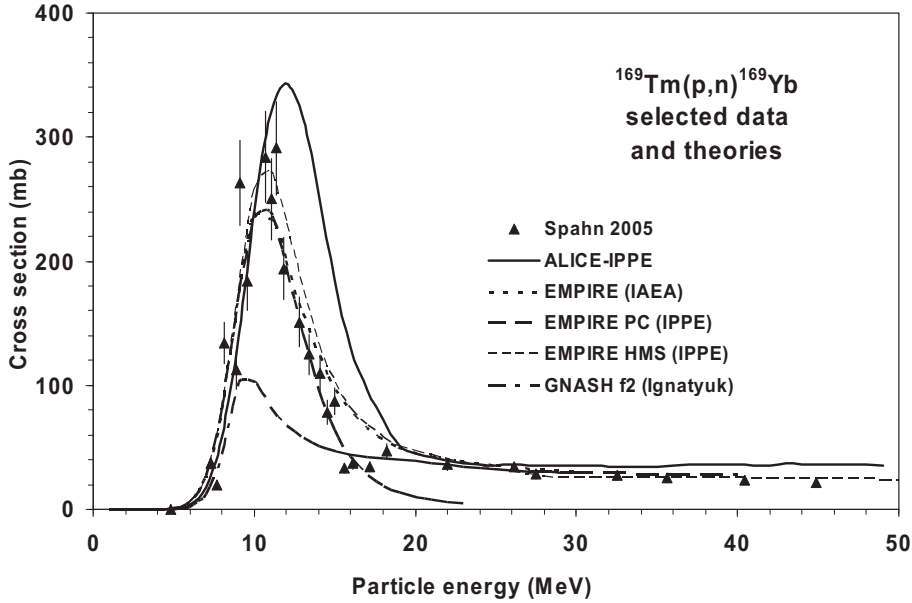

FIG. 7.106. Selected experimental data and theoretical calculations.

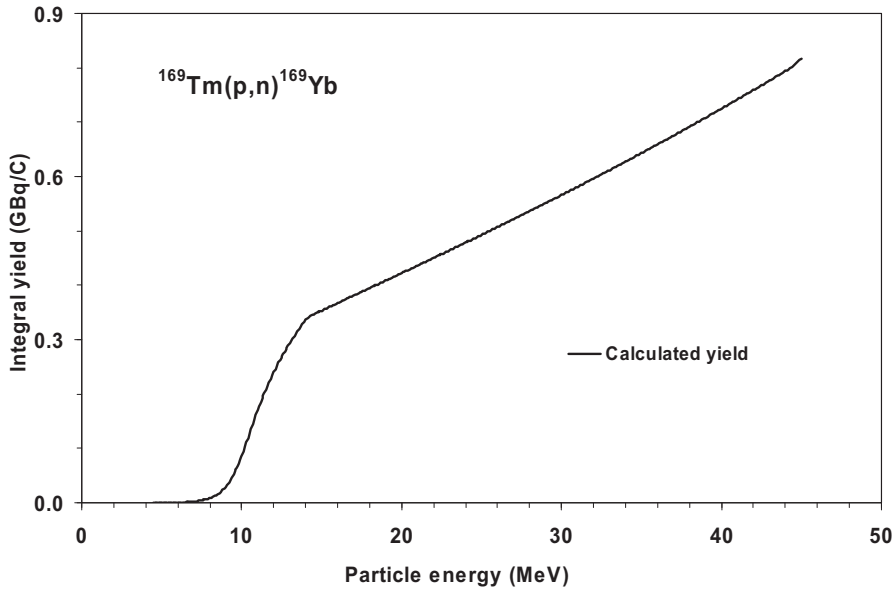

FIG. 7.107. Calculated integral yield curve based on the recommended cross-sections.

TABLE 7.44. RECOMMENDED CROSS-SECTIONS AND INTEGRAL YIELDS

$^{169}Tm(p, n)^{169}Yb$ energy (MeV)	Cross-section (mb)	Integral yield (μCi/μAh)	
4.5	0.0	0.00	0.0000
5.0	0.5	0.00	0.0000
5.5	1.5	0.01	0.0001
6.0	3.5	0.04	0.0004
6.5	7.0	0.1	0.001
7.0	13.1	0.2	0.002
7.5	23.6	0.4	0.004
8.0	41.8	0.8	0.008
8.5	73.0	1.6	0.016
9.0	124.1	2.9	0.029
9.5	195.7	5.1	0.052
10.0	264.2	8.4	0.086
10.5	288.9	12.4	0.128
11.0	266.3	16.5	0.170
11.5	226.2	20.2	0.208
12.0	188.8	23.4	0.240
12.5	159.5	26.1	0.268
13.0	137.8	28.5	0.293
13.5	122.3	30.7	0.316
14.0	111.7	32.7	0.336
14.5	40.1	33.7	0.347
15.0	36.5	34.4	0.353
15.5	35.6	35.1	0.360
16.0	34.8	35.7	0.367
16.5	34.0	36.4	0.374
17.0	33.3	37.1	0.381
17.5	32.6	37.7	0.388
18.0	32.0	38.4	0.395
18.5	31.4	39.1	0.402
19.0	30.9	39.8	0.409
19.5	30.4	40.4	0.416

TABLE 7.44. RECOMMENDED CROSS-SECTIONS AND INTEGRAL YIELDS (cont.)

$^{169}Tm(p, n)^{169}Yb$ energy (MeV)	Cross-section (mb)	Integral yield (μCi/μAh)	
20.0	29.9	41.1	0.422
20.5	29.4	41.8	0.429
21.0	29.0	42.5	0.436
21.5	28.6	43.1	0.443
22.0	28.3	43.8	0.450
22.5	27.9	44.5	0.457
23.0	27.6	45.2	0.464
23.5	27.3	45.9	0.471
24.0	27.0	46.6	0.478
24.5	26.7	47.2	0.486
25.0	26.4	47.9	0.493
25.5	26.1	48.6	0.500
26.0	25.9	49.3	0.507
26.5	25.7	50.0	0.514
27.0	25.4	50.8	0.522
27.5	25.2	51.5	0.529
28.0	25.0	52.2	0.536
28.5	24.8	52.9	0.544
29.0	24.6	53.6	0.551
29.5	24.5	54.3	0.559
30.0	24.3	55.1	0.566
30.5	24.1	55.8	0.574
31.0	24.0	56.5	0.581
31.5	23.8	57.3	0.589
32.0	23.7	58.0	0.596
32.5	23.5	58.8	0.604
33.0	23.4	59.5	0.612
33.5	23.3	60.3	0.620
34.0	23.1	61.1	0.627
34.5	23.0	61.8	0.635
35.0	22.9	62.6	0.643

TABLE 7.44. RECOMMENDED CROSS-SECTIONS AND INTEGRAL YIELDS (cont.)

$^{169}Tm(p, n)^{169}Yb$ energy (MeV)	Cross-section (mb)	Integral yield (μCi/μAh)	
35.5	22.8	63.4	0.651
36.0	22.7	64.1	0.659
36.5	22.6	64.9	0.667
37.0	22.5	65.7	0.675
37.5	22.4	66.5	0.684
38.0	22.3	67.3	0.692
38.5	22.2	68.1	0.700
39.0	22.1	68.9	0.708
39.5	22.0	69.7	0.717
40.0	21.9	70.6	0.725
40.5	21.8	71.4	0.734
41.0	21.8	72.2	0.742
41.5	21.7	73.0	0.751
42.0	21.6	73.9	0.759
42.5	21.5	74.7	0.768
43.0	21.5	75.5	0.776
43.5	21.4	76.4	0.785
44.0	21.3	77.3	0.794
44.5	28.1	78.3	0.805
45.0	27.6	79.4	0.816

BIBLIOGRAPHY, EVALUATION AND SELECTION

Cross-sections

TÁRKÁNYI, F., et al., Activation cross sections of the ^{169}Tm(d,2n) reaction for production of the therapeutic radionuclide ^{169}Yb, Appl. Radiat. Isot **65** (2007) 663–668.
EXFOR: D4180

HERMANNE, A., et al., Excitation functions for production of medically relevant radioisotopes in deuteron irradiations of Pr and Tm targets, J. Labelled Compd Radiopharm. Suppl. **50** (2007) 102.
EXFOR: no
The numerical data are still preliminary, and are not included in this CRP.

Yield

No data were found

Tárkányi (2007) measurements are compared with the resulting statistical fit to these data in Fig. 7.108. Excitation functions have been calculated by means of the ALICE-IPPE, EMPIRE and GNASH nuclear reaction modelling codes, and results are compared with all of the selected experimental data in Fig. 7.109. Yields determined from the recommended cross-sections are presented in Fig. 7.110, while corresponding numerical values for the recommended cross-sections and yields are listed in Table 7.45.

7.11. CHARGED PARTICLE PRODUCTION OF ^{177g}Lu

Lutetium-177 has excellent properties for application in therapy (498 keV β^- emission of 79.4%), and the photon emissions are ideally suited for imaging and localization with gamma cameras. A simplified decay scheme is shown in Fig. 7.111, and the main emissions, as defined in Table 7.46, were taken from NuDat 2.4 [7.3]. All rare earth radionuclides are useful or potentially useful for the treatment of bone metastases. More specifically, ^{177}Lu is attracting great attention for the labelling of monoclonal antibodies in therapeutic applications.

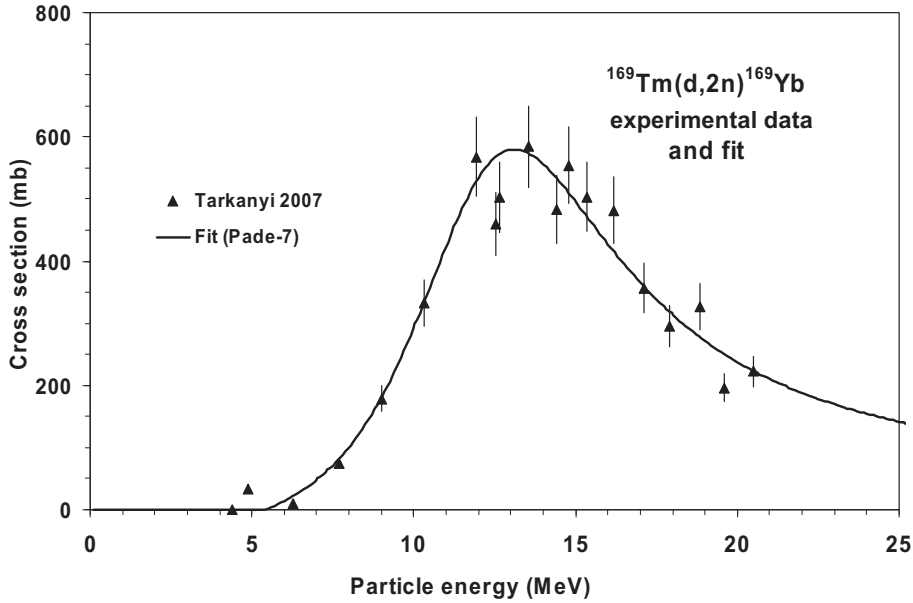

FIG. 7.108. Experimental data and the recommended curve (fit).

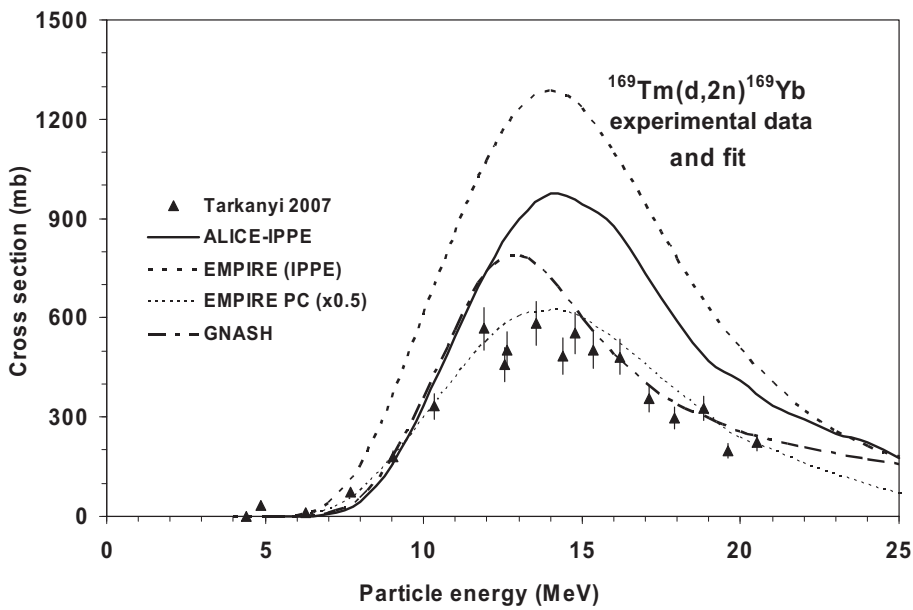

FIG. 7.109. Experimental data and theoretical calculations.

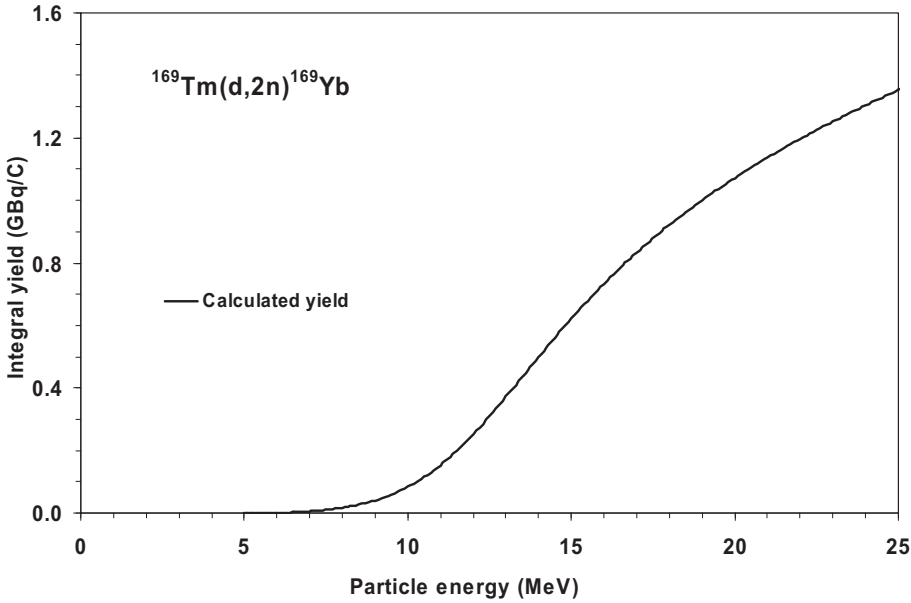

FIG. 7.110. Calculated integral yield curve based on the recommended cross-sections.

TABLE 7.45. RECOMMENDED CROSS-SECTIONS AND INTEGRAL YIELDS

^{169}Tm(d, 2n)^{169}Yb energy (MeV)	Cross-section (mb)	Integral yield	
		(μCi/μAh)	(GBq/C)
5.0	0	0.0	0.000
5.5	2	0.0	0.000
6.0	14	0.1	0.001
6.5	29	0.2	0.002
7.0	48	0.5	0.005
7.5	71	1.0	0.010
8.0	100	1.6	0.017
8.5	137	2.6	0.027
9.0	180	4.0	0.041
9.5	232	5.8	0.059
10.0	292	8.1	0.084
10.5	357	11.2	0.11

TABLE 7.45. RECOMMENDED CROSS-SECTIONS AND INTEGRAL YIELDS (cont.)

^{169}Tm(d, 2n)^{169}Yb energy (MeV)	Cross-section (mb)	Integral yield	
		(μCi/μAh)	(GBq/C)
11.0	423	14.9	0.15
11.5	485	19.4	0.20
12.0	534	24.5	0.25
12.5	566	30.2	0.31
13.0	580	36.2	0.37
13.5	575	42.4	0.44
14.0	556	48.6	0.50
14.5	528	54.7	0.56
15.0	495	60.5	0.62
15.5	461	66.1	0.68
16.0	427	71.3	0.73
16.5	395	76.3	0.78
17.0	365	81.0	0.83
17.5	338	85.5	0.88
18.0	313	89.6	0.92
18.5	291	93.6	0.96
19.0	271	97.4	1.00
19.5	254	100.9	1.04
20.0	238	104.3	1.07
20.5	223	107.6	1.11
21.0	210	110.7	1.14
21.5	199	113.6	1.17
22.0	188	116.5	1.20
22.5	178	119.2	1.23
23.0	170	121.9	1.25
23.5	162	124.4	1.28
24.0	154	126.9	1.30
24.5	148	129.3	1.33
25.0	141	131.6	1.35

A. Decay data

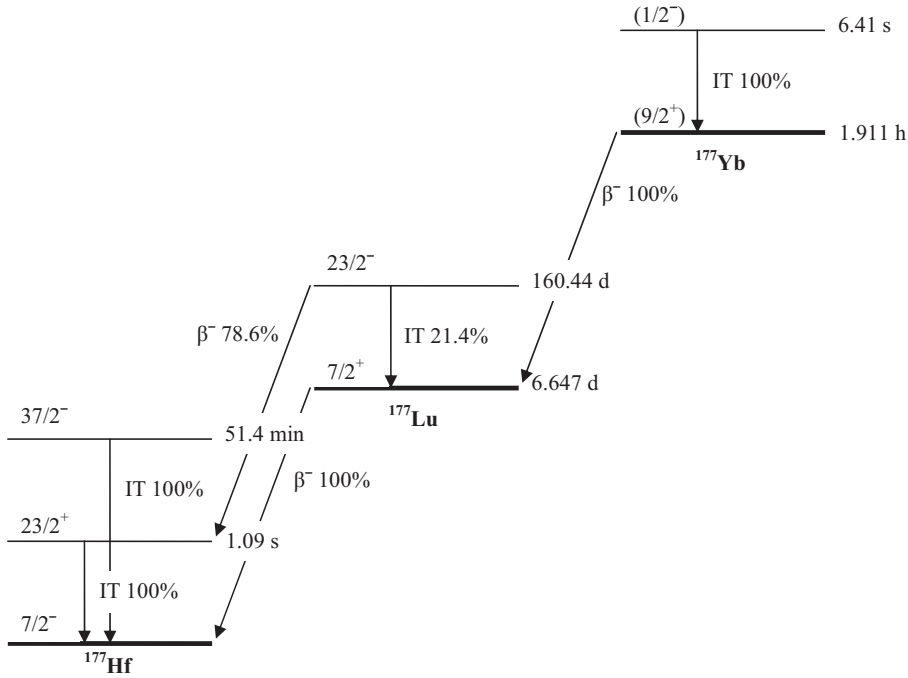

FIG. 7.111. Simplified decay scheme of ^{177}Lu [7.3].

TABLE 7.46. MAIN EMISSIONS [7.3]

Lu-177g	Decay mode: $T_{1/2}$:	β^- 100% 6.647 d	
Radiation	Energy (keV)	End point energy (keV)	Intensity (%)
β^-	47.66	177.0	11.61
β^-	78.61	248.6	0.006
β^-	111.69	385.3	9.0
β^-	149.35	498.3	79.4
g	112.9498		6.17
g	208.3662		10.36

B. Production routes

Lutetium-177 is predominantly produced in reactors by neutron capture on ^{nat}Lu or enriched ^{176}Lu. However, since efficient labelling of the biomolecules requires very high specific activity, production is confined to high flux reactors. A possible alternative involves employing the ^{176}Yb(n, γ)^{177}Yb → ^{177}Lu reaction to give a nearly carrier-free product, and this route has been studied. Possible increases in the yield of high activity, carrier-free ^{177g}Lu by means of deuteron induced reactions on Yb targets have also been investigated, as defined in Table 7.47.

TABLE 7.47. INVESTIGATED PRODUCTION ROUTES [7.3, 7.4]

Target isotope	Natural abundance	Reaction	Q-value (MeV)	Threshold energy (MeV)
Yb-176	12.76%	(d, n)^{177g}Lu	4.0	0.0
Yb-176	12.76%	(d, p)^{177}Yb → ^{177g}Lu	3.3	0.0

C. ^{176}Yb(d, n)^{177g}Lu reaction

The measurements of Hermanne (2006) are compared with the resulting statistical fit to these data in Fig. 7.112. Excitation functions have been calculated by means of the ALICE-IPPE and EMPIRE nuclear reaction modelling codes, and results are compared with all of the selected experimental data in Fig. 7.113. Yields determined from the recommended cross-sections are presented in Fig. 7.114, while corresponding numerical values for the recommended cross-sections and yields are listed in Table 7.48.

BIBLIOGRAPHY, EVALUATION AND SELECTION

Cross-sections

HERMANNE, A., et al., Deuteron-induced reactions on Yb: Measured cross sections and rationale for production pathways of carrier-free, medically relevant radionuclides, Nucl. Instrum. Methods B **247** (2006) 223–231.
EXFOR: D4175

Cross-sections for the $^{176}Yb(d, n)^{177g}Lu$ reaction were deduced by subtracting the contribution of the directly measured $^{176}Yb(d, p)^{177}Yb$ reaction from the $^{176}Yb(d, x)^{177g}Lu$ reaction determined after the decay of ^{177}Yb. The resulting excitation function of the $^{176}Yb(d, n)^{177g}Lu$ reaction with respect to energy scale, tendency and magnitude is highly disputable. However, taking into account the small contribution of the (d, n) process to the production of ^{177g}Lu (compared with the indirect (d, p) route), the (d, p) and (d, x) data could effectively be used.

Yield

No data were found.

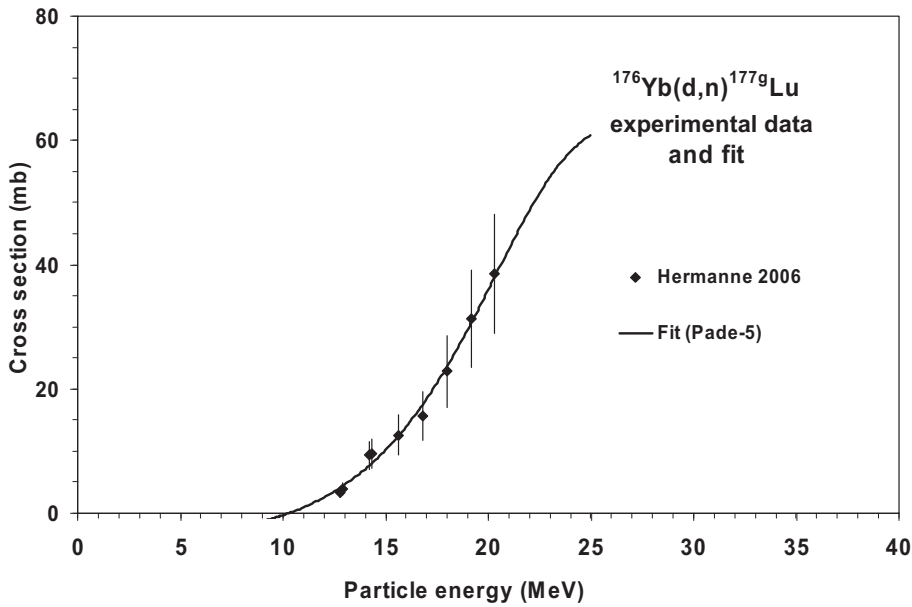

FIG. 7.112. Experimental data and the recommended curve (fit).

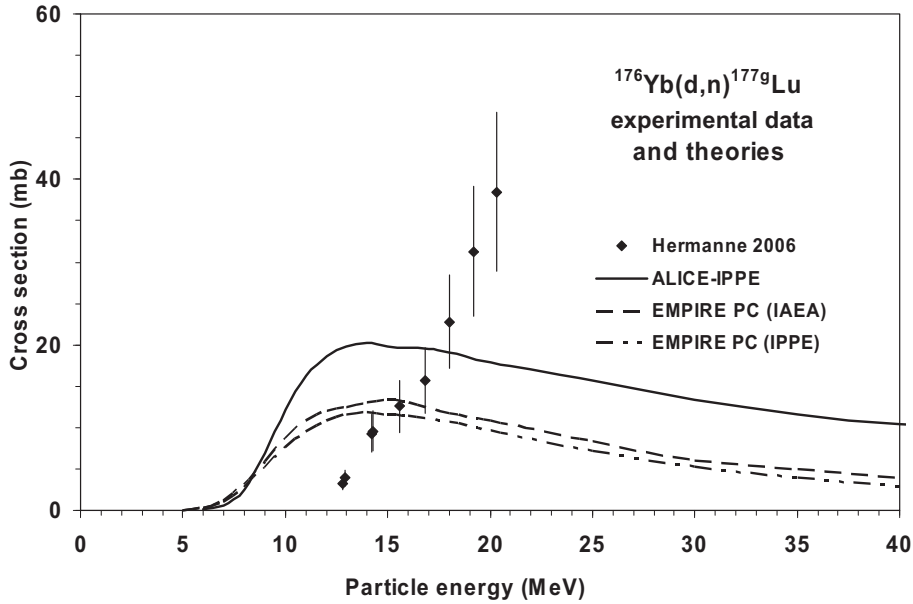

FIG. 7.113. Experimental data and theoretical calculations.

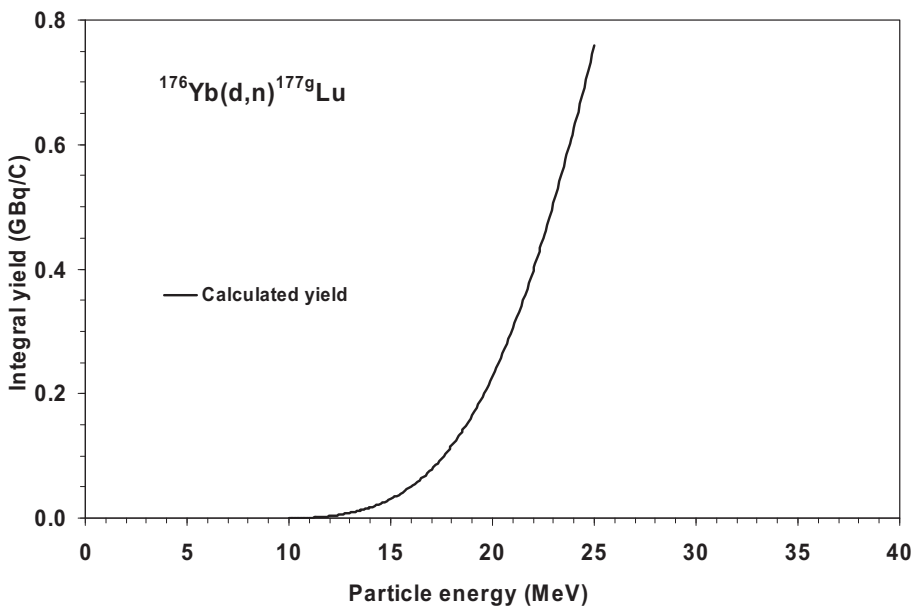

FIG. 7.114. Calculated integral yield curve based on the recommended cross-sections.

TABLE 7.48. RECOMMENDED CROSS-SECTIONS AND INTEGRAL YIELDS

$^{176}Yb(d, n)^{177g}Lu$ energy (MeV)	Cross-section (mb)	Integral yield	
		(μCi/μAh)	(GBq/C)
10.0	0.0	0.0	0.000
10.5	0.3	0.0	0.000
11.0	1.0	0.0	0.001
11.5	1.7	0.1	0.001
12.0	2.6	0.3	0.003
12.5	3.5	0.5	0.005
13.0	4.6	0.8	0.008
13.5	5.8	1.2	0.012
14.0	7.1	1.7	0.017
14.5	8.6	2.3	0.023
15.0	10.2	3.0	0.031
15.5	12.0	3.9	0.040
16.0	14.0	4.9	0.051
16.5	16.1	6.2	0.063
17.0	18.4	7.6	0.078
17.5	21.0	9.3	0.096
18.0	23.7	11.3	0.116
18.5	26.5	13.5	0.139
19.0	29.6	16.0	0.165
19.5	32.7	18.9	0.194
20.0	36.0	22.1	0.228
20.5	39.2	25.7	0.264
21.0	42.5	29.7	0.305
21.5	45.7	34.0	0.349
22.0	48.7	38.7	0.398
22.5	51.5	43.8	0.450
23.0	54.1	49.2	0.506
23.5	56.3	54.9	0.565
24.0	58.2	61.0	0.627
24.5	59.7	67.3	0.692
25.0	60.8	73.8	0.759

D. ^{176}Yb(d, p)^{177}Yb reaction

The measurements of Hermanne (2006) are compared with the resulting statistical fit to these data in Fig. 7.115. Excitation functions have been calculated by means of the ALICE-IPPE, EMPIRE and GNASH nuclear reaction modelling codes, and results are compared with all of the selected experimental data in Fig. 7.116. Yields determined from the recommended cross-sections are presented in Fig. 7.117, while corresponding numerical values for the recommended cross-sections and yields are listed in Table 7.49.

BIBLIOGRAPHY, EVALUATION AND SELECTION

Cross-sections

HERMANNE, A., et al., Deuteron-induced reactions on Yb: Measured cross sections and rationale for production pathways of carrier-free, medically relevant radionuclides, Nucl. Instrum. Methods B **247** (2006) 223–231.
EXFOR: D4175
Cross-sections for the ^{176}Yb(d, n)^{177g}Lu reaction were deduced by subtracting the contribution of the directly measured ^{176}Yb(d, p)^{177}Yb reaction from the ^{176}Yb(d, x)^{177g}Lu reaction determined after the decay of ^{177}Yb. The resulting excitation function of the ^{176}Yb(d, n)^{177g}Lu reaction with respect to energy scale, tendency and magnitude is strongly disputable. However, taking into account the small contribution of the (d, n) process to the production of ^{177g}Lu (compared with the indirect (d, p) route), the (d, p) and (d, x) data could effectively be used.

Yield

No data were found.

E. ^{176}Yb(d, x)^{177g}Lu cumulative process

A cumulative process is feasible which involves the production of ^{177g}Lu via the (d, n) reaction and decay of ^{177}Yb.

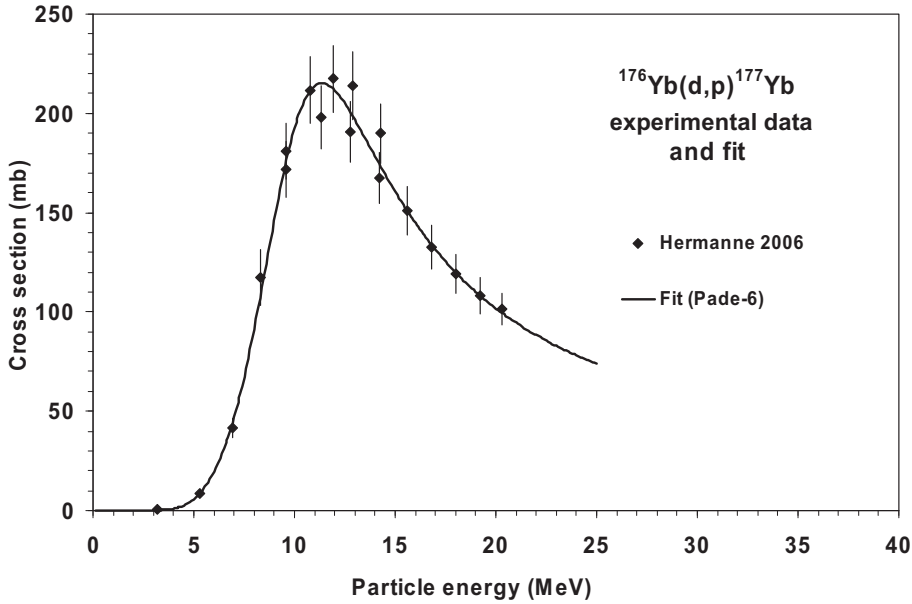

FIG. 7.115. Experimental data and the recommended curve (fit).

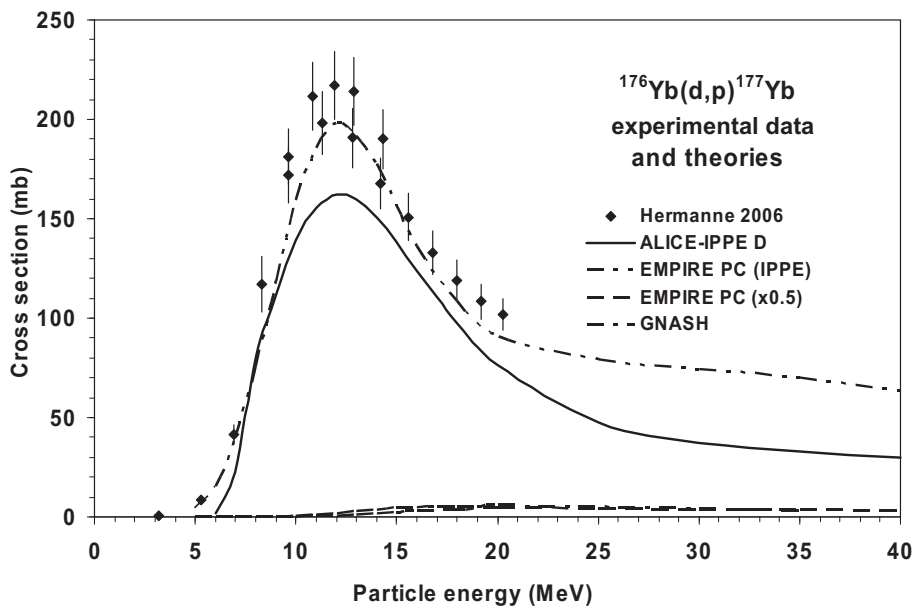

FIG. 7.116. Experimental data and theoretical calculations.

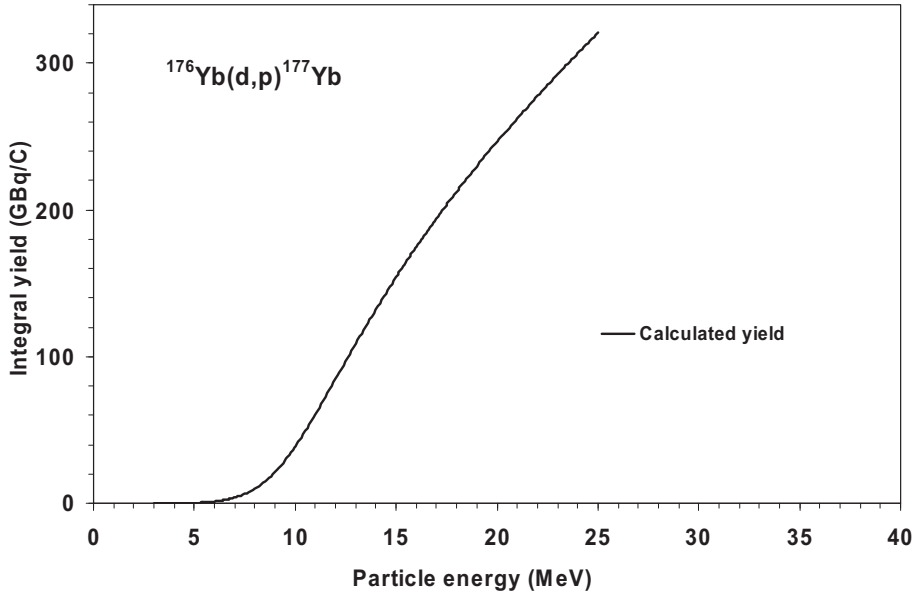

FIG. 7.117. Calculated integral yield curve based on the recommended cross-sections.

TABLE 7.49. RECOMMENDED CROSS-SECTIONS AND INTEGRAL YIELDS

^{176}Yb(d, p)^{177}Yb energy (MeV)	Cross-section (mb)	Integral yield	
		(μCi/μAh)	(GBq/C)
3.0	0.0	0	0.0
3.5	0.4	0	0.0
4.0	0.8	2	0.0
4.5	2.4	7	0.1
5.0	5.7	21	0.2
5.5	11.2	51	0.5
6.0	19.4	109	1.1
6.5	31.1	209	2.1
7.0	46.9	369	3.8
7.5	67.0	612	6.3
8.0	91.2	962	9.9
8.5	118.3	1442	14.8
9.0	146.2	2068	21.3

TABLE 7.49. RECOMMENDED CROSS-SECTIONS AND INTEGRAL YIELDS (cont.)

^{176}Yb(d, p)^{177}Yb energy (MeV)	Cross-section (mb)	Integral yield	
		(μCi/μAh)	(GBq/C)
9.5	171.8	2843	29.2
10.0	192.5	3757	38.6
10.5	206.6	4785	49.2
11.0	213.8	5893	60.6
11.5	214.9	7051	72.5
12.0	211.5	8235	84.6
12.5	205.1	9418	96.8
13.0	196.8	10 586	108.8
13.5	187.7	11 730	120.6
14.0	178.4	12 844	132.0
14.5	169.3	13 929	143.2
15.0	160.6	14 980	154.0
15.5	152.5	15 998	164.4
16.0	144.9	16 985	174.6
16.5	137.8	17 942	184.4
17.0	131.3	18 875	194.0
17.5	125.4	19 780	203.3
18.0	119.8	20 661	212.3
18.5	114.8	21 519	221.2
19.0	110.1	22 356	229.8
19.5	105.7	23 176	238.2
20.0	101.7	23 977	246.4
20.5	98.0	24 761	254.5
21.0	94.6	25 529	262.4
21.5	91.3	26 283	270.1
22.0	88.3	27 022	277.7
22.5	85.5	27 749	285.2
23.0	82.9	28 465	292.6
23.5	80.4	29 169	299.8
24.0	78.1	29 862	306.9
24.5	75.9	30 545	313.9
25.0	73.9	31 218	320.9

BIBLIOGRAPHY, EVALUATION AND SELECTION

Cross-sections

HERMANNE, A., et al., Deuteron-induced reactions on Yb: Measured cross sections and rationale for production pathways of carrier-free, medically relevant radionuclides, Nucl. Instrum. Methods B **247** (2006) 223–231.
EXFOR: D4175
Cross-sections for the ^{176}Yb(d, n)^{177g}Lu reaction were deduced by subtracting the contribution of the directly measured ^{176}Yb(d, p)^{177}Yb reaction from the ^{176}Yb(d, x)^{177g}Lu reaction determined after the decay of ^{177}Yb. The resulting excitation function of the ^{176}Yb(d, n)^{177g}Lu reaction with respect to energy scale, tendency and magnitude is strongly disputable. However, taking into account the small contribution of the (d, n) process to the production of ^{177g}Lu (compared with the indirect (d, p) route), the (d, p) and (d, x) data could effectively be used.

Yield

No data were found.

The measurements of Hermanne (2006) are compared with the resulting statistical fit to these data in Fig. 7.118. Excitation functions have been calculated by means of the EMPIRE nuclear reaction modelling code, and results are compared with all of the selected experimental data in Fig. 7.119. Yields determined from the recommended cross-sections are presented in Fig. 7.120, while corresponding numerical values for the recommended cross-sections and yields are listed in Table 7.50.

7.12. CHARGED PARTICLE PRODUCTION OF ^{186g}Re

Rhenium has similar chemical properties to those of technetium, and can be used to label hydroxyethylidenediphosphonate (HEDP) with ^{186}Re after reduction to perrhenate by stannous ions. ^{186}Re(Sn-)HEDP has also been successfully used for palliation of skeletal metastases. Furthermore, ^{186}Re has great potential in the labelling of monoclonal antibodies for radio-immunotherapy. A simplified decay scheme is shown in Fig. 7.121, and the main emissions, as defined in Table 7.51, were taken from NuDat 2.4 [7.3].

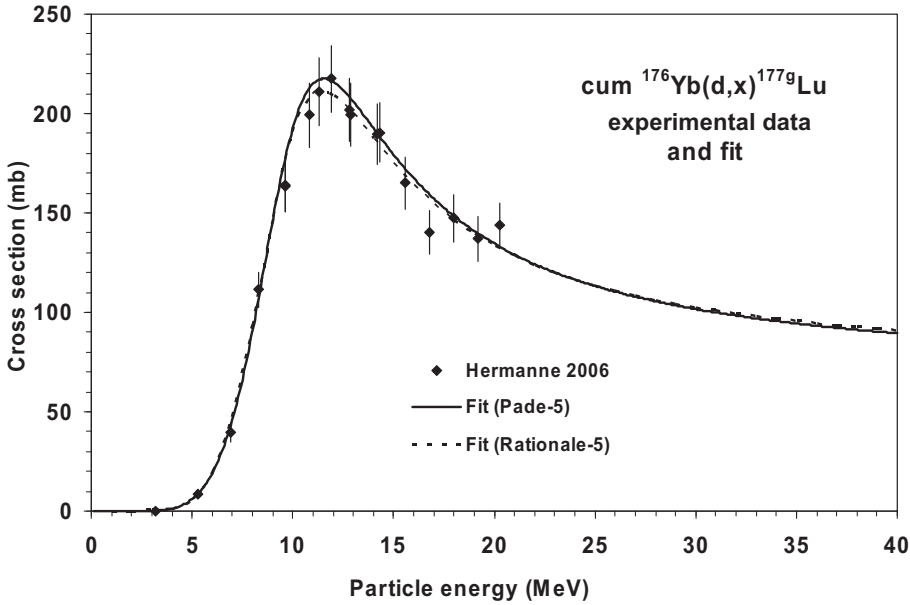

FIG. 7.118. Experimental data and the recommended curve (fit).

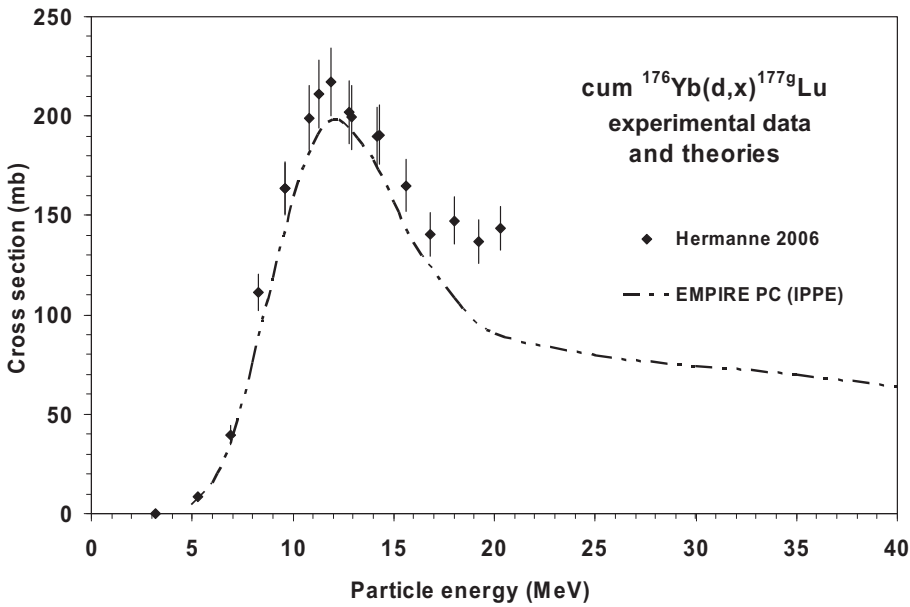

FIG. 7.119. Experimental data and theoretical calculations.

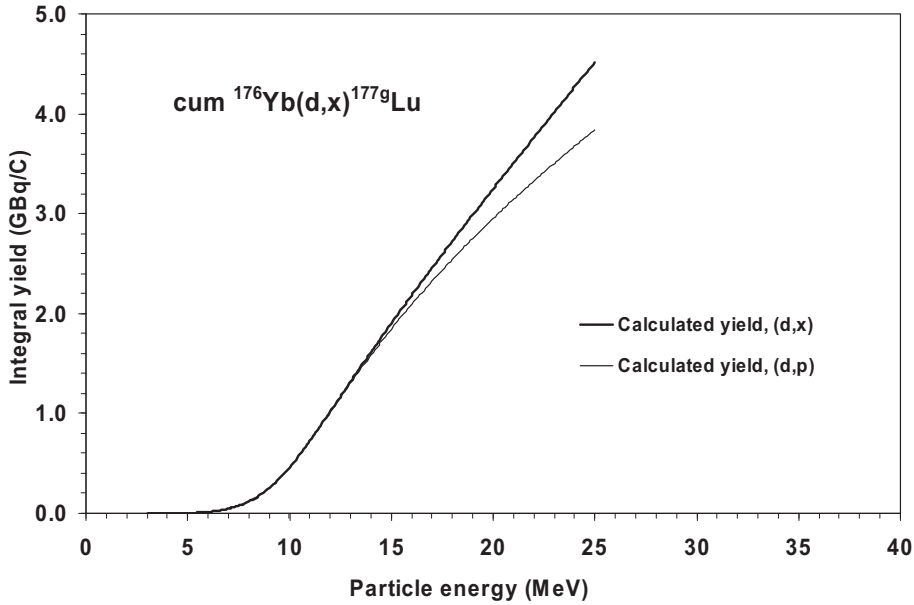

FIG. 7.120. Calculated integral yield curve based on the recommended cross-sections.

TABLE 7.50. RECOMMENDED CROSS-SECTIONS AND INTEGRAL YIELDS

cum ^{176}Yb(d, x)^{177g}Lu energy (MeV)	Cross-section (mb)	Integral yield	
		(μCi/μAh)	(GBq/C)
3.0	0	0.0	0.00
3.5	1	0.0	0.00
4.0	1	0.1	0.00
4.5	3	0.1	0.00
5.0	6	0.3	0.00
5.5	11	0.7	0.01
6.0	19	1.4	0.01
6.5	30	2.5	0.03
7.0	46	4.4	0.05
7.5	66	7.3	0.07
8.0	91	11.4	0.12
8.5	118	17.2	0.18
9.0	146	24.7	0.25

TABLE 7.50. RECOMMENDED CROSS-SECTIONS AND INTEGRAL YIELDS (cont.)

cum ^{176}Yb(d, x)^{177g}Lu energy (MeV)	Cross-section (mb)	Integral yield	
		(μCi/μAh)	(GBq/C)
9.5	172	34.0	0.35
10.0	193	44.9	0.46
10.5	207	57.3	0.59
11.0	215	70.6	0.73
11.5	217	84.6	0.87
12.0	216	99.0	1.02
12.5	212	113.6	1.17
13.0	206	128.1	1.32
13.5	200	142.6	1.47
14.0	193	156.9	1.61
14.5	186	171.1	1.76
15.0	179	185.1	1.90
15.5	173	198.8	2.04
16.0	168	212.4	2.18
16.5	162	225.8	2.32
17.0	157	239.1	2.46
17.5	153	252.2	2.59
18.0	148	265.2	2.73
18.5	145	278.0	2.86
19.0	141	290.8	2.99
19.5	138	303.5	3.12
20.0	135	316.1	3.25
20.5	132	328.6	3.38
21.0	129	341.1	3.51
21.5	127	353.5	3.63
22.0	124	365.9	3.76
22.5	122	378.3	3.89
23.0	120	390.6	4.01
23.5	118	402.9	4.14
24.0	116	415.2	4.27
24.5	115	427.5	4.39
25.0	113	439.8	4.52

A. Decay data

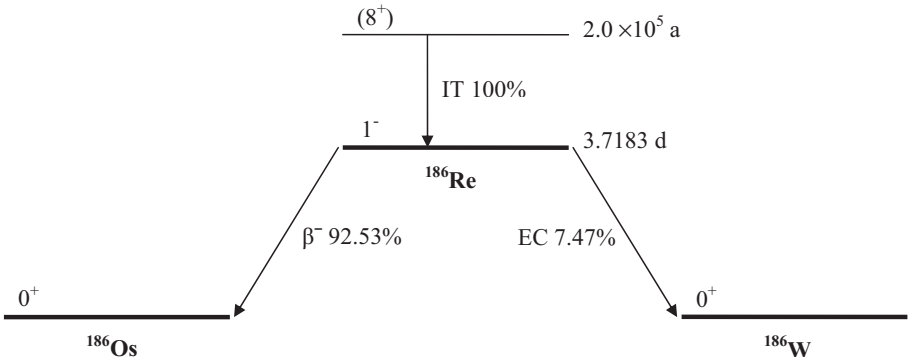

FIG. 7.121. Simplified decay scheme of ^{186}Re [7.3].

TABLE 7.51. MAIN EMISSIONS [7.3]

Re-186g	Decay mode: $T_{1/2}$:	β^- 92.53% 3.7183 d	
Radiation	Energy (keV)	End point energy (keV)	Intensity (%)
β^-	48.4	158.8	2.6E–5
β^-	84.9	302.0	0.0625
β^-	306.1	932.3	21.54
β^-	359.2	1069.5	70.99
g	137.157		9.47

B. Production routes

Rhenium-186 is routinely produced in nuclear reactors by neutron activation of metallic rhenium enriched with ^{185}Re via the ^{185}Re(n, γ)^{186}Re nuclear reaction. An evaluation of the data for this reaction is given in Section 6.3.1. However, alternative charged particle routes of production have been developed because of the low specific activity achieved in the neutron activation process, as specified in Table 7.52.

TABLE 7.52. INVESTIGATED PRODUCTION ROUTES [7.3, 7.4]

Target isotope	Natural abundance	Reaction	Q-value (MeV)	Threshold energy (MeV)
W-186	28.43%	(p, n)	–1.4	1.4
W-186	28.43%	(d, 2n)	–3.6	3.6

C. ^{186}W(p, n)^{186g}Re reaction

BIBLIOGRAPHY, EVALUATION AND SELECTION

The data were corrected for absolute intensity of the measured 137 keV gamma line (Miyahara et al. (2000), $I_\gamma = 0.0947$) and for data of the used monitor reactions. The correction factors are given in the list of references (detailed explanation in Tárkányi et al. (2007)).

Decay data

MIYAHARA, H., et al., Precise measurements of the gamma-ray emission probabilities of ^{186}Re and ^{188}Re, Appl. Radiat. Isot. **52** (2000) 573–579.
EXFOR: no

Cross-sections

SHIGETA, N., et al., Production method of no-carrier-added ^{186}Re, J. Radioanal. Nucl. Chem. **205** (1996) 85–92.
EXFOR: no
Correction factor of 0.987.

SHIGETA ISHIOKA, N., SEKINE, T., LAMBRECHT, R.M., Comments on the cross sections of ^{186}Re in the ^{186}W(p,n) and ^{186}W(d,2n) reactions in connection to the paper given by Zhu et al. and correction of the calculated yields of ^{186}Re in the ^{186}W(p,n) reaction, J. Radioanal. Nucl. Chem. **241** (1999) 383.
EXFOR: no
Correction of Shigeta et al. (1996).

ZHANG, X., et al., Excitation functions for ^{nat}W(p,xn)$^{181-186}$Re reactions and production of no-carrier-added ^{186}Re via ^{186}W(p,n)^{186}Re reaction, Radiochim. Acta **86** (1999) 11.
EXFOR: no
Correction factor of 1.434.

MIAH, M.H., KUHNHENN, J., HERPERS, U., MICHEL, R., KUBIK, P., Production of residual nuclides by proton-induced reactions on target W at an energy of 72 MeV, Int. Conf. Nucl. Data for Science and Technology (Proc. Int. Conf. Tsukuba, 2001), (SHIBATA, K. et al., Eds), J. Nucl. Sci. Technol. Suppl. **2** (2002) 369, Rhenium 372.
EXFOR: O1100
Correction factor of 0.971.

SZELECSÉNYI, F., TAKÁCS, S., TÁRKÁNYI, F., SONCK, M., HERMANNE, A., Study of production possibility of no-carrier-added ^{186}Re via proton induced reaction on tungsten for use in radiotherapy, 6th Int. Symp. Synthesis and Applications of Isotopically Labeled Compounds (Proc. Int. Symp. Philadelphia, 1997), (HEYS, J.R., MELLILO, D.G., Eds), John Wiley and Sons, Chichester (1998) 701.
EXFOR: D4087
Preliminary data of Tárkányi et al. (2006).

TÁRKÁNYI, F., et al., Excitation functions of proton induced nuclear reactions on natural tungsten up to 34 MeV, Nucl. Instrum. Methods B **252** (2006) 160–174.
EXFOR: D4163
Correction factor of 0.897.

LAPI, S., et al., Production cross sections of $^{181–186}$Re isotopes from proton bombardment of natural tungsten, Appl. Radiat. Isot. **65** (2007) 345–349.
EXFOR: C1501
Correction factor of 0.971.

MENAPACE, E., et al., Experimental and calculated nuclear reaction data relative to innovative production of medical radioisotopes, Int. Conf. Nuclear Data for Science and Technology, Nice, 2007, AID#655.
EXFOR: no
Correction factor of 0.868.

TÁRKÁNYI, F., et al., New measurement and evaluation of the excitation function of the ^{186}W(p,n) nuclear reaction for production of the therapeutic radioisotope ^{186}Re, Nucl. Instrum. Methods B **264** (2007) 389–394.
EXFOR: D4193
Correction factor of 1.0.

KHANDAKER, M.U., et al., Excitation functions of proton induced nuclear reactions on ^{nat}W up to 40 MeV, Nucl. Instrum. Methods B **266** (2008) 1021–1029.
EXFOR: D0282
Correction factor of 0.994.

Yield

ZHANG, X., LI, W., FANG, K., HE, W., Preparation of carrier free ^{186}Re, J. Nucl. Radiochem. **21** (1999) 178–183.
EXFOR: no

MOUSTAPHA, M.E., et al., Preparation of cyclotron-produced ^{186}Re and comparison with reactor-produced ^{186}Re and generator-produced ^{188}Re for the labeling of bombesin, Nucl. Med. Biol. **33** (2006) 81–89.
EXFOR: no

DMITRIEV, P.P., MOLIN, G.A., Yields of ^{181}Re, ^{182m}Re, ^{182}Re, ^{183}Re, ^{184m}Re, ^{184}Re and ^{186}Re when irradiating tungsten with protons and deuterons, and tantalum with alpha particles, Atomnaya Energiya **48** (1980) 122–124.
EXFOR: A0070
The yields were determined from excitation functions obtained by calculation and, therefore, were rejected.

Selected measurements with corrections are compared with the resulting statistical fit to these data in Fig. 7.122. Excitation functions have been calculated by means of the ALICE-IPPE, EMPIRE and GNASH nuclear reaction modelling codes, and results are compared with all of the selected experimental data in Fig. 7.123. Yields determined from the recommended cross-sections are presented in Fig. 7.124, while corresponding numerical values for the recommended cross-sections and yields are listed in Table 7.53.

D. ^{186}W(d, 2n)^{186g}Re reaction

These data sets were not corrected according to the new decay data as was carried out for the ^{186}W(p, n) reaction.

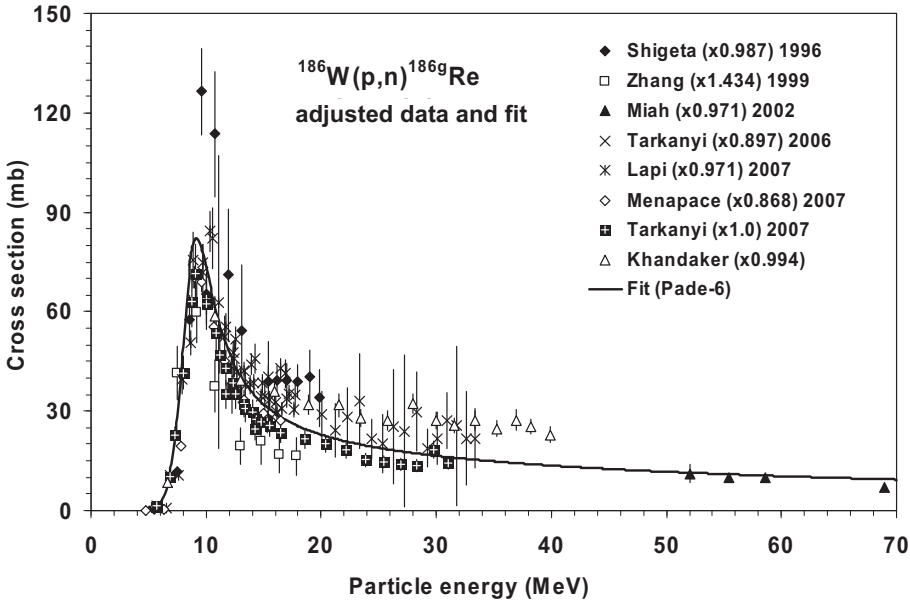

FIG. 7.122. Adjusted experimental data and the recommended curve (fit).

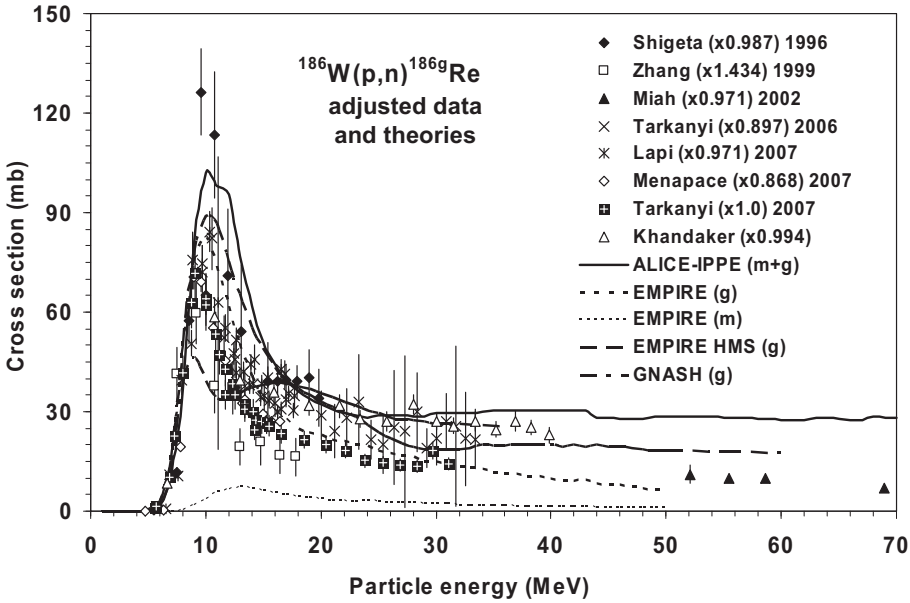

FIG. 7.123. Adjusted experimental data and theoretical calculations.

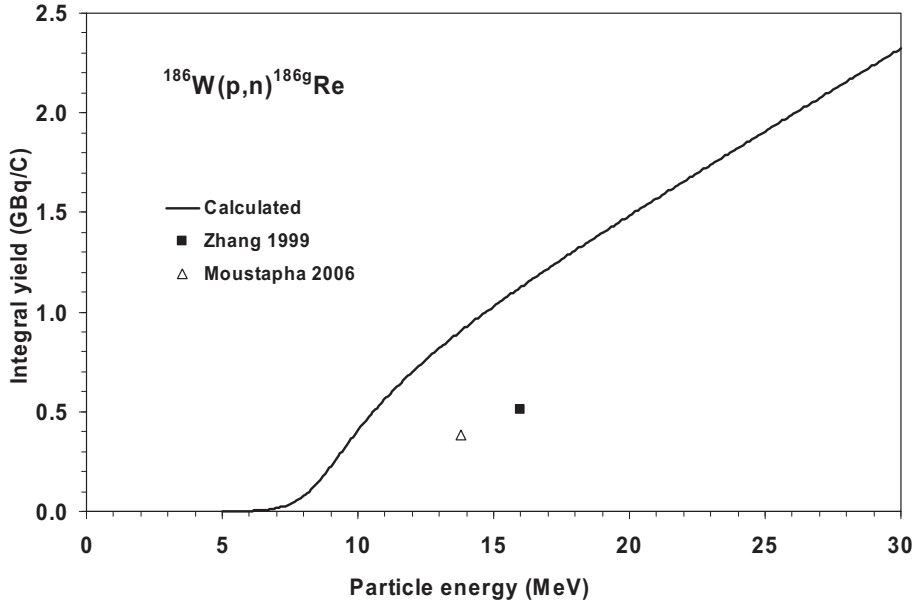

FIG. 7.124. Calculated integral yield curve based on the recommended cross-sections.

TABLE 7.53. RECOMMENDED CROSS-SECTIONS AND INTEGRAL YIELDS

^{186}W(p, n)^{186g}Re energy (MeV)	Cross-section (mb)	Integral yield	
		(μCi/μAh)	(GBq/C)
5.0	0.0	0.0	0.00
5.5	1.2	0.1	0.00
6.0	2.5	0.2	0.00
6.5	6.1	0.6	0.01
7.0	13.9	1.5	0.02
7.5	28.2	3.6	0.04
8.0	49.4	7.5	0.08
8.5	70.6	13.8	0.14
9.0	81.3	22.1	0.23
9.5	80.3	30.9	0.32
10.0	73.5	39.6	0.41
10.5	65.6	47.6	0.49

TABLE 7.53. RECOMMENDED CROSS-SECTIONS AND INTEGRAL YIELDS (cont.)

$^{186}W(p, n)^{186g}Re$ energy (MeV)	Cross-section (mb)	Integral yield	
		(μCi/μAh)	(GBq/C)
11.0	58.5	54.9	0.56
11.5	52.5	61.7	0.63
12.0	47.7	68.1	0.70
12.5	43.8	74.0	0.76
13.0	40.5	79.6	0.82
13.5	37.8	85.0	0.87
14.0	35.6	90.2	0.93
14.5	33.7	95.2	0.98
15.0	32.0	100.1	1.03
15.5	30.6	104.8	1.08
16.0	29.3	109.5	1.12
16.5	28.2	114.0	1.17
17.0	27.2	118.5	1.22
17.5	26.3	122.9	1.26
18.0	25.5	127.3	1.31
18.5	24.8	131.6	1.35
19.0	24.1	135.9	1.40
19.5	23.5	140.1	1.44
20.0	22.9	144.4	1.48
20.5	22.4	148.5	1.53
21.0	21.9	152.7	1.57
21.5	21.4	156.9	1.61
22.0	21.0	161.0	1.65
22.5	20.6	165.1	1.70
23.0	20.2	169.2	1.74
23.5	19.9	173.3	1.78
24.0	19.5	177.4	1.82
24.5	19.2	181.4	1.86
25.0	18.9	185.5	1.91
25.5	18.6	189.6	1.95

TABLE 7.53. RECOMMENDED CROSS-SECTIONS AND INTEGRAL YIELDS (cont.)

^{186}W(p, n)^{186g}Re energy (MeV)	Cross-section (mb)	Integral yield	
		(μCi/μAh)	(GBq/C)
26.0	18.3	193.6	1.99
26.5	18.1	197.7	2.03
27.0	17.8	201.7	2.07
27.5	17.6	205.8	2.11
28.0	17.4	209.8	2.16
28.5	17.1	213.8	2.20
29.0	16.9	217.9	2.24
29.5	16.7	221.9	2.28
30.0	16.5	225.9	2.32

BIBLIOGRAPHY, EVALUATION AND SELECTION

Cross-sections

PEMENT, F.W., WOLKE, R.L., Compound-statistical features of deuteron-induced reactions: (II) The compound nucleus and stripping-evaporation mechanisms in (d,2n) reactions, Nucl. Phys. **86** (1966) 429–442.
EXFOR: P0115

NASSIFF, S.J., MUNZEL, H., Cross sections for the reactions ^{66}Zn(d,n)^{67}Ga, ^{52}Cr(d,2n)^{52g}Mn and ^{186}W(d,2n)^{186}Re, Radiochim. Acta **19** (1973) 97.
EXFOR: A0202
This data set was rejected because of a large difference in the shape and values compared with the other measurements.

ZHENLAN, T., FUYING, Z., HUIYUAN, Q., GONGQING, W., Excitation functions for $^{182-186}$W(d,2n)$^{182-186}$Re and ^{186}W(d,p)^{187}W reactions, Chin. J. Nucl. Phys. **3** (1981) 242.
EXFOR: S0014

SZELECSÉNYI, F., TAKÁCS, S., TÁRKÁNYI, F., SONCK, M., HERMANNE, A., Study of production possibility of ^{186}Re via the ^{186}W(d,2n)^{186}Re nuclear reaction for use of radiotherapy, J. Labelled Compd Radiopharm. Suppl. **42** (1999) 912.
EXFOR: no
Preliminary data of Tárkányi et al. (2006).

ISHIOKA, N.S., et al., Excitation functions of rhenium isotopes on the ^{nat}W(d,xn) reactions and production of no-carrier added ^{186}Re, Int. Conf. Nucl. Data for Science and Technology (Proc. Int. Conf. Tsukuba, 2001), (SHIBATA, K., et al., Eds), J. Nucl. Sci. Technol. Suppl. **2** (2002) 1334–1337.
EXFOR: no

TÁRKÁNYI, F., et al., Excitation functions of deuteron induced nuclear reactions on natural tungsten up to 50 MeV, Nucl. Instrum. Methods B **211** (2003) 319–330.
EXFOR: D4141

ALEKSEEV, I.E., LAZAREV, V.V., Cyclotron production and radiochemical isolation of the therapeutical radionuclide ^{186}Re, Soviet Radiochem. **48** (2006) 446–449.
EXFOR: no

Yield

DMITRIEV, P.P., MOLIN, G.A., Yields of ^{181}Re, ^{182m}Re, ^{182}Re, ^{183}Re, ^{184m}Re, ^{184}Re and ^{186}Re when irradiating tungsten with protons and deuterons, and tantalum with alpha particles, Atomnaya Energiya **48** (1980) 122–124.
EXFOR: A0070
Yields were determined from excitation functions obtained by calculation and, therefore, these data were rejected.

MUKHAMMEDOV, S., VASIDOV, A., PARDAEV, E., Application of proton and neutron activation method of analysis for the determination of elements with Z greater than 42, Atomnaya Energiya **56** (1984) 50–53.
EXFOR: A0212

ZHANG, X., LI, Q., LI, W., SHENG, R., SHEN, S., Production of no-carrier-added ^{186}Re via deuteron induced reactions on isotopically enriched ^{186}W, Appl. Radiat. Isot. **54** (2001) 89–92.
EXFOR: no

All experimental cross-section data are shown in Fig. 7.125, and the selected measurements are compared with the resulting statistical fit to these data in Fig. 7.126. Excitation functions have been calculated by means of the ALICE-IPPE, EMPIRE and GNASH nuclear reaction modelling codes, and results are compared with all of the selected experimental data in Fig. 7.127. Yields determined from the recommended cross-sections are presented in Fig. 7.128, while corresponding numerical values for the recommended cross-sections and yields are listed in Table 7.54.

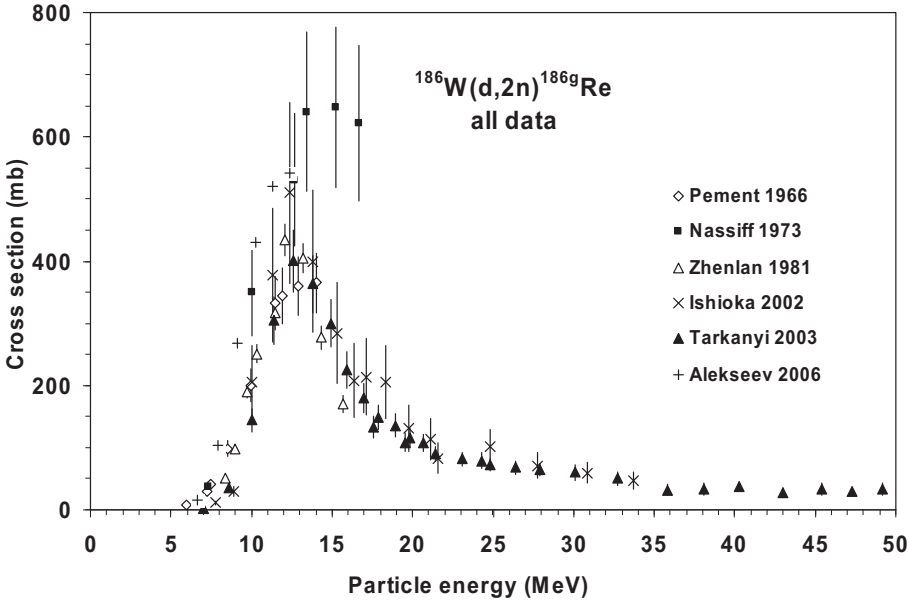

FIG. 7.125. All experimental data.

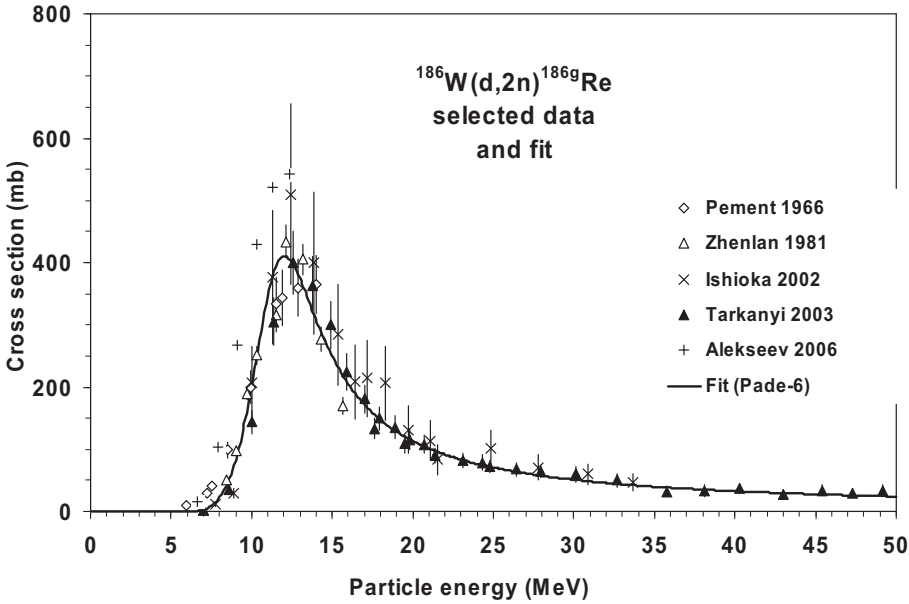

FIG. 7.126. Selected experimental data and the recommended curve (fit).

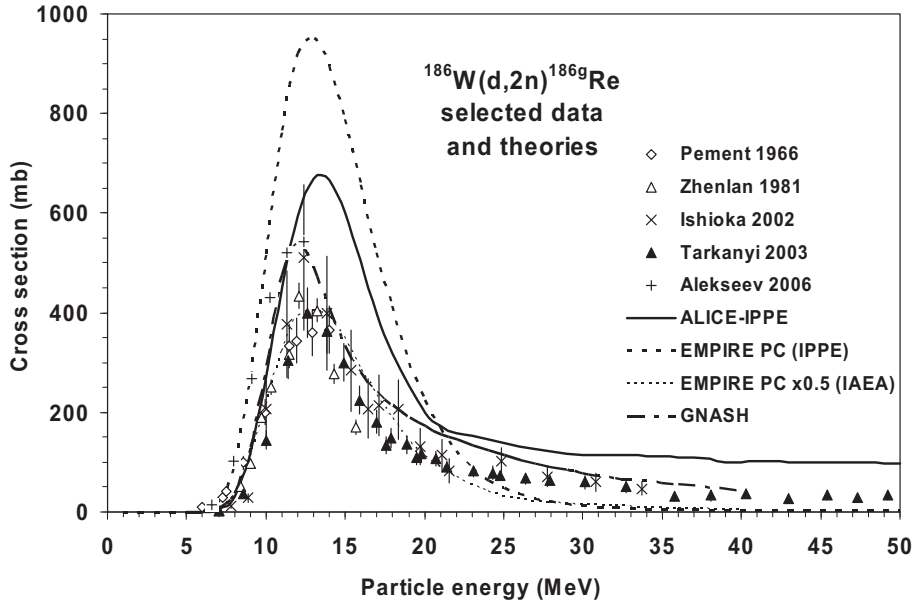

FIG. 7.127. Selected experimental data and theoretical calculations.

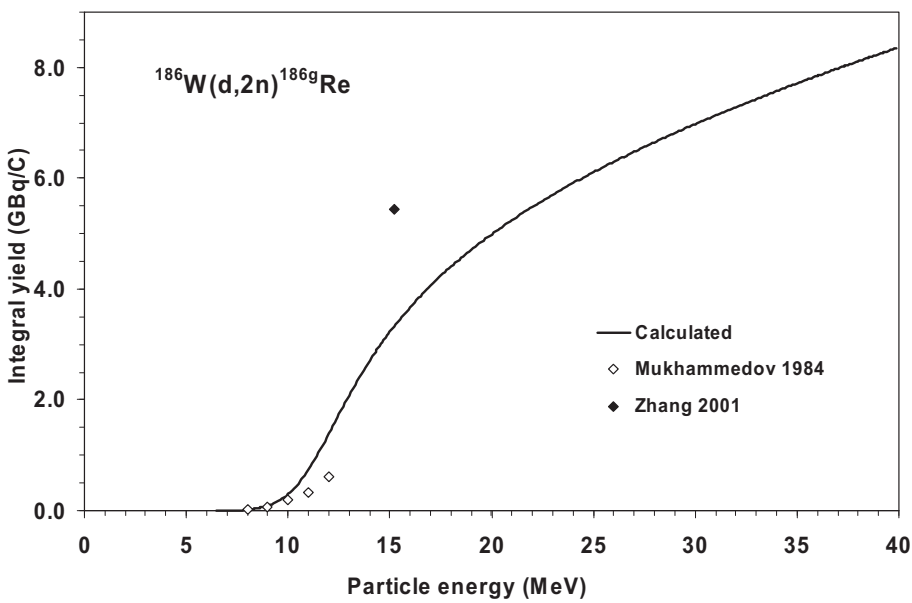

FIG. 7.128. Calculated integral yield curve based on the recommended cross-sections.

TABLE 7.54. RECOMMENDED CROSS-SECTIONS AND INTEGRAL YIELDS

$^{186}W(d, 2n)^{186g}Re$ energy (MeV)	Cross-section (mb)	Integral yield	
		(μCi/μAh)	(GBq/C)
6.5	0.0	0.0	0.00
7.0	2.4	0.1	0.00
7.5	8.9	0.4	0.00
8.0	22.7	1.5	0.02
8.5	46.1	3.9	0.04
9.0	82.1	8.4	0.09
9.5	133.4	16.3	0.17
10.0	200.0	29.0	0.30
10.5	275.6	47.4	0.49
11.0	345.7	72.1	0.74
11.5	393.4	102.1	1.05
12.0	410.2	135.4	1.39
12.5	400.1	169.5	1.74
13.0	373.8	202.6	2.08
13.5	341.0	233.9	2.40
14.0	307.6	262.8	2.70
14.5	276.8	289.5	2.98
15.0	249.4	314.1	3.23
15.5	225.5	336.7	3.46
16.0	205.0	357.7	3.68
16.5	187.2	377.2	3.88
17.0	171.9	395.4	4.06
17.5	158.7	412.5	4.24
18.0	147.1	428.6	4.41
18.5	137.0	443.9	4.56
19.0	128.0	458.4	4.71
19.5	120.1	472.2	4.85
20.0	113.1	485.5	4.99
20.5	106.8	498.1	5.12
21.0	101.1	510.3	5.24
21.5	95.9	522.0	5.37
22.0	91.3	533.4	5.48
22.5	87.0	544.3	5.59

TABLE 7.54. RECOMMENDED CROSS-SECTIONS AND INTEGRAL YIELDS (cont.)

$^{186}W(d, 2n)^{186g}Re$ energy (MeV)	Cross-section (mb)	Integral yield	
		(μCi/μAh)	(GBq/C)
23.0	83.2	554.9	5.70
23.5	79.6	565.3	5.81
24.0	76.3	575.3	5.91
24.5	73.3	585.0	6.01
25.0	70.5	594.5	6.11
25.5	67.9	603.8	6.21
26.0	65.5	612.8	6.30
26.5	63.2	621.7	6.39
27.0	61.1	630.4	6.48
27.5	59.2	638.9	6.57
28.0	57.3	647.2	6.65
28.5	55.6	655.3	6.74
29.0	53.9	663.4	6.82
29.5	52.4	671.2	6.90
30.0	50.9	679.0	6.98
30.5	49.5	686.6	7.06
31.0	48.2	694.1	7.13
31.5	47.0	701.4	7.21
32.0	45.8	708.7	7.28
32.5	44.7	715.9	7.36
33.0	43.6	723.0	7.43
33.5	42.6	729.9	7.50
34.0	41.6	736.8	7.57
34.5	40.7	743.6	7.64
35.0	39.8	750.4	7.71
35.5	38.9	757.0	7.78
36.0	38.1	763.5	7.85
36.5	37.3	770.0	7.91
37.0	36.6	776.4	7.98
37.5	35.8	782.8	8.05
38.0	35.2	789.1	8.11
38.5	34.5	795.3	8.17
39.0	33.8	801.4	8.24
39.5	33.2	807.5	8.30

7.13. CHARGED PARTICLE PRODUCTION OF ^{192g}Ir

Iridium-192 is an important radionuclide commonly used in brachytherapy as a sealed source or activated Ir wire, possessing highly suitable decay properties for therapy (relatively low energy, high intensity beta radiation and sufficiently long half-life). A simplified decay scheme is shown in Fig. 7.129, and the main emissions, as defined in Table 7.55, were taken from NuDat 2.4 [7.3].

A. Decay data

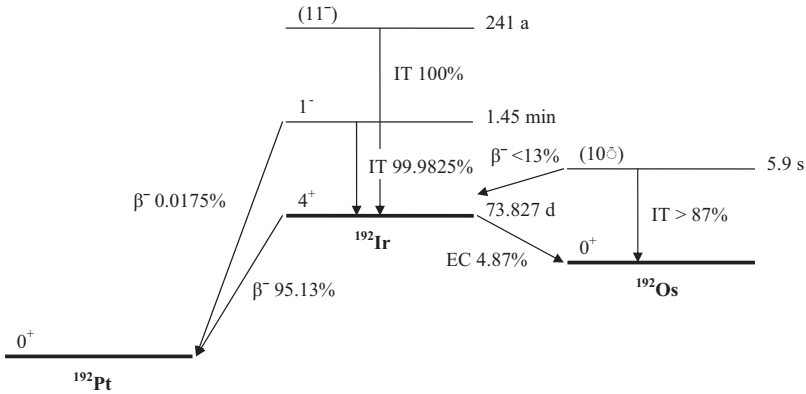

FIG. 7.129. Simplified decay scheme of ^{192}Ir [7.3].

TABLE 7.55. MAIN EMISSIONS [7.3]

Re-186g	Decay mode: $T_{1/2}$:	β⁻ 95.13% 73.827 d	
Radiation	Energy (keV)	End point energy (keV)	Intensity (%)
β⁻	13.6	53.5	0.0035
β⁻	19.5	75.7	0.0039
β⁻	21.1	81.7	0.103
β⁻	71.6	258.7	5.60
β⁻	162.1	538.8	41.43
β⁻	209.9	675.1	48.0
g	295.95650		28.72
g	308.45507		29.68
g	316.50618		82.71
g	468.0688		47.81

B. Production routes

Although the specific activity of the product is rather low, it is routinely produced in a nuclear reactor via the $^{191}Ir(n, \gamma)^{192}Ir$ reaction by irradiating Na_2IrCl_6 or iridium wire. Neutron activation in a medium or high flux reactor would considerably enhance the specific activity by means of the (n, γ) process. However, ^{192}Ir cannot be produced in a non-carrier-added form. An evaluation of the data for this reaction is given in Section 6.5.5. Alternative charged particle induced routes of production have been developed to address the specific activity problem, as defined in Table 7.56.

TABLE 7.56. INVESTIGATED PRODUCTION ROUTES [7.3, 7.4]

Target isotope	Natural abundance	Reaction	Q-value (MeV)	Threshold energy (MeV)
Os-192	40.93%	(p, n)	–1.8	1.8
Os-192	40.93%	(d, 2n)	–4.1	4.1

C. $^{192}Os(p, n)^{192m1+g}Ir$ reaction

The reaction cross-section includes the contribution of the short lived metastable state in addition to the formation of the ground state. Only one set of cross-section data exists in the literature as reported by Hilgers et al. (2005) as part of this CRP initiative.

BIBLIOGRAPHY, EVALUATION AND SELECTION

Cross-sections

HILGERS, K., SUDÁR, S., QAIM, S.M., Experimental study and nuclear model calculations on the $^{192}Os(p,n)^{192}Ir$ reaction: Comparison of reactor and cyclotron production of the therapeutic radionuclide ^{192}Ir, Appl. Radiat. Isot. **63** (2005) 93–98.
EXFOR: O1274

Yield

No data were found.

Hilgers (2005) measurements are compared with the resulting statistical fit to these data in Fig. 7.130. Excitation functions have been calculated by means of the ALICE-IPPE, EMPIRE and GNASH nuclear reaction modelling codes, and results are compared with experimental data in Fig. 7.131. Yields determined from the recommended cross-sections are presented in Fig. 7.132, while corresponding numerical values for the recommended cross-sections and yields are listed in Table 7.57.

D. ^{192}Os(d, 2n)$^{192m1+g}$Ir reaction

The reaction cross-section includes the contribution of the short lived metastable state in addition to the formation of the ground state. Only one set of cross-section data exists in the literature as reported by Tárkányi et al. (2007), and undertaken as part of this CRP initiative.

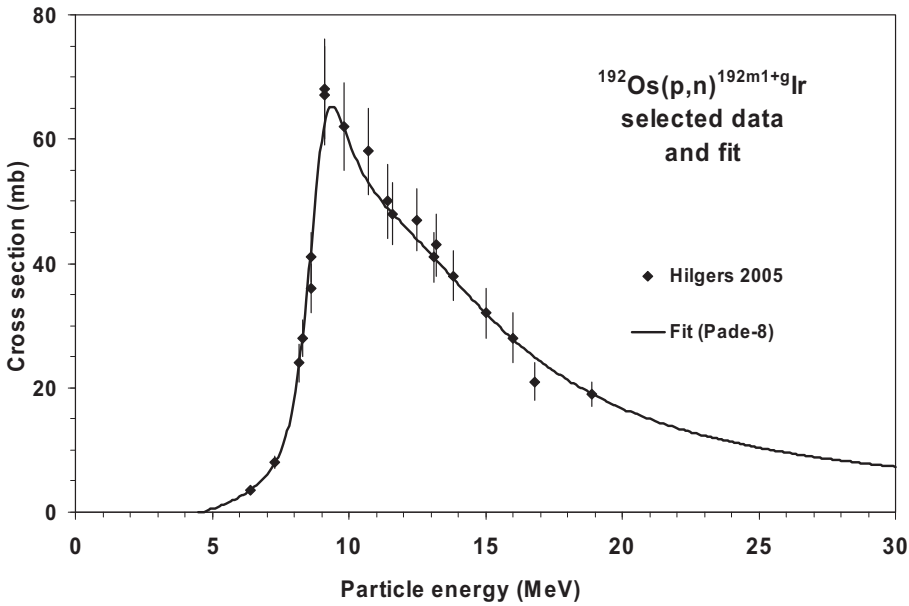

FIG. 7.130. Experimental data and the recommended curve (fit).

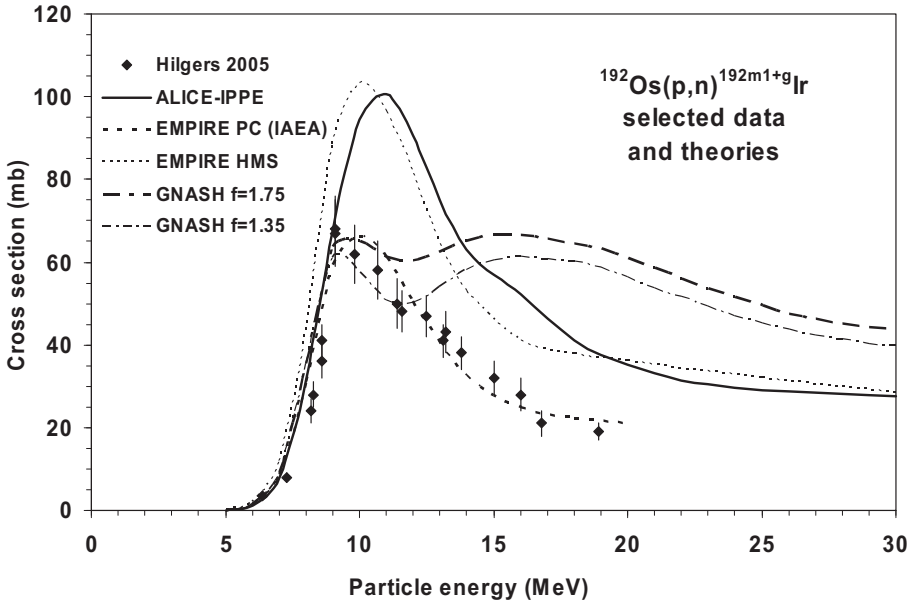

FIG. 7.131. Experimental data and theoretical calculations.

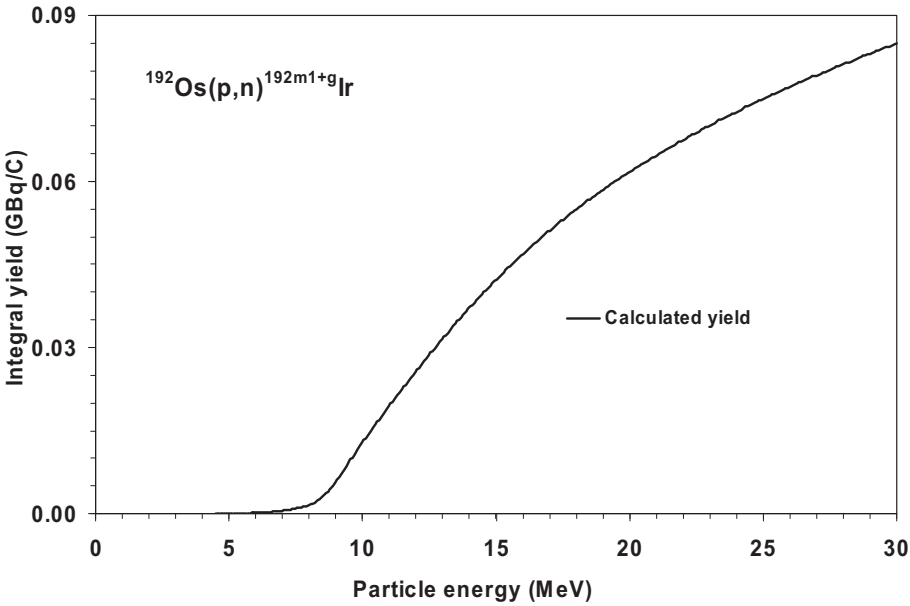

FIG. 7.132. Calculated integral yield curve based on the recommended cross-sections.

TABLE 7.57. RECOMMENDED CROSS-SECTIONS AND INTEGRAL YIELDS

$^{192}Os(p, n)^{192m1+g}Ir$ energy (MeV)	Cross-section (mb)	Integral yield	
		(μCi/μAh)	(GBq/C)
4.5	0.0	0.00	0.0000
5.0	0.5	0.00	0.0000
5.5	1.4	0.00	0.0000
6.0	2.5	0.01	0.0001
6.5	3.9	0.03	0.0003
7.0	6.0	0.05	0.0005
7.5	9.8	0.09	0.0009
8.0	18.1	0.16	0.0016
8.5	36.6	0.30	0.0031
9.0	59.6	0.56	0.0058
9.5	64.9	0.91	0.0094
10.0	59.7	1.26	0.0129
10.5	54.7	1.58	0.0163
11.0	51.1	1.90	0.0195
11.5	48.5	2.20	0.0226
12.0	46.1	2.50	0.0257
12.5	43.8	2.79	0.0287
13.0	41.5	3.07	0.0316
13.5	39.1	3.35	0.0344
14.0	36.7	3.61	0.0371
14.5	34.3	3.87	0.0397
15.0	32.0	4.11	0.0422
15.5	29.8	4.34	0.0446
16.0	27.8	4.56	0.0469
16.5	26.0	4.77	0.0490
17.0	24.3	4.97	0.0511
17.5	22.7	5.16	0.0531
18.0	21.3	5.35	0.0550
18.5	20.0	5.52	0.0568

TABLE 7.57. RECOMMENDED CROSS-SECTIONS AND INTEGRAL YIELDS (cont.)

$^{192}Os(p, n)^{192m1+g}Ir$ energy (MeV)	Cross-section (mb)	Integral yield	
		(μCi/μAh)	(GBq/C)
19.0	18.8	5.69	0.0585
19.5	17.7	5.85	0.0601
20.0	16.7	6.00	0.0617
20.5	15.8	6.15	0.0632
21.0	15.0	6.30	0.0647
21.5	14.2	6.43	0.0661
22.0	13.5	6.57	0.0675
22.5	12.9	6.70	0.0688
23.0	12.3	6.82	0.0701
23.5	11.8	6.94	0.0713
24.0	11.3	7.06	0.0725
24.5	10.8	7.17	0.0737
25.0	10.4	7.28	0.0749
25.5	9.9	7.39	0.0760
26.0	9.6	7.50	0.0771
26.5	9.2	7.60	0.0781
27.0	8.9	7.70	0.0792
27.5	8.6	7.80	0.0802
28.0	8.3	7.90	0.0812
28.5	8.0	7.99	0.0821
29.0	7.8	8.08	0.0831
29.5	7.5	8.17	0.0840
30.0	7.3	8.26	0.0849

BIBLIOGRAPHY, EVALUATION AND SELECTION

Cross-sections

TÁRKÁNYI, F., et al., Study of the ^{192}Os(d,2n) reaction for production of the therapeutic radionuclide ^{192}Ir in no-carrier added form, Appl. Radiat. Isot. **65** (2007) 1215–1220.
EXFOR: D4192

Yield

No data were found.

Tárkányi (2007) measurements are compared with the resulting statistical fit to these data in Fig. 7.133. Excitation functions have been calculated by means of the ALICE-IPPE, EMPIRE and GNASH nuclear reaction modelling codes, and results are compared with experimental data in Fig. 7.134. Yields determined from the recommended cross-sections are presented in Fig. 7.135, while corresponding numerical values for the recommended cross-sections and yields are listed in Table 7.58.

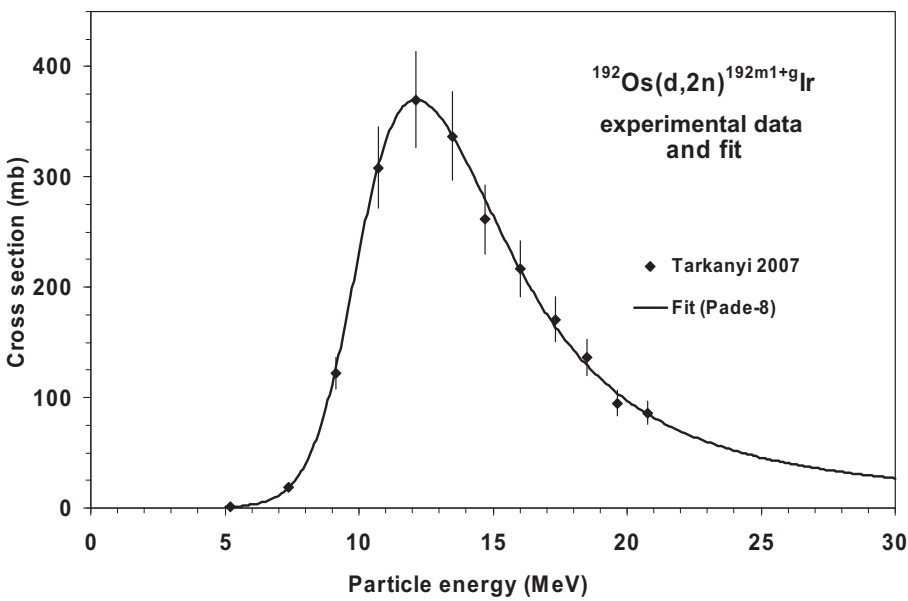

FIG. 7.133. Experimental data and the recommended curve (fit).

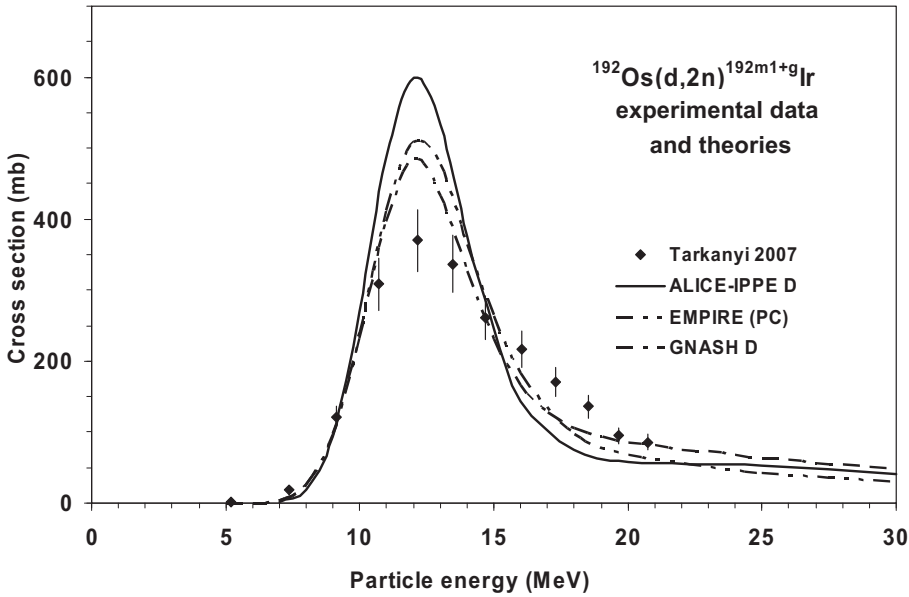

FIG. 7.134. Experimental data and theoretical calculations.

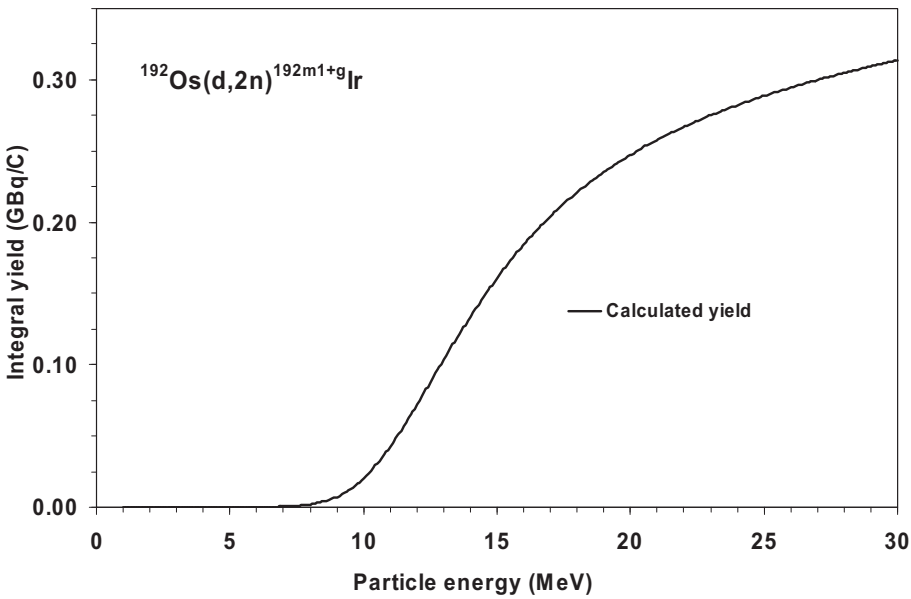

FIG. 7.135. Calculated integral yield curve based on the recommended cross-sections.

TABLE 7.58. RECOMMENDED CROSS-SECTIONS AND INTEGRAL YIELDS

$^{192}Os(d, 2n)^{192m1+g}Ir$ energy (MeV)	Cross-section (mb)	Integral yield	
		(μCi/μAh)	(GBq/C)
1.0	0.0	0.000	0.0000
1.5	0.1	0.000	0.0000
2.0	0.1	0.000	0.0000
2.5	0.2	0.000	0.0000
3.0	0.2	0.001	0.0000
3.5	0.3	0.001	0.0000
4.0	0.3	0.002	0.0000
4.5	0.4	0.003	0.0000
5.0	0.7	0.004	0.0000
5.5	1.4	0.007	0.0001
6.0	2.8	0.012	0.0001
6.5	5.7	0.025	0.0003
7.0	11.3	0.050	0.0005
7.5	21.5	0.102	0.0010
8.0	39.4	0.201	0.0021
8.5	68.5	0.383	0.0039
9.0	111.7	0.699	0.0072
9.5	168.0	1.204	0.0124
10.0	230.6	1.946	0.0200
10.5	288.4	2.934	0.0302
11.0	332.4	4.142	0.0426
11.5	359.0	5.515	0.0567
12.0	369.6	6.996	0.0719
12.5	367.2	8.526	0.0876
13.0	355.4	10.057	0.1034
13.5	337.0	11.555	0.1188
14.0	314.5	12.996	0.1336
14.5	289.9	14.364	0.1476
15.0	264.8	15.644	0.1608
15.5	240.2	16.831	0.1730
16.0	217.0	17.928	0.1843

TABLE 7.58. RECOMMENDED CROSS-SECTIONS AND INTEGRAL YIELDS (cont.)

^{192}Os(d, 2n)$^{192m1+g}$Ir energy (MeV)	Cross-section (mb)	Integral yield	
		(μCi/μAh)	(GBq/C)
16.5	195.6	18.938	0.1946
17.0	176.1	19.867	0.2042
17.5	158.7	20.719	0.2129
18.0	143.2	21.501	0.2210
18.5	129.5	22.221	0.2284
19.0	117.4	22.884	0.2352
19.5	106.7	23.498	0.2415
20.0	97.3	24.067	0.2474
20.5	89.0	24.594	0.2528
21.0	81.7	25.085	0.2578
21.5	75.2	25.544	0.2625
22.0	69.5	25.974	0.2670
22.5	64.3	26.377	0.2711
23.0	59.7	26.758	0.2750
23.5	55.6	27.117	0.2787
24.0	52.0	27.456	0.2822
24.5	48.6	27.778	0.2855
25.0	45.6	28.084	0.2886
25.5	42.9	28.375	0.2916
26.0	40.5	28.653	0.2945
26.5	38.2	28.919	0.2972
27.0	36.1	29.174	0.2998
27.5	34.3	29.418	0.3024
28.0	32.5	29.653	0.3048
28.5	31.0	29.879	0.3071
29.0	29.5	30.096	0.3093
29.5	28.1	30.306	0.3115
30.0	26.9	30.509	0.3136

7.14. CHARGED PARTICLE PRODUCTION OF ^{211}At

Astatine-211 has recently generated great interest for adoption in targeted radiotherapy. Radionuclides such as ^{211}At and ^{212}Bi decay by the emission of alpha particles that penetrate only a few cell diameters of the tissue, offering the possibility of combining cell-specific targeting with radiation of a similar range. Unlike beta particles, alpha particles are radiation of high linear energy transfer and greater biological effectiveness. Astatine-211 is the most often discussed radionuclide for α therapy, although the At–C bond is rather weak and the chemistry very challenging. Simplified decay schemes of ^{211}At and ^{210}At, and their respective daughters are shown in Figs 7.136(a) and 7.136(b), respectively, while their main emissions are listed in Tables 7.59(a) to 7.59(d) (^{211}At and ^{211g}Po; ^{210}At and ^{210}Po).

A. Decay data

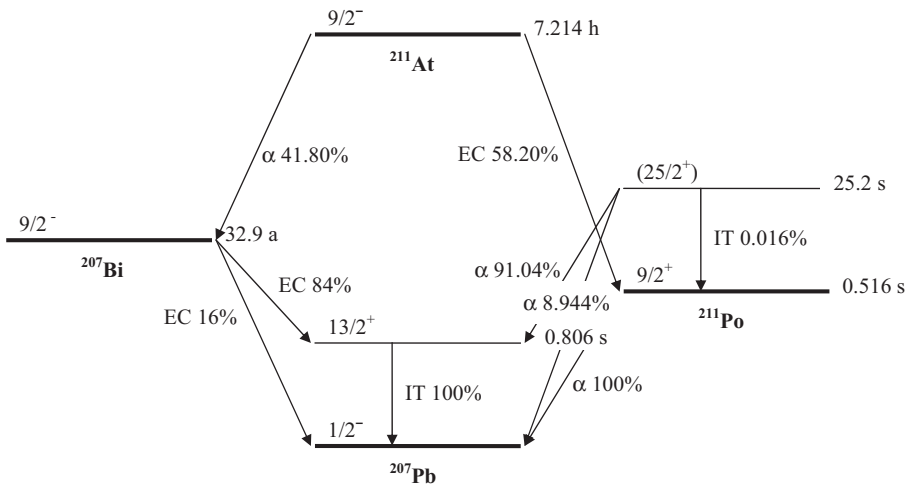

FIG. 7.136(a). Simplified decay scheme of ^{211}At and daughters [7.3].

TABLE 7.59(a). MAIN EMISSIONS OF ^{211}At [7.3]

At-211	Decay mode: $T_{1/2}$:	α 41.80% 7.214 h
Radiation	Energy (keV)	Intensity (%)
a	4997	0.000418
a	5141	0.0010
a	5210.0	0.0036
a	5869.5	41.80
g	669.6	0.0035
g	742.7	0.0010

TABLE 7.59(b). MAIN EMISSIONS OF ^{211g}Po [7.3]

Po-211g	Decay mode: $T_{1/2}$:	α 100% 0.516 s
Radiation	Energy (keV)	Intensity (%)
a	6568.3	0.544
a	6891.5	0.557
a	7450.3	98.890
g	569.65	0.545
g	897.8	0.561

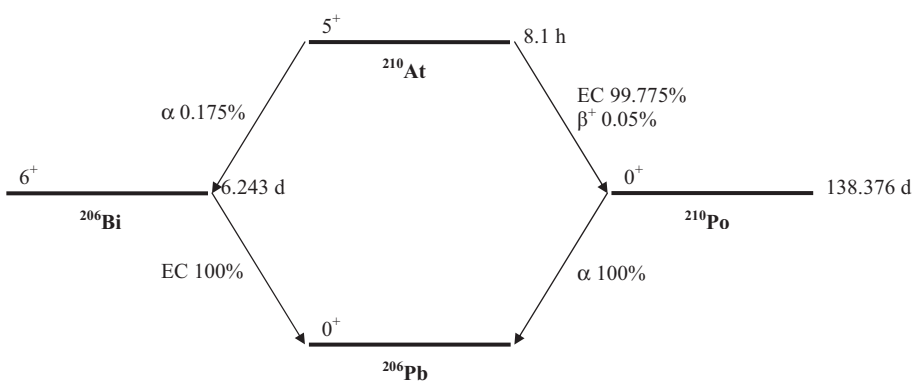

FIG. 7.136(b). Simplified decay scheme of ^{210}At and daughters [7.3].

TABLE 7.59(c). MAIN EMISSIONS OF ^{210}At [7.3]

At-210	Decay mode: $T_{1/2}$:	EC 99.775% β^+ 0.05% 8.1 h
Radiation	Energy (keV)	Intensity (%)
g	245.3	79
g	1181.4	99
g	1436.7	29.0
g	1483.3	46.5
g	1599.5	13.4

TABLE 7.59(d). MAIN EMISSIONS OF ^{210}Po [7.3]

Po-210	Decay mode: $T_{1/2}$:	α 100% 138.376 d
Radiation	Energy (keV)	Intensity (%)
a	4516.53	0.00122
a	5304.33	100
g	803.10	0.00121

B. Production routes

Astatine-211 is routinely produced at cyclotrons via the ^{209}Bi(α, 2n)^{211}At reaction. The major impurity is ^{210}At, generated by the ^{209}Bi(α, 3n)^{210}At reaction, which undergoes EC decay (99.775%) to the long lived ^{210}Po that decays by alpha decay to stable ^{206}Pb. An important requirement is to minimize the production of ^{210}At (or ^{210}Po daughter) and, therefore, evaluated data for both the main and the side reactions, as defined in Table 7.60, are presented.

TABLE 7.60. INVESTIGATED PRODUCTION ROUTES [7.3, 7.4]

Target isotope	Natural abundance	Reaction	Q-value (MeV)	Threshold energy (MeV)
Bi-209	100%	$(\alpha, 2n)^{211}At$	–20.3	20.7
Bi-209	100%	$(\alpha, 3n)^{210}At$ impurity	–28.1	28.6

C. $^{209}Bi(\alpha, 2n)^{211}At$ reaction

BIBLIOGRAPHY, EVALUATION AND SELECTION

Cross-sections

KELLY, E.L., SEGRÈ, E., Some excitation functions of bismuth, Phys. Rev. **75** (1949) 999–1005.
EXFOR: no

RAMLER, W.J., WING, J., HENDERSON, D.J., HUIZENGA, J.R., Excitation functions of bismuth and lead, Phys. Rev. **114** (1959) 154–162.
Exfor: A0246

STICKLER, J.D., HOFSTETTER, K.J., Comparison of ^{3}He-, ^{4}He-, and ^{12}C-induced nuclear reactions in heavy-mass targets at medium excitation energies (I), Experimental cross sections, Phys. Rev. C **9** (1974) 1064–1071.
EXFOR: no
Data were rejected because of an order of magnitude difference with all other measurements.

DECONNINCK, G., LONGRÉE, M., Fonctions d'excitation des réactions induites par particules alpha sur ^{209}Bi entre 40 et 100 MeV, Ann. Soc. Sci. Brux. Ser. 1 **88** (1974) 341–346.
EXFOR: no

LAMBRECHT, R.M., MIRZADEH, S., Cyclotron isotopes and radiopharmaceuticals – XXXV Astatine-211, Int. J. Appl. Radiat. Isot. **36** (1985) 443–450.
EXFOR: A0249

HERMANNE, A., et al., Experimental study of the cross sections of α-particle induced reactions on ^{209}Bi, Appl. Radiat. Isot. **63** (2005) 1–9.
Exfor: O1272
Direct measurement of α of ^{211}At and indirect measurement through α of ^{211g}Po.

HERMANNE, A., TÁRKÁNYI, F., TAKÁCS, S., SZÜCS, Z., Experimental study of the cross sections of alpha-particle induced reactions on ^{209}Bi, Int. Conf. on Nuclear Data for Science and Technology (Proc. Int. Conf. Santa Fe, 2004), (HAIGHT, R.C., CHADWICK, M.B., TALOU, P., KAWANO, T., Eds), AIP Conf. Proc. **769** (2005) 957–960.
Same as Hermanne et al. (2005) above.

Yield

BEYER, G.J., DREYER, R., ODRICH, H., ROSCH, F., Production of ^{211}At at the Rossedorf-Cyclotron U-120, Radiochem. Radioanal. Lett. **47** (1981) 63–65.
EXFOR: A0115
Data are not comparable.

LAMBRECHT, R.M., MIRZADEH, S., Cyclotron isotopes and radiopharmaceuticals – XXXV Astatine-211, Int. J. Appl. Radiat. Isot. **36** (1985) 443–450.
EXFOR: no

LARSEN, R.H., WIELAND, B.W., ZALUTSKY, M.R., Evaluation of an internal cyclotron target for the production of ^{211}At via the ^{209}Bi(α,2n)^{211}At reaction, Appl. Radiat. Isot. **47** (1996) 135–143.
EXFOR: no

HENRIKSEN, G., MESSELT, S., OLSEN, E., LARSEN, R.H., Optimisation of cyclotron production parameters for the ^{209}Bi(α,2n)^{211}At reaction related to biomedical use of ^{211}At, Appl. Radiat. Isot. **54** (2001) 839–844.
EXFOR: D0167

LEBEDA, O., JIRAN, R., RÁLIŠ, J., ŠTURSA, J., A new internal target system for production of ^{211}At on the cyclotron U-120M, Appl. Radiat. Isot. **63** (2005) 49–53.
EXFOR: O1275

ALFARANO, A., et al., Thick target yield measurement of ^{211}At through the nuclear reaction ^{209}Bi(α,2n), J. Phys. Conf. Ser. **41** (2006) 115–122.
EXFOR: D0413

All experimental cross-section data are shown in Fig. 7.137, and the selected measurements are compared with the resulting statistical fit to these data in Fig. 7.138. Excitation functions have been calculated by means of the ALICE-IPPE, EMPIRE and GNASH nuclear reaction modelling codes, and results are compared with all of the selected experimental data in Fig. 7.139. Yields determined from the recommended cross-sections are presented in Fig. 7.140, while corresponding numerical values for the recommended cross-sections and yields are listed in Table 7.61.

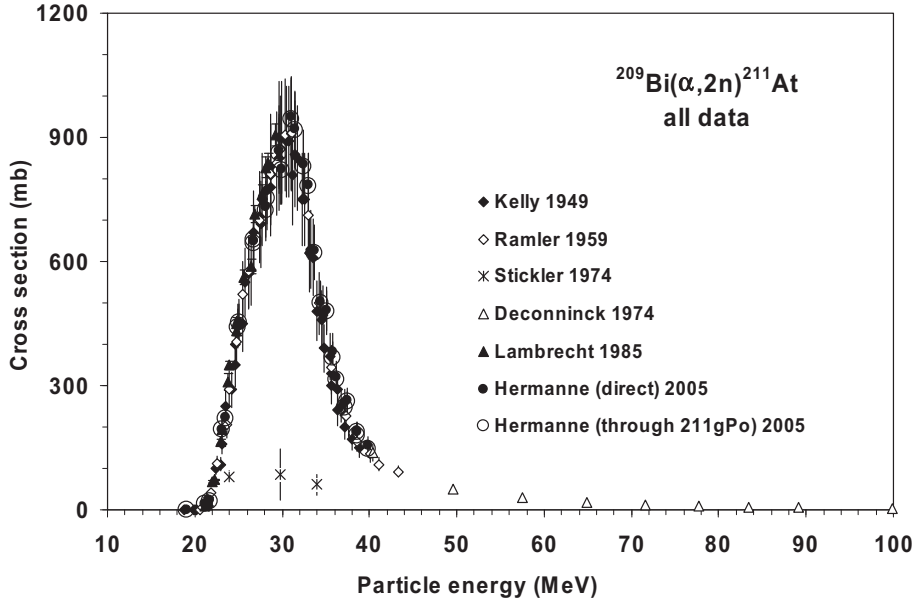

FIG. 7.137. All experimental data.

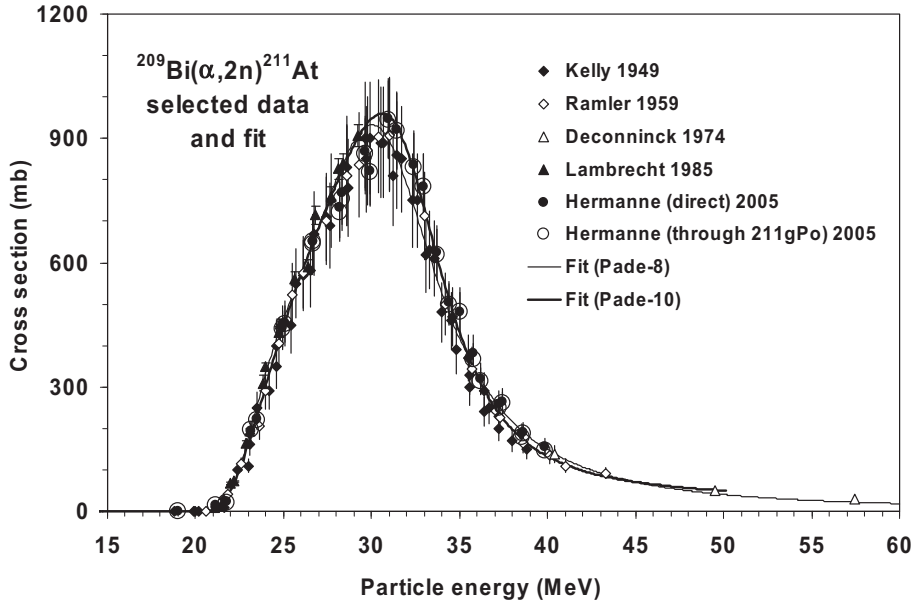

FIG. 7.138. Selected experimental data and the recommended curve (fit).

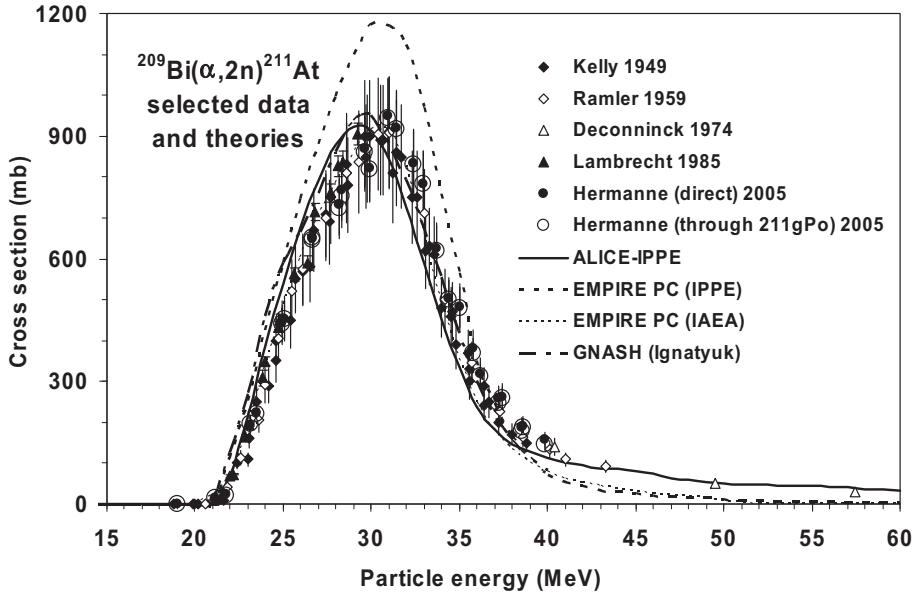

FIG. 7.139. Selected experimental data and theoretical calculations.

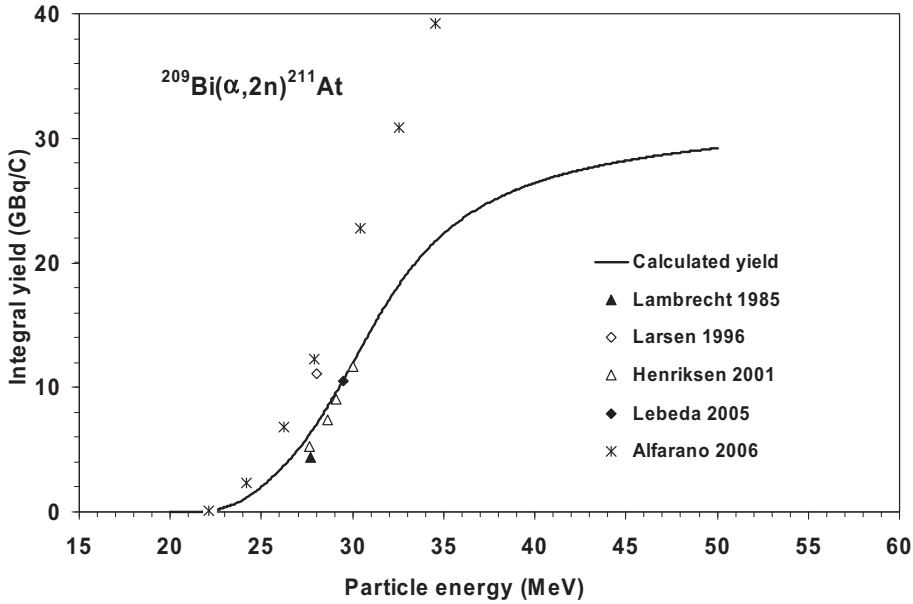

FIG. 7.140. Calculated integral yield curve based on the recommended cross-sections.

TABLE 7.61. RECOMMENDED CROSS-SECTIONS AND INTEGRAL YIELDS

$^{209}Bi(\alpha, 2n)^{211}At$ energy (MeV)	Cross-section (mb)	Integral yield	
		(μCi/μAh)	(GBq/C)
20.0	0	0	0.0
20.5	1	0	0.0
21.0	6	0	0.0
21.5	21	2	0.0
22.0	53	6	0.1
22.5	107	16	0.2
23.0	178	33	0.3
23.5	258	60	0.6
24.0	334	96	1.0
24.5	403	141	1.5
25.0	464	195	2.0
25.5	521	257	2.6
26.0	576	326	3.4
26.5	631	403	4.1
27.0	688	488	5.0
27.5	745	582	6.0
28.0	800	684	7.0
28.5	851	794	8.2
29.0	893	911	9.4
29.5	922	1035	10.6
30.0	933	1162	11.9
30.5	924	1291	13.3
31.0	894	1417	14.6
31.5	848	1540	15.8
32.0	789	1656	17.0
32.5	723	1764	18.1
33.0	655	1863	19.1
33.5	588	1953	20.1
34.0	526	2035	20.9
34.5	468	2108	21.7
35.0	417	2174	22.3

TABLE 7.61. RECOMMENDED CROSS-SECTIONS AND INTEGRAL YIELDS (cont.)

$^{209}Bi(\alpha, 2n)^{211}At$ energy (MeV)	Cross-section (mb)	Integral yield	
		(μCi/μAh)	(GBq/C)
35.5	372	2233	23.0
36.0	332	2287	23.5
36.5	297	2335	24.0
37.0	266	2378	24.4
37.5	239	2418	24.8
38.0	216	2454	25.2
38.5	196	2486	25.6
39.0	178	2516	25.9
39.5	162	2544	26.1
40.0	148	2569	26.4
40.5	136	2593	26.6
41.0	125	2614	26.9
41.5	115	2634	27.1
42.0	107	2653	27.3
42.5	99	2670	27.4
43.0	92	2687	27.6
43.5	86	2702	27.8
44.0	80	2717	27.9
44.5	75	2730	28.1
45.0	70	2743	28.2
45.5	66	2755	28.3
46.0	62	2767	28.4
46.5	58	2778	28.5
47.0	55	2788	28.7
47.5	52	2798	28.8
48.0	49	2807	28.9
48.5	47	2816	28.9
49.0	45	2825	29.0
49.5	42	2833	29.1
50.0	40	2841	29.2

D. $^{209}Bi(\alpha, 3n)^{210}At$ reaction: radioisotope impurity

Long lived, strong α emitting ^{210}Po is formed mainly through the EC decay of ^{210}At, and is the main contaminant in the possible radiotherapeutic use of ^{211}At. Direct production is small and any ^{210}Po can be chemically separated from ^{211}At.

BIBLIOGRAPHY, EVALUATION AND SELECTION

Cross-sections

KELLY, E.L., SEGRÈ, E., Some excitation functions of bismuth, Phys. Rev. **75** (1949) 999–1005.
EXFOR: no

RAMLER, W.J., WING, J., HENDERSON, D.J., HUIZENGA, J.R., Excitation functions of bismuth and lead, Phys. Rev. **114** (1959) 154–162.
Exfor: A0246

STICKLER, J.D., HOFSTETTER, K.J., Comparison of ^{3}He-, ^{4}He-, and ^{12}C-induced nuclear reactions in heavy-mass targets at medium excitation energies (I), Experimental cross sections, Phys. Rev. C **9** (1974) 1064–1071.
EXFOR: no

DECONNINCK, G., LONGRÉE, M., Fonctions d'excitation des réactions induites par particules alpha sur ^{209}Bi entre 40 et 100 MeV, Ann. Soc. Sci. Brux. Ser. I **88** (1974) 341–346.
EXFOR: no
Cumulative cross-section of ^{210}Po was measured, which is almost the same as the cross-section of ^{210}At because the direct production of ^{210}Po through the (d, t) reaction is negligible — rejected.

LAMBRECHT, R.M., MIRZADEH, S., Cyclotron isotopes and radiopharmaceuticals — XXXV Astatine-211, Int. J. Appl. Radiat. Isot. **36** (1985) 443–450.
EXFOR: no

RATTAN, S.S., SINGH, R.J., SAHAKUNDU, S.M., PRAKASH, S., RAMANIAH, M.V., Alpha particle induced reactions of ^{209}Bi and $^{63,65}Cu$, Radiochim. Acta **39** (1986) 61–63.
EXFOR: A0353

RIZVI, I.A., BHARDWAJ, M.K., AFZAL ANSARI, M., CHAUBEY, A.K., Non-equilibrium reaction mechanism in alpha-particle induced excitation function for ^{209}Bi up to 60 MeV, Appl. Radiat. Isot. **41** (1990) 215–219.
EXFOR: no
Rejected because of the significant differences compared with all other data.

RATTAN, S.S., CHAKRAVARTY, N., RAMASWAMI, A., SINGH, R.J., Alpha particle induced reactions of ^{209}Bi at 55.7 and 58.6 MeV, Radiochim. Acta **57** (1992) 7–9.
EXFOR: O1300

SINGH, N.L., MUKHERJEE, S., SOMAYAJULU, D.R.S., Non-equilibrium analysis of (α,xn) reactions on heavy nuclei, Nuovo Cimento A **107** (1994) 1635–1645.
EXFOR: O1119

PATEL, H.B., SHAH, D.J., SINGH, N.L., Study of (α,xn) reactions on ^{169}Tm, ^{181}Ta and ^{209}Bi up to 70 MeV, Nuovo Cimento **112** (1999) 1439–1452.
EXFOR: no

HERMANNE, A., et al., Experimental study of the cross sections of α-particle induced reactions on ^{209}Bi, Appl. Radiat. Isot. **63** (2005) 1–9.
EXFOR: O1272
The excitation function of ^{210}At and the cumulative cross-section of ^{210}Po were measured. The cumulative cross-section of ^{210}Po is almost the same as the cross-section of ^{210}At because the direct production of ^{210}Po by means of the (d, t) reaction is negligible. Results for ^{210}Po have been rejected.

HERMANNE, A., TÁRKÁNYI, F., TAKÁCS, S., SZÜCS, Z., Experimental study of the cross sections of alpha-particle induced reactions on ^{209}Bi, Int. Conf. on Nuclear Data for Science and Technology (Proc. Int. Conf. Santa Fe, 2004), (HAIGHT, R.C., CHADWICK, M.B., TALOU, P., KAWANO, T., Eds), AIP Conf. Proc. **769** (2005) 957–960.
Same as the above.

Yield

HENRIKSEN, G., MESSELT, S., OLSEN, E., LARSEN, R.H., Optimisation of cyclotron production parameters for the ^{209}Bi(α,2n)^{211}At reaction related to biomedical use of ^{211}At, Appl. Radiat. Isot. **54** (2001) 839–844.
EXFOR: D0167

ALFARANO, A., et al., Thick target yield measurement of ^{211}At through the nuclear reaction ^{209}Bi(α,2n), J. Phys. Conf. Ser. **41** (2006) 115–122.
EXFOR: D0413

All experimental cross-section data are shown in Fig. 7.141, and the selected measurements are compared with the resulting statistical fit to these data in Fig. 7.142. Excitation functions have been calculated by means of the ALICE-IPPE and EMPIRE nuclear reaction modelling codes, and results are compared with all of the selected experimental data in Fig. 7.143. Yields determined from the recommended cross-sections are presented in Fig. 7.144, while corresponding numerical values for the recommended cross-sections and yields are listed in Table 7.62.

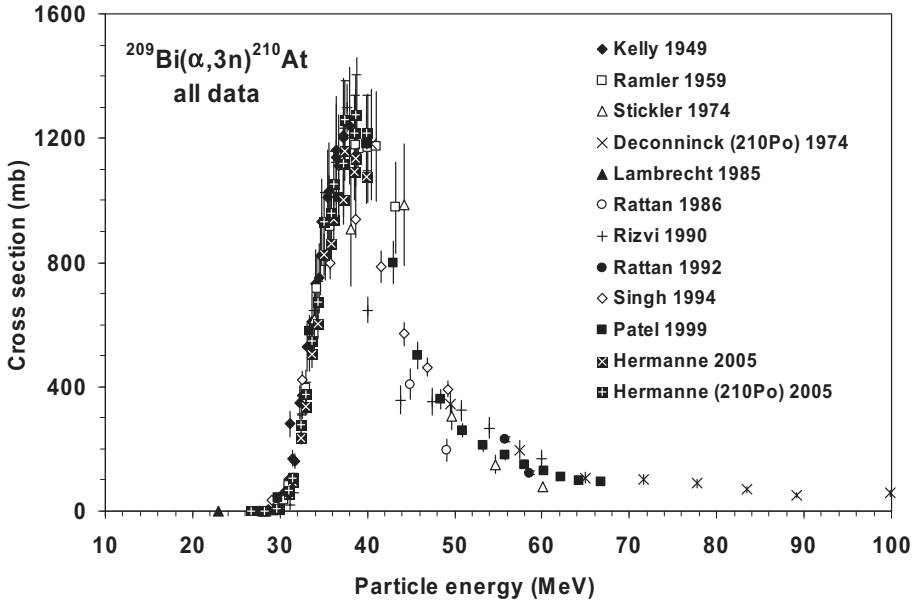

FIG. 7.141. All experimental data.

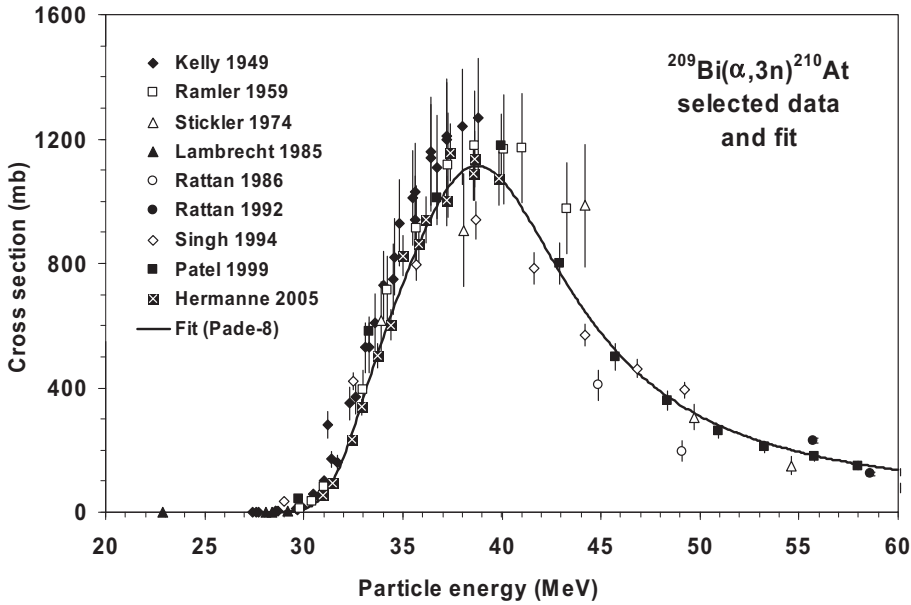

FIG. 7.142. Selected experimental data and the recommended curve (fit).

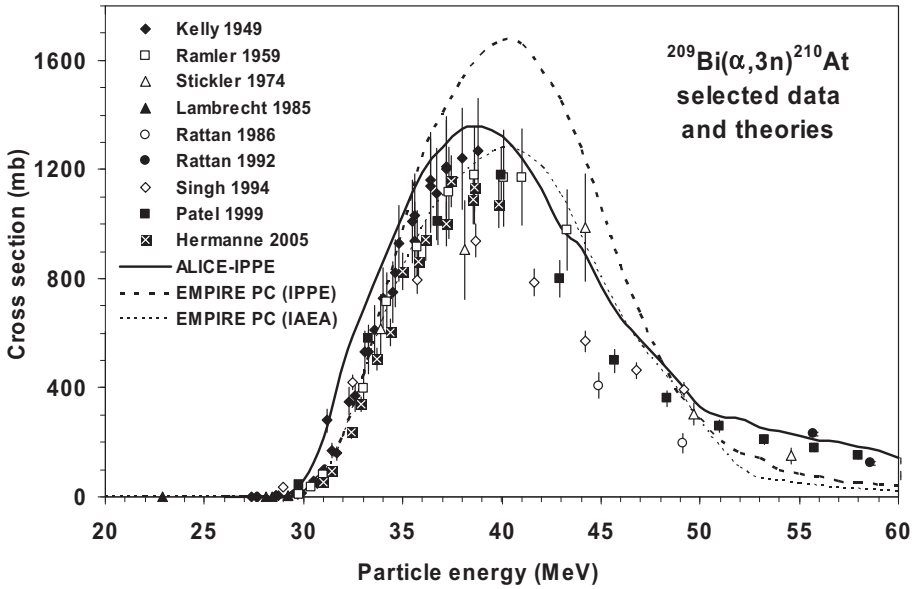

FIG. 7.143. Selected experimental data and theoretical calculations.

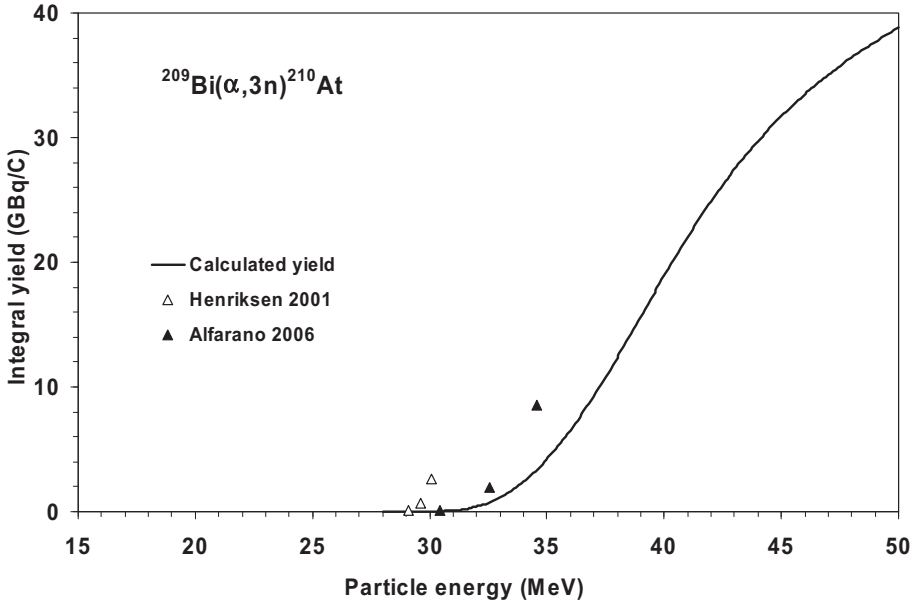

FIG. 7.144. Calculated integral yield curve based on the recommended cross-sections.

TABLE 7.62. RECOMMENDED CROSS-SECTIONS AND INTEGRAL YIELDS

$^{209}Bi(\alpha, 3n)^{210}At$ energy (MeV)	Cross-section (mb)	Integral yield	
		(μCi/μAh)	(GBq/C)
28.0	0	0	0.00
28.5	0	0	0.00
29.0	1	0	0.00
29.5	3	0	0.00
30.0	10	1	0.01
30.5	25	3	0.04
31.0	55	9	0.09
31.5	105	19	0.20
32.0	177	38	0.39
32.5	267	67	0.69
33.0	366	109	1.12
33.5	465	165	1.70
34.0	561	234	2.40
34.5	651	316	3.25
35.0	735	410	4.22
35.5	816	517	5.31
36.0	890	635	6.52
36.5	958	763	7.85
37.0	1016	902	9.27
37.5	1063	1049	10.78
38.0	1095	1203	12.36
38.5	1112	1361	13.99
39.0	1112	1522	15.64
39.5	1096	1682	17.29
40.0	1067	1841	18.92
40.5	1027	1995	20.51
41.0	980	2144	22.04
41.5	927	2287	23.50
42.0	872	2422	24.90
42.5	817	2550	26.21
43.0	764	2671	27.46

TABLE 7.62. RECOMMENDED CROSS-SECTIONS AND INTEGRAL YIELDS (cont.)

$^{209}Bi(\alpha, 3n)^{210}At$ energy (MeV)	Cross-section (mb)	Integral yield	
		(μCi/μAh)	(GBq/C)
43.5	712	2785	28.62
44.0	664	2891	29.72
44.5	618	2992	30.75
45.0	576	3086	31.71
45.5	538	3174	32.62
46.0	502	3257	33.48
46.5	470	3335	34.28
47.0	440	3409	35.04
47.5	413	3479	35.76
48.0	388	3545	36.43
48.5	366	3607	37.08
49.0	345	3667	37.69
49.5	326	3723	38.26
50.0	309	3777	38.82

7.15. CHARGED PARTICLE PRODUCTION OF ^{225}Ac

Several alpha particle emitting radioisotopes have been studied for use in radio-immunotherapy. Actinium-225 has the potential advantages of a relatively long half-life of 10 d, and four alpha particle emitters in the resulting decay chain, with a total energy release of ~28 MeV. Potentially, this radioisotope is a very important α emitter, and efforts are underway to extend application in radiotherapy. The decay chain of ^{225}Ac is shown in Fig. 7.145, and the main emissions are listed in Table 7.63.

A. Decay data

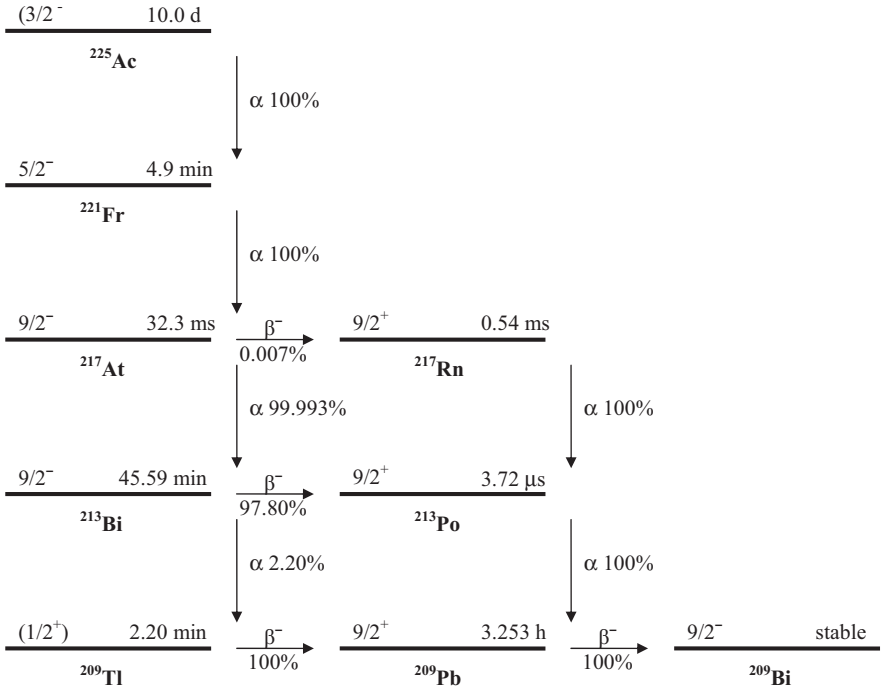

FIG. 7.145. Decay scheme of ^{225}Ac [7.3].

B. Production routes

Presently, ^{225}Ac can be obtained only in limited quantities (approx. 1 Ci/a) by radiochemical separation from ^{229}Th sources. Alternative methods of producing ^{225}Ac have been proposed, mainly through the irradiation of ^{226}Ra targets using protons, neutrons or gamma rays in order to meet the increasing radioisotope demands of large scale clinical studies, and the treatment of a large number of patients. The ^{226}Ra(p, 2n) reaction is defined in Table 7.64.

TABLE 7.63. MAIN EMISSIONS [7.3]

Parent	Decay mode	$T_{1/2}$	Radiation	Energy (keV)	End point energy (keV)	Intensity (%)
Ac-225	α 100%	10.0 d	a	5580		1.20
			a	5609		1.10
			a	5637		4.4
			a	5682		1.30
			a	5724		3.1
			a	5732		8.0
			a	5732		1.32
			a	5790.6		8.6
			a	5792.5		18.1
			a	5830		50.7
Fr-221	α 100%	4.9 min	a	6126.3		15.10
			a	6243.0		1.34
			a	6341.0		83.4
			g	218.12		11.4
At-217	α 99.993%	32.3 ms	a	7066.9		99.89
Bi-213	β^- 97.80%	45.59 min	β^-	320.4	983	30.74
			β^-	492.2	1423	65.8
			g	440.45		25.94
	α 2.20%	45.59 min	a	5869		1.94
Tl-209	β^- 100%	2.20 min	β^-	660	1827	98.80
			g	117.211		84.3
			g	465.130		96.9
			g	1567.09		99.8
Rn-217	α 100%	0.54 ms	a	7741		100
Po-213	α 100%	3.72 μs	a	8375.9		100
Pb-209	β^- 100%	3.253 h	β^-	197.5	644.4	100

TABLE 7.64. INVESTIGATED PRODUCTION ROUTE [7.3, 7.4]

Target isotope	Natural abundance	Reaction	Q-value (MeV)	Threshold energy (MeV)
Ra-226	1600 a	(p, 2n)	–6.8	6.9

C. ^{226}Ra(p, 2n)^{225}Ac reaction

The measurements of Apostolidis (2005) are compared with the resulting statistical fit to experimental cross-section data in Fig. 7.146. Excitation functions have been calculated by means of the ALICE-IPPE and EMPIRE nuclear reaction modelling codes, and results are compared with all of the selected experimental data in Fig. 7.147. Yields determined from the recommended cross-sections are presented in Fig. 7.148, while corresponding numerical values for the recommended cross-sections and yields are listed in Table 7.65.

BIBLIOGRAPHY, EVALUATION AND SELECTION

Decay data

XIAOLONG, H., BAOSONG, W., Evaluation of ^{225}Ac decay data, Appl. Radiat. Isot. **65** (2007) 712–723.
New results.

Cross-sections

APOSTOLIDIS, C., et al., Cyclotron production of ^{225}Ac for targeted alpha therapy, Appl. Radiat. Isot. **62** (2005) 383–387.
EXFOR: O1236

Yield

No data were found.

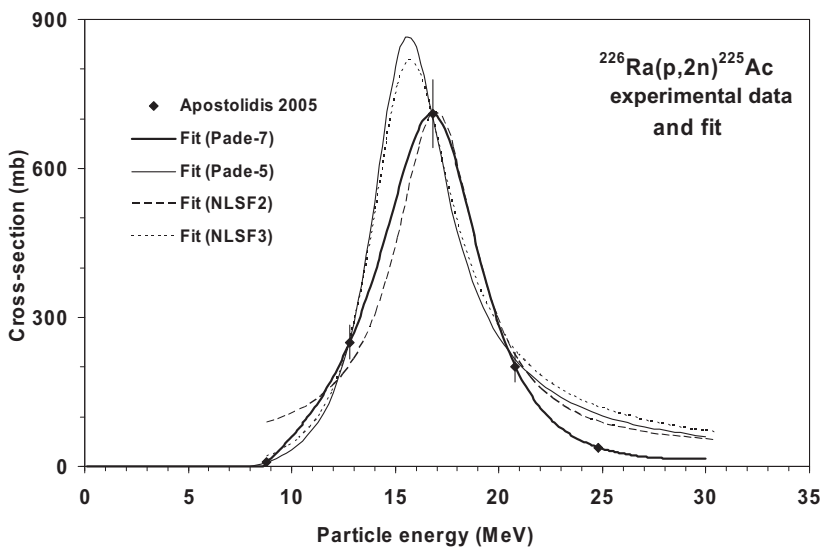

FIG. 7.146. Experimental data and the recommended curve (fit).

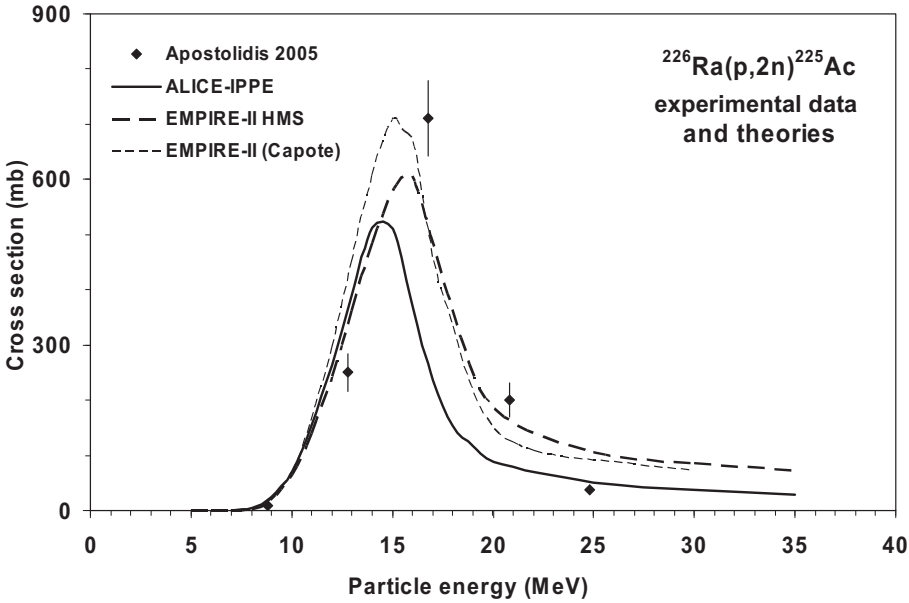

FIG. 7.147. Experimental data and theoretical calculations.

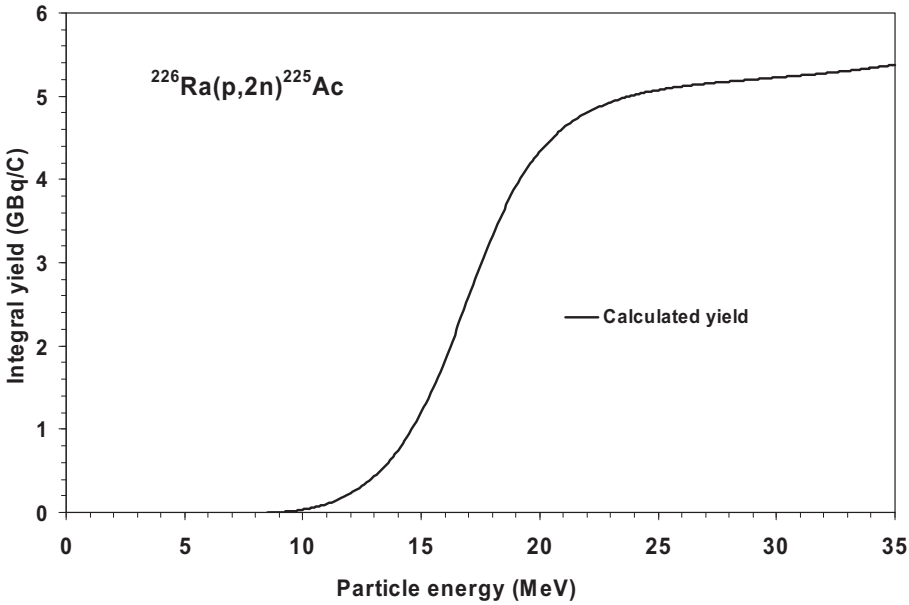

FIG. 7.148. Calculated integral yield curve based on the recommended cross-sections.

TABLE 7.65. RECOMMENDED CROSS-SECTIONS AND INTEGRAL YIELDS

$^{226}Ra(p, 2n)^{225}Ac$ energy (MeV)	Cross-section (mb)	Integral yield	
		(μCi/μAh)	(GBq/C)
8.5	0	0	0.00
9.0	16	0	0.00
9.5	37	1	0.01
10.0	59	3	0.03
10.5	84	6	0.06
11.0	112	10	0.10
11.5	144	15	0.16
12.0	180	22	0.23
12.5	222	31	0.32
13.0	270	42	0.43
13.5	325	56	0.57
14.0	389	72	0.74
14.5	459	93	0.95
15.0	534	117	1.20
15.5	607	146	1.50
16.0	668	179	1.84
16.5	705	215	2.20
17.0	706	252	2.59
17.5	669	289	2.97
18.0	601	324	3.33
18.5	518	355	3.64
19.0	432	381	3.92
19.5	353	404	4.15
20.0	285	422	4.34
20.5	229	437	4.49
21.0	183	449	4.62
21.5	147	459	4.72
22.0	118	467	4.80
22.5	95	474	4.87
23.0	77	480	4.93
23.5	63	484	4.98

TABLE 7.65. RECOMMENDED CROSS-SECTIONS AND INTEGRAL YIELDS (cont.)

$^{226}Ra(p, 2n)^{225}Ac$ energy (MeV)	Cross-section (mb)	Integral yield	
		(μCi/μAh)	(GBq/C)
24.0	51	488	5.01
24.5	42	491	5.05
25.0	35	494	5.07
25.5	30	496	5.10
26.0	25	498	5.12
26.5	22	500	5.13
27.0	19	501	5.15
27.5	18	502	5.16
28.0	16	504	5.18
28.5	15	505	5.19
29.0	15	506	5.20
29.5	14	507	5.21
30.0	14	508	5.22
30.5	15	509	5.24
31.0	15	511	5.25
31.5	16	512	5.26
32.0	16	513	5.27
32.5	17	515	5.29
33.0	18	516	5.30
33.5	19	518	5.32
34.0	20	519	5.34
34.5	21	521	5.36
35.0	22	523	5.38

REFERENCES

[7.1] QAIM, S.M., BISINGER, T., HILGERS, K., NAYAK, D., COENEN, H.H., Positron emission intensities in the decay of ^{64}Cu, ^{76}Br and ^{124}I, Radiochim. Acta **95** (2007) 67–73.

[7.2] Medical Internal Radiation Dose (MIRD) Database, http://www.nndc.bnl.gov/mird

[7.3] http://www-nds.iaea.org/ensdf/ and http://www.nndc.bnl.gov/ensdf/ for ENSDF, NuDat 2.4, National Nuclear Data Center, Brookhaven Natl Lab., http://www.nndc.bnl.gov/nudat2/

[7.4] Q-value Calculator (QCalc), National Nuclear Data Center (NNDC), Brookhaven Natl Lab., http://www.nndc.bnl.gov/qcalc/

CONTRIBUTING AUTHORS

Běták, E.	Slovak Academy of Science, Slovakia
Caldeira, A.D.	Centro Técnico Aeroespacial, Brazil
Capote, R.	International Atomic Energy Agency
Carlson, B.V.	Instituto Tecnologico de Aeronáutica, Brazil
Choi, H.D.	Seoul National University, Republic of Korea
Guimarães, F.B.	Centro Técnico Aeroespacial, Brazil
Ignatyuk, A.V.	Institute of Physics and Power Engineering, Russian Federation
Kim, S.K.	Seoul National University, Republic of Korea
Kiraly, B.	Hungarian Academy of Sciences, Hungary
Kovalev, S.F.	Institute of Physics and Power Engineering, Russian Federation
Menapace, E.†	ENEA, Italy
Nichols, A.L.	International Atomic Energy Agency
Nortier, M.	Los Alamos National Laboratory, United States of America
Pompeia, P.	Centro Técnico Aeroespacial, Brazil
Qaim, S.M.	Forschungszentrum Jülich, Germany
Scholten, B.	Forschungszentrum Jülich, Germany
Shubin, Yu.N.†	Institute of Physics and Power Engineering, Russian Federation
Sublet, J.-Ch.	CEA Cadarache, France
Tárkányi, F.	Hungarian Academy of Sciences, Hungary

† Deceased.

IAEA
International Atomic Energy Agency

Where to order IAEA publications

In the following countries IAEA publications may be purchased from the sources listed below, or from major local booksellers. Payment may be made in local currency or with UNESCO coupons.

AUSTRALIA
DA Information Services, 648 Whitehorse Road, MITCHAM 3132
Telephone: +61 3 9210 7777 • Fax: +61 3 9210 7788
Email: service@dadirect.com.au • Web site: http://www.dadirect.com.au

BELGIUM
Jean de Lannoy, avenue du Roi 202, B-1190 Brussels
Telephone: +32 2 538 43 08 • Fax: +32 2 538 08 41
Email: jean.de.lannoy@infoboard.be • Web site: http://www.jean-de-lannoy.be

CANADA
Bernan Associates, 4501 Forbes Blvd, Suite 200, Lanham, MD 20706-4346, USA
Telephone: 1-800-865-3457 • Fax: 1-800-865-3450
Email: customercare@bernan.com • Web site: http://www.bernan.com

Renouf Publishing Company Ltd., 1-5369 Canotek Rd., Ottawa, Ontario, K1J 9J3
Telephone: +613 745 2665 • Fax: +613 745 7660
Email: order.dept@renoufbooks.com • Web site: http://www.renoufbooks.com

CHINA
IAEA Publications in Chinese: China Nuclear Energy Industry Corporation, Translation Section, P.O. Box 2103, Beijing

CZECH REPUBLIC
Suweco CZ, S.R.O., Klecakova 347, 180 21 Praha 9
Telephone: +420 26603 5364 • Fax: +420 28482 1646
Email: nakup@suweco.cz • Web site: http://www.suweco.cz

FINLAND
Akateeminen Kirjakauppa, PO BOX 128 (Keskuskatu 1), FIN-00101 Helsinki
Telephone: +358 9 121 41 • Fax: +358 9 121 4450
Email: akatilaus@akateeminen.com • Web site: http://www.akateeminen.com

FRANCE
Form-Edit, 5, rue Janssen, P.O. Box 25, F-75921 Paris Cedex 19
Telephone: +33 1 42 01 49 49 • Fax: +33 1 42 01 90 90
Email: formedit@formedit.fr • Web site: http://www. formedit.fr

Lavoisier SAS, 145 rue de Provigny, 94236 Cachan Cedex
Telephone: + 33 1 47 40 67 02 • Fax +33 1 47 40 67 02
Email: romuald.verrier@lavoisier.fr • Web site: http://www.lavoisier.fr

GERMANY
UNO-Verlag, Vertriebs- und Verlags GmbH, Am Hofgarten 10, D-53113 Bonn
Telephone: + 49 228 94 90 20 • Fax: +49 228 94 90 20 or +49 228 94 90 222
Email: bestellung@uno-verlag.de • Web site: http://www.uno-verlag.de

HUNGARY
Librotrade Ltd., Book Import, P.O. Box 126, H-1656 Budapest
Telephone: +36 1 257 7777 • Fax: +36 1 257 7472 • Email: books@librotrade.hu

INDIA
Allied Publishers Group, 1st Floor, Dubash House, 15, J. N. Heredia Marg, Ballard Estate, Mumbai 400 001,
Telephone: +91 22 22617926/27 • Fax: +91 22 22617928
Email: alliedpl@vsnl.com • Web site: http://www.alliedpublishers.com

Bookwell, 2/72, Nirankari Colony, Delhi 110009
Telephone: +91 11 23268786, +91 11 23257264 • Fax: +91 11 23281315
Email: bookwell@vsnl.net

ITALY
Libreria Scientifica Dott. Lucio di Biasio “AEIOU”, Via Coronelli 6, I-20146 Milan
Telephone: +39 02 48 95 45 52 or 48 95 45 62 • Fax: +39 02 48 95 45 48
Email: info@libreriaaeiou.eu • Website: www.libreriaaeiou.eu

JAPAN
Maruzen Company, Ltd., 13-6 Nihonbashi, 3 chome, Chuo-ku, Tokyo 103-0027
Telephone: +81 3 3275 8582 • Fax: +81 3 3275 9072
Email: journal@maruzen.co.jp • Web site: http://www.maruzen.co.jp

REPUBLIC OF KOREA
KINS Inc., Information Business Dept. Samho Bldg. 2nd Floor, 275-1 Yang Jae-dong SeoCho-G, Seoul 137-130
Telephone: +02 589 1740 • Fax: +02 589 1746 • Web site: http://www.kins.re.kr

NETHERLANDS
De Lindeboom Internationale Publicaties B.V., M.A. de Ruyterstraat 20A, NL-7482 BZ Haaksbergen
Telephone: +31 (0) 53 5740004 • Fax: +31 (0) 53 5729296
Email: books@delindeboom.com • Web site: http://www.delindeboom.com

Martinus Nijhoff International, Koraalrood 50, P.O. Box 1853, 2700 CZ Zoetermeer
Telephone: +31 793 684 400 • Fax: +31 793 615 698
Email: info@nijhoff.nl • Web site: http://www.nijhoff.nl

Swets and Zeitlinger b.v., P.O. Box 830, 2160 SZ Lisse
Telephone: +31 252 435 111 • Fax: +31 252 415 888
Email: infoho@swets.nl • Web site: http://www.swets.nl

NEW ZEALAND
DA Information Services, 648 Whitehorse Road, MITCHAM 3132, Australia
Telephone: +61 3 9210 7777 • Fax: +61 3 9210 7788
Email: service@dadirect.com.au • Web site: http://www.dadirect.com.au

SLOVENIA
Cankarjeva Zalozba d.d., Kopitarjeva 2, SI-1512 Ljubljana
Telephone: +386 1 432 31 44 • Fax: +386 1 230 14 35
Email: import.books@cankarjeva-z.si • Web site: http://www.cankarjeva-z.si/uvoz

SPAIN
Díaz de Santos, S.A., c/ Juan Bravo, 3A, E-28006 Madrid
Telephone: +34 91 781 94 80 • Fax: +34 91 575 55 63
Email: compras@diazdesantos.es, carmela@diazdesantos.es, barcelona@diazdesantos.es, julio@diazdesantos.es
Web site: http://www.diazdesantos.es

UNITED KINGDOM
The Stationery Office Ltd, International Sales Agency, PO Box 29, Norwich, NR3 1 GN
Telephone (orders): +44 870 600 5552 • (enquiries): +44 207 873 8372 • Fax: +44 207 873 8203
Email (orders): book.orders@tso.co.uk • (enquiries): book.enquiries@tso.co.uk • Web site: http://www.tso.co.uk

On-line orders
DELTA Int. Book Wholesalers Ltd., 39 Alexandra Road, Addlestone, Surrey, KT15 2PQ
Email: info@profbooks.com • Web site: http://www.profbooks.com

Books on the Environment
Earthprint Ltd., P.O. Box 119, Stevenage SG1 4TP
Telephone: +44 1438748111 • Fax: +44 1438748844
Email: orders@earthprint.com • Web site: http://www.earthprint.com

UNITED NATIONS
Dept. I004, Room DC2-0853, First Avenue at 46th Street, New York, N.Y. 10017, USA
(UN) Telephone: +800 253-9646 or +212 963-8302 • Fax: +212 963-3489
Email: publications@un.org • Web site: http://www.un.org

UNITED STATES OF AMERICA
Bernan Associates, 4501 Forbes Blvd., Suite 200, Lanham, MD 20706-4346
Telephone: 1-800-865-3457 • Fax: 1-800-865-3450
Email: customercare@bernan.com · Web site: http://www.bernan.com

Renouf Publishing Company Ltd., 812 Proctor Ave., Ogdensburg, NY, 13669
Telephone: +888 551 7470 (toll-free) • Fax: +888 568 8546 (toll-free)
Email: order.dept@renoufbooks.com • Web site: http://www.renoufbooks.com

Orders and requests for information may also be addressed directly to:

Marketing and Sales Unit, International Atomic Energy Agency
Vienna International Centre, PO Box 100, 1400 Vienna, Austria
Telephone: +43 1 2600 22529 (or 22530) • Fax: +43 1 2600 29302
Email: sales.publications@iaea.org • Web site: http://www.iaea.org/books

11-09421

PRODUCTION OF LONG LIVED PARENT RADIONUCLIDES FOR GENERATORS: ^{68}Ge, ^{82}Sr, ^{90}Sr AND ^{188}W
IAEA Radioisotopes and Radiopharmaceuticals Series No. 2
STI/PUB/1436 (116 pp.; 2010)
ISBN 978-92-0-101110-7 Price: €50.00

CYCLOTRON PRODUCED RADIONUCLIDES: GUIDELINES FOR SETTING UP A FACILITY
Technical Reports Series No. 471
STI/DOC/010/471 (213 pp.; 2009)
ISBN 978-92-0-103109-9 Price: €45.00

THERAPEUTIC RADIONUCLIDE GENERATORS: ^{90}Sr/^{90}Y AND ^{88}W/^{188}Re GENERATORS
Technical Reports Series No. 470
STI/DOC/010/470 (233 pp.; 2009)
ISBN 978-92-0-111408-2 Price: €45.00

CYCLOTRON PRODUCED RADIONUCLIDES: PHYSICAL CHARACTERISTICS AND PRODUCTION METHODS
Technical Reports Series No. 468
STI/DOC/010/468 (266 pp.; 2009)
ISBN 978-92-0-106908-5 Price: €52.00

CYCLOTRON PRODUCED RADIONUCLIDES: PRINCIPLES AND PRACTICE
Technical Reports Series No. 465
STI/DOC/010/465 (215 pp.; 2009)
ISBN 978-92-0-100208-2) Price: €45.00

TRENDS IN RADIOPHARMACEUTICALS (ISTR-2005) (2 volumes)
STI/PUB/1294 (408 pp.; 2008)
ISBN 92-0-101707-3 Price: €120.00

CHARGED PARTICLE CROSS-SECTION DATABASE FOR MEDICAL RADIOISOTOPE PRODUCTION: DIAGNOSTIC RADIOISOTOPES AND MONITOR REACTIONS
IAEA-TECDOC-1211 Price: €15.00

Nuclear reactors, cyclotrons and accelerators are used for the production of radionuclides for both diagnostic and therapeutic purposes in nuclear medicine. The physical basis of their production routes is described through the interaction of neutrons and charged particles with matter. These processes have to be well understood in order to produce radionuclides of high purity in an efficient manner. This technical report summarizes the results of an IAEA coordinated research project devoted to comprehensive measurements and evaluations of neutron and charged particle induced cross-sections for the production of therapeutic radionuclides for medical applications.

INTERNATIONAL ATOMIC ENERGY AGENCY
VIENNA
ISBN 978–92–0–115010–3
ISSN 0074–1914